Tectonic history, microtopography and bottom water circulation of the Natal Valley and Mozambique Ridge, southwest Indian Ocean.

By:

Errol Avern Wiles

Submitted in fulfilment of the degree Doctor of Philosophy

In the Discipline of Geological Sciences

School of Agricultural, Earth and Environmental Sciences

College of Agriculture, Engineering and Science

University of KwaZulu Natal,

Durban

South Africa

2014

Preface

The experimental work described in this thesis was carried out in the Discipline of Geological Sciences, University of KwaZulu-Natal, Westville, from July 2010 to November 2014, under the supervision of Prof. Watkeys, Dr. Green and Prof. Jokat.

These studies represent original work by the author and have not otherwise been submitted in any form for any degree or diploma to any tertiary institution. Where use has been made of the work of others it is duly acknowledged in the text.

*Signed:*_____ *Name:*_____ *Date:*_____

Declaration 1 – Plagiarism

I, Errol Avern Wiles, declare that:

1. The research reported in this thesis, except where otherwise indicated, is my original research.

2. This thesis has not been submitted for any degree or examination at any other university.

3. This thesis does not contain other persons' data, graphs or other information, unless specifically acknowledged as being sourced from other persons.

4. This thesis does not contain any other persons writing, unless specifically acknowledged as being sourced from other researchers. Where other written sources have been quoted then:

a. *Their words have been re-written but the general information attributed to them has been referenced*

b. *Where their exact words have been used, then their writing has been placed in italics and inside quotation marks, and referenced.*

5. This thesis does not contain text, graphics or tables copied from the Internet, unless specifically acknowledged, and the source being detailed in the thesis and in the References section.

*Signed:*_____ *Name:*_____ *Date:*_____

Declaration 2 – Publications

A detailed account of the contributions by the authors of published work is given in section 1.4 Structure and layout of Thesis (page 5). Published, peer reviewed papers comprise the following:

- *Article I, Chapter 3: Anomalous seafloor mounds in the northern Natal Valley, southwest Indian Ocean: Implications for the East African Rift System. Tectonophysics, 630:300–312. dx.doi.org/10.1016/j.tecto.2014.05.030.*

Errol Wiles [a], Andrew Green [a], Mike Watkeys [a], Wilfried Jokat [b], Ralf Krocker [b]

[a] Geological Sciences, School of Agricultural, Earth and Environmental Sciences, University of KwaZulu-Natal, Private Bag X 54001, Durban 4000, South Africa.

[b] Alfred-Wegener-Institute for Polar and Marine Research, Am Alten Hafen 26, D-27568 Bremerhaven, Germany.

- *Article II, Chapter 4: The evolution of the Tugela Canyon and submarine fan: A complex interaction between margin erosion and bottom current sweeping, southwest Indian Ocean, South Africa. Marine and Petroleum Geology 44 (2013) 60 – 70.*

Errol Wiles [a], Andrew Green [a], Mike Watkeys [a], Wilfried Jokat [b], Ralph Krocker [b]

[a] Geological Sciences, School of Agricultural, Earth and Environmental Sciences, University of KwaZulu-Natal, Private Bag X 54001, Durban 4000, South Africa.

[b] Alfred-Wegener-Institute for Polar and Marine Research, Am Alten Hafen 26, D-27568 Bremerhaven, Germany.

- *Article III, Chapter 5: A new pathway for Deep water exchange between the Natal Valley and Mozambique Basin. Accepted by Geo-Marine Letters (JrnlID 367_ArtID 383).*

Errol Wiles [a], Andrew Green [a], Mike Watkeys [a], Wilfried Jokat [b], Ralf Krocker [b]

[a] Geological Sciences, School of Agricultural, Earth and Environmental Sciences, University of KwaZulu-Natal, Private Bag X 54001, Durban 4000, South Africa.

[b] Alfred-Wegener-Institute for Polar and Marine Research, Am Alten Hafen 26, D-27568 Bremerhaven, Germany.

In each case E. A. Wiles drafted the manuscripts and figures/tables for submission as the primary and corresponding author based on research carried out by the first author (E.A. Wiles). Subsequent authors (Prof. Mike Watkeys, Dr. Green, Prof. Dr. Wilfried Jokat and Ralph Krocker) represent advisory and editorial roles played by the Supervisor, Co-supervisors, and technical personnel.

*Signed:*_____ *Name:*_____ *Date:*_____

Acknowledgements

This thesis is the culmination of a journey which began in 2005 when I enrolled as an undergraduate at the University of KwaZulu-Natal. I never imagined it would come this far. The thought of going beyond Honours was daunting, and anyway, who in their right mind wants to study for that long?? However, after beginning this study in 2011 time seems to have flown.

Many people and institutions have been involved is this work and I thank them all. In particular I must thank the Alfred Wegner Institute for marine and polar research. The data used in this study were made available by the Alfred Wegner Institute, without which this study would not have been possible. The National Research Foundation is acknowledged and thanked for granting scholarships (Innovation Scholarship) throughout this Doctoral study. Without this financial support this study would not have been sustainable.

My supervisors, Professor Michael Watkeys, Doctor Andrew Green and Professor Wilfried Jokat are thanked for their valued guidance, support and input (academic and in general) throughout this study, as well as during my time at the University of KwaZulu Natal, on research cruises, at conferences and abroad. I have learnt a lot more from these people than this thesis can possibly show. Prof. Watkeys inspired an interest in Geology from the first lecture I took in the subject and ignited a passion for rocks and the stories they tell. Dr. Green exposed me to the world of marine geology and set me on this marine course early in my undergraduate degree, and has continued to expose me to new facets of marine geoscience. Prof. Watkeys introduced me to Prof. Jokat and the AWI in 2009. I have not looked back since. Prof. Jokat has generously allowed me access to the data used in this study, as well as providing me with fantastic practical experience through two research cruises in the southwest Indian Ocean (although both these cruises involved several weeks of seasickness).

To the post-grad team from Geology Alex Metz, Carlos Loreio, Lauren Hoyer, Lauren Pretoriuos, Shannon Dixon, Leslee Salzmann, Nku Dladla, Jannie Weitz, Riaan Botha and Warwick Hastie, you all have had an impact on this thesis in one way or another, be it practical advice, as a sounding board, or a much needed distraction when my mind went AWOL. Warwick Hastie, in particular, set the tone of post-graduate research for me as a Masters student (although he likely does not realise this). His work ethic and focus is something I have tried to emulate throughout this study, and it has done me well.

To my non-varsity friends and family, in particular Craig Howie, Miguel Rodriges, Allen Foster, and my brothers Graham Wiles and Bryan Paynter, who have hiked, fished, cycled and surfed (and eaten junk-food when there was no surf) with me, I cannot thank you enough. You guys all helped me keep on track.

On a professional note I must also thank Doug Slograve, Michael MacHutchon, Hayley Cawthra, Rio Lueci and Zane Thakerey for offering me the opportunity to gain practical experience associated with the marine geology/survey industry. I learnt a hell of a lot from you all, and I appreciate the time spent in this regard. It has left me with a far more well-rounded understanding than what purely academic work would have afforded me.

To my family Wendy Wiles, Laura Jaggard and Matt Jaggard, thank you for standing by me through these years of study (it has been a good few years…), stressful times (there were many…), and for celebrating the good times (including, but not limited to, the submission of this thesis). Without this support life would have been a lot more difficult.

We thank the BMBF (Bundesministerium fur Bildung und Forschung) for funding the scientific projects (contract number 03G0183A, 03G0730A). The crews of RV Sonne (AISTEK II) and RV Pelagia (AISTEK III) are acknowledged for their excellent support and expertise in the data acquisition phases. The financial assistance of the National Research Foundation (DAAD-NRF) towards this research is hereby acknowledged (Innovation Scholarship: 83799). Opinions expressed and conclusions arrived at, are those of the author and are not necessarily to be attributed to the DAAD-NRF. The Petroleum Agency of South Africa are thanked for allowing us access to multichannel seismic data.

Lastly I thank my mind for always coming back and not disintegrating during the course of this research.

Abstract

This thesis focuses on aspects of the tectonic history, sediment delivery and subsequent sediment redistribution within the Natal Valley and Mozambique Basin of the southwest Indian Ocean. It aims to 1) better constrain the tectonic history of these basins based on anomalous seafloor features, 2) understand the timing, evolution and formative processes of sediment delivery systems within the Natal Valley and Mozambique Basin, 3) account for the redistribution of seafloor sediments within the southwest Indian Ocean. The southwest Indian Ocean opened during the Gondwana breakup event giving rise to two north/south orientated rectangular basins separated by the Mozambique ridge. Early research (1980's) within these basins discussed basin features in terms of the available data at the time. By modern standards these data sets are relatively low resolution, and did not allow early researchers to fully account for the existence, development or evolution of many morphological features within the southwest Indian Ocean. This study uses recently acquired multibeam bathymetry and PARASOUND/3.5 kHz seismic data sets to describe and account for the geomorphology of the southwest Indian Ocean. Antecedent geology is discussed with respect to its development, in association with regional regimes, and role in provision of accommodation space and sediment redistribution within the study area. Sediment delivery pathways from the continental shelf to the deep marine basins are discussed, outlining the evolution of these systems under the control of antecedent geology and regional uplift. The redistribution of sediment is then discussed from the microtopography observed within the southwest Indian Ocean. Results show anomalous seafloor mounds in the northern Natal Valley, and extensional structures within the Mozambique Basin, are likely linked to the southward propagation of the East African Rift System. Dynamic current regimes and antecedent geology have played a significant role in the availability of sediment and subsequent delivery of sediment to the Natal Valley and Mozambique Basin via submarine canyons and channels. Once delivered to the basins, sediments are redistributed by deep and bottom water thermohaline Circulation. In the Natal Valley this is manifest as an atypical, current swept and winnowed, submarine fan (associated with the Tugela Canyon). While in the Mozambique Basin significant sediment wave fields reflect the influence of Thermohaline Circulation within this basin, and interaction with the seafloor. This relationship between Thermohaline Circulation and seafloor sediments has allowed existing deep and bottom water pathways to be better constrained and, in some instances, modified to better represent the actual circulation within specific regions of the study area.

Contents

Chapter 1 –

1. Introduction **1**

1.1. *Introduction and rationale* **1**

1.2. Aims of research **2**

1.3. Materials and methods **4**

1.4 Structure and layout of Thesis **5**

Chapter 2 –

2. Regional setting **10**

2.1. Geology and physiography **10**

2.1.1. Natal Valley **10**

2.1.2. Northern Mozambique Basin and Channel **12**

2.2. Oceanography **14**

2.2.1 Natal Valley **14**

2.2.2. Northern Mozambique Basin and Channel **16**

Chapter 3 – *Anomalous seafloor mounds in the northern Natal Valley, southwest Indian Ocean: Implications for the East African Rift System*

3.1. Introduction **18**

3.1.1. Previous bathymetric work **19**

3.2. Material and Methods **21**

3.3. Results **22**

3.3.1 Bathymetry **22**

3.3.2 High frequency seismic character **26**

3.3.3 Morphological character **27**

3.4. Discussion **33**

3.4.1 Bathymetry **33**

3.4.2 High frequency seismic character **33**

3.4.3 Mound origins **34**

3.4.3.1 Salt **34**

3.4.3.2 Bottom water circulation **35**

3.4.3.3 Submarine igneous activity **36**

3.4.4 Seamount geomorphology **36**

3.4.4.1 Alkaline igneous activity **38**

3.5 Timing and tectonic significance ***40***

Chapter 4 – *The evolution of the Tugela Canyon and submarine fan: A complex interaction between margin erosion and bottom current sweeping, southwest Indian Ocean, South Africa.*

4.1. Introduction **43**

4.2 Results **45**

4.3 Discussion **52**

4.3.1 Erosional styles **52**

4.3.2. Timing and mechanisms of canyon development **54**

4.3.3. Modern canyon and fan activity **55**

Chapter 5 – *A new pathway for Deep water exchange between the Natal Valley and Mozambique Basin?*

5.1. Introduction **58**

5.2. Results **60**

5.3. Discussion **68**

5.3.1 Echo character contrasts **68**

5.3.2 Interpretation of bathymetric and 3.5 kHz data **69**

5.3.3. Significance of creep **71**

5.3.4 Sediment redistribution via the Agulhas Current or NADW? **72**

5.3.4.1 Oceanographic constraints to potential NADW flow and a revised pathway **73**

5.3.5 The relevance of a revised deep water pathway **74**

Chapter 6 – *Surface expression of East African Rift System propagation in the Mozambique Channel, southwest Indian Ocean.*

6.1. Introduction **77**

6.2 Material and Methods **78**

6.3. Results **78**

6.3.1 Bathymetry **78**

6.3.2 High frequency seismic character **80**

6.3.3 Seismicity **82**

6.4. Discussion **84**

6.4.1 Bathymetry **84**

6.4.2 High frequency seismic character **84**

6.4.3 Seismicity **85**

6.4.3.1 Seafloor expression of southeasterly extension? **85**

Chapter 7 – *Anatomy, high frequency seismic character and depositional processes of the lower Zambezi Channel, Mozambique Basin, SWIO.*

7.1. Introduction **88**

7.2. Results **89**

7.2.1 Zambezi Channel **89**

7.2.2 Tsiribihina Channel **94**

7.2.3 Confluence of Zambezi and Tsiribihina Channels **95**

7.3 Discussion **97**

7.3.1 Current classification of deep sea channels **97**

7.3.1.1 The Zambezi Channel system **98**

7.3.2. Shallow seismic character of the Zambezi Channel **100**

7.3.3. Comparison of the Zambezi Channel with empirical results **101**

7.3.4. Evolution of the Zambezi Channel system **103**

Chapter 8 – *Microtopography and Bottom Water circulation of the northern Mozambique Basin.*

8.1 Introduction **109**

8.2 Results **109**

8.2.1 Distribution of seafloor types **109**

8.2.2 Description of seafloor types **110**

8.2.3 Echo character classification **117**

8.2.3.1 Echo character types **117**

8.3 Discussion **120**

8.3.1 Relating microtopography to basin processes **120**

8.3.1.1 Microtopography **121**

8.3.1.2 Current circulation, turbidity currents and relationship to bathymetric character **123**

Chapter 9

9.1. Concluding remarks **126**

9.1.1. Tectonic history Natal Valley **126**

9.1.2. Sediment delivery Natal Valley **126**

9.1.3. Seafloor characteristics of the Natal Valley **127**

9.1.4. Tectonics within the Mozambique Basin **128**

9.1.5 The Zambezi Channel **128**

9.1.6. Seafloor characteristics of the northern Mozambique Basin **129**

References **130**

Appendix A **156**

Appendix B **198**

Appendix C **227**

Appendix D **290**

Chapter 1

1. Introduction

1.1. Introduction and rationale

The primary objective of this study was to account for sediment delivery and redistribution in two adjacent marine basins, taking into account certain aspects of the basins' tectonic regime and the associated regional context (Fig. 1.1). The basins in question are the Natal Valley and Mozambique Basin of the southwest Indian Ocean (SWIO) (Fig. 1.2). The majority of sediment input to these basins is shed from the African continent and introduced into either basin. Both are north-south orientated, rectangular confined basins that deepen to the south and provide relatively restricted topographic accommodation space (negative relief areas) to incoming sediments.

The three factors mentioned above account for much of the macro/microtopography within general ocean basins. Whereas macrotopography describes large basin scale (ca. > 10 km) basin topography, typically defined by oceanic crust protuberances, microtopography is the result of bedforms developing in the sedimentary cover, draped over the oceanic crust, that are not typically resolved in basin scale studies. The microtopography that develops is dependent on the form of the antecedent geology (oceanic/continental crust), sediment in-put/out-put and the interaction between the seafloor and bottom water circulation (Fig. 1.1). The resulting bedforms are largely produced through the movement of bottom water currents, but are also influenced by sediments introduced into the basin by turbidity currents cascading down from continental shelves, submarine channels or bathymetric highs.

Until the 1960's, these microtopographic features were regarded as being of too small a scale to be mapped in deep ocean basins because of the poor resolution of the mapping equipment. Pioneering research into bottom water currents and the associated microtopography initially commenced in the Atlantic Ocean and was then extended into the SW Indian Ocean and Mozambique Basin (Damuth, 1980; Kolla et al., 1980) (Fig. 1.2). However, in the past three decades this aspect of the ocean floor evolution in the latter regions has been neglected, despite the considerable improvement in resolution of geophysical imaging of the ocean floor through techniques such as multibeam bathymetry. New bathymetric data collected during recent research cruises over the Natal Valley and Mozambique Basin have provided much higher resolution data sets, concerning

microtopography, than available in the past, allowing new microtopographic interpretations to be made and considered in terms of antecedent geology and bottom water circulation.

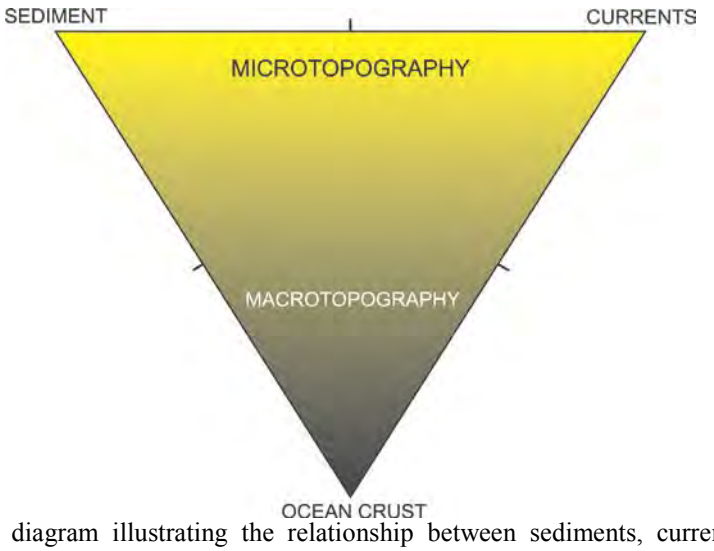

Fig.1.1: A schematic diagram illustrating the relationship between sediments, currents (bottom water and turbidity currents) and the ocean crust. Macrotopography is controlled primarily by the morphology of the ocean crust (antecedent geology), while microtopography reflects the dynamic relationship between sediments and currents within the macrotopographic framework.

1.2 Aims of research

The main aims of this research project are to better constrain the tectonic history of the Natal Valley and Mozambique Basin, understand the timing and evolution of sediment delivery to the Natal Valley and Mozambique Basin, and to document and account for the redistribution of sediments within the Natal Valley and Mozambique Basin, micro\macrotopography of the southwest Indian Ocean, offshore of SE Africa as well as the significance of antecedent geological control through the study of bathymetric and shallow seismic datasets (Fig. 1.2). The objective is to use this understanding to establish the tectonic history of, sediment delivery to, and bottom water circulation within the SWIO.

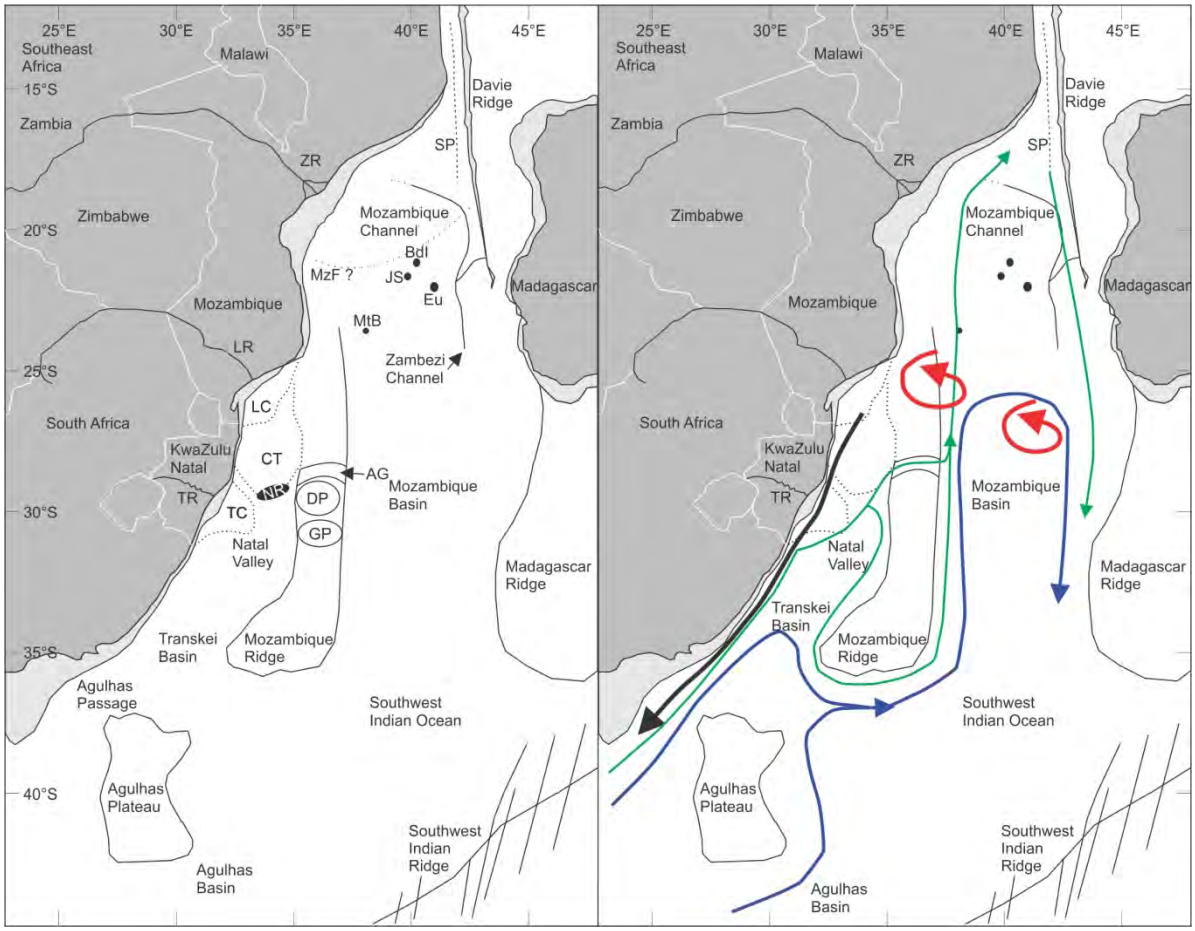

Fig. 1.2. The general format and circulation of the southwest Indian Ocean. Left: International borders within southeast Africa, major rivers (TR = Thukela River, LR = Limpopo Rivers, ZR = Zambezi River), and significant features of the southwest Indian Ocean (MzF = Mozambique Fan, CT = Central Terrace, LP = Limpopo Cone, TC = Tugela Cone, NR = Naudé Ridge, SP = Serpa Pinto Channel, AG = Ariel Graben, DP = Dana Plateau, GP = Galathea Plateau). Right: General circulation; Agulhas Current (Black), North Atlantic Deep Water (Green), Antarctic Bottom Water (Purple), eddies associated with the East Madagascar and Mozambique Current (Red). Significant seamounts are shown as black circles (MtB = Mount Bourcart, JS = Jaguar Seamount, BdI = Bassas da India, Eu = Europa Island).

To this end, the following questions are asked:

1. What is the regional significance of anomalous macrotopographic features within the southwest Indian Ocean?
2. What sediment delivery mechanisms exist within the Natal Valley and Mozambique Basin?
3. When and how did these sediment delivery systems develop and evolve?
4. What role does antecedent geology play in sediment delivery, redistribution and accommodation space within the SWIO?
5. What microtopography exists within the Natal Valley and Mozambique Basin?

6. Are the formative controls of the microtopography associated with Thermohaline Circulation or gravity driven processes (e.g., turbidity currents)?
7. In areas where the microtopography is due to bottom current circulation, is it possible to differentiate between the influences of various water masses on the seafloor sediments?
8. Can the Thermohaline Circulation pathways be better constrained based on macrotopographic controls and microtopography distribution?

To answer these questions recently acquired multibeam bathymetry and 3.5 kHz PARASOUND single-channel seismic data will be used. These data are described and discussed in section *1.3* below.

1.3 Materials and methods

The overall materials and methods pertinent to this thesis are outlined below. The data referred to below are used in part for each chapter and are not presented in a materials and methods section within each chapter. Rather, specific methods associated with individual chapters are outlined in those respective chapters.

Data from two recent research cruises, AISTEK II (20th of May – 7th of July, 2005) aboard the R/V Sonne (Jokat, 2006) and AISTEK III (9th of April – 1st June, 2009) aboard the R/V Pelagia (Jokat, 2009), were used in this study. AISTEK II investigated the Mozambique Basin and Ridge using a SIMRAD EM120 multibeam echosounder. A Kongsberg EM300 multibeam echosounder was used to acquire bathymetry data over the Mozambique Ridge and Natal Valley during the AISTEK III survey. Both multibeam data sets were processed onboard using CARIS HIPS and exported as xyz ASCII files. Interactive Visualization Systems' DMagic (version 7.3.1a) was used to grid the data, which were then displayed in Fledermaus (version 7.3.1a) for interpretation. The final bathymetry data have an output matrix of ~35 m, providing a relatively high resolution dataset. Specific portions of these data are presented in this study to illustrate the results and discussion graphically.

A 3.5 kHz (AISTEK III) and a parametric ATLAS PARASOUND echosounder (AISTEK II) were used to collect seafloor and sub-bottom seismic reflection data during the respective cruises. These data sets provide very high frequency seismic data with a vertical resolution ca. 1 m. Due to technical difficulties, complete seismic coverage along track was in some instances not achievable. In-house designed software, in addition to SEISEE

(version 2.17.1.), were used to process the data. These data were incorporated into SEISEE for visualization and interpretation of the echo character. Band pass filter adjustments and colour gains were applied to the data.

The echo character classification used in this thesis is based on that of Damuth (1975). These works represent some of the most extensive deep marine echo character-based studies from varied settings to date. The echo character types described by Damuth (1975; 1978) and summarily related to formative processes are a significant baseline against which the echo character of the Natal Valley and northern Mozambique Basin can be compared.

Although these bathymetric and shallow seismic data do not yield information relating to the opening history of the basins concerned, they provide insight into the contemporary and recent basin dynamics in terms of both sedimentary and current regimes. They also offer new insight into the significance of some macrotopographic features within the study area. The importance of 3.5 kHz and PARASOUND (shallow seismic) data in the study of microtopography was demonstrated by many workers (such as Damuth, 1975; 1978; Johnson and Damuth, 1979; Damuth, 1980; Kolla et al., 1980; Lee et al., 2002) who maintain that the study of echo-character can yield significant results with respect to understanding sedimentation processes of the deep sea (Johnson and Damuth, 1979; Damuth, 1980).

1.4 Structure and layout of Thesis

This thesis comprises a series of papers published in international peer-review journals and collated as individual chapters (Chapters 3, 4 and 5), as well as papers that are still in the manuscript preparation stage and envisioned for future submission (Chapters 6, 7 and 8).

The thesis first discusses the Natal Valley (Chapters 3, 4 and 5) in terms of its tectonic setting and attributes, the mechanisms of sediment delivery to the basin, and finally the redistribution of sediment. Chapters 6, 7 and 8 follow the same structure and discuss the Mozambique Basin/Channel in terms of the tectonic attributes, delivery of sediment, and finally sediment redistribution. The distinction between these two basins is made as each represents a discrete system that has evolved under different tectonic regimes and fed by different source areas.

Published, peer reviewed papers comprise the following:

- Article I, Chapter 3: *Anomalous seafloor mounds in the northern Natal Valley, southwest Indian Ocean: Implications for the East African Rift System.* Tectonophysics, 630: 300–312. dx.doi.org/10.1016/j.tecto.2014.05.030.
  Errol Wiles [a], Andrew Green [a], Mike Watkeys [a], Wilfried Jokat [b], Ralf Krocker [b]
  [a] Geological Sciences, School of Agricultural, Earth and Environmental Sciences, University of KwaZulu-Natal, Private Bag X 54001, Durban 4000, South Africa.
  [b] Alfred-Wegener-Institute for Polar and Marine Research, Am Alten Hafen 26, D-27568 Bremerhaven, Germany.
- Article II, Chapter 4: *The evolution of the Tugela Canyon and submarine fan: A complex interaction between margin erosion and bottom current sweeping, southwest Indian Ocean, South Africa*. Marine and Petroleum Geology, 44 (2013) 60 – 70.
  Errol Wiles [a], Andrew Green [a], Mike Watkeys [a], Wilfried Jokat [b], Ralph Krocker [b]
  [a] Geological Sciences, School of Agricultural, Earth and Environmental Sciences, University of KwaZulu-Natal, Private Bag X 54001, Durban 4000, South Africa.
  [b] Alfred-Wegener-Institute for Polar and Marine Research, Am Alten Hafen 26, D-27568 Bremerhaven, Germany.
- Article III, Chapter 5: *A new pathway for Deep water exchange between the Natal Valley and Mozambique Basin*. Geo-Marine Letters, 34(6): 525-540.
  Errol Wiles [a], Andrew Green [a], Mike Watkeys [a], Wilfried Jokat [b], Ralf Krocker [b]
  [a] Geological Sciences, School of Agricultural, Earth and Environmental Sciences, University of KwaZulu-Natal, Private Bag X 54001, Durban 4000, South Africa.
  [b] Alfred-Wegener-Institute for Polar and Marine Research, Am Alten Hafen 26, D-27568 Bremerhaven, Germany.

Appendix A contains the articles comprising chapters 3, 4 and 5 as they appear in each respective journal. Appendix B contains an article (Breitzke et al., subm.) for which the author (E. A. Wiles) is the second author. This research paper (appendix B) represents collaborative research between the first two authors (Breitzke M. and Wiles E.A.), based on initial interpretations made by Wiles (2009). Further explanation is provided in Appendix B.

It should be noted that Articles I, II, III, as well as those in preparation, are entirely the result of research carried out by the first author (E.A. Wiles), and that the subsequent authors represent advisory and editorial roles played by the Supervisor, Co-supervisors (Prof.

Mike Watkeys, Dr. Green and Prof. Dr. Wilfried Jokat), and technical personnel (Ralph Krocker). In all cases, the basis of the research was conceptualised by the first author (E.A. Wiles). The writing, preparation of the manuscripts and drawing of figures was completed by the author (E. A. Wiles), unless otherwise stated. Similarly, the submission and revision of accepted work for publication was carried out by the author, with guidance from Prof. Mike Watkeys, Dr. Andrew Green and Prof. Dr. Wilfried Jokat.

Appendix C contains other research outputs produced during the authors Doctoral studies. The author was involved in field work and initial interpretations on which these publications are based. As these topics fall outside the main aims and objectives of this thesis they are not included in the main text.

There is no main "Results" or "Discussion" section in this thesis. All results are presented and discussed within the relevant chapters in order to maintain the integrity of the published work. Concluding remarks relevant to chapters 1 – 8, within the thesis, are provided in the final chapter (Chapter 9).

Portions of this work have been presented (by Wiles, E) at the following international and national conferences (Appendix D):

- European Geosciences Union Annual Congress, 2014. *Soft sediment deformation associated with the passage of North Atlantic Deep Water through the deep Ariel Graben, Mozambique Ridge, SWIO.* Vienna, Austria. 27 April – 2 May, 2014.
  Errol Wiles [a], Andrew Green [a], Mike Watkeys [a], Wilfried Jokat [b], Ralph Krocker [b]
  [a] Geological Sciences, School of Agricultural, Earth and Environmental Sciences, University of KwaZulu-Natal, Private Bag X 54001, Durban 4000, South Africa.
  [b] Alfred-Wegener-Institute for Polar and Marine Research, Am Alten Hafen 26, D-27568 Bremerhaven, Germany.
- South African Marine Science Symposium, 2014. *Anatomy, high frequency seismic character and depositional processes of the lower Zambezi Channel, Mozambique Basin, SWIO.* Stellenbosch, South Africa. 15 – 18 July, 2014.
  Errol Wiles [a], Andrew Green [a], Mike Watkeys [a], Wilfried Jokat [b], Ralf Krocker [b]
  [a] Geological Sciences, School of Agricultural, Earth and Environmental Sciences, University of KwaZulu-Natal, Private Bag X 54001, Durban 4000, South Africa.
  [b] Alfred-Wegener-Institute for Polar and Marine Research, Am Alten Hafen 26, D-27568 Bremerhaven, Germany.

The following presentations were made by Dr. M. Breitzke using portions of the dataset initially interpreted by Wiles (2009) and culminating in the submitted work of appendix B.

- Dialogue between Contourite and Oceanography Processes, International Workshop, 28 – 29 January, University of Hull, Hull, UK, 2013. *Seafloor morphology in the Mozambique Channel: Evidence for long-term persistent bottom-current flow and deep-reaching eddy activity*.

  Monika Breitzke[a], Errol Wiles [b], Ralf Krocker [a] , Mike Watkeys [b], Wilfried Jokat [a]

  [a] Geological Sciences, School of Agricultural, Earth and Environmental Sciences, University of KwaZulu-Natal, Private Bag X 54001, Durban 4000, South Africa.

  [b] Alfred-Wegener-Institute for Polar and Marine Research, Am Alten Hafen 26, D-27568 Bremerhaven, Germany.
- Seminar Geophysik, 19 June, Universität Bremen, Bremen (2012). Evidence for current-controlled sedimentation in the southern Mozambique Channel inferred from high-resolution bathymetric and sub-bottom profiler data.

  Monika Breitzke[a], Errol Wiles [b], Ralf Krocker [a] , Mike Watkeys [b], Wilfried Jokat [a]

  [a] Alfred-Wegener-Institute for Polar and Marine Research, Am Alten Hafen 26, D-27568 Bremerhaven, Germany.

  [b] Geological Sciences, School of Agricultural, Earth and Environmental Sciences, University of KwaZulu-Natal, Private Bag X 54001, Durban 4000, South Africa.
- AGU Chapman Conference on the Agulhas System and its Role in Changing Ocean Circulation, Climate, and Marine Ecosystems, 08 – 12 October, Stellenbosch, South Africa, 2012. *Morphology of the seafloor in the Southern Mozambique Channel: Evidence for long-term persistent bottom-current flow and deep reaching eddy activity.*

  Monika Breitzke[a], Errol Wiles [b], Ralf Krocker [a] , Mike Watkeys [b], Wilfried Jokat [a]

  [a] Alfred-Wegener-Institute for Polar and Marine Research, Am Alten Hafen 26, D-27568 Bremerhaven, Germany.

  [b] Geological Sciences, School of Agricultural, Earth and Environmental Sciences, University of KwaZulu-Natal, Private Bag X 54001, Durban 4000, South Africa.
- AGU Fall Meeting, 05 – 09 December, San Francisco, USA. 2011. *Does the seafloor morphology of the southern Mozambique Channel provide evidence for persistent bottom-current flow and deep reaching eddy activity?*

  Monika Breitzke[a], Errol Wiles [b], Ralf Krocker [a] , Mike Watkeys [b], Wilfried Jokat [a]

[a] Alfred-Wegener-Institute for Polar and Marine Research, Am Alten Hafen 26, D-27568 Bremerhaven, Germany.

[b] Geological Sciences, School of Agricultural, Earth and Environmental Sciences, University of KwaZulu-Natal, Private Bag X 54001, Durban 4000, South Africa.

- European Geosciences Union General Assembly, 03 – 08 April, Vienna, Austria, 2011. *High-resolution bathymetry and shallow acoustic images of current-controlled sedimentary processes in the Southern Mozambique, Channel.*

  Monika Breitzke[a], Errol Wiles [b], Ralf Krocker [a], Mike Watkeys [b], Wilfried Jokat [a]

  [a] Alfred-Wegener-Institute for Polar and Marine Research, Am Alten Hafen 26, D-27568 Bremerhaven, Germany.

  [b] Geological Sciences, School of Agricultural, Earth and Environmental Sciences, University of KwaZulu-Natal, Private Bag X 54001, Durban 4000, South Africa.

Chapter 2

2. Regional setting

2.1. Geology and physiography

2.1.1. Natal Valley

The Natal Valley is bound to the east by the Mozambique Ridge and to the west by the south east coast of southern Africa (Fig. 1.2). The adjacent continental shelf is straight and narrow (4 – 15 km) compared to global standards (Dingle and Robson, 1985; Green, 2011a, b) but widens substantially to 45 km offshore the Thukela River. On average the continental shelf in this region dips at 0.2° toward a poorly defined shelf-break at ca. 100 m (Goodlad, 1986; Martin and Flemming, 1988). The Natal Valley deepens toward the south where it merges with the deep Transkei Basin at 4000 m depth (Fig. 1.2). Sediment input to the basin occurred at ca. 4.9 $x10^6$ m^3/yr, over the past 65 Myr (Dingle et al., 1987) and was attributed to rivers along the KwaZulu-Natal coast. These rivers, the most prominent being the Thukela River (Fig. 1.2), have been in existence since mid-Cretaceous times (Partridge and Maud, 2000) and presently deliver sediment (4.405 – 106 m^3) to the coast on a seasonal time scale (Flemming, 1980).

This sedimentary basin can be subdivided into a northern and southern area at 30° south (Fig. 1.2). The basement of the northern Natal Valley is oceanic in origin, the result of a SW – NE spreading centre (now the present-day southern Mozambique coastline) that produced the initial basin during early Gondwana break-up ca. 183 – 159 Ma (Leinweber and Jokat, 2011a). The southern Natal Valley, also floored by an oceanic basement, opened ca. 138.9 – 130.3 Ma via a southwest/northeast spreading centre to the east of the present-day basin (Leinweber and Jokat, 2011b). Spreading in the Natal Valley was complete by 90 Ma (Martin and Hartnady, 1986; Ben Avraham et al., 1993).

The sedimentary fill of the Natal Valley comprises sedimentary rocks of the Zululand Group's Makhatini Formation; fossiliferous shallow marine clays of mid Barremian to lower Aptian age that represent the rift succession. Uncomformably overlying this is the mid Aptian to lower Cenomanian Mzinene Formation that comprises fossiliferous shallow marine silts, sands and interbedded hardgrounds (Shone, 2006). Basin deposition was interrupted by a hiatus spanning the mid Cenomanian to upper Turonian times. This is defined by a regional

seismic reflection termed "McDuff" by Dingle et al. (1978). Deposition of fossiliferous shallow marine silts, sands and conglomerates of the St. Lucia Formation resumed from this point to upper Maastrichtian times. Another regional reflection, "Angus", marks the top of the St. Lucia Formation and defines another hiatus (Dingle et al., 1978; Shone, 2006). Post-Angus deposits are associated with the construction of the Tugela Cone (Fig. 1.2), the large (180 x 250 km) subaqueous delta of the Thukela River that displays a complex onlap/offlap configuration in the offshore stratigraphy (Goodlad, 1986). A Lower Pliocene unconformity, marked by regional reflection "Jimmy" truncates the underlying units. Post-Jimmy, sediments continue to exhibit an onlap/offlap configuration, with bottom current interaction noted in seismic records (cf. Goodlad, 1986). Overall Pleistocene aged deposits are rare. Lower Pleistocene unconsolidated sediments occur on the outer shelf (Green et al., 2008) and mid-upper Pleistocene aeolianite cordons span the inner to outer shelf. These cordons are mantled by thin unconsolidated Holocene sediments that are reworked and redistributed by energetic gyres and eddies associated with the southward flowing Agulhas Current (Flemming, 1980; Green, 2009).

Bathymetric features of the Natal Valley pertinent to this study are the Central Terrace, Naudé Ridge, Mozambique Ridge (Dana Plateau in particular), Ariel Graben, Tugela Cone and Limpopo Cone (Fig. 1.2). The Central Terrace is a north-south orientated basement high that provides the initial northern bathymetric depth constraint within the northern Natal Valley (Fig. 1.2). The Central Terrace has a smooth convex surface flanked to the east and west by prominent valleys, whereas the southern flank comprises a steep, smooth slope that extends southward to the deep central northern Natal Valley (Dingle et al. 1978). The steep southern slope is the topographic expression of the Naudé Ridge, a prominent basement high now overlain by sediment (thickness of 1 sec TTWT) (Dingle et al. 1978). The Tugela and Limpopo cones represent fan shaped features prograding into the Natal Valley from offshore of the Thukela and Limpopo rivers respectively (Fig. 1.2). The Tugela Cone exhibits a steep, west/east orientated southern flank, while the eastern flank has a more moderate gradient and hummocky surface. Numerous terraces create complex bathymetry over the surface of the cone, which is crosscut by the Tugela Canyon (Dingle et al. 1978; Chapter 4). The Limpopo Cone lies north of the Tugela Cone, and northwest of the Central Terrace, extending 300 km south of the Limpopo River (Martin 1981a). This sedimentary cone is separated from the continental shelf of southern Mozambique by a narrow valley, similar to that of the Central Terrace to the southeast (Dingle et al. 1978). To the east of the

Natal Valley, the north/south orientated Mozambique Ridge provides further bathymetric constraint in the form of numerous submarine plateaus. Of importance to this study are the Dana and Galathea plateaus of the northern Mozambique Ridge (Fig. 1.2). The northern Dana Plateau is the larger or the two, measuring 120 x 130 km in dimension, and rising to a depth of 1795 m below the sea surface. The northern flanks of the Dana Plateau deepen into the Ariel Graben (comprising the southern flank of the Ariel Graben), a west/east orientated 12 km wide saddle that crosses the Mozambique Ridge at 28°30"S (Fig. 1.2). South of the Dana Plateau, the Galathea Plateau rises to shallower depths (1600 m) extending 150 km in a west/east orientation and 80 km north/south.

2.1.2. Northern Mozambique Basin and Channel

Located in the southwest Indian Ocean, the Mozambique Basin is a north/south orientated rectangular marine basin (Fig. 1.2). The Mozambique Basin shoals from a depth of 5500 m in the south to a depth of 2500 m where it enters the Mozambique Channel in the north. Flanking the Mozambique Basin are the Mozambique and Madagascar ridges. The Mozambique Basin is the product of the second stage of Gondwana break-up (167 M.y), although two stages of extensional development have been noted off the southern coast of Mozambique (Leinweber, and Jokat, 2011; Mahanjan, 2012). The development of the Mozambique Ridge, to the west of the Mozambique Basin, took place at a later stage (Leinweber, and Jokat, 2011).

The Mozambique Channel is confined by the east coast of Mozambique and the west coast of Madagascar (Fig. 1.2). Within the Mozambique Channel there are two significant topographic features; the Davie Ridge and the Bassas da India/Europa islands and associated volcanic seamounts, including the Jaguar Seamount and Mount Bourcart (Fig. 1.2). The Davie Ridge is a curvilinear fracture zone that facilitated the relative southward migration of Madagascar away from Africa in the Late Jurassic to Early Cretaceous (Bassias, 1992; Scrutton, 1978). This north/south orientated feature divides the northern Mozambique Channel longitudinally, interfering with bottom water circulation and sediment transport regimes in the region. To the southwest of the southern Davie Ridge, the Bassas da India/Europa islands and associated seamounts provide further restrictions to deep water and bottom water flow, in addition to restricting sediment transport.

Laterally discontinuous, stratified to chaotic reflectors have been recognised as overlying the stretched continental basement. These represent pre-rift sedimentation and are

truncated to the northeast by either break-up or rift-onset unconformities, and pinch out to seaward (Mahanjan, 2012). The Mozambique fan comprises the main sedimentary body covering much of the Mozambique Channel and northern Mozambique Basin at present (Droz and Mougenot, 1987; Kolla et al., 1980). Several canyons along the Mozambique continental margin transport sediments to the upper fan region which is considered the main staging area for sediment delivery to the deeper basin (Droz and Mougenot, 1987; Kolla et al., 1980; Walford et al., 2005). Sediment transport to the lower fan is facilitated by the Zambezi Channel, with input from the Tsiribihina Channel which sheds sediment from the west Madagascan margin (Droz and Mougenot, 1987) (Fig. 1.2). Previous accounts of the Zambezi Channel describe it as being the deep extension of the Zambezi Valley. This is considered to originate ca. 50 km southwest of Pembane, southern Mozambique (Droz and Mougenot, 1987; Schulz, et al., 2011). Unlike the Amazon, Zaire, Indus and Bengal systems (cf. Kolla, 2007); the Zambezi Canyon/Channel system is not directly connected to a significant fluvial source (Schulz, et al., 2011). The most significant source of sediment is the Zambezi River, ca. 200 km to the southwest of the suggested location of the Zambezi Canyon head (Schulz, et al., 2011). The Serpa Pinto Channel, now inactive, was once considered as the primary deliverer of sediment to the proto Zambezi Channel system (Droz and Mougenot, 1987) (Fig. 1.2).

Seismicity in the Mozambique Channel originates offshore of Tanzania and northern Mozambique by virtue of the southeastern branch of the East African Rift System (EARS). This branch follows the Davie fracture zone, making use of Cretaceous-age grabens associated with the southward shearing of Madagascar from Africa. The marine extension of the EARS along this southeastern branch, first discussed by Mougenot et al. (1986) and Grimison and Chen (1988), is considered to continue into the southern Mozambique Channel. Despite being included in recent kinematic models, this zone in the Mozambique Channel is described as diffuse with respect to extensional deformation and is difficult to define (Horner-Johnson et al., 2007, Déprez et al., 2013; Saria et al., 2013; 2014). Plate boundaries, tectonic regimes and their relation to the southward propagation of the EARS thus remain unclear. Some aspects of the EARS are discussed in relation to the SWIO (Chapters 3 and 6).

2.2. Oceanography

2.2.1 Natal Valley

Circulation within the Natal Valley, and surrounding SWIO, is complex owing to the macrotopography of the basins and the adjacent narrow continental shelf (Fig. 1.2). Two main circulation systems are recognised, the Agulhas Current and the North Atlantic Deep Water (NADW) current.

The Agulhas Current is a fast (4 knots), poleward-flowing, wide (ca. 100 km) geostrophic current that dominates the upper ocean flow along the western boundary of the Natal Valley (Bang and Pearce, 1976; Dingle et al., 1987, Martin, 1981a; 1981b; Donohue and Toole, 2003; Lutjeharms, 2007, McDonagh et al., 2008) (Fig. 1.2). The precise source area for the Agulhas Current is unknown; however sedimentological studies suggest this source area occurs between 26°S and 30°S offshore the east African coast (Flemming, 1980; Martin, 1981a; 1981b; Lutjeharms, 2006a; 2006b). This is a dynamic region influenced by several water masses. Southward flowing eddies from the Mozambique Channel meet with eddies of the East Madagascar Current, with additional input from the Agulhas Return Current (Stramma and Lutjeharms, 1997; de Ruijter et al., 2003; Quartly and Srokosz, 2004; Quartly et al., 2006; Lutjeharms, 2007). A deep-reaching current, the Agulhas Current is considered by some to progressively extend to depths of as much as 2500 m by 32°S along South Africa's southeast coast (Bang and Pearce, 1976; Pearce, 1977; Dingle et al., 1987; Beal and Bryden, 1999; Donohue and Toole, 2003). However, in some instances it has only been the upper 500 m of the Agulhas Current that was intensely studied (Pearce, 1977), whereas the structure below 1000 m was estimated or shown to be shallower than the sea bottom (Donohue et al., 2000). As such a complete understanding of the variability of depth changes and the influencing factors of the Agulhas Current remains elusive (Lutjeharms, 2006a).

The northern section of the current system is remarkably stable, owing to the steep, linear continental shelf of the northern South African margin that steers the current flow (de Ruijter et al., 1999; Lutjeharms, 2006a; Lutjeharms, 2007). A consequence of this stable linear flow path is that the southward flow associated with the Agulhas Current terminates ca. 200 km offshore (Lutjeharms, 2006b). Inshore of this northern Agulhas Current, Beal and Bryden (1997) describe an undercurrent at ca. 31°S flowing northward along the continental slope at 1200 m depth, and directly beneath the surface core of the Agulhas Current.

Numerical models have produced comparable flows at ca. 34°S, with the depth of the undercurrent varying from 300 – 2500 m (see Lutjeharms, 2006a).

Other authors (Toole and Warren, 1993; van Aken et al., 2004; Schlüter and Uenzelmann-Neben, 2008a) consider the bottom water circulation within the Natal Valley to be governed by the northeasterly flowing NADW, a deep western boundary current. Two possibly contemporaneous pathways have been proposed to describe the passage of NADW (ca. $1.2x10^6$ $ms^{-1)}$ into the Natal Valley (Fig. 1.2). The first (southern) pathway is facilitated by the South Atlantic Current. This pathway is envisaged as transporting NADW around the southern tip of Africa. The NADW core then bifurcates; the northern branch (confined to a depth of 2000 – 3500 m, and salinity of 34.83%) continuing northeast-ward, via the Agulhas and Transkei basins, into the Natal Valley. In contrast, the southern branch of NADW continues eastward beneath the meandering Agulhas Return Current and does not enter the Natal Valley (Toole and Warren, 1993; van Aken et al., 2004).

The second (northern) NADW pathway is considered to flow along the African continental slope at depths between 2000 – 2500 m. This NADW core passes, via the Agulhas Passage, into the Transkei Basin on its pathway into the Natal Valley (Toole and Warren, 1993; Aken et al., 2004; Schlüter and Uenzelmann-Neben, 2008a). Confined by shoaling bathymetry within the Natal Valley, the NADW is believed to return southward along the eastern boundary of the Natal Valley (constrained by the western slopes of the Mozambique Ridge) (Dingle et al., 1987; McDonagh et al., 2008). Van Aken et al. (2004) considered some leakage across a saddle in the Mozambique Ridge at ca. 31°S and at depths of 2500 – 3000 m.

Within the southern Natal Valley a net northeastward flow of NADW, west of 32°E was confirmed (Beal and Bryden, 1999; Donohue et al., 2000; Donohue and Toole, 2003, McDonagh et al., 2008). It is this deep northward flow of the NADW which is likely responsible for winnowing of the Tugela fan in the mid-western Natal Valley (Chapter 4).

In the northernmost and shallowest portions of the Natal Valley, seafloor/current interactions were recorded as areas of non-deposition on the Limpopo Cone and Central Terrace (Martin, 1981a; 1981b; Preu et al., 2011). This interaction between the Agulhas Current and the northernmost Natal Valley has a minimum age of Early/Middle Miocene (Martin, 1981a; Preu et al., 2011). Although initially variable, the Agulhas Current pathways

were thus fairly stable following the Early Miocene. Erosion and redistribution of sediment on the Limpopo Cone and Central Terrace, between depths of 400 – 1500 m, can therefore be attributed to the net southward flow of the Agulhas Current.

Deeper into the Natal Valley (ca. 2500 – 3000 m) and further south (ca. 33°S), Dingle et al. (1987) recognise recirculation of NADW within the Natal Valley based on the location, orientation, depth and character of sediment drifts in the basin. Through interactions with the seafloor sediments, the NADW has developed two elongate, north/south orientated, sediment drifts. The western drift and eastern drift associated with northward and southward flow respectively since the Late Eocene (Dingle et al., 1987).

2.2.2. Northern Mozambique Basin and Channel

Similar to the Natal Valley, circulation within the northern Mozambique Basin and Channel is complex owing to the setting of the basin and the macrotopography of the basin floors (Fig. 1.2). The southern Mozambique Channel is particularly variable, with two main currents (Mozambique Current and East Madagascar Current) converging in this region (de Ruijter et al., 2002; Ridderinkhof and de Ruijter, 2003, Quartly and Srokosz, 2004; Ullgren et al., 2012) (Fig 1.2). The Mozambique Current is best described as a repetitive series of anti-cyclonic eddies, with a net southward transport of water through the Mozambique Channel, rather than a steady western boundary current (de Ruijter et al., 2002; Ridderinkhof and de Ruijter, 2003). The East Madagascar Current is less stable, being defined by various transient eddie pathways originating at the southern tip of Madagascar (de Ruijter et al., 2003; Quartly and Srokosz, 2004). These eddies, both cyclonic and anti-cyclonic, propagate westward toward the Agulhas Current source region (Quartly and Srokosz, 2002; Quartly et al., 2006). This dynamic region in the southern Mozambique Channel and northern Natal Valley is the source area for the Agulhas Current (Stramma and Lutjeharms, 1997; de Ruijter et al., 2003; Quartly and Srokosz, 2004; Lutjeharms, 2007). The formation of anti-cyclonic eddies, and the transient nature of transport pathways facilitate variations in the Agulhas Current which manifest as Natal Pulses, and ultimately the shedding of Agulhas rings into the south Atlantic (van Leeuwen et al., 2000).

Further north, hydrographic observations from the Mozambique Channel show a variable northward flowing undercurrent along the western channel at 1500 – 2400 m depth, inshore of the southward migrating Mozambique Current eddies (de Ruijter et al., 2002; DiMarco et al., 2002; Ullgren et al., 2012). The deep core of this undercurrent comprises

NADW (flowing at $4x10^6 m^3 s^{-1}$) which, at 2000 m, is able to cross the shallow sill of the Mozambique Channel (2500 m) and continue into the Somali Basin (Donohue and Toole, 2003; van Aken et al., 2004). The NADW that does not cross this sill is considered to return southward along the eastern side of the Mozambique Channel and Basin (Donohue and Toole, 2003).

Chapter 3

Anomalous seafloor mounds in the northern Natal Valley, southwest Indian Ocean: Implications for the East African Rift System

3.1. Introduction

The geological evolution of ocean basins is reflected in the shape and form of the deep seafloor (Dietz, 1963; Norton and Sclater, 1979; Cochran; 1981; Goff and Jordan, 1988). This typically comprises a variety of features that range in horizontal scales from the micro (10^{-3} km) to basin-scale (10^{4} km) level. At the macro scale (10 km and above), seafloor features are usually determined by the nature of the basin margins (passive vs. active), the location of oceanic ridges (including past spreading centres and abyssal hills) (cf. Goff et al., 1997; Leinweber and Jokat, 2011a; 2011b), fracture zones (Cochran, 1981; Courtillot, et al., 1999), and sediment input to the basin over time.

With respect to the shape and form of the deep seafloor, morphological characteristics may vary with the type of feature encountered. Parameters such as the height to width ratio, length to width ratio, slope angle and flatness are useful measures for the morphological comparison of different features. Furthermore, these parameters are suggestive of general formative processes related to the origin of seafloor features (Das et al., 2007; Smith, 1988; Mukhopadhyay and Khadge, 1990; Mukhopadhyay and Batiza, 1994: Kodagali, 1989).

This chapter describes a series of macro scale (ca. 30 km) seafloor mounds in the Natal Valley, southwest Indian Ocean (SWIO). The Natal Valley has a complicated and protracted opening history, during the Jurassic and Cretaceous, which is reflected in the mixture of rifting, shearing and drifting of the margin, coupled with episodic submarine volcanism. The adjacent African continent, too, has a long tectonic and seismic history. Following the break-up of Gondwana (Watkeys, 2006), the EARS is by far the most dominant active feature on the continent (Chorowicz, 2005). The EARS represents a 3000 km long discrete intracontinental rift zone initiated some 30 million years ago between the Nubian and Somalian plates (Calais, 2006). EARS rift kinematics have resulted in the development of two microplates, the northern Victoria plate, and southern Rovuma Plate, with a possible third microplate, Lwandle, developing further south (Calais, 2006; Stamps et al., 2008) through the interaction of several rift segments comprising the EARS (Koehn et al., 2008). The East African Rift is comparable in size to the West Antarctic Rift, and far more

accessible as it lacks the ice cover of the West Antarctic Rift (Fig. 3.1, insets, lower right). Since the initiation of the EARS in the Afar region (NE Africa), rift propagation has been southward (Burke, 1996), developing two distinct southern extensions, the older eastern branch and younger western branch (Ebinger, 1989; Ruppel, 1995; Wolfeden, 2004). Both of these branches avoid the Archean cratons, taking advantage of Proterozoic orogenic belts which represent preferential avenues for rift propagation (Morley, 1999). The possible seaward extension of the eastern branch of the EARS was discussed by Mougenot et al. (1986). These workers suggested that the eastern branch joins up with submerged Cretaceous age grabens (located on the Tanzanian continental shelf) associated with the drift of Madagascar away from Africa. Similarly, this chapter discusses the possible southward extension of the western branch (southern Malawi Rift) into the Natal Valley.

The Natal Valley Mounds have been previously partly documented (cf. Martin, 1984; Goodlad, 1986); however their significance was not recognised at that time and they were considered non-descript basement outcrop within the Natal Valley. Their significance as recorders of the geological history of the Natal Valley and SE African margin has been over-looked with little attempt made to identify their origin, evolution and tectonic significance. This chapter aims to describe these features from a morphological and shallow seismic perspective and to use their occurrence as a means to better understand the geological and/or oceanographic evolution of this basin.

3.1.1. Previous bathymetric work

As in all other basins, early work in the Natal Valley relied heavily on high frequency seismic echo-character to describe the bathymetry and shallow sub-bottom characteristics of the seafloor (cf. Dingle et al., 1978; Dingle and Camden-Smith, 1979; Kolla et al., 1980). The primary focus of this was to establish the acoustic stratigraphy and magnetic character of the Natal Valley. The bathymetric and seismic data sets were of sufficiently high resolution to resolve basin-scale features but insufficient to resolve the scale and complexity of complicated seafloor features that are easily revealed with modern multibeam and high resolution seismic tools. With the introduction of multibeam bathymetry systems to scientific research (in conjunction with high frequency seismic systems), the capacity to document and describe the deep-seafloor at far higher resolutions has been greatly increased.

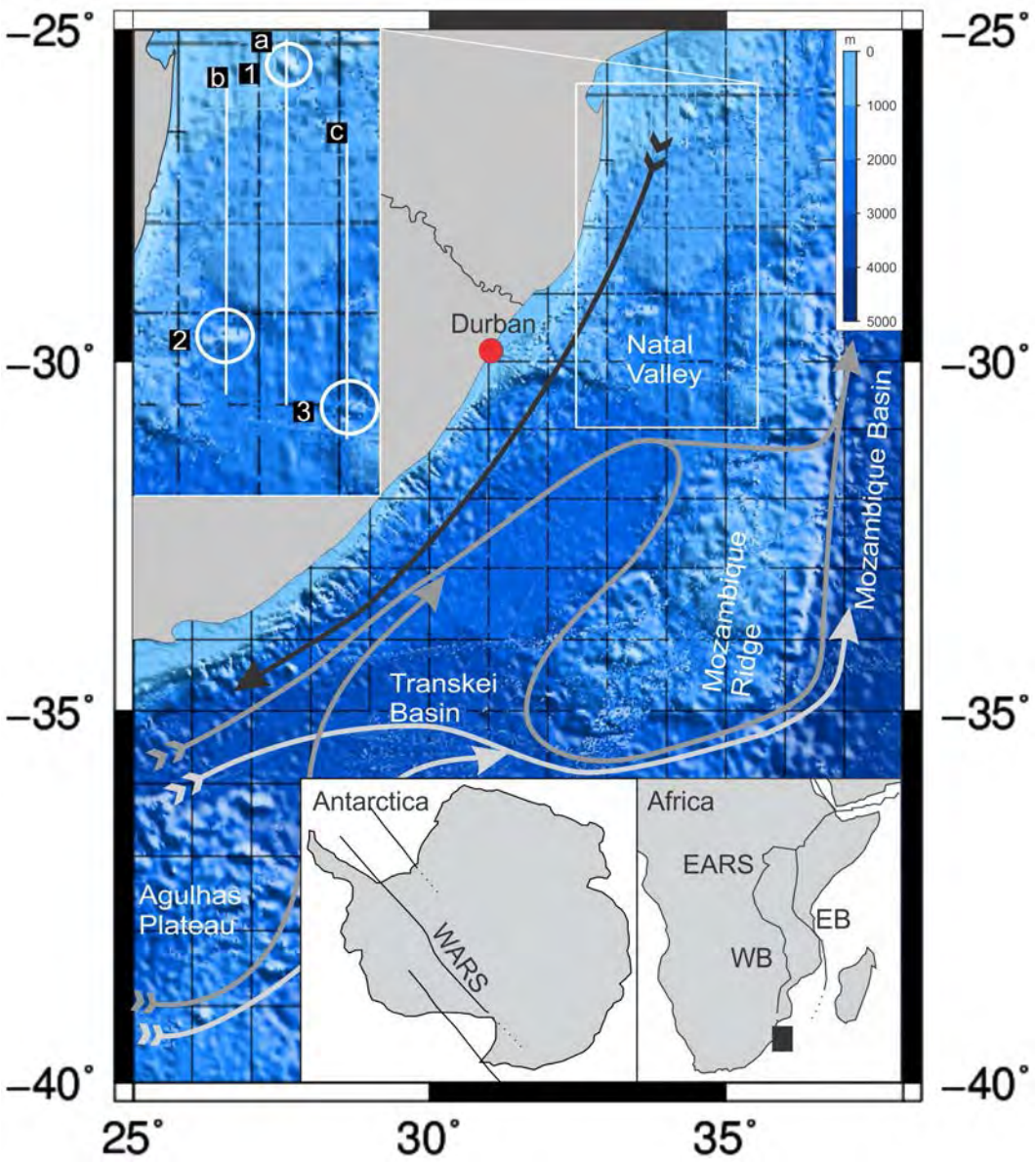

Fig. 3.1. The south-west Indian Ocean (The GEBCO_08 Grid, version 20091120), showing notable basin features. The black arrow shows passage of the Agulhas Current, the dark-grey arrow shows the NADW pathways, while the light grey arrows describe the route of the AABW. The study area (white box), offshore of Durban (red circle), is enlarged showing the location of the mounds. The mounds are identified as follows: 1 - northernmost, 2- southwestern and 3- southeastern. North-south transects (a, b and c) through the northern Natal Valley are depicted by white lines. West Antarctic Rift System (WARS) inset modified after Schmidt and Rowley (1986).

Compared to Dingle et al. (1978), Martin (1984) and Goodlad (1986) were able to resolve significantly more of the Natal Valley, providing 20 m interval bathymetry charts, and seismic reflection profiles (with 10, 40, 300 cubic inch air-guns). Seismic coverage was such that the majority of the seafloor mounds were inadvertently missed, while the 20 m interval bathymetric charts could not resolve the complex seafloor in sufficient detail. Present technologies and techniques allow data to be acquired at far higher resolutions. It is

from the perspective of increased resolution in both bathymetry and seismic data that this chapter re-investigates aspects of the Natal Valley seafloor and shallow subsurface geomorphology.

3.2. Material and Methods

Morphological parameters for slope (average change in elevation over distance), flatness, height to width ratios (H/W), and length to width ratios (L/W) were measured (Fig. 3.2). The use of such parameters is common practice when investigating the morphology of seafloor features (cf. Smith, 1988; Mukhopadhyay and Khadge, 1990; Mukhopadhyay and Batiza, 1994; Kodagali, 1989; Das et al., 2007). The slope angle is calculated as an average value describing the change in elevation over horizontal distance. The flatness parameter reflects the ratio of summit width to basal width. Changes in flatness are typically manifest in changes in slope angle, basal width and summit width, but not necessarily height. The H/W ratio is symptomatic of the flatness and slope parameters, thus changes in this ratio are associated with changes in flatness and slope angle (Das et al., 2007). The H/W ratio allows comparisons of submarine igneous features to be made and is suggestive of formative processes, varying from point to fissure type igneous sources (Smith, 1988; Mukhopadhyay and Khadge, 1990; Mukhopadhyay and Batiza, 1994; Kodagali, 1989). Das et al. (2007) describe four types of relationships between flatness and slope, with varying H/W ratio. Type one, for low H/W (< 0.08) typically indicates low slope angles (<10°) and low flatness (<0.12). Varied slope angles (6 – 15°) and flatness (0.08 – 0.3) are associated with H\W ratios of 0.081 to 0.16 (Type 2). Type 3 intermediate H\W ratios (0.161 – 0.23) suggest high slope angles (>10°) and high flatness (>0.2). Height to width ratios of >0.23 are associated with high slope angles (>10°) and low to moderate flatness (<0.2) are typical of type 4.

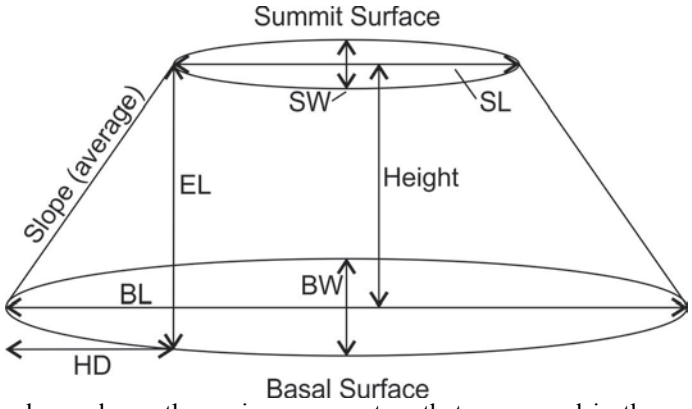

Fig. 3.2. The schematic above shows the various parameters that were used in the morphological analysis of seafloor features. Flatness represents the ratio of summit width (SW) to basal width (BW), as measured from the summit and basal surfaces respectively. The height to width ratios is determined by the features elevation in relation to its basal width. Basal length (BL) versus basal width (BW) gives the length to width ratio. While the slope angle is given by the average change in elevation (EL) over horizontal distance (HD) recorded from the feature.

3.3. Results

3.3.1 Bathymetry

The multibeam bathymetry data reveal three laterally extensive, macro scale, seafloor mounds in the northern Natal Valley (Figs. 3.3 – 3.5). One is located in the northern portion of the northern Natal Valley (Fig. 3.3), while two occur in the southern portion (Figs. 3.3 and 3.4). The bathymetric character of these mounds varies greatly from the character of the adjacent bathymetry. In general, the Natal Valley is typified by smooth seafloor with gradual changes in gradient, punctuated by rugged basement outcrop (mostly confined to the north). The Tugela Cone (mid Natal Valley) provides a notable departure from the gentle gradient of the Natal Valley as it progrades into the basin from the South African east coastline.

Partial coverage of the northernmost mound (Fig. 3.3) shows a north-south orientated feature, 25.4 km in length and at least 3000 m wide, standing 472 m proud of the surrounding seafloor sediments. The crown occurs at a depth of 502 m. The flanks (crown to base) average a gradient of 7.3° with localised steepening of up to 30° on the northern flank. A moat, 25 m deep in the south, and 240 m deep in the north, is observed at the base of the mound. The moat merges with the shoaling bathymetry to the north.

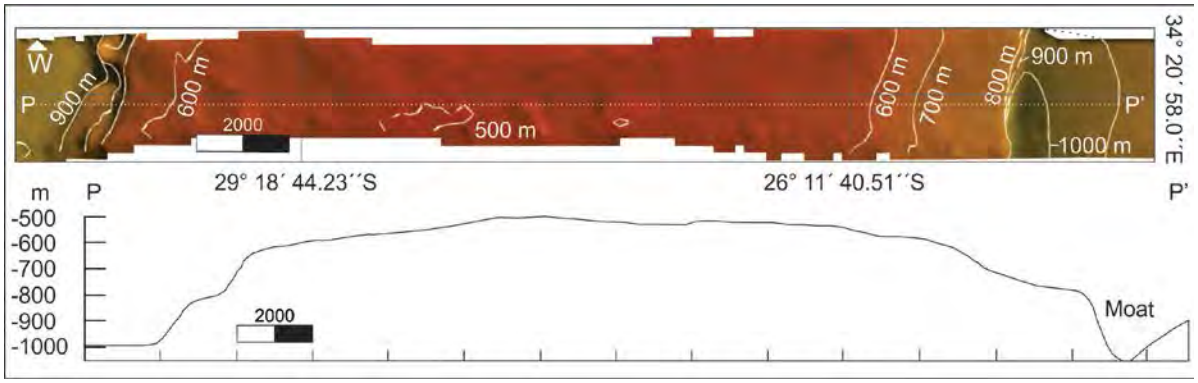

Fig. 3.3. The northernmost mound in plan-view (north to the right). The convex crown, with off centre (to the south) apex is evident, as are the steepened flanks. There is very little distinction between the bathymetric character of the mound crown and adjacent smooth seafloor. The S – N profile (P – P') below the bathymetry image clearly shows the mounded morphology of the feature.

Figure 3.4 shows bathymetry data associated with the second mound, situated in the southwestern portion of the northern Natal Valley. Orientated east-west, this mound is 33 km in length and 17.5 km wide. The shallowest mapped portion of the mound is 420 m above the adjacent seafloor, at 1959 m deep. A discontinuous moat, 34 m deep, fronts the northern flanks of the mound. The moat is less prevalent in the east, where it merges with the smooth low gradient seafloor typical of the greater Natal Valley. The average gradient of the mound (crown to base) is 8.5° with a maximum of 44° on the steepened flanks.

The third mound (Fig. 3.5) is located in the southeastern portion of the Natal Valley, the crown lying at a depth of 1845 m. Like the previous mound, this is similarly east-west orientated. Overall it is 29.7 km long, with a width of 16.2 km and height of 422 m above the surrounding seafloor sediments. A discontinuous moat, 255 m deep, is observed along the northern flanks of the mound. More prevalent in the west, the moat narrows toward the east, terminating at the eastern extent of the mound with a relief of 50 m. The flanks of the mound have an average gradient of 11.3°, steepening to 31° in places.

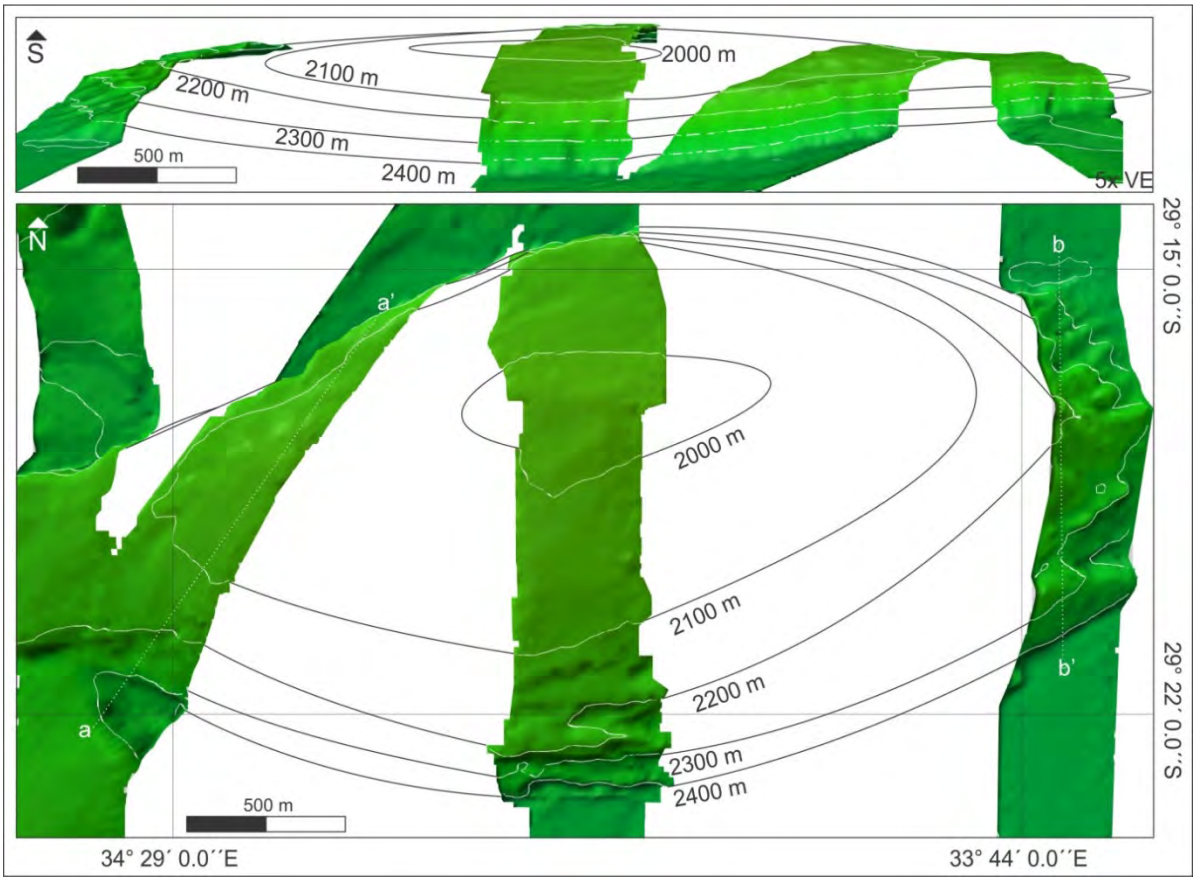

Fig. 3.4. The south western mound (perspective view above, plan view below), and locations of 3.5 kHz profiles (a – a' and b – b'). Ridges are evident on the eastern and southern flank of the mound.

Figure 3.6 shows a perspective and plan view of rugged as well as smooth seafloor of the Natal Valley. The rugged seafloor is dominated by elongated conical features 100 – 350 m in height, reaching local maximums of 65° in gradient. The adjacent smooth seafloor shows gentle changes in gradient.

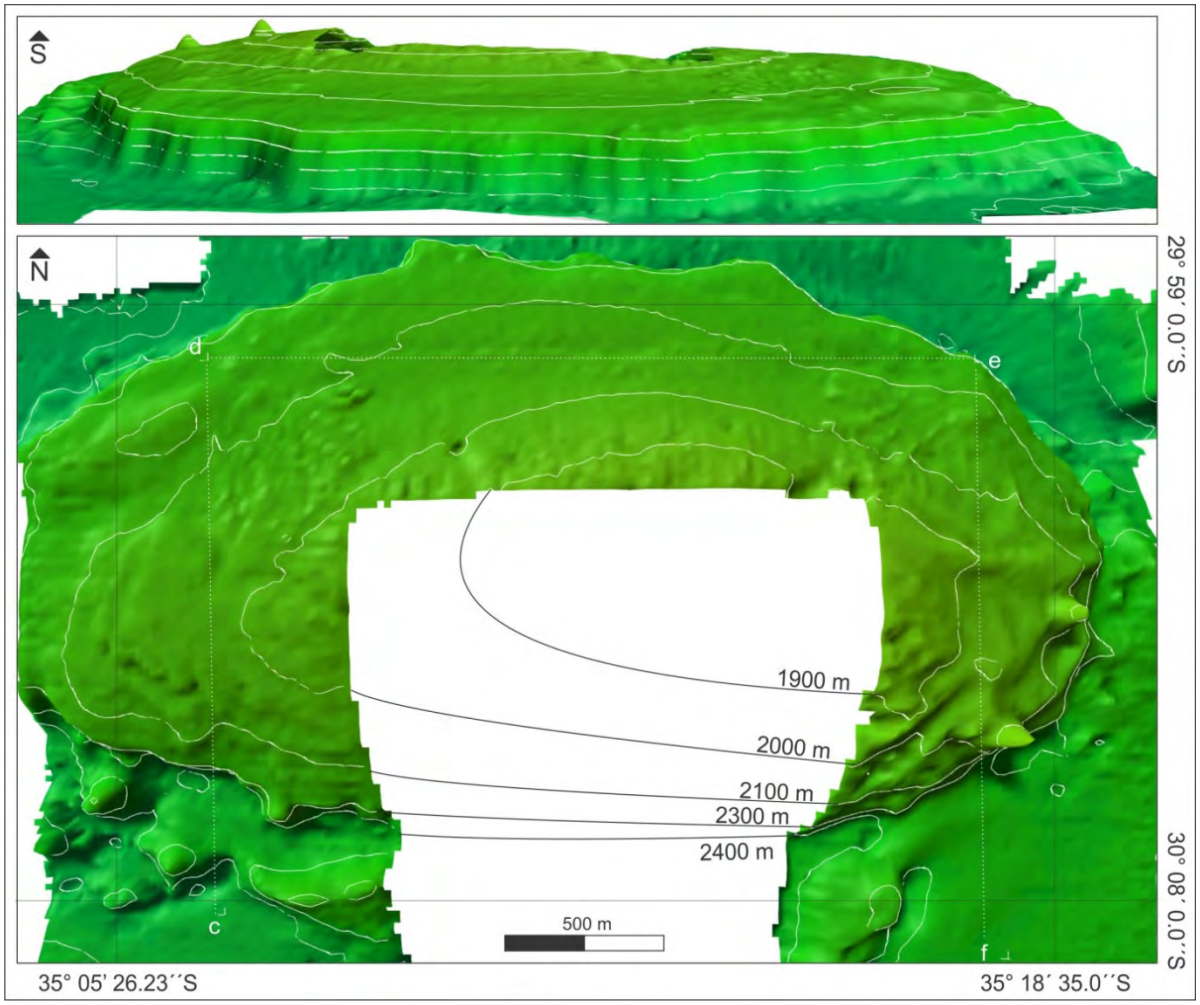

Fig. 3.5. Bathymetry of the south-eastern mound. The mound flanks, and convex crown are clearly evident in the perspective view (top), while in plan (bottom) the oval west\east orientation of the mound is clear. The location of 3.5 kHz profiles (c – d, d – e and e – f) is shown.

Figure 3.7 depicts three profiles (a, b, and c) from transects through the bathymetry data, as well as a slope angle map for better discrimination of the seafloor types found in the area. The profiles are N – S transects through areas of smooth, rugged and mounded bathymetry (see figure 3.1 for profile locations). The overall smooth seafloor with gradual changes in gradient of the northern Natal Valley is clearly evident, as are the anomalous mounds. Rugged basement outcrop is shown in the enlargement of box ii, on profile a. This type of bathymetry is largely confined to the northern extent of the basin. The slope map showing a northern portion of profile a (box i) illustrates the distinct character of the mound, compared to smooth and rugged seafloor. Bands of steepened gradient are found on the mound flanks, while cones of steepened gradient (including the steepest gradients, ca. 65°) are associated with the flanks of rugged seafloor. The intervening smooth seafloor is fairly uniform in slope showing gentle changes in an overall low gradient, similar in character to the mound crown area. Areas of gentle slope are confined to the smooth seafloor and mound

crowns. These are not typically associated with the crowns of the rugged seafloor, although smooth seafloor is noted in the valley floors between peaks of rugged bathymetry (Fig. 3.7).

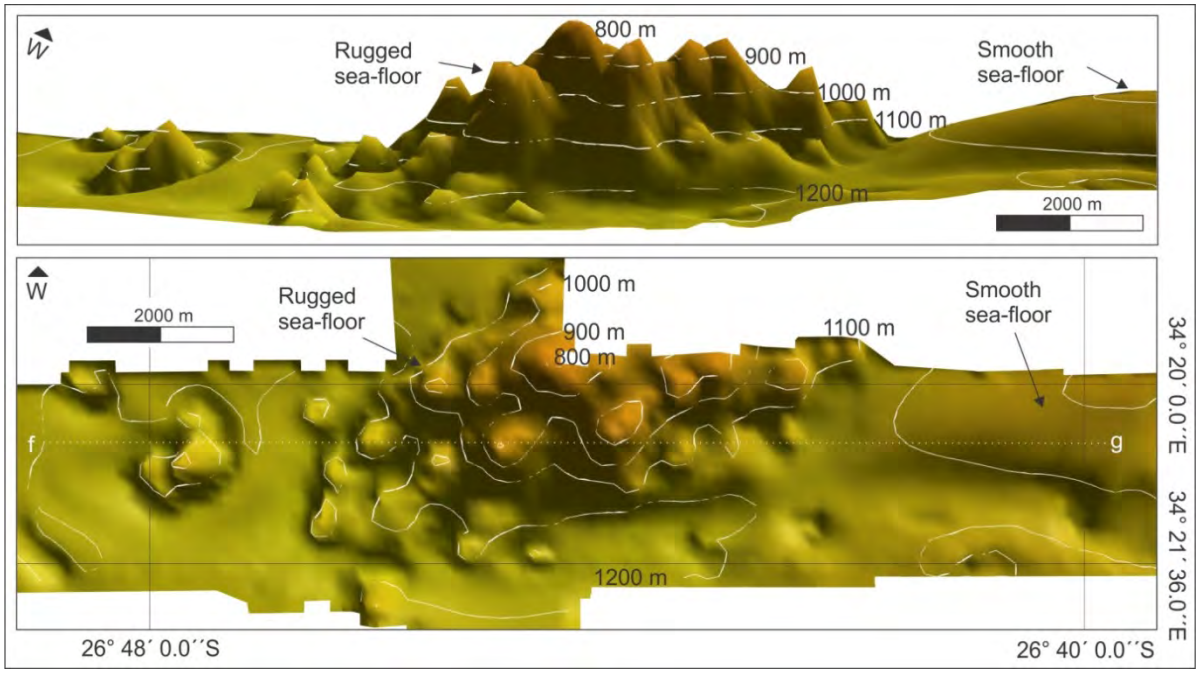

Fig. 3.6. Typical morphology of rugged seafloor, confined to the northern portion of the Natal Valley. The basement outcrop is conical in appearance. Note perspective view on top and plan view on bottom. The 3.5 kHz seismic record associated with profile f – g is shown in figure 3.10. This outcrop is located 38 km south of the northernmost mound, along the same ship track.

3.3.2 High frequency seismic character

Figures 3.8 – 3.10 show high frequency seismic records collected across two of the mounds. The echo character from the southwestern mound (Fig. 3.8, profiles a – a' and b – b') show limited penetration, semi-prolonged echoes as well as broad hyperbolic reflectors with little variance in vertex depth below the seafloor and low angle sub-parallel reflectors (see figure 4 for profile locations).

The seismic profiles in figure 3.9 are associated with the southeastern mound (see figure 3.5 for profile locations). Three profiles (c – d, d – e, and e – f) show the varied reflector characteristics between different areas of the mound. Semi-prolonged echoes are noted once more, in conjunction with continuous isolated reflectors, discontinuous sub-parallel, continuous sub-parallel reflectors and chaotic reflectors. Continuous isolated reflectors are confined to the main body of the mound, while discontinuous and chaotic reflectors are observed toward the rim of the mound.

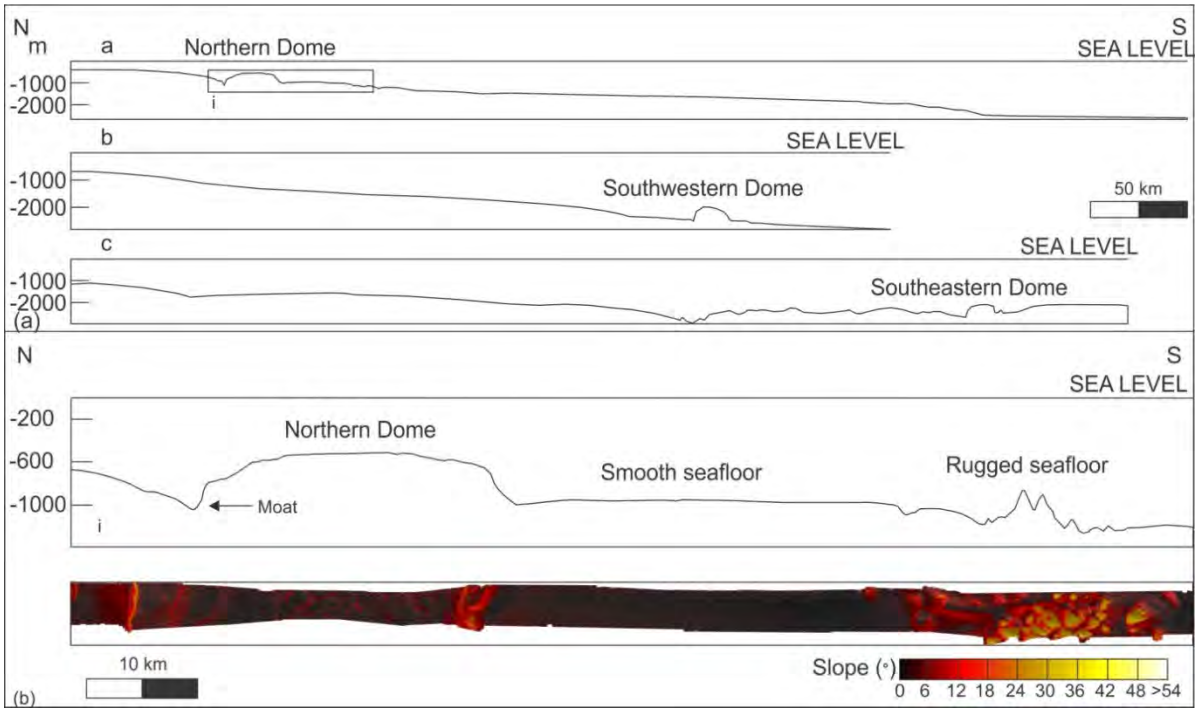

Fig. 3.7. (a) Three N – S transects through the northern Natal Valley are shown (see Fig. 3.1. for location). Note the contrast in morphology between the mounds, smooth and rugged seafloor over each transect. Typical rugged seafloor (see Fig. 5) is shown by the enlarged portion of Profile "a". (b) Box i is enlarged to better illustrate the contrasting morphology of the mounded and rugged bathymetry. The accompanying slope map highlights the change in slope, and so morphological character, across smooth, mounded and rugged seafloor.

Vastly different echo character is observed elsewhere in the northern Natal Valley. Rugged seafloor shows distinct hyperbolic reflectors (Fig. 3.10), while smooth seafloor exhibits continuous to discontinuous sub-parallel reflectors (Fig. 3.9, southern portion of profile e – f). The hyperbolic echoes associated with rugged bathymetry display varied vertex elevations above the seafloor as well as varied amounts of overlap. Continuous to discontinuous sub-parallel reflectors are noted either side of the rugged terrain, and are prevalent throughout areas of smooth seafloor within the Natal Valley.

3.3.3 Morphological character

The morphological characteristics of the Natal Valley mounds are listed in Table 3.1, along with the morphological characteristics of similar mound-like features, and seamounts located along the eastern African margin. Selected characteristics are plotted in figure 3.11. Slope angle is plotted as an average against flatness (Flatness = summit width/basal width) for all the features (Fig. 3.11a). Although there is no clearly defined trend, the Natal Valley mounds have higher flatness values with lower slope angles than the seamountTB and seamountsIOB (Fig. 3.11), for which the inverse is true. Terrestrial alkaline complexes

display varied slope and flatness characteristics, scattered between those of the seamounts and Natal Valley mounds. Plotted height-width and length-width ratios (figure 3.11b) reveal that the Natal Valley mounds and alkaline complexes are comparable in terms of these parameters, while other features are more varied in character.

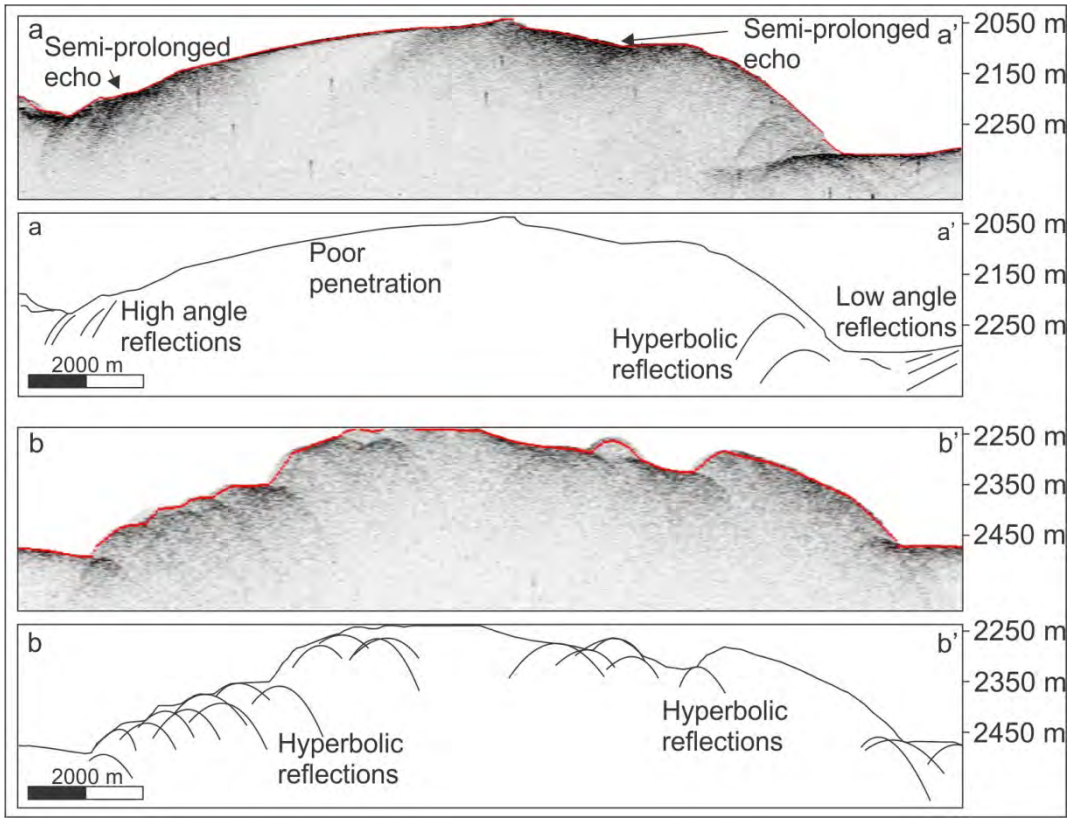

Fig. 3.8. A 3.5 kHz seismic record crossing the south western mound. Semi-prolonged echoes, as well as high, low and hyperbolic reflectors are evident. See figure 3.4 for profile locations.

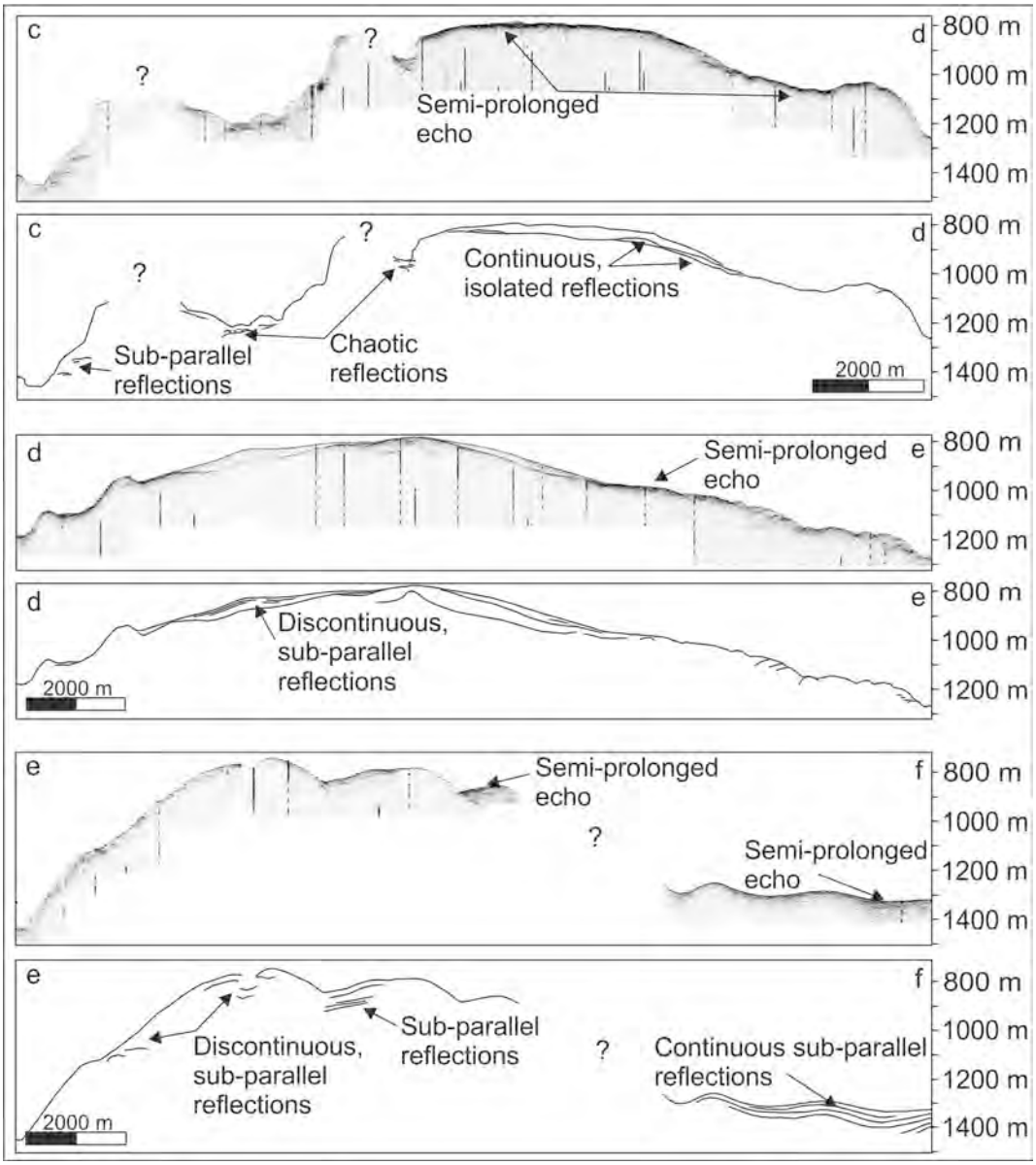

Fig. 3.9. 3.5 kHz seismic record crossings of the southeastern mound. Note the difference in character between the mounds and adjacent smooth seafloor (profile e – f). Figure 3.5 shows the profile locations.

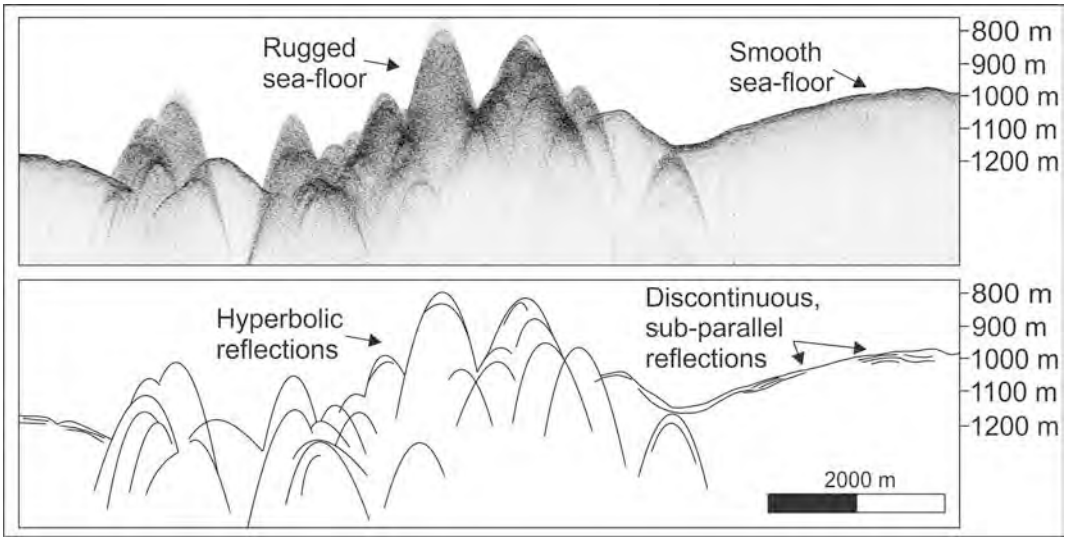

Fig. 3.10. A 3.5 kHz seismic record crossing of the rough terrain south of the northern mound. This 3.5 kHz record shows the echo character associated with both rugged and smooth seafloor. Note the conical expression of the rugged basement outcrop typical of the northern Natal Valley. See figure 3.6 for location.

Table 3.1. Morphological characteristics for the various mounded features discussed in this study. The northern mound has an estimated width due to a lack of data coverage. Overall, the similarity in geomorphology between the terrestrial features, and those of the Natal Valley is noteworthy. Ns, Nepheline syenites; Gs, Granite/Syenite; Ns/S/Qs, Nepheline syenite, Syenite and Quartz syenite; SeamountTB: Lone seamount from the Transkei Basin; SeamountIOB: Large seamounts of Das et al., 2007.

Name	Length (km)	Width (km)	Height (km)	(H/W)	(L/W)	Volume (km3)	Flatness	Slope (°)	Lithology	Location
Gorongosa	30	19	1.046	0.06	1.58	1891.02	0.52	12.12	Ns/S/Qs	Mozambique
Salambidwe	10.08	7.31	0.318	0.04	1.38	97.91	0.46	10.11	G/S	Mozambique
Morrumbala	16.5	9.2	0.795	0.09	1.79	504.24	0.46	10.63	G/S	Mozambique
Muljane	30	16.5	1.258	0.08	1.82	2601.88	0.56	12.31	G/S	Malawi
Zomba	22	13	0.859	0.07	1.69	1026.5	0.55	12.05	G/S	Malawi
Junguni	4.6	4.4	0.12	0.03	1.05	10.15	0.78	14.73	Ns	Malawi
Mongolowe	13.39	8.47	0.429	0.05	1.58	203.29	0.63	10.55	NS	Malawi
Chaone	11.63	9.62	0.448	0.05	1.21	209.43	0.62	11.9	Ns	Malawi
Chikala	9.17	5.55	0.523	0.09	1.64	111.22	0.38	15.78	Ns	Malawi
Nuanetsi	52.96	38.1	0.158	0.01	1.39	1328.94	0.29	3.25	G/S	Zimbabwe
Marungudzi	12.47	8.33	0.1	0.01	1.50	31.25	0.39	11.4	G/S	Zimbabwe
SE Mound (3)	29.7	17	1.12	0.07	1.75	2362.79	0.86	11.3	?	Natal Valley
Mid Mound (1)	25.4	16	1.272	0.08	1.59	1079.97	0.79	7.3	?	Natal Valley
SW Mound (2)	31	18	1.22	0.07	1.72	2844.43	0.62	8.5	?	Natal Valley
Sedom	11	1.25	5	4.00	8.80	68	0.15	7.02	Salt	Dead Sea
Lisan diapir	13	10	6	0.60	1.30	780	?	?	Salt	Dead Sea
SeamountTB	15	13	2.24	0.17	1.15	145.6	0.06	16.75	?	Transkei Basin
SeamountsIOB	16.21	12.59	1.33	0.24	1.29	54.3	0.16	13.25	?	Indian Ocean
Giant contourite	200	45	0.9	0.02	4.44	3870	0.08	1.3	Sediment	Argentine Basin

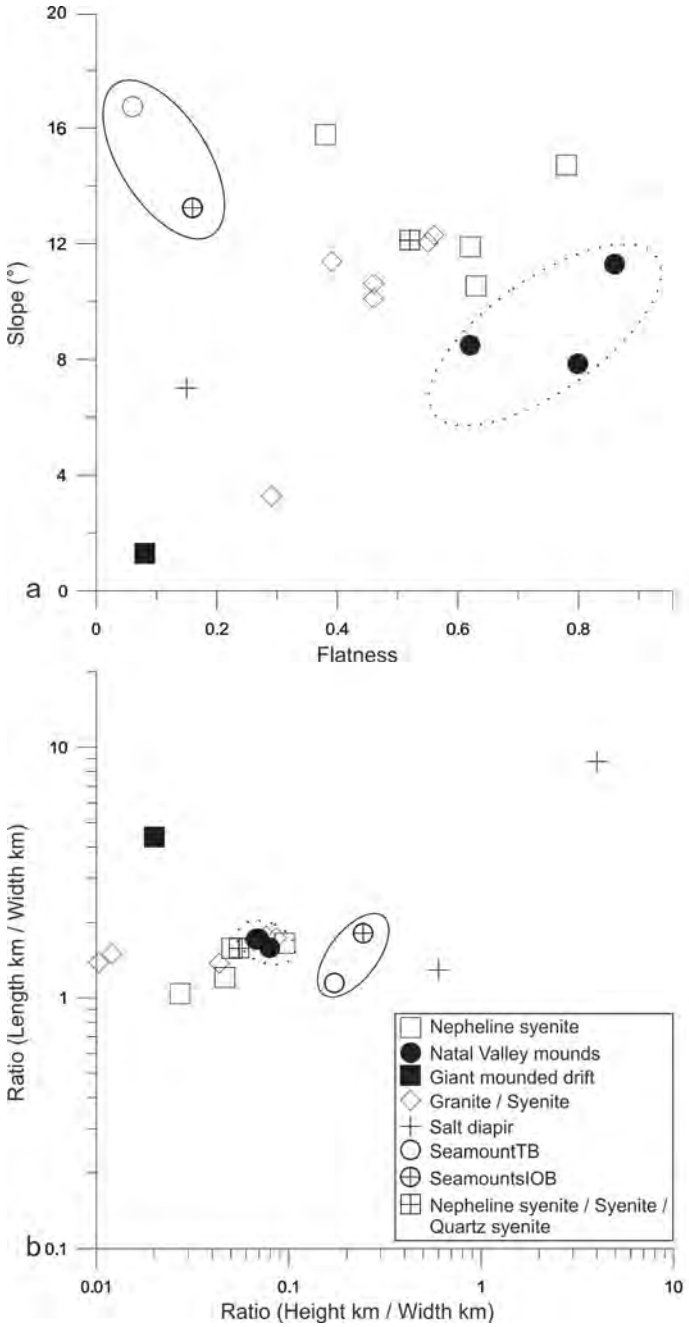

Fig. 3.11. Plots of selected morphological parameters associated with mounded features. a) The mounds (solid black circles), generally plot away from traditional seamounts (open and crossed circles), while terrestrial alkaline complexes of varied lithologies (Nepheline syenites, open square; Granite/Syenite, open diamond, and Nepheline syenite, Syenite and Quartz syenite, crossed square) show a scattered distribution between the seamount morphologies. b) Nepheline syenites (open square), Granite/Syenite (open diamond) and Nepheline syenite, Syenite and Quartz syenite (crossed square) show strong morphological similarities with the Natal Valley mounds (solid black circles). Salt related features (cross), as well as giant mounded drifts (solid black square) do not exhibit comparable morphological characteristics.

3.4. Discussion

3.4.1 Bathymetry

These mound features create oval-like (plan view), positive dome-shaped (cross-section) features on the seafloor of the Natal Valley. These features are distinct from the typical bathymetry of the Natal Valley, which includes irregular rugged and smooth seafloor (Fig. 3.7). The mounds rise over 400 m above the surrounding seafloor sediments and similar features are not evident elsewhere in the Natal Valley. The three mounds have off-centre high points; the gradient from these high points is gentle (2.3° average), until an abrupt change is noted at the mound flanks (9° average for the three mounds). The rugged seafloor, typically associated with oceanic crust outcrop (Fig. 3.5), exhibits an average gradient of 13.15° (mounds average 7.2°, from crown to base), steeper on the upper portion of the feature with the gradient lessening toward the base, in contrast to the mounds for which the inverse is true. By comparison, the smooth seafloor, a product of depositional / erosional processes on the basin floor (Damuth, 1980), generally deepens toward the south with an average gradient of 0.2° (Fig. 3.6). It is clear that these mounds represent anomalous bathymetric features, dissimilar in character from adjacent bathymetry.

This dissimilarity is highlighted by the distribution of areas of seafloor affected by significant changes in slope (Fig. 3.6). In plan-view, rugged seafloor displays grouped circular patterns of steepening slope amidst low gradient seafloor of fairly uniform slope. Whilst little distinction can be made between the smooth seafloor and crown of the mounds, the mound flanks are notably different. The flanks are seen as bands of steepened bathymetry between the smooth seafloor and mound crowns. Similarities between the smooth seafloor and mound crowns can be described by sediment draping during deposition, and reworking by currents (e.g., NADW), whereas the flanks (which provide a significant change in gradient and substrate) are prone to current scouring and moat development.

3.4.2 High frequency seismic character

With respect to echo character, there is a marked difference between typical rugged seafloor of the Natal Valley and the mounds (Figs. 3.6 – 3.8). The rugged features exhibit large, individual to overlapping, irregular hyperbolae with varied vertex elevations about the seafloor. Such a strongly reflective echo character is characteristic of basement highs or outcrop (Damuth, 1980; Lee et al., 2002). On either side of the rugged basement outcrop,

like the mounds, smooth seafloor occurs (Figs. 3.9, profile e – f, and 3.10). Semi-prolonged echoes, with continuous to discontinuous sub-parallel sub-bottom reflectors characterise this smooth seafloor. Such echo character is common to deep seafloor globally; the product of depositional/erosional processes on the basin floor (cf. Damuth, 1980).

In contrast to the smooth and rugged seafloor, the mounds show prolonged, semi-prolonged and continuous isolated echoes, with lesser discontinuous, sub-parallel and chaotic echoes. Broad hyperbolic (Fig. 3.8, profile b – b') and high angle (Fig. 3.9, profile e – e') echoes are associated with hard ridges (Fig. 3.4), rather than irregular rugged bathymetry (Fig. 3.6). The regularly overlapping hyperbolae lie below the seafloor, with little variation in depth. As such; these echoes are distinct from those associated with the rugged basement outcrop discussed above.

Of particular interest are the continuous isolated echoes, the lowermost of which drape the pre-existing bathymetry of the mound while the upper (shallower) reflectors encompass packages of homogenous sediment. This type of echo character is not observed in areas of rugged seafloor associated with typical basement highs (small seamounts) in the Natal Valley. Furthermore it is atypical of seafloor-penetrating salt diapirs as described by Kelling et al. (1979); rather salt diapirs return isolated transparent hyperbolic echoes amidst continuous seafloor reflectors with multiple parallel sub-bottom reflectors. In addition, continuous isolated echoes are not associated with areas of smooth seafloor.

With respect to morphological and seismic character, these mounds are distinct from the surrounding seafloor. It is highly unlikely, then, that they were produced by the same processes responsible for the development of either smooth or rugged seafloor types.

3.4.3 Mound origins

There are three plausible options that could account for the presence of these mounds within the Natal Valley. These formative processes and factors are discussed below, while the corresponding morphological characteristics are shown in Table 3.1.

3.4.3.1 Salt

Salt, as described by Hudec and Jackson (2007), is often associated with deformation when it is present in significant volumes within the stratigraphy. Salt is a common stratigraphic constituent of passive margins, deposited both during and following continental

rifting (Brun and Fort, 2011). Inherently weak, salt is relatively easily mobilised in accordance with regional tectonic and/or gravity driven regimes (Hudec and Jackson, 2007; Brun and Fort, 2011).

Along the passive west coast of Africa, salt tectonics have played a role in the development of the contemporary bathymetry (Hudec and Jackson, 2007; Davison, 2005; Davison and Dailly, 2010; Liu and Li, 2011; Gee and Gawthorpe, 2006). Diapiric features ranging from round to elongate in plan are well documented (cf. Hudec, 2007). The geometry of salt diapirs can, most simply, be described by three end-member forms; upward-narrowing, columnar, and upward-widening (Koyi, 1997). Each end-member is associated with particular sedimentary and tectonic settings (cf. Koyi, 1997). Most favourable in this instance would be the columnar end-member, as this is most likely to produce circular mounds or oval mounds on the seafloor. The shortcomings of this hypothesis are several-fold. Firstly, the morphological character of the Natal Valley mounds is at odds with that expected of salt diapirs. Surface penetrating salt diapirs are not known to reach the size of the mounds described in the Natal Valley from multibeam bathymetry data. Additionally, the echo character of the mounds is distinct from the echo character associated with salt diaper related structures (cf. Kelling et al., 1979). Furthermore, there is insufficient salt to produce significant diapirs. The basin, as inspected from the onshore portions where boreholes intersect both the rift and drift phase of margin development, is devoid of evaporite deposits (cf. Shone, 2006). As such these features appear unrelated to salt tectonics by virtue of an absence of salt and will thus not be discussed further. It is, however, incorporated within the morphological plots provided in figure 3.11 for simple comparison.

3.4.3.2 Bottom water circulation

The second option is that these anomalous mounds are the result of current activity. Bottom current activity in the basins off the southeast coast of South Africa has been shown to have a significant effect on sedimentation in both the Natal Valley (Chapter 4), and neighbouring Transkei Basin (Schlüter, 2007; Schlüter, 2008). Bedforms produced by bottom water currents may cover extensive (>1000 km^2) tracts of seafloor. However, despite the impressive wavelengths associated with these features (>10 km), the amplitude is typically on a scale of tens of meters (Wynn and Masson, 2008) and clearly does not approach the scale of the mounds discussed here. Giant contourite drifts, as described by Hernández-Molina et al. (2010) (ca. 40 – 50 km wide and 250 – 300 km long), by far exceed

the horizontal scale of the Natal Valley mounds, in addition to other contrasting morphological characteristics (Table 3.1). Additionally, such bedforms are not typified by abrupt scarps or moats, features characteristic of the anomalous mounds. Consequently, they are not comparable to these mounds found in the Natal Valley and current activity may be regarded as an unlikely origin for the Natal Valley mounds.

3.4.3.3 Submarine igneous activity

Submarine igneous activity is the third option. Dingle et al. (1978) tentatively alluded to this as a possible cause for the mounds (described by these authors as basement highs) in the Natal Valley, but without more detailed bathymetric imagery this has not been possible to confirm nor refute. On the basis of the size and position of these mounds, igneous activity appears to be a plausible factor in their genesis.

Leinweber and Jokat (2011a) identified an extinct spreading centre at 30°S, extending eastward from ~34°E to ~35° 30' E. The southeastern mound coincides exactly with this extinct spreading centre (Fig. 3.1). The northern mound (Fig. 3.1) is located in the vicinity of the northernmost magnetic lineaments associated with an early spreading centre identified by Leinweber and Jokat (2011a). Furthermore, the mounds lie in the north/south (30° E – 40° E) corridor of igneous activity associated with the southern portion of the EARS's western branch, as well as Karoo age alkaline igneous activity (Fig. 3.12).

3.4.4 Seamount geomorphology

In terms of their size and shape (bearing in mind sediment accumulation in the Natal Valley), the Natal Valley mounds bear a striking resemblance to several igneous complexes of south-east Africa (Fig. 3.13). These terrestrial features relate to three distinct periods; those of Jurassic age are associated with Karoo igneous activity, the late Jurassic to early Cretaceous are associated with the breakup of Gondwana, while the Tertiary features are related to the southward propagation of the EARS. The H/W ratio of features has been used as a means of morphological classification that is suggestive of formative processes (Smith, 1988; Mukhopadhyay and Khadge, 1990; Mukhopadhyay and Batiza, 1994; Kodagali, 1989; Das et al., 2007). In comparison, the L/W ratio is useful in relating the plan-view shape of features (from circular to oblate). Both the H/W and L/W ratios, along with flatness and slope are useful morphological measures when comparing various features of differing origins. When compared in terms of slope angle vs. flatness, and height to width (H/W) vs

length to width (L/W), the mounds of the Natal Valley are well placed within the spread of possible morphological character associated with other similar features from the African continent (Fig. 3.11). Included in figure 3.11 are examples of salt diapirs, giant contourite mounds, and other seamounts for comparison. Seamounts from the central Indian Ocean Basin (seamountsIOB hereafter), described by Das et al. (2007) and plotted as an average (in terms of measured morphological parameters) for all large single peaked seamounts, plot away from the Natal Valley mounds illustrating differences in the morphological character between these features. A lone (the only one for which the bathymetry is known), single peaked, seamount (seamountTB hereafter) from the Transkei Basin also plots away from the Natal Valley mounds, with morphological character more akin to the seamounts of Das et al. (2007). These plots illustrate the similarities in morphological character between these types of seamounts, and differences when compared to the Natal Valley mounds.

The Natal Valley mounds have H/W ratios of <0.08, a class defined as low by Das et al. (2007). This morphological class is said to be associated with low flatness ratios (<0.12) and low slope angles (<10°), suggestive of a point source of magma, that flows along the slope of the seamount. In contrast to these findings, the Natal Valley mounds exhibit high averaged flatness ratios (0.74), and average slopes of 9.03° (local maximum slopes reach up to 44°). It is clear that the Natal Valley mounds are morphologically distinct from those observed by Das et al. (2007), based on these morphologic parameters. The lone seamountTB from the Transkei Basin has a flatness of 0.06, slope angle of 16.75°, and intermediate H/W ratio (0.17). As the H/W ratio is indicative of the mode of origin of seamounts (Smith, 1988; Mukhopadhyay and Khadge, 1990; Mukhopadhyay and Batiza, 1994; Kodagali, 1989; Das et al., 2007), it appears that the origins of the Natal Valley mounds differ from those of the Central Indian Ocean Basin seamounts, as well as the lone seamount from the Transkei Basin.

Comparison of volume to L/W reveals a similar trend (Table 3.1); seamounts in general differ from the Natal Valley mounds, whereas terrestrial alkaline features are more comparable to the Natal Valley mounds. Differences in morphological character between conventional seamounts and the Natal Valley mounds are most evident when comparing flatness and slope angle, with alkaline complexes grouped toward the Natal Valley mounds, while the seamounts occupy a zone of inverse slope/flatness character (Fig. 3.11a). This trend is more evident in the second plot where the total morphology (X, Y, and Z axes) of the features is compared (Fig. 3.11b). Here the Natal Valley mounds and alkaline complexes are

tightly grouped, whereas the traditional seamounts occupy a slightly different zone in the plot. Again, this illustrates the variation in morphological character between the Natal Valley mounds and other seamounts.

3.4.4.1 Alkaline igneous activity

A great deal of the igneous activity in this area is associated with the southern portion of the western branch of the EARS (southern Malawi Rift) (Fig. 3.12), which lies directly north of the Natal Valley. Alkaline igneous activity is common to the EARS, and there are many documented cases with volcanic features ranging from metres to tens of kilometres in scale (Chorowicz, 2005; Mollel and Swisher, 2012). The area around and south of Lake Malawi hosts numerous igneous features on a scale directly comparable to the mounds of the Natal Valley. In particular, alkaline complexes bear the greatest resemblance in terms of geomorphology to the Natal Valley mounds (Fig. 3.13) with the long axis profiles of the features displaying a similar morphological character. The greatest geomorphological departure is the seafloor mounds lack of erosional features that are evident in the subaerial setting (e.g. streams and gullies). Of interest too is the possibility that a few smaller features could be combined to create one large feature. The alkaline complexes Mongolowe, Chaone and Chikala (Fig. 3.13), if draped with sediment and not eroded (to the extent that terrestrial features are naturally) would provide another possible analogue to the mounds of the Natal Valley. The average H/W ratio for these terrestrial mounds is 0.05, with a flatness of 0.51, and slope of 11.35°. The Natal Valley mounds plot in similar morphological zones to these terrestrial features, suggesting similar formative processes and origins. Such alkaline igneous activity in a marine setting is not uncommon and is usually associated with rift systems. The Cameroon line, a series of Tertiary to Recent (generally alkaline volcanoes), is a good example of this (cf. Fitton and Dunlop, 1985; Barfod and Fitton, 2013).

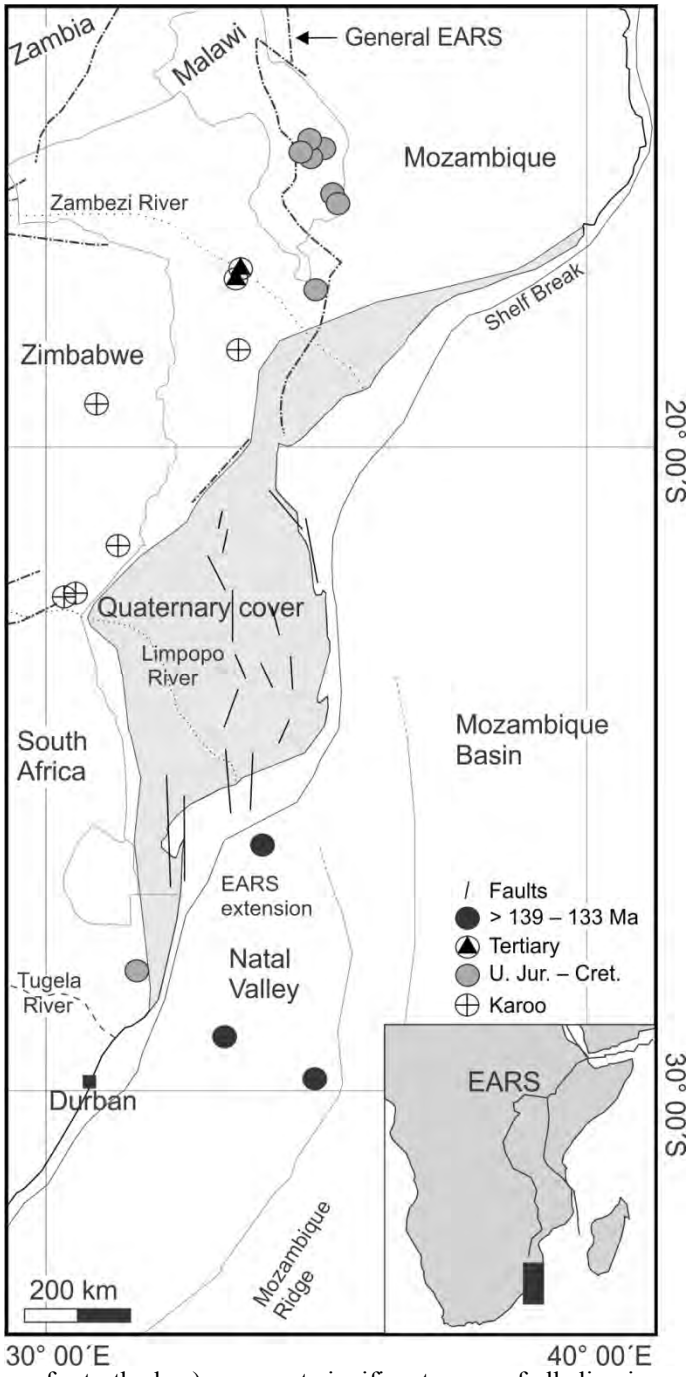

Fig. 3.12. Circles (please refer to the key) represent significant cases of alkaline igneous activity of south-east Africa, black circles show the relative position of mounds in the Natal Valley. The present accepted extent of the EARS (black dot-dash lines) lies to the north of the southern coastal plains of Mozambique, an area that shows evidence of E – W extension (see location of normal faults). Black lines (main figure and inset) show the location of the major rift features of the EARS. The Natal Valley mounds are located directly south of this area, within the northern Natal Valley. The city of Durban is shown, for reference, by the black square. This map is modified after Chorowicz, 2005, and the Geological Map of Mozambique (Ministerio dos Recursos Minerais, 1987).

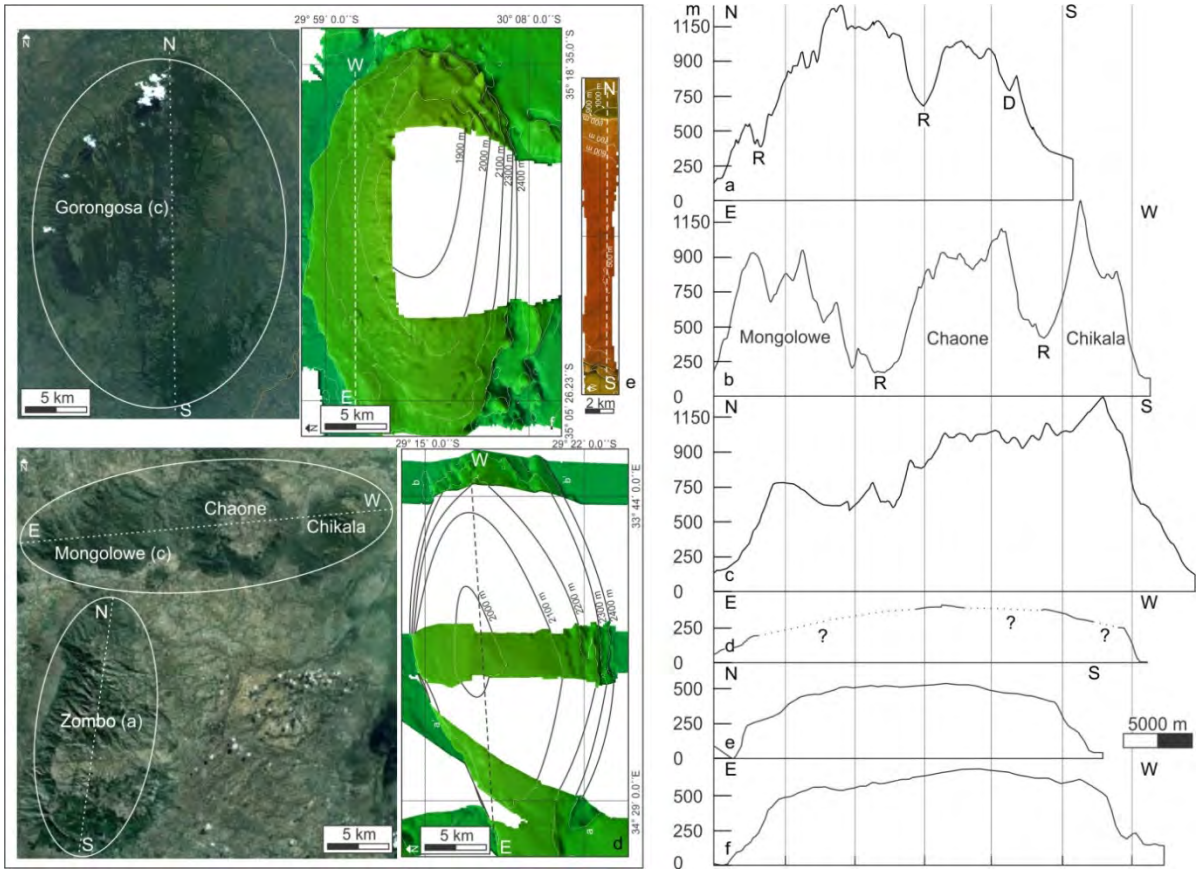

Fig. 3. 13. Google Earth images of alkaline complexes compared to bathymetry data showing the mounds of the Natal Valley (left). The overall morphological similarity is striking, particularly if one removes the effects of weathering and erosion by fluvial and similar processes, from the subaerial alkaline complexes. Profiles across the long axis of the alkaline complexes, and Natal Valley mounds are shown on the left. The effect of subaerial weathering and erosion on the alkaline complexes is evident. The mounds have not been affected by subaerial processes, however, the Natal Valley basin has accumulated ca. 800 m of sediment since deposition commenced (a = Zomba; b = Mongolowe-Chaone-Chikala; c = Gorongosa; d = SW mound; e = N mound; f = SE mound).

3.5 Timing and tectonic significance

It may be hypothesised that these mounds may be related to the southward propagation of the East African Rift system during the Neogene period. The EARS is typified by, among other characteristics, elongate zones of thinned continental crust. Weaknesses in the crustal structure are further exploited by rift propagation and associated volcanism (Chorowicz, 2005). Corti (2009) and Stamps et al. (2008) outline the location of plate boundaries associated with the Victoria, Rovuma and Lwandle microplates which developed in response to regional extensional regimes; the Victoria and Rovuma microplates being continental expressions of deformation related to the EARS. In contrast, the Lwandle microplate occurs in a marine setting between the Nubian and Somalian plates, thus representing rift associated deformation in that environment. It is therefore apparent that the

region south of the EARS is active, and that the activity is associated with zones of predefined weakness (Morley, 1999).

In addition, the lowlands of southern Mozambique mark the southern extension of the Pan-African Mozambique Belt, another zone of weakness. This area lies to the east of the Kaapvaal craton, through which a rift is unlikely to propagate. Additionally, along the eastern boundary of the Kaapvaal craton lies the Lebombo monocline of the Mesozoic Karoo Igneous Province, a further zone of weakness (Klausen, 2009). The transitional crust along the western Natal Valley is located east and south of these zones of weakness, representing another zone marked by a weak crust with continental affinities (cf. Leinweber, and Jokat, 2011a). These factors combined present a considerable north-south zone of crust predisposed to rifting with a long history of activity.

Igneous activity in the southern EARS began at ca. 10 Ma, sometime after the initiation of the EARS (30 Ma) and shows a definitive southward younging of the rift kinematics as the rift propagated in that direction (Chorowicz, 2005; Albaric et al., 2009). Recent seismic activity in the south confirms this (Fairhead and Stuart, 1982; Albaric et al., 2009). Although it has low overall seismicity, the Natal Valley does show some recent activity in the northern portion of the basin (Fig. 3.14). To the north of the study area, seismic activity is focused along two main N – S orientated regions. These regions mark the eastern, western and southeastern boundaries of the Rovuma Plate (Stamps et al., 2008), defined by the western and southeastern branches of the EARS (Chorowicz, 2005). The intersection of these plate boundaries is proximal to the study area (Fig. 3.14). The northern and southwestern mounds are located close (within 50 km) to epicentres ranging in magnitude from 3 – 4.6 ML, while elsewhere in the basin earthquakes of 6.8 ML have been recorded (International Seismological Centre, On-line Bulletin, 2011).

This argument suggests that these mounds may mark a southerly extension of the EARS into the Natal Valley and show the progression of rifting into a deep (~ 2400 m) ocean system. This appears to be contrary to the typical propagation of continental rift systems that open seawards and spread into the continental interior (Cratchley et al., 1984). No other such examples have been documented for rift systems elsewhere. Beyond this unique point, there are also implications for the oil and gas industry. Exploration for petroleum could be affected by elevated thermal gradients in this region, raising temperatures through the oil/gas window.

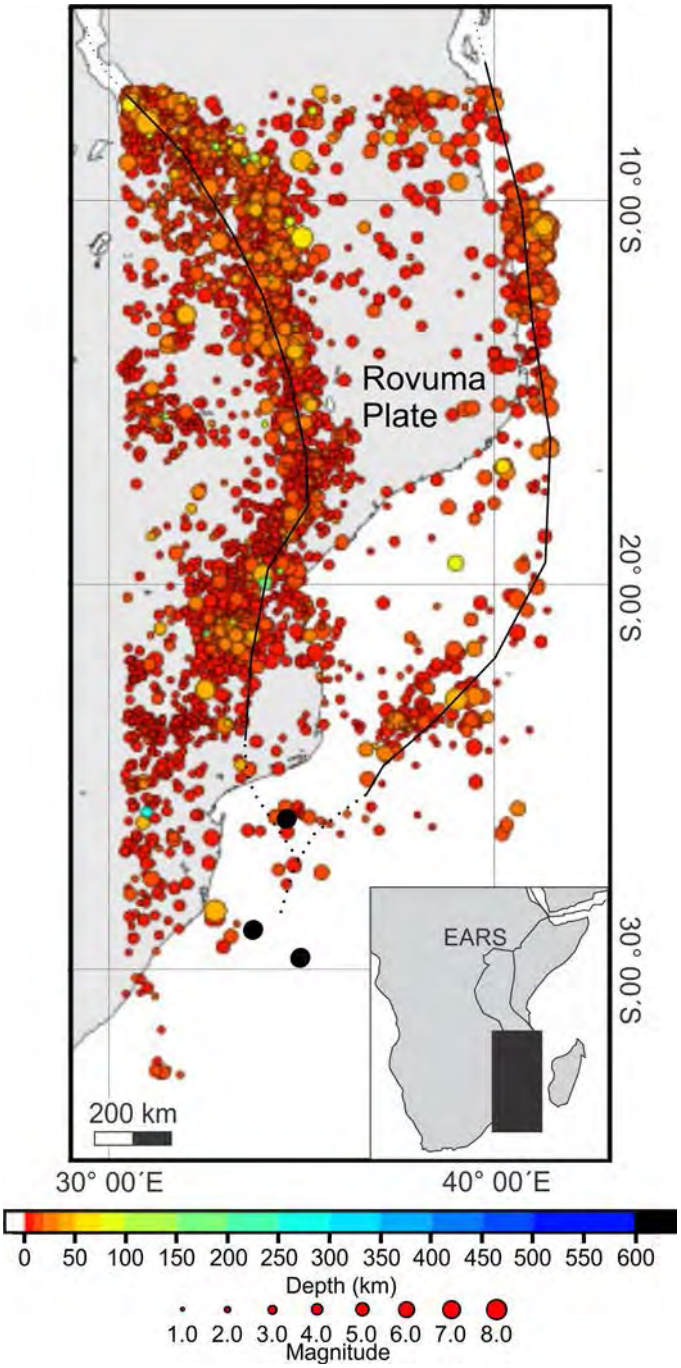

Fig. 3.14. Earthquake epicenter data from the vicinity of the study area for the period 1904 – Present are plotted, along with the locations of the mounds (black circles). Interestingly, activity is focused along the boundaries of the Rovuma Plate. The study area is located at the southern edge of this plate, proximal to the intersection of the western and southeastern plate boundaries. Epicentre Data were sourced from the International Seismological Centre, On-line Bulletin (2011), and the Rovuma Plate boundaries after Stamps et al. (2008).

Chapter 4

The evolution of the Tugela Canyon and submarine fan: A complex interaction between margin erosion and bottom current sweeping, southwest Indian Ocean, South Africa.

4.1. Introduction

Submarine canyons are known the world over as significant morphological features that have modified continental margins over significant periods of time via erosion and ultimately the deposition of fan complexes. Typically, submarine canyons are classified as either "shelf-breaching", "shelf-indenting" or "slope-confined" based on their relationship with the continental shelf (Farre et al., 1983). The mechanism responsible for the former is believed to be a combination of eustatic sea level change and submarine erosion, often associated with subaerial exposure of the shelf to fluvial processes. Slope-confined and shelf-indenting categories are likely the result of retrogressive failure, fluid venting and tide-driven bottom currents (Ridente et al., 2007). Submarine canyons, particularly the shelf-breaching class, represent preferential sediment transport pathways (via tectonosedimentary processes) to the World's major sedimentary basins, albeit episodic in nature (Dingle and Robson, 1985; Ridente et al., 2007; Lastras et al., 2011).

Very few examples of across slope transport pathways in deep water have been documented from the passive eastern margin of South Africa. This is in comparison to the notable examples from North America (Farre et al., 1983; Pratson et al., 1994; Vachtman et al., 2012) and Europe (Lastras et al., 2011). Deep water studies of the South African continental slope and rise have tended to focus on bottom water flows and sedimentation rather than the role submarine canyons play in the delivery of sediment to the deep oceans (cf. Dingle et al., 1978, 1987; Martin et al., 1982; Schlüter and Uenzelmann-Neben, 2007, 2008). In the Natal Valley, offshore the east coast of South Africa, only a single very large submarine canyon (120 km long, 50 km offshore of the Thukela River) has been identified (Dingle et al., 1978; Goodlad, 1986). This is an example of a large submarine canyon restricted to the mid-lower slope and attributed with the delivery of detrital material from the Thukela River (South Africa's second largest river) to the deep ocean basin. Despite having no contemporary connection to the upper slope and shelf, the canyon is deeply incised and the exact structure and origin of this canyon is unknown. Similarly, the associated fan is

poorly understood; previous sampling efforts having been frustrated by the lack of geophysical data required to accurately delineate this feature (Türkay and, Pätzold, 2009).

This study incorporates new multibeam bathymetric and sub-bottom data collected in the Natal Valley, located in the SWIO (Fig. 4.1) in an attempt to understand the evolution of the Tugela Canyon and fan system. By examining the geomorphology of these features, insights into the sedimentary processes responsible for sculpting the southeast African margin can be made. As such, this chapter aims to present a model for a submarine canyon-fan system with a sediment starved upper limit and a bottom current swept lower region.

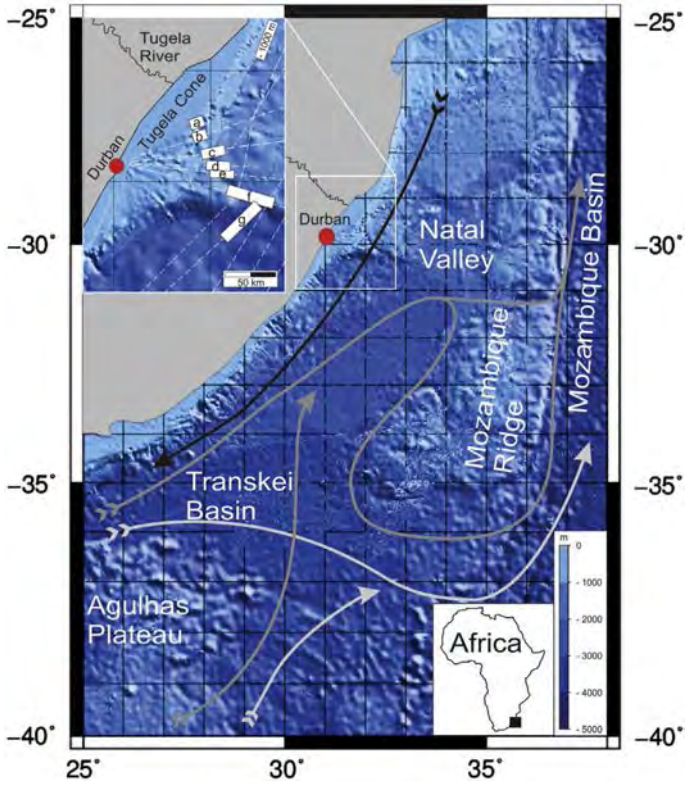

Fig. 4.1. GEBCO (30 s grid) DTM showing the study area (white box and inset) and adjacent southwest Indian Ocean bathymetry. Note the location of the Natal Valley, Mozambique Ridge and the Transkei Basin. The black arrow illustrates Agulhas Current flow, mid-gray arrows illustrate North Atlantic Deep Water flow, light grey arrows shows the passage of Antarctic Bottom Water (Flow paths compiled after: Toole and Warren, 1993; Schlüter and Uenzelmann-Neben, 2008; Bang and Pearce, 1976; Dingle et al., 1987). Ship tracks (white dashed lines) are overlain with white rectangles delineating portions of the Tugela Canyon discussed in this study, see main text for further detail.

4.2 Results

The Tugela Canyon is intersected by five lines of multibeam bathymetry. Partial coverage spanning depths of 644m (at the canyon head) to 2828 m (where the canyon ends in the Natal Valley) was achieved.

Swath TC1 (TC being an identifier of the swath in question) displays an area of the canyon between 842 m and 990 m depth (Figs. 4.1, box b and 4.2). In this section, the canyon incises 240 m into the adjacent slope and exhibits an average axial gradient of 3.7°. Closer to the canyon axis, wall gradients of 20° are apparent. Slump scarps (five) and rills (six) occur and are interspersed with sporadic, high relief basement outcrop. Slump scarps are more prevalent on the western margin, with rills and basement exposure confined to the eastern canyon margin. A gradient knickpoint, associated with a 1.81° change in gradient, is noted above the confluence of the Tugela Canyon and a canyon tributary.

Very high resolution 3.5 kHz records show a distinct contrast between the eastern and western margins of the canyon (Fig. 4.2, profile T – T1). The latter is dominated by parallel reflectors, truncated by a well-defined scarp. At the foot of the scarp parallel reflectors are once again visible within a cohesive landslide block. The eastern margin is defined by extensive hyperbolic returns draped with isolated thin packages of parallel reflectors. These reconcile with the rugged portions of seafloor identified as basement outcrop.

Approximately 15 km southeast of TC1 the Tugela Canyon (Figs. 4.1, box c and 4.3) now possesses a “U”-shaped cross-sectional profile. The canyon has incised 492 m into the surrounding slope (gradient ca. 1°) and steepens to a maximum slope of 28°. Mass wasting is evident on both sides of the canyon. On either side of the canyon the seafloor is relatively smooth, although basement does crop out to the west. Notably, axial incision is evident from a depth of 1490 m, a feature not observed inshore of this point.

Southeast of TC2 (ca. 10.5 km), the overall morphology of the Tugela Canyon changes drastically although the bottom of the canyon remains “U”-shaped (TC3). Terraces, separated by substantial escarpments, dominate the western margin (Figs. 4.1, box d and 4.4). The upper terrace is littered with blocky debris while the lower terraces appear free from debris. The eastern margin is dominated by slide/slump scarps. A canyon axis gradient of 0.6° is observed here. While the canyon walls reach a gradient of up to 30° locally, the escarpments within the terraces attain gradients of up to 39°. Beyond the canyon walls, the seafloor is smooth with no signs of basement cropping out.

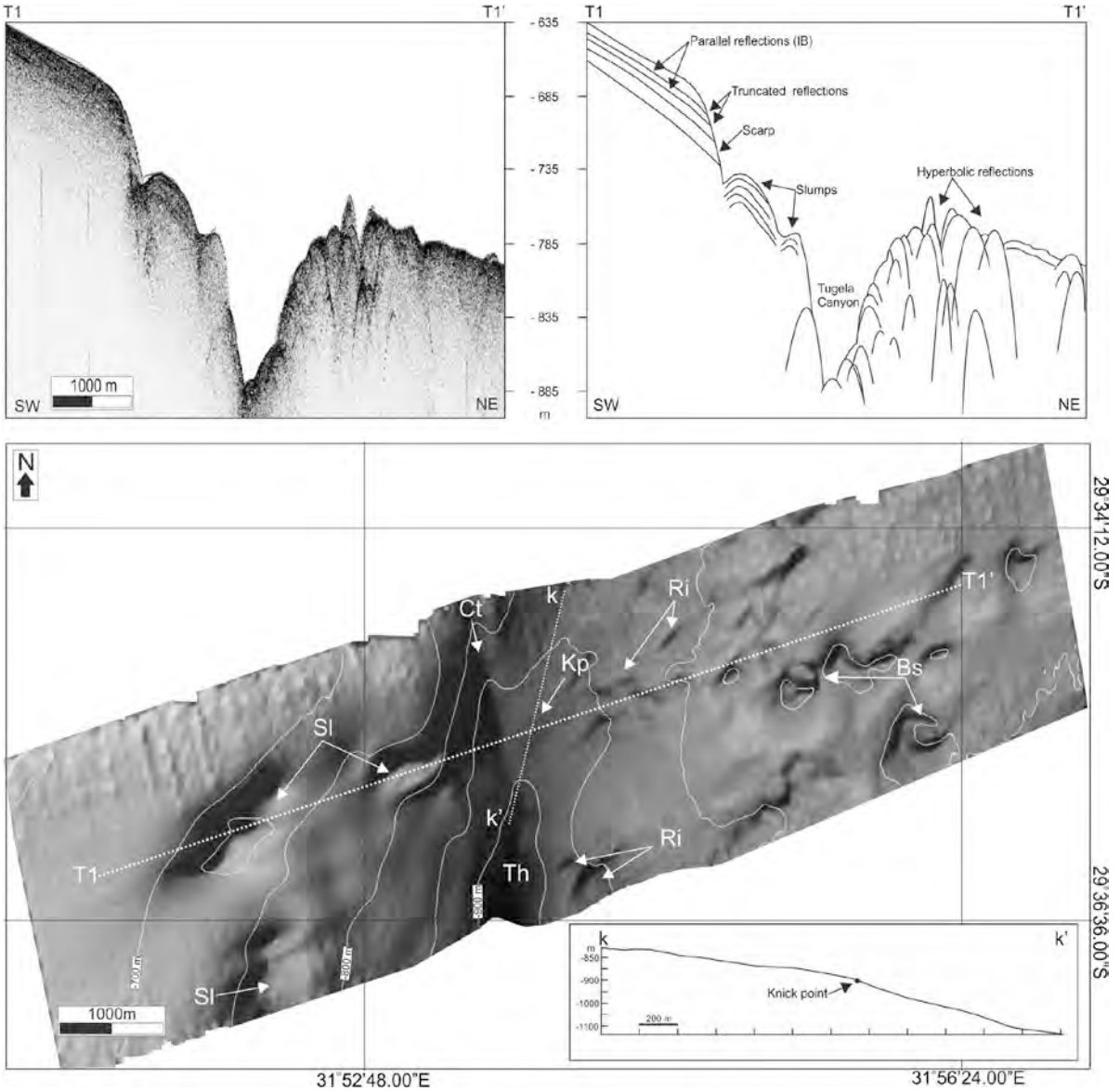

Fig. 4.2. Swath TC1 from the innermost portion of the Tugela Canyon. Note apparent basement outcrop (Bs), and rill (Ri) development, associated with the eastern canyon wall. Slide/slump scarps (Sl) are evident either side of the canyon axis. The thalweg (Th) is well defined below the knickpoint (Kp) and confluence of the main canyon and canyon tributary (Cr). Profiles k-k' and T1-T1' illustrate the change in gradient across the knickpoint and 3.5 kHz echo trace across the Tugela Canyon respectively.

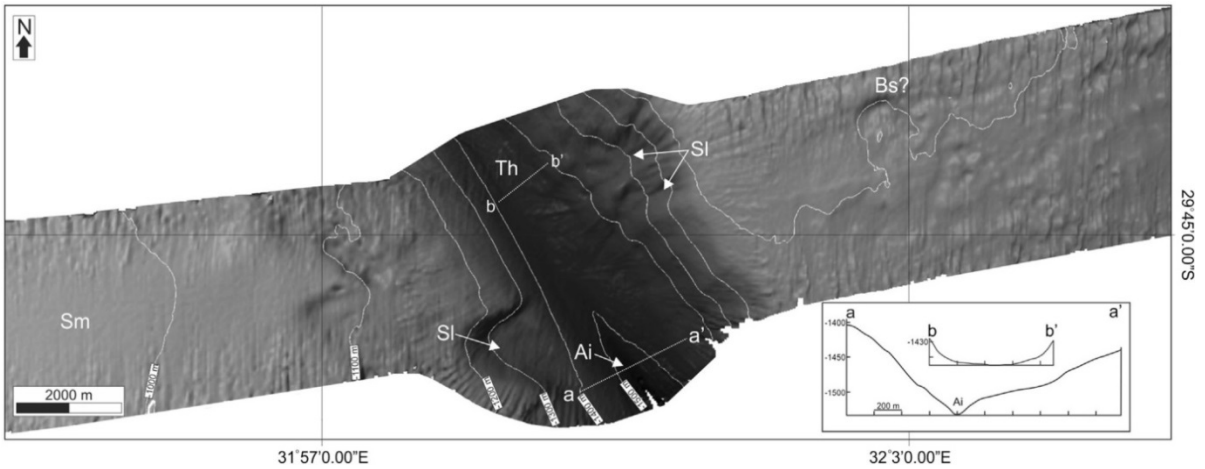

Fig. 4.3. A distinct change in canyon morphology is illustrated by Swath TC2. The profile is now decidedly "U"-shaped and shows evidence of minor axial incision (Ai) at 1490 m (profile a – a'). This is not apparent upslope at 1450 m (b – b'). Slump/slide scarps (Sl) are common to both canyon flanks. Note the difference in the character of the seafloor either side of the canyon. Smooth (Sm) seafloor on the west is markedly different from rough seafloor in the east, suggesting some basement (Bs) outcrop or subcrop.

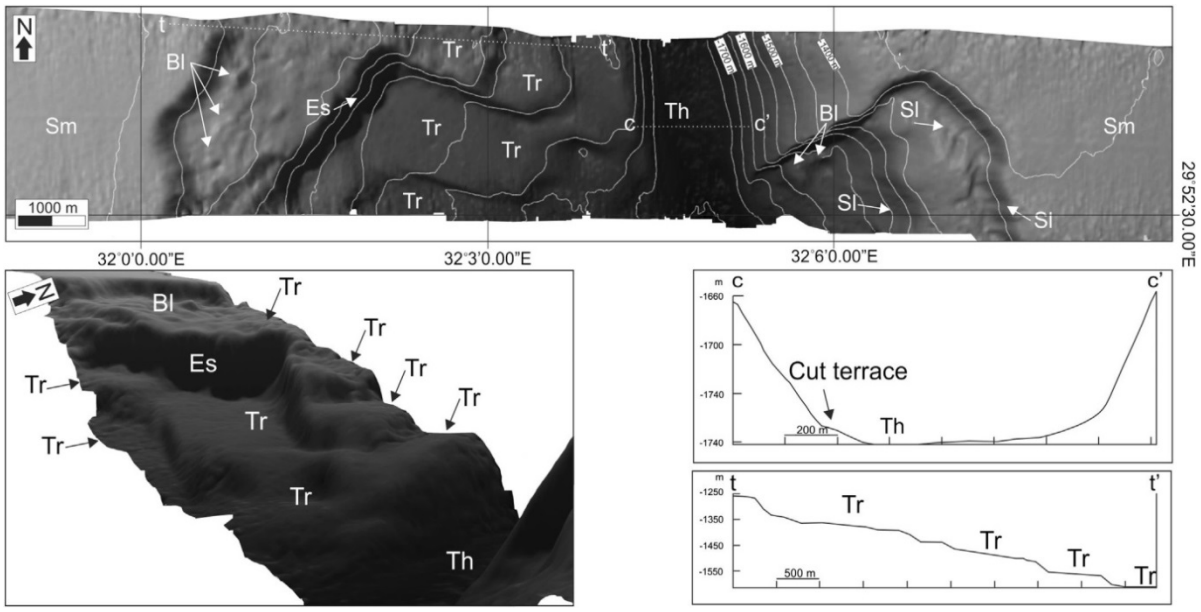

Fig. 4.4. Swath TC3 from the mid-slope. Note the development of terraces (Tr) along the western canyon wall (profile t – t'), Escarpments (Es), blocky debris (Bl) and slide/slump scarps (Sl) are also evident. Smooth seafloor (Sm) occurs on either side of the Tugela Canyon. A minor cut terrace denotes flow bias toward the western side of the main canyon floor, associated erosion and incision (profile c – c'). The 3D inset illustrates the terraced nature of this portion of the canyon.

Directly south of swath TC3 (ca. 4 km), swath TC4 (Fig. 4.1, box e) reveals a vastly different morphology from the upper reaches of the Tugela Canyon. Despite still possessing a "U" shape with terraces (Fig. 4.5a), the lowest terrace now supports an inner branch of the canyon which enters the main canyon floor at 32°40'E/29°55'S (Fig. 4.5b). Four smaller

channels feed into the inner branch near the base of the lowest escarpment. Interestingly, two channels are evident in the main canyon floor, one on the eastern side directly related to the upper reaches of the canyon and one on the western side associated with the inner branch (Fig. 4.5, profile e – e'). The two are initially separated by a longitudinally orientated mound of material that elevates the central portion of the canyon 40 m above the canyon floor and extends for at least 4 km, narrowing from 750 m to 350 m wide downstream (at the limit of data coverage).

3.5 kHz echosounder traces over the blocky deposits adjacent to the inner gorge area reveal significant hyperbolic echoes. The central portion of the line exhibits a package characterised by chaotic reflectors, while further east discontinuous parallel reflectors are evident (Fig. 4.5, profile d – d').

Terraces are no longer evident in swath TC5 (21 km southeast of TC4) (Figs. 4.1, box f and 4.6). Here the Tugela Canyon reaches its maximum degree of incision (1000 m) into the surrounding slope. Two minor hanging branches (cf. Lastras et al., 2011) enter the canyon. Cut-terraces are a feature of the main canyon floor showing at least five periods of axial incision (Fig. 4.6, profile g – g').

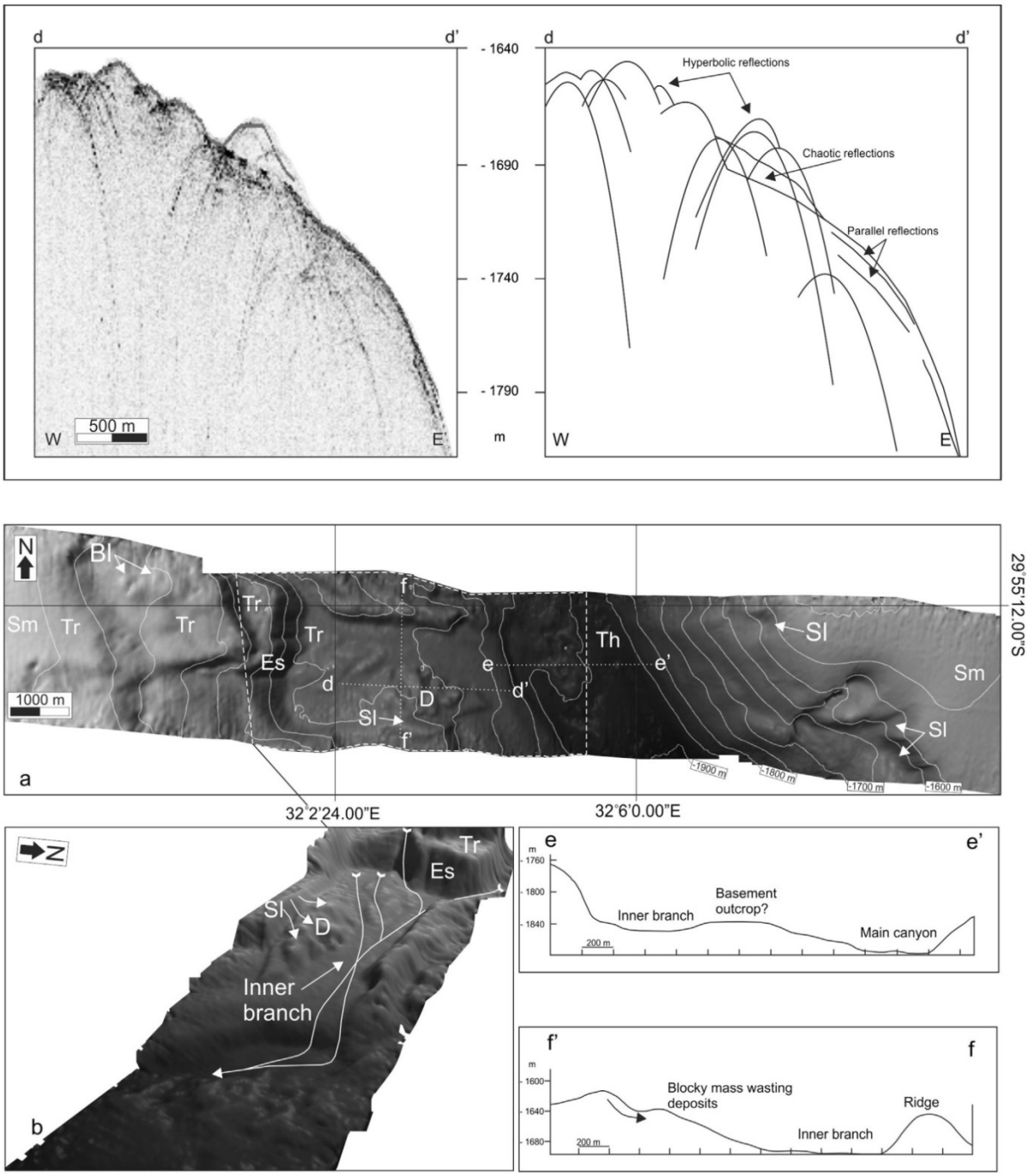

Fig. 4.5. 3.5 kHz seismic profile and bathymetry of Swath TC4 (a). The canyon's inner branch (dashed box in (a)) is shown from a 3D perspective in the inset (b). Echo character, associated with mass-wasting debris (D) is illustrated in profile d – d'. Profile f – f' is orientated north-south across the inner branch. The location of the main canyon floor relative to the inner branch canyon can be seen in profile e – e'.

The Tugela Canyon widens into the abyssal Natal Valley, where a crude sub-horizontal (0.12°) terrace extends 100 km to the south west (Fig. 4.1, box g and 4.7). The echo character of the 3.5 kHz record is dominated by regular overlapping hyperbolae with varied vertex elevations extending ca. 40 km to the south west (Fig. 4.7b). This irregular seafloor extends distally into smooth seafloor. Another package of reflectors is apparent underlying the smooth seafloor. These high amplitude parallel reflectors appear to interfinger

with the adjacent hyperbolae-dominated seismic unit (Fig. 4.7a). No distributary channels, lobes or levees are evident in either the bathymetry or 3.5 kHz record.

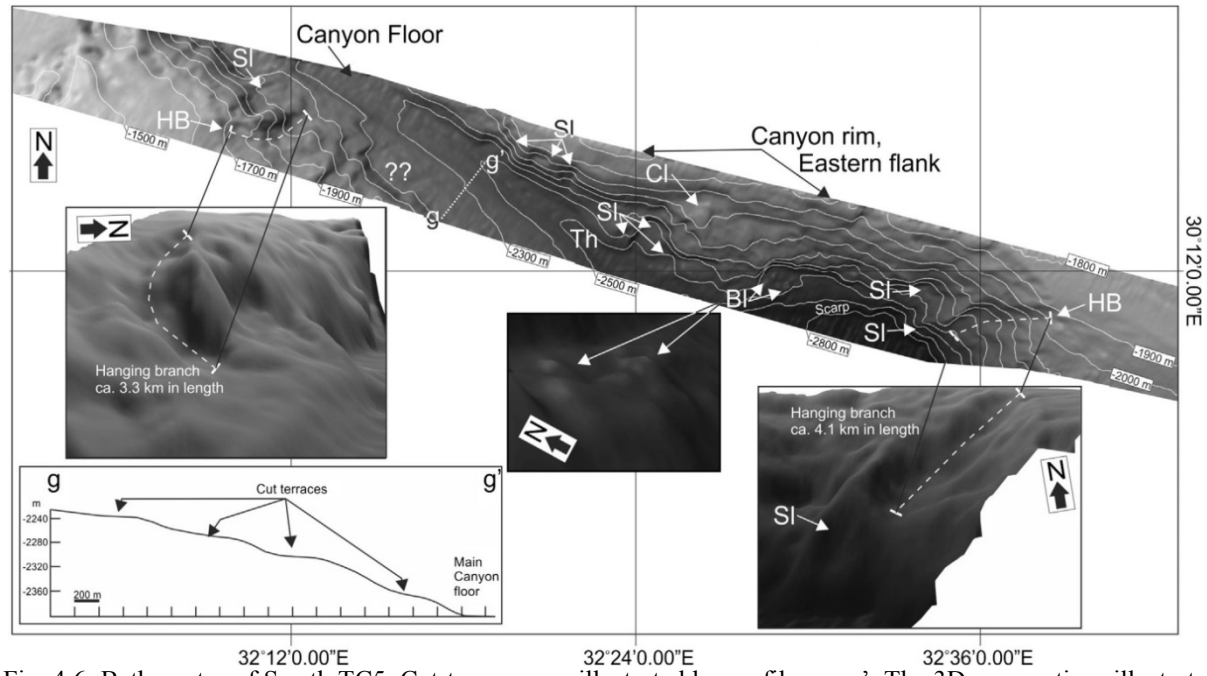

Fig. 4.6. Bathymetry of Swath TC5. Cut-terraces are illustrated by profile g – g'. The 3D perspectives illustrate hanging branches (Hb) and blocky debris (Bl) along the canyon flanks.

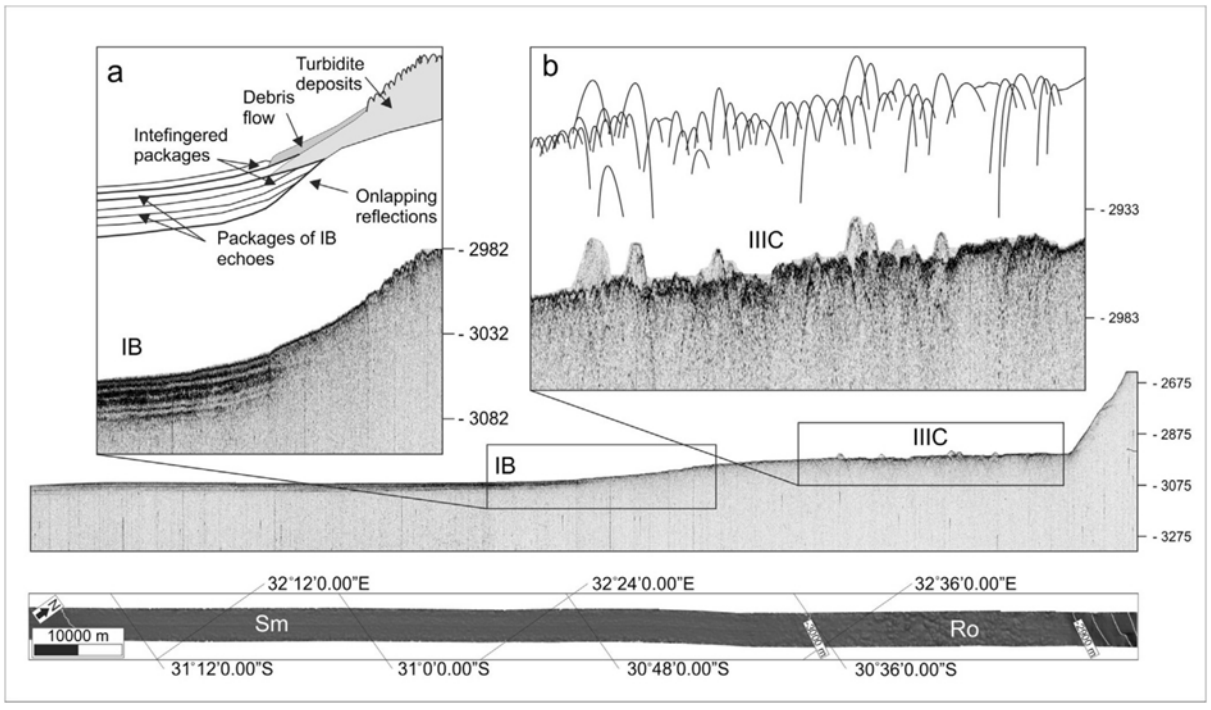

[*Previous page*] Fig. 4.7. Multibeam bathymetry and 3.5 kHz profile from the Tugela Canyon fan region. Inset (a) shows the distal transition from type IIIC echoes (cf. Damuth and Hayes, 1977) to IB echoes further south. Inset (b) illustrates the overlapping hyperbolae of IIIC echoes. A crude terrace is dominated by IIIC echoes. The character of the seafloor noted in the 3.5 kHz record is confirmed in the bathymetry, rough seafloor (Ro) changes abruptly to smooth seafloor (Sm) as it extends southwest into the deep Natal Valley.

The deep penetration multichannel seismics from the mid slope reveal several phases of canyon incision and fill that underlie the head of the Tugela Canyon (Figs. 4.1, box a and 4.8). These occur as a series of high amplitude reflectors that incise into the underlying stratigraphy and are truncated by successively younger reflectors, the overall incision pattern of which is nested within the deepest incised reflector. On the basis of these discordant relationships, three phases of canyon incision and fill can be recognised: the youngest canyon fill, is characterised by an onlapping drape relationship with the palaeo-canyon walls. The contemporary Tugela Canyon head is located in the topographic low preserved within these series of drapes.

Table 4.1 shows down-canyon characteristics associated with canyon width, relief, margin and gradient for the areas covered by multibeam bathymetry. Canyon relief and width were noted at the up-canyon and down-canyon limits of data coverage in order to best describe the canyon long-profile. Overall, the Tugela Canyon shows an increase in width and relief with increasing distance from the continental shelf, and increasing water depth. The gradient of the canyon floor varies but, generally decreases with increasing distance from the continental shelf, and increasing water depth.

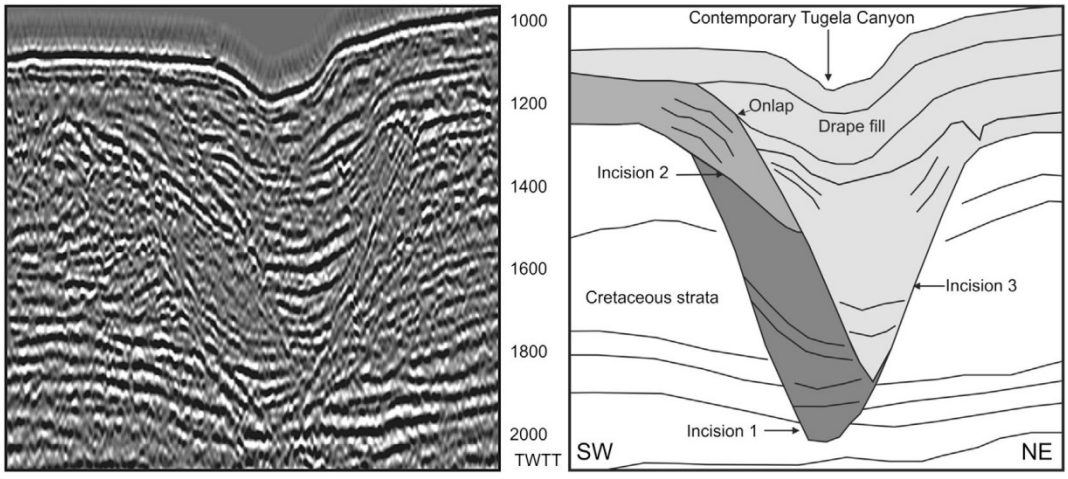

[*Previous page*] Fig. 4.8. Along strike multi-channel seismic record and interpretation from the mid-slope portion of the Tugela Canyon. Note the three stacked paleo-canyons, the youngest of which is dominated by an onlapping drape fill. Note the stacked nature of the canyons and the position of the contemporary Tugela Canyon within the low point of the drape succession.

Table 4.1 Down-canyon comparison of relief, width and gradient.

Swath	TC1	TC2	TC3	TC4	TC5
Width (km)	3.1	6.4	11.5	12.2	18.3
Relief (m)	72	435	572	579	874
Width (km)	6	6.8	13	13.8	19.6
Relief (m)	260	458	599	615	1028
Margins (km)	Straight	Straight, diverging	Meandering, diverging	Meandering, diverging	Meandering, diverging
Gradient (°)	3.7	0.3	0.6	0.6	0.6

4.3 Discussion

4.3.1 Erosional styles

The canyon morphologies of the northern KwaZulu-Natal continental margin, (Green et al., 2007; Green and Uken, 2008; Green, 2011a), differ significantly from the expression of the Tugela Canyon. Notably absent from the slope confined Tugela Canyon is the amphitheatre-shaped canyon head morphology, associated with upslope eroding retrogressive failure (cf. Farre et al., 1983). Furthermore, the Tugela Canyon displays a marked increase in relief and width with increased distance from the continental shelf and water depth (Table 4.1). Gradient, although variable, shows a decreasing trend in angle with increasing distance from the shelf (concave upward profile) and water depth (Table 4.1). This suggests that downslope erosive processes dominated the formation of this canyon (cf. Goff, 2001; Mitchell, 2004). When compared to other slope canyon systems such as the submarine canyons of the American Atlantic (Vachtman et al., 2012) or Argentinian margins (Lastras et al., 2011), the Tugela Canyon is particularly isolated from other erosive features. These other canyons show a significant number of tributary branches whereas no significant tributaries exist for the Tugela Canyon. This character approaches the "Type Ia" (straight slope systems) morphological class of Vachtman et al. (2012) and linear canyon class of Mitchell (2005). Such systems are associated with fluvial-like erosion dominated by bypassing of sedimentary flows, particularly during lowstand intervals. The absence of mass wasting debris along the thalweg of the Tugela Canyon further reinforces the notion of downslope excavation as the principal factor in canyon formation (Vachtman et al., 2012).

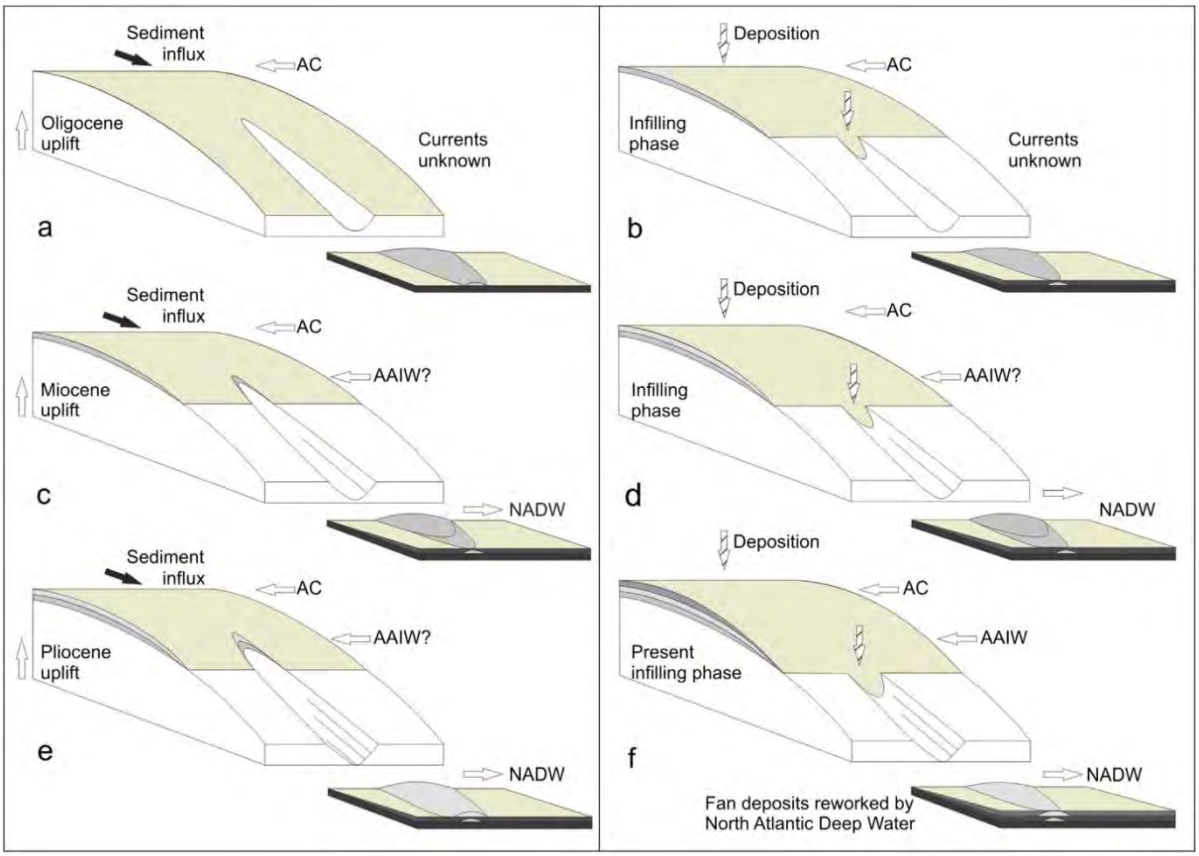

Fig. 4.9. An evolutionary model for the Tugela Canyon and fan evolution. Note periods of uplift (a, c, e) set-apart by infilling (b, d, f) of the upper canyon, stagnation of the mid to lower reaches during quiet phases, and interfingered fan/pelagic sediments in the deep Natal Valley.

Axial incision (Fig. 4.3) noted at 1490 m further illustrates the significance of downslope erosion as a contributor to canyon formation. Baztan et al. (2005) found axial incision in canyons of the Gulf of Lion to be associated with river connection during lowstands. Hyperpycnal plumes generated by flooding rivers provide the necessary energy to develop axial incisions of considerable downslope length (>50 km) (Baztan et al., 2005), an attribute not associated with axial incision within the Tugela Canyon. In this instance dilute turbidity currents (cf. Laberg et al., 2007; Jobe et al., 2011), rather than hyperpycnal plumes, are believed to be responsible for limited axial incision present in the Tugela Canyon. Such turbidity currents can ignite from an over steepened muddy/silty upper slope (Pratson et al., 1994; Mitchell, 2005). It is highly unlikely that a river connection existed, certainly not at -1490 m, furthermore incision is limited to less than 10 km alluding to short lived erosive events. Axial incision was, however, sufficient to induce further instability resulting in mass wasting of the canyon flanks down slope. Cut-terraces evident in the lower course (Fig. 4.6, profile g – g') illustrate five lesser periods of vertical erosion, while two significant periods of incision are envisioned for the canyon system as a whole (discussed in Section 4.3.2).

Escarpments (Figs. 4.4 and 4.5), formed by the erosion of sedimentary strata as opposed to displacement via faulting, are confined to the western flank of the Tugela Canyon. This is likely controlled by bed geometry, a topic discussed by McGregor (1981). In this instance, SE dipping strata of the western flank are inherently unstable. These strata dip in towards the void excavated by the Tugela Canyon, resulting in preferential erosion of these strata. Conversely, strata of the eastern flank are less susceptible to erosion and more stable, given that these strata dip into the eastern flank. This accounts for the canyon wall asymmetry depicted in figures 4.4 and 4.5. Basement outcrop becomes less evident down canyon; certainly by swath TC3 no basement outcrop is apparent. The prominent outcrop up canyon from this point suggests an increase in basement control, over canyon development, toward the continental shelf.

4.3.2. Timing and mechanisms of canyon development

The cross-cutting relationship between the Tugela Canyon and Cretaceous units (Fig. 4.8) clearly shows that the formation of the Tugela Canyon post-dates the deposition of the upper Maastrichtian age basin fill (Goodlad, 1986). The multi-channel seismic sections upslope of the modern canyon head show several phases of incision. Here it is proposed that the earliest of these corresponds to a mid-Oligocene stage of hinterland uplift, the first to occur during the Neogene (Walford et al., 2005). Uplift, combined with regressive conditions (Fig. 4.9a), resulted in considerable sediment shedding in the hinterland, and transport across the shelf. Sediment was thus provided directly to the slope where downslope-eroding mass wasting processes associated with sediment loading and over-steepening initiated the proto-Tugela Canyon (Figs. 4.9a and 4.10). Subsequent transgression would subsequently reduce downslope eroding sediment flows to the canyon, resulting in a period of dormancy corresponding to the first stage of infilling (Fig. 4.9b).

The Tugela Canyon was later reactivated during the subsequent early Miocene uplift (Fig. 4.9c), as evidenced in the second canyon incision in the upslope seismic sections (Fig. 4.8) and an associated second phase of terracing in the lower canyon portions. This is reconciled to the early hiatus documented in the shallow shelfal portions of the Tugela Cone and suggests a significant period of regression, sediment bypass and associated incision in the shelf (Green and Garlick, 2011). This is likely to have translated downslope and thus substantially rejuvenated the Tugela Canyon. This is linked to the generation of a modified "U" profile (Figs. 4.4 and 4.5) and the hanging branches depicted in figure 4.6.

Another period of quiescence followed this and was associated with infilling (Fig. 4. 9d) prior to a third stage of late Pliocene uplift occurred on a scale greater than that of the Miocene phase (Fig. 4.9e) (Walford et al., 2005; Moore and Blenkinsop, 2006). This resulted in canyon incision into both the previous palaeo-canyons, pronounced axial incision and additional terracing in the walls (Figs. 4.4 and 4.6).

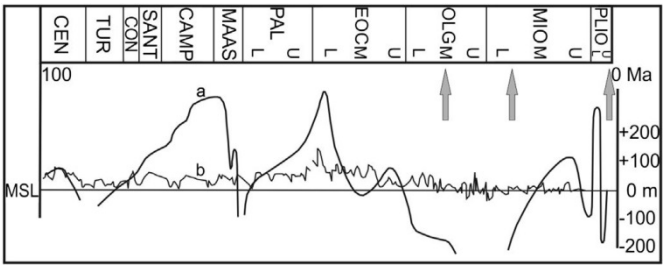

Fig. 4.10. Mid Cretaceous to Pliocene sea-level curve (a, modified after Dingle et al., 1983) compared to the global eustatic sea-level curve (b, modified after Miller et al., 2005). Grey arrows denote uplift episodes. Note the poorly constrained Tertiary sealevel curve.

Comparable studies from the western South African margin indicate similar erosional periods. A protracted early to mid-Oligocene hiatus is recognised by Wigley and Compton (2006) and is contemporaneous with a recognised global sea level lowstand of the mid Oligocene (Miller et al., 1998). It is likely that off-shelf shedding of sediment during regression to this lowstand (cf. Compton and Wiltshire, 2009) would have resulted in downslope erosion. Overall, the most protracted amount of uplift occurred during the Pliocene (Partridge and Maud, 2000). This is considered to have caused several slumps on the southern African margin (Dingle, 1980), initiated the head of the Cape Canyon on the western South African margin (Wigley and Compton, 2006) and caused several submarine canyons to form on the northern KwaZulu-Natal margin (Green, 2011a).

4.3.3. Modern canyon and fan activity

Given the age and the amount of sediment that was likely to have passed through the Tugela Canyon since its inception; the absence of a well-developed submarine fan prograding into the Natal Valley is surprising. A situation similar to the Congo deep-sea fan would be expected (cf. Anka et al., 2009), however fan deposits directly offshore the Tugela river are completely absent (Türkay and Pätzold, 2009). Instead a poorly developed fan extending from the sudden opening of the Tugela Canyon is present (Fig. 4.7). Echosounder records show the fan as a crude terrace dominated by regular overlapping hyperbolae with varied vertex elevations extending ca.40 km to the south west (Fig. 4.7b). These correspond to the

Type IIIC echo facies of Damuth and Hayes (1977). Such echo character is associated with erosional/depositional bedforms, either the result of erosion in the bottom boundary layer (Flood, 1980) and syndeposition (Tucholke, 1979) related to bottom water circulation or gravity driven processes (Damuth, 1975) depending on the setting. This irregular seafloor extends distally into smooth seafloor as the Natal Valley deepens toward the south (Fig. 4.7).

Another package of reflectors is apparent underlying the smooth seafloor (Fig. 4.7a). These comprise distinct high amplitude parallel reflectors (echo facies IB of Damuth, 1975) that appear to interfinger with the adjacent hyperbolae-dominated seismic unit. Such seismic facies have been recognised by Damuth (1975) and interpreted to be the proximal variant of turbidites on the abyssal rise, or the result of pelagic sedimentation. Such flat lying deposits (in this area the slope is sub-horizontal, averaging 0.12°) have been recognised by others as pelagic deposits and their flat parallel nature is indicative of bottom current winnowing and episodic seafloor smoothing in association with drift development (Schlüter and Uenzelmann-Neben, 2008). Contrary to what one might expect, there are no surface expressions of distributary channels or levees etc. The interfingering of hyperbolae-dominated IIIC facies with parallel, flat-lying facies (IB) is likely the result of intermittent unconfined turbidite introduction to the area (Fig. 4.7a).

This suggests that there is significant interaction between the two systems whereby sporadic and energetic turbidites overprint NADW deposition before being winnowed and redistributed into an echo facies 1B configuration. No other features associated with deep-sea fans, lobes, or distributaries are recognised in the Tugela Canyon fan region. It should therefore be described as an atypical, sediment starved deep-sea fan that is strongly modified by the NADW. Other examples of such fans are poorly described. Eschard (2001) maintains that such interactions between deep-sea fans and bottom water circulation (erosion and redistribution of sediment) are underrated.

In the proximal staging grounds for downslope eroding flows, the overspilling of sediment from the shelf to the slope is limited by the Agulhas Current. In these areas, the current re-organises sediment in a coast parallel manner and it only overspills the shelf break where major inflection points in the coast occur (Flemming, 1980). Despite these being a possible source for turbidity currents (Boyd et al., 2008) the wholesale starvation of the shelf has occurred to the extent that the submarine canyons along the northern KZN coast have been quiescent since the late Pliocene (Green, 2011b). Since then an overall period of

starvation has prevailed and has limited the primary canyon driving mechanism, namely upper slope sediment loading and resultant mass wasting. During these times, pelagic sedimentation on the upper and mid-slope has been dominant (Fig. 4.9f). This is responsible for the development of the most recent onlapping drape fill in the upper canyon which has not fully filled the palaeo-canyon form (Fig. 4.8). Further down canyon, erosion may still be occurring (as evidenced by some smaller cut terraces developed in the canyon walls) but is limited in comparison to that of the Neogene.

During the current highstand where sediment delivery is commonly not as prominent as lowstand periods, even less sediment is released to the shelf. This is further held up in the poleward moving sediment conveyor of the Agulhas Current thereby starving the upper slope region. The fan deposits that are preserved from periods of canyon activity are currently in the process of being reworked by the NADW, a scenario similarly encountered in the adjacent Transkei Basin (Schlüter and Uenzelmann-Neben, 2007, 2008).

Chapter 5

A new pathway for deep water exchange between the Natal Valley and Mozambique Basin?

5.1. Introduction

The global transfer of heat and nutrients is driven by THC within the ocean basins. The THC system comprises a network of bottom, deep and surface currents that conserve mass and energy in the World's oceans by the creation of a complex system of circulation cells. The southwest Indian Ocean (SWIO) is a dynamic region of ocean exchange between the Indian, Atlantic and Southern Oceans representing a pivotal component of the THC system. In general, both bottom and deep water circulation pathways around the globe and within the SWIO are well known and constrained. The residence times of these deep and bottom waters have significant implications for long-term climate state as well as CO_2 sequestration (Martin, 1981a; 1981b; Ben-Averaham et al., 1994; Srinivasan et al., 2009). As a result, the greater THC system has garnered increased attention over the past two decades, particularly in light of their potential roles driving both palaeo and future climate change (Martin 1981a; 1981b; Raymo et al., 1990; Winter and Martin, 1990; Raymo et al., 1997; Schmieder et al., 2000; Srinivasan et al., 2009; Gutjahr et al., 2010). However, at a more localised scale, THC pathways are often poorly constrained. Many factors, including the Earth's rotation (Coriolis Effect), ocean basin macrotopography, ocean gateways, prevailing winds, and glacial/ inter-glacial cycles have a direct impact on THC circulation and transport volumes. This research examines deep water bottom currents in the context of seafloor macrotopography and interprets these in light of several possible deep water circulation systems in the Natal Valley, SWIO.

Since the initial research thrust in the Natal Valley (cf. Martin 1981a; 1981b; Dingle et al., 1978; Dingle et al., 1987, Winter and Martin, 1990), little additional research associated with the Natal Valley has been undertaken; this is especially true for the deep, northern portions of the Natal Valley. Notable exceptions include studies on the interactions between bottom water currents (those deep currents in contact with the seafloor) and sediments from the Natal Valley (Niemi et al., 2000; Chapter 4), and submarine canyons of the upper slope (Green et al., 2007; Green and Uken, 2008; Green, 2011a).

This chapter presents a new, higher resolution dataset of the area, highlighting several key seafloor and subsurface features that reveal a potential new deep water pathway across the Mozambique Ridge (via the Ariel Graben) to the Mozambique Basin, as described by new multibeam bathymetry and high frequency seismic data from the Natal Valley, SWIO. The aim of this chapter is to reconcile this with the major THC systems in the area.

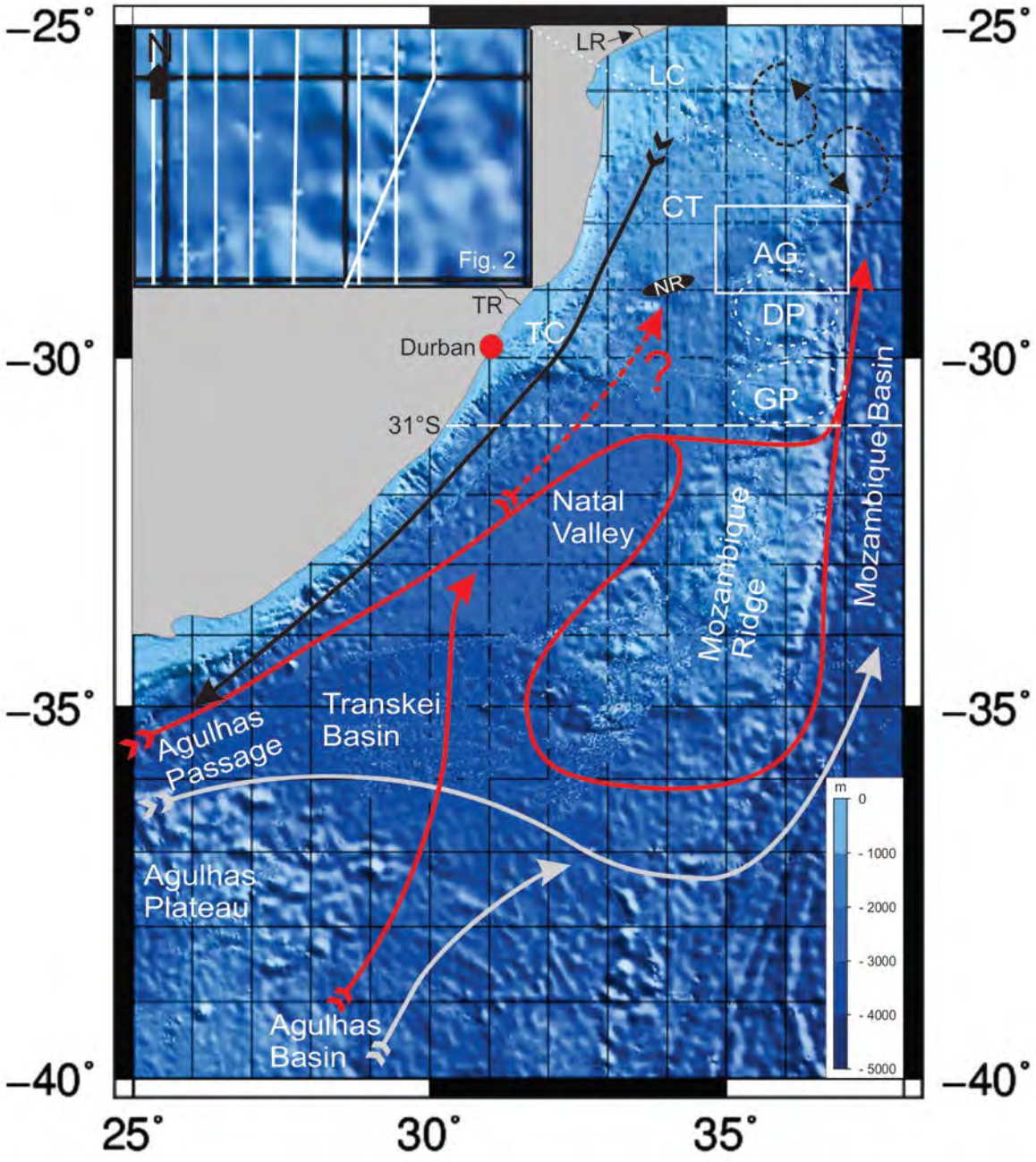

[*Previous page*] Fig. 5.1 The general bathymetry (The GEBCO_08 Grid, version 20091120) of the southwest Indian Ocean. Presently known THC pathways are shown; black arrow illustrates the Agulhas Current, red - the North Atlantic Deep Water, and grey - the Antarctic Bottom Water (after Bang and Pearce, 1976; Casal et al. 2006; Dingle et al., 1987; Toole and Warren, 1993; Schlüter and Uenzelmann-Neben, 2008a; van Aken et al. 2004). Eddies associated with the Mozambique and East Madagascar Currents are shown by dashed circular arrows (Quartly and Srokosz, 2004). The Tugela Cone (TC), Limpopo Cone (LC) and Central Terrace (CT) are located west of the study area (white box), which is enlarged to show the ship tracks. The Dana (DP) and Galathea Plateaus (GP) of the northern Mozambique Ridge are indicated by dashed circles. North of the Dana Plateau lies the Ariel Graben (AG), a west/east saddle across the Mozambique Ridge. The most prominent rivers flowing into this Natal Valley region are the Thukela River (TR) in South Africa, and the Limpopo River (LR) in Mozambique. The Naudé Ridge (NR) is a buried basement high. A more detailed overview of the study area is provided in figure 5.2.

5.2. Results

A wide, channel-like feature is evident in the multibeam bathymetric data, leading from the mid-Natal Valley across the Mozambique Ridge toward the Mozambique Basin (Fig. 5.2). Confined to the north-west by the Central Terrace, and the south-east by the Dana Plateau (Mozambique Ridge), the channel is located in the bathymetric depression associated with the Ariel Graben (Fig. 5.2). Rugged bathymetry is more common on the northern flanks of the Dana Plateau (i.e., southern flank of the Ariel Graben) than on the Central Terrace, where seafloor is smooth (Fig. 5.2). This rugged bathymetry is confined to depths of 2000 – 3000 m on the northern flank of the Dana Plateau where there is a significant amount of basement control on topography. Evidence of this is manifest in the highly irregular, rugged bathymetry, and seismic character presented in figures 5.3 and 5.4. Although the Ariel Graben has created an overall west to east orientated saddle, the actual depression follows a curved path (Fig. 5.2). The degree of change in channel axis orientation increases more rapidly in the west in the vicinity of box c (Fig. 5.2).

Boxes a and b (Fig. 5.2.) are enlarged in figures 5.3 and 5.4 respectively. These figures illustrate in detail the bathymetry and shallow seismic character of this portion of the Mozambique Ridge. The northern flanks of the channel return distinct bottom echoes, with several discontinuous sub-bottom echoes (profile A – A' in Fig. 5.3, and profile B – B' in Fig. 5.4). The seafloor is smooth, with no apparent basement outcrop or subcrop visible within the limit of penetration (20 m) and coverage. The gradient of the northern flank is variable, (0.3° – 2.1°, total slope average is 1°), typically increasing with depth (north/south

toward the channel) to a maximum of 5.7° nearest the channel. Steepest gradients (5° – 6°) are noted in the central region of the saddle across the Mozambique Ridge (Figs. 5.3 and 5.4).

The channel floor ranges in width from 4385 m to 5100 m with a variable echo character. In the western portions of the channel, hyperbolic reflectors are evident in the 5.5 kHz profile (profile A –A' in Fig. 5.3). The hyperbolae are of a similar height above the seafloor, and vary from individual to overlapping in organisation. Bathymetric data show this area to be rough/undulating. Smooth seafloor in the bathymetry is associated with distinct seafloor returns and continuous and sub-parallel sub-bottom reflector packages (profile B – B' in Fig. 5.4). An elongate terrace, orientated parallel to the base of the southern flank, is evident in both the bathymetry and shallow seismic data suggesting some degree of lateral and vertical erosion (profile B – B' in Fig. 5.4).

The southern flanks of the channel are distinct from the northern flanks in both bathymetric and seismic character. Large, irregular, hyperbolae, ranging in size, amplitude and spacing (over-lapping to 1 km) dominate the seismic profiles (Figs. 5.3 and 5.4). Intense overlapping is focused on the more rugged areas, while individual hyperbolae are observed where the bathymetry is less complex. Rugged bathymetry associated with such echoes, exhibit highly variable gradients (0.3° – 19.6°). Overall, the channel floor is relatively flat, while the profile of the channel is "U"-shaped. Scouring has modified this "U" shape in certain areas of the lower channel flanks suggesting sustained reworking and removal of sediment (Fig. 5.3).

There is a notable eastward change in character of the seafloor on the northern flanks of the channel (Fig. 5.5). At depths between 2100 m and 3000 m, the seafloor displays an undulating morphology (Fig. 5.5 and profile C – C' in Fig. 5.6). These undulations are straight crested and parallel/sub-parallel to the local isobaths, with crest long axes orientated west to east. Spacing between the crests is variable. The middle zone (2330 – 2677 m) is typified by undulations with 600 – 900 m wavelengths, whereas the upper and lower zones have distances of 1000 – 1200 m between crests. Cross- sectional symmetry of these features varies from symmetrical to asymmetrical, with broad crests and narrow troughs (Fig. 5.5). When asymmetrical, the downslope (south-facing) limb is longer (511.76 m average) than the up-slope (north-facing) limb (323.53 m average) (Table 5.1). The lower limbs are also steeper than the upper limbs; calculated averages being 3.80° and 1.55°, respectively (Table 5.1). Overall the total slope on which the undulations are found is south-facing with a

gradient of 1.54°, however, the area affected by undulations is slightly steeper with an average slope of 1.75°. Beyond 3000 m (the lower limit of the undulations), the gradient increases to 4.71° at the flank/channel floor transition. North of the undulations (above 2100 m) the seafloor becomes smooth once more, reflecting similar characteristics to that of the western portion of the study area (Fig. 5.5 and profile D – D' in Fig. 5.6). The total slope average in this eastern region is 0.54°, thus steeper than to the west. The channel floor, no longer flat, is ca. 440 m wide at 3160 m depth. The profile now has a more "V"-shaped section.

The southern flank of the channel is more rugged than the northern flank (Fig. 5.5). Hyperbolic echoes (from the 3.5 kHz echo trace) are associated with rugged bathymetry (profile E – E' in Fig. 5.6). Distinct bottom echoes, with several sub-parallel sub-bottom reflector packages are noted in areas of flat lying bathymetry (profile E – E' in Fig. 5.6). These packages onlap the rugged subcrop, showing varied package thickness and amplitude. The lowermost packages comprise low amplitude, transparent packages that thicken from south to north, while toward the seafloor surface, high amplitude packages of uniform thickness are evident. The gradient of the southern flank is highly variable, reaching a maximum of 10.5° in the rugged areas, whereas areas of subdued bathymetry exhibit low gradients (0.18°). The total gradient is 1.34° but is a poor indicator of the seafloor character due to marked variability in the gradient of the area (Fig. 5.7). The variation of the rugged southern flank is far greater and widespread than that of the north (Fig. 5.7). Only in the eastern portions of the study area, on the northern flank, does the gradient begin to vary as the undulation field is encountered (Fig. 5.7).

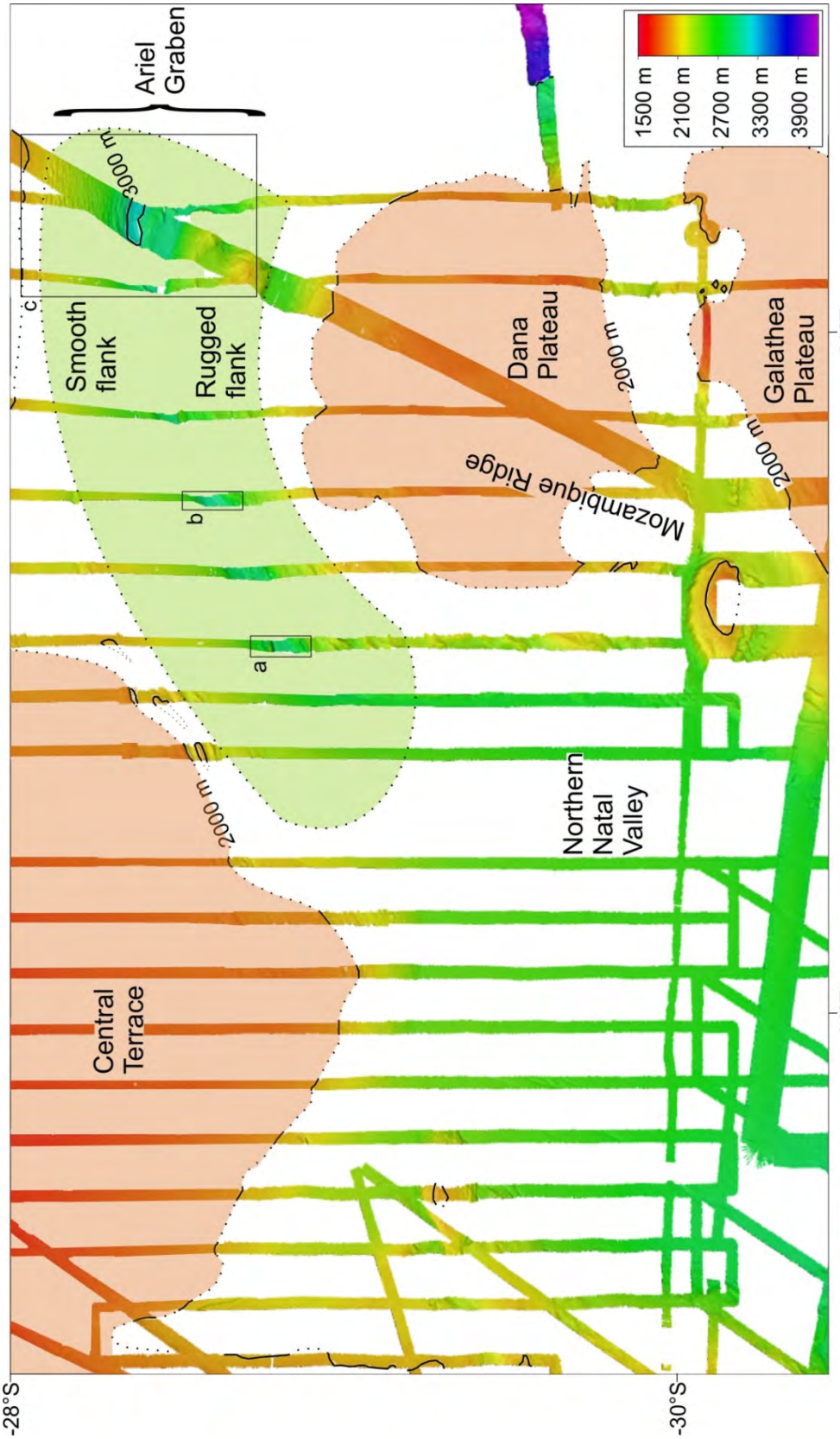

Fig. 5.2. An overview of the northern Natal Valley and northern Mozambique Ridge. Note the 2000 m isobaths to the NW (Central Terrace) and SE (Dana Plateau), as well as the saddle created by the Ariel Graben. Boxes a, b, and c show areas enlarged in figures 5.3, 5.4, 5.5 and 5.6, and are referred to in text.

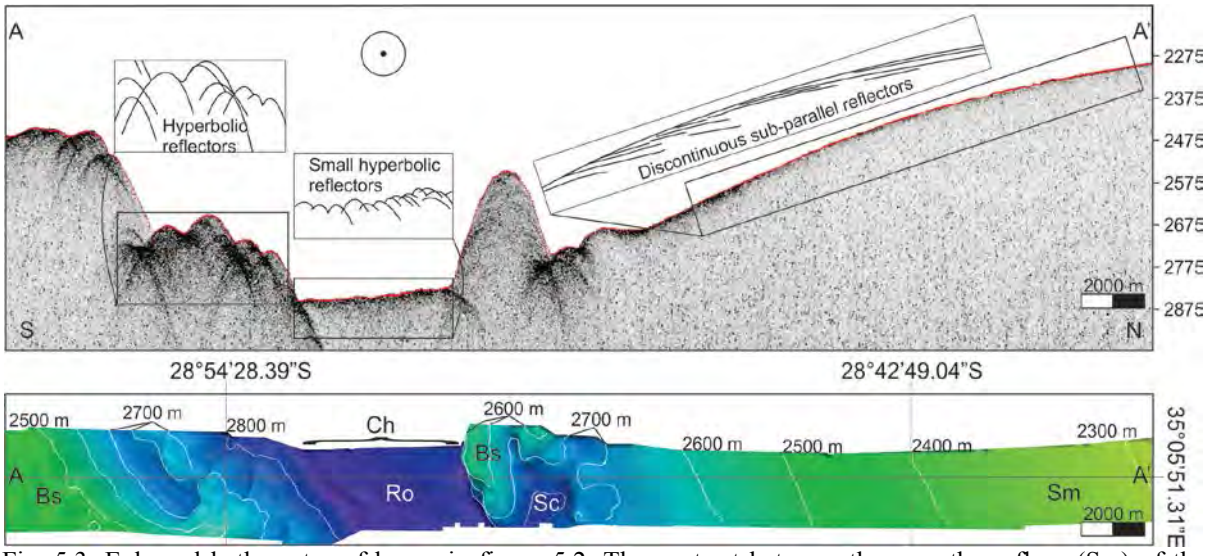

Fig. 5.3. Enlarged bathymetry of box a in figure 5.2. The contrast between the smooth seafloor (Sm) of the northern flank and the rugged seafloor (Bs), reflecting some basement control, of the southern flank is evident in the multibeam bathymetry (bottom) and high frequency seismic record (profile A – A', top). Note the apparent scouring (Sc) around basement outcrop in the saddle floor.

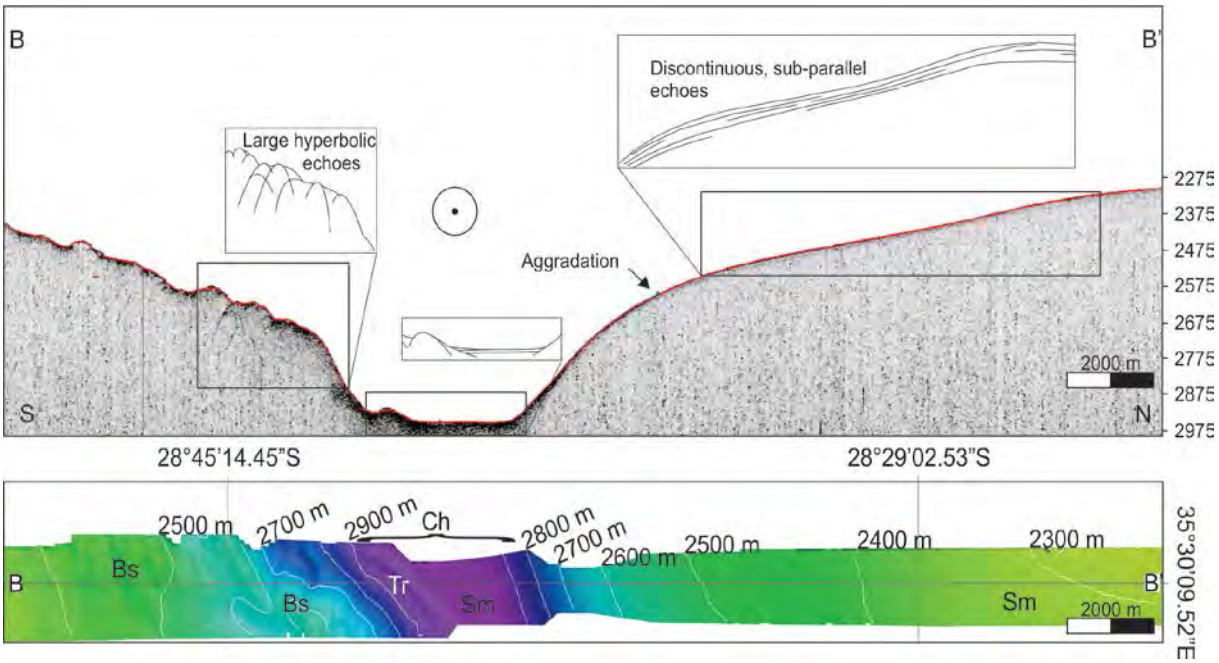

Fig. 5.4. Enlarged bathymetry of box b in figure 5.2. The contrast between the smooth seafloor (Sm) of the northern flank and the rugged seafloor (Bs) of the southern flank of the Ariel Graben is clear in the multibeam bathymetry (bottom) and high frequency seismic record (profile B – B', top). Note the change in character of the floor of the saddle. A terrace (Tr) is apparent at the base of the southern flank.

Table 5.1. Length and gradient characteristics of undulations.

ID	Upslope limb (m)	Downslope limb (m)	Upslope limb (°)	Downslope limb (°)
1	550	650	1.66	-3.88
2	500	550	0.86	-5.64
3	400	600	2.81	-3.17
4	500	700	0.54	-3.15
5	400	600	2.11	-4.66
6	400	600	1.71	-2.80
7	400	450	0.65	-4.25
8	200	450	0.86	-5.09
9	200	400	1.18	-4.62
10	300	300	1.79	-3.28
11	300	400	0.41	-3.98
12	150	350	4.21	-5.59
13	200	350	0.26	-2.87
14	200	350	0.16	-3.15
15	200	800	3.04	-3.48
16	200	400	2.26	-5.46
17	200	750	1.78	-5.84
Average	323.53	511.76	1.55	-3.80

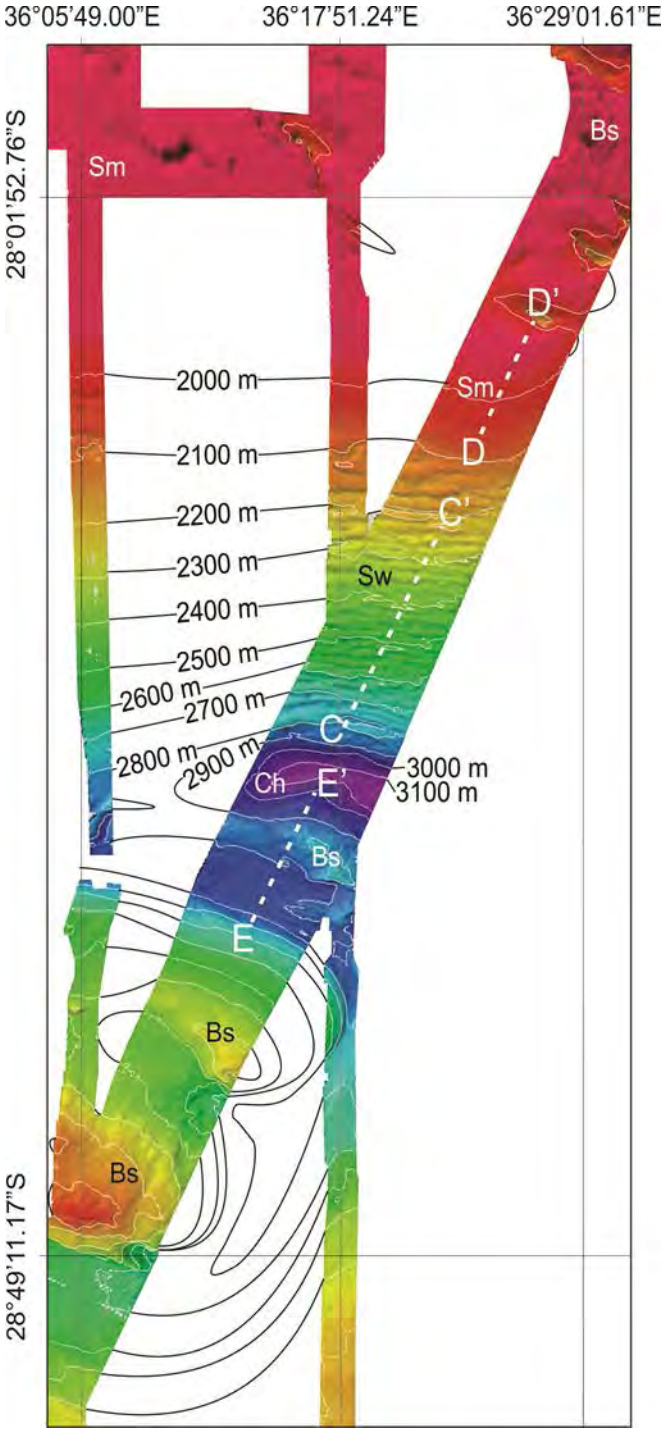

Fig. 5.5. The eastern region of the Ariel Graben revealed in the multibeam data (See figure 5.2, Box c for location). Note elements of basement control (Bs), smooth seafloor (Sm), and undulation field (Sw). The channel floor (Ch) is now narrower than in the west toward the Natal Valley. Profiles C – C', D – D', and E – E' shown in figure 5.6.

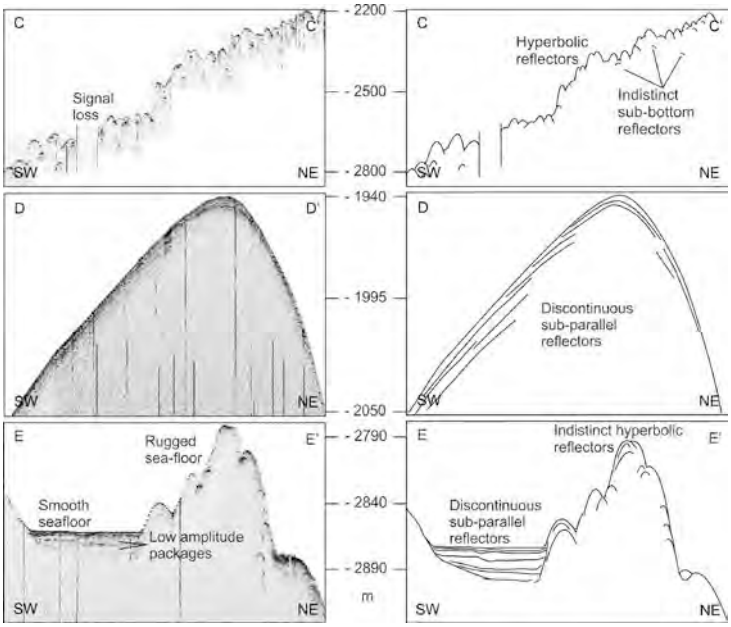

Fig. 5.6. Seismic character of profiles C – C', D – D', and E – E' (see figure 2, Box c, and figure 5 for location). Undulating seafloor is associated with hyperbolic echoes with indistinct sub-bottom returns. This is in contrast to the discontinuous sub-parallel reflectors of profile D – D', which is associated with smooth seafloor. On the southern flank of the Ariel Graben, hyperbolic echoes are similarly associated with rugged seafloor (Bs in figure 5.5), while horizontal, discontinuous sub-parallel echoes are evident in troughs adjacent to the rugged seafloor.

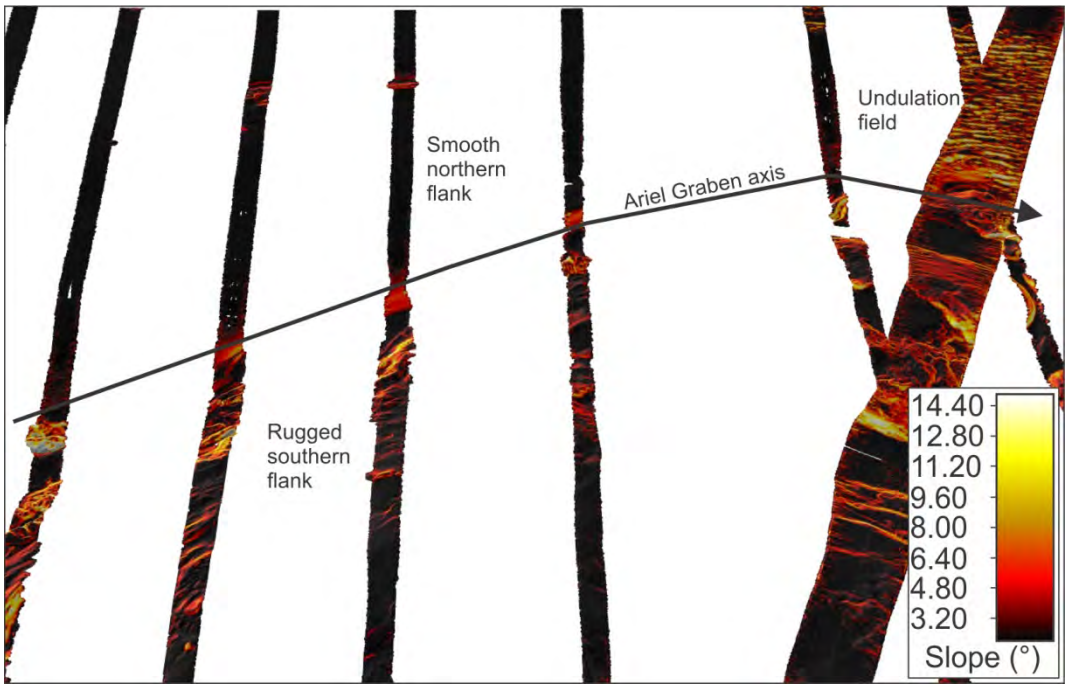

[*Previous page*] Fig. 5.7. 3D perspective view slope map for the Ariel Graben looking south to north from the Dana plateau across the Ariel Graben. The strips of data reflect the slope of the seafloor as calculated from the bathymetry data from the same area. Note the difference in slope and relief between the northern and southern flanks of the Ariel Graben. The northern flank is relatively uniform, the exception being the undulations to the east which exhibit regular variance in gradient over short distances. In contrast, the southern flank exhibits varied gradients throughout the study area reflecting an irregular seafloor relief. The change in the orientation of the Ariel Graben (from west to east) is shown by the black arrow.

5.3. Discussion

5.3.1 Echo character contrasts

There is distinct contrast in the echo character of the Ariel Graben's northern and southern flanks. The northern flank (western area) shows distinct, high amplitude, bottom echoes with several discontinuous parallel/sub-parallel sub-bottom reflectors. This echo character is synonymous with the development of crude plastered drifts, as described from other regions (cf. Damuth, 1975; Damuth, 1980; Jacobi, 1982; Faugères et al., 1999; Stow and Mayall, 2000; Masson et al., 2002; Maldonado et al., 2003; Stow et al., 2008), and the same deposit is envisioned in this study (Figs. 5.3, 5.4 and 5.6). This is further demonstrated by the areas of smooth seafloor (Sm in figures 5.3, 5.4 and 5.5) where current-plastering has created a uniform surface relief. This seafloor character has similar associations to plastered drifts, discussed from other regions by multiple authors (Damuth, 1975; Damuth, 1980; Jacobi, 1982; Faugères et al., 1999; Stow and Mayall, 2000; Masson et al., 2002; Maldonado et al., 2003; Stow et al., 2008). Along the northern flanks of the eastern Ariel Graben, seafloor undulations (Fig. 5.5) are associated with large, individual hyperbolic echoes (Fig. 5.6) that approach the IIB-2 character of Damuth's (1975) scheme. The origin of this echo character is said to be varied; bottom current and gravity-driven processes are postulated as possible formative processes, with setting being an important consideration. In the case presented by Damuth (1975) IIB-2 echoes are located adjacent to levees and distributary channels of the Amazon cone. However, more consolidated gravity controlled flows and mass movements may also result in type IIB-2 echoes being recorded from the respective deposits.

The floor of the Ariel Graben (Ch in figures 5.3, 5.4, and 5.5) has a varied echo character. In the west it is rough, with small overlapping hyperbolae (IIIC of Damuth, 1975) showing evidence of erosional/depositional bedforms. Such bedforms from other basins have been ascribed to erosion in the bottom boundary layer (Flood, 1980) and syndeposition

(Tucholke, 1979) related to bottom water circulation or gravity driven processes (Damuth, 1975) depending on the setting.

The southern flank of the Ariel Graben is rugged, dominated by large hyperbolae. Such a strongly reflective, hyperbolic echo character typifies basement highs or outcrop (Damuth and Hayes, 1977; Damuth, 1980; Lee et al., 2002). In this case, the lower northern flank of the Dana Plateau is cropping out due to an overall lack of sediment deposition on the southern flank. As shown in figure 5.6 (profile E – E'), ponds of sediment (discontinuous sub-parallel reflectors) are present in troughs and depressions of the southern flank. This suggests a sediment-starved environment on the southern flank of the Ariel Graben, and implies differential deposition within the study area

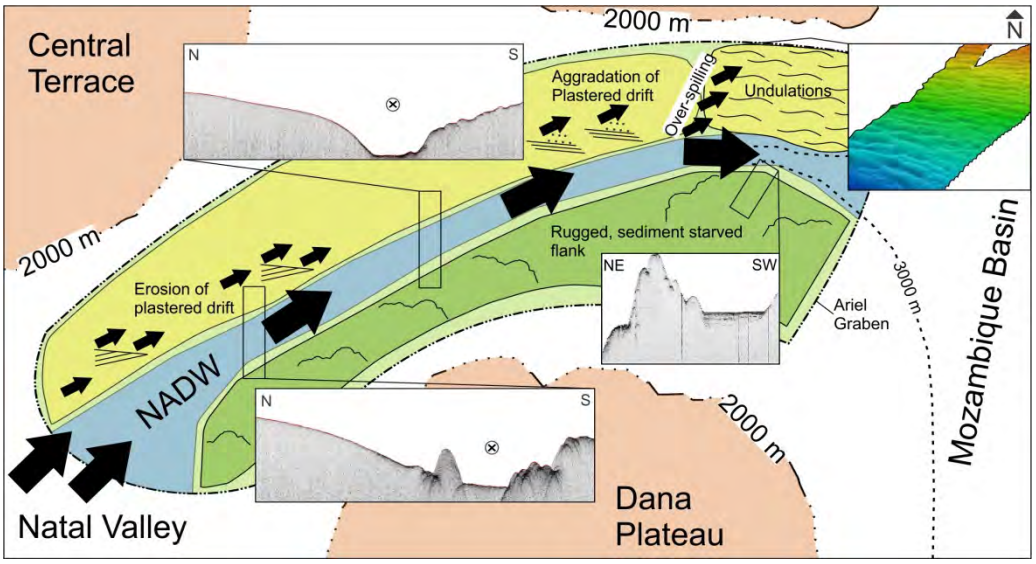

Fig. 5.8. Schematic of the study area (refer to figures 5.1 and 5.2) illustrating the proposed NADW pathway through the Ariel Graben. Once the water mass has entered the Ariel Graben its passage is determined by the axis of the graben. Proximally northeast orientated, the graben axis changes to east-southeast towards the distal areas in the east.

5.3.2 Interpretation of bathymetric and 3.5 kHz data

The development of a crude plastered sediment drift in the west (on the northern flank) gives way to soft sediment deformation fields in the east of the northern flank of the Ariel Graben. This demonstrates changes in the depositional/erosional setting from west to east through the Ariel Graben along the northern flank. The plastered drifts are typical of depositional features associated with bottom water current circulation (Stow et al., 2008), yet the transition to the field of undulations is atypical and requires that others factors be involved in their formation.

The presence of these undulations could be explained by several processes including contour current/seafloor interactions, turbidity current activity and mass-wasting/soft sediment deformation. Although the undulation dimensions are similar to features created by turbidity currents (see Table 5.2 for a comparison). In the setting presented here, the formative process associated with IIB-2 echoes is potentially related to deposition by turbidity currents. However, the undulation field is not associated with any deep sea canyon/channel/fan system. The nearest continental shelf that could shed sediment directly to the Ariel Graben is 380 km to the west. Apart from being sediment starved (Green, 2009; Flemming, 1980), this margin is separated from the Ariel Graben by the Central Terrace, disrupting the pathway of sediment by turbidity current. The Mozambique Ridge is obviously a feature which could play host to turbidity currents, however, in the setting of the Ariel Graben this is unlikely. There is no suitable staging area/source, directly to the north of the Ariel Graben, for the generation of turbidity driven flows. Hence, given the location of the undulation field of this study, deposits associated with turbidity currents are highly improbable.

Furthermore, from a morphological perspective, the character of the undulations is atypical of the surface expression of turbidites (Faugères et al., 2002; Wynn and Stow, 2002). The wave-form (i.e., the general morphology of the undulations) dimensions of the undulations are larger in the upslope and downslope areas, decreasing in dimension toward the middle of the flank as opposed to the general decrease in wave dimension downslope (i.e., with distance from the source) expected of turbidity current-fed bedforms.

With regards the genesis of sediment waves by bottom current interaction, the dimensions of the wave-forms observed in this study are similar to those of fine-grained bottom sediment waves (cf. Wynn and Stow, 2002; Table 5.2 this study). Such fine-grained bottom sediment waves are found in sediment drift environments on the basin floor, lower slope and rise. At odds with this interpretation are the general orientations of the wave-form crests themselves. Typically, the crests of fine-grained bottom current sediment wave systems are oblique to the slope, or perpendicular to the flow direction of the current, with evidence of upslope and up-current migration of bedforms. In this study, the crests are parallel/sub-parallel to the maximum slope, orientated west/east; ca. 90° to the expected orientation (north-south) had they been directly developed by a current flowing west to east through the graben. As with a turbidity current-induced setting, the decrease then increase of the wave-form dimensions is in contrast to that of a bottom current sediment wave setting

that generally produces decreasing wave-form dimensions with increased transport distance (Faugères et al., 2002; Wynn and Stow, 2002).

The final alternative of downslope creep appears to be a viable option for the genesis of these features. There has been much discussion concerning the distinction between current generated sediment waves and undulations generated by creep/soft sediment deformation (Dillon et al., 1993; Gardner et al., 1999; Holbrook, 2001; Lee and Cough, 2001; Holbrook et al., 2002; Lee et al., 2002; Trincardi et al., 2004; Schwehr et al., 2007; Shillington et al., 2012). The debate stems from the similarities in bathymetry and seismic characteristics of these features. However, having excluded generation by bottom or turbidity current, soft sediment deformation is a likely formative process. In addition, the dimensions and characteristics of the seafloor undulations in this study (Table 5.2) are comparable to those associated with creep as described by Wynn and Stow (2002).

In keeping with the discussion in section 5.3.1 and in the context of the bathymetry signatures discussed above, it is clear that the northern flank of the Ariel Graben is dominated by sediment cover, whereas the southern flank of the Ariel Graben exhibits basement control on sedimentation in a sediment starved setting with ponds of sediment filling low lying areas amidst the rugged bathymetry of the Dana Plateau's northern flank. The local outcrop of basement is likely to increase turbulence and promote the resuspension and redistribution of sediment rather than deposition. The net result is preferential deposition on the northern, rather than southern flank of the Ariel Graben. The resultant uneven depositional regime is at odds with the uniform distribution of sediment thicknesses attributed to pelagic deposition. Preferential drift deposition on the northern flank of the Ariel Graben is thus the likely driver of downslope creep here.

5.3.3. Significance of creep

Seafloor undulations generated by soft sediment deformation are often related to seismic activity. Examples from the Adriatic and Californian continental slopes describe such occurrences of seismically induced soft sediment deformation. However, such settings are far removed from the deep Ariel Graben of the Mozambique Ridge. The former two regions have recent and sustained seismic histories accounting for extensive soft sediment deformation fields (cf. Dengler, 1993; Tinti et al., 1995), whereas the Mozambique Ridge is comparatively stable (Leinweber and Jokat, 2012). Recent findings suggest that there may be some tectonic activity associated with the southward propagation of the East African Rift

System (Saria et al., 2014; Chapter 3). However, seismically induced deformation seems unlikely at this location as the soft sediment deformation is restricted to a specific area within the region rather than a wide-spread occurrence in line with seismically-induced deformation fields. High sedimentation rates, storm waves, and biological processes may also induce downslope movements through the increase of applied shear stress or reduction of the critical shear strength of sediments (Stow et al., 1996). At the depth of the undulations, storm waves are not considered, while biological activity is an unknown variable. A high sedimentation rate is therefore suggested as the most prominent factor in this instance, likely delivered by deep water bottom-interacting currents in the area.

5.3.4 Sediment redistribution via the Agulhas Current or NADW?

In the northernmost Natal Valley, sediment redistribution at depths of between 400 – 1500 m on the Central Terrace, Limpopo Cone and adjacent continental shelf has been attributed to action of the Agulhas Current (Flemming and Hay, 1988; Martin, 1981a; 1981b; Preu et al., 2011). However, it is unlikely that the Agulhas Current at 27°S is as deep seated as it is to the south (32°S), where it reaches depths of 2500 m (Bang and Pearce, 1976; Dingle et al., 1987, Beal and Bryden, 1997; Donohue and Toole, 2003). Three reasons account for this. Firstly, in this source region the Agulhas Current is still forming from the amalgamation of eddies from the north and east (Preu et al., 2011). Secondly, the Central Terrace lies in ca. 1500 m of water, so a deeper extension of the current to 2500 m is not possible. Thirdly, the observation by previous authors of a northerly flowing NADW in the west and a southerly flowing NADW in the east of the Natal Valley implies recirculation of this current system whereby NADW passes beneath the Agulhas Current at a deeper level. On this basis the alternative hypothesis is considered valid, bottom current activity and sediment re-organisation by the NADW.

5.3.4.1 Oceanographic constraints to potential NADW flow and a revised pathway

As a deep western boundary current plastered up against the east coast of South Africa by the Coriolis Effect, it is unlikely that its northward passage would be impeded until

obstacles to that flow are encountered (Dingle et al., 1987; van Aken et al., 2004; Martínez-Méndez et al., 2008; McDonagh et al., 2008). The shoaling of the northern Natal Valley provides the necessary bathymetric restriction to change the pathway of the NADW. However, this restriction within the known depth range of NADW is gradual and asymmetrical. The northern Natal Valley does not terminate in a horseshoe between 2000 m – 3500 m (Fig. 5.8), but rather the Tugela Cone and Central Terrace (fronted by the Naude' Ridge) provide initial restrictions from the west and northwest respectively (Fig. 5.8). These restrictions would force the NADW to shift from its original north northeast flow direction towards the northeast. The 2000 m isobath marks the shallow edge of the Central Terrace, and consequently the northward limit of NADW flow in the northern Natal Valley. Continuing to the northeast, the 2000 m isobaths of the Central Terrace merges with the top of the Ariel Graben's northern flank (Figs. 5.2 and 5.8). The Dana Plateau, located south east of the Central Terrace, rises to a minimum depth of 1795 m and consequently restricts the direct eastward flow of NADW into the Mozambique Basin (Fig. 5.8). The Dana Plateau thus offers a potential point divergence for NADW flow whereby a portion of the water mass can continue northeast into the Ariel Graben, while the remainder recirculates southward along the eastern margin of the Natal Valley.

Once the NADW enters the Ariel Graben its passage is likely defined by the graben long-axis; the orientation of which is not constant. From west to east the axis migrates in a clockwise manner, not confined to the orientation of the saddle axis. The average gradient of the graben flanks, particularly the northern flank, typically increases from west to east with the steepest gradient found where the saddle axis changes direction to the east (Fig. 5.7). It is in the east that the maximum axis curvature takes place and it is here that the upper portion of the NADW is likely to over-spill on to the northern flank, effectively over-shooting the bend in the graben axis. This over-spilling results in reduced velocity, and deposition of suspended load on the northern flank. Coriolis Effect is likely to also play a role. Deflection to the left (north in this case) further promotes preferential deposition of the northern flank of the Ariel Graben thereby compounding the result of over-spilling in the region of undulations. Such rapid sedimentation is said elevate pore pressure, and create weak planes within the deposited sediments (Shillington et al., 2012). Subsequent slow gravity-driven downslope motion and deformation generates the region of seafloor undulations on the northern flank of the Ariel Graben. Hence, this area represents an over-steepened plastered drift, developed in response

to over-spilling of NADW in the Ariel Graben, the failure of which is manifest as seafloor undulations generated by down slope creep (Fig. 5.8).

5.3.5 The relevance of a revised deep water pathway

The complex macrotopography of the SWIO, as demonstrated by Dingle et al. (1987), van Aken et al. (2004) and Casal et al. (2006), represents a significant factor in the control of deep THC flow (Donohue and Toole 2003). In this study, a previously unrecognised northern-most pathway for deep water exchange between the Natal Valley and the Mozambique Basin at 28°S is proposed (Fig. 5.9). The recognition of this pathway means the Natal Valley system and its effect on the SWIO region should be re-evaluated as the THC system and global climate are strongly linked (Martin 1981b; Martin 1987; Martin and Flemming 1988; Winter and Martin 1990; Martínez-méndez et al., 2008; Blome et al., 2012; Li et al., 2013; Menary and Scaife, 2014).

With respect to NADW circulation interglacial periods typically see increased flow of NADW, while glacial periods are associated with reduced flow (Ben-Averaham et al., 1994; Alley et al., 1999; Rutberg et al., 2000). Increased flow, especially the proposed northern incursion of NADW, has implications for the ocean basins in which this water body is found, affecting deep water exchange between sub-basins within the SWIO (Fig. 5.9). The forcing of this deep water mass into rugged regions of shoaling bathymetry of the northern Natal Valley and Mozambique Ridge has the potential to increase upwelling in these regions, resulting in increased diapycnal mixing between water masses (Polzin et al., 1997).

As long-lived CO_2 sinks, such diapycnal mixing could be of ecological and climatological significance. It is suggested that CO_2 flushing from deep water masses is a step-wise process that includes elevated nutrient supply to the mid-depths, subsequently resulting rapid rage expansion of species, increased productivity and CO_2 sequestration within the mid-Ocean (Galbraith et al., 2007; Henry et al., 2014). These have important ramifications for the east coast of Africa's future fishery potentials.

Table 5.2 Summary of characteristics for different types of sediment waves, and also soft sediment deformation features (modified after Wynn and Stow, 2002).

Wave-forming process	Turbidity current	Turbidity current	Bottom current	Bottom current	Soft sediment deformation (e.g. creep folds)	This study
Sediment grain Size	Fine-grained (mud and silt dominated)	Coarse-grained (sand and gravel dominated)	Fine-grained (mud and silt dominated)	Coarse-grained (sand and gravel dominated)	Varied: usually fine-grained (mud/silt dominated)	Unknown: presumed fine-grained
Environment	Channel levees, continental slope/rise	Canyons, channels and canyon/channel mouths	Sediment drifts on basin floor/lower slope/rise	Topographic ridges, continental slopes, b-c passages	Varied: potentially any submarine slope	Ariel Graben northern flank
Wavelength	Up to 7 km	Usually up to 1 km, rarely larger	Up to 10 km	Up to 200 m	Up to 10 km	600 m – 1.2 km
Wave height	Up to 80 m	Up to 10 m	Up to 150 m	A few metres	Up to 100 m	35 – 70 m
Key features	Usually on slopes of 0.1 to 0.7° Wave dimensions progressively decrease downslope Wave asymmetry usually decreases downslope Crests are roughly parallel to regional slope	Crests aligned perpendicular to flow direction Can show decrease in dimensions at channel margin Morphology is often irregular/disrupted Migration direction variable	Wave dimensions decrease near edge of wave field Wave symmetry decreases near edge of wave field Waves on slopes are aligned oblique to slope Most waves on slopes migrate upcurrent and upslope Crests are straight or slightly sinuous	Can occur as straight waves or barchans Both types aligned perpendicular to flow Barchans common where sediment supply is poor, migration is upcurrent Ripple patterns show peak flow near barchan crest	Most common on slopes of >2° Orientated perpendicular to maximum slope Do not show true lateral migration Usually show broard crests and narrow troughs Typically random scatter of dimensions	Orientated perpendicular to maximum slope Usually show board crests and narrow troughs Dimensions increase toward the edges, up and down slope.
Key examples	Monterey Fan levees (Normark et al., 1980) Bounty Channel levees (Carter et al., 1990) Toyama Channel levees (Nakajima and Satoh, 2001) Var Fan levees (Migeon et al., 2000, 2001) Canary Islands slopes (Wynn et al., 2000a,b)	Var Canyon (Malinverno et al., 1988) Stromboli Canyon (Kidd et al., 1998) Valencia Channel mouth (Morris et al., 1998) Canary Islands (Wynn et al., 2000a) Laurentian Fan (Piper et al., 1985)	Argentine Basin (Flood et al., 1993) Rockall Trough (Howe, 1996) Blake-Bahama Ridge (Flood, 1994) Gardar Drift (Manley and Caress, 1994) Falkland Trough (Cunningham and Barker, 1996)	NW European slope (Kenyon, 1986) Iceland-Faroe Ridge (Dorn and Werner, 1993) Carnegie Ridge (Lonsdale and Malfait, 1974) Gulf of Cadiz (Kenyon and Belderson, 1973) Various sites (Lonsdale and Speiss, 1977)	South Korea Plateau (Lee and Chough, 2001) Beaufort Sea (Hill et al., 1982) Tingin Fjord (Syvitski et al., 1987) Landes Marginal Plateau (Kenyon et al., 1978) New England slope (O'Leary and Laine, 1996)	

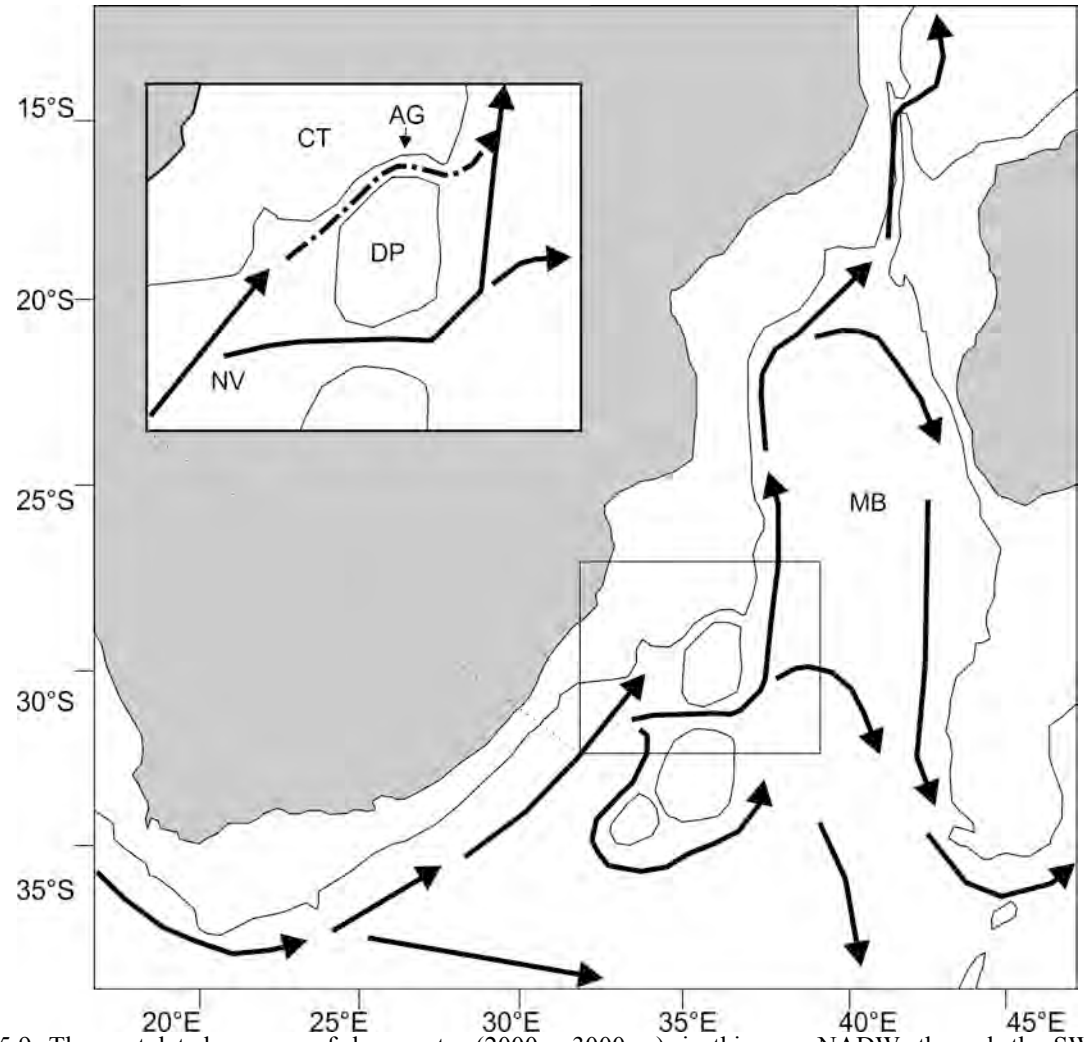

Fig. 5.9. The postulated passage of deep water (2000 – 3000 m), in this case NADW, through the SWIO is shown by black arrows, after van Aken et al. (2004). The 2000 m isobaths are shown for reference by the solid black line. The inset shows the study area, where the Ariel Graben creates a saddle across the Mozambique Ridge. The suggested NADW pathway across this saddle, through the Ariel Graben, is illustrated by the black dot-dash line. Abbreviations in insert: CT = Central Terrace, AG = Ariel Graben, DP = Dana Plateau, NV = Natal Valley.

Chapter 6

Surface expression of East African Rift System propagation in the Mozambique Channel, southwest Indian Ocean.

6.1. Introduction

The EARS is currently the dominant tectonic feature on the African continent. It is manifest as a series of long axis aligned rift valleys orientated north/south through east and southern Africa (Chorowicz, 2005; Saria et al., 2014) (Figs. 3.1 and 6.14). The EARS is typically characterised by elongate zones of thinned continental crust, where weaknesses in the crustal structure of the African plate are exploited allowing rift propagation, seismic activity and associated volcanism to extend southward (Fairhead et al., 1982; Chorowicz, 2005). Two main terrestrial branches, the older eastern and younger western branches respectively, characterise the EARS which was initiated in the Afar region 30 Ma ago and now extends ca.3000 km across Africa, defining a zone of extension between the Nubian and Somalian plates (Calais, 2006). Between the main Nubian and Somalian plates two microplates, the northern Victoria and southern Rovuma plates, have developed in response to rift kinematics with a third, the Lwandle microplate, developing further south in a marine setting (Hartnady, 2002; Calais, 2006; Stamps et al., 2008; Saria et al., 2014).

A lack of data has hampered efforts to fully understand seismicity in the diffuse region represented by the Mozambique Channel. This is especially so in the context of the EARS. However, neotectonic activity in the Natal Valley and Mozambique Basin/Channel has been associated with a postulated link between the African continent and the southwest Indian Ridge (Figs. 1.2, 3.12 and 3.14) (Hartnady et al., 1992; Ben-Avraham et al., 1995; Calais et al., 2006).

The terrestrial portions of the EARS have received much attention when compared to the southeastern marine branch, particularly in light of modern geophysical and positioning techniques that can better be used to explain the present-day kinematics (Déprez 2013; Saria et al., 2013; 2014). Efforts to examine the submarine aspects of the EARS have received far less attention. Chapter 3 outlined the formation of a series of mounds in the Natal Valley and ascribed them to the southward propagation of the EARS during the Neogene. This zone of activity was located at the postulated plate boundary of the southern Rovuma and northern Lwandle microplates as defined by Corti (2009) and Stamps et al. (2008). Although the kinematics of the Nubia-Somalia-Victoria-Rovuma plate system have recently been

discussed, the Lwandle microplate kinematics are more difficult to model (Déprez 2013; Saria et al., 2013, 2014) and the southward propagation of the EARS in the SWIO thus remains uncertain (Saria et al., 2014).

In this chapter, the seafloor and shallow subsurface geomorphology within the northern Mozambique Basin are investigated with an aim to identifying and reconciling various geomorphic features with the current tectonic regime, as defined by the EARS.

6.2 Material and Methods

Seismicity data were acquired online from the International Seismological Centre (ISC) using the latest ISC Bulletin. Only those data relevant to the study area are presented. These data are plotted together with significant plate boundaries within the study area, the outlines of which have been lifted from the latest literature.

6.3. Results

6.3.1 Bathymetry

The bathymetry of the general area ranges from smooth seafloor, to sediment waved and/or irregular seafloor (Fig. 6.2). Two seamounts to the west (Mt Bourcart - MtB) and east (Unnamed seamount - Smt) of the study area are also noted (Fig. 6.2). Smooth seafloor is restricted to the northern reaches of the site, while irregular and sediment wave dominated areas are located in the central and southern portions of the site respectively. The smooth seafloor gradients range between 0.170 and 0.2 degrees at depths typically below 3000 m. Above 3000 m sediment waves, with wave lengths of 1000 – 1400 m and amplitudes of between 15 – 35 m are interspersed with irregular seafloor (Fig. 6.2). The irregular seafloor in the central area occurs atop a west/east orientated, broad crested ridge (Fig. 6.2). A west/east bathymetric depression has formed within this ridge (Fig. 6.2, profiles M1 – M1' and M2 – M2'). The depression ranges in width from 12 – 14 km, and 100 – 160 m deep. The inner flanks of the depression reach gradients of 18°, although the average is 4 – 7°. Either side of this depression the gradient is reduced to <1° as the seafloor deepens away from the ridge and depression.

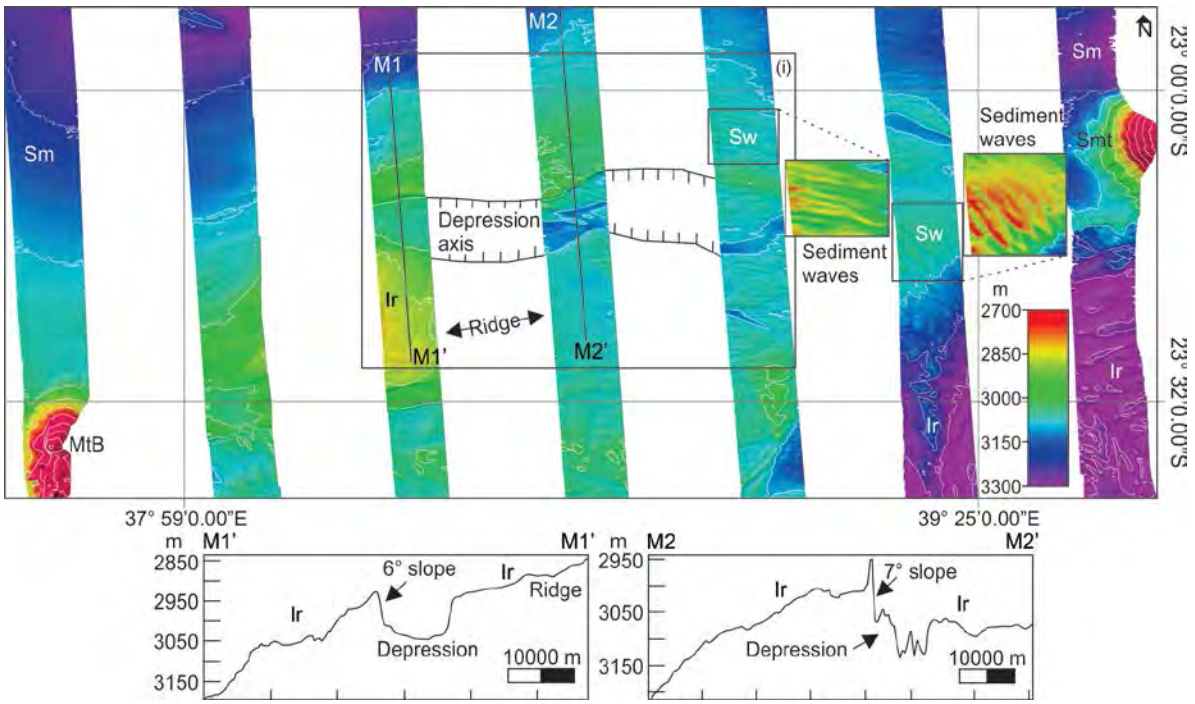

Fig. 6.2. Bathymetric data from the general study area shows the northern portion dominated by smooth seafloor (Sm). Sediment waves (Sw) and irregular (Ir) seafloor are restricted to the central and southern areas. Two seamounts (Smt) are located in the southwest and northeast respectively. Profiles M1 – M1' and M2 – M2' show the irregular seafloor north and south of the west/east orientated depression in section. Note the steeper northern flank. (Box i in shown in Fig. 6.3.)

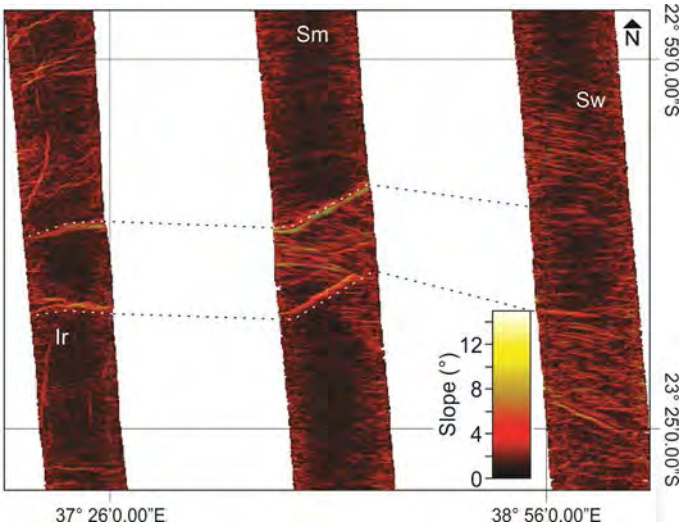

Fig. 6.3. Slope map extracted from bathymetric data, showing the variation in slope around the depression (enlarged from Box i, Fig. 6.2). Sediment waves (Sw) manifest as regular, linear changes in slope, whereas irregular seafloor (Ir) shows a non-uniform pattern with an irregular distribution of slope variation. Smooth seafloor (Sm), in contrast, shows little variation in slope as one would expect.

The area depicted in box i from figure 6.2 is enlarged and presented in figure 6.3 as a slope map. The slope map shows the variation in slope around the depression and ridge area. Areas of sediment waves manifest as regular slope changes describing the linear crest and trough of these features. Areas of smooth seafloor show little variation in slope as to be expected. Irregular seafloor, which includes the depression, is associated with markedly irregular changes in slope, unlike that of the sediment waves. The steepened flanks of the depression are clearly noticeable, and can be followed across the data gap as significant features forming the margins of the depression.

6.3.2 High frequency seismic character

Sub-bottom profile lines are shown in figure 6.2 for comparison with the bathymetry data. The echo character across the depression shows various reflectors and surface characteristics. In the east, the smooth basin floor is characterised by a distinct bottom echo followed by several continuous to discontinuous sub-parallel sub-bottom returns (Fig. 6.4). At the basin margin (signified by the toe of the ridge), sub-bottom reflectors onlap onto prolonged echoes and are associated with an abrupt change in slope angle (although it remains <1°). The seafloor continues to shoal southwards, and the echo character changes to display crude, semi-prolonged hyperbolic echoes (associated with irregular seafloor in the bathymetry data). This echo character continues until the edge of the depression's northern flank where there is a distinct reduction in signal amplitude upon entering the depression. The floor of the depression has a distinct bottom return, however the sub-bottom returns are poorly defined comprising discontinuous sub-parallel to diverging reflectors. Beyond the steep southern flank of the depression, the seafloor return remains distinct, however reflector style changes to a more discontinuous parallel reflector configuration.

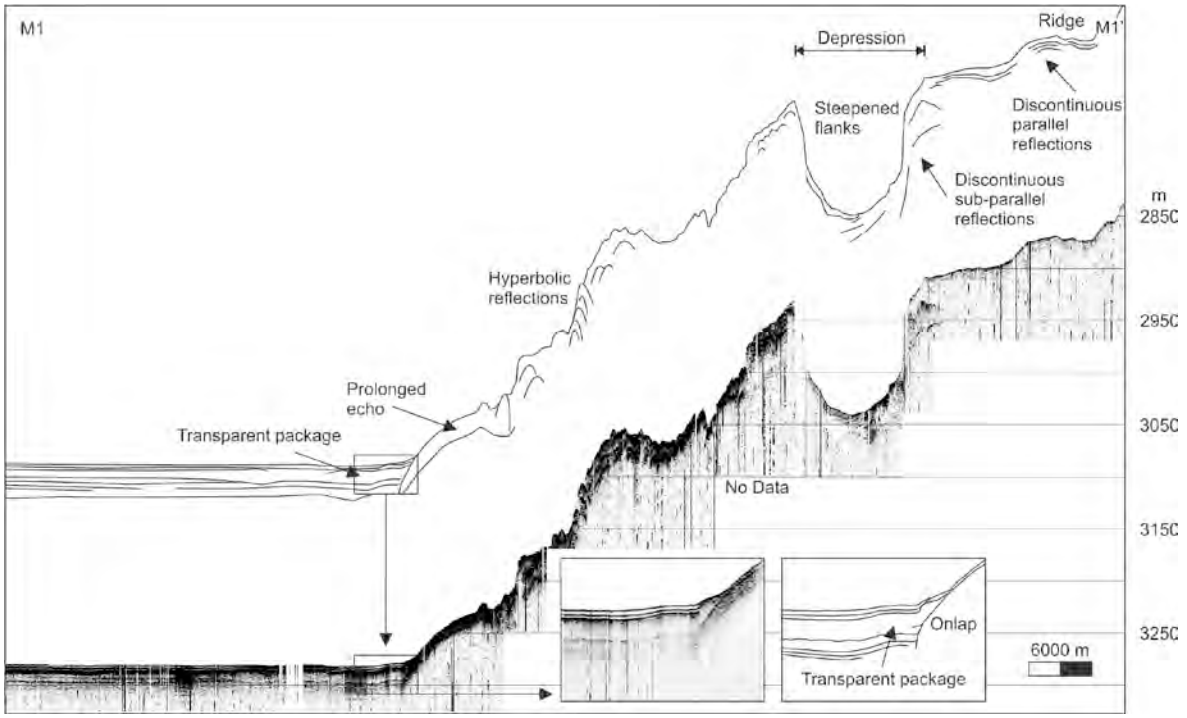

Fig. 6.4. A PARASOUND profile across the depression (M1 – M1') and surrounding area shows varied echo character associated with this region. Basin deposits on lap onto the ridge core. There is an abrupt increase in gradient at this point, and the seafloor character changes from smooth to irregular.

To the east a palaeo-surface lies beneath the smooth seafloor and the prolonged echoes associated with the present-day deposits (Fig. 6.5). The prolonged echo character continues upslope; however, the seafloor now displays asymmetrical undulations. This undulating surface is dissimilar from sediment waves observed elsewhere (Chapter 5), and is associated with irregular seafloor in the bathymetry data. The undulations have longer steepened downslope limbs (ca. 1520 m at 1°), with low gradient upslope limbs (ca. 310 m at 0.6°), and a separation of ca. 2000 m between crests. The internal geometry of these undulating features is not discernable. Further south the undulating seafloor abuts against a region of transparent packages. The sub-surface shows two distinct reflectors of similar geometry, over which a transparent package is draped (Fig. 6.5, inset). This transparent package overfills depressions in the underlying surface, smoothing off the topography. The upper unconformity surface of the transparent package onlaps an upper transparent package, the upper surface of which downlaps onto the sub-bottom reflectors. North of the depression flanks, the subsurface displays discontinuous sub-parallel reflectors beneath a distinct seafloor reflector. The depression area is characterised by large individual hyperbolic echoes with varied vertex elevations above the seafloor.

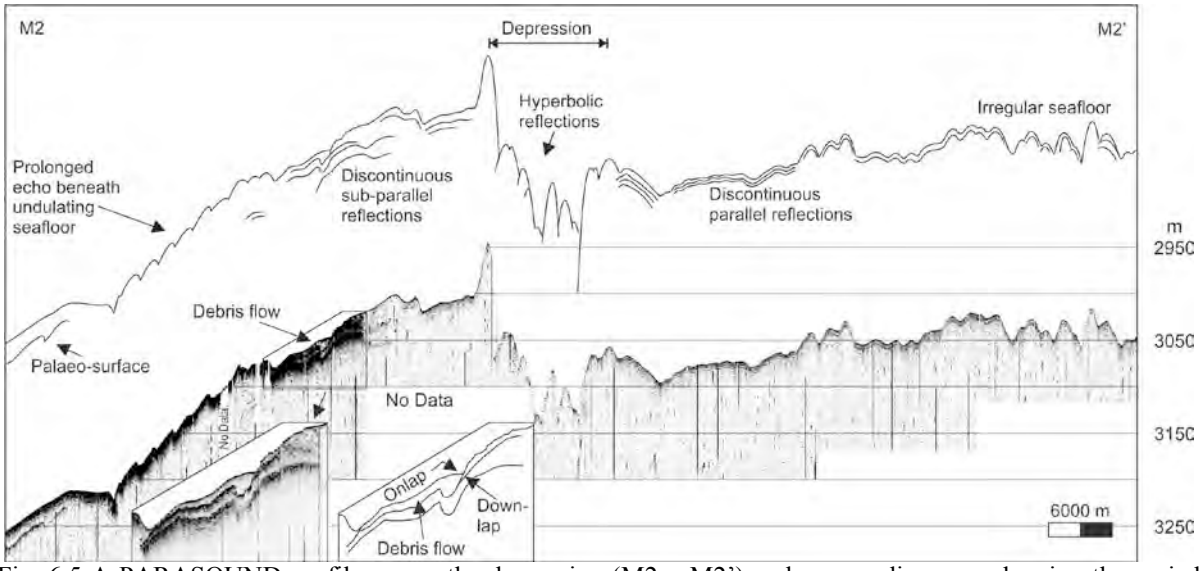

Fig. 6.5 A PARASOUND profile across the depression (M2 – M2') and surrounding area showing the varied echo character associated with the depression. Undulating seafloor is evident in the north, shoaling toward transparent packages beneath a smooth seafloor. The depression is marked by steep flanks and hyperbolic seafloor echoes.

6.3.3 Seismicity

The study area shows a long history of seismic activity within a region that hosts significant seismic activity both in the marine and terrestrial settings (Fig. 6.6). Within the Mozambique Channel the general trend of seismic activity between 10 – 19°S is elongate, and orientated north/south at ca. 41°E. At ca. 19°S, the zone of activity rotates clockwise, orientated northeast/southwest and maintaining the elongate character of the most active zone. The study area itself is marked by a zone of seismic activity. Despite this active zone maintaining an overall linear arrangement, the area itself broadens. The depression discussed above is located within this broadened zone of seismic activity (Fig. 6.6, inset). Here, epicentres associated with earthquakes ranging in magnitude from 3 – 6.5 (n=41 recorded events) are scattered around the depression, ridge, and Mt. Bourcart. Several events are recorded from beneath Mt. Bourcart, while the remainder occur across the ridge and depression.

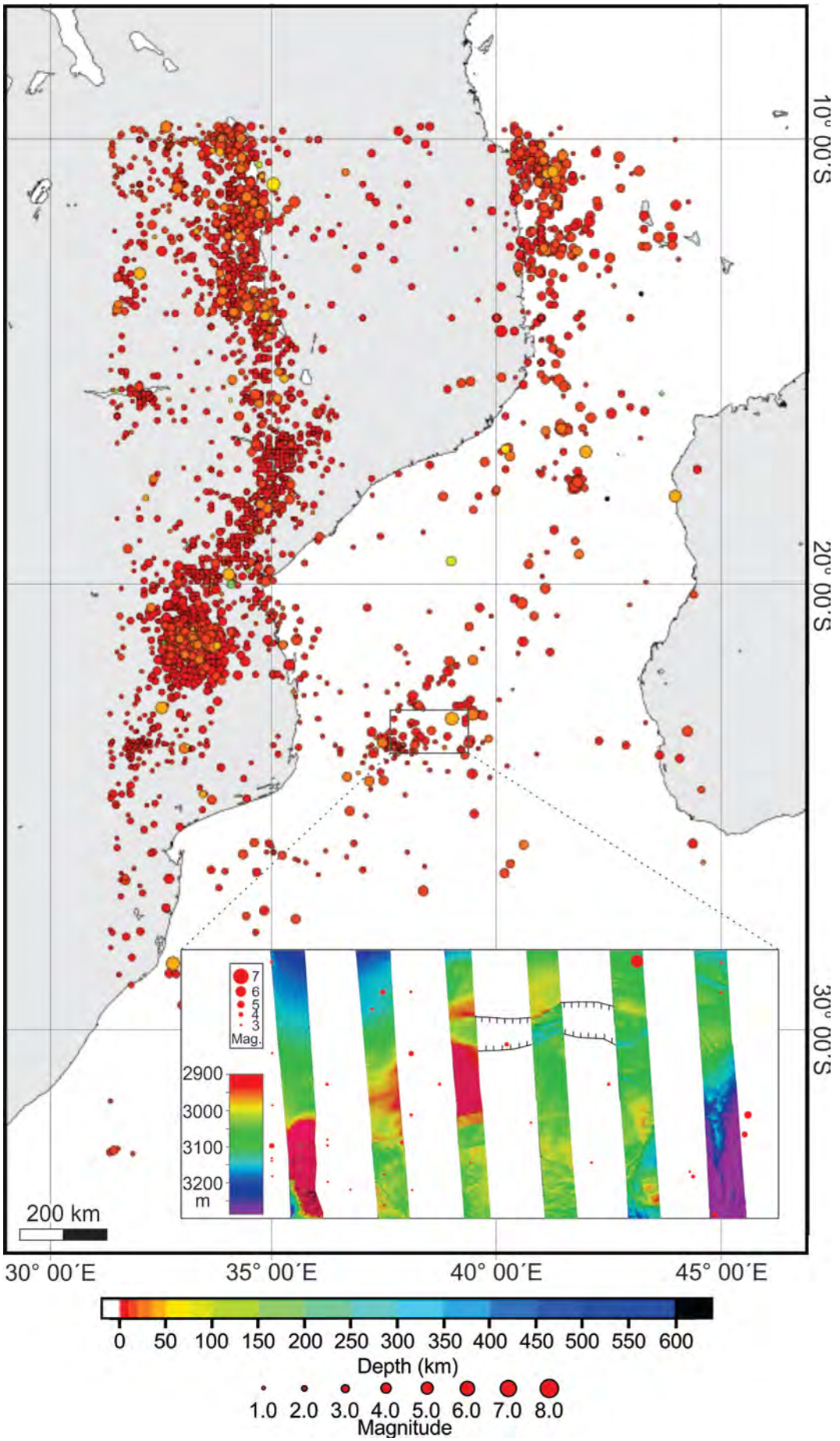

Fig. 6.6. Seismicity of the Mozambique Channel and surrounding region (ICS Bulletin). Inset shows study area.

6.4. Discussion

6.4.1 Bathymetry

Bathymetry data from the study area display a varied seafloor topography (Fig. 6.2) comprising smooth seafloor in the northeast and northwest, irregular seafloor in the central and southeastern regions and areas of sediment waves in the central zone. Much of the seafloor in this region is swept by bottom water circulation associated with the Global THC system (as discussed in Chapter 5). The AABW is credited with creating giant northwest/southeast orientated erosional scours in the seafloor sediment to the south of the study area, associated with recirculation of the water mass in this region (Brietzke et al., subm.). Although similar in morphology to the west/east depression observed in the study area, no comparable giant scours were identified as being associated with either the NADW or Mozambique Current eddies (Brietzke et al., subm.).

6.4.2 High frequency seismic character

Several echo character types are recorded in the study area. The distinct seafloor returns with several distinct parallel sub-bottom reflectors are common to deep marine basins. Such echoes, described by Damuth (1975) as type IB echoes, are typically associated with either turbidite deposits, or pelagic sedimentation. Others attribute such echo character to seafloor smoothing by bottom water circulation and winnowing of the deposit. Within the study area, these IB echoes (after Damuth, 1975) have an onlapping relationship with the ridge in which the depression is located. To the north of the study area, a relatively large basin is characterised by comparable reflectors intercalated with transparent lenses associated with mass wasting deposits (Brietzke et al., subm.). The geometry and nature of these basin deposits (Fig. 6.4, transparent package) when in contact with the base of the ridge as well as the transparent packages noted on the ridge flanks (Fig. 6.5) suggest that turbidity and mass wasting flows are common to the area. The smooth seafloor is the likely result of distal gravity flows, later winnowed by deep seated circulation.

Hyperbolic echoes are observed on the northern flank of the ridge, as well as within the eastern depression. The character of these hyperbolic echoes, however, differs with the setting. On the ridge flanks (Fig. 6.4) the hyperbolic echoes are smaller and lie at or below the seafloor, whereas within the depression the hyperbolic echoes are large and distinct, extending above the seafloor (Fig. 6.5). This suggests they are returned from different

seafloor/sub-bottom features, and likely result from different formative processes. The echoes returned from the northern flank are similar in character to the IIB-2/IIB-4 echoes of Damuth (1975) from the abyssal western equatorial Atlantic. Such echoes were ascribed to bedforms generated in response to bottom water circulation. The same is considered likely in this instance. The hyperbolic echoes from within the depression approach the IIB-1 character of Damuth (1975), and are associated with rugged seafloor morphology typically associated with seamounts and fracture zones (Damuth, 1978; Lee et al., 2005).

The undulating, asymmetric, seafloor features with a prolonged echo character noted on the northern flank (Fig. 6.5) are similar to features associated with downslope creep discussed from the Ariel Graben (Chapter 5) as well as features described from the Adriatic and Californian continental slopes (Dengler, 1993; Tinti et al., 1995). Given the mass wasting-related deposits noted elsewhere on the northern flank, as well as at the base of the ridge, the area appears to be prone to the downslope movement of material. Whether the instability is brought on by oversteepening of the flank deposits, or seismicity is unclear.

6.4.3 Seismicity

The study area occurs in a region of the Mozambique Channel where there is a higher density of seismic activity than elsewhere in the basin (Fig. 6.6). Comparison with previous research shows that the study area falls in the vicinity of the postulated southeastern Rovuma microplate boundary (Fig. 6.7). Saria et al. (2014) recently discussed seismicity in the Mozambique Channel as associated with the movement of the Rovuma microplate. In the region considered in this study, plate movement is to the southeast, suggesting extension is the same direction, presently occurring at 0.7 mm/yr (Saria et al., 2014). To the southwest, along the Nubian-Lwandle plate boundary, southeast extension is estimated at 1.1 mm/yr (Fig. 6.7). Clearly this region is tectonically active and the activity is associated with the kinematics of the East African Rift System.

6.4.3.1 Seafloor expression of southeasterly extension?

Of the bathymetric and PARASOUND data, many features are accounted for based on circulation/erosional/depositional processes within the Mozambique Channel. The formative processes associated with the asymmetric undulations and particularly the west/east depression, remain unclear. The depression flanks mark areas of steepened seafloor topography. Given the seismicity in the area, the asymmetric undulations may be generated

through seismically induced soft sediment deformation on the flanks of the ridge extending east from Mt. Bourcart. The floor of the depression, despite representing a basin, lacks significant sedimentary fill. Rather, the depression floor exhibits character associated with basement outcrop and sparse sedimentary cover, usually corresponding to seamounts and rifts. Furthermore, the depression flanks have developed as mirror images of each other. Tentatively, these flanks could reflect northwest/southeast divergence (Fig. 6.7). If so, given the location of the depression and postulated Rovuma microplate boundary, this depression could represent a surface expression of southeast extension associated with the EARS kinematics described by Saria et al. (2014). Such a case of extension could account for the complementary orientation of the depression flanks, as well as the lack of sedimentary cover in the floor of the depression. As the floor represents more recently exposed outcrop, sedimentation has not yet had time to drape the floor with deposits of significant thickness.

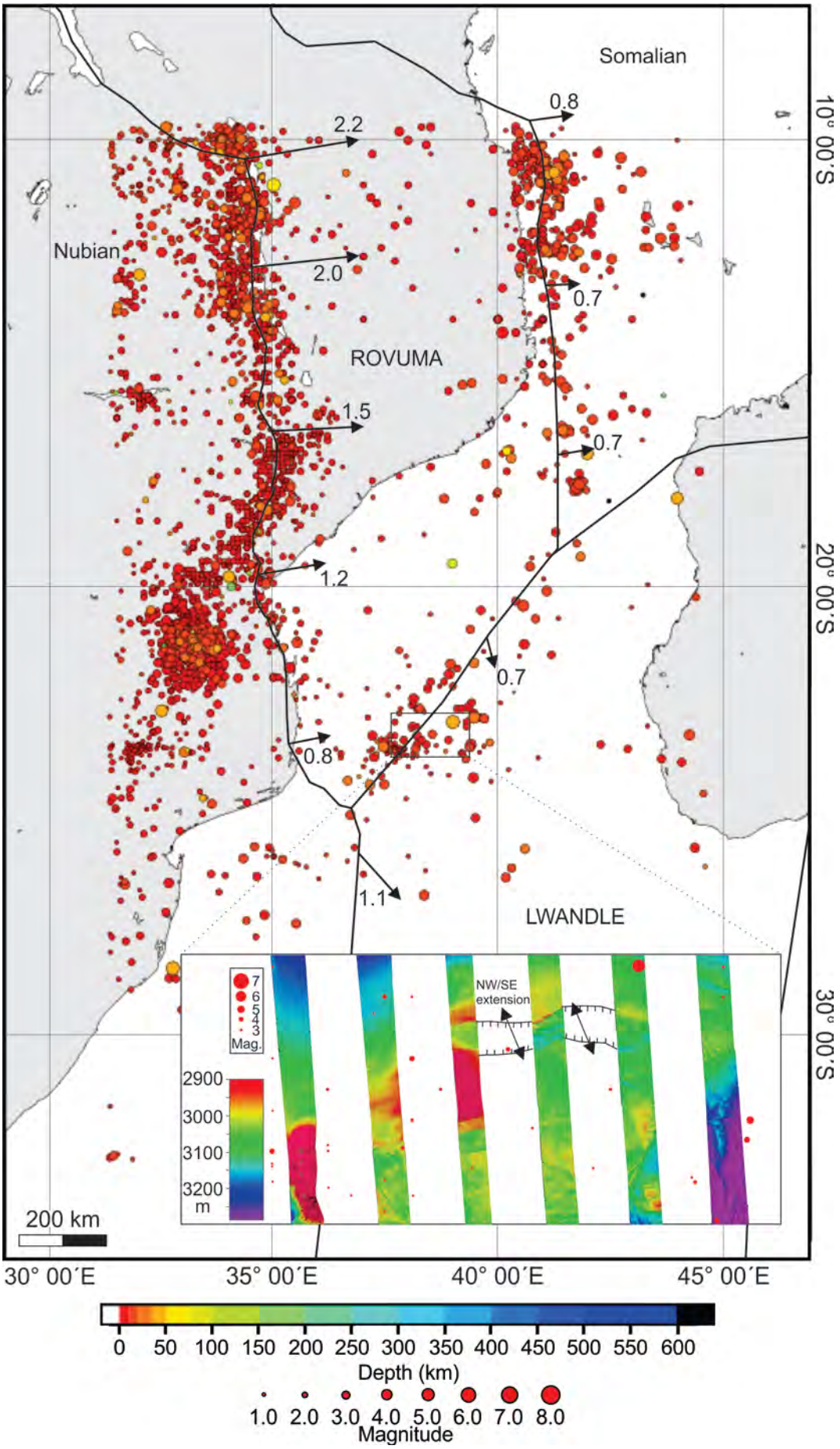

Fig. 6.7. Location of the Rovuma/Lwandle microplate boundaries. Units in mm/yr (after Saria et al., 2014).

Chapter 7

Anatomy, high frequency seismic character and depositional processes of the lower Zambezi Channel, Mozambique Basin, SWIO

7.1. Introduction

Deep-sea channels represent preferential sediment transport conduits to the deep ocean floor, funnelling gravity flows from canyons towards deep-sea fans. After their existence was first noted in the 1950's they have become the focus of numerous studies globally since the 1980's as interest in deep-sea processes grows and technology advances (Garrison et al., 1982; Damuth et al., 1983). Deposits associated with these deep-sea channels may accumulate over millions of years, providing longstanding records of changing climate, hinterland tectonics, and ocean circulation (Mutti et al., 1999; Zhang et al., 2001). Not only of academic value, such systems are of particular interest to the hydrocarbon industry as a potential hydrocarbon source, thus an understanding of their evolution and architecture is imperative across a variety of disciplines (Stow and Mayall, 2000).

Submarine channels are typically located in distal regions of the slope, where they form meandering systems as a result of erosional/depositional processes (Abreu et al., 2003; Deptuck et al., 2003; Mayall et al., 2006; McHargue et al., 2011; Pirmez et al., 2000). The initiation and evolution of these systems is complex, resulting from a combination of factors associated with basin tectonics, climate and sea-level changes, as well as local controls on the type, supply and deposition of sediment from the source region (Bouma, 2004; Kolla, 2007; Richards et al., 1998; Chapter 4).

New multibeam bathymetric and sub-bottom data collected in the northern Mozambique Basin and Channel reveal an unprecedented view of the Zambezi Channel. Due to apparent morphological differences between the Zambezi Channel and other deep-sea channels, a number of questions are raised regarding the evolution of this system as well as how it should be classified. This research investigates the anatomy and shallow seismic character of the lower Zambezi Channel system, outlining its possible evolution in relation to basin opening, sediment load and current activity (Fig. 1.2).

7.2. Results

Four lines of bathymetric and sub-bottom data that cover a 530 km long portion of the Zambezi Channel were acquired parallel to the channel axis. The lower portion of the Tsiribihina Channel, where it joins the Zambezi Channel, is also included in these results. Data quality of the eastern-most line was affected by inclement weather, although the reduced record still portrays several discrete seafloor features. Overall, the Zambezi Channel has a sinuosity of 1.08 with a variable channel width 5 km in the north to 7 km downstream. At 28° 16'S the main channel branches into several distributaries which extend for approximately 230 km southward into the Mozambique Basin, and beyond the data coverage.

7.2.1 Zambezi Channel

Initially "U"-shaped (and symmetrical), with a near horizontal floor (Fig. 7.1), the channel profile at the northern limit of data has a steeper eastern bank that reaches a maximum gradient of 18° as compared to a maximum of 16° for the western flank. Zones of maximum gradient are confined to the lower flanks, below a series of terraces and reach elevations of up to 200 m above the channel floor. The terraces are 0.5 – 1.4 km wide, with gradients of 1 – 3°. Side wall scarps, between terraces are not well defined. These features have gradients of 7 – 9°, are 0.3 – 0.6 km wide, and have a vertical distance of 0.1 – 0.2 km between terraces. The channel floor is 4.2 km wide with a downslope gradient of 0.16°, the thalweg occupying the centre of the channel. The channel floor displays semi prolonged seafloor echoes, as well as chaotic reflectors with no apparent layered reflectors (Fig. 7.1). Distinct bottom echoes, with discontinuous sub-bottom reflectors characterise the channel flanks, which have a hummocky character at elevations above the terraces.

Continuing downslope (Fig. 7.2), the 3.5 kHz echo character records show undulations in the 4.2 km wide channel floor surface. Overall the channel floor here is relatively smooth with a downslope gradient of ca. 1.4°. The channel floor deepens slightly from west to east with an average gradient (across channel) of 0.1°. The eastern flank of the channel displays a smooth inclined surface, which becomes crudely terraced as it nears the channel floor. The terraces are not as well defined as in the north (Fig. 7.1). With respect to shallow seismic character, the seafloor of the channel is characterised by a diffuse seafloor return pattern, while the subsurface echoes are either prolonged or transparent (Fig. 7.2). The western floor of the channel is characterised by an acoustically transparent mound. In contrast, the shallow seismic character of the eastern flank differs from the character of the

flank to the north as it is smooth (not hummocky) and with no sub-bottom echoes. The western flank (outer bank) is steeper (with an average of 10°, reaching 34° toward the channel floor), than the eastern flank (average of 2° reaching a maximum of 4°), as shown by the canyon profile (Fig. 7.2).

In contrast, the central portion of the lower Zambezi Channel displays a smooth channel floor (still 4.2 km wide), with both sub-parallel sub-bottom reflectors, and prolonged echoes present (Fig. 7.3), rather than the undulations found in the north. There is no district across channel change in depth. A pool (zone of channel deepened through erosion) is evident, extending downstream toward the subsequent bend apex, downstream of the bend's maximum point of inflection (maximum inflection point not covered by data) (Fig. 7.3). The outer (upslope) bank gradient is slightly reduced (7.3°), with local maximums of 24° toward the channel floor. The inner (downslope) bank has an average gradient of 2.3°, while the maximum gradient has increased to 9° in the vicinity of the terraces. The terraces range from 0.2 – 0.6 km wide, with gradients of 0.1 – 0.6°. The terraces shoal toward an area of levee development, apparently perched on one of the terraced surfaces (Fig. 7.3). The levee is an elongate, crescent shaped feature, which follows the curved inner bank of the channel. Although there are no apparent bedforms visible in the bathymetry, the shallow seismic character shows a distinct, undulating seafloor on the levee surface, while internally the levee displays several continuous sub-bottom echoes. Side wall scarps are not a prominent feature and range in gradient from 3 – 7°. Their heights can vary between 25 – 55 m between the terraces. Mass wasting features are uncommon in this portion of the channel with only one significant mass wasting scar apparent.

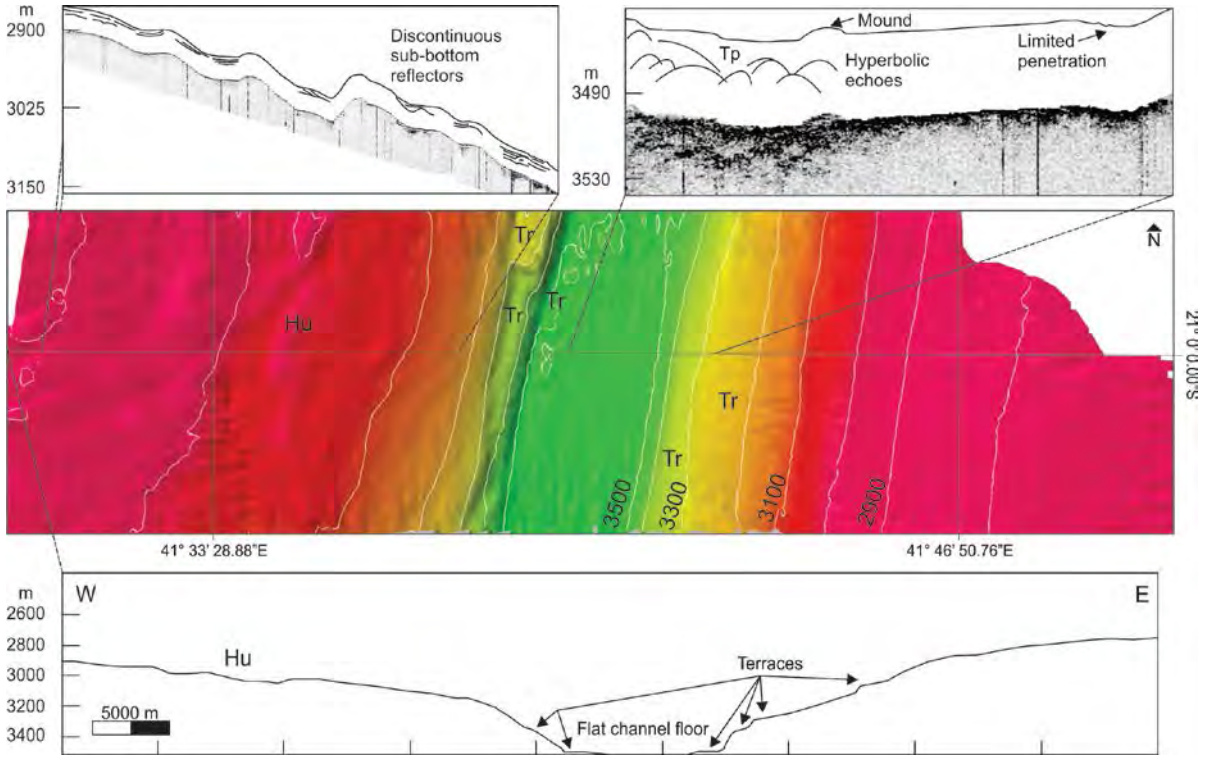

Fig. 7.1 The northern limit of data coverage shows a "U" shaped channel, with a hummocky western flank, and smooth eastern flank. The channel floor is distinct from the flanks in that the subsurface exhibits indistinct hyperbolic echoes and mounds.

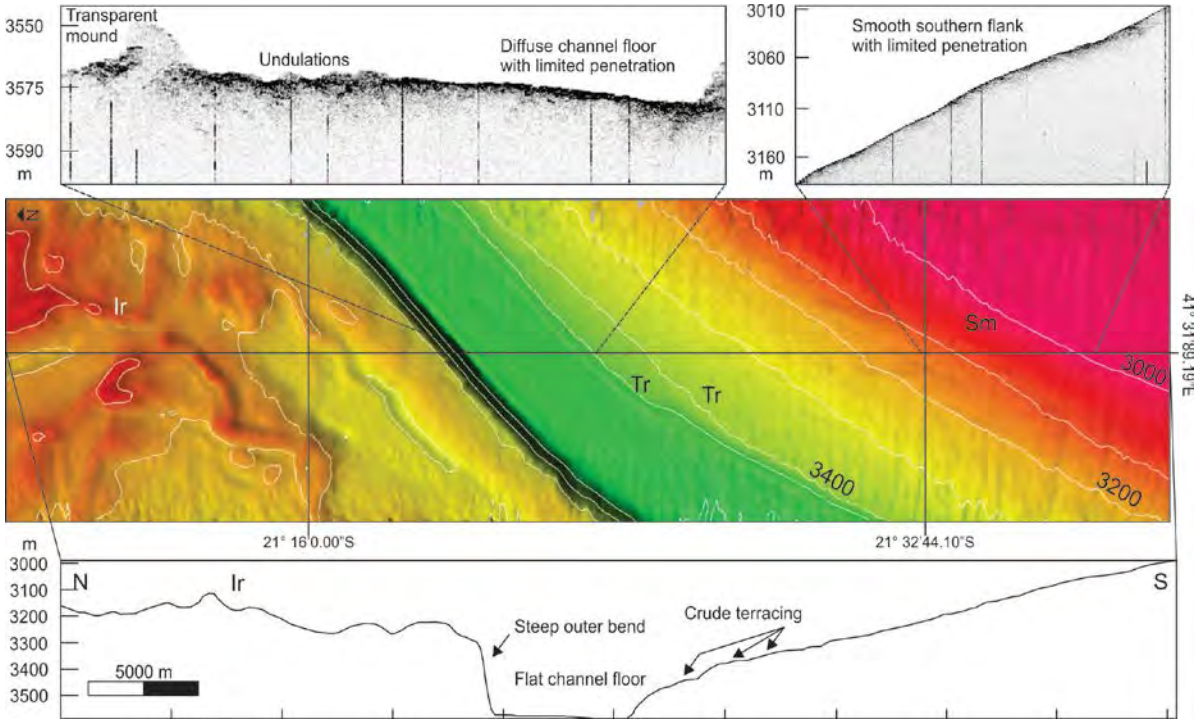

[*Previous* page]Fig. 7.2. The bathymetric and shallow seismic character of the northern portion of the Zambezi Channel. Note the varied echo-character across the channel floor, in contrast to the uniform echo-character of eastern flank. Hummocky seafloor is restricted the west of the channel, while smooth seafloor lies to the east.

The southern Zambezi Channel debouches into a frontal splay (Fig. 7.4). Here the main trunk of the channel widens and shallows, becoming less distinct as it merges with the Zambezi Cone. At the mouth of the frontal splay, the Zambezi Channel floor is ca. 10 km wide. The channel floor still deepens toward the east as it does upstream, although it is now steeper (0.3° across channel). The downslope bank, although steeper than the upslope (1.2° average gradient, 2.5° local maximum) averages 2.1° (5.5° local maximum), thus having a more subdued morphologic character than in the north. Numerous distributary channels (10 – 20 m deep) now extend south and southwest across the poorly defined sediment cone. East of the mouth there are no distributaries present. Given the lack of distributaries to the east, an asymmetrical distributary system exists at present. Many of the northern distributaries are located at a shallower depths than, and perched above the series of distributaries that exit the main trunk of the Zambezi Channel. As such, these northern distributaries are likely abandoned channels resulting from avulsion and incision of new active distributary channels farther south. Approximately 200 km south of the Zambezi Channel mouth, the bathymetry shoals by 20 m, causing a divergence in distributary channel pathways around this slight bathymetric high. In this area, the western Zambezi cone area has an irregular seafloor surface, while to the north undulating bedforms (orientated west/east) are common. Overall, the cone deepens to the southwest (average gradient of 0.04° over 287 km) (Fig. 7.4).

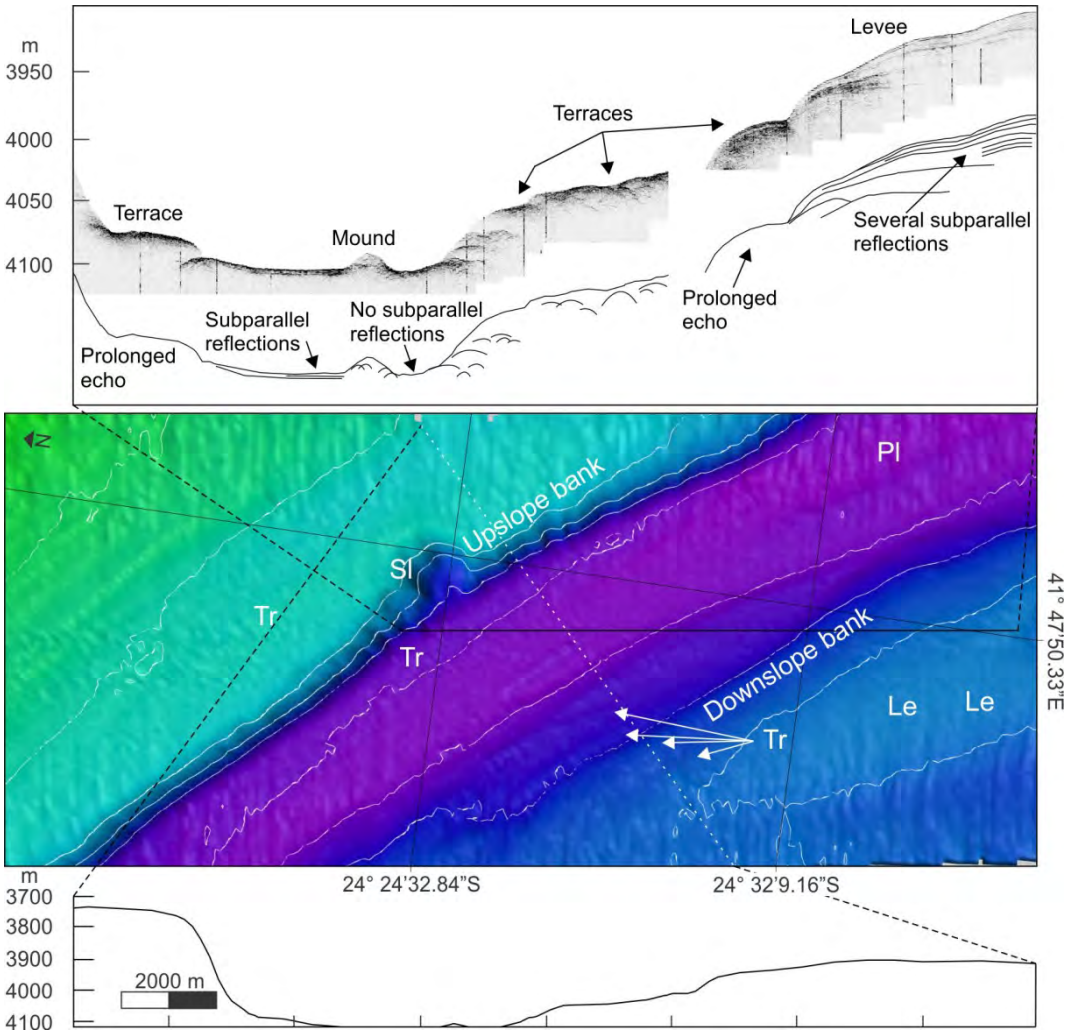

Fig. 7.3.Still "U"shaped, the Zambezi Channel flanks now exhibit mass wasting scars (Sl) in the terraces (Tr) of the steepened upslope (outer bank) flanks. The subsurface echo character is now more varied reflecting indistinct and sub-parallel echoes. Terraces are clearly evident in both the bathymetry and subsurface data, and extend beneath the levee (Le). A pool (PL) is evident downstream of the upslope bank.

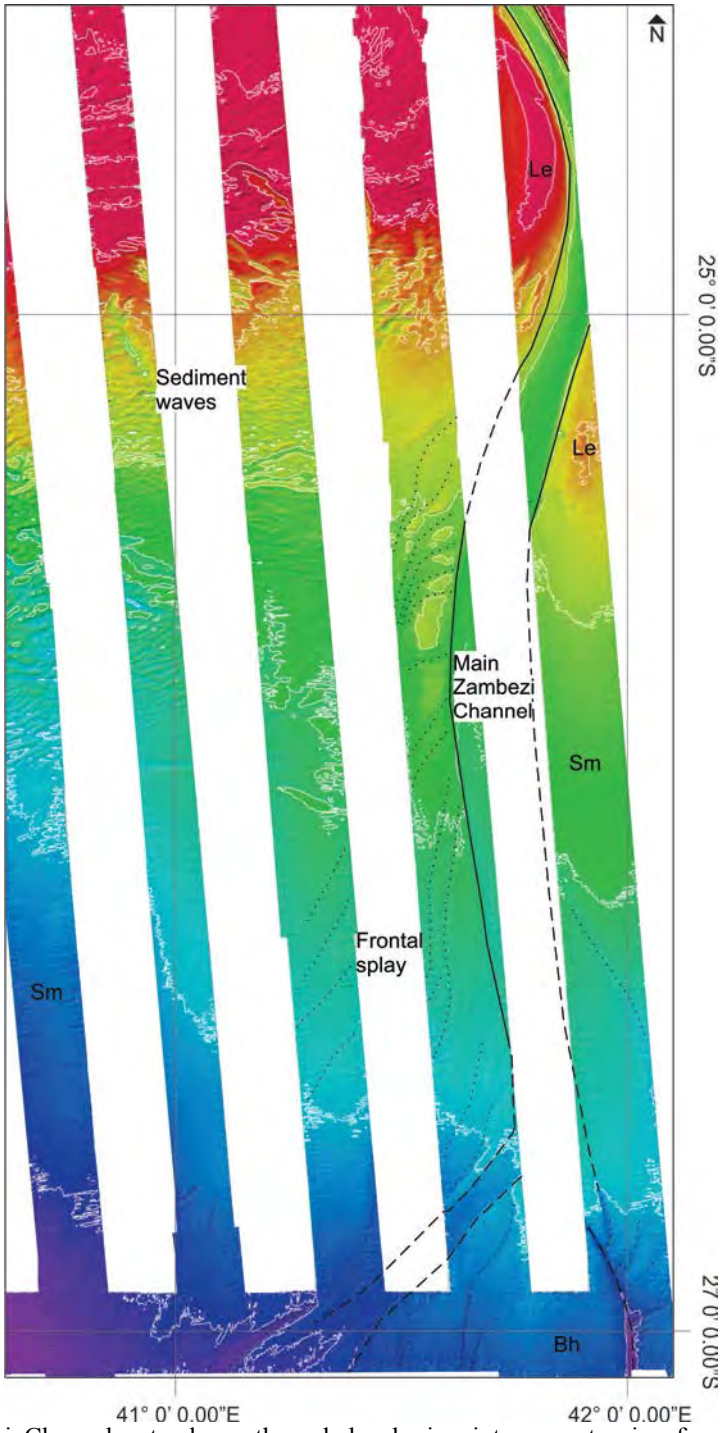

Fig. 7.4. The Zambezi Channel extends southward developing into an extensive frontal splay. Distributary channels continue south and west beyond the data coverage, while the main Zambezi Channel bifurcates around a topographic high to the south. Sediment waves, associated with Antarctic Bottom Water circulation are evident in the northwest (Breitzke et al., Subm.).

7.2.2 Tsiribihina Channel

The Tsiribihina Channel represents the only significant tributary to the lower Zambezi Channel (Fig. 7.5). In the east (limit of data coverage), the Tsiribihina Channel floor is 2 km wide, deepening slightly across channel to the north (across channel gradient of 0.4°). The

inner bank has an average gradient of 7° (maximum 15°), while the cut bank averages 11° (maximum 22°). The downstream gradient in the east is 0.2°; this gradient steepens to 0.3° as the Tsiribihina Cannel approaches the Zambezi Channel, where the channel widens to 3 km. In profile, the channel is decidedly "U"-shaped, although there are various examples of mass wasting scars and terraces which modify the profile locally (Fig. 7.5, profile P4 – P4'). Terraces range from 0.3 – 1 km wide, with gradients of 0.9 – 2.7°.

A crude levee has been developed midway along the channel's southern side. Superimposed on the lower to mid-levee are a series of elongate, slope oblique bedforms (wave length ca. 1 km, amplitude ca. 80 m) which grade into smooth seafloor further south (Fig. 7.5). These undulating bedforms are manifest as obtuse overlapping hyperbolae, which display occasional sub-surface bowtie reflectors (Fig. 7.5, box i; Fig. 7.6). These hyperbolic reflectors transition abruptly to several continuous parallel sub-bottom reflectors beneath a distinct seafloor reflector in the south.

7.2.3 Confluence of Zambezi and Tsiribihina Channels

The southwest/northeast orientated Tsiribihina Channel joins the main trunk of the Zambezi Channel as a tributary at 22° 10'S (Fig. 7.5). The "Y" shaped junction is asymmetrical with the Tsiribihina Channel entering (ca. 20 m above the main channel floor) from the east (Fig. 7.7, profile W – E). A gradient knick point, associated with a 1.1° change in gradient (0.3° to 1.4°) where the Tsiribihina Channel enters the main Zambezi Channel, is evident ca. 1 km upstream of the confluence. This defines the confluence as a pure, unequal, asymmetrical type confluence.

Upstream of the confluence, the Tsiribihina Channel shoals more rapidly than the Zambezi Channel. Approximately 100 km upstream (the limit of Tsiribihina Channel coverage) there is a difference of 220 m between the depths of the two channel floors, with the Zambezi Channel thalweg at 3577 m depth (Fig. 7.5). Downstream of the confluence the Zambezi Channel immediately deepens, associated with a downstream increase in gradient of 0.7°. The confluence width to tributary width ratio of the Zambezi/Tsiribihina confluence is 1.05.

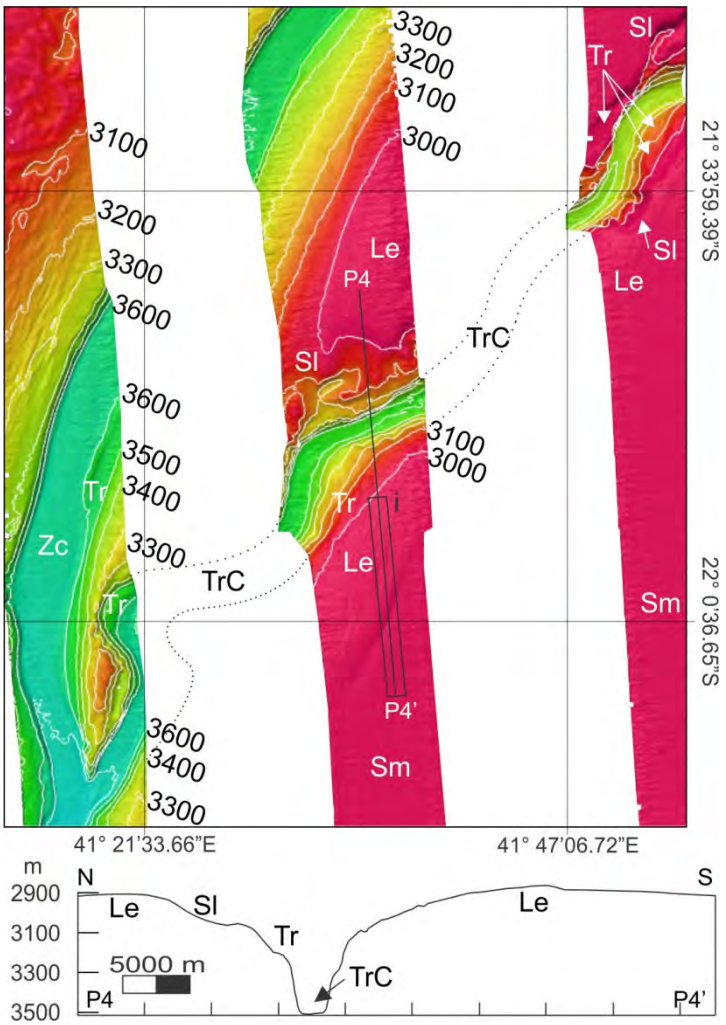

Fig. 7.5. The Tsiribihina Channel (TrC), the only significant tributary to the lower Zambezi Channel. The channel flanks are terraced (Tr), with slump scars (Sl) in channel bends. Box i is enlarged in Fig. 7.6.

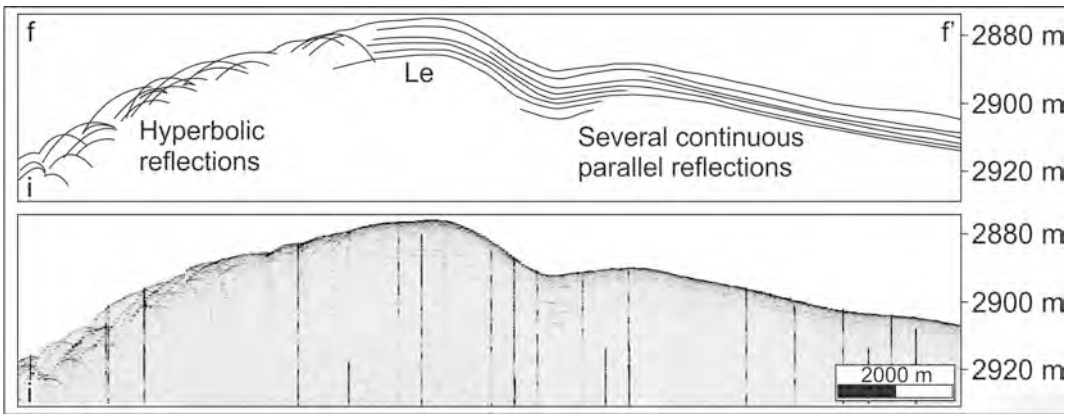

Fig. 7.6. PARASOUND (3.5 kHz) record for box i (Fig. 7.4). Individual to overlapping hyperbolic reflectors with occasional bow-tie reflectors transition abruptly to several continuous sub-bottom echoes below a distinct seafloor echo. The levee (Le) shows varied character, with hyperbolic reflectors returned in the north, and continuous parallel reflectors returned from the southern portion of the feature.

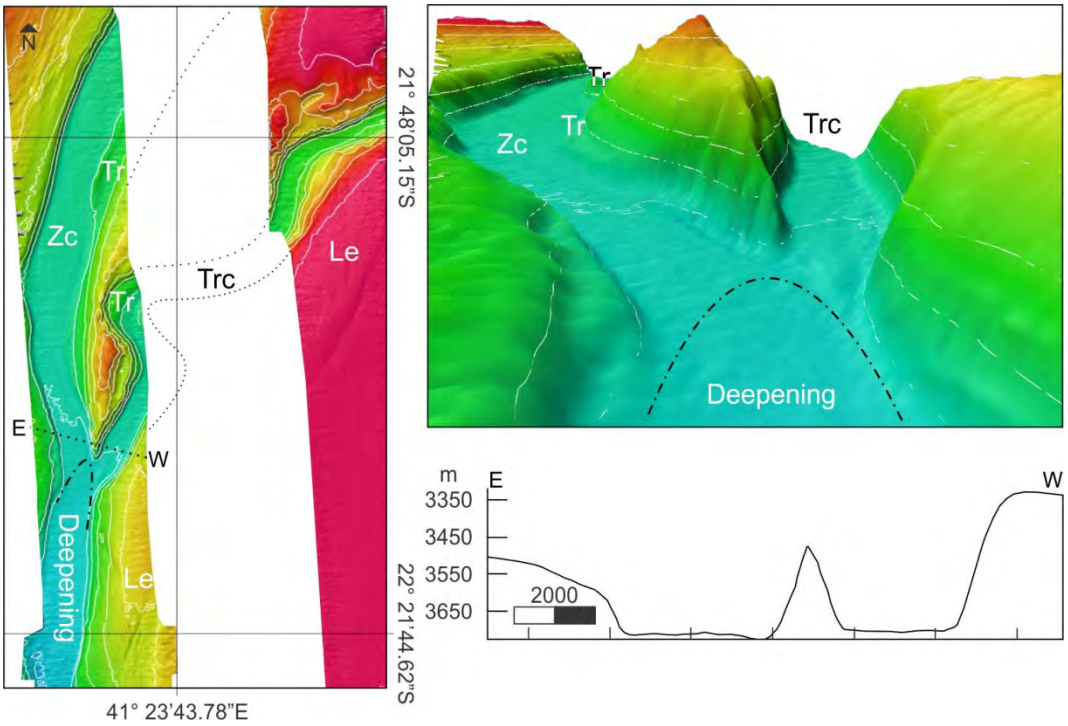

Fig. 7.7. The "Y" shaped confluence between the Zambezi (Zc) and Tsiribihina (TrC) channels is distinct in both plan (left) and three dimensional perspective (right, looking northwards). The cross sectional profile shows the slight elevation of the Tsiribihina Channel over the main trunk of the Zambezi Channel.

7.3 Discussion

7.3.1 Current classification of deep sea channels

Submarine channels are currently classified by channel geometry (Clark et al., 1992), sinuosity, slope gradient, and sediment type (Reading and Richards, 1994), and in some instances, sediment cohesion (Clark and Pickering, 1996; Piper and Normark, 2001). Based on this classification scheme, high-sinuosity, low-gradient, fine-grained systems, commonly occurring in equatorial regions (Gee et al., 2007; Wynn et al., 2007; Peakall et al., 2012), are distinct from low-sinuosity, high-gradient, coarse grained systems, typically located in higher latitude regions (Clark and Pickering, 1996; Klaucke et al., 1997; Peakall et al., 2012) (Table 7.1). Coriolis force appears to be a dominant control on sinuosity as it acts to restrict perturbations on channel bends, this effect thus increasing with increasing latitude (cf. Peakall et al., 2012 for a full discussion).

Flow nature (velocity structure, stratification, rheology, size of downslope flow within the channel) and sediment type are secondary factors to the Coriolis force. Flow type appears to be linked to the source and manner of sediment delivery. Low latitude submarine channels are typically directly or indirectly fed by river input (Mulder and Syvitski, 1995; Peakall,

2012), while high latitude submarine channels are affected by a range of factors, comprising glacial meltwater outbursts (Shaw and Lesemann, 2003; Piper and Normark, 2009), dense cold water underflows (Dowdeswell et al., 2002), and shifting ice streams (Escutia et al., 2000) giving rise to significant flux in sediment delivery periods and volumes.

Based on these factors, dynamic and changeable conditions, sediment supply and source type, channel sinuosity may be influenced by episodic increases in sediment supply. These can be from dynamic indirect supply sources and result in straight channel morphologies, whereas regular sediment supply from direct stable sources promotes the formation of meanders and increased sinuosity (Peakall et al., 2012). Coriolis force exerts a further control in the higher latitudes as previously discussed. The Zambezi Channel has a history of variable fluvial sediment sources and volumes (Droz and Mougenot, 1987; Walford et al., 2005). As such, one might expect the low latitude indirectly river fed Zambezi Channel to exhibit low gradient, high sinuosity characteristics akin to other equatorial channels. This does not appear to be the case as the Zambezi Channel has attributes of both high and low latitude systems (Figs. 7.9), yet does not fall within the bounds of Skene and Piper's (2006) classification (Fig. 7.9) (see Skene and Piper, 2006 for a full discussion). The following sections demonstrate the unique character of the Zambezi Channel when compared to such models.

Table 7.1. Typical character of high and low latitude submarine channels (after Peakall et al. 2014)

Latitude	Sinuosity	Gradient	Grain size	Sediment supply	Coriolis force effect
Low	High	Low	Fine	Constant (River)	Low
High	Low	High	Coarse	Intermittent (Glacial)	High

7.3.1.1 The Zambezi Channel system

In contrast to the Amazon, Zaire, Indus and Bengal systems (cf. Kolla, 2007) the Zambezi canyon/channel system is not directly connected to a significant fluvial source (Schulz, et al., 2011). The Zambezi River, is located 200 km to the southwest of the suggested location of the Zambezi Canyon head, and represents the most significant source of sediment to the shelf system (Schulz, et al., 2011). Furthermore, the sinuosity of other equatorial deep sea channels is typically greater than 1.2, and morphologically they exhibit numerous cut-off meanders associated with channel migration, and multiple lobes that spread unimpeded into the associated deep ocean basins (with apparently little oceanographic control). This is in stark contrast to the Zambezi Channel which is not sinuous (sinuosity of 1.08), does not

exhibit meanders, "Ox-bow" lakes, abandoned channels (except in the frontal splay area), nor multiple lobes. Elevated channel levee complexes are also a common feature of typical deep sea channels, developed by aggradational overbank sedimentation. Although levees associated with the Zambezi Channel are evident, they are not elevated above the surrounding bathymetry. In contrast the Zambezi Channel and its levees rest below the majority of the northern Mozambique basins bathymetry (see Chapter 8).

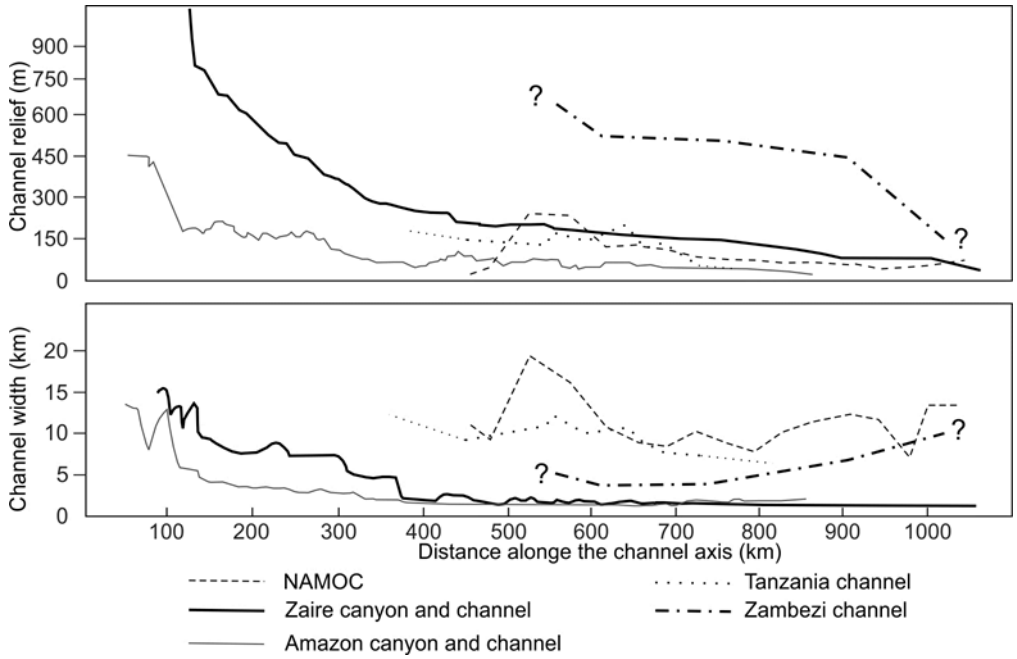

Fig. 7.8. Comparison of channel width and relief over distance along the channel axis, using data from this study, Skene and Piper (2006) and Bourcart et al. (2008).

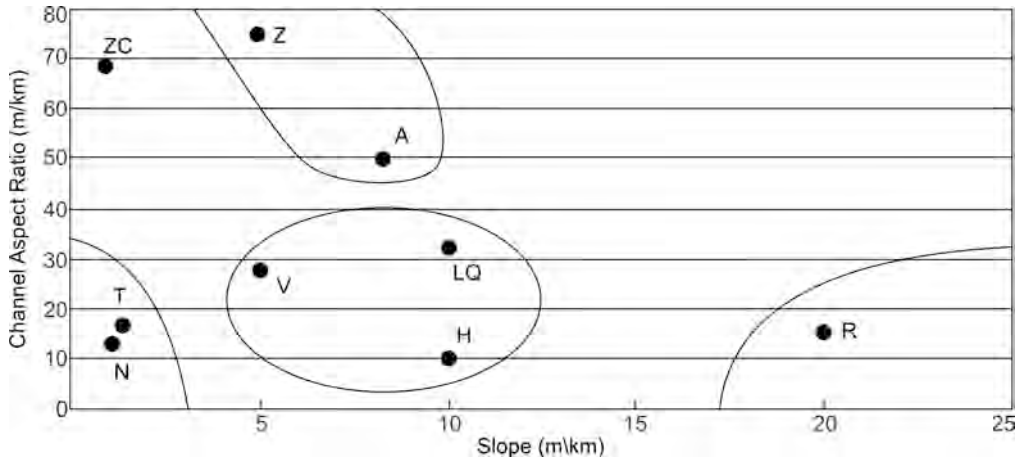

Fig. 7.9. Comparison of channel aspect ratio and slope. (ZC = Zambezi Channel, Z = Zaire Channel, T = Tanzania Channel, N = NAMOC, A= Amazon Channel, V = Var Channel, LQ = Laurentian Quaternary Channel, H= Hueneme Channel (H), R = Reserve Fan after Skene and Piper (2006) and Bourcart et al. (2008)).

The nature of the margin (passive Vs. active) precludes a simple classification of the Zambezi Channel as the passive margin in question has a complex opening history, the result

of several spreading phases dictated by both transform and normal faulting (Jokat, 2011). The resulting macrotopography is unlike most passive margins from which other deep-sea channels are described (cf. Kolla, 2007). Instead the Mozambique and Madagascar Ridge's various seamounts (e.g., Jaguar Seamount, Mount Bourcart, Bassas da India and Europa Island) and sub-bottom structures (e.g., Beira High) offer significant control over basin shape in the form of inheritance of antecedent geology by the bathymetry. This is dissimilar to most margins where the abyssal reaches of typical channel systems are essentially unconfined, allowing erosional/depositional processes to act unimpeded as channel evolution occurs within a largely unobstructed accommodation space.

7.3.2. Shallow seismic character of the Zambezi Channel

PARASOUND data show a variation in the echo character associated with the different components of the lower Zambezi Channel. The channel floor typically shows prolonged echoes with no sub-bottom reflectors (Figs. 7.1, 7.2, 7.4) and is associated with small, regular erosional/depositional bedforms less than 100 m in wavelength. Coarse bedded sediments, associated with high velocity currents, have been found to return such echoes (Damuth and Hayes 1977; Damuth 1975; 1980). This suggests that given the location of these echoes along the main channel floor, they represent rapid downslope flows (in accordance with the bedform/upper flow regime bedded interpretation). In this light, the lower Zambezi Channel is likely still active, fed from tributaries originating in the north. If it were inactive, these areas would be zones of pelagic settling, however, finely laminated planar reflectors with considerable thickness are absent from the channel.

Terraces show two dominant echo characteristics along the length of the lower Zambezi Channel; both Type IIB and IIIC (after Damuth and Hayes 1977; Damuth 1975; 1980) are evident (Fig. 7.3) and suggest a mix of processes that affect these areas. These are represented by a lower assemblage and an upper assemblage. Type IIB, discussed above, reflects periods where high volume and velocity flows reach the level of some terraces, thereby producing seafloor characteristics associated with coarse, bedded sediment. Type IIID echoes, are also associated with finer grained non-migrating erosional/depositional features. Areas of strong contour or downslope flows often reflect this echo character (Damuth and Hayes 1977; Damuth 1975; 1980). Given the location of these echoes within the Zambezi Channel, contour currents are an unlikely proposition. In this case, this echo character likely represents finer grained overflow deposits on the upper terraces; these

terraces thus represent relict features associated with a downslope progradational wave as described by Métvier et al. (2005). These have been subsequently left perched above the present-day channel floor. These terraces are periodically overlain by overflow deposits represented by a distinct seafloor reflector with several continuous to discontinuous sub-parallel sub-bottom reflectors (IB) (Fig. 7.3). Lower terraces show less of the Type IIID character, and are likely swept by the coarse fraction of high volume downslope flows thus accounting for their echo-character similarity with those of the channel floor.

Levee echo character is predominantly restricted to type IB echoes (Fig. 7.3). Such echo character has been associated with sediments that contain only very minor amounts of bedded sand/silt (Damuth and Hayes 1977; Damuth 1975) and indicate lower energy processes. This echo character is most common in the submarine setting covering hundreds of kilometres of the continental slope, rise and abyssal plain in numerous marine basins associated with pelagic and hemipelagic deposition, together with deposition by bottom water currents and the distal-most (low energy) deposits of turbidity currents (Damuth and Hayes 1977; Damuth 1975; 1980). In this instance, the deposition of the fine fraction by overtopping the main channel, generally at channel bends, seems a plausible mechanism for their genesis. In this light, settling of this sediment creates levees of finer material, which overlie a series of relict terraces (see Fig. 7.3). A departure from the typical Type IB levee echo character is observed only along the Tsiribihina Channel where echoes approaching type IIIA are observed. The bathymetry shows a series of related bedforms that are superimposed on the levee of the Tsiribihina Channel. The change in echo character is associated with a change in bedform orientation, as well as the presence/absence of bedforms, across the levee from north to south. Where bedform crests are orientated oblique to the ship track, hyperbolic echoes, with occasional bow tie reflectors, are present. The bedform crest orientation changes across the levee, eventually becoming parallel with the ship track, associated with sediment waves characterised by IIIA echoes (Fig. 7.6).

7.3.3. Comparison of the Zambezi Channel with empirical results

With respect to the anatomy of the channel, it approaches the character of experimental channel results obtained by Métvier et al. (2005) (Fig. 7.10). In many instances, the locations and geometries of the side wall scarps, terraces, levees and pools are directly comparable between the experimental model and the Zambezi Channel. The model of Métvier et al. (2005) was created with a significant degree of control over the

"depositional setting" responsible for the formation of the channel; the associated formative processes thus responsible for the anatomy and geometry of the experimental channel can be inferred for the Zambezi Channel. To this end, Métvier et al. (2005) suggest that a progradational wave of downslope sediment movement and aggradation, may precede an erosional wave of downslope sediment erosion during the formation of the channel. The progradational waves are responsible for the build-up of sediment (i.e., development of lobes on the channel flanks), while the subsequent erosional wave removes these progradational deposits along the channel thalweg leaving the lobes as relict, perched, features on the channel flanks in the form of terraces. This model still allows for the formation of cut-terraces, in accordance with thalweg migration and axial incision, within the main channel. In light of the terraces may represent relict progradational wave lobes subsequently eroded by the erosional wave propagating downslope, rather than the result of lateral channel migration. Métvier et al. (2005) also show that there is a distinct relationship between sediment flux and slope where low sinuosity channels are more likely to develop on moderate slopes with low sediment flux. However, as sediment flux increases straight channels can develop on higher gradient slopes. The low sinuosity Zambezi Channel has experienced a significant degree of sediment flux throughout its evolution within the Mozambique Basin (discussed in *7.3.5. Evolution of the Zambezi Channel system*). This highlights another similarity between the behaviour of the modelled result and the likely evolution of the Zambezi Channel.

Departures from the model experiments and the Zambezi Channel do exist. There are several reasons for the departure in morphological character and genesis of the Zambezi Channel. Firstly, the particle size and density in the experimental channel was strictly controlled, the result was little variation in grain size and density. Turbidity currents that were released down the model profile would not have a clear enough distinction between the flow traction carpet and the tail to promote the process of overspilling or flow stripping (cf. Parsons et al., 2007). As such, fine grained levee deposits would not be expected in the experimental result.

Secondly, the sediment delivery along the southeastern Mozambique continental margin and deep Mozambique Channel is affected by a dynamic current regime (Walford et al., 2005; Schulz, et al., 2011) that controls sediment dispersal and delivery to the slope and abyssal plain. Recent studies show that the sedimentation to the west of the Zambezi Channel, within the northern Mozambique Basin, is dominated by reworking in accordance with bottom-water circulation (Kolla et al., 1980; Breitzke et al., Subm.; Chapter 8). Thus

not all the sediment delivered to the shelf reaches the slope. A portion of the sediment that does reach the slope is redistributed by deep reaching circulation, effectively removing this sediment from the Zambezi Channel system.

Thirdly, the underlying structural control on accommodation space by antecedent geology must play some role in the morphology of the Zambezi Channel. The Zambezi Channel is not free to develop in an unconfined manner. Rather, the course is initially directed from the Zambezi continental shelf region, coast perpendicular, toward the southern Davie Ridge. However, this course is not sustainable and is subsequently forced to migrate clockwise continuing southwards, in an elongate north/south topographic low, now confined between the west coast of Madagascar, the Madagascar Ridge and the aforementioned islands and seamounts (Fig. 7.10). Thus, antecedent geology acts to confine the development of the Zambezi Channel, resulting in the "dog-leg" morphology exhibited by the present-day channel system.

7.3.4. Evolution of the Zambezi Channel system

The present-day anatomy of the Zambezi Channel is linked to the evolution of the system as a whole. Droz and Mougenot (1987) suggest that the Zambezi Channel was initiated in the Oligocene to early Miocene as the downslope, southern extension of the Serpa Pinto Channel (Fig. 7.11). It was during this time that Walford et al. (2005) postulate the initiation of the Mozambique Current. Over this period sediment loads to the Zambezi delta show a marked increase, associated with hinterland uplift that affected southeastern Africa (Walford et al. 2005). This period of uplift, associated with forced regression and increased sediment transport past the shelf-edge, was also recorded along the east coast of South Africa by the development of the Tugela Canyon along the east coast of KwaZulu Natal (Dingle et al., 1983; Chapter 4).

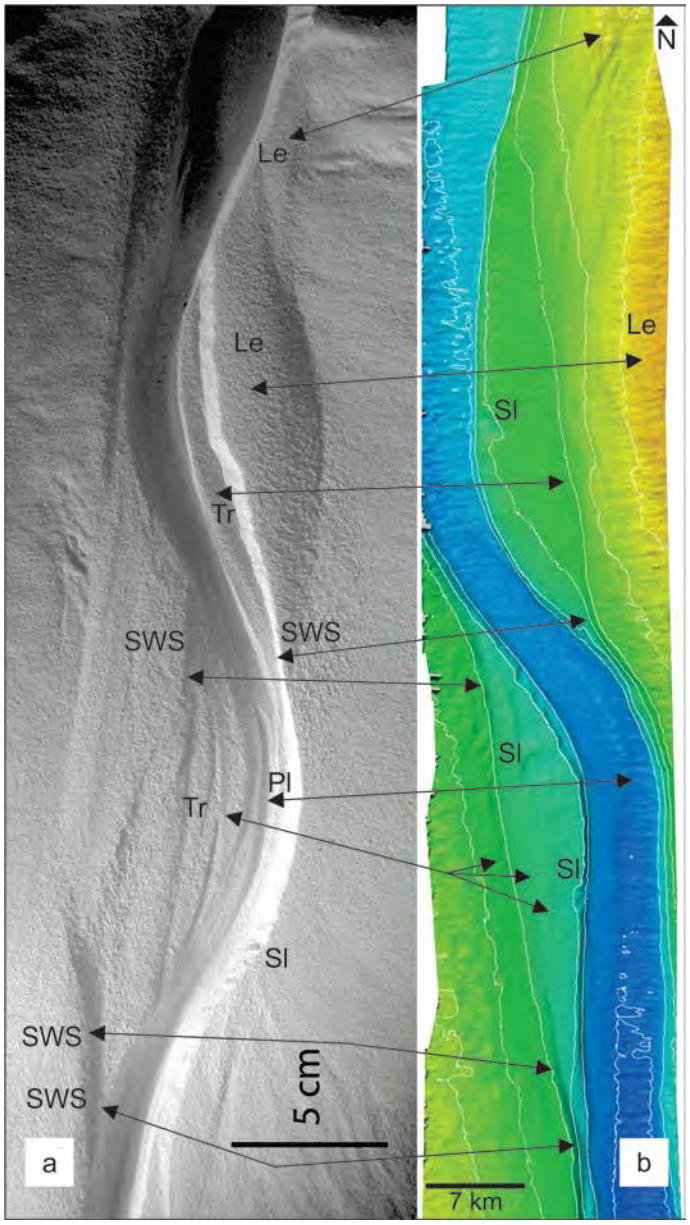

Fig. 7.10. a) Experimental channel of Métvier et al. (2005). b) Zambezi Channel, this study. Note the location, and relative position, of side wall scarps (SWS), terraces (Tr), channel pools (Pl) and levees (Le) in each figure.

By the mid-Miocene, activity in the Serpa Pinto valley decreased and the dominant sediment supply to the Zambezi Channel switched to the Zambezi Valley (mid-Miocene to Pliocene) rather than the northern sources (via the Serpa Pinto Channel) (Droz and Mougenot, 1987) (Fig. 7.11). With the development of the EARS, and uplift of southern Africa, the sediment load delivered to the Zambezi delta and shelf once more increased (Dingle et al., 1983; Droz and Mougenot, 1987, Walford et al. 2005). This developed a new staging area for sediment supply that would ultimately be transported via the Zambezi valley to the Zambezi Channel. During this period, river capture upstream of the Victoria Falls took place and resulted in elevated sediment flux to the continental margin (Walford et al., 2005).

The contemporaneous southerly transport of sediment via the Serpa Pinto Channel continued to decrease, being dominated by infilling, rather than transport of sediment to the Zambezi Channel (Droz and Mougenot, 1987). Major channel building periods, during which progradational/erosional waves are the dominant process in channel development, are likely linked to these periods of hinterland uplift in which sediment delivery to the Mozambique continental shelf (Walford et al., 2005).

The period of increased sediment flux to the Zambezi margin is mirrored along the east coast of South Africa where a second phase of incision on the shelf and increased sediment transport from the hinterland to the Natal Valley was recorded in the Tugela Canyon (Chapter 4, Fig. 4.10). The protracted late-Miocene to Pliocene uplift (Partridge and Maud, 2000), also resulted in the initiation of the Cape canyon (Wigley and Compton, 2006), caused several submarine canyons to form on the northern KwaZulu-Natal margin (Green, 2011a), and is considered to have caused several slumps on the southern African margin (Dingle, 1980). Relatively minor flows, during the intervening periods of reduced sediment delivery, are likely responsible for channel maintenance, rather than modification.

As a tributary to the Zambezi Channel the Tsiribihina Channel must have played a role in the evolution of the Zambezi Channel, downslope of the confluence. Droz and Mougenot (1987) posit that the Tsiribihina channel only became a tributary to the Zambezi Channel in the Pleistocene. This would suggest overtopping of the confining Davie Ridge in this region during the Pleistocene, thus allowing the westward transport of sediment to occur. This was sourced from Madagascar and directed toward the Zambezi Channel (Droz and Mougenot, 1987). Given the nature of the confluence between the Zambezi and Tsiribihina channels, the latter must have been very energetic for a considerable period of time in order for it to have incised to the approximate level of the Zambezi Channel at the confluence, despite the time delay (Oligocene to Pleistocene) in the initiation of the Tsiribihina Channel as a tributary.

The 1.05 confluence width to tributary width ratio of the Zambezi/Tsiribihina confluence is above the average ratio of 0.9 calculated from various margins globally, and ideal value of 1 (Fig. 7.12), and similar to channel C1 of the Espirinto Santos Basin, channels of the Niger Delta, and examples from the US Atlantic margin. A value of 1 indicates that the combined pre-confluence channel width is equal to the width of the confluence junction. This in turn suggests synchronous activity (equal development) of the pre-confluence

channels. Deviation from this ideal value of 1 reflects variation in channel activity through the lifespan of the channels in question. With respect to the Zambezi/Tsiribihina channel confluence this deviation from the ideal value is reflected in the tributary/confluence width ratio of 1.05, the unequal morphology of the channel floor depth at the confluence, and the asymmetrical nature of the confluence junction. The locations of submarine channel confluences are often associated with regions of lateral confinement (Gamboa et al., 2012). In this study, the antecedent geology of the Mozambique Basin acts to confine the available transport pathways influencing the location of the confluence.

Thus, throughout the development of the Zambezi Channel the setting and conditions in which the system exists have been in constant flux. Sediment input volumes to the margin, changes in sediment source, a complex circulation system and accommodation space under significant structural control by antecedent geology (in association with regional tectonics) creates a setting comparable to the dynamic settings of the high latitudes. It is this dynamic source and flux of sediment that accounts, in part, for the straight channels in these high latitude regions, along with Coriolis force (Peakall et al., 2012). In this instance, the dynamic source and flux of sediment, along with accommodation space, that promote the straight morphology of the Zambezi Channel. While the channel anatomy likely results from the formative processes directly, and are comparable to experimental results.

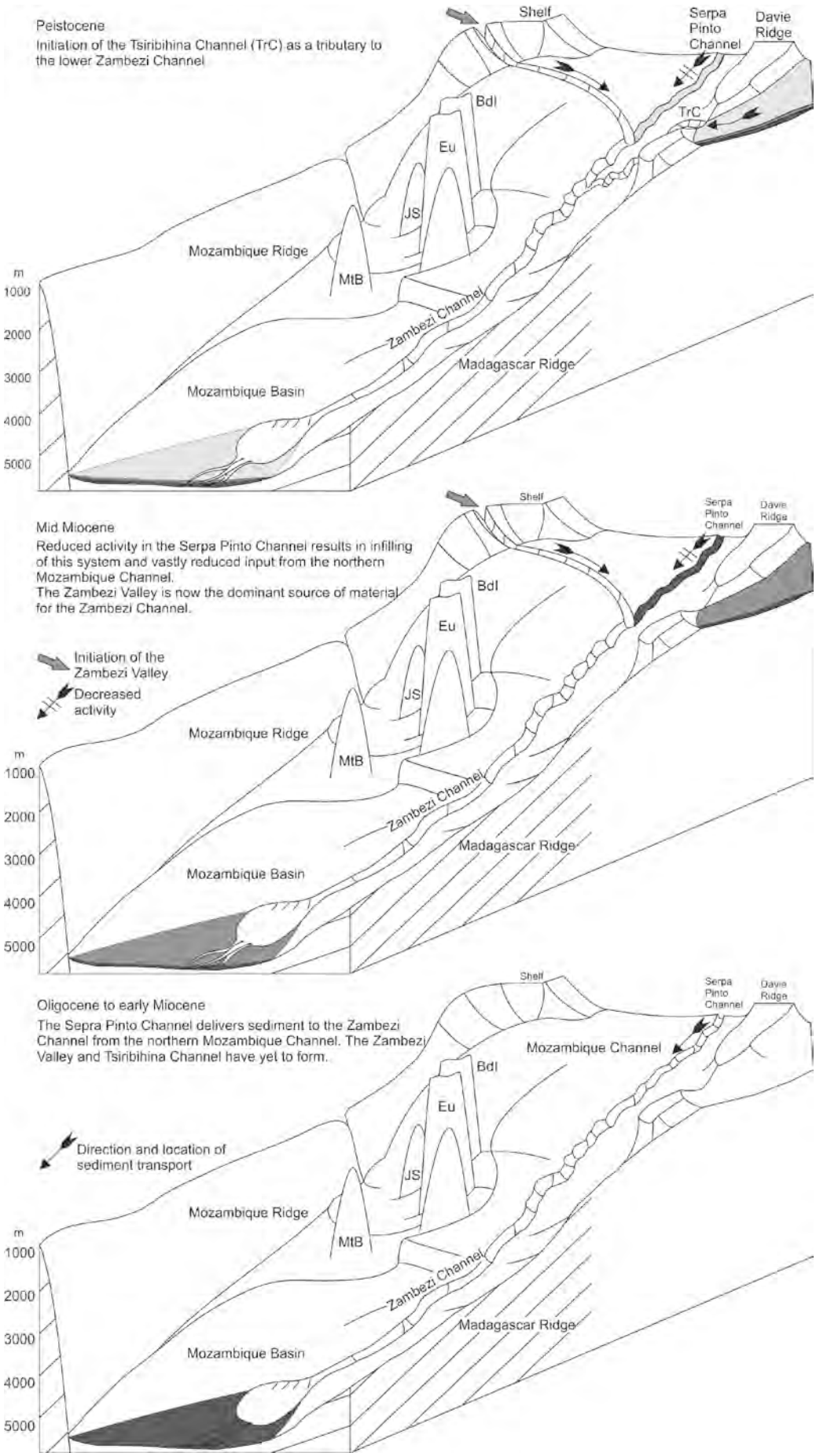

Fig. 7. 11. The proposed evolution of the Zambezi Channel from the Oligocene to present.

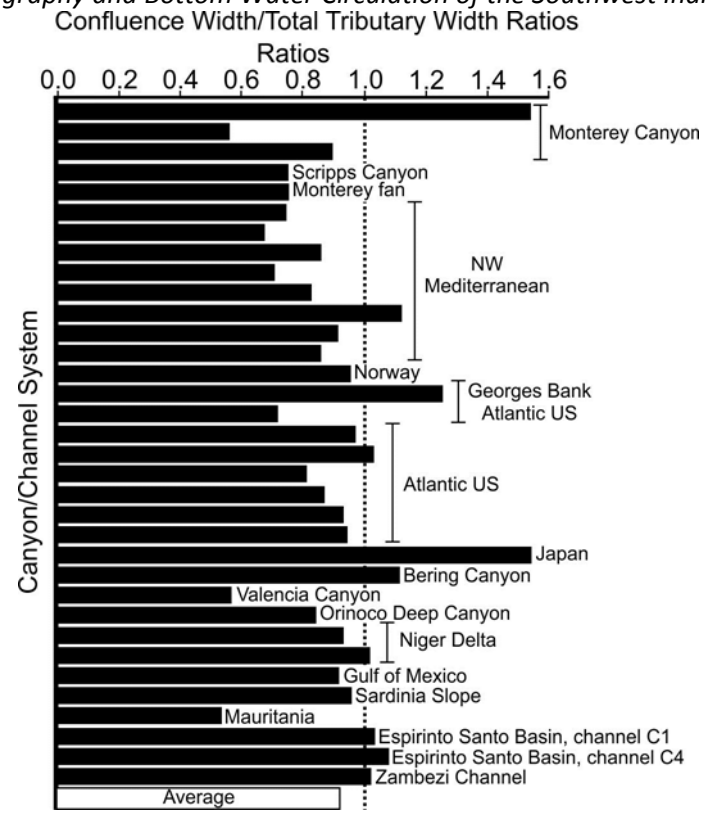

Fig. 7.12. Global confluence width to tributary width ratios vary greatly. The Zambezi/Tsiribihina confluence lies slightly above the global average.

Chapter 8

Microtopography and Bottom Water circulation of the northern Mozambique Basin.

8.1 Introduction

The purpose of this chapter is to provide an overview of the sedimentary dynamics and geomorphology of the northern Mozambique Basin. The basin occurs between southeast Africa and western Madagascar (Fig. 1.2) and is unique with regards the complex interactions between basin floor sediment, bottom water circulation, antecedent geology and hinterland tectonism. Despite several promising investigations of the southwest Indian Ocean and Mozambique Basins in the 1960s – 1970s (Damuth, 1980; Kolla et al., 1980; Martin 1981a; Dingle et al., 1987; Droz and Mougenot, 1987), little further research has been undertaken. However, over the past several years renewed interest has been shown in the area (Saria et al., 2014; Chapter 3 and 4) thus prompting a call to re-examine and interpret the complex seafloor morphology and shallow geomorphology.

8.2 Results

8.2.1 Distribution of seafloor types

Seafloor Type BI, smooth seafloor, dominates the northern Mozambique Basin (Fig. 8.1 for all seafloor type distributions, Table 8.1 for summary). Approximately east-west orientated, 3D (bifurcating) sediment waves, with a wavelength of ca. 2.3 km, comprise seafloor Type BII. Type BIII is characterised by a rough seafloor, comprising discontinuous, well-defined, narrow 3D sediment waves (λ= ca. 4.5 km). The fourth type, BIV, consists of southeast-northwest orientated 3D sediment waves (λ = ca. 1.85 km). Type BV shows randomly distributed 3D sediment waves, with two dominant orientations, east-west and southwest-northeast, throughout the zone (λ = ca. 1.4 km). Southwest-northeast orientated, 2D sediment waves comprise Type BVI (λ = ca. 1.23 km). Type BVII seafloor is characterised by an irregular distribution of mixed scale bedforms and features. The final type, BVIII, comprises contour parallel 2D sediment waves.

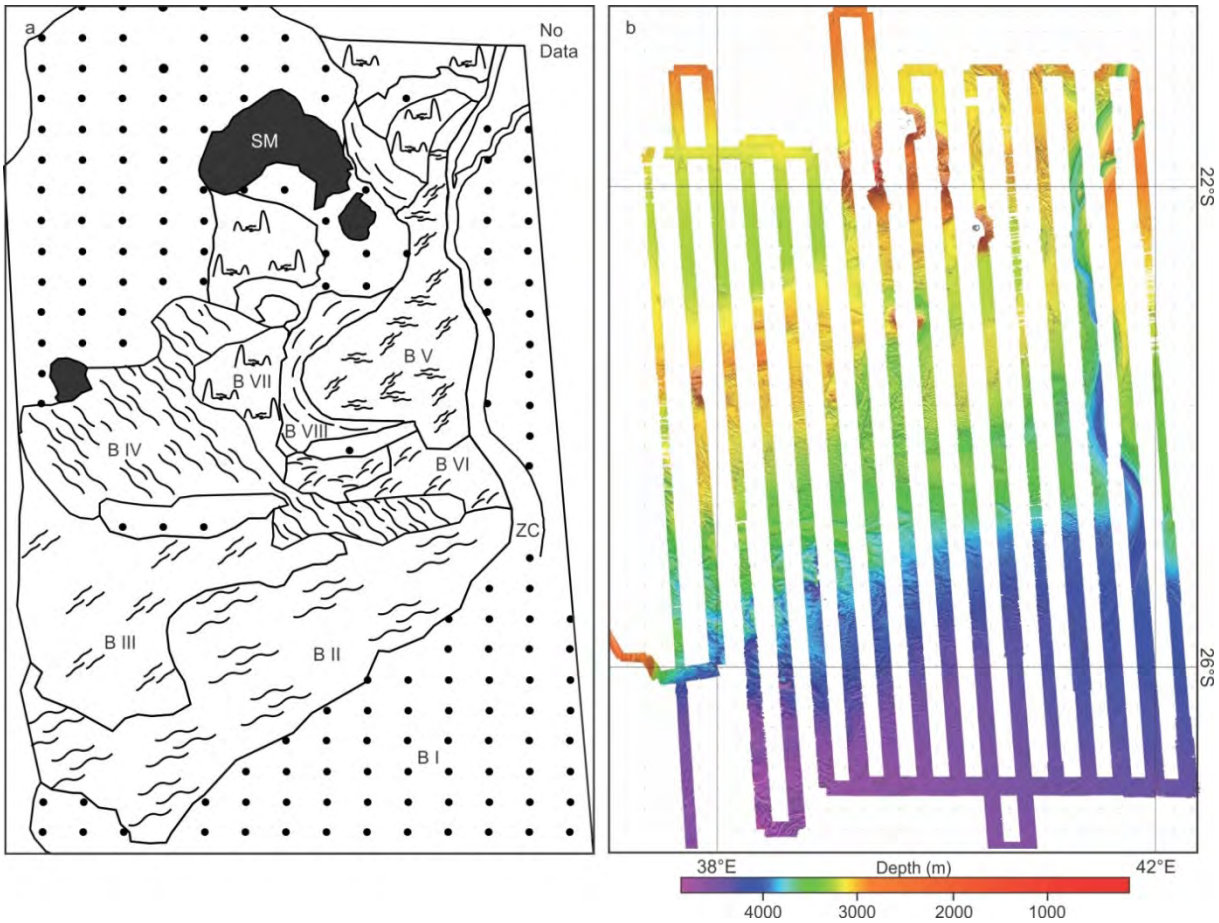

Fig. 8.1: Eight (BI – BVIII) types of seafloor were recognised in the multibeam bathymetry data. The zones (II smooth, III sediment waves, and IV regular hyperbolae) delineated by Kolla et al. (1980) are shown for comparison (dotted white lines).

8.2.2 Description of seafloor types

Type BI, figure 8.3, seafloor occurs predominantly along the eastern, southeastern and northwestern boundary of the study zone, with isolated diagonal patches across the middle of the area (Fig. 8.1, Table 8.1). The eastern boundary of this seafloor type contains the lower reaches of the Zambezi Channel and its associated channel-levee complex. The southeastern portion, although smooth, is cut by a number of relatively small canyons/channels which trend northeast-southwest. Levees and lobes of sediment associated with these features are evident in some instances (Chapter 7).

In the northwest, the Type BI seafloor is essentially featureless with only minor channels crossing the shallower margins (2900 – 3150 m) of a wide and flat seafloor basin (roughly 240 km north-south by 180 km east-west, approaching 3400 m at its centre). Smaller, isolated patches of Type BI seafloor are found at depths of 3200 – 3700 m,

comprising either depressions or wide "valleys" between the adjacent seafloor types. The "valleys" show defined channels orientated along the valley floor toward the deeper regions.

Type BII seafloor is orientated southwest-northeast across the southern portion of the study area (Figs. 8.1 and 8.3, Table 8.1). The 3D sediment waves with crests (aligned southwest-northeast) roughly parallel to local isobaths diminish in size toward the north and in aerial extent toward the south, where Type BI seafloor is mostly prevalent. This type of seafloor is not evident elsewhere in the basin.

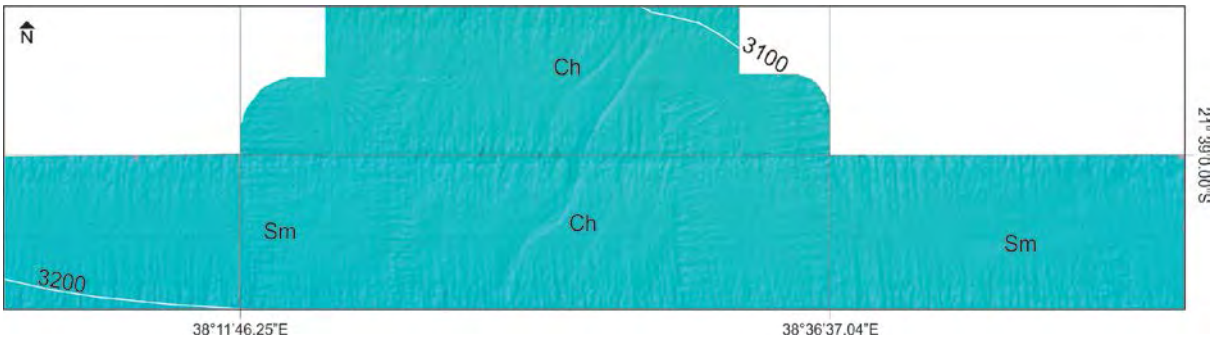

Fig. 8.2. Type BI seafloor, characterised by smooth seafloor (Sm) and occasional channels (Ch).

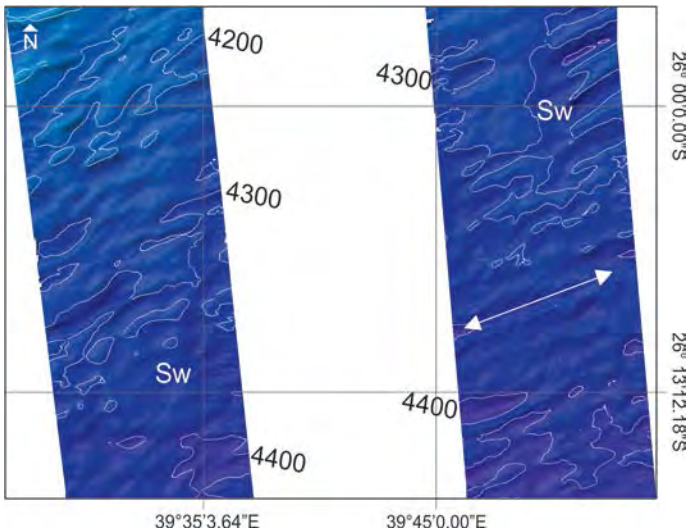

Fig. 8.3. Type BII seafloor associated with northeast-southwest sediment waves (Sw).

Type BIII is found in the southwest of the study area, covering a region of ca. 230 x 120 km within the northern Mozambique Basin (Figs. 8.1 and 8.4, Table 8.1). Sediment waves observed within these zones are orientated (crests aligned southwest-northeast) roughly parallel to local isobaths. Rugged seafloor occupies the area between sediment wave fields.

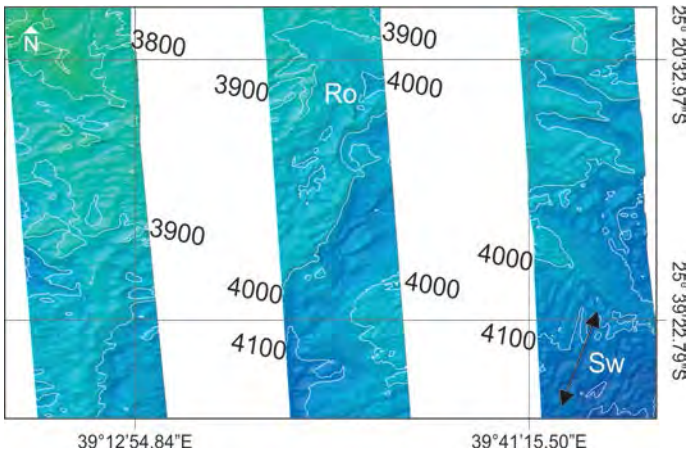

Fig. 8.4. Sediment waves (Sw) and rugged (Ro) seafloor typifies Type BIII seafloor zones.

Type BIV seafloor occurs from the western boundary eastwards, diminishing in extent towards the eastern boundary of the basin where it terminates ca. 50 km west of the Zambezi Channel (Figs. 8.1 and 8.5, Table 8.1). This is the only example of this seafloor in the study area, covering a region of seafloor 360 x 220 km in extent. Sediment wave crests are aligned oblique to the local isobaths.

Type BV seafloor is found at a depth of ca. 3100 – 3300 m and extends north-south in the central study area, covering an area 310 x 150 km in dimension (Figs. 8.1 and 8.6, Table 8.1). This seafloor type is dominated by sediment waves of two primary orientations, west-east and northeast-southwest (Table 8.1).

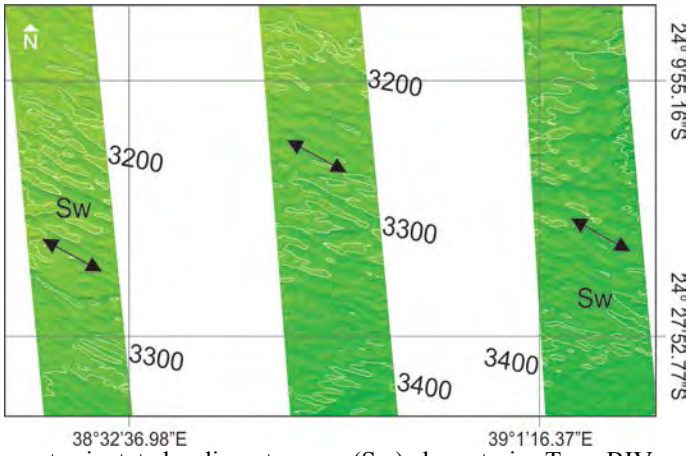

Fig. 8.5. Southeast-northwest orientated sediment waves (Sw) characterise Type BIV seafloor.

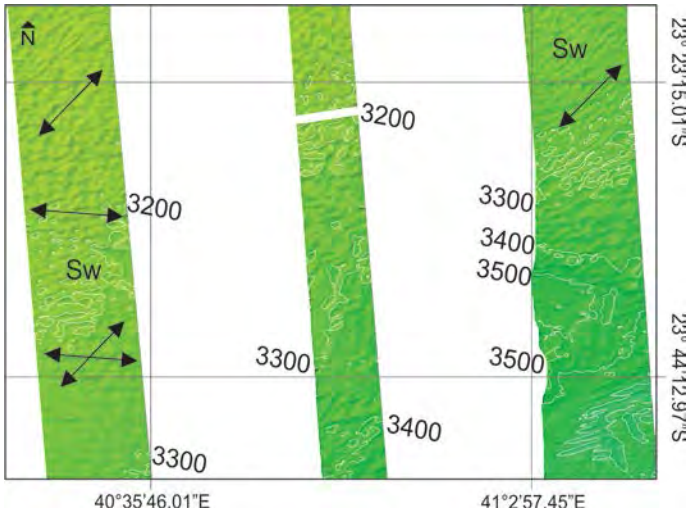

Fig. 8.6. East-west and southwest-northeast orientated sediment waves (Sw) of Type BV seafloor.

Seafloor Type BVI is one of the least aerially extensive of the seafloor zones recognised, covering 146 x 72 km, (Figs. 8.1 and 8.7, Table 8.1) and is wholly confined by five other types of seafloor (Types BI, BII, BIV, BV and BVIII). Bound by levees of the distal Zambezi Canyon to the east, it extends west toward the centre of the study area where it terminates against Type BV and BVI seafloor zones. Sediment wave crests, associated with this seafloor type, are orientated oblique to local isobaths (Table 8.1).

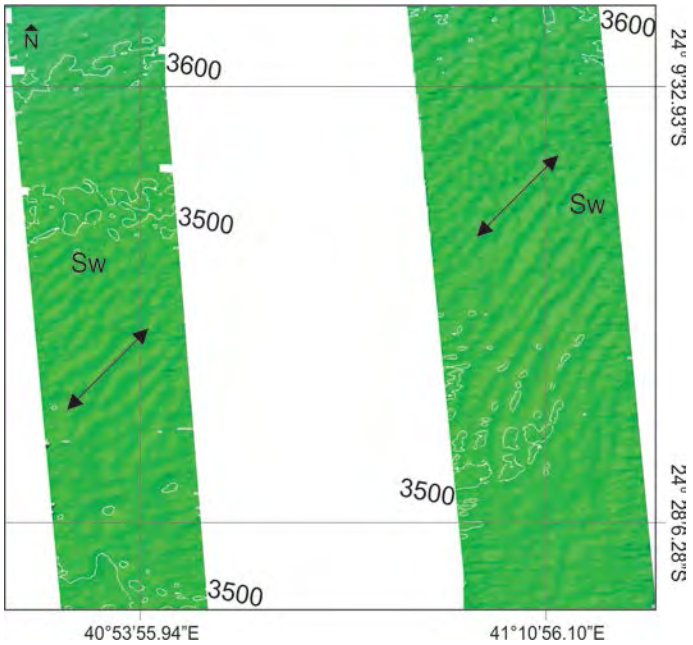

Fig. 8.7. Southwest-northeast orientated sediment waves (Sw) associated with the isolated Type BVI seafloor zone.

The Type BVII seafloor occupies four main zones, two in the central region, and two in the northeast portion of the study area (Figs. 8.1 and 8.8, Table 8.1). This seafloor zone is typified by rugged, irregular seafloor features with no particular orientation. Each of these areas are approximately 100 – 120 km long and 80 – 100 km wide, at depths 3000 – 3300 m.

Bordering the western portion of the larger Type BV seafloor zone, seafloor Type BVIII is encountered (Figs. 8.1 and 8.9, Table 8.1). This seafloor type is confined to the gentle slopes of the central basin dropping westward away from the 3200 m isobaths in a crescent-shaped form. It occupies and area 115 x 22 km in size. The crests of the sediment waves associated with Type BV seafloor are orientated parallel to the local isobaths (Table 8.1).

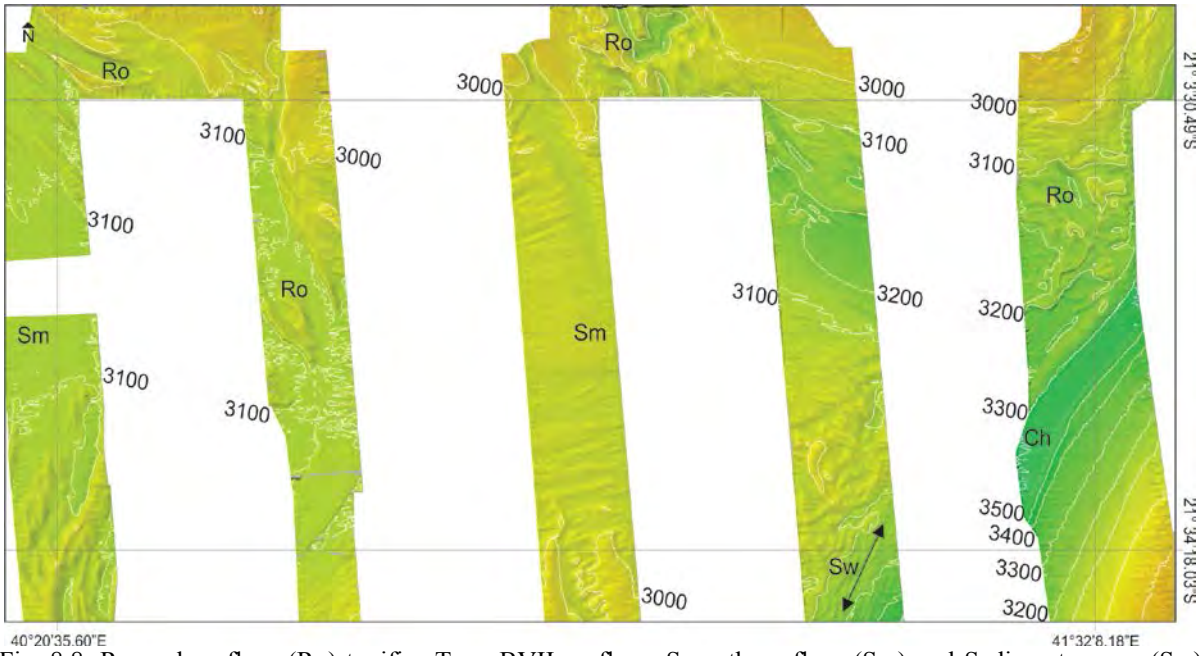

Fig. 8.8. Rugged seafloor (Ro) typifies Type BVII seafloor. Smooth seafloor (Sm) and Sediment waves (Sw) occupy the intervening areas. Ch denotes a seafloor channel.

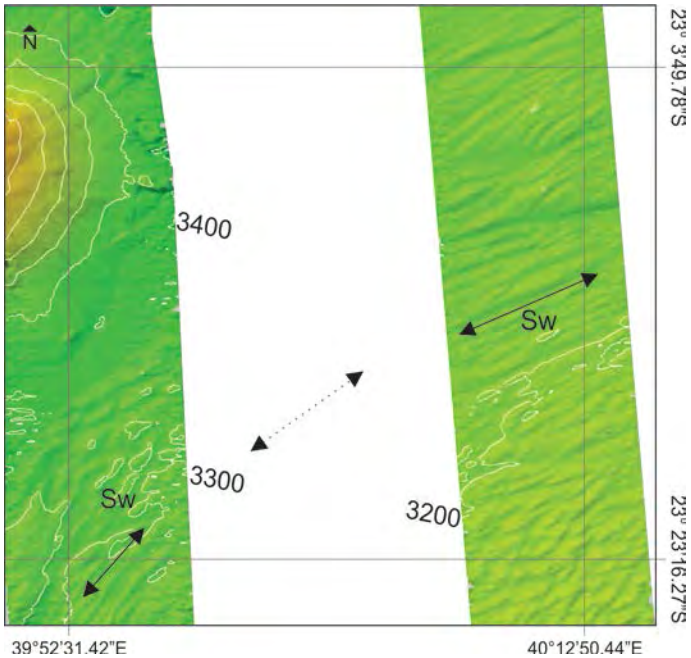

Fig. 8.9. Sediment waves (Sw) parallel to isobaths on the western slopes of a bathymetric high characterise Type BVIII seafloor.

Table 8.1. Summary of seafloor types, distribution and prominent features.

Seafloor Type	Locality	Features	Wavelength	Amplitude
Type BI	Eastern, southeastern, northwestern regions.	Smooth seafloor, cross-cut by channels. Recognised on levees.	n/a	n/a
Type BII	Southern region.	3D bifurcating sediment waves, crests parallel to isobaths.	ca. 2.3 km	ca. 60 m
Type BIII	Southwest regions.	Sediment waves, crests parallel to isobaths.	ca. 4.5 km	ca. 50 m
Type BIV	Western and central regions.	3D sediment waves, crests oblique to isobaths.	ca. 1.85 km	20 – 90 m
Type BV	Central region, extending northwards.	Sediment waves, west-east and northeast-southwest sets, with crests oblique to isobaths.	ca. 1.4 km	ca.40 m
Type BVI	Central regions, confined by Types BI, BII, BIV, BV and BVIII.	Sediment waves, crests oblique to isobaths.	ca. 1.23 km	ca. 45 m
Type BVII	Central and northeastern regions.	Rugged, irregular seafloor.	n/a	n/a
Type BVIII	Central regions.	Sediment waves with crest parallel to isobaths.	ca. 1.5 km	ca. 35 m

8.2.3 Echo character classification

A total of ten echo types were identified within the study area, these types are listed in Table 8.2., and described below.

Table 8.2: Summary of Broad and Localised echo character types.

Echo category	Echo type	Echo character
Distinct echoes	Type (IB)	Sharp, continuous echoes with several sharp continuous parallel sub-bottom reflectors.
Indistinct echoes: Prolonged	Type (IIA)	Very prolonged echoes with no sub-bottom reflectors.
	Type (IIB)	Semi-prolonged echoes with intermittent sub-bottoms.
	Type (IIC)	Irregular, semi-prolonged echoes with several discontinuous sub-bottom reflectors.
Indistinct echoes: Hyperbolic	Type (IIIA)	Distinct, undulating bottom echoes with semi-prolonged to discontinuous parallel sub-bottoms.
	Type (IIIB)	Large, single hyperbola with varying vertex elevations.
Localised echoes	Type (IVA)	Regular, intense overlapping hyperbola with little to no vertex elevation.
	Type (IVB)	Oblate to elongate bodies with no defined internal structure and a low amplitude irregular/hummocky upper surface.
	Type (IVC)	Lumpy to botryoidal bodies with prolonged echo to transparent internal structure.
	Type (IVD)	Blocky bodies associated with scarps/slip planes.

8.2.3.1 Echo character types

Type IB echoes exhibit distinct, sharp and continuous bottom echoes with several parallel sub-bottom reflectors (Fig. 8.10). The number of sub-bottom reflectors may vary. There are generally at least four but can reach up to seventeen.

Type II echoes are indistinct, though three sub-types are recognised: IIA are very prolonged with no sub-bottom reflectors (Fig. 8.11a), while IIB are semi-prolonged with intermittent sub-bottom reflectors (Fig. 8.4b). Irregular, semi-prolonged bottom echoes (20m penetration), with several discontinuous sub-bottom echoes characterise Type IIC (Fig. 8.11c).

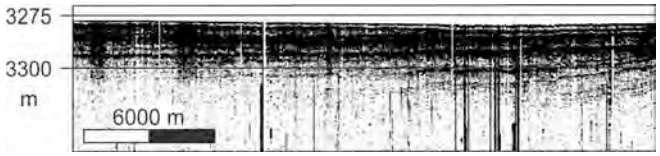

Fig. 8.10. Type IB echo character. Several parallel sub-bottom reflectors underlie a distinct seafloor return.

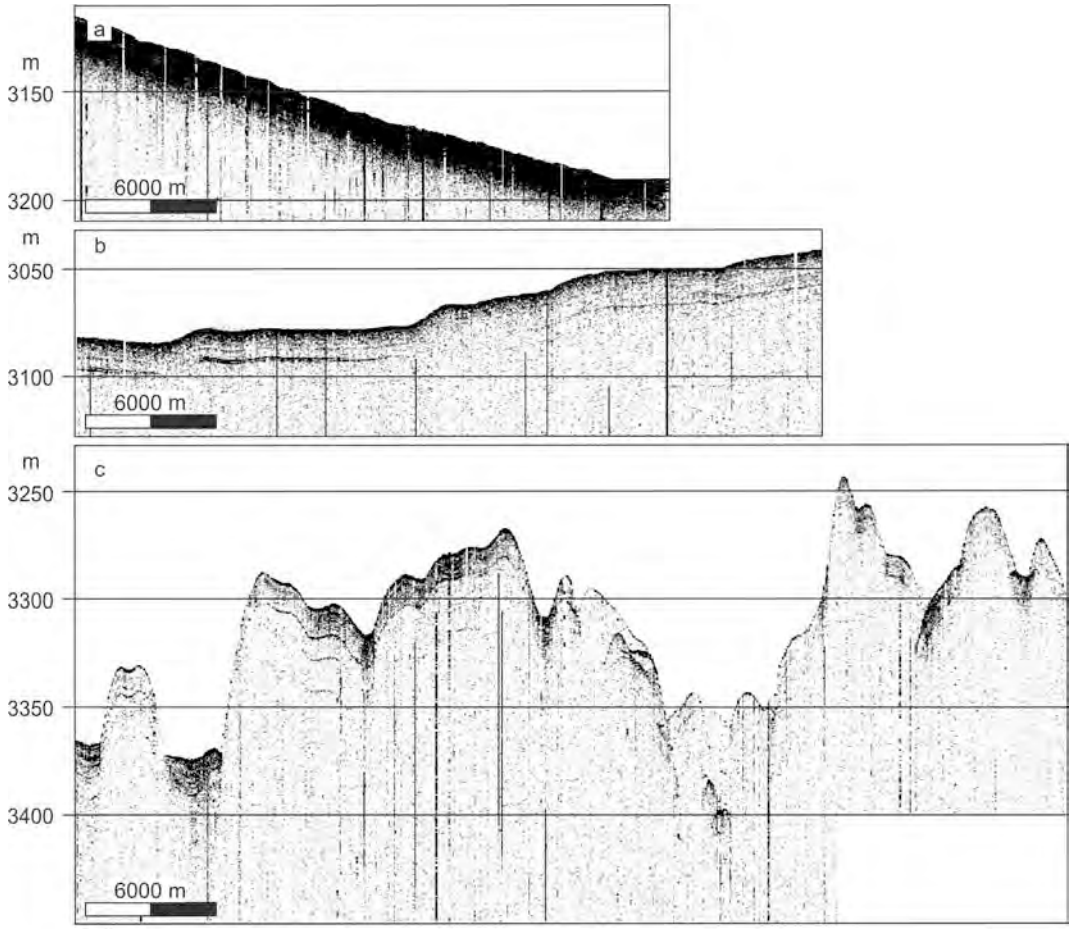

Fig. 8.11. a) *Type IIA echoes are very prolonged with no sub-bottom reflectors. b) Semi prolonged with intermittent sub-bottoms characterise Type IIB echoes. c) Irregular, semi-prolonged bottom echoes (20m), with several discontinuous sub-bottom echoes characterise Type IIC.*

Distinct, undulating bottom echoes (individual hyperbola) with semi-prolonged to discontinuous parallel sub-bottoms are classified as Type IIIA echo character, a modification of Type IIIC of Damuth (1980) (Fig. 8.12a). Large, regular, single hyperbolic echoes (at times indistinct), with slightly varied vertex elevations above the seafloor are classified as Type IIIB echoes (Fig. 8.12b).

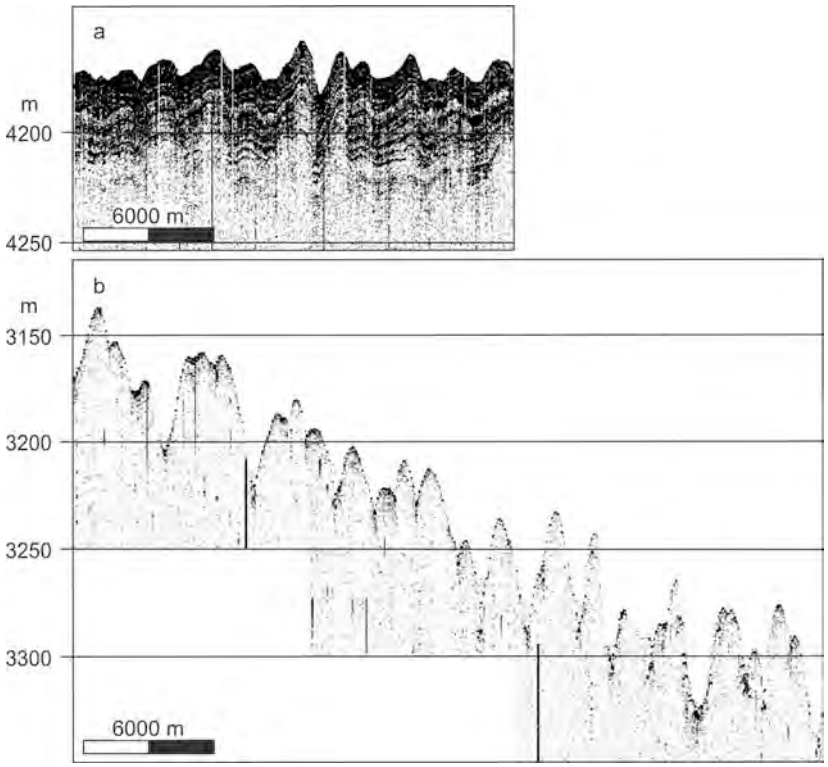

Fig. 8.12. a) Distinct, undulating bottom echoes (individual hyperbolic echoes) with semi-prolonged to discontinuous parallel sub-bottoms represent the Type IIIA echo character class. b) Large, single hyperbola (at times indistinct, with marginal overlapping of forms), displaying varied vertex elevations above the seafloor were classified as Type IIIB echoes.

Three localised echo character types are also described. These echo types are found in laterally confined areas and are uncommon throughout the study area. They occur as isolated surface and sub-bottom returns within the areas dominated by the broad echo types mentioned above. Small (ca. 10 m), regular, intense overlapping hyperbolae, with little to no vertex variation about the seafloor, were classed as Type IVA echoes (Fig. 8.13a), whereas oblate to elongate bodies with no defined internal structure and a low amplitude irregular/hummocky upper surface characterise Type IVB echoes. Typically the base of these Type IVB packages, in contact with the underlying seafloor, is clearly visible (Fig. 8.13b). Type IVC echoes manifest as lumpy, or botryoidal bodies, that showing a prolonged echo and at times may have a transparent internal structure (Fig. 8.13c). Type IVD echoes represent the final class, and comprise blocky bodies of various scale which have scarps or potential slip planes above them (Fig. 8.13d).

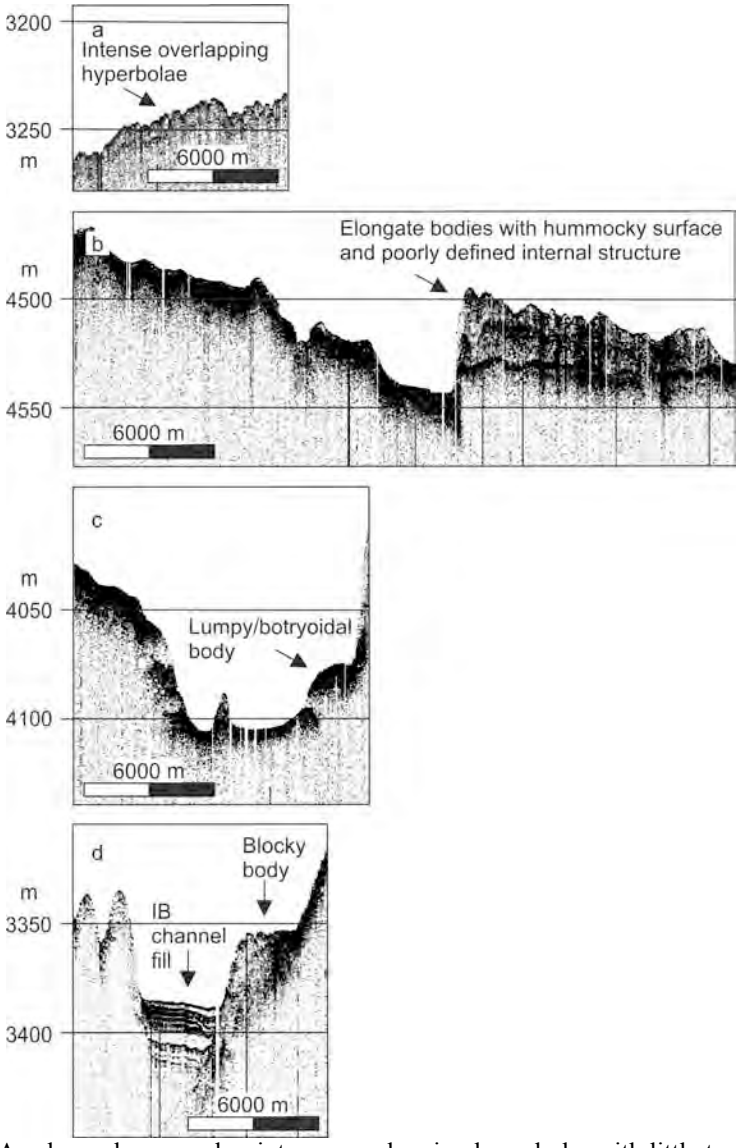

Fig. 8.13. a) Type IVA echoes show regular, intense overlapping hyperbola, with little to no vertex variation. b) Oblate to elongate bodies with no defined internal structure (chaotic) and a low amplitude irregular/hummocky upper surface characterise Type IVB echoes. c) Type IVC echoes are denoted by lumpy, or botryoidal bodies showing a prolonged echo to transparent/indistinct internal structure. d) Blocky bodies, of varied scale, represent Type IVD echoes. Note the Type IB echoes returned from the channel fill in this case.

8.3 Discussion

8.3.1 Relating microtopography to basin processes

The previous seafloor boundaries described by Kolla et al.(1980) are overlaid on the final seafloor character map of this study for ease of comparison (Fig. 8.14). It is clear that the northern Mozambique Basin can be divided into eight seafloor types based on the character of bedforms, as distinguished from bathymetric and PARASOUND data. This is a major advance on the four broad microtopographical zones delineated by Kolla et al. (1980).

Overall, the findings of this study are similar to those of Kolla et al. (1980) (Fig. 8.14). Zones II and III ((BI) and (BII) this study) defined by Kolla et al. (1980) were recognised and appeared to occupy the same position as identified in 1980. The formative processes associated with these two zones, turbidity currents and bottom water currents (Kolla et al., 1980), also appear to be the same. The existence of smooth seafloor to the east of the Zambezi Channel, as suggested by Kolla et al. (1980), is similarly confirmed in this study. Zone IV, the regular hyperbolae of Kolla et al. (1980), was actually found to comprise a number of distinct seafloor types, a notable deviation from the single zone described previously. This study found that areas were instead dominated by sediment waves of various orientations and origins, in addition to smooth and irregular seafloor. The increased resolution of the multi-beam bathymetry data was key to the differentiation of seafloor types in this instance.

8.3.1.1 Microtopography

The most prevalent bedforms within the study area are sediment waves. These features showed a range of spacing from ca. 1 km to several kilometres. The orientation (long axis parallel to the crest of bedforms) of the sediment waves also varies within the study area, in addition to the bedform shape. Some orientations appear to be parallel to the local isobaths, while others are offset from these isobaths with sediment wave crests aligned oblique to local isobaths. Portions of the seafloor not covered by sediment waves are either relatively smooth or irregular in character. The Zambezi Channel and levee complex dominates the eastern portion of the study area. This feature is discussed in detail in Chapter 7.

The area under investigation was initially delineated into zones on the basis of spacing and orientation of bedforms identified using multibeam bathymetry data. There is good agreement between the type of microtopography delineated, with reference to the multibeam bathymetry data, and the echo character of the shallow seismic data from the same areas (Table 8.3). The location and attitude (orientation in relation to bathymetry) of sediment waves suggest two different formative processes for these features in the northern Mozambique Basin.

Wynn and Stow (2002) maintain that currents, either as downslope-flowing turbidity currents or along slope-flowing bottom currents may interact with the seafloor to produce

sediment waves. This appears to be the case in the northern Mozambique Basin as discussed below.

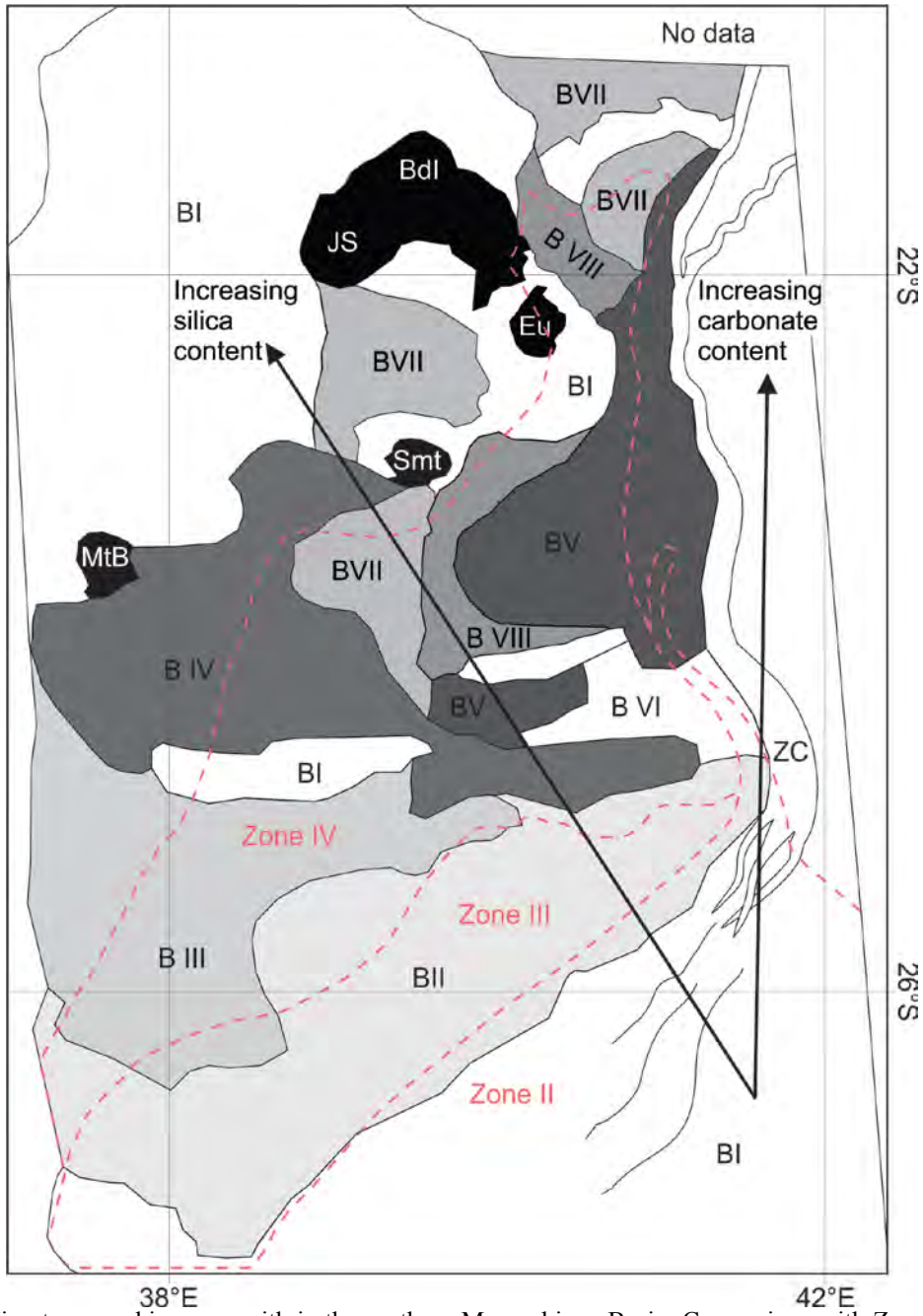

Fig. 8.14. Microtopographic zones with in the northern Mozambique Basin. Comparison with Zones II, III, and IV of Kolla et al. (1980) illustrated by the white dotted lines. Silica and carbonate content of sediment (after Kolla et al., 1980) is also shown. The delineated Zones II and III of Kolla et al. (1980) are roughly comparable to those of this study, allowances being made for a lack of multibeam bathymetry data and positioning inaccuracies in the case of the earlier interpretation. See Table 8.1 for seafloor type details. (MtB = Mount Bourcart, Smt = Unnamed seamount, JS = Jaguar Seamount, BaI = Bassas da India, Eu = Europa Island, ZC = Zambezi Channel)

Table 8.3: A summary of multibeam and 3.5 kHz PARASOUND classification of the seafloor of the northern Mozambique Basin.

Multibeam	Echo character	Microtopographic description	Interpretation
Type (BI)	Type (IIA); (IIB) and (IB)	Flat	Deposition by turbidity currents.
Type (BII) – (BVI)	Type (IIIA)	Sediment waves	Sediment wave dominated sheeted drifts influenced by bottom water circulation.
Type (BVII)	Type (IIC); (IIIB). Lesser (IB); (IIA).	Irregular seafloor morphology.	Scoured/sediment starved regions.
Type (BVIII)	(IIIA)	Sediment waves	Deposition by turbidity currents.

8.3.1.2 Current circulation, turbidity currents and relationship to bathymetric character

The passage of THC within the Mozambique Basin is known from hydrographic research and THC pathways have been postulated previously by many authors (cf. Ridderinkhof and de Ruijter, 2003; van Aken et al., 2004; Schott et al., 2009), however, this is the first time the resultant bedforms have been discussed, and found to support these previous studies (Breitzke et al., subm.) (Fig. 8.15).

As both deep seated THC and turbidity currents may form sediment waves, careful attention must be paid to the setting and character (i.e., crest orientation) of these sediment waves (Table 5.2). As both AABW and NADW are in contact with the seafloor of the northern Mozambique Basin as it shoals from south to north (van Aken, 2004), these currents are thus viable options as formative controls on sediment waves in certain areas of the Mozambique Basin. The regions of seafloor influenced by the AABW and NADW currents are characterised by low gradients and are unlikely to generate turbidity currents of regional extent. First to come into contact with the seafloor, as it shoals northward, at ca. 4500 m is the deeper AABW current (van Aken 2004; Breitzke et al., subm.). Within the depth range of AABW, three dimensional southwest/northeast orientated sediment waves on a sheeted drift dominate the seafloor (Type BII seafloor, Figs. 8.2 and 8.4). As regionally extensive turbidity currents are unlikely, these sediment waves may represent the interaction of AABW with sediments of the seafloor.

The basin continues to shoal northwards into depths of 2000 – 3500 m, occupied by NADW flowing northeastwards (van Aken, 2004). Sediment waves in this region are orientated southeast/northwest (Type BIII and BIV seafloor), their crests oblique to local

isobaths and perpendicular to NADW flow. It is likely that these sediment waves have developed in response to the passage of NADW over the seafloor surface. These sediment wave fields are interrupted by areas of irregular bathymetry (Type BVII seafloor) which suggests the reorganisation of sediments into sediment waves in some areas, with nondeposition or scour in others reflecting more basement control in the irregular seafloor surface that is essentially sediment-starved. As turbidity currents are not typically associated with irregular seafloor deposits of this scale, such currents are unlikely to be responsible for creating this seafloor type. Given that this seafloor type occurs amongst various seamounts past which the NADW flows, turbulence associated with the proximal passage of NADW to these seamounts is proposed to account for seafloor scour and development of irregular seafloor character, thereby removing and redistributing the sediments downcurrent.

Zones BV and BVI represent areas that host two sets of sediment waves in close proximity. Southwest/northeast orientated (crests) sediment waves characterise Type BV and BVI seafloor, additionally west-east sediment waves are associated with Type BV seafloor. These areas may be under the influence of eddies and bifurcation within the NADW current (van Aken et al., 2004), Mozambique Current Eddies (Ridderinkhof and de Ruijter, 2003; Schott et al., 2009; Breitzke et al., subm.), or East Madagascar Current Eddies spilling over the Madagascar ridge (Chapman et al., 2003; de Ruijter et al., 2003; Quartly and Srokosz, 2004; Quartly et al., 2006). Occupying the western flanks of the Zambezi Channel, levee breaching turbidity currents may also be responsible for the southwest/northeast orientated sediment waves. In reality it is likely a combination of all these formative processes. With the available data it is difficult to separate them. Type BVIII seafloor, dominated by slope parallel sediment waves (crests aligned parallel to isobaths) is typically confined to slopes surrounding Type BVII seafloor describing a crescent shaped area within the region. Given the parallel orientation of these sediment wave's crests to the local isobaths downslope rather than downcurrent processes are likely the controls on formation.

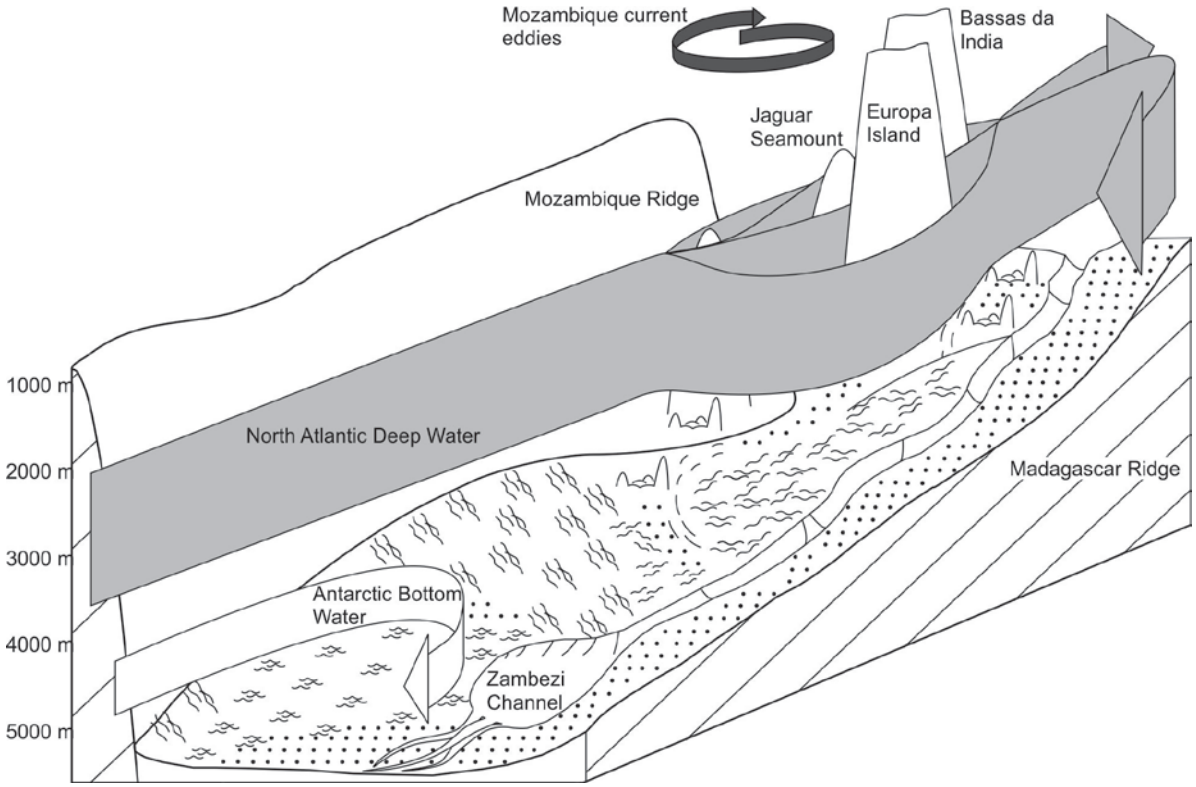

Fig. 8.15. A schematic illustration of the interaction between deep ocean circulation (a-NADW; b-AABW) and the surficial sediments of the northern Mozambique Basin. Field of sediment waves are associated with THC. At deeper levels, AABW is responsible for large three dimensional sediment waves, while at shallower levels NADW circulation have developed southeast/northwest orientated bedforms. Irregular seafloor around the Jaguar seamounts is associated with turbulent scouring reorganisation of sediments as the NADW navigates between the seamounts.

Chapter 9

9.1. Concluding remarks

The southwest Indian Ocean has had a protracted and complex evolution beginning with the break-up of Gondwana 146 million years ago. Since the initiation of the first beak-up event, several other significant events (including the formation of the Mozambique Ridge, several phases of hinterland uplift, and southward propagation of the EARS) have sculpted two major southwest Indian Ocean basins, the Natal Valley, and the Mozambique Basin. Despite these basins being located adjacent to each other, they have each responded differently to these regional events.

9.1.1. Tectonic history Natal Valley

Anomalous seafloor mounds in the Natal Valley represent a morphological class that is distinct from other seamounts, sharing more similarities with terrestrial alkaline complexes on the adjacent African continent than other submarine features. They mark a line of continuation of several alkaline complexes likely related to development of the East African Rift System and associated igneous activity. The mounds, compared to their terrestrial counterparts, show evidence of recent sediment draping and smoothing of their topographic profiles. These features may represent an offshore extension of the East African Rift igneous activity, implying a southward propagation of the East African Rift into a mature ocean basin, a phenomenon previously unrecognised from continental rift systems. As proximal to the western and southeastern plate boundaries of the Rovuma plate, these mounds have implications for the movement of the Rovuma plate, better defining the southern plate boundaries and allowing for better constrained models of plate dynamics in this region to be produced.

9.1.2. Sediment delivery Natal Valley

The Tugela Canyon, responsible for the delivery of sediment to the Natal Valley, has evolved via downslope erosion, primarily driven by sediment gravity flows or dilute turbidity currents. These initiated from periods of upper slope progradation whereby the oversteepened upper slope acted as a source for these flows. These periods can be linked to uplift of the hinterland and are interposed with periods of pelagic canyon infilling.

Two minor periods of hinterland uplift in the mid Oligocene and mid Miocene caused the canyon to incise into the same palaeo-canyon surface. A major period of uplift in the late Pliocene caused protracted incision and the development of the main lower slope canyon. Upslope, this created a compound feature of nested palaeo-canyons, the most recent (late Pliocene) incision is now filled by pelagic deposition during a long period of quiescence. The contemporary Tugela Canyon rests within this infilled palaeo-canyon and appears to be moribund with respect to canyon forming processes.

The contemporary canyon morphology is controlled to some extent by basement outcrop, though bed geometry also plays a role in the evolution of the canyon through preferential erosion of the western flank and levee development on the eastern flank. The associated contemporary Tugela Canyon fan appears to represent a mixed turbidity and bottom current smoothed pelagic system. The lack of sediment input from the shelf is a result of sweeping by the Agulhas Current. Along the abyssal rise, the fan's limited extent and the lack of features such as lobes and channel levee complexes define it as an atypical sediment starved and bottom current winnowed system. Winnowed sediment is driven northward into the northern Natal Valley, controlled largely by NADW.

9.1.3. Seafloor characteristics of the Natal Valley

The Ariel Graben creates a deep west to east saddle across the Mozambique Ridge at ca. 28°S. This deep saddle in the Mozambique Ridge provides the potential for deep water exchange between the northern Natal Valley and Mozambique Basin. A west to east change in character in the Ariel Graben is recorded in the sub-surface and expressed in the morphology of the seafloor and linked to deep water sediment transport. Evidence of this transport is manifest as crudely developed plastered drifts in the west and a field soft sediment deformation, of limited extent, in the east of the study area. Here current flow stripping due to increased curvature of the graben axis, results in preferential deposition of suspended load in accordance with reduced current velocity in an area of limited accommodation space. This results in an over-steepened plastered drift. Deposited sediments overcome the necessary shear stresses, resulting in soft sediment deformation in the form of downslope growth faulting (creep) and generation of undulating seafloor morphology. The observed seafloor and subseafloor characteristics are considered to be associated with a newly postulated NADW passage through the Ariel Graben, as opposed to influence by deep-reaching Agulhas Current activity.

9.1.4. Tectonics within the Mozambique Basin

The data presented in Chapter 9 show an unusual west-east depression within the Mozambique Channel, in an area of relatively high seismic activity on the southeastern boundary of the Rovuma microplate. Many attributes of the surrounding area, excluding the depression, are explained by typical deep sea processes, including erosion/deposition by deep reaching currents. The depression marks a west-east orientated elongate zone bordered by steepened flanks. The basin floor is devoid of significant sedimentary deposits, and reflects a character associated with rugged basement outcrop. This depression is likely the surficial expression of the southeasterly extension related to the present-day kinematics of the East African Rift System. To the east of this zone of extension, the Zambezi Channel funnels sediment from the African continent into the Mozambique Basin, loading the Rovuma and Lwandle microplates.

9.1.5 The Zambezi Channel

The lower submarine Zambezi Channel is not comparable to other systems from similar equatorial latitudes, and varies in character from the Tanzania channel, which shares a similar setting. Some characteristics are similar to high latitude systems (e.g., low sinuosity, relatively wide channel in the distal reaches), including the NAMOC system. Thus the Zambezi Channel does not fit into the general classification scheme for deep ocean channels, and represents a modified character with characteristics of both high and low latitude submarine channels.

The development of the Zambezi Channel is linked to major periods of sediment influx associated with hinterland uplift. The periodic nature of sediment flux, lack of direct connection to a significant fluvial source, and vigorous current regime resulted in a dynamic setting not conducive to the formation of a sinuous system comparable to other equatorial channels. Episodes of progradational/erosional waves passing downstream through the system, associated with periods of increased sediment supply had a significant effect on the anatomy of the channel within the limited accommodation space provided by the structurally controlled northern Mozambique Basin. At present, the Zambezi Channel exists within a sedimentary basin dominated by sediment waves, controlled by antecedent geology and a dynamic hydrographic regime.

9.1.6. Seafloor characteristics of the northern Mozambique Basin

The northern Mozambique Basin is divided into eight microtopographic seafloor types based on the morphology and echo character of the seafloor. Sediment wave fields with crest orientations oblique to local isobaths, and within the depth range of deep and bottom water currents, are attributed to deep THC. Whereas sediment wave fields where crests are orientated parallel the local isobaths, and in proximal to the Zambezi Channel, are attributed to down-slope sediment transport by turbidity currents. Areas of rugged, mixed scale, seafloor morphology represent current swept and sediment starved regions proximal to seamounts in the central region of the study area. The microtopography of the northern Mozambique Basin is influenced by both bottom water circulation and turbidity currents. The circulation of bottom water has developed sediment wave-dominated sheeted drifts within the study area, while turbidity currents are responsible for the development of large areas of relatively smooth seafloor, as well as some sediment wave zones proximal to the Zambezi Channel.

References

Abreu, V., Sullivan, M., Pirmez, C., Mohrig, D., 2003. Lateral accretion packages (LAPs): an important reservoir element in deep water sinuous channels. Marine and Petroleum Geology 20, 631–648.

Albaric, J., Déverchère, J., Petit, C., Perrot, J., Le Gall, B., 2009. Crustal rheology and depth distribution of earthquakes: Insights from the central and southern East African Rift System. Tectonophysics 468(1–4), 28–41.

Alley, R.B., Clark, P.U., Keigwin, L.D., Webb, R.S., 1999. Making sense of millennial-scale climate change. In: Clark PU, Webb R.S., Keigwin L.D., (eds.), Mechanisms of Global Climate Change at Millennial Time Scales. AGU Geophys. Monogr. 112, pp. 385–494.

Anka, Z., Séranne, M., Lopez, M., Scheck-Wenderoth, M., Savoye, B., 2009. The long term evolution of the Congo deep-sea fan: a basin-wide view of the interaction between a giant submarine fan and a mature passive margin (ZaiAngo project). Tectonophysics 470, 42–56.

Arhan, M., Mercier, H., Park, P., 2003. On the deep water circulation of the eastern South Atlantic Ocean. Deep-Sea Research I 50, 889–916.

Backeberg, B.C., Reason, C., 2010. A connection between the South Equatorial current north of Madagascar and Mozambique Channel eddies. Geophys. Res. Lett. 37, L04604.

Bang, N.D., Pearce A.F., 1976. Large-scale circulation of surface water of the south Indian Ocean. In: Heydorn, A.E.F., (eds.), Ecology of the Agulhas Current Region–an Assessment of Biological Responses to Environmental Parameters in the South-West Indian Ocean. Proceedings of the Marine Freshwater Conference, Port Elizabeth. CSIR, Pretoria pp. 4–10.

Barfod, D.N., Fitton, J.G., 2013. Pleistocene volcanism on São Tomé, Gulf of Guinea, West Africa. Quaternary Geochronology, 1–13.

Bassias, Y., 1992. Petrological and geochemical investigation of rocks from the Davie fracture zone (Mozambique Channel) and some tectonic implications. Journal of African Earth Sciences (and the Middle East) 15(3–4), 321–339.

Baztan, J., Berne, S., Olivet, J., Rabineau, M., Aslanian, D., Gaudin, M., Rehault, J., Canals, M., 2005. Axial incision: the key to understand submarine canyon evolution (in the western Gulf of Lion). Marine and Petroleum Geology 22, 805–826.

Beal, L.M., Bryden, H.L., 1997. Observations of an Agulhas Undercurrent, Deep Sea Res I 44, 1715–1724. doi:10.1016/S0967-0637(97)00033-2

Beal, L.M., Bryden, H.L., 1999. The velocity and vorticity structure of the Agulhas Current at 32° S. Journal of Geophysical Research 104(C3), 5151–5176.

Beiersdorf, H., Kudrass, H.R., von Stackelberg, U., 1980. Placer deposits of Ilmenite and Zircon on the Zambezi Shelf. Geologisches Jahrbuch, Reihe D 36, 5–85.

Ben-Avraham, Z., Hartnady, C.H.J., Malan, J.A., 1993. Early tectonic extension between the Agulhas Bank and Falkland Plateau due to the rotation of the Lafonia microplate. Earth and Planetary Science Letters 117, 43–58.

Ben-Avraham, Z., Niemi, T.M., Hartnady, C.J.H., 1994. Mid-Tertiary changes in deep ocean circulation patterns in the Natal Valley and Transkei basin, Southwest Indian Ocean. Earth and Planetary Science Letters 121(3–4), 639–646.

Ben-Avraham, Z., Hartnady, C.J.H., le Roex, A.P., 1995. Neotectonic activity on continental fragments in the Southwest Indian Ocean: Agulhas Plateau and Mozambique Ridge. Journal of Geophysical Research 100, 6199–6211.

Biastoch, A., Krauss, W., 1999. The role of mesoscale eddies in the source regions of the Agulhas Current. J. Phys.Oceanogr. 29, 2303–2317.

Bouma, A.H., 2004. Key controls on the characteristics of turbidite systems. In: Lomas, S.A., Joseph, P. (eds.), Confined Turbidite Systems. Geological Society of London, Special Publication 222, pp. 9–22.

Bourget, J., Zaragosi, S., Gabelotaud, I., Guyomard, P., Dennielou, B., Ellouz-Zimmermann, N., Schneide, J.L., the FanIndien 2006 survey crew, 2008. Discovery of a giant deep-sea valley in the Indian Ocean, off eastern Africa: The Tanzania channel. Marine Geology 255, 179–185.

Boswell, S. M., Smythe-Wright, D., 2002. The tracer signature of Antarctic Bottom Water and its spread in the Southwest Indian Ocean: Part I—CFC-derived translation rate

and topographic control around the Southwest Indian Ridge and the Conrad Rise. Deep Sea Research Part I: Oceanographic Research Papers 49, 555–573.

Boyd, R., Ruming, K., Goodwin, I., Sandstrom, M., Schröder-Adams, C., 2008. Highstand transport of coastal sand to the deep ocean: a case study from Fraser Island, southeast Australia. Geology 36, 15–18.

Breitzke, M., Wiles, E., Krocker, R., Watkeys, M., Jokat, W. (subm.). Seafloor morphology in the Mozambique Channel: Evidence for long-term persistent bottom-current flow and deep-reaching eddy activity, submitted to Marine Geology, 2014.

Brun, J., Fort, X., 2011. Salt tectonics at passive margins: Geology versus models. Marine and Petroleum Geology 28, 1123–1145.

Burke, K., 1996. The African plate. South African Journal of Geology 99, 339–409.

Carter, L., Carter, R.M., Nelson, C.S., Fulthorpe, C.S., Neil, H.L., 1990. Evolution of Pliocene to recent abyssal sediment waves on Bounty Channel levees, New Zealand. Marine Geology 95, 97–109.

Calais, E., Hartnady, C., Ebinger, C., Nocquet, J.M., 2006. Kinematics of the East African Rift from GPS and earthquake slip vector data. In: Yirgu, G., Ebinger, C.J., Maguire, P.K.H. (eds.), Structure and Evolution of the Rift Systems within the Afar volcanic province, Northeast Africa. Geological Society Special Publications 259, pp. 9–22.

Casal, T.G.D., Beal, L, M., Lumpkin, R., 2006. A North Atlantic deep-water eddy in the Agulhas Current system Deep-Sea Research I 53, 1718–1728.

Cawthra, H.C., Neumann, F.H., Uken, R., Smith, A.M., Guastella, L., Yates, A.M., 2012. Sedimentation on the narrow (8 km wide), oceanic current-influenced continental shelf off Durban, KwaZulu-Natal, South Africa. Marine Geology 323–325, 107–122.

Chapman, P., Di Marco, S.F., Davis, R.E., Coward, A.C., 2003. Flow at intermediate depths around Madagascar based on ALACE float trajectories. Deep Sea Research II 50, 1957–1986.

Chorowicz, J., 2005. The East African Rift System. Journal of African Earth Sciences 43(1–3), 379–410.

Corti, G., 2009. Continental rift evolution: From rift initiation to incipient break-up in the Main Ethiopian Rift, East Africa. Earth-Science Reviews 96 (1–2), 1–53.

Clark, J.D., Pickering, K.T., 1996. Submarine channels: Process and architecture: London, Vallis Press, pp. 231.

Clark, J.D., Kenyon, N.H., Pickering, K.T., 1992. Quantitative analysis of the geometry of submarine channels: Implications for the classification of submarine fans: Geology, 20, 633–636.

Cochran, J.R., 1981. The Gulf of Aden: Structure and Evolution of a Young Ocean Basin and Continental Margin. Journal of Geophysical Research 86, 263–287.

Compton, J.S., Wiltshire, J.G., 2009. Terrigenous sediment export from the western margin of South Africa on glacial to interglacial cycles. Marine Geology 266, 212–222.

Courtillot, V., Jaupart, C., Manighetti, I., Tapponnier, P., Besse, J., 1999. On causal links between flood basalts and continental breakup. Earth and Planetary Science Letters 166, 177–195.

Cunningham, A.P., Barker, P.F., 1996. Evidence for westward-flowing Weddell Sea Deep Water in the Falkland Trough, western South Atlantic. Deep-Sea Res. 43, 643–654.

Cratchley, C. R., Louis, P., Ajakaiye, D. E., 1983. Geophysical and geological evidence for the Benue-Chad Basin Cretaceous rift valley system and its tectonic implications. Journal of African Earth Sciences 2, 141–150.

Damuth, J.E., 1975. Echo characters of the western equatorial Atlantic floor and its relationship to the dispersal and distribution of terrigenous sediments. Marine Geology 18, 17–45.

Damuth, J.E., Hayes, D.E., 1977. Echo character of the east Brazilian continental margin and its relationship to sedimentary processes. Marine Geology 24, 73–95.

Damuth, J.E., 1978. Echo character of the Norwegian-Greenland Sea: Relationship to Quaternary sedimentation. Marine Geology 28, 1–36.

Damuth, J.E., 1980. Use of high-frequency (3.5–12 kHz) echograms in the study of near-bottom sedimentation processes in the deep sea: A review. Marine Geology 38, 51–75.

Damuth, J.E., Kolla, V., Flood, R.D., Kowsmann, R.O., Montei, M.C., Gorini, A., Palma, J.J.C., Belderson, R.H., 1983. Distributary channel meandering and bifurcation patterns on the Amazon deep-sea fan as revealed by long-range side-scan sonar (GLORIA). Geology 11, 94–98.

Das, P., Iyer, S.D., Kodagali, V.N., 2007. Morphological characteristics and emplacement mechanism of the seamounts in the Central Indian Ocean Basin. Tectonophysics, 443(1–2), 1–18.

Davison, I., 2005. Central Atlantic margin basins of North West Africa: Geology and hydrocarbon potential (Morocco to Guinea). Journal of African Earth Sciences 43, (1–3), 254–274.

Davison, I., Dailly, P., 2010. Salt tectonics in the Cap Boujdour Area, Aaiun Basin, NW Africa. Marine and Petroleum Geology 27(2), 435–441.

Dengler, L., Carver, G.A., McPherson, R., 1993. Sources of north coast seismicity. Calif. Geol. 45, 40–53.

Déprez, A., Doubre, C., Masson, F., Ulrich, P., 2013. Seismic and aseismic deformation along the East African Rift System from a reanalysis of the GPS velocity field of Africa, Geophys. J. Int. 193, 1353–1369.

Deptuck, M.E., Steffens, G.S., Barton, M., Pirmez, C., 2003. Architecture and evolution of upper fan channel-belts on the Niger Delta slope and in the Arabian Sea. Marine and Petroleum Geology 20, 649–676.

de Ruijter, W.P.M., Biastoch, A., Drijfhout, S.S., Lutjeharms, J.R.E., Matano, R.P., Pichevin, T., van Leeuwen, P.J., Weijer, W., 1999. Indian-Atlantic interocean exchange: Dynamics, estimation and impact. Journal of Geophysical Research 104, 20885–20910.

de Ruijter, W.P.M., Ridderinkhof, H., Lutjeharms, J.R.E., Schouten, M.W., Veth, C., 2002. Observations of the flow in the Mozambique Channel. Geophysical Research Letters 29(10), 1401–1403.

de Ruijter, W.P.M., van Aken, H.M., Beier, E.J., Lutjeharms, J.R.E., Matano, R.P., Schouten, M.W., 2003. Eddies and dipoles around south Madagascar: Formation, pathways and large-scale impact. Deep Sea Res I 51, 383–400.

Dietz, R.S., 1963. Continent and Ocean Basin Evolution by Sea Floor Spreading. Tulsa Geological Society Digest 31, 241–242.

Dillon, W.P., Lee, M.W., Fehlhaber, K., Coleman, D.F., 1993. Gashydrates on the Atlantic margin of the United States—Controls on concentration. In Howell, D.G., (ed.), The Future of Energy Gases. Geol. Surv. Prof. Pap. 1570, 313–330.

DiMarco, S.F., Chapman, P., Nowlin, Jr. W.D., Hacker, P., Donohue, K., Luther, M., Johnson, G.C., Toole, J., 2002. Volume transport and property distributions of the Mozambique Channel. Deep Sea Res II: Topical Studies in Oceanography 49(7–8), 1481–1511.

Dingle, R.V., Goodlad, S.W., Martin, A.K., 1978. Bathymetry and Stratigraphy of the northern Natal Valley (SW Indian Ocean): A preliminary account. Marine Geology 28, 89–106.

Dingle, R.V., Camden-Smith, F., 1979. Acoustic stratigraphy and current-generated bedforms in deep ocean basins off southeastern Africa. Marine Geology 33, 239–260.

Dingle, R.V., 1980. Large allochthonous sediment masses and their role in the construction of the continental slope and rise of southwestern Africa. Marine Geology 37, 33–35.

Dingle, R.V., Siesser, W.G., Newton, A.R., 1983. Mesozoic and Tertiary Geology of Southern Africa. Balkema, Rotterdam, pp. 375.

Dingle, R.V., Robson, S., 1985. Slumps, canyons and related features on the continental margin off East London, SE Africa (SW Indian Ocean). Marine Geology 67, 37–54

Dingle, R.V., Birch, G.F., Bremner, J.M., de Decker, R.H., du Plessis, A., Engelbrecht, J.C., Fincham, M.J., Fitton, T., Flemming, B.W., Goodlad, S.W., Gentle, R.I., Martin, A.K., Mills, E.G., Moir, G.J., Parker, R.J., Robson, S.H., Rogers, J., Salmon, D.A.,

Siesser, W.G., Simpson, E.S.W., Summerhayes, C.P., Westall, F., Winter, A., Woodborne, M.W., 1987. Deep-sea sedimentary environments around southern Africa (SE-Atlantic & SW-Indian Oceans). Annals South African Museum 98, 1–27.

Donohue, K.A., Firing, E., Beal, L., 2000. Comparison of three velocity sections of the Agulhas Current and Agulhas Undercurrent. Journal of Geophysical Research: Oceans 105(C12), 28585–28593.

Donohue, K.A., Toole. J.M., 2003. A near-synoptic survey of the Southwest Indian Ocean. Deep-Sea Research II 50, 1893–1931.

Dowdeswell, J.A., O'Cofaigh, C., Taylor, J., Kenyon, N.H., Mienert, J., and Wilken, M., 2002, On the architecture of high-latitude continental margins: The infl uence of ice-sheet and sea-ice processes in the Polar North Atlantic, In: Dowdeswell, J.A., and O'Cofaigh, C., (eds.), Glacier-influenced sedimentation on high-latitude continental margins: Geological Society of London Special Publication 203, 33–54, doi:10.1144/GSL.SP.2002.203.01.03.

Droz, L., Mougenot, D., 1987. Mozambique Upper Fan: Origin of depositional units. AAPG Bulletin 71, 1355–1365.

Ebinger, C. J., 1989. Tectonic development of the western branch of the East African Rift System. Geological Society of America Bulletin 101, 885–903.

Eschard, R., 2001. Geological factors controlling sediment transport from platform to deep basin: a review. Marine and Petroleum Geology 18, 487–490.

Escutia, C., Eittreim, S.L., Cooper, A.K., Nelson, C.H., 2000. Morphology and acoustic character of the Antarctic Wilkes Land turbidite systems: Ice-sheet-sourced versus river-sourced fans: Journal of Sedimentary Research 70, 84–93.

Fairhead, J.D., Stuart, G.W., 1982. The seismicity of the East Africa rift system and comparison with others continental rifts. In: Palmason, G. (ed.), Continental and Oceanic Rifts. Geodynamics Series 8, 41–61.

Farre, J.A., McGregor, B.A., Ryan, W.B.F., Robb, J.M., 1983. Breaching the shelfbreak; passage from youthful to mature phase in submarine canyon evolution. In: Stanley,

D.J., Moore, G.T., (Eds.), The Shelfbreak: Critical Interface on Continental Margins. Soc. Econ. Palaeontol. Mineral. Spec. Pub. 33, 25–39.

Faugères, J.C., Stow, D.A.V., Imbert, P., Viana, A., 1999. Seismic features diagnostic of contourite drifts. Marine Geology 162, 1–38.

Faugères, J.C., Gonthier, E., Mulder, T., Kenyon, N., Cirac, P., Griboulard, R., Berné, S., Lesuavé, R., 2002. Multi-process generated sediment waves on the Landes Plateau (Bay of Biscay, North Atlantic). Marine Geology 182(3–4), 279–302

Fitton, J.G., Dunlop, H.M., 1985. The Cameroon line, West Africa, and its bearing on the origin of oceanic and continental alkali basalt. Earth and Planetary Science Letters 72(1), 23–38.

Flemming, B.W., 1978. Underwater sand dunes along the southeast African continental margin–observations and implications. Marine Geology 26, 177–198.

Flemming, B.W., 1980. Sand transport and bedform patterns on the continental shelf between Durban and Port Elizabeth (southeast African continental margin). Sedimentary Geology 26(1–3), 179–205.

Flemming, B, Hay, R., (1988) Sediment distribution and dynamics of the Natal continental shelf, in Coastal Ocean Studies off Natal, South Africa, Lecture Notes. In: Schumann, E.H., (ed.), Coastal Estuarine Stud. Springer, Berlin 26, 47–80.

Flood, R.D., 1980. Deep-sea sedimentary morphology: modelling and interpretation of echo-sounding profiles. Marine Geology 38, 77–92.

Flood, R.D., 1994. Abyssal bedforms as indicators of changing bottom current flow: Examples from the U.S. East Coast continental rise. Paleoceanography 9, 1049–1060.

Galbraith, E.D., Jaccard, S.L., Pedersen, T.F., Sigman, D.M., Haug, D.H., Cook, M., Southon, J.R., Francois, R., 2007. Carbon dioxide release from the North Pacific abyss during the last deglaciation. Nature 449, 890–893.

Gamboa, D., Alves, T.M., Cartwright, J., 2012. A submarine channel confluence classification for topographically confined slopes. Marine and Petroleum Geology 35, 176–189.

Gardner, J., Prior, D., Field, M., 1999. Humboldt Slide–a large shear dominated retrogressive slope failure. Marine Geology 154, 323–338.

Garrison, L.E., Kenyon, N.H., Bouma, A.H., 1982. Channel systems and lobe construction in the Mississippi Fan. Geo-Marine Letters 2, 31–39.

Gee, M.J.R., Gawthorpe, R.L., 2006. Submarine channels controlled by salt tectonics: Examples from 3D seismic data offshore Angola. Marine and Petroleum Geology 23, 443–458.

Gee, M.J.R., Gawthorpe, R.L., Bakke, K., Friedmann, S.J., 2007. Seismic geomorphology and evolution of submarine channels from the Angolan continental margin: Journal of Sedimentary Research 77, 433–446. doi:10.2110/jsr.2007.042.

Goff, J.A., Jordan, T.H., 1988. Stochastic Modeling of Sea floor Morphology: Inversion of Sea Beam data for second-order statistics. Journal of Geophysical Research 93, 13589–13608.

Goff, J.A., Ma, Y., Shah, A., Cochran, J. R., Sempéré, C., 1997. Stochastic analysis of sea floor morphology on the flank of the Southeast Indian Ridge: The influence of ridge morphology on the formation of abyssal hills, Journal of Geophysical Research 102, 15521–15534.

Goff, J.A., 2001. Quantitative classification of canyon systems on continental slopes and a possible relationship to slope curvature. Geophysical Research Letters 28, 4359–4362.

Goff, J.A., Swift, D.J.P., Duncan, C.S., Mayer, L.A., Hughes-Clarke, J., 1999. High-resolution swath sonar investigation of sand ridge, dune and ribbon morphology in the offshore environment of the New Jersey margin. Marine Geology 161, 307–337.

Goodlad, S.W., 1986. Tectonic and Sedimentary History of the Mid-Natal Valley (SW Indian Ocean). In: Marine Geoscience Unit Bulletin. Joint Geological Survey/University of Cape Town 15, pp. 415.

Green, A.N., Goff, J.A., Uken, R., 2007. Geomorphological evidence for upslope canyon forming processes on the northern KwaZulu-Natal shelf, South Africa. Geo-Marine Letters 27, 399–409.

Green, A.N., Uken, R., 2008. Submarine landsliding and canyon evolution on the northern KwaZulu-Natal continental shelf, South Africa, SW Indian Ocean. Marine Geology 254, 152–170.

Green, A.N., Uken, R., Ovechkina, M., 2008. Nannofossil age constraints for the northern KwaZulu-Natal shelf-edge wedge: implications for continental margin dynamics, South Africa, SW Indian Ocean. Continental Shelf Research 28, 2442–2449.

Green, A.N., 2009. Sediment dynamics on the narrow, canyon-incised and currentswept shelf of the northern KwaZulu-Natal continental shelf, South Africa. Geo- Marine Letters 29, 201–219.

Green, A.N., 2011a. Submarine canyons associated with alternating sediment starvation and shelf-edge wedge development: northern KwaZulu-Natal continental margin, South Africa. Marine Geology 289, 114–126.

Green, A.N., 2011b. The late Cretaceous to Holocene sequence stratigraphy of a sheared passive upper continental margin, northern KwaZulu-Natal, South Africa. Marine Geology 289, 17–28.

Green, A.N., Garlick, G.L., 2011. Sequence stratigraphic framework for a narrow, current-swept continental shelf: the Durban Bight, central KwaZulu-Natal, South Africa. Journal of African Earth Sciences 60, 303–314.

Grimison, N.L. Chen, W.-P., 1988. Earthquakes in the Davie Ridge-Madagascar region and the southern Nubian-Somalian plate boundary. Journal of Geophysical Research: Solid Earth 93(B9), 10439–10450.

Gutjahr, M., Hoogakker, B.A.A., Frank, M., McCave, I.N., 2010. Changes in North Atlantic Deep Water strength and bottom water masses during Marine Isotope Stage 3 (45–35 ka BP). Quaternary Science Reviews 29, 2451–2461. doi:10.1016/j.quascirev.2010.02.024

Hartnady C.J.H., Ben-Avraham Z. and Rogers J., 1992. Deep-ocean basins and submarine rises off the continental margin of south-eastern Africa: new geological research. S. Afr. J. Sci. 88, 534–539.

Henry, L.A., Frank, N., Hebbeln, D., Wienberg, C., Robinson, L., de Flierdt, T.v., Dahl, M., Douarin, M., Morrison, C.L., Correa, M.L., Rogers, A.D., Ruckelshausen, M., Roberts, J.M., 2014. Global ocean conveyor lowers extinction risk in the deep sea. Deep Sea Research Part I: Oceanographic Research Papers 88, 8–16.

Hernández-Molina, F.J., Paterlini.M., Somoza, L., Violante, R., Arecco, M.A., de Isasi, M., Rebesco, M., Uenzelmann-Neben, G., Neben, S., Marshall, P., 2010. Giant mounded drifts in the Argentine Continental Margin: Origins, and global implications for the history of thermohaline circulation. Marine and Petroleum Geology 27, 1508–1530.

Holbrook, W., 2001. Seismic studies of the Blake Ridge: implications for hydrate distribution, methane expulsion, and free gas dynamics. In: Paull, C., Dillon, W., (eds.), Natural Gas Hydrates: Occurrence, Distribution, and Detection. American Geophysical Union, Geophysical Monograph 124, 235–256.

Holbrook, W., Lizarralde, D., Pecher, I., Gorman, A., Hackwith, K., Hornbach, M., Saffer, D., 2002. Escape of methane gas through sediment waves in a large methane hydrate province. Geology 30(5), 467–470.

Horner-Johnson, B.C., Gordon, R.G., Argus, D.F., 2007. Plate kinematic evidence for the existence of a distinct plate between the Nubian and Somalian plates along the Southwest Indian Ridge. Journal of Geophysical Research 112, B05418. doi:10.1029/2006JB004519.

Howe, J.A., 1996. Turbidite and contourite sediment waves in the northern Rockall Trough, North Atlantic Ocean. Sedimentology 43, 219–234.

Hudec, M.R., Jackson, M.P.A., 2007. Terra infirma: Understanding salt tectonics. Earth-Science Reviews 82, 1–28.

Ikehara, K., Kinoshita, Y., 1994. Distribution and origin of subaqueous dunes on the shelf of Japan. Marine Geology 120, 75–87.

International Seismological Centre, On-line Bulletin, 2011. http://www.isc.ac.uk, International Seismological Centre, Thatcham, United Kingdom.

Jacobi, R.D., 1982. Microphysiographie du Sud-Est de l'Atlantique Nord et ses conse´quences pour la distribution des processus pre`s du fond marin et des facie`s associe´s. Bull. Inst. Geol. Bassin Aquitaine, Bordeaux 31, 31–46.

Jobe, Z.R., Lowe, D.R., Uchytil, S.J., 2011. Two fundamentally different types of submarine canyons along the continental margin of Equatorial Guinea. Marine and Petroleum Geology 28(3), 843–860.

Johnson, D.A., Damuth, J.E., 1979. Deep thermohaline flow and current controlled sedimentation in the Amirante Passage: western Indian Ocean. Marine Geology 33, 1–44.

Jokat, W., 2006. Southeastern Atlantic and Southwestern Indian Ocean: Reconstruction of the Sedimentary and Tectonic Development Since the Cretaceous, AISTEK-II: Mozambique Ridge and Mozambique Basin. Report of the RV "Sonne" Cruise SO-183, Project AISTEK-II 20 May to 7 July 2005 Reports on Polar and Marine Research. Alfred-Wegener-Institute for Polar and Marine Research, Bremerhaven, pp. 71.

Jokat, W., 2009. The Expedition of the Research Vessel "Pelagia" to the Natal Basin and the Mozambique Ridge in 2009 (Project AISTEK III). Alfred-Wegener-Institute for Polar and Marine Research, Bremerhaven, pp. 67.

Kelling, G., Maldonado, A., Stanley, D.J., 1979. Salt Tectonics and Basement Fractures: Key Controls of Recent Sediment Distribution on the Balearic Rise, Western Mediterranean. Smithsonian Institute Press, pp. 1–52.

Kenyon, N.H., Belderson, R.H., 1973. Bedforms of the Mediterranean undercurrent observed with sidescan sonar. Sediment. Geol. 9, 77–99.

Kenyon, N.H., Belderson, R.H., Stride, A.H., 1978. Channels, canyons and slump folds on the continental slope between south-west Ireland and Spain. Oceanol Acta 1, 369–380.

Kenyon, N.H., 1986. Evidence from bedforms for a strong poleward current along the upper continental slope of NW Europe. Marine Geology 72, 187–198

Klaucke, I., Hesse, R., Ryan, W.B.F., 1997. Flow parameters of turbidity currents in a low-sinuosity giant deep-sea channel. Sedimentology 44, 1093 – 1102.

Klausen, M.B., 2009. The Lebombo monocline and associated feeder dyke swarm: Diagnostic of a successful and highly volcanic rifted margin? Tectonophysics, 468(1–4), 42–62.

Kodagali, V.N., 1989. Morphometric studies on a part of Central Indian Ocean. J. Geol. Soc. India 33, 89–94.

Koehn, D., Aanyu, K., Haines, S., Sachau, T., 2008. Rift nucleation, rift propagation and the creation of basement micro-plates within active rifts. Tectonophysics 458, 105–116.

Kolla, K., Sullivan, L., Streeter, S., and Langseth, M., 1976. Spreading of Antarctic bottom water and its effects on the floor of the Indian Ocean inferred from bottom-water potential temperature, turbidity and sea-floor photography. Marine Geology 21, 171–189.

Kolla, V., Eittreim, S., Sullivan, L., Kostecki, J.A., Burckle, L.H., 1980.Current-controlled, abyssal microtopography and sedimentation in Mozambique Basin, Southwest Indian Ocean. Marine Geology 34, 171–206.

Kolla, V., 2007. A reviewof sinuous channel avulsion patterns in some major deep-sea fans and factors controlling them. Marine and Petroleum Geology 24, 450–469.

Koyi, H., 1997. The shaping of salt diapirs. Journal of Structural Geology 20, 321–338.

Laberg, J.S., Guidard, S., Mienert, J., Vorren, T.O., Haflidason, H., Nygard, A., 2007. Morphology and morphogenesis of a high-latitude canyon; the Andøya canyon, Norwegian Sea. Marine Geology 246, 68–85.

Lastras, G., Acosta, J., Muñoz, A., Canals, M., 2011. Submarine canyon formation and evolution in the Argentine Continental Margin between 44°30'S and 48°S. Geomorphology 128, 116–136.

Lee, S.H., Choughs S.K., 2001. High-resolution (2-7 kHz) acoustic and geometric characters of submarine creep deposits in the South Korea Plateau, East Sea. Sedimentology 48, 629–644.

Lee, S.H., Chough S.K., Back G.G., Kim, Y.B., 2002. Chirp (2–7 kHz) echo characters of the South Korea Plateau, East Sea: styles of mass movement and sediment gravity flow. Marine Geology 3042, 1–21.

Lee, H.J., Syvitski, J.P.M., Parker, G., Orange, D., Locat, J., Hutton, E.W.H., Imran, J., 2002. Distinguishing sediment waves from slope failure deposits: field examples, including the ‘‘Humboldt Slide”, and modelling results. Marine Geology 192, 79–104.

Lee, T.-G., Hein, J.R., Lee, K., Moon, J.-W., Ko, Y.-T., 2005. Sub-seafloor acoustic characterization of seamounts near the Ogasawara Fracture Zone in the western Pacific using chirp (3–7 kHz) subbottom profiles. Deep Sea Research Part I: Oceanographic Research Papers 52(10), 1932–1956.

Leinweber, V.T., Jokat, W., 2011. Is there continental crust underneath the northern Natal Valley and the Mozambique Coastal Plains? Geophysical Research Letters 38, L14303.

Leinweber, V.T., Jokat, W., 2012. The Jurassic history of the Africa-Antarctica Corridor: new constraints from magnetic data on the conjugate continental margins. Tectonophysics. http://dx.doi.org/10.1016/j.tecto.2011.11.008.

Li, C., von Storch, J.S., Marotzke, J., 2013. Deep-ocean heat uptake and equilibrium climate response. Climate Dynamics 40(5-6), 1071–1086

Liu, Z., Li, J., 2011. Control of salt structures on hydrocarbons in the passive continental margin of West Africa. Petroleum Exploration and Development 38(2), 196–202.

Lonsdale, P., Malfait, B., 1974. Abyssal dunes of foraminiferal sand on the Carnegie Ridge. GSA Bull 85, 1697–1712.

Lonsdale, P.F., Speiss, F.N. 1977. Abyssal bedforms explored with a deeply towed instrument package. Marine Geology 23, 57–75.

Lu, H., Moran, C.J., Prosser, I.P., 2006. Modelling sediment delivery ratio over the Murray Darling Basin. Environmental Modelling& Software 21, 1297–1308.

Lutjeharms, J.R.E., 2006a. The Agulhas Current. Springer-Verlag, Berlin pp. 329.

Lutjeharms, J.R.E., 2006b. The coastal oceans of south-eastern Africa. In: Robinson A.R., Brink, K.H., (eds.), The Sea. Harvard University Press Cambridge MA 14B, 783–834.

Lutjeharms, J.R.E., 2007. Three decades of research on the greater Agulhas Current. Ocean Sci. 3(1), 129–147.

Mahanjan, E.S., 2012. A geotectonic history of the northern Mozambique Basin including the Beira High - A contribution for the understanding of its development. Marine and Petroleum Geology 36, 1–12.

Maia, M., Diament, M., Recq, M., 1990. Isostatic response of the lithosphere beneath the Mozambique Ridge (SW Indian Ocean) and geodynamic implications. Geophysical Journal International 100, 337–348.

Maina, J., de Moel, H., Vermaat, J.E., Henrich Bruggemann, J., Guillaume, M.M.M., Grove, C.A., Madin, J.S., Mertz-Kraus, R. and Zinke, J., 2012. Linking coral river runoff proxies with climate variability, hydrology and land-use in Madagascar catchments. Marine Pollution Bulletin 64(10), 2047–2059.

Maldonado, A., Barnolas, A., Bohoyo, F., Galindo-Zaldívar, J., Hernández-Molina, J., Lobo, F., Rodríguez-Fernández, J., Somoza, L., Tomás Vázquez, J., 2003. Contourite deposits in the central Scotia Sea: the importance of the Antarctic Circumpolar Current and the Weddell Gyre flows. Palaeogeography, Palaeoclimatology, Palaeoecology 198(1–2), 187–221.

Malinverno, A., Ryan, W.B.F., Auffret, G., Pautot, G., 1998. Sonar images of the path of recent failure events on the continental margin off Nice, France. GSA Spec. Pap. 229, 59–76.

Manley, P.L., Caress, D.W., 1994. Mudwaves on the Gardar sediment drift, NE Atlantic Paleoceanography 9, 973–988.

Martin, A.K., 1981a. The influence of the Agulhas Current on the physiographic development of the northernmost Natal Valley (SW Indian Ocean). Marine Geology 39, 259–276.

Martin, A.K., 1981b. Evolution of the Agulhas Current and its palaeoecological implications. South African Journal of Science 77, 547–554.

Martin, A.K., Goodlad, S.W., Hartnady, C.J.H., du Plessis, A., 1982. Cretaceous palaeopositions of the Falkland Plateau relative to southern Africa using Mesozoic seafloor spreading anomalies. The Geophysical Journal of the Royal Astronomical Society 71, 567–579.

Martin, A.K., 1984. Plate tectonic status and sedimentary basin in-fill of the Natal Valley (S.W. Indian Ocean). Joint Geological Survey/University of Cape Town. Marine Geoscience Unit Bulletin 14, pp. 209.

Martin, A.K., Hartnady, C.J.H., 1986. Plate tectonic development of the south-west Indian Ocean: a revised reconstruction of East Antarctica and Africa. Journal of Geophysical Research 91, 4767–4786.

Martin, A.K., 1987. A comparison of sedimentation rates in the Natal Valley, S.W. Indian Ocean, with modern sediment yields in east coast rivers, Southern Africa. South African Journal of Science 83, 716–724.

Martin, A.K., Flemming, B.W., 1988. Physiography, structure and geological evolution of the Natal continental shelf. In: Schumann, E., (ed.), Lecture Notes on Coastal and Estuarine Studies off Natal, South Africa. Springer, New York, pp. 11–46.

Martínez-Méndez, G., Zahn, R., Hall, I.R., Pena, L.D., Cacho, I., 2008. 345,000-year-long multi-proxy records off South Africa document variable contributions of Northern versus Southern Component Water to the Deep South Atlantic. Earth and Planetary Science Letters 267(1–2), 309–321.

Masson, D.G., Watts, A.B., Gee, M.J.R., Urgeles, R., Mitchell, N.C., Le Bas, T.P., Canals, M., 2002. Slope failures on the flanks of the western Canary Islands. Earth Sci. Rev. 57(1–2), 1–35. dx.doi.org/10.1016/S0012-8252(01)00069-1

Mayall, M., Lonergan, L., Bowman, A., James, S., Mills, K., Primmer, T., Pope, D., Rogers, L., Skeene, R., 2010. The response of turbidite slope channels to growth induced seabed topography. AAPG Bulletin 94, 1011–1030.

McCave, I.N., Hollister, C.D., 1985. Sedimentation under deep-sea current systems: Pre-HEBBLE ideas. In: Nowell, A.R.M., Hollister, C.D., (eds.), Deep Ocean Sediment Transport- Prelimenary Results of the High Energy Benthic Boundary Layer Experiment. Marine Geology 66, 13–34.

McDonagh, E.L., Bryden, H.L., King, B.A., Sanders, R.J. 2008. The circulation of the Indian Ocean at 32°S. Progress in Oceanography 79, 20–36.

McGregor, B.A., 1981. Smooth seaward-dipping horizons - an important factor in sea-floor stability? Marine Geology 34, 3–4.

McHargue, T., Pyrcz, M.J., Sullivan, M.D., Clark, J.D., Fildani, A., Romans, B.W., Covault, J.A., Levy, M., Posamentier, H.W., Drinkwater, N.J., 2011. Architecture of turbidite channel systems on the continental slope: patterns and predictions. Marine and Petroleum Geology 28, 728–743.

Menary, M., Scaife, A., 2014. Naturally forced multidecadal variability of the Atlantic meridional overturning circulation. Climate Dynamics 42(5–6), 1347–1362.

Migeon. S., Savoye, B., Faugeres, J-C., 2000. Quaternary development of migrating sediment waves in the Var deep-sea fan: distribution, growth pattern, and implication for levee evolution. Sediment. Geol. 133, 265–293.

Migeon, S., Savoye, B., Zanella, E., Mulder, T., Faugeres, J-C., Weber, O., 2001. Detailed seismic-reflection and sedimentary study of turbidite sediment waves on the Var Sedimentary Ridge (SE France): significance for sediment transport and deposition and for the mechanics of sediment-wave construction. Mar. Pet. Geol. 18,179–208.

Miller, K.G., Mountain, G.S., Browning, J.V., Kominz, M., Sugarman, P.J., Christie-Blick, N., Katz, M.E., Wright, J.D., 1998. Cenozoic global sea level, sequences, and the New Jersey transect: results from coastal plain and continental slope drilling. Reviews of Geophysics 36, 569–601.

Miller, K.G., Kominz, M., Browning, J.V., Wright, J.D., Mountain, G.S., Katz, M.E., Sugarman, P.J., Cramer, B.S., Christie-Blick, N., Pekar, S.F., 2005. The Phanerozoic record of global sea-level change. Science 310, 1293–1298.

Mitchell, N.C., 2004. Form of submarine erosion from confluences in Atlantic USA continental slope canyons. American Journal of Science 304, 590–611.

Mitchell, N.C., 2005. Interpreting long-profiles of canyons in the USA Atlantic continental slope. Marine Geology 214, 75–99.

Mollel, G.F., Swisher, C.C., 2012. The Ngorongoro Volcanic Highland and its relationships to volcanic depositsat Olduvai Gorge and East African Rift volcanism. Journal of Human Evolution 63, 275–283.

Moore, A.E., Blenkinsop, T.G., 2006. Scarp retreat versus pinned drainage divide in the formation of the Drakensberg escarpment, southern Africa. South African Journal of Geology 109, 455–456.

Morley, C.K., 1999. Geoscience of rift systems-evolution of East Africa. AAPG Studies in Geology 44 pp. 242.

Morris, S.A., Kenyon, N.H., Limonov, A.F., Alexander, J., 1998. Downstream changes of large-scale bedforms in turbidites around the Valencia channel mouth, north-west Mediterranean: implications for paleoflow reconstruction. Sedimentology 45, 365–377.

Mougenot, D., Recq, M., Virlogeux, P., Lepvrier, C., 1986. Seaward extension of the East African Rift. Nature 321, 599–603.

Mukhopadhyay, R., Batiza, R., 1994. Basinal seamounts and seamount chain of the Central Indian Ocean: probable near-axis origin from fast spreading ridge. Mar. Geophys. Res. 16, 303–314.

Mukhopadhyay, R., Khadge, N.H., 1990. Seamount in the Central Indian Ocean Basin: indicator of the Indian plate movement. Proc. Indian Acad. Sci., Earth Planet. Sci. 99(3), 357–365.

Mulder, T., 2011. Gravity Processes and Deposits on Continental Slope, Rise and Abyssal Plains. In: Huneke, H., Mulder, T., (eds.), Developments in Sedimentology 63, pp. 1–850.

Mulder, T., Syvitski, J.P.M., 1995, Turbidity currents generated at river mouths during exceptional discharges to the world oceans. Journal of Geology 103, 285–299. doi:10.1086/629747.

Mutti, E., Tinterri, R., Remacha, E., Mavilla, N., Angella, S., Fava, L., 1999. An introduction to the analysis of ancient turbiditic basins from an outcrop perspective: AAPG, Continuing Education, Course Note Series 39.

Nakajima, T., Satoh, M., 2001. The formation of large mudwaves by turbidity currents on the levees of the Toyama deep-sea channel, Japan Sea. Sedimentology 48, 435–463.

Niemi, T.M., Ben-Avraham, Z., Hartnady, C.J.H., Reznikov, M., 2000. Post-Eocene seismic stratigraphy of the deep ocean basin adjacent to the southeast African continental margin: a record of geostrophic bottom current systems. Marine Geology 162(2–4), 237–258.

Normark, W.R., Hess, G.R., Stow, D.A.V., Bowen, A.J., 1980. Sediment waves on the Monterey Fan levee: a preliminary physical interpretation. Marine Geology 37, 1–18.

Norton, I. O., Sclater, J. G., 1979. A model for the evolution of the Indian Ocean and the breakup of Gondwanaland. J. Geophys. Res., 84(B12), 6803–6830.

O'Leary, D.W.O., Laine, E., 1996. Proposed criteria for recognizing intrastratal deformation features in marine high resolution seismic reflection profiles. Geo-Mar. Lett. 16, 305–312.

Orsi, A.H., Johnson, G.C., Bullister, J.L., 1999. Circulation, mixing, and production of Antarctic Bottom Water. Progress in Oceanography 43, 55–109.

Ovechkina, M.N., Watkeys, M.K., Kretzinger, W.R., 2009. Nannoplankton in the manganese deposits of the Mozambique Ridge and Mozambique Basin, SW Indian Ocean. Palaeontologica Africana 44, 126–128.

Partridge, T.C., Maud, R.R., 2000. Macro-scale geomorphic evolution of southern Africa. In: Partridge, T.C., Maud, R.R., (eds.), The Cenozoic of Southern Africa. Oxford University Press, New York, pp. 3–18.

Peakall, J., Kane, I.A., Masson, D.G., Keevil, G., McCaffrey, W.D., Corney, R., 2012. Global (latitudinal) variation in submarine channel sinuosity. Geology 40, 11–14. doi:10.1130/G32295.1.

Pearce, A.F., 1977. Some features of the upper 500m of the Agulhas Current. Journal of Marine Research 35(4), 731–753.

Perritt, S., Watkeys, M.K., 2007. The effects of environmental controls on the metal content in ferromanganese encrustations and nodules from the Mozambique Ridge and in the

Mozambique Basin, southwestern Indian Ocean. South African Journal of Geology 110, 295–310.

Piper, D.J.W., Shor, A.N., Farre, J.A., O'Connell, S., Jacobi, R., 1985. Sediment slides and turbidity currents on the Laurentian Fan: sidescan sonar observations near the epicentre of the 1929 Grand Banks earthquake. Geology 13, 538–541

Piper, D.J.W., Normark, W.R., 2001, Sandy fans—From Amazon to Hueneme and beyond: American Association of Petroleum Geologists Bulletin 85, 1407–1438. doi:10.1306/8626CACD-173B-11D7-8645000102C1865D.

Piper, D.J.W., Normark, W.R., 2009. Processes that initiate turbidity currents and their influence on turbidites: A marine geology perspective. Journal of Sedimentary Research 79, 347–362. doi:10.2110/jsr.2009.046.

Pirmez, C., Beaubouef, R.T., Friedmann, S.J., Mohrig, D.C., 2000. Equilibrium profile and baselevel in submarine channels: examples from Late Pleistocene systems and implications for the architecture of deepwater reservoirs, Deepwater Reservoirs of the World, GCSSEPM Foundation 20th Annual Research Conference, 782–805.

Polzin, K.L., Toole, J.M., Ledwell, J.R., Schmitt, R.W., 1997. Spatial Variability of Turbulent Mixing in the Abyssal Ocean. Science 276, 93–96.

Pratson, L.F., Ryan, W.B.F., Mountain, G.S., Twitchell, D.C., 1994. Submarine canyon initiation by downslope-eroding sediment flows: evidence in late Cenozoic strata on the New Jersey continental slope. Geological Society of America, Bulletin 106, 395–412.

Preu, B., Spieß, V., Schwenk, T., Schneider, R.R., 2011. Evidence for current-controlled sedimentation along the southern Mozambique continental margin since Early Miocene times. Geo-Marine Letters 31(5-6), 427–435. doi:10.1007/s00367-011-0238-y

Quartly, G.D., Srokosz, M.A., 2004. Eddies in the Southern Mozambique Channel. Deep-Sea Research II 51, 69–83.

Quartly, G.D., Buck, J.J.H., Srokosz, M.A., Coward, A.C., 2006. Eddies around Madagascar - The retroflection re-considered. Journal of Marine Systems 63, 115–129.

Ramsay, P., Smith, A.M., Mason, T.R., 1996. Geostrophic sand ridge, dune fields and associated bedforms. International Association of Sedimentologists 43, 407–419.

Raymo, M.E., Ruddiman, W.F., Shackleton, N.J., Oppo, D.W. 1990. Evolution of Atlantic-Pacific gradients over the last 2.5 m.y. Earth and Planetary Science Letters 97. 353–368.

Raymo, M.E., Oppo, D.W., Curry, W., 1997. The mid-Pleistocene climate transition: A deep sea carbon isotopic perspective. Paleoceanography 12, 546–559.

Reading, H.G., Richards, M., 1994. Turbidite systems in deep-water basin margins classified by grain size and feeder system. American Association of Petroleum Geologists Bulletin 78, 792–822.

Richards, M., Bowman, M., Reading, H., 1998. Submarine-fan systems i: characterization and stratigraphic prediction. Marine and Petroleum Geology 15, 689–717.

Ridderinkhof, H., de Ruijter, W.P.M., 2003. Moored current observations in the Mozambique Channel. Deep Sea Research Part II. Topical Studies in Oceanography 50(12–13), 1933–1955.

Ridente, D., Foglini, F., Minisini, D., Trincardi, F., Verdicchio, G., 2007. Shelf-edge erosion, sediment failure and inception of Bari canyon on the Southwestern Adriatic Margin (Central Mediterranean). Marine Geology 246, 193–207.

Ridderinkhof, H., VanderWerf, P.M., Ullgren, J.E., Van Aken, H.M., Van Leeuwen, P.J., De Ruijter, W.P.M., 2010. Seasonal and interannual variability in the Mozambique Channel from moored current observations. J. Geophys. Res.115, C06010.

Rutberg, R.L., Hemming, S.R., Goldstein, S.L., 2000. Reduced North Atlantic Deep Water flux to the glacial Southern Ocean inferred from neodymium isotope ratios. Nature 405, 935–938.

Ruppel, C., 1995. Extensional processes in continental lithosphere. Journal of Geophysical Research 100(24), 187–215.

Saria, E., Calais, E., Altamimi, Z., Willis, P. Farah, H., 2013. A new velocity field for Africa from combined GPS and DORIS space geodetic Solutions: Contribution to the

definition of the African reference frame (AFREF). Journal of Geophysical Research: Solid Earth 118(4), 1677–1697.

Saria, E., Calais, E., Stamps, D.S., Delvaux, D., Hartnady, C.J.H., 2014. Present-day kinematics of the East African Rift. J. Geophys. Res. Solid Earth 119, 3584–3600. doi:10.1002/2013JB010901

Schlüter, P., Uenzelmann-Neben G., 2007. Seismostratigraphic analysis of the Transkei Basin: A history of deep sea current controlled sedimentation. Marine Geology 240, 99–111.

Schlüter, P., Uenzelmann-Neben, G., 2008. Indications for bottom current activity since Eocene times: the climate and ocean gateway archive of the Transkei Basin, South Africa. Global and Planetary Change 60, 416–428.

Schmidt, D.L., Rowley, P.D., 1986. Continental rifting and transform faulting along the Jurassic Transantarctic Rift, Antarctica. Tectonics 5(2), 279–291.

Schmieder, F., von Dobeneck, T., Bleil, U., 2000. The Mid-Pleistocene climate transition as documented in the deep South Atlantic Ocean: initiation, interim state and terminal event. Earth and Planetary Science Letters 179, 539–549.

Schouten, M.W., DeRuijter, W.P.M., Van Leeuwen, P.J., Ridderinkhof, H., 2003. Eddies and variability in the Mozambique Channel. Deep-Sea Res. II 50, 1987–2003.

Schulz, H., Lückge, A., Emeis, K., Mackensen, A., 2011. Variability of Holocene to Late Pleistocene Zambezi riverine sedimentation at the upper continental slope off Mozambique, 15°–21°S. Marine Geology 286, 21–34.

Schwehr, K., Driscoll, N., Tauxe, L., 2007. Origin of continental margin morphology: Submarine-slide or downslope current-controlled bedforms, a rock magnetic approach: Marine Geology 240, 19–41. doi:10.1016/j.margeo.2007.01.012.

Scrutton, R.A., 1978. Davie Fracture Zone and the Movement of Madagascar. Earth and planetary science letters, 39(1), 84–88.

Shaw, J., Lesemann, J.-E., 2003, Subglacial outburst floods and extreme sedimentary events in the Labrador Sea. In: Chan, M.A., Archer, A.W., (eds.), Extreme depositional

environments: Mega end members in geologic time. Geological Society of America Special Paper 370, pp. 25–41. doi:10.1130/0-8137-2370-1.25.

Shillington, D.J., Seeber, L., Sorlien, C.C., Steckler, M.S., Kurt, H., Dondurur, D., Çifçi, G., İmren, C., Cormier, M.H., McHugh, C.M.G., Gürçay, S., Poyraz, D., Okay, S., Atgın, O., Diebold, J.B., 2012. Evidence for widespread creep on the flanks of the Sea of Marmara transform basin from marine geophysical data. Geology 40(5), 439–442.

Simpson, E.S.W., Sclater, J.G., Parsons, B., Norton, I., Meinke, L., 1979. Mesozoic magnetic lineations in the Mozambique Basin. Earth and Planetary Science Letters 43, 260–264.

Shone, R.W., 2006. Onshore post-Karoo Mesozoic deposits. In: Johnson, M.R., Anheuser, C.R., Thomas, R.J., (eds.), The Geology of South Africa. The Geological Society of South Africa, Johannesburg/Council for Geoscience, Pretoria pp. 541–553.

Smith, D.K., 1988. Shape analysis of Pacific seamounts. Earth Planet.Sci. Lett. 90, 457–466.

Srinivasan, A., Garraffo, Z., Iskandarani, M., 2009. Abyssal circulation in the Indian Ocean from a resolution global hindcast. Deep Sea Research I: Oceanographic Research Papers 56(11), 1907–1926.

Stamps, D.S., Calais, E., Saria, E., Hartnady, C., Nocquet, J.-M., Ebinger, C. J., Fernandes, R. M., 2008. A kinematic model for the East African Rift, Geophys. Res. Lett., 35, L05304.

Stramma, L., Lutjeharms, J.R.E., 1997. The flow field of the subtropical gyre of the South Indian Ocean. J. Geophys. Res. 102, 5513-5530.

Stow, D.A.V., Reading, H.G., Collison, J.D., 1996. Deep seas. In: Reading H.G., (ed.) Sedimentary Environments: Processes, Facies and Stratigraphy. Blackwell Science Oxford, pp. 395–453.

Stow, D.A.V., Mayall, M., 2000. Deep-water sedimentary systems: New models for the 21st century. Marine and Petroleum Geology 17(2), 125–135.

Syvitski, J.P.M., Burrell, D.C., Skei, J.M., 1987. Fjords: Processes and Products. Springer Verlag, New York, pp. 379.

Thompson, G., Bryan, W.B., Frey, F.A., Dickey, J.S., Davies, H., 1982. Petrology, geochemistry and original tectonic setting of basalts from the Mozambique Basin and Ridge (DSDP sites 248, 249 and 250), and from the southwest Indian Ocean. Marine Geology 48, 175–195.

Toole, J.M., Warren, B.A., 1993. A hydrographic section across the subtropical South Indian Ocean. Deep Sea Research I 40, 1973–2019.

Tinti, S., Maramai, A., Favali, P., 1995. The Gargano Promontory: an important Italian seismogenetic–tsunamigenic area. Marine Geology 122, 227–241.

Trincardi, F., Cattaneo, A., Correggiari, A., Ridente, D., 2004. Evidence of soft sediment deformation, fluid escape, sediment failure and regional weak layers within the late Quaternary mud deposits of the Adriatic Sea. Marine Geology 213(1–4), 91–119

Tucholke, B.E., 1979. Furrows and focuses echoes on the Blake Outer Ridge. Marine Geology 31, 13–20.

Türkay, M., Pätzold, J., (eds.), 2009. Southwestern Indian Ocean e Eastern Atlantic Ocean, Cruise No 63, January 24–March 30, 2005. METEOR-Berichte 09-3,Universität Hamburg, pp. 98.

Uenzelmann-Neben, G., Watkeys, M. K., Kretzinger, W., Frank, M., Heuer, L., 2010. Palaeoceanographic changes identified using seismic and radiogenic isotope data from the Mozambique Ridge, SW Indian Ocean. Geo-Temas 11, 173–174.

Ullgren, J.E., van Aken, H.M., Ridderinkhof, H., de Ruijter, W.P.M., 2012. The hydrography of the Mozambique Channel from six years of continuous temperature, salinity, and velocity observations. Deep Sea Research I Oceanographic Research Papers 69(0), 36–50.

Vachtman, D., Mitchell, N.C., Gawthorpe, R., 2012. Morphologic signatures in submarine canyons and gullies, central USA Atlantic continental margins. Marine and Petroleum Geology, 1–14.

van Aken, H.M., Ridderinkhof, H., de Ruijter, W.P.M., 2004. North Atlantic deep water in the south-western Indian Ocean. Deep-Sea Research I 51, 755–776.

Watkeys, M. K., 2006. Gondwana Break-up: A South African perspective. In: Johnson, M.R., Anheuser, C.R., Thomas, R.J., (eds.), The Geology of South Africa. The Geological Society of South Africa. Johannesburg/Council for Geoscience, Pretoria, pp. 531–539.

Walford, H.L., White, N.J., Sydow, J.C., 2005. Solid sediment load history of the Zambezi Delta. Earth and Planetary Science Letters 238, 49–63.

Wigley, R.A., Compton, J.S., 2006. Late Cenozoic evolution of the outer continental shelf at the head of the Cape Canyon, South Africa. Marine Geology 226, 1–23.

Wiles, E.A., 2009, Microtopography and bottom water circulation of the northern Mozambique Basin, southwest Indian Ocean. Unpublished honours thesis. Department of Geology, University of KwaZulu Natal, pp 62.

Wiles, E., Green, A., Watkeys, M., Jokat, W., Krocker, R., 2013. The evolution of the Tugela canyon and submarine fan: A complexinteraction between margin erosion and bottom current sweeping, southwest Indian Ocean, South Africa. Marine and Petroleum Geology 44, 60–70.

Wiles, E., Green, A., Watkeys, M., Jokat, W., Krocker, R., 2014. Anomalous seafloor mounds in the northern Natal Valley, southwest Indian Ocean: Implications for the East African Rift System. Tectonophysics 630, 300–312. dx.doi.org/10.1016/j.tecto.2014.05.030

Winter, A., Martin, A.K., 1990. Late Quaternary history of the Agulhas Current. Paleoceanography, 5(4), 479–486.

Wolfeden, E., Ebinger, C., Yirgu, G., Deino, A., Ayalew, D., 2004. Evolution of the northern Main Ethiopian Rift: Birth of a triple junction. Earth Planetary Science Letters 224, 213–228.

Wynn, R.B., Stow, D.A.V., 2002. Classification and characterisation of deep-water sediment waves. Marine Geology 192, 7–22.

Wynn, R.B., Masson, D.G., Stow, D.A.V., Weaver, P.P.E., 2000a. Turbidity current sediment waves on the submarine slopes of the western Canary Islands. Marine Geology 163, 185–198.

Wynn, R.B., Weaver, P.P.E., Ercilla, G., Stow, D.A.V., Masson, D.G., 2000b. Sedimentary processes in the Selvage sediment-wave field, NE Atlantic: new insights into the formation of sediment waves by turbidity currents. Sedimentology 47, 1181–1197.

Wynn, R.B., Cronin, B.T., Peakall, J., 2007, Sinuous deep-water channels: Genesis, geometry and architecture: Marine and Petroleum Geology 24, 341–387. doi:10.1016/j.marpetgeo.2007.06.001.

Wynn, R. B., Masson, D.G., 2008. Sediment waves and bedforms. In: Rebesco, M., Camerlenghi, A., (eds), Contourites. Developments in Sedimentology 60, pp. 289–300.

Zachos, J., Pangani, M., Sloan, L., Thomas, E., Billups, K., 2001. Trends, rhythms and aberrations in global climate 65 Ma to present. Science 292, 686–693.

Zhang, P., Molnar, P., Downs, W., 2001. Increased sedimentation rates and grain sizes 2–4 myr ago due to the influence of climate change on erosion rates. Nature 410, 891–897.

Appendix A

Tectonophysics 630 (2014) 300–312

Contents lists available at ScienceDirect

Tectonophysics

journal homepage: www.elsevier.com/locate/tecto

Anomalous seafloor mounds in the northern Natal Valley, southwest Indian Ocean: Implications for the East African Rift System

Errol Wiles [a,*], Andrew Green [a], Mike Watkeys [a], Wilfried Jokat [b], Ralph Krocker [b]

[a] Discipline of Geological Sciences, School of Agricultural, Earth and Environmental Sciences, University of KwaZulu-Natal, Private Bag X 54001, Durban 4000, South Africa
[b] Alfred-Wegener-Institute for Polar and Marine Research, Am Alten Hafen 26, D-27568 Bremerhaven, Germany

ARTICLE INFO

Article history:
Received 13 September 2013
Received in revised form 27 May 2014
Accepted 28 May 2014
Available online 2 June 2014

Keywords:
Natal Valley
Seafloor mounds
Southwest Indian Ocean
East African Rift System
Tectonics
Passive margin

ABSTRACT

The Natal Valley (southwest Indian Ocean) has a complicated and protracted opening history, as has the surrounding southwest Indian Ocean. Recently collected multibeam swath bathymetry and 3.5 kHz seismic data from the Natal Valley reveal anomalous seafloor mounds in the northern Natal Valley. The significance, of these domes, as recorders of the geological history of the Natal Valley and SE African Margin has been overlooked with little attempt made to identify their origin, evolution or tectonic significance. This paper aims to describe these features from a morphological perspective and to use their occurrence as a means to better understand the geological and oceanographic evolution of this basin. The seafloor mounds are distinct in both shallow seismic and morphological character from the surrounding seafloor of the Natal Valley. Between 25 km and 31 km long, and 16 km and 18 km wide, these features rise some 400 m above the sedimentary deposits that have filled in the Natal Valley. Such macro-scale features have not previously been described from the Natal Valley or from other passive margins globally. They are not the result of bottom water circulation, salt tectonics; rather, igneous activity is favoured as the origin for these anomalous seafloor features. We propose a hypothesis that the anomalous seafloor mounds observed in the Natal Valley are related to igneous activity associated with the EARS. The complicated opening history and antecedent geology, coupled with the southward propagation of the East African Rift System creates a unique setting where continental rift associated features have been developed in a marine setting.

1. Introduction

The geological evolution of the ocean basins is reflected in the shape and form of the deep seafloor (Cochran, 1981; Dietz, 1963; Goff and Jordan, 1988; Norton and Sclater, 1979). This typically comprises a variety of features that range in horizontal scales from the micro (10^{-3} km) to basin-scale (10^{4} km) level. At the macro scale (10 km and above), seafloor features are usually determined by the nature of the basin margins (passive vs. active), the location of oceanic ridges (including past spreading centres and abyssal hills) (cf. Goff et al., 1997; Leinweber and Jokat, 2011a,b), fracture zones (Cochran, 1981; Courtillot et al., 1999), and sediment input to the basin over time.

With respect to the shape and form of the deep seafloor, morphological characteristics may vary with the type of feature encountered. Parameters such as the height to width ratio, length to width ratio, slope angle and flatness are useful measures for the morphological comparison of different features. Furthermore, these parameters are suggestive of general formative processes related to the origin of seafloor features (Das et al., 2007; Kodagali, 1989; Mukhopadhyay and Batiza, 1994; Mukhopadhyay and Khadge, 1990; Smith, 1988).

This paper describes a series of macro scale (ca. 30 km) seafloor mounds in the Natal Valley, southwest Indian Ocean (SWIO). The Natal Valley has a complicated and protracted opening history, during the Jurassic and Cretaceous, which is reflected in the mixture of rifting, shearing and drifting of the margin, coupled with episodic submarine volcanism. The adjacent African continent, too, has a long tectonic and seismic history. Following the break-up of Gondwana (Watkeys, 2006), the East African Rift System (hereafter EARS) is by far the most dominant active feature on the continent (Chorowicz, 2005). The EARS represents a 3000 km long discrete intracontinental rift zone initiated some 30 Ma ago between the Nubian and Somalian plates (Calais et al., 2006). EARS rift kinematics have resulted in the development of two micro-plates, the northern Victoria plate, and southern Rovuma Plate, with a possible third micro-plate, Lwandle, developing further south (Calais et al., 2006; Stamps et al., 2008) through the interaction of several rift segments comprising the EARS (Koehn et al., 2008). The East African Rift is comparable in size to the West Antarctic Rift, and far more accessible as it lacks the ice cover of the West Antarctic Rift (Fig. 1, insets, lower right). Since the initiation of the EARS in the Afar region (NE Africa), rift propagation has been southward (Burke, 1996), developing

* Corresponding author. Tel./fax: +27 312602801.

http://dx.doi.org/10.1016/j.tecto.2014.05.030
0040-1951/

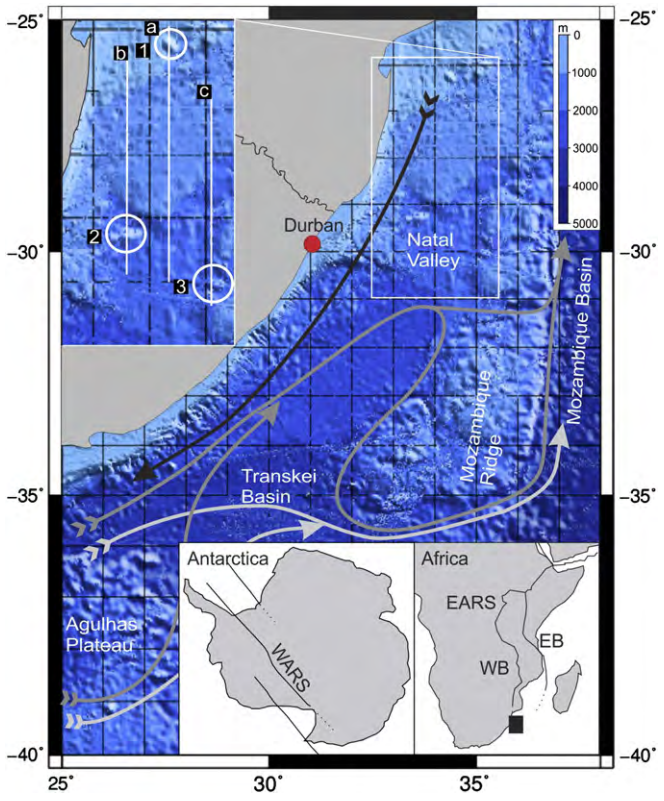

Fig. 1. The south-west Indian Ocean (The GEBCO_08 Grid, version 20091120), showing notable basin features. The black arrow shows passage of the Agulhas Current, the dark-grey arrow shows the NADW pathways, while the light grey arrows describe the route of the AABW. The study area (white box), offshore of Durban (red circle), is enlarged showing the location of the mounds. The mounds are identified as follows: 1 — northernmost, 2 — southwestern and 3 — southeastern. N–S transects (a, b and c) through the northern Natal Valley are depicted by white lines.
West Antarctic Rift System (WARS) inset modified after Schmidt and Rowley (1986).

two distinct southern extensions, the older eastern branch and younger western branch (Ebinger, 1989; Ruppel, 1995; Wolfeden et al., 2004). Both of these branches avoid the Archean cratons, taking advantage of Proterozoic orogenic belts which represent preferential avenues for rift propagation (Morley, 1999). The possible seaward extension of the eastern branch of the EARS was discussed by Mougenot et al. (1986). These workers suggested that the eastern branch joins up with the submerged Cretaceous age grabens (located on the Tanzanian continental shelf) associated with the drift of Madagascar away from Africa. There is renewed interest in this area, particularly in the vicinity of the Kerimbas Graben in the northern Mozambique Channel. Similarly, we discuss the possible southward extension of the western branch (southern Malawi Rift) into the Natal Valley.

The Natal Valley Mounds were partly documented previously (cf. Goodlad, 1986; Martin, 1984); however the significance of the mounds was not recognised at that time and were considered non-descript basement outcrop within the Natal Valley. Their significance as recorders of the geological history of the Natal Valley and SE African margin has been over-looked with little attempt made to identify their origin, evolution and tectonic significance. This paper aims to describe these features from a morphological and shallow seismic perspective and to use their occurrence as a means to better understand the geological and/or oceanographic evolution of this basin.

1.1. Previous bathymetric work

As in all other basins, early work in the Natal Valley relied heavily on high frequency seismic echo-character to describe the bathymetry and shallow sub-bottom characteristics of the seafloor (cf. Dingle and Camden-Smith, 1979; Dingle et al., 1978; Kolla et al., 1980). The primary focus of this was to establish the acoustic stratigraphy and magnetic character of the Natal Valley. The bathymetric and seismic data sets were of sufficiently high resolution to resolve basin-scale features but insufficient to resolve the scale and complexity of complicated seafloor features that are easily revealed with modern multibeam and high resolution seismic tools. With the introduction of multibeam swath bathymetry systems to scientific research (in conjunction with high frequency seismic systems); our capacity to document and describe the deep-sea floor at far higher resolutions has been greatly increased. Compared to Dingle et al. (1978), Goodlad (1986) and Martin (1984) were able to resolve significantly more of the Natal Valley, providing 20 m interval bathymetry charts, and seismic reflection profiles (with 10, 40, 300 cubic inch air-guns). Seismic coverage was such that the majority of the seafloor mounds were inadvertently missed, while the 20 m interval bathymetric charts could not resolve the complex seafloor in sufficient detail. Present technologies and techniques allow data to be acquired at far higher resolutions. The recent acquisition of multibeam swath bathymetry and high frequency seismic data in the Natal Valley is testament to this (cf. Wiles et al., 2013). It is from the perspective of increased resolution in both bathymetry and seismic data that we re-investigate aspects of the Natal Valley seafloor and shallow subsurface geomorphology.

2. Regional setting

2.1. Geology and physiography

The Natal Valley is a N–S orientated basin located in the SWIO (Fig. 1). Bound to the west by the south-eastern margin of southern Africa and to the east by the Mozambique Ridge, the Natal Valley shoals north from the deep Transkei Basin toward the extensive coastal plains of southern Mozambique (Dingle et al., 1978; Goodlad, 1986). Although both floored by an oceanic crust, the northern and the southern Natal Valley (Fig. 1) are the product of two distinct spreading centres. The former was created ca. 183–158 Ma (Leinweber and Jokat, 2011a) while the latter opened ca. 138.9–130.3 Ma (Leinweber and Jokat, 2011b). By 90 Ma spreading within the Natal Valley had ceased (Ben Avraham et al., 1993; Martin and Hartnady, 1986).

The western continental margin boundary of the Natal Valley exhibits a narrow, 4–15 km wide, coast-parallel shelf (Dingle and Robson, 1985; Green, 2011a,b). Departure from the narrow shelf is observed offshore of the Zambezi, Limpopo and Tugela rivers where sedimentary cones prograde into the Natal Valley (Dingle et al., 1978). Over the past 65 Ma, sediment input into the Natal Valley has been estimated at ca. 23 m^3/km^2/year; the Limpopo and Tugela rivers delivering the bulk of sediment to the basin which amounts to the deposition of approximately 800 m of sediment in the basin (Flemming, 1980; Partridge and Maud, 2000).

2.2. Oceanography

Bottom water (a deep current in contact with the seafloor) circulation within the Natal Valley is dominated by the equatorward flowing North Atlantic Deep Water (NADW). The passage of NADW (ca. 1.2×10^6 m^3 s^{-1}) into the Natal Valley is controlled by two, likely contemporaneous, systems (Fig. 1). The South Atlantic Current (SAC) facilitates the first (southern) pathway, transporting NADW around the southern tip of Africa. The NADW core then bifurcates; one branch (depth of 2000–3500 m, salinity of 34.83‰) continuing northeastward into the Natal Valley via the Agulhas and Transkei basins respectively. The second branch continues east beneath the meandering Agulhas Return Current (Toole and Warren, 1993).

The second (northern) NADW pathway flows along the continental slope, at depths between 2000 and 2500 m as it rounds the African

continent passing via the Agulhas Passage into the Transkei Basin on its approach to the Natal Valley (Schlüter and Uenzelmann-Neben, 2008; Toole and Warren, 1993). A component of NADW returns southward along the eastern boundary of the Natal Valley (constrained by the western slopes of the Mozambique Ridge), while a portion of it crosses a saddle (2500–3000 m depth) in the Mozambique Ridge at approximately 31°S latitude.

Antarctic Bottom Water does not enter the Natal Valley. Rather, it passes through the Transkei Basin and around the southern edge of the Mozambique Ridge entering the southern Mozambique Basin beneath the northward flowing NADW core (Toole and Warren, 1993).

3. Material and methods

Data from two recent research cruises are used in this study; AISTEK II aboard the R/V Sonne (Jokat, 2006) and AISTEK III aboard the R/V Pelagia (Jokat, 2009). The Mozambique Basin was the focus of AISTEK II, where bathymetric data were collected using a Kongsberg SIMRAD EM120 (12 kHz) system. AISTEK III focused on the Mozambique Ridge and Natal Valley, data were collected using a Kongsberg SIMRAD EM300 (30 kHz) system. Both data sets were processed using CARIS HIPS and exported as xyz ASCII files. The data were gridded using Interactive Visualization Systems' DMagic (version 7.3.1a) and displayed in Fledermaus (version 7.3.1a) for interpretation. The final bathymetric chart has an output matrix of ~35 m capable of resolving seafloor features at that approximate scale.

Very high frequency seismic data (vertical resolution ca. 1 m) were simultaneously collected using both a 3.5 kHz (AISTEK III) and a parametric ATLAS PARASOUND echosounder (AISTEKII). Complete seismic coverage along the track was in some instances not achievable due to technical difficulties. Data were processed using in-house designed software, in addition to SEISEE (version 2.17.1.). These data were incorporated into SEISEE for visualization and interpretation of the echo character. Band pass filter was adjusted and colour gains were applied to the data.

Morphological parameters for slope (average change in elevation over distance), flatness, height to width ratios (H/W), and length to width ratios (L/W) were measured (Fig. 2). The use of such parameters is common practice when investigating the morphology of sea-floor features (cf. Das et al., 2007; Kodagali, 1989; Mukhopadhyay and Batiza, 1994; Mukhopadhyay and Khadge, 1990; Smith, 1988). The slope angle is calculated as an average value describing the change in elevation over horizontal distance. The flatness parameter reflects the ratio of summit width to basal width. Changes in flatness are typically manifest in changes in slope angle, basal width and summit width, but not necessarily height. The H/W ratio is symptomatic of the flatness and slope parameters, thus changes in this ratio are associated with changes in flatness and slope angle (Das et al., 2007). The H/W ratio allows comparisons of submarine igneous features to be made and is suggestive of formative processes, varying from point to fissure type igneous sources (Kodagali, 1989; Mukhopadhyay and Batiza, 1994; Mukhopadhyay and Khadge, 1990; Smith, 1988). Das et al. (2007) describe four types of relationships between flatness and slope, with varying H/W ratio. Type one, for low H/W (<0.08) typically indicates low slope angles (<10°) and low flatness (<0.12). Varied slope angles (6–15°) and flatness (0.08–0.3) are associated with H/W ratios of 0.081 to 0.16 (Type 2). Type 3 intermediate H/W ratios (0.161–0.23) suggest high slope angles (>10°) and high flatness (>0.2). Height to width ratios of >0.23 are associated with high slope angles (>10°) and low to moderate flatness (<0.2) are typical of Type 4.

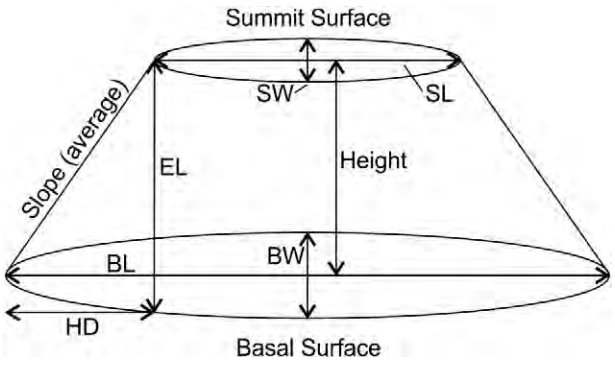

Fig. 2. The schematic above shows the various parameters that were used in the morphological analysis of sea-floor features. Flatness represents the ratio of summit width (SW) to basal width (BW), as measured from the summit and basal surfaces respectively. The height to width ratios is determined by the feature elevation in relation to its basal width. Basal length (BL) versus basal width (BW) gives the length to width ratio. While the slope angle is given by the average change in elevation (EL) over horizontal distance (HD) recorded from the feature.

4. Results

4.1. Bathymetry

The collected multibeam swath bathymetry data reveal three laterally extensive, macro scale, seafloor mounds (Figs. 3–5) in the northern Natal Valley. One is located in the northern portion of the northern Natal Valley (Fig. 3), while the two occur in the southern portion (Figs. 3 and 4). The bathymetric character of these mounds varies greatly from the character of the adjacent bathymetry. In general, the Natal Valley is typified by smooth seafloor with gradual changes in gradient, punctuated by rugged basement outcrop (mostly confined to the north). The Tugela cone (mid Natal Valley) provides a notable departure from the gentle gradient of the Natal Valley as it progrades into the basin from the South African east coastline.

Partial coverage of the northernmost mound (Fig. 3) shows a N–S orientated feature, 25.4 km in length and at least 3000 m wide, standing 472 m proud of the surrounding seafloor sediments. The crown occurs at a depth of 502 m. The flanks (crown to base) average a gradient of 7.3° with localised steepening of up to 30° on the northern flank. A moat, 25 m deep in the south, and 240 m deep in the north, is observed at the base of the mound. The moat merges with the shoaling bathymetry to the north.

Fig. 4 shows bathymetry data associated with the second mound, situated in the southwestern portion of the northern Natal Valley. Orientated E–W, this mound is 33 km in length and 17.5 km wide. The shallowest mapped portion of the mound is 420 m above the adjacent seafloor, at 1959 m deep. A discontinuous moat, 34 m deep, fronts the northern flanks of the mound. The moat is less prevalent in the east, where it merges with the smooth low gradient seafloor typical of the greater Natal Valley. The average gradient of the mound (crown to base) is 8.5° with a maximum of 44° on the steepened flanks.

The third mound (Fig. 5) is located in the southeastern portion of the Natal Valley, the crown lying at a depth of 1845 m. Like the previous mound, this is similarly E–W orientated. Overall it is 29.7 km long, with a width of 16.2 km and height of 422 m above the surrounding seafloor sediments. A discontinuous moat, 255 m deep, is observed along the northern flanks of the mound. More prevalent in the west, the moat narrows toward the east, terminating at the eastern extent of the mound with a relief of 50 m. The flanks of the mound have an average gradient of 11.3°, steepening to 31° in places.

Fig. 6 shows a perspective and plan view of rugged as well as smooth seafloor of the Natal Valley. The rugged seafloor is dominated by elongated conical features 100–350 m in height, reaching local maximums of 65° in gradient. The adjacent smooth seafloor shows gentle changes in gradient.

Fig. 7 depicts three profiles (a, b, and c) from transects through the bathymetry data, as well as a slope angle map for better discrimination of the seafloor types found in the area. The profiles are N–S transects

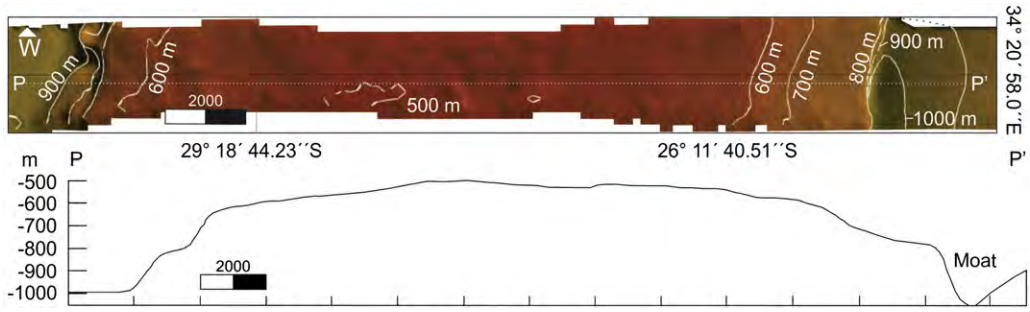

Fig. 3. The northernmost mound in plan view (north to the right). The convex crown, with off centre (to the south) apex is evident, as are the steepened flanks. There is very little distinction between the bathymetric character of the mound crown and adjacent smooth seafloor. The S–N profile (P–P′) below the bathymetry image clearly shows the mounded morphology of the feature.

through areas of smooth, rugged and mounded bathymetry (see Fig. 1 for profile locations). The overall smooth seafloor with gradual changes in gradient of the northern Natal Valley is clearly evident, as are the anomalous mounds. Rugged basement outcrop is shown in the enlargement of box ii, on profile a. This type of bathymetry is largely confined to the northern extent of the basin. The slope map showing a northern portion of profile a (box i) illustrates the distinct character of the mound, compared to smooth and rugged seafloor. Bands of steepened gradient are found on the mound flanks, while cones of steepened gradient (including the steepest gradients, ca. 65°) are associated with the flanks of rugged seafloor. The intervening smooth seafloor is fairly uniform in slope showing gentle changes in an overall low gradient, similar in character to the mound crown area. Areas of gentle slope are confined to the smooth seafloor and mound crowns. These are not typically associated with the crowns of the rugged seafloor, although smooth seafloor is noted in the valley floors between peaks of rugged bathymetry (Fig. 7).

4.2. High frequency seismic character

Figs. 8–10 show high frequency seismic records collected across two of the mounds. The echo character from the southwestern mound (Fig. 8, profiles a–a′ and b–b′) show limited penetration, semi-prolonged echoes as well as broad hyperbolic reflections with little variance in vertex depth below the seafloor and low angle sub-parallel reflectors (see Fig. 4 for profile locations).

The seismic profiles in Fig. 9 are associated with the southeastern mound (see Fig. 5 for profile locations). Three profiles (c–d, d–e, and e–f) show the varied reflector characteristics between different areas of the mound. Semi-prolonged echoes are noted once more, in conjunction with continuous isolated reflectors, discontinuous sub-parallel, continuous sub-parallel reflectors and chaotic reflectors. Continuous isolated reflectors are confined to the main body of the mound, while discontinuous and chaotic reflections are observed toward the rim of the mound.

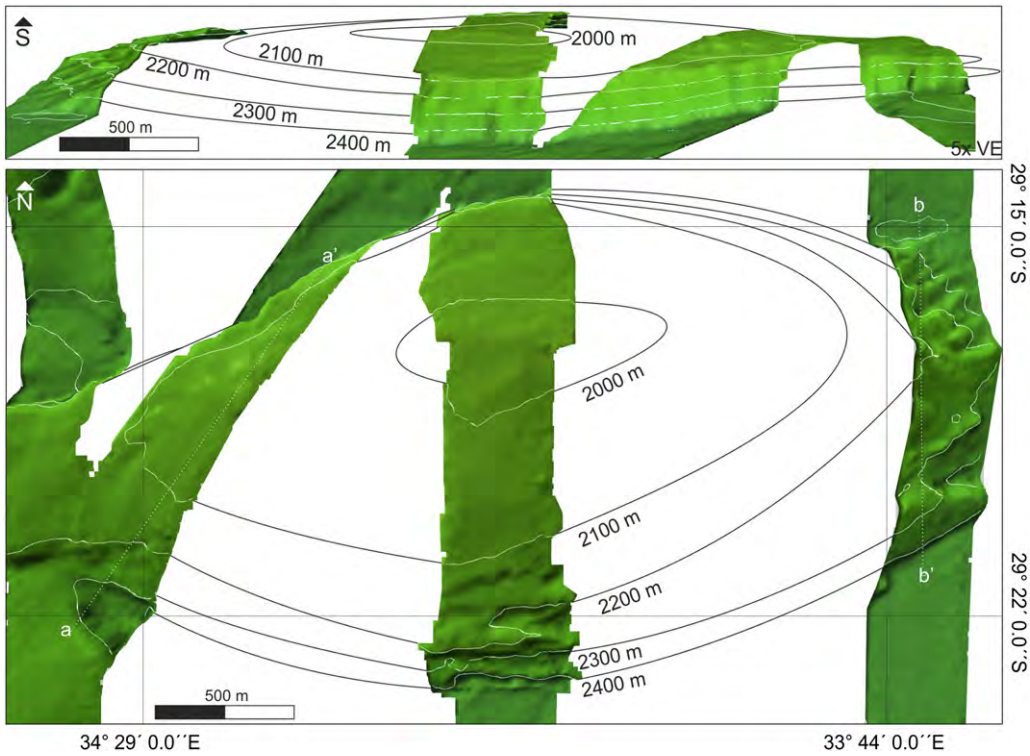

Fig. 4. The south western mound (perspective view above, plan view below), and locations of 3.5 kHz profiles (a–a′ and b–b′). Ridges are evident on the eastern and southern flanks of the mound.

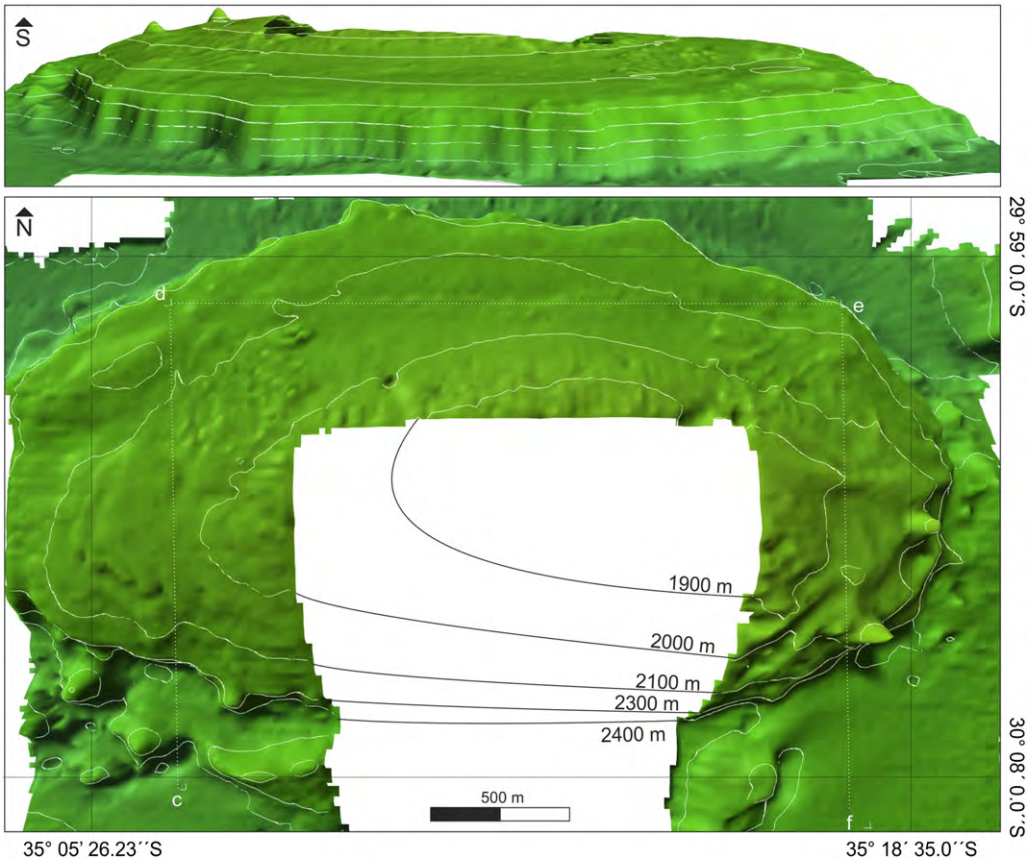

Fig. 5. Bathymetry of the south-eastern mound. The mound flanks, and convex crown are clearly evident in the perspective view (top), while in plan (bottom) the oval W–E orientation of the mound is clear. The location of 3.5 kHz profiles (c–d, d–e and e–f) is shown.

Vastly different echo character is observed elsewhere in the northern Natal Valley. Rugged seafloor shows distinct hyperbolic reflectors (Fig. 10), while smooth seafloor exhibits continuous to discontinuous sub-parallel reflectors (Fig. 9, southern portion of profile e–f). The hyperbolic echoes associated with rugged bathymetry display varied vertex elevations above the seafloor as well as varied amounts of overlap. Continuous to discontinuous sub-parallel reflectors are noted either side of the rugged terrain, and are prevalent throughout areas of smooth seafloor within the Natal Valley.

4.3. Morphological character

The morphological characteristics of the Natal Valley mounds are listed in Table 1, along with the morphological characteristics of similar

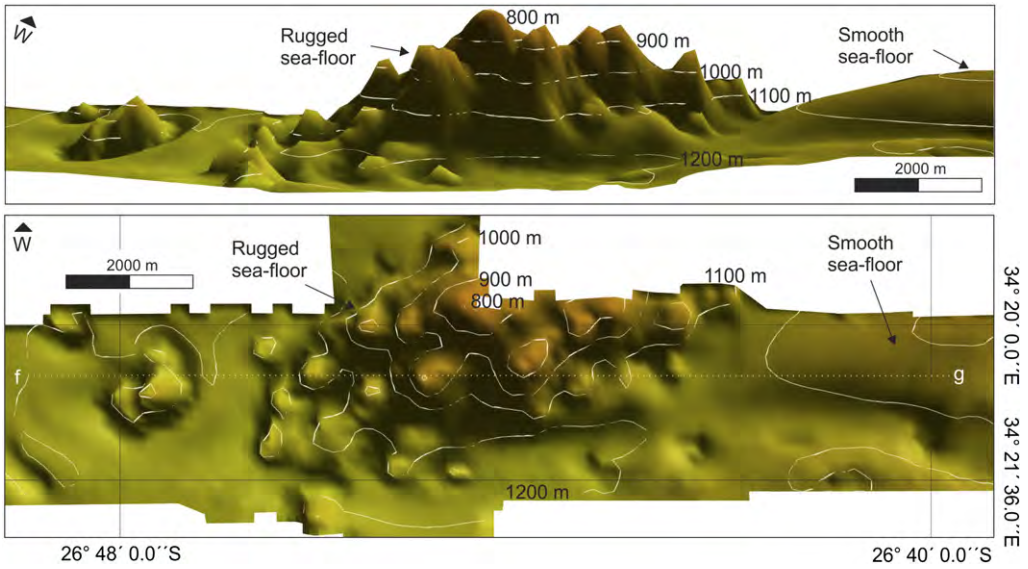

Fig. 6. Typical morphology of rugged seafloor, confined to the northern portion of the Natal Valley. The basement outcrop is conical in appearance. Note the perspective view on top and plan view on bottom. The 3.5 kHz seismic record associated with profile f–g is shown in Fig. 9. This outcrop is located 38 km south of the northernmost mound, along the same ship track.

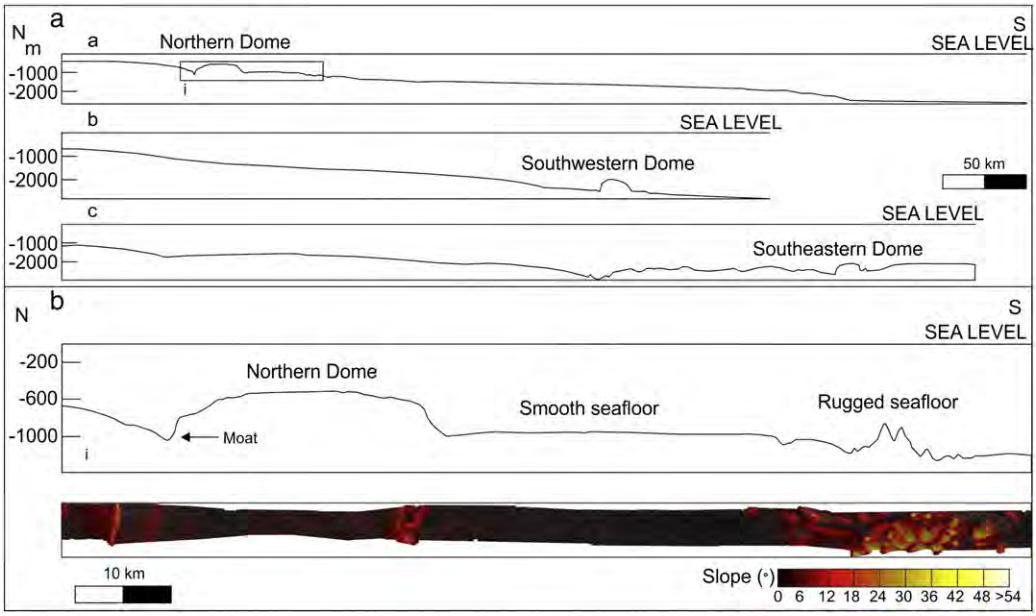

Fig. 7. (a) Three N–S transects through the northern Natal Valley are shown (see Fig. 1. for location). Note the contrast in morphology between the mounds, smooth and rugged seafloor over each transect. Typical rugged seafloor (see Fig. 5) is shown by the enlarged portion of profile "a". (b) Box i is enlarged to better illustrate the contrasting morphology of the mounded and rugged bathymetry. The accompanying slope map highlights the change in slope, and so morphological character, across smooth, mounded and rugged seafloor.

mound-like features, and seamounts located along the eastern African margin. Selected characteristics are plotted in Fig. 11. Slope angle is plotted as an average against flatness (flatness = summit width / basal width) for all the features (Fig. 11a). Although there is no clearly defined trend, the Natal Valley mounds have higher flatness values with lower slope angles than the seamount TB and seamounts IOB (Fig. 11), for which the inverse is true. Terrestrial alkaline complexes display varied slope and flatness characteristics, scattered between those of the seamounts and Natal Valley mounds. Plotted height–width and length–width ratios (Fig. 11b) reveal that the Natal Valley mounds and alkaline complexes are comparable in terms of these parameters, while other features are more varied in character.

5. Discussion

5.1. Bathymetry

These mound features create oval-like (plan view), positive dome-shaped (cross-section) features on the seafloor of the Natal Valley. These features are distinct from the typical bathymetry of the Natal Valley, which includes irregular rugged and smooth seafloor (Fig. 7). The mounds rise over 400 m above the surrounding seafloor sediments and similar features are not evident elsewhere in the Natal Valley. The three mounds have off-centre high points; the gradient from these high points is gentle (2.3° average), until an abrupt change is noted at the

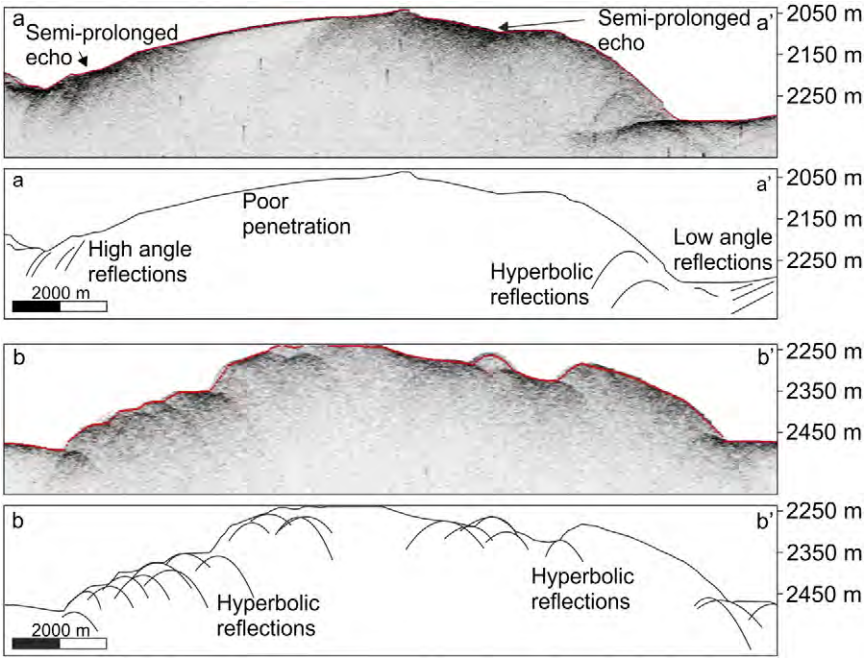

Fig. 8. A 3.5 kHz seismic record crossing the south western mound. Semi-prolonged echoes, as well as high, low and hyperbolic reflections are evident. See Fig. 3 for profile locations.

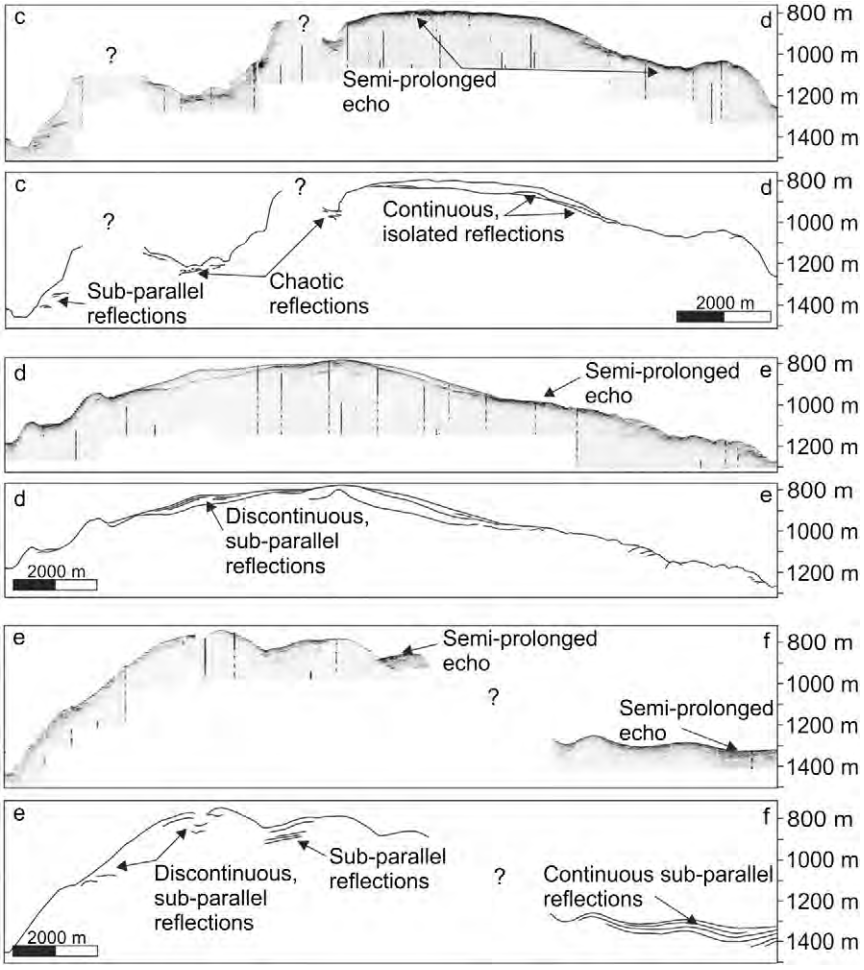

Fig. 9. 3.5 kHz seismic record crossings of the southeastern mound. Note the difference in character between the mounds and adjacent smooth seafloor (profile e–f). Fig. 4 shows the profile locations.

mound flanks (9° average for the three mounds). The rugged seafloor, typically associated with oceanic crust outcrop (Fig. 5), exhibits an average gradient of 13.15° (mounds average 7.2°, from crown to base), steeper on the upper portion of the feature with the gradient lessening toward the base, in contrast to the mounds for which the inverse is true. By comparison, the smooth seafloor, a product of depositional/erosional processes on the basin floor (Damuth, 1980), generally deepens toward the south with an average gradient of 0.2° (Fig. 6). It is clear that these mounds represent anomalous bathymetric features, dissimilar in character from adjacent bathymetry.

This dissimilarity is highlighted by the distribution of areas of seafloor affected by significant changes in slope (Fig. 6). In plan-view, rugged seafloor displays grouped circular patterns of steepening slope amidst low gradient seafloor of fairly uniform slope. While little distinction can be made between the smooth seafloor and crown of the mounds, the mound flanks are notably different. The flanks are seen as bands of

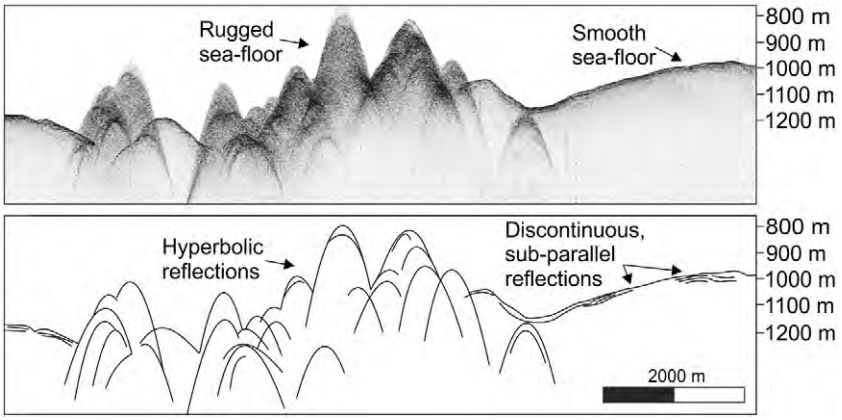

Fig. 10. A 3.5 kHz seismic record crossing of the rough terrain south of the northern mound. This 3.5 kHz record shows the echo character associated with both rugged and smooth seafloor. Note the conical expression of the rugged basement outcrop typical of the northern Natal Valley. See Fig. 5 for location.

Table 1
Morphological characteristics for the various mounded features discussed in this study. The northern mound has an estimated width due to a lack of data coverage. Overall, the similarity in geomorphology between the terrestrial features, and those of the Natal Valley is noteworthy. Ns, nepheline syenites; Gs, granite/syenite; Ns/S/Qs, nepheline syenite, syenite and quartz syenite; Seamount TB: lone seamount from the Transkei Basin; Seamount IOB: large seamounts of Das et al., 2007.

Name	Length (km)	Width (km)	Height (km)	(H/W)	(L/W)	Volume (km^3)	Flatness	Slope (°)	Lithology	Location
Gorongosa	30	19	1.046	0.06	1.58	1891.02	0.52	12.12	N s/S/Q s	Mozambique
Salambidwe	10.08	7.31	0.318	0.04	1.38	97.91	0.46	10.11	G/S	Mozambique
Morrumbala	16.5	9.2	0.795	0.09	1.79	504.24	0.46	10.63	G/S	Mozambique
Mulanje	30	16.5	1.258	0.08	1.82	2601.88	0.56	12.31	G/S	Malawi
Zomba	22	13	0.859	0.07	1.69	1026.5	0.55	12.05	G/S	Malawi
Junguni	4.6	4.4	0.12	0.03	1.05	10.15	0.78	14.73	N s	Malawi
Mongolowe	13.39	8.47	0.429	0.05	1.58	203.29	0.63	10.55	N s	Malawi
Chaone	11.63	9.62	0.448	0.05	1.21	209.43	0.62	11.9	N s	Malawi
Chikala	9.17	5.55	0.523	0.09	1.65	111.22	0.38	15.78	N s	Malawi
Nuanetsi	52.96	38.1	0.158	0.01	1.39	1328.94	0.29	3.25	G/S	Zimbabwe
Mamngudzi	12.47	8.33	0.1	0.01	1.50	31.25	0.39	11.4	G/S	Zimbabwe
SE mound (3)	29.7	17	1.12	0.07	1.75	2362.79	0.86	11.3	?	Natal Valley
Mid mound (1)	25.4	16	1.272	0.08	1.59	1079.97	0.79	7.3	?	Natal Valley
SW mound (2)	31	18	1.22	0.07	1.72	2844.43	0.62	8.5	?	Natal Valley
Sedom	11	1.25	5	4.00	8.80	68	0.15	7.02	Salt	Dead Sea
Lisan diapir	13	10	6	0.60	1.30	780	?	?	Salt	Dead Sea
Seamount TB	15	13	2.24	0.17	1.15	145.6	0.06	16.75	?	Transkei Basin
Seamounts IOB	16.21	12.59	1.33	0.24	1.29	54.3	0.16	13.25	?	Indian Ocean
Giant contourite	200	45	0.9	0.02	4.44	3870	0.08	1.3	Sediment	Argintine Basin

steepened bathymetry between the smooth seafloor and mound crowns. Similarities between the smooth seafloor and mound crowns can be described by sediment draping during deposition, and reworking by currents (e.g., NADW), whereas the flanks (which provide a significant change in gradient and substrate) are prone to current scouring and moat development.

5.2. High frequency seismic character

With respect to echo character, there is a marked difference between typical rugged seafloor of the Natal Valley and the mounds (Figs. 6–8). The rugged features exhibit large, individual to overlapping, irregular hyperbolae with varied vertex elevations about the seafloor. Such a strongly reflective echo character is characteristic of basement highs or outcrop (Damuth, 1980; Lee et al., 2002). On either side of the rugged basement outcrop, like the mounds, smooth seafloor occurs (Figs. 9, profile e–f, and 10). Semi-prolonged echoes, with continuous to discontinuous sub-parallel sub-bottom reflectors characterise this smooth seafloor. Such echo character is common to deep seafloor globally; the product of depositional/erosional processes on the basin floor (cf. Damuth, 1980).

In contrast to the smooth and rugged seafloor, the mounds show prolonged, semi-prolonged and continuous isolated echoes, with lesser discontinuous, sub-parallel and chaotic echoes. Broad hyperbolic (Fig. 8, profile b–b′) and high angle (Fig. 8, profile a–a′) echoes are associated with hard ridges (Fig. 4), rather than irregular rugged bathymetry (Fig. 6). The regularly overlapping hyperbolae lie below the seafloor, with little variation in depth. As such; these echoes are distinct from those associated with the rugged basement outcrop discussed above.

Of particular interest are the continuous isolated echoes, the lowermost of which drape the pre-existing bathymetry of the mound while the upper (shallower) reflectors encompass packages of homogenous sediment. This type of echo character is not observed in areas of rugged seafloor associated with typical basement highs (small seamounts) in the Natal Valley. Furthermore it is atypical of seafloor-penetrating salt diapirs as described by Kelling et al. (1979); rather salt diapirs return isolated transparent hyperbolic echoes amidst continuous seafloor reflectors with multiple parallel sub-bottom reflectors. In addition, continuous isolated echoes are not associated with areas of smooth seafloor.

With respect to morphological and seismic character, these mounds are distinct from the surrounding seafloor. It is highly unlikely, then, that they were produced by the same processes responsible for the development of either smooth or rugged seafloor types.

5.3. Mound origins

There are three plausible options that could account for the presence of these mounds within the Natal Valley. These formative processes and factors are discussed below, while the corresponding morphological characteristics are shown in Table 1.

5.3.1. Salt

Salt, as described by Hudec and Jackson (2007), is often associated with deformation when it is present in significant volumes within the stratigraphy. Salt is a common stratigraphic constituent of passive margins, deposited both during and following continental rifting (Brun and Fort, 2011). Inherently weak, salt is relatively easily mobilised in accordance with regional tectonic and/or gravity driven regimes (Brun and Fort, 2011; Hudec and Jackson, 2007).

Along the passive west coast of Africa, salt tectonics has played a role in the development of the contemporary bathymetry (Davison, 2005; Davison and Dailly, 2010; Gee and Gawthorpe, 2006; Hudec and Jackson, 2007; Liu and Li, 2011). Diapiric features ranging from round to elongate in plan are well documented (cf. Hudec and Jackson, 2007). The geometry of salt diapirs can, most simply, be described by three end-member forms; upward-narrowing, columnar, and upward-widening (Koyi, 1997). Each end-member is associated with particular sedimentary and tectonic settings (cf. Koyi, 1997). Most favourable in this instance would be the columnar end-member, as this is most likely to produce circular mounds or oval mounds on the seafloor. The shortcomings of this hypothesis are several-fold. Firstly, the morphological character of the Natal Valley mounds is at odds with that expected of salt diapirs. Surface penetrating salt diapirs are not known to reach the size of the mounds described in the Natal Valley from multibeam bathymetry data. Additionally, the echo character of the mounds is distinct from the echo character associated with salt diaper related structures (cf. Kelling et al., 1979). Furthermore, there is insufficient salt to produce significant diapirs. The basin, as inspected from the onshore portions where boreholes intersect both the rift and drift phase of margin development, is devoid of evaporite deposits (cf.

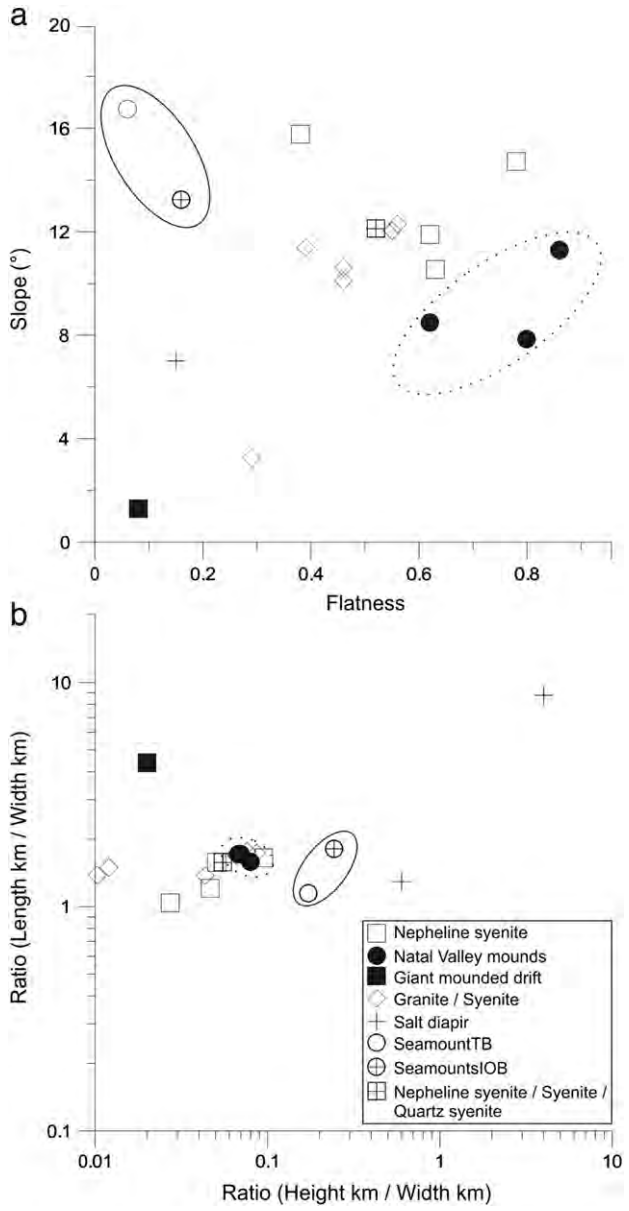

Fig. 11. Plots of selected morphological parameters associated with mounded features. a) The mounds (solid black circles), generally plot away from traditional seamounts (open and crossed circles), while terrestrial alkaline complexes of varied lithologies (nepheline syenites, open square; granite/syenite, open diamond, and nepheline syenite, syenite and quartz syenite, crossed square) show a scattered distribution between the seamount morphologies. b) Nepheline syenites (open square), granite/syenite (open diamond) and nepheline syenite, syenite and quartz syenite (crossed square) show strong morphological similarities with the Natal Valley mounds (solid black circles). Salt related features (cross), as well as giant mounded drifts (solid black square) do not exhibit comparable morphological characteristics.

Shone, 2006). As such these features appear unrelated related to salt tectonics by virtue of an absence of salt and will thus not be discussed further. It is however incorporated within the morphological plots provided in Fig. 11 for simple comparison.

5.3.2. Bottom water circulation

The second option is that these anomalous mounds are the result of current activity. Bottom current activity in the basins off south east coast of South Africa has been shown to have a significant effect on sedimentation in both the Natal Valley (Wiles et al., 2013), and neighbouring Transkei Basin (Schlüter and Uenzelmann-Neben, 2007, 2008). Bedforms produced by bottom water currents may cover extensive (>1000 km^2) tracts of seafloor. However, despite the impressive wave-lengths associated with these features (>10 km), the amplitude is typically on a scale of tens of metres (Wynn and Masson, 2008) and clearly does not approach the scale of the mounds discussed here. Giant contourite drifts, as described by Hernández-Molina et al. (2010) (ca. 40–50 km wide and 250–300 km long), by far exceed the horizontal scale of the Natal Valley mounds, in addition to other contrasting morphological characteristics (Table 1). Additionally, such bedforms are not typified by abrupt scarps or moats, features characteristic of the anomalous mounds. Consequently, they are not comparable to these mounds found in the Natal Valley and current activity may be regarded as an unlikely origin for the Natal Valley mounds.

5.3.3. Submarine igneous activity

Submarine igneous activity is the third option. Dingle et al. (1978) tentatively alluded to this as a possible cause for the mounds (described by these authors as basement highs) in the Natal Valley, but without more detailed bathymetric imagery this has not been possible to confirm nor refute. On the basis of the size and position of these mounds, igneous activity appears to be a plausible factor in their genesis.

Leinweber and Jokat (2011a) identified an extinct spreading centre at 30°S, extending eastward from ~34°E to ~35° 30′ E. The southeastern mound coincides exactly with this extinct spreading centre (Fig. 1). The northern mound (Fig. 1) is located in the vicinity of the northernmost magnetic lineaments associated with an early spreading centre identified by Leinweber and Jokat (2011a). Furthermore, the mounds lie in the N–S (30° E–40° E) corridor of igneous activity associated with the southern portion of the EARS's western branch, as well as Karoo age alkaline igneous activity (Fig. 12).

5.4. Seamount geomorphology

In terms of their size and shape (bearing in mind sediment accumulation in the Natal Valley), the Natal Valley mounds bear a striking resemblance to several igneous complexes of south-east Africa (Fig. 13). These terrestrial features relate to three distinct periods; those of Jurassic age are associated with Karoo igneous activity, the late Jurassic to early Cretaceous are associated with the breakup of Gondwana, while the Tertiary features are related to the southward propagation of the EARS. The H/W ratio of features has been used as a means of morphological classification that is suggestive of formative processes (Das et al., 2007; Kodagali, 1989; Mukhopadhyay and Batiza, 1994; Mukhopadhyay and Khadge, 1990; Smith, 1988). In comparison, the L/W ratio is useful in relating the plan-view shape of features (from circular to oblate). Both the H/W and L/W ratios, along with flatness and slope are useful morphological measures when comparing various features of differing origins. When compared in terms of slope angle vs. flatness, and height to width (H/W) vs length to width (L/W), the mounds of the Natal Valley are well placed within the spread of possible morphological character associated with other similar features from the African continent (Fig. 11). Included in Fig. 11 are examples of salt diapirs, giant contourite mounds, and other seamounts for comparison. Seamounts from the central Indian Ocean Basin (seamounts IOB hereafter), described by Das et al. (2007) and plotted as an average (in terms of measured morphological parameters) for all large single peaked seamounts, plot away from the Natal Valley mounds illustrating differences in the morphological character between these features. A lone (the only one for which the bathymetry is known), single peaked, seamount (seamount TB hereafter) from the Transkei Basin also plots away from the Natal Valley mounds, with morphological character more akin to the seamounts of Das et al. (2007). These plots illustrate the similarities in morphological character between these types of seamounts, and differences when compared to the Natal Valley mounds.

The Natal Valley mounds have H/W ratios of <0.08, a class defined as low by Das et al. (2007). This morphological class is said to be associated

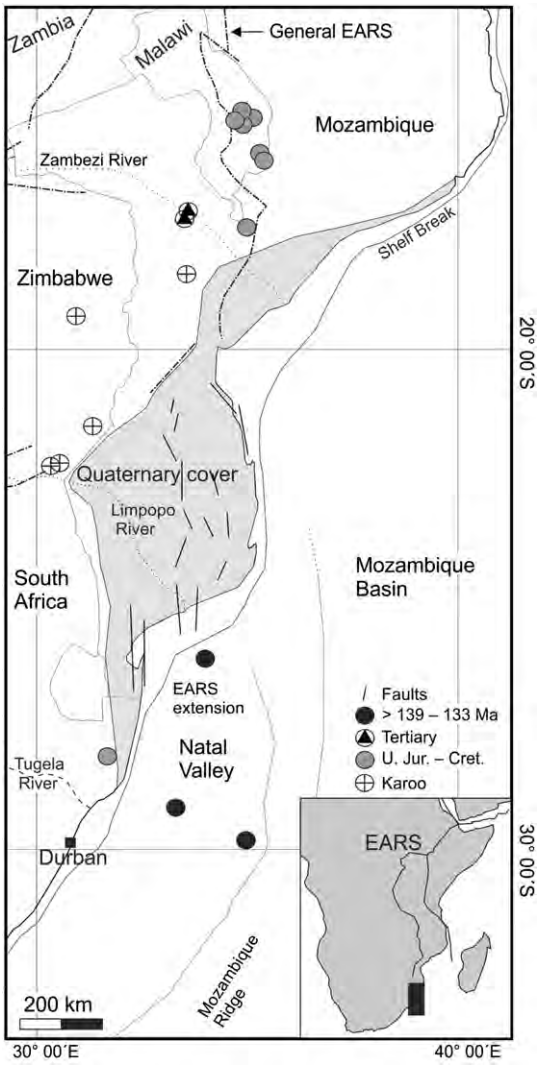

Fig. 12. Circles (please refer to the key) represent significant cases of alkaline igneous activity of south-east Arica, black circles show the relative position of mounds in the Natal Valley. The present accepted extent of the EARS (black dot–dash lines) lies to the north of the southern coastal plains of Mozambique, an area that shows evidence of E–W extension (see location of normal faults). Black lines (main figure and inset) show the location of the major rift features of the EARS. The Natal Valley mounds are located directly south of this area, within the northern Natal Valley. The city of Durban is shown, for reference, by the black square.
This map is modified after Chorowicz, 2005, and the Geological Map of Mozambique (Ministerio dos Recursos Minerais, 1987).

with low flatness ratios (<0.12) and low slope angles (<10°), suggestive of a point source of magma, that flows along the slope of the seamount. In contrast to these findings, the Natal Valley mounds exhibit high averaged flatness ratios (0.74), and average slopes of 9.03° (local maximum slopes reach up to 44°). It is clear that the Natal Valley mounds are morphologically distinct from those observed by Das et al. (2007), based on these morphologic parameters. The lone seamount TB from the Transkei Basin has a flatness of 0.06, slope angle of 16.75°, and intermediate H/W ratio (0.17). As the H/W ratio is indicative of the mode of origin of seamounts (Das et al., 2007; Kodagali, 1989; Mukhopadhyay and Batiza, 1994; Mukhopadhyay and Khadge, 1990; Smith, 1988), it appears that the origins of the Natal Valley mounds differ from those of the Central Indian Ocean Basin seamounts, as well as the lone seamount from the Transkei Basin.

Comparison of volume to L/W reveals a similar trend (Table 1); seamounts in general differ from the Natal Valley mounds, whereas terrestrial alkaline features are more comparable to the Natal Valley mounds. Differences in morphological character between conventional seamounts and the Natal Valley mounds are most evident when comparing flatness and slope angle, with alkaline complexes grouped toward the Natal Valley mounds, while the seamounts occupy a zone of inverse slope/flatness character (Fig. 11a). This trend is more evident in the second plot where the total morphology (X, Y, and Z axes) of the features is compared (Fig. 11b). Here the Natal Valley mounds and alkaline complexes are tightly grouped, whereas the traditional seamounts occupy a slightly different zone in the plot. Again, this illustrates the variation in morphological character between the Natal Valley mounds and other seamounts.

5.4.1. Alkaline igneous activity

A great deal of the igneous activity in this area is associated with the southern portion of the western branch of the EARS (southern Malawi Rift), which lies directly north of the Natal Valley. Alkaline igneous activity is common to the EARS, and there are many documented cases with volcanic features ranging from metres to tens of kilometres in scale (Chorowicz, 2005; Mollel and Swisher, 2012). The area around and south of Lake Malawi hosts numerous igneous features on a scale directly comparable to the mounds of the Natal Valley. In particular, alkaline complexes bear the greatest resemblance in terms of geomorphology to the Natal Valley mounds (Fig. 13) with the long axis profiles of the features displaying a similar morphological character. The greatest geomorphological departure is the seafloor mounds lack of erosional features that are evident in the subaerial setting (e.g. streams and gullies). Of interest too is the possibility that a few smaller features could be combined to create one large feature. The alkaline complexes Mongolowe, Chaone and Chikala (Fig. 13), if draped with sediment and not eroded (to the extent that terrestrial features are naturally) would provide another possible analogue to the mounds of the Natal Valley. The average H/W ratio for these terrestrial mounds is 0.05, with a flatness of 0.51, and slope of 11.35°. The Natal Valley mounds plot in similar morphological zones to these terrestrial features, suggesting similar formative processes and origins. Such alkaline igneous activity in a marine setting is not uncommon and is usually associated with rift systems. The Cameroon line, a series of Tertiary to Recent (generally alkaline volcanoes), is a good example of this (cf. Barfod and Fitton, 2013; Fitton and Dunlop, 1985).

5.5. Timing and tectonic significance

It may be hypothesised that these mounds may be related to the southward propagation of the East African Rift System during the Neogene period. The EARS is typified by, among other characteristics, elongate zones of thinned continental crust. Weaknesses in the crustal structure are further exploited by rift propagation and associated volcanism (Chorowicz, 2005). Corti (2009) and Stamps et al. (2008) outline the location of plate boundaries associated with the Victoria, Rovuma and Lwandle micro-plates which developed in response to regional extensional regimes; the Victoria and Rovuma microplates being continental expressions of deformation related to the EARS. In contrast, the Lwandle micro-plate occurs in a marine setting between the Nubian and Somalian plates, thus representing rift associated deformation in that environment. It is therefore apparent that the region south of the EARS is active, and that the activity is associated with zones of predefined weakness (Morley, 1999).

In addition, the lowlands of southern Mozambique mark the southern extension of the Pan-African Mozambique Belt, another zone of weakness. This area lies to the east of the Kaapvaal craton, through which a rift is unlikely to propagate. Additionally, along the eastern boundary of the Kaapvaal craton lies the Lebombo monocline of the Mesozoic Karoo Igneous Province, a further zone of weakness (Klausen, 2009). The transitional crust along the western Natal Valley is located east and south of these zones of weakness, representing another zone

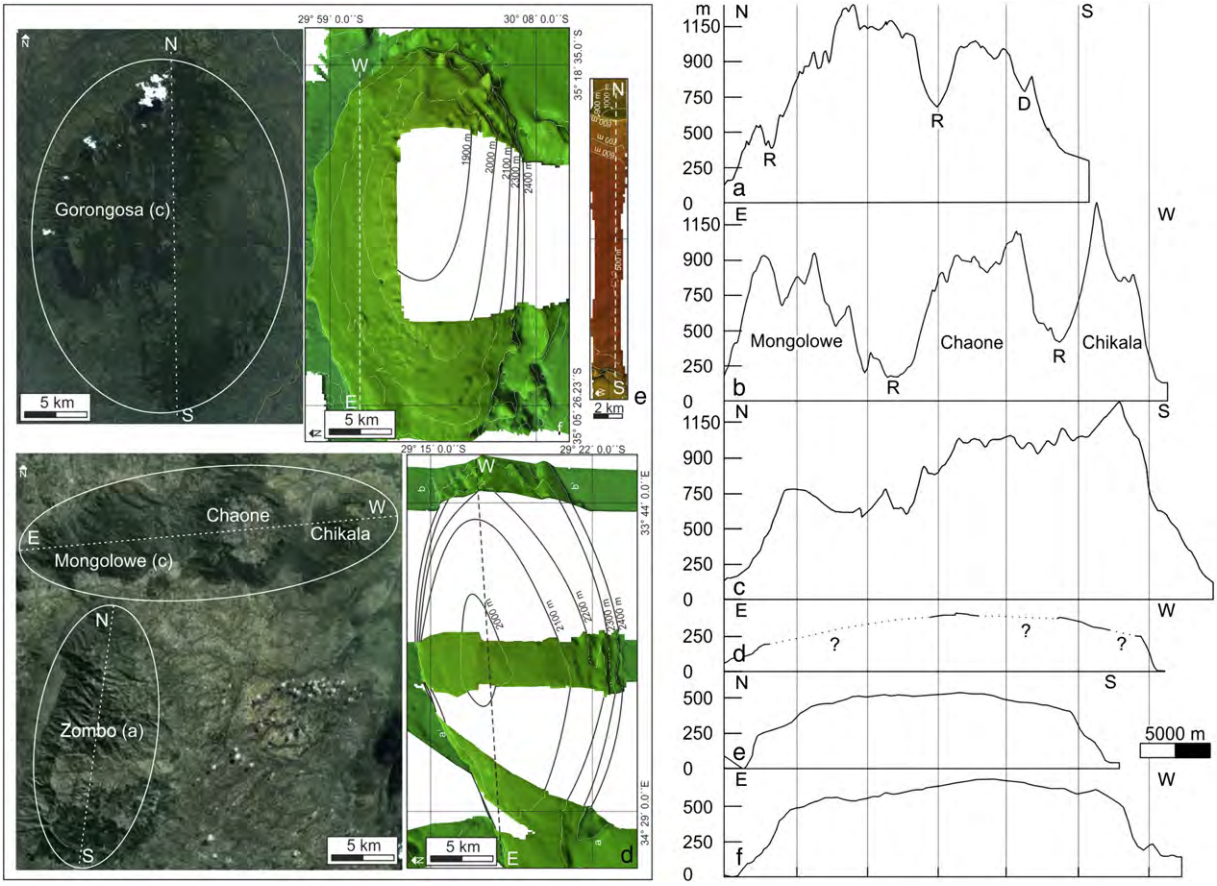

Fig. 13. Google Earth images of alkaline complexes compared to bathymetry data showing the mounds of the Natal Valley (left). The overall morphological similarity is striking, particularly if one removes the effects of weathering and erosion by fluvial and similar processes, from the subaerial alkaline complexes. Profiles across the long axis of the alkaline complexes, and Natal Valley mounds are shown on the left. The effect of subaerial weathering and erosion on the alkaline complexes is evident. The mounds have not been affected by subaerial processes, however, the Natal Valley basin has accumulated ca. 800 m of sediment since deposition commenced (a, Zomba; b, Mongolowe–Chaone–Chikala; c, Gorongosa; d, SW mound; e, N mound; f, SE mound).

marked by a weak crust with continental affinities (cf. Leinweber and Jokat, 2011a). These factors combined present a considerable N–S zone of crust predisposed to rifting with a long history of activity.

Igneous activity in the southern EARS began at ca. 10 Ma, sometime after the initiation of the EARS (30 Ma) and shows a definitive southward younging of the rift kinematics as the rift propagated in that direction (Albaric et al., 2009; Chorowicz, 2005). Recent seismic activity in the south confirms this (Albaric et al., 2009; Fairhead and Stuart, 1982). Although it has low overall seismicity, the Natal Valley does show some recent activity in the northern portion of the basin (Fig. 14). To the north of the study area, seismic activity is focused along two main N–S orientated regions. These regions mark the eastern, western and southeastern boundaries of the Rovuma Plate (Stamps et al., 2008), defined by the western and southeastern branches of the EARS (Chorowicz, 2005). The intersection of these plate boundaries is proximal to the study area (Fig. 14). The northern and southwestern mounds are located close (within 50 km) to epicentres ranging in magnitude from 3 to 4.6 ML, while elsewhere in the basin Earthquakes of 6.8 ML have been recorded (International Seismological Centre, On-line Bulletin, 2011).

This argument suggests that these mounds may mark a southerly extension of the EARS into the Natal Valley and show the progression of rifting into a deep (~2400 m) ocean system. This appears to be contrary to the typical propagation of continental rift systems that open seawards and spread into the continental interior (Cratchley et al., 1983). No other such examples have been documented for rift systems elsewhere. Beyond this unique point, there are also implications for the oil and gas industry. Exploration for petroleum could be affected by elevated thermal gradients in this region, raising temperatures through the oil/gas window.

6. Conclusion

Anomalous seafloor mounds in the Natal Valley represent a morphological class that is distinct from other seamounts, sharing more similarities with terrestrial alkaline complexes on the adjacent African continent than other submarine features. As such, they are believed to mark a line of continuation of several alkaline complexes likely related to development of the East African Rift System and associated igneous activity. The mounds, compared to their terrestrial counterparts, show evidence of recent sediment draping and smoothing of their topographic profiles. We hypothesise that these features may represent an offshore extension of the East African Rift igneous activity. This implies a southward propagation of the East African Rift into a mature ocean basin, a phenomenon previously unrecognised from continental rift systems. These mounds are proximal to the western and southeastern plate boundaries of the Rovuma plate. This has implications for the movement of the Rovuma plate, better defining the southern plate boundaries thus allowing for better constrained models of plate dynamics in this region to be produced. Furthermore, igneous and tectonic activity in this region associated with the formation of the mounds could have significant implications for petroleum exploration as the local thermal gradient may have increased beyond the oil and/or gas windows rendering the region barren in this respect.

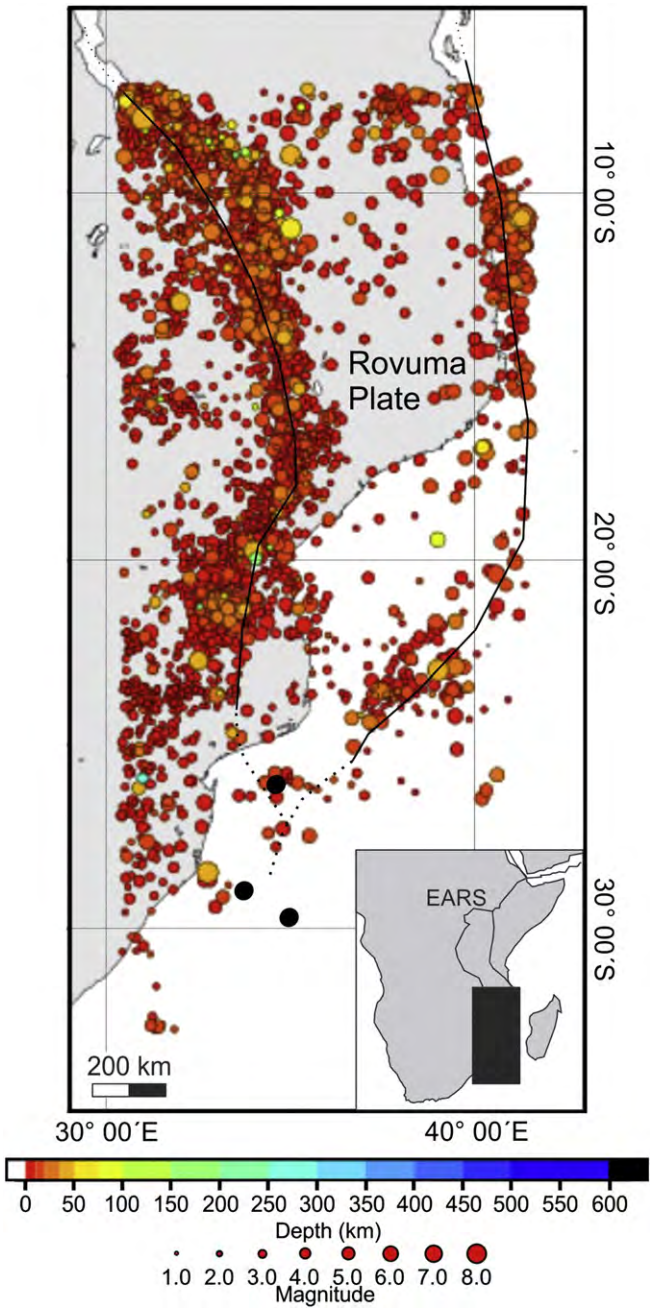

Fig. 14. Earthquake epicentre data from the vicinity of the study area for the period 1904–present are plotted, along with the locations of the mounds (black circles). Interestingly, activity is focused along the boundaries of the Rovuma Plate. The study area is located at the southern edge of this plate, proximal to the intersection of the western and southeastern plate boundaries.
Epicentre data were sourced from the International Seismological Centre, On-line Bulletin (2011), and the Rovuma Plate boundaries after Stamps et al., 2008.

Acknowledgements

We wish to thank the critical reviews of two anonymous reviewers and the input of the editor that helped to clarify this paper significantly. We further thank the BMBF (Bundesministerium fur Bildung und Forschung) for funding the scientific projects (contract numbers 03G0183A, 03G0730A). The crews of RV Sonne (AISTEK II) and RV Pelagia (AISTEK III) are acknowledged for their excellent support and expertise in the data acquisition phases. The financial assistance of the National Research Foundation (Innovation Scholarship) (83799) towards this research is hereby acknowledged. Opinions expressed and conclusions arrived at, are those of the authors and are not necessarily to be attributed to the DAAD-NRF.

References

Albaric, J., Déverchère, J., Petit, C., Perrot, J., Le Gall, B., 2009. Crustal rheology and depth distribution of earthquakes: Insights from the central and southern East African Rift System. Tectonophysics 468 (1–4), 28–41.
Barfod, D.N., Fitton, J.G., 2013. Pleistocene volcanism on São Tomé, Gulf of Guinea, West Africa. Quat. Geochronol. 1–13.
Ben Avraham, Z., Hartnady, C.H.J., Malan, J.A., 1993. Early tectonic extension between the Agulhas Bank and Falkland Plateau due to the rotation of the Lafonia microplate. Earth Planet. Sci. Lett. 117, 43–58.
Brun, J., Fort, X., 2011. Salt tectonics at passive margins: Geology versus models. Mar. Pet. Geol. 28, 1123–1145.
Burke, K., 1996. The African plate. S. Afr. J. Geol. 99, 339–409.
Calais, E., Hartnady, C., Ebinger, C., Nocquet, J.M., 2006. Kinematics of the East African Rift from GPS and earthquake slip vector data. In: Yirgu, G., Ebinger, C.J., Maguire, P.K.H. (Eds.), Structure and Evolution of the Rift Systems within the Afar volcanic province, Northeast Africa. Geological Society Special Publications, vol. 259, pp. 9–22.
Chorowicz, J., 2005. The East African Rift System. J. Afr. Earth Sci. 43 (1–3), 379–410.
Cochran, J.R., 1981. The Gulf of Aden: Structure and Evolution of a Young Ocean Basin and Continental Margin. J. Geophys. Res. 86, 263–287.
Corti, G., 2009. Continental rift evolution: From rift initiation to incipient break-up in the Main Ethiopian Rift, East Africa. Earth-Science Reviews 96 (1–2), 1–53.
Courtillot, V., Jaupart, C., Manighetti, I., Tapponnier, P., Besse, J., 1999. On causal links between flood basalts and continental breakup. Earth Planet. Sci. Lett. 166, 177–195.
Cratchley, C.R., Louis, P., Ajakaiye, D.E., 1983. Geophysical and geological evidence for the Benue-Chad Basin Cretaceous rift valley system and its tectonic implications. J. Afr. Earth Sci. 2, 141–150.
Damuth, J.E., 1980. Use of high-frequency (3.5–12 kHz) echograms in the study of near-bottom sedimentation processes in the deep-sea: a review. Mar. Geol. 38, 51–75.
Das, P., Iyer, S.D., Kodagali, V.N., 2007. Morphological characteristics and emplacement mechanism of the seamounts in the Central Indian Ocean Basin. Tectonophysics 443 (1–2), 1–18.
Davison, I., 2005. Central Atlantic margin basins of North West Africa: Geology and hydrocarbon potential (Morocco to Guinea). J. Afr. Earth Sci. 43 (1–3), 254–274.
Davison, I., Dailly, P., 2010. Salt tectonics in the Cap Boujdour Area, Aaiun Basin, NW Africa. Mar. Pet. Geol. 27 (2), 435–441.
Dietz, R.S., 1963. Continent and Ocean Basin Evolution by Sea Floor Spreading. Tulsa Geol. Soc. Dig. 31, 241–242.
Dingle, R.V., Camden-Smith, F., 1979. Acoustic stratigraphy and current-generated bedforms in deep ocean basins off southeastern Africa. Mar. Geol. 33, 239–260.
Dingle, R.V., Robson, S., 1985. Slumps, canyons and related features on the continental margin off East London, SE Africa (SW Indian Ocean). Mar. Geol. 67, 37–54.
Dingle, R.V., Goodlad, S.W., Martin, A.K., 1978. Bathymetry and stratigraphy of the northern Natal Valley (SW Indian Ocean): a preliminary account. Mar. Geol. 28, 89–106.
Ebinger, C.J., 1989. Tectonic development of the western branch of the East African Rift System. Geol. Soc. Am. Bull. 101, 885–903.
Fairhead, J.D., Stuart, G.W., 1982. The seismicity of the East Africa rift system and comparison with others continental rifts. In: Palmason, G. (Ed.), Continental and Oceanic Rifts. Geodynamics Series, 8, pp. 41–61.
Fitton, J.G., Dunlop, H.M., 1985. The Cameroon line, West Africa, and its bearing on the origin of oceanic and continental alkali basalt. Earth Planet. Sci. Lett. 72 (1), 23–38.
Flemming, B.W., 1980. Sand transport and bedform patterns on the continental shelf between Durban and Port Elizabeth (southeast African continental margin). Sediment. Geol. 26 (1–3), 179–205.
Gee, M.J.R., Gawthorpe, R.L., 2006. Submarine channels controlled by salt tectonics: Examples from 3D seismic data offshore Angola. Mar. Pet. Geol. 23, 443–458.
Goff, J.A., Jordan, T.H., 1988. Stochastic Modeling of Sea floor Morphology: Inversion of Sea Beam data for second-order statistics. J. Geophys. Res. 93, 13589–13608.
Goff, J.A., Ma, Y., Shah, A., Cochran, J.R., Sempéré, C., 1997. Stochastic analysis of sea floor morphology on the flank of the Southeast Indian Ridge: The influence of ridge morphology on the formation of abyssal hills. J. Geophys. Res. 102, 15521–15534.
Goodlad, S.W., 1986. Tectonic and sedimentary history of the mid-Natal Valley (SW Indian Ocean). Marine Geoscience Unit Bulletin, 15. Joint Geological Survey/University of Cape Town, p. 415.
Green, A.N., 2011a. Submarine canyons associated with alternating sediment starvation and shelf-edge wedge development: Northern KwaZulu-Natal continental margin, South Africa. Mar. Geol. 289, 114–126.
Green, A.N., 2011b. The late Cretaceous to Holocene sequence stratigraphy of a sheared passive upper continental margin, northern KwaZulu-Natal, South Africa. Mar. Geol. 289, 17–28.
Hernández-Molina, F.J., Paterlini, M., Somoza, L., Violante, R., Arecco, M.A., de Isasi, M., Rebesco, M., Uenzelmann-Neben, G., Neben, S., Marshall, P., 2010. Giant mounded drifts in the Argentine Continental Margin: Origins, and global implications for the history of thermohaline circulation. Mar. Pet. Geol. 27, 1508–1530.
Hudec, M.R., Jackson, M.P.A., 2007. Terra infirma: Understanding salt tectonics. Earth Sci. Rev. 82, 1–28.
International Seismological Centre, On-line Bulletin, 2011. http://www.isc.ac.uk, International Seismological Centre, Thatcham, United Kingdom.
Jokat, W., 2006. Southeastern Atlantic and Southwestern Indian Ocean: Reconstruction of the Sedimentary and Tectonic Development Since the Cretaceous, AISTEK-II: Mozambique Ridge and Mozambique Basin. Report of the RV "Sonne" Cruise SO-183,

Project AISTEK-II 20 May to 7 July 2005 Reports on Polar and Marine Research. Alfred-Wegener-Institute for Polar and Marine Research, Bremerhaven, p. 71.
Jokat, W., 2009. The Expedition of the Research Vessel "Pelagia" to the Natal Basin and the Mozambique Ridge in 2009 (Project AISTEK III). Alfred-Wegener-Institute for Polar and Marine Research, Bremerhaven, p. 67.
Kelling, G., Maldonado, A., Stanley, D.J., 1979. Salt Tectonics and Basement Fractures: Key Controls of Recent Sediment Distribution on the Balearic Rise, Western Mediterranean. Smithsonian Institute Press, pp. 1–52.
Klausen, M.B., 2009. The Lebombo monocline and associated feeder dyke swarm: Diagnostic of a successful and highly volcanic rifted margin? Tectonophysics 468 (1–4), 42–62.
Kodagali, V.N., 1989. Morphometric studies on a part of Central Indian Ocean. J. Geol. Soc. India 33, 89–94.
Koehn, D., Aanyu, K., Haines, S., Sachau, T., 2008. Rift nucleation, rift propagation and the creation of basement micro-plates within active rifts. Tectonophysics 458, 105–116.
Kolla, V., Eittreim, S., Sullivan, L., Kostecki, J.A., Burckle, L.H., 1980. Current-controlled, abyssal microtopography and sedimentation in Mozambique Basin, Southwest Indian Ocean. Mar. Geol. 34, 171–206.
Koyi, H., 1997. The shaping of salt diapirs. J. Struct. Geol. 20, 321–338.
Lee, S.H., Chough, C.K., Back, G.G., Kim, Y.B., 2002. Chirp (2–7-kHz) echo characters of the South Korea Plateau, East Sea: styles of mass movement and sediment gravity flow. Mar. Geol. 3042, 1–21.
Leinweber, V.T., Jokat, W., 2011a. Is there continental crust underneath the Northern Natal Valley and the Mozambique Coastal Plains? Geophys. Res. Lett. 38, L14303.
Leinweber, V.T., Jokat, W., 2012b. The Jurassic history of the Africa–Antarctica Corridor — new constraints from magnetic data on the conjugate continental margins. Tectonophysics 530, 87–101.
Liu, Z., Li, J., 2011. Control of salt structures on hydrocarbons in the passive continental margin of West Africa. Pet. Explor. Dev. 38 (2), 196–202.
Ministerio dos Recursos Minerais, 1987. Carta Geologica 1:1 000 000. Instituto Nacional De Geologia.
Martin, A.K., 1984. Plate tectonic status and sedimentary basin in-fill of the Natal Valley (S.W. Indian Ocean). Marine Geoscience Unit Bulletin, 14. Joint Geological Survey/University of Cape Town, p. 209.
Martin, A.K., Hartnady, C.J.H., 1986. Plate tectonic development of the south-west Indian Ocean: a revised reconstruction of East Antarctica and Africa. J. Geophys. Res. 91, 4767–4786.
Mollel, G.F., Swisher, C.C., 2012. The Ngorongoro Volcanic Highland and its relationships to volcanic deposits at Olduvai Gorge and East African Rift volcanism. J. Hum. Evol. 63, 275–283.
Morley, C.K., 1999. Geoscience of rift systems—evolution of East Africa. AAPG Stud. Geol. 44, 242.
Mougenot, D., Recq, M., Virlogeux, P., Lepvrier, C., 1986. Seaward extension of the East African Rift. Nature 321, 599–603.
Mukhopadhyay, R., Batiza, R., 1994. Basinal seamounts and seamount chain of the Central Indian Ocean: probable near-axis origin from fast spreading ridge. Mar. Geophys. Res. 16, 303–314.
Mukhopadhyay, R., Khadge, N.H., 1990. Seamount in the Central Indian Ocean Basin: indicator of the Indian plate movement. Proc. Indian Acad. Sci. A Earth Planet. Sci. 99 (3), 357–365.
Norton, I.O., Sclater, J.G., 1979. A model for the evolution of the Indian Ocean and the breakup of Gondwanaland. J. Geophys. Res. 84 (B12), 6803–6830.
Partridge, T.C., Maud, R.R., 2000. Macro-scale geomorphic evolution of southern Africa. In: Partridge, T.C., Maud, R.R. (Eds.), The Cenozoic of Southern Africa. Oxford University Press, New York, pp. 3–18.
Ruppel, C., 1995. Extensional processes in continental lithosphere. J. Geophys. Res. 100 (24), 187–215.
Schlüter, P., Uenzelmann-Neben, G., 2007. Seismostratigraphic analysis of the Transkei Basin: A history of deep sea current controlled sedimentation. Mar. Geol. 240, 99–111.
Schlüter, P., Uenzelmann-Neben, G., 2008. Indications for bottom current activity since Eocene times: The climate and ocean gateway archive of the Transkei Basin, South Africa. Glob. Planet. Chang. 60, 416–428.
Schmidt, D.L., Rowley, P.D., 1986. Continental rifting and transform faulting along the Jurassic Transantarctic Rift, Antarctica. Tectonics 5 (2), 279–291.
Shone, R.W., 2006. Onshore post-Karoo Mesozoic deposits. In: Johnson, M.R., Anheuser, C. R., Thomas, R.J. (Eds.), The Geology of South Africa. The Geological Society of South Africa. Johannesburg/Council for Geoscience, Pretoria, pp. 541–553.
Smith, D.K., 1988. Shape analysis of Pacific seamounts. Earth Planet. Sci. Lett. 90, 457–466.
Stamps, D.S., Calais, E., Saria, E., Hartnady, C., Nocquet, J.-M., Ebinger, C.J., Fernandes, R.M., 2008. A kinematic model for the East African Rift. Geophys. Res. Lett. 35, L05304.
Toole, J.M., Warren, B.A., 1993. A hydrographic section across the subtropical South Indian Ocean. Deep Sea Res. I 40, 1973–2019.
Watkeys, M.K., 2006. Gondwana Break-up: A South African perspective. In: Johnson, M.R., Anheuser, C.R., Thomas, R.J. (Eds.), The Geology of South Africa. The Geological Society of South Africa. Johannesburg/Council for Geoscience, Pretoria, pp. 531–539.
Wiles, E., Green, A., Watkeys, M., Jokat, W., Krocker, R., 2013. The evolution of the Tugela canyon and submarine fan: A complex interaction between margin erosion and bottom current sweeping, southwest Indian Ocean, South Africa. Mar. Pet. Geol. 44, 60–70.
Wolfeden, E., Ebinger, C., Yirgu, G., Deino, A., Ayalew, D., 2004. Evolution of the northern Main Ethiopian Rift: Birth of a triple junction. Earth Planet. Sci. Lett. 224, 213–228.
Wynn, R.B., Masson, D.G., 2008. Sediment waves and bedforms. In: Rebesco, M., Camerlenghi, A. (Eds.), Contourites. Developments in Sedimentology, 60, pp. 289–300.

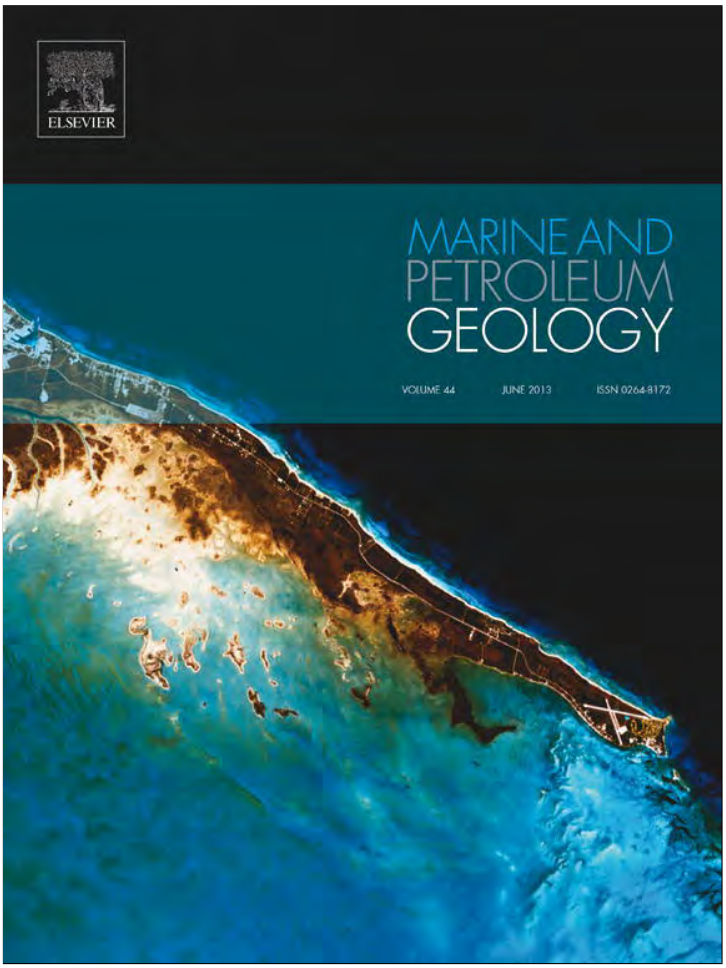

Marine and Petroleum Geology 44 (2013) 60–70

Contents lists available at SciVerse ScienceDirect

Marine and Petroleum Geology

journal homepage: www.elsevier.com/locate/marpetgeo

The evolution of the Tugela canyon and submarine fan: A complex interaction between margin erosion and bottom current sweeping, southwest Indian Ocean, South Africa

Errol Wiles [a,*], Andrew Green [a], Mike Watkeys [a], Wilfred Jokat [b], Ralph Krocker [b]

[a] Geological Sciences, School of Agricultural, Earth and Environmental Sciences, University of KwaZulu-Natal, Private Bag X 54001, Durban 4000, South Africa
[b] Alfred-Wegener-Institute for Polar and Marine Research, Am Alten Hafen 26, D-27568 Bremerhaven, Germany

ARTICLE INFO

Article history:
Received 22 September 2012
Received in revised form
7 March 2013
Accepted 21 March 2013
Available online 2 April 2013

Keywords:
Submarine canyons
Deep-sea fans
Current sweeping

ABSTRACT

The transfer of sediment from the upper continental slope to rise is poorly documented along the southeast African passive margin. New swath bathymetric and sub-bottom data collected in the Natal Valley, southwest Indian Ocean, provide insight into the evolution of the Tugela canyon and fan system. Several distinct downslope changes in canyon morphology are noted. The canyon increases in relief and widens with depth. Basement outcrop is restricted to the head of the canyon becoming less prominent with depth. Step-like terracing of the canyon walls and floor becomes prominent in the mid-slope portions of the canyon and is related to a marked increase in the cross sectional asymmetry of the canyon profile. The contemporary Tugela canyon rests within a depression of the last phase of infilling. The canyon is the product of downslope erosion, and incision, caused by several phases of hinterland uplift in the mid Oligocene, mid Miocene and late Pliocene. Each phase was followed by pelagic infilling of the palaeo-canyon form. Downslope, the uplift phases are preserved in the cut-terraces and axial incisions within the main canyon thalweg. The contemporary canyon is a moribund feature, sediment starvation of the shelf area by current sweeping of the Agulhas current has decreased the material available for canyon incision and fan development. Additional current sweeping by the North Atlantic Deep Water current has stunted the development of the associated fan complex.

1. Introduction

Submarine canyons are known the world over as significant morphological features that have modified continental margins over significant periods of time via erosion and ultimately the deposition of fan complexes. Typically, submarine canyons are classified as either “shelf-breaching”, “shelf-indenting” or “slope-confined” based on their relationship with the continental shelf (Farre et al., 1983). The mechanism responsible for the former is believed to be a combination of eustatic sea level change and submarine erosion, often associated with subaerial exposure of the shelf to fluvial processes. Slope-confined and shelf-indenting categories are likely the result of retrogressive failure, fluid venting and tide-driven bottom currents (Ridente et al., 2007). Submarine canyons, particularly the shelf-breaching class, represent preferential sediment transport pathways (via tectono-sedimentary processes) to the World’s major sedimentary basins, albeit episodic in nature (Dingle and Robson, 1985; Ridente et al., 2007; Lastras et al., 2011).

Very few examples of across slope transport pathways in deep water have been documented from the passive eastern margin of South Africa. This is in comparison to the notable examples from North America (Farre et al., 1983; Pratson et al., 1994; Vachtman et al., 2012) and Europe (Lastras et al., 2011). Deep water studies of the South African continental slope and rise have tended to focus on bottom water flows and sedimentation rather than the role submarine canyons play in the delivery of sediment to the deep oceans (cf. Dingle et al., 1978, 1987; Martin et al., 1982; Schlüter and Uenzelmann-Neben, 2007, 2008). In the Natal Valley, offshore the east coast of South Africa, only a single very large submarine canyon (120 km long, 50 km offshore of the Tugela, river) has been identified (Dingle et al., 1978; Goodlad, 1986). This is an example of a large submarine canyon restricted to the mid–lower slope and attributed with the delivery of detrital material from the Tugela

* Corresponding author. Tel.: +27 031 260 2801.
E-mail addresses: 205514699@stu.ukzn.ac.za, eawiles@yahoo.com (E. Wiles).

0264-8172/$ – see front matter © 2013 Elsevier Ltd. All rights reserved.
http://dx.doi.org/10.1016/j.marpetgeo.2013.03.012

river (South Africa's second largest river) to the deep ocean basin. Despite having no contemporary connection to the upper slope and shelf, the canyon is deeply incised and the exact structure and origin of this canyon is unknown. Similarly, the associated fan is poorly understood; previous sampling efforts having been frustrated by the lack of geophysical data required to accurately delineate this feature (Türkay and, Pätzold, 2009).

This study incorporates new swath bathymetric and sub-bottom data collected in the Natal Valley, located in the southwest Indian Ocean (SWIO) (Fig. 1) in an attempt to understand the evolution of the Tugela canyon and fan system. By examining the geomorphology of these features, insights into the sedimentary processes responsible for sculpting the southeast African margin can be made. As such, this paper aims to present a model for a submarine canyon-fan system with a sediment starved upper limit and a bottom current swept lower region.

2. Regional setting

2.1. Geological setting

The Natal Valley is located off the southeastern seaboard of southern Africa. This sedimentary basin can be subdivided, at 30° south, into a northern and southern area (Fig. 1). The basement of the northern Natal Valley is oceanic in origin, the result of a SW–NE spreading centre (now the present day southern Mozambique coastline) that produced the initial basin during early Gondwana break-up ~ 183–159 Ma (Leinweber and Jokat, 2011a). The southern Natal Valley, also floored by an oceanic basement, opened ca. 138.9–130.3 Ma via a SW–NE spreading centre to the east of the present day basin (Leinweber and Jokat, 2011b). Spreading in the Natal Valley was complete by 90 Ma (Martin and Hartnady, 1986; Ben Avraham et al., 1993).

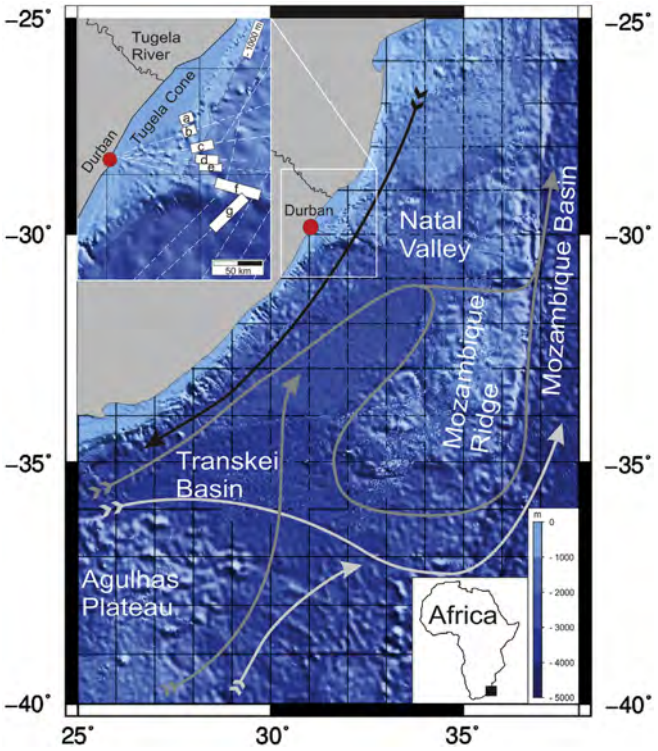

Figure 1. GEBCO (30 s grid) DTM showing the study area (white box and inset) and adjacent southwest Indian Ocean bathymetry. Note the location of the Natal Valley, Mozambique Ridge and the Transkei Basin. The black arrow illustrates Agulhas Current flow, mid-gray arrows illustrate North Atlantic Deep Water flow, light grey arrows shows the passage of Antarctic Bottom Water (Flow paths compiled after: Toole and Warren, 1993; Schlüter and Uenzelmann-Neben, 2008; Bang and Pearce, 1976; Dingle et al., 1987). Ship tracks (Dashed lines) are overlain with white rectangles delineating portions of the Tugela canyon discussed in this study, see main text for further detail.

The sedimentary fill comprises sedimentary rocks of the Zululand Group's Makhatini Formation; fossiliferous shallow marine clays of mid Barremian to lower Aptian age that represent the rift succession. Uncomformably overlying this is the mid Aptian to lower Cenomanian Mzinene Formation that comprises fossiliferous shallow marine silts, sands and interbedded hardgrounds (Shone, 2006). Basin deposition was interrupted by a hiatus spanning the mid Cenomanian to upper Turonian times. This is defined by a regional seismic reflection somewhat whimsically termed "McDuff" by Dingle et al. (1978). Deposition of fossiliferous shallow marine silts, sands and conglomerates of the St. Lucia Formation resumed from this point to upper Maastrichtian times. Another regional reflection, "Angus" marks the top of the St. Lucia Formation and defines another hiatus (Dingle et al., 1978; Shone, 2006).

Post-Angus deposits are associated with the construction of the Tugela Cone, a large subaqueous delta of the Tugela river that displays a complex onlap/offlap configuration in the offshore stratigraphy (Goodlad, 1986). A Lower Pliocene unconformity, marked by regional reflection "Jimmy" truncates the underlying units. Post-Jimmy, sediments continue to exhibit an onlap/offlap configuration, with bottom current interaction noted in seismic records (cf. Goodlad, 1986). Pleistocene aged deposits are rare. Lower Pleistocene unconsolidated sediments occur on the outer shelf (Green et al., 2008) and mid–upper Pleistocene aeolianite cordons span the inner to outer shelf. These cordons are mantled by thin unconsolidated Holocene sediments that are reworked and redistributed by energetic gyres and eddies associated with the poleward flowing Agulhas current (Flemming, 1980; Green, 2009).

2.2. Physiography and oceanography

The Natal Valley is bound to the east by the Mozambique Ridge and to the west by the south east coast of southern Africa. The adjacent continental shelf is straight and narrow (4–15 km) compared to global standards (Dingle and Robson, 1985; Green, 2011a, b) but widens substantially to 45 km offshore the Tugela river. On average the continental shelf in this region dips at 0.2° toward a poorly defined shelf-break at −100 m (Goodlad, 1986; Martin and Flemming, 1988).

The Natal Valley deepens toward the south where it merges with the deep Transkei Basin at 4000 m depth (Fig. 1). Sediment input to the basin occurred at ~23 $m^3/km^2/yr$ over the past 65 Ma (Dingle et al., 1978) and was attributed to rivers along the KwaZulu-Natal coast. These rivers, the most prominent being the Tugela river (Fig. 1), have been in existence since mid Cretaceous times (Partridge and Maud, 2000), and deliver vast quantities of sediment (4.405×10^6 m^3) to the coast on a seasonal time scale (Flemming, 1980).

Circulation within the Natal Valley is complex, particularly when considering the smaller scale shallow currents of the adjacent narrow continental shelf. Upper ocean flow in the basin is dominated by the polewards flowing Agulhas Current (with contributions from Red Sea Water), a fast moving (4 knots), wide (ca. 100 km) poleward flowing western boundary current (Fig. 2). This is considered to extend to depths as much as 2500 m along South Africa's south east coast (Bang and Pearce, 1976; Dingle et al., 1987).

Bottom currents (those in contact with the sea-floor) in the Natal Valley are dominated by the equatorward flowing North Atlantic Deep Water (NADW). Passage of the NADW into the Natal Valley (ca. 1.2×10^6 m^3 s^{-1}) is considered to be controlled by two

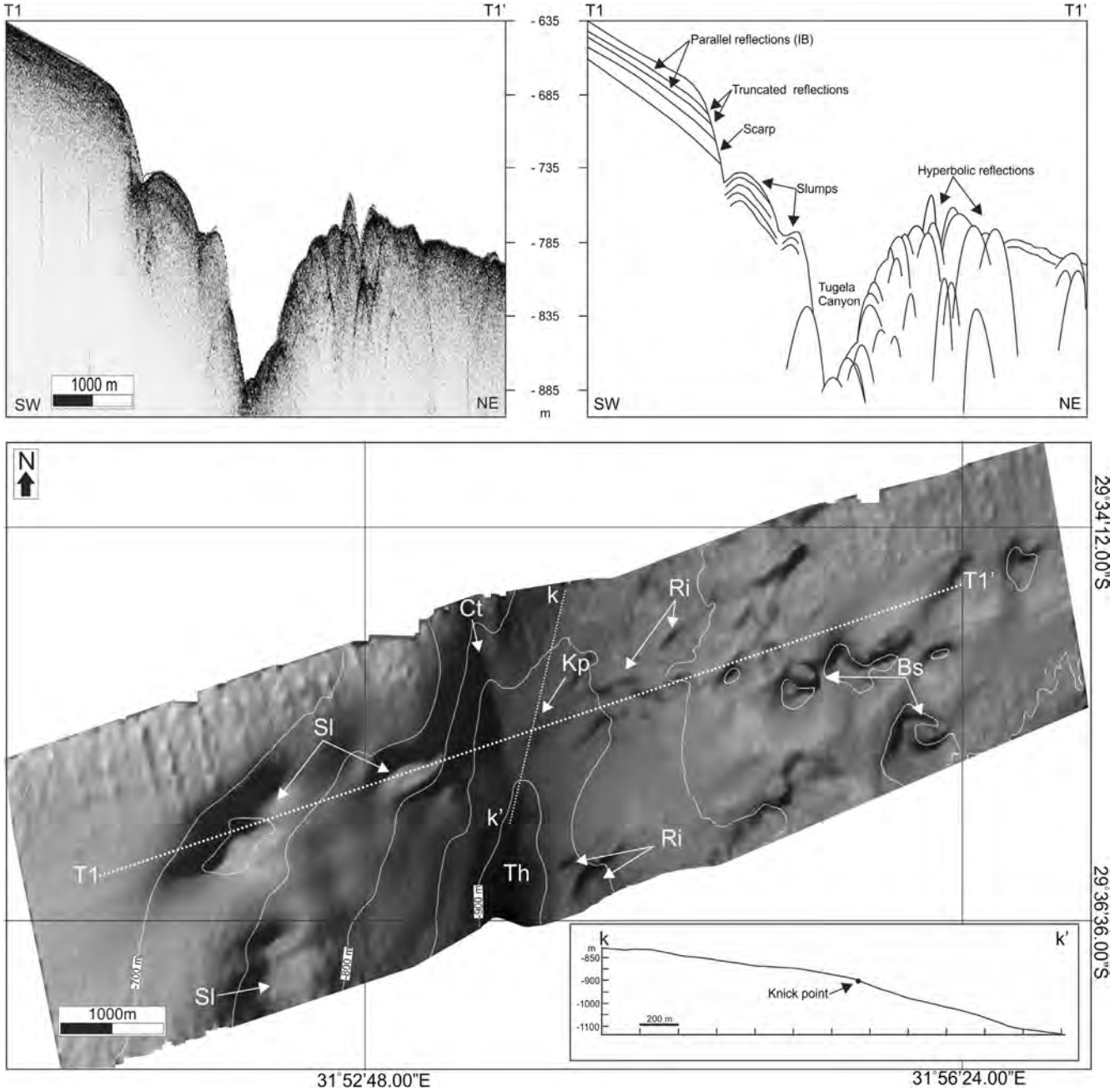

Figure 2. Swath TC1 from the innermost portion of the Tugela canyon. Note apparent basement outcrop (Bs), and rill (Ri) development, associated with the eastern canyon wall. Slide/slump scarps (Sl) are evident either side of the canyon axis. The thalweg (Th) is well defined below the knickpoint (Kp) and confluence of the main canyon and canyon tributary (Cr). Profiles k–k′ and T1–T1 illustrate the change in gradient across the knickpoint and 3.5 kHz echo trace across the Tugela canyon respectively.

likely contemporaneous systems. The first is facilitated by the South Atlantic Current (SAC) where flow comes from south of the Agulhas Plateau (Fig. 1). The SAC transports NADW around the southern tip of Africa, thereafter the NADW core bifurcates; one branch (depth of −2000 to −3500 m, salinity of 34.83‰) continuing northeastward, with the Agulhas Under Current deep flow, into the Natal Valley and Mozambique Basin via the Agulhas and Transkei basins respectively. The other branch continues east with the meandering Agulhas Return Current (Toole and Warren, 1993).

The second NADW pathway is by a continental-margin inflow. This system rounds the African continent at depths of between 2000 and 2500 m along the continental slope into the Transkei Basin on its approach to the Natal Valley (Toole and Warren, 1993; Schlüter and Uenzelmann-Neben, 2008). Some of the NADW returns along the eastern boundary of the Natal Valley (constrained by the western slopes of the Mozambique Ridge), while a portion of it crosses a saddle (2500–3000 m) in the Mozambique Ridge at approximately 31°S latitude.

Antarctic Bottom Water (AABW) does not enter the Natal Valley. Instead it rounds the southern edge of the Mozambique Ridge as it leaves the Transkei Basin, entering the Mozambique Basin beneath the northward flowing NADW core (Toole and Warren, 1993).

3. Material and methods

The data used in this study were collected during two research cruises; AISTEK II aboard the R/V Sonne (Jokat, 2006) and AISTEK III aboard the R/V Pelagia (Jokat, 2009).

AISTEK II focused on the Mozambique Basin where bathymetric data were collected using a SIMRAD EM120 system. Data acquired during AISTEK III (Mozambique Ridge and Natal Valley) were collected using a Kongsberg EM300 system. Both data sets were processed using CARIS HIPS and exported as xyz ASCII files. The data were gridded using Interactive Visualization Systems' DMagic (version 7.3.1a) and displayed in Fledermaus (version 7.3.1a) for interpretation. The final bathymetric chart has an output matrix of ~35 m capable of resolving seafloor features at that approximate scale.

Very high resolution seismic data (vertical resolution ca. 1 m) were simultaneously collected using both a 3.5 kHz (AISTEK III) and a parametric ATLAS PARASOUND echosounder (AISTEK II). Complete ship coverage along track was in some instances not achievable due to technical difficulties. Data were processed using in-house designed software, in addition to SEISEE (version 2.17.1). Higher penetration (4400 s TWTT), lower vertical resolution multichannel seismic data were sourced from the Petroleum Agency of South Africa. These data were incorporated into SEISEE for visualization and interpretation of the upslope canyon extensions. Band pass filter was adjusted and colour/wiggle gains were applied to the data.

4. Results

The Tugela canyon is intersected by five lines of swath bathymetry. Partial coverage spanning depths of 644 m (at the canyon head) to 2828 m (where the canyon ends in the Natal Valley) was achieved.

Swath TC1 (TC being an identifier of the swath in question) displays an area of the canyon between 842 m and 990 m depth (Figs. 1, box b and 2). In this section, the canyon incises 240 m into the adjacent slope and exhibits an average axial gradient of 3.7°. Closer to the canyon axis, wall gradients of 20° are apparent. Slump scarps (five) and rills (six) occur and are interspersed with sporadic, high relief basement outcrop. Slump scarps are more prevalent on the western margin, with rills and basement exposure confined to the eastern canyon margin. A gradient knickpoint, associated with a 1.81° change in gradient, is noted above the confluence of the Tugela canyon and a canyon tributary.

Very high resolution 3.5 kHz records show a distinct contrast between the eastern and western margins of the canyon (Fig. 2, profile T–T1). The latter is dominated by parallel reflections, truncated by a well-defined scarp. At the foot of the scarp parallel reflections are once again visible within a cohesive landslide block. The eastern margin is defined by extensive hyperbolic returns draped with isolated thin packages of parallel reflections. These reconcile with the rugged portions of seafloor identified as basement outcrop.

Approximately 15 km southeast of TC1 the Tugela canyon (Figs. 1, box c and 3) now possesses a "U"-shaped cross-sectional profile. The canyon has incised 492 m into the surrounding slope (gradient ~ 1°) and steepens to a maximum slope of 28°. Mass wasting is evident on both sides of the canyon. On either side of the canyon the sea-floor is relatively smooth, although basement does crop out to the west. Notably, axial incision is evident from a depth of 1490 m, a feature not observed inshore of this point.

Southeast of TC2 (~10.5 km), the overall morphology of the Tugela canyon changes drastically although the bottom of the canyon remains "U"-shaped (TC3). Terraces, separated by substantial escarpments, dominate the western margin (Figs. 1, box d and 4). The upper terrace is littered with blocky debris while the lower terraces appear free from debris. The eastern margin is dominated by slide/slump scarps. A canyon axis gradient of 0.6° is observed here. While the canyon walls reach a gradient of up to 30° locally, the escarpments within the terraces attain gradients of up to 39°. Beyond the canyon walls, the sea-floor is smooth with no signs of basement cropping out.

Directly south of swath TC3 (~4 km), swath TC4 (Fig. 1, box e) reveals a vastly different morphology from the upper reaches of the Tugela canyon. Despite still possessing a "U" shape with terraces (Fig. 5a), the lowest terrace now supports an inner branch of the canyon which enters the main canyon floor at 32°4′E/29°55′S (Fig. 5b). Four smaller channels feed into the inner branch near the base of the lowest escarpment. Interestingly, two channels are evident in the main canyon floor, one on the eastern side directly related to the upper reaches of the canyon and one on the western side associated with the inner branch (Fig. 5, e–e′). The two are initially separated by a longitudinally orientated mound of material that elevates the central portion of the canyon 40 m above the canyon floor and extends for at least

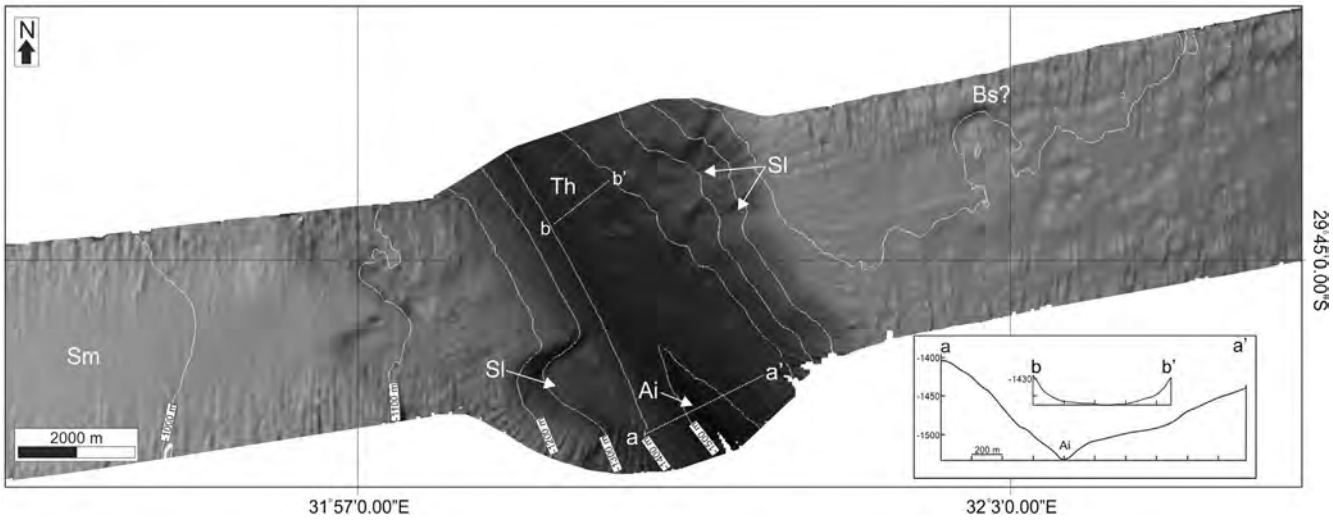

Figure 3. A distinct change in canyon morphology is illustrated by Swath TC2. The profile is now decidedly "U"-shaped and shows evidence of minor axial incision (Ai) at −1490 m (profile a–a′). This is not apparent upslope at −1450 m (b–b′). Slump/slide scarps (Sl) are common to both canyon flanks. Note the difference in the character of the seafloor either side of the canyon. Smooth (Sm) seafloor on the west is markedly different from rough seafloor in the east, suggesting some basement (Bs) outcrop or subcrop.

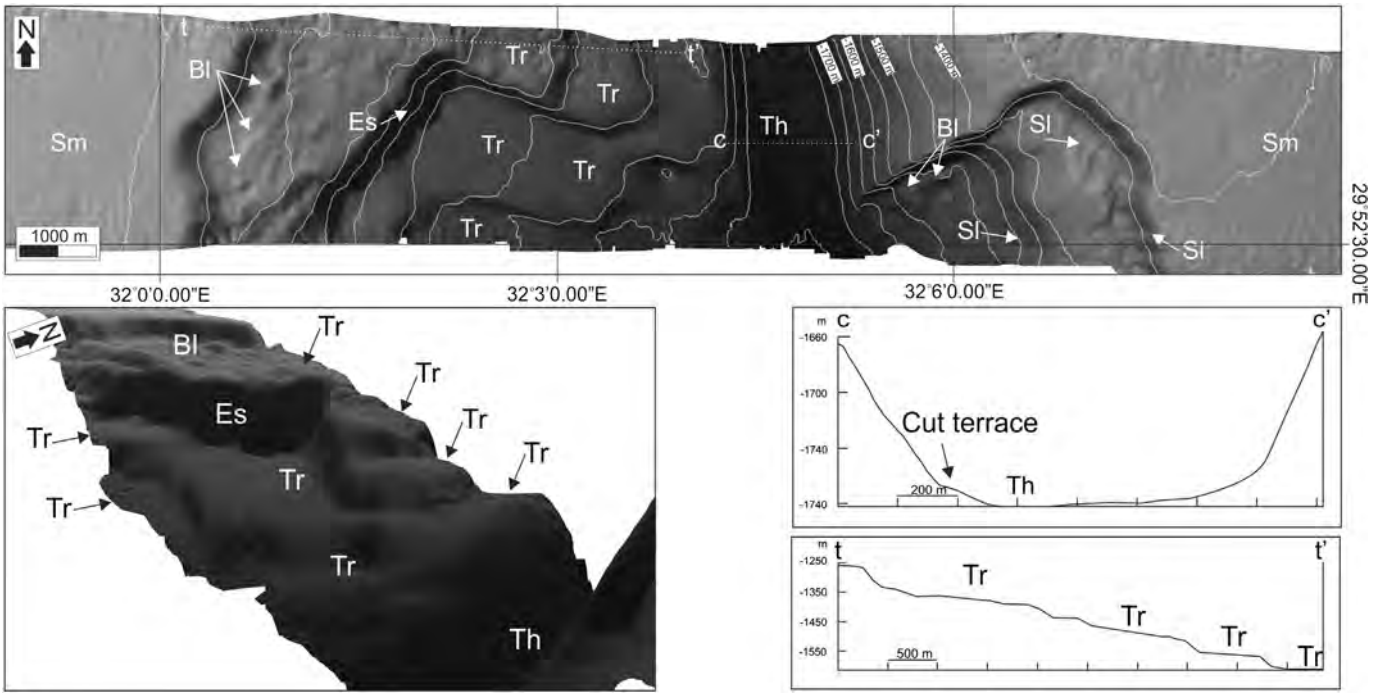

Figure 4. Swath TC3 from the mid-slope. Note the development of terraces (Tr) along the western canyon wall (profile t–t′), Escarpments (Es), blocky debris (Bl) and slide/slump scarps (Sl) are also evident. Smooth sea-floor (Sm) occurs on either side of the Tugela canyon. A minor cut terrace denotes flow bias toward the western side of the main canyon floor, associated erosion and incision (profile c–c′). The 3D inset illustrates the terraced nature of this portion of the canyon.

4 km, narrowing from 750 m to 350 m wide downstream (at the limit of data coverage).

3.5 kHz echosounder traces over the blocky deposits adjacent to the inner gorge area reveal significant hyperbolic echoes. The central portion of the line exhibits a package characterised by chaotic reflections, while further east discontinuous parallel reflections are evident (Fig. 5, profile d–d′).

Terraces are no longer evident in swath TC5 (21 km southeast of TC4) (Figs. 1, box f and 6). Here the Tugela canyon reaches its maximum degree of incision (1000 m) into the surrounding slope. Two minor hanging branches (cf. Lastras et al., 2011) enter the canyon. Cut-terraces are a feature of the main canyon floor showing at least five periods of axial incision (Fig. 6, profile g–g′).

The Tugela canyon widens into the abyssal Natal Valley, where a crude sub-horizontal (0.12°) terrace extends 100 km to the south west (Fig. 1, box g and 7). The echo character of the 3.5 kHz record is dominated by regular overlapping hyperbolae with varied vertex elevations extending ~40 km to the south west (Fig. 7b). This irregular sea-floor extends distally into smooth sea-floor. Another package of reflections is apparent underlying the smooth sea-floor. These high amplitude parallel reflections appear to interfinger with the adjacent hyperbolae-dominated seismic unit (Fig. 7a). No distributary channels, lobes or levees are evident in either the bathymetry or 3.5 kHz record.

The deep penetration multichannel seismics from the mid slope reveal several phases of canyon incision and fill that underlie the head of the Tugela canyon (Figs. 1, box a and 8). These occur as a series of high amplitude reflections that incise into the underlying stratigraphy and are truncated by successively younger reflections, the overall incision pattern of which is nested within the deepest incised reflection. On the basis of these discordant relationships, three phases of canyon incision and fill can be recognised: the youngest canyon fill, is characterised by an onlapping drape relationship with the palaeo-canyon walls. The contemporary Tugela canyon head is located in the topographic low preserved within these series of drapes.

Table 1 shows down-canyon characteristics associated with canyon width, relief, margin and gradient for the areas covered by multibeam bathymetry. Canyon relief and width were noted at the up-canyon and down-canyon limits of data coverage in order to best describe the canyon long-profile. Overall, the Tugela canyon shows an increase in width and relief with increasing distance from the continental shelf, and increasing water depth. The gradient of the canyon floor varies but, generally decreases with increasing distance from the continental shelf, and increasing water depth.

5. Discussion

5.1. Erosion styles

The canyon morphologies of the northern KwaZulu-Natal continental margin, (Green et al., 2007; Green and Uken, 2008; Green, 2011a), differ significantly from the expression of the Tugela canyon. Notably absent from the slope confined Tugela canyon is the amphitheatre-shaped canyon head morphology, associated with upslope eroding retrogressive failure (cf. Farre et al., 1983). Furthermore, the Tugela canyon displays a marked increase in relief and width with increased distance from the continental shelf and water depth (Table 1). Gradient, although variable, shows a decreasing trend in angle with increasing distance from the shelf (concave upward profile) and water depth (Table 1). This suggests that down-slope erosive processes dominated the formation of this canyon (cf. Goff, 2001; Mitchell, 2004). When compared to other slope canyon systems such as the submarine canyons of the American Atlantic (Vachtman et al., 2012) or Argentinian margins (Lastras et al., 2011), the Tugela canyon is particularly isolated from other erosive features. These other canyons show a significant number of tributary branches whereas no significant tributaries

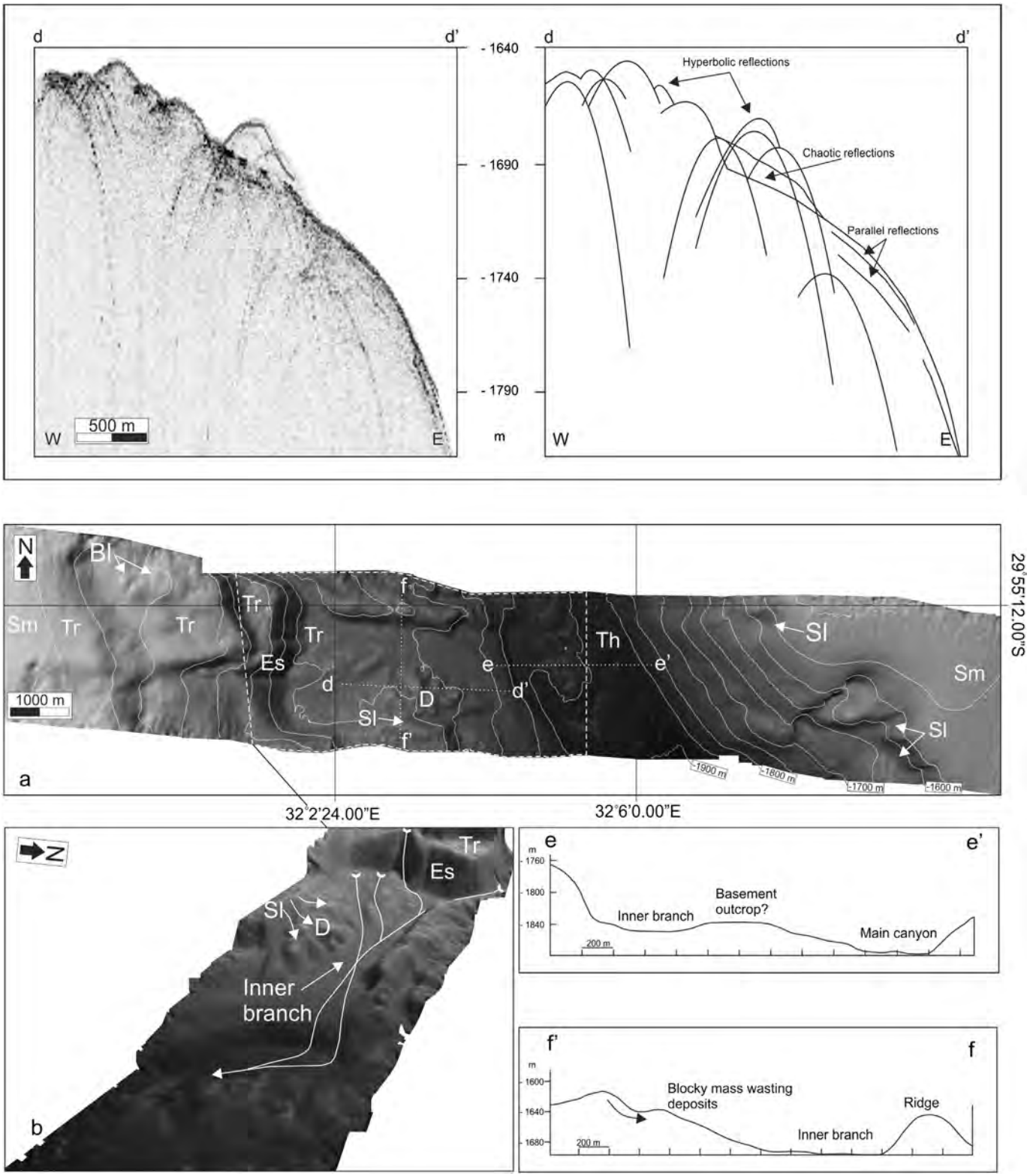

Figure 5. 3.5 kHz seismic profile and bathymetry of Swath TC4 (a). The canyon's inner branch (dashed box in (a)) is shown from a 3D perspective in the inset (b). Echo character, associated with mass-wasting debris (D) is illustrated in profile d–d′. Profile f–f′ is orientated north–south across the inner branch. The location of the main canyon floor relative to the inner branch canyon can be seen in profile e–e′.

exist for the Tugela canyon. This character approaches the "Type Ia" (straight slope systems) morphological class of Vachtman et al. (2012) and linear canyon class of Mitchell (2005). Such systems are associated with fluvial-like erosion dominated by bypassing of sedimentary flows, particularly during lowstand intervals. The absence of mass wasting debris along the thalweg of the Tugela canyon further reinforces the notion of downslope excavation as the principal factor in canyon formation (Vachtman et al., 2012).

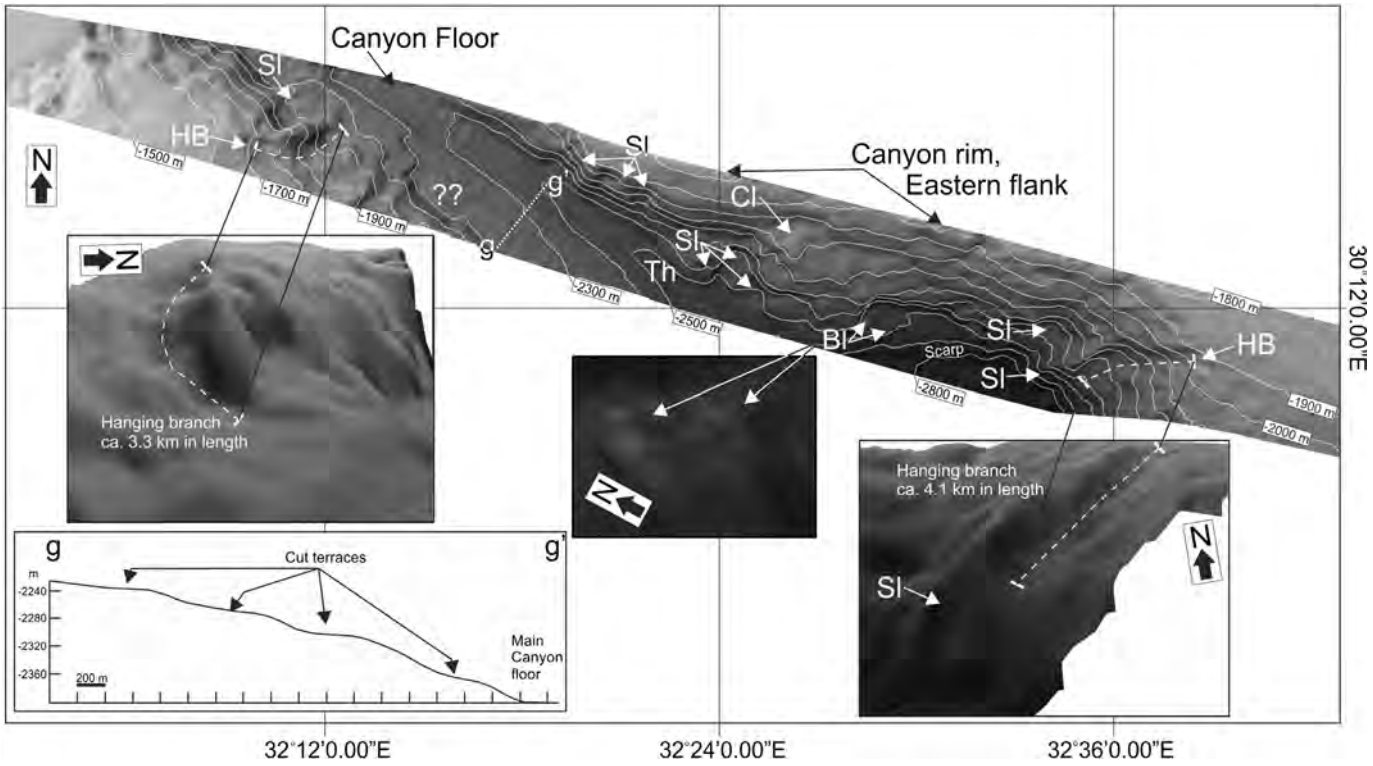

Figure 6. Bathymetry of Swath TC5. Cut-terraces are illustrated by profile g–g′. The 3D perspectives illustrate hanging branches (Hb) and blocky debris (Bl) along the canyon flanks.

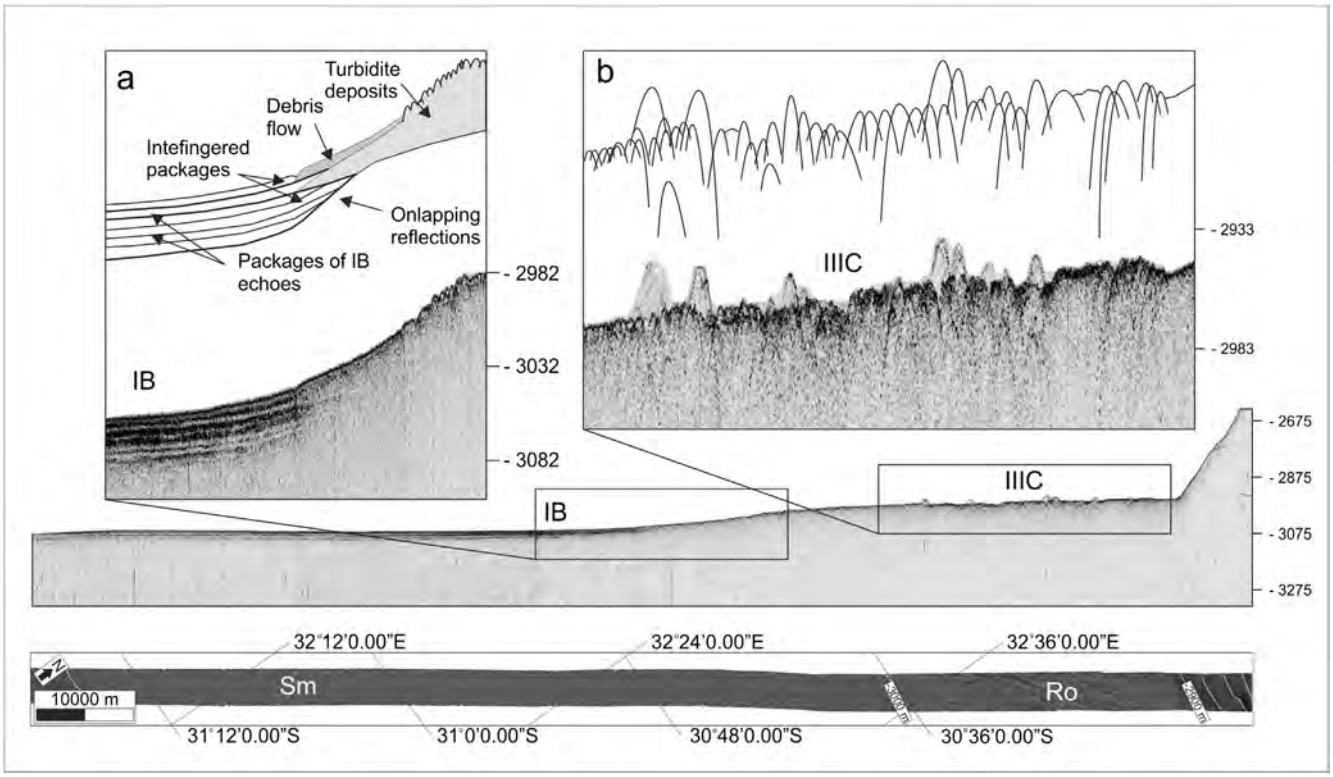

Figure 7. Swath bathymetry and 3.5 kHz profile from the Tugela canyon fan region. Inset (a) shows the distal transition from type IIIC echoes (cf. Damuth and Hayes, 1977) to IB echoes further south. Inset (b) illustrates the overlapping hyperbolae of IIIC echoes. A crude terrace is dominated by IIIC echoes. The character of the sea-floor noted in the 3.5 kHz record is confirmed in the bathymetry, rough sea-floor (Ro) changes abruptly to smooth sea-floor (Sm) as it extends southwest in to the deep Natal Valley.

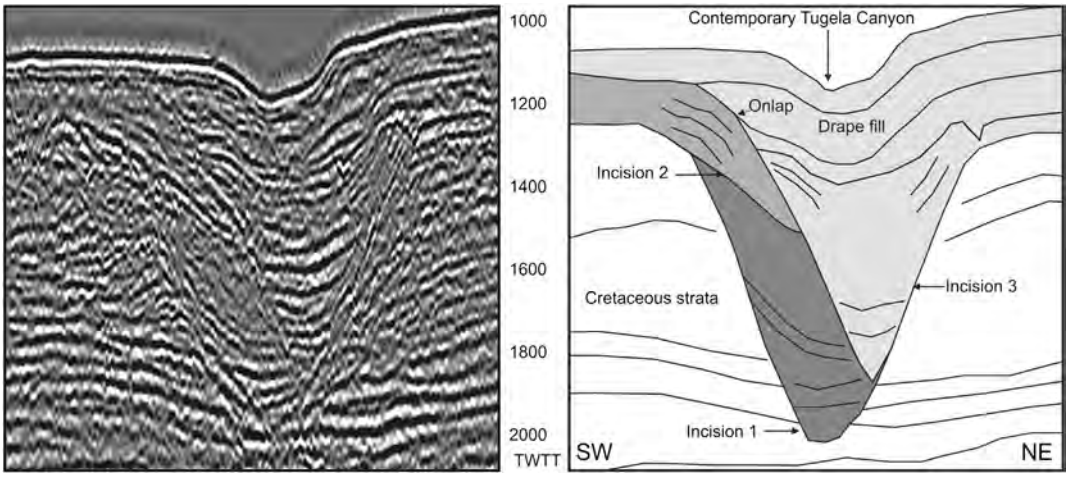

Figure 8. Along strike multi-channel seismic record and interpretation from the mid-slope portion of the Tugela Canyon. Note the three stacked paleo-canyons, the youngest of which is dominated by an onlapping drape fill. Note the stacked nature of the canyons and the position of the contemporary Tugela canyon within the low point of the drape succession.

Axial incision (Fig. 3) noted at −1490 m further illustrates the significance of down-slope erosion as a contributor to canyon formation. Baztan et al. (2005) found axial incision in canyons of the Gulf of Lion to be associated with river connection during lowstands. Hyperpycnal plumes generated by flooding rivers provide the necessary energy to develop axial incisions of considerable downslope length (>50 km) (Baztan et al., 2005), an attribute not associated with axial incision within the Tugela canyon. In this instance dilute turbidity currents (cf. Laberg et al., 2007; Jobe et al., 2011), rather than hyperpycnal plumes, are believed to be responsible for limited axial incision present in the Tugela canyon. Such turbidity currents can ignite from an over steepened muddy/silty upper slope (Pratson et al., 1994; Mitchell, 2005). It is highly unlikely that a river connection existed, certainly not at −1490 m, furthermore incision is limited to less than 10 km alluding to short lived erosive events. Axial incision was, however, sufficient to induce further instability resulting in mass wasting of the canyon flanks down slope. Cut-terraces evident in the lower course (Fig. 6, profile g–g′) illustrate five lesser periods of vertical erosion, while two significant periods of incision are envisioned for the canyon system as a whole (discussed in Section 5.2). Escarpments (Figs. 4 and 5), formed by the erosion of sedimentary strata as opposed to displacement via faulting, are confined to the western flank of the Tugela canyon. This is likely controlled by bed geometry, a topic discussed by McGregor (1981). In this instance, SE dipping strata of the western flank are inherently unstable. These strata dip in towards the void excavated by the Tugela canyon, resulting in preferential erosion of these strata. Conversely, strata of the eastern flank are less susceptible to erosion and more stable, given that these strata dip into the eastern flank. This accounts for the canyon wall asymmetry depicted in Figures 4 and 5. Basement outcrop becomes less evident down canyon; certainly by swath TC3 no basement outcrop is apparent. The prominent outcrop up canyon from this point suggests an increase in basement control, over canyon development, toward the continental shelf.

5.2. Timing and mechanisms of canyon development

The cross-cutting relationship between the Tugela canyon and Cretaceous units (Fig. 8) clearly shows that the formation of the Tugela canyon post-dates the deposition of the upper Maastrichtian age basin fill (Goodlad, 1986). The multi-channel seismic sections upslope of the modern canyon head show several phases of incision. Here it is proposed that the earliest of these corresponds to a mid Oligocene stage of hinterland uplift, the first to occur during the Neogene (Walford et al., 2005). Uplift, combined with regressive conditions (Fig. 9a), resulted in considerable sediment shedding in the hinterland, and transport across the shelf. Sediment was thus provided directly to the slope where downslope-eroding mass wasting processes associated with sediment loading and over-steepening initiated the proto-Tugela canyon (Figs. 9a and 10). Subsequent transgression would subsequently reduce downslope eroding sediment flows to the canyon, resulting in a period of dormancy corresponding to the first stage of infilling (Fig. 9b).

The Tugela canyon was later reactivated during the subsequent early Miocene uplift (Fig. 9c), as evidenced in the second canyon incision in the upslope seismic sections (Fig. 8) and an associated second phase of terracing in the lower canyon portions. This is reconciled to the early hiatus documented in the shallow shelfal portions of the Tugela Cone and suggests a significant period of regression, sediment bypass and associated incision in the shelf (Green and Garlick, 2011). This is likely to have translated downslope and thus substantially rejuvenated the Tugela canyon. This is

Table 1
Down-canyon comparison of relief, width and gradient.

Swath	TC1	TC2	TC3	TC4	TC5
Width U	3.1 km	6.4 km	11.5 km	12.2 km	18.3 km
Relief U	72 m	435 m	572 m	579 m	874 m
Width L	6 km	6.8 km	13 km	13.8 km	19.6 km
Relief L	260 m	458 m	599 m	615 m	1028 m
Margins	Straight, converging	Straight, diverging	Meandering, diverging	Meandering, diverging	Meandering, diverging
Gradient	3.7°	0.3°	0.6°	0.6°	0.6°

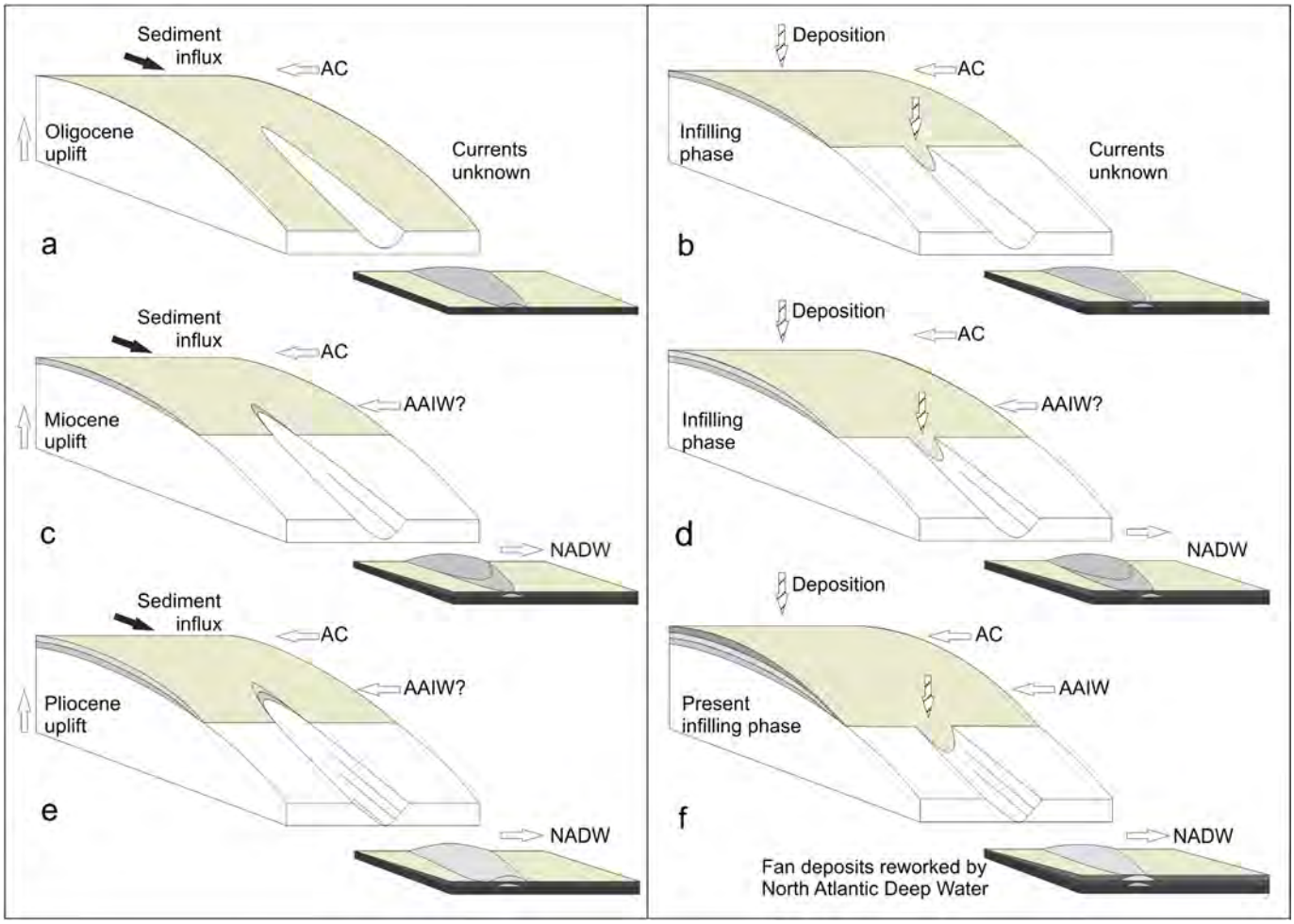

Figure 9. An evolutionary model for the Tugela canyon and fan evolution. Note periods of uplift (a, c, e) set-apart by infilling (b, d, f) of the upper canyon, stagnation of the mid to lower reaches during quiet phases, and interfingered fan/pelagic sediments in the deep Natal Valley.

linked to the generation of a modified "U" profile (Figs. 4 and 5) and the hanging branches depicted in Figure 6.

Another period of quiescence followed this and was associated with infilling (Fig. 9d) prior to a third stage of late Pliocene uplift occurred on a scale greater than that of the Miocene phase (Fig. 9e) (Walford et al., 2005; Moore and Blenkinsop, 2006). This resulted in canyon incision into both the previous palaeo-canyons, pronounced axial incision and additional terracing in the walls (Figs. 4 and 6).

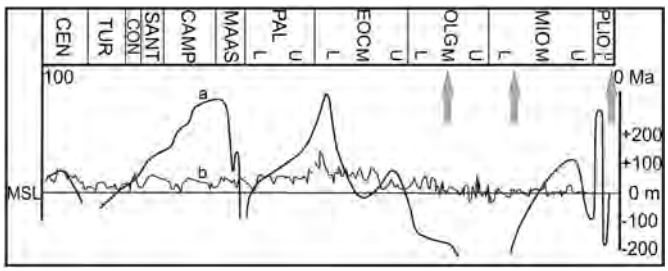

Figure 10. Mid Cretaceous to Pliocene sea-level curve (a, modified after Dingle et al., 1983) compared to the global eustatic sea-level curve (b, modified after Miller et al., 2005). Grey arrows denote uplift episodes. Note the poorly constrained Tertiary sea-level curve.

Comparable studies from the western South African margin indicate similar erosional periods. A protracted early to mid Oligocene hiatus is recognised by Wigley and Compton (2006) and is contemporaneous with a recognised global sea level lowstand of the mid Oligocene (Miller et al., 1998). It is likely that off-shelf shedding of sediment during regression to this lowstand (cf. Compton and Wiltshire, 2009) would have resulted in downslope erosion. Overall, the most protracted amount of uplift occurred during the Pliocene (Partridge and Maud, 2000). This is considered to have caused several slumps on the southern African margin (Dingle, 1980), initiated the head of the Cape Canyon on the western South African margin (Wigley and Compton, 2006) and caused several submarine canyons to form on the northern KwaZulu-Natal margin (Green, 2011a).

5.3. Modern canyon and fan activity

Given the age and the amount of sediment that was likely to have passed through the Tugela canyon since its inception; the absence of a well-developed submarine fan prograding into the Natal Valley is surprising. A situation similar to the Congo deep-sea fan would be expected (cf. Anka et al., 2009), however fan deposits directly offshore the Tugela river are completely absent (Türkay and Pätzold, 2009). Instead a poorly developed fan extending from the sudden opening of the Tugela canyon is present (Fig. 7).

Echosounder records show the fan as a crude terrace dominated by regular overlapping hyperbolae with varied vertex elevations extending ~40 km to the south west (Fig. 7b). These correspond to the Type IIIC echo facies of Damuth and Hayes (1977). Such echo character is associated with erosional/depositional bedforms, either the result of erosion in the bottom boundary layer (Flood, 1980) and syndeposition (Tucholke, 1979) related to bottom water circulation or gravity driven processes (Damuth, 1975) depending on the setting. This irregular sea-floor extends distally into smooth sea-floor as the Natal Valley deepens toward the south (Fig. 7).

Another package of reflections is apparent underlying the smooth sea-floor (Fig. 7a). These comprise distinct high amplitude parallel reflections (echo facies IB of Damuth, 1975) that appear to interfinger with the adjacent hyperbolae-dominated seismic unit. Such seismic facies have been recognised by Damuth (1975) and interpreted to be the proximal variant of turbidites on the abyssal rise, or the result of pelagic sedimentation. Such flat lying deposits (in this area the slope is sub-horizontal, averaging 0.12°) have been recognised by others as pelagic deposits and their flat parallel nature is indicative of bottom current winnowing and episodic sea-floor smoothing in association with drift development (Schlüter and Uenzelmann-Neben, 2008). Contrary to what one might expect, there are no surface expressions of distributary channels or levees etc. The interfingering of hyperbolae-dominated IIIC facies with parallel, flat-lying facies (IB) is likely the result of intermittent unconfined turbidite introduction to the area (Fig. 7a).

This suggests that there is significant interaction between the two systems whereby sporadic and energetic turbidites overprint NADW deposition before being winnowed and redistributed into an echo facies 1B configuration. No other features associated with deep-sea fans, lobes, or distributaries are recognised in the Tugela canyon fan region. It should therefore be described as an atypical, sediment starved deep-sea fan that is strongly modified by the NADW. Other examples of such fans are poorly described. Eschard (2001) maintains that such interactions between deep-sea fans and bottom water circulation (erosion and redistribution of sediment) are underrated.

In the proximal staging grounds for downslope eroding flows, the overspilling of sediment from the shelf to the slope is limited by the Agulhas Current. In these areas, the current re-organises sediment in a coast parallel manner and it only overspills the shelf break where major inflection points in the coast occur (Flemming, 1980). Despite these being a possible source for turbidity currents (Boyd et al., 2008) the wholesale starvation of the shelf has occurred to the extent that the submarine canyons along the northern KZN coast have been quiescent since the late Pliocene (Green, 2011b). Since then an overall period of starvation has prevailed and has limited the primary canyon driving mechanism, namely upper slope sediment loading and resultant mass wasting. During these times, pelagic sedimentation on the upper and mid-slope has been dominant (Fig. 9f). This is responsible for the development of the most recent onlapping drape fill in the upper canyon which has not fully filled the palaeo-canyon form (Fig. 8). Further down canyon, erosion may still be occurring (as evidenced by some smaller cut terraces developed in the canyon walls) but is limited in comparison to that of the Neogene.

During the current highstand where sediment delivery is commonly not as prominent as lowstand periods, even less sediment is released to the shelf. This is further held up in the polewards moving sediment conveyor of the Agulhas Current thereby starving the upper slope region. The fan deposits that are preserved from periods of canyon activity are currently in the process of being reworked by the NADW, a scenario similarly encountered in the adjacent Transkei Basin (Schlüter and Uenzelmann-Neben, 2007, 2008).

6. Conclusions

The Tugela canyon has evolved via downslope erosion, primarily driven by sediment gravity flows or dilute turbidity currents. These initiated from periods of upper slope progradation whereby the oversteepened upper slope acted as a source for these flows. These periods can be linked to uplift of the hinterland and are interposed with periods of pelagic canyon infilling.

Two minor periods of hinterland uplift in the mid Oligocene and mid Miocene caused the canyon to incise into the same palaeo-canyon surface. A major period of uplift in the late Pliocene caused protracted incision and the development of the main lower slope canyon. Upslope, this created a compound feature of nested palaeo-canyons, the most recent (late Pliocene) incision now filled by pelagic deposition during a long period of quiescence.

The contemporary Tugela canyon now rests within this infilled palaeo-canyon and appears to be moribund with respect to canyon forming processes. The contemporary canyon morphology is controlled to some extent by basement outcrop, though bed geometry also plays a role in the evolution of the canyon through preferential erosion of the western flank and levee development on the eastern flank.

The associated Tugela canyon fan appears to represent a mixed turbidite and bottom smoothed pelagic system. The lack of sediment input from the shelf is a result of sweeping by the Agulhas current. Along the abyssal rise, the fan's limited extent and the lack of features such as lobes and channel–levee complexes defines it as an atypical sediment starved and bottom current winnowed system.

Acknowledgements

We thank the BMBF (Bundesministerium fur Bildung und Forschung) for funding the scientific projects (contract number 03G0183A, 03G0730A). The crews of RV Sonne (AISTEK II) and RV Pelagia (AISTEK III) are acknowledged for their excellent support and expertise in the data acquisition phases. The financial assistance of the National Research Foundation (DAAD-NRF) towards this research is hereby acknowledged. Opinions expressed and conclusions arrived at, are those of the author and are not necessarily to be attributed to the DAAD-NRF. The Petroleum Agency of South Africa are thanked for allowing us access to multichannel seismic data.

References

Anka, Z., Séranne, M., Lopez, M., Scheck-Wenderoth, M., Savoye, B., 2009. The long-term evolution of the Congo deep-sea fan: a basin-wide view of the interaction between a giant submarine fan and a mature passive margin (ZaiAngo project). Tectonophysics 470, 42–56.

Bang, N.D., Pearce, A.F., 1976. Large-scale circulation of surface water of the south Indian Ocean. In: Heydorn, A.E.F. (Ed.), Ecology of the Agulhas Current Region – an Assessment of Biological Responses to Environmental Parameters in the South-West Indian Ocean. Proceedings of the Marine Freshwater Conference, Port Elizabeth. CSIR, Pretoria, pp. 4–10.

Baztan, J., Berne, S., Olivet, J., Rabineau, M., Aslanian, D., Gaudin, M., Rehault, J., Canals, M., 2005. Axial incision: the key to understand submarine canyon evolution (in the western Gulf of Lion). Marine and Petroleum Geology 22, 805–826.

Ben Avraham, Z., Hartnady, C.H.J., Malan, J.A., 1993. Early tectonic extension between the Agulhas Bank and Falkland Plateau due to the rotation of the Lafonia microplate. Earth and Planetary Science Letters 117, 43–58.

Boyd, R., Ruming, K., Goodwin, I., Sandstrom, M., Schröder-Adams, C., 2008. Highstand transport of coastal sand to the deep ocean: a case study from Fraser Island, southeast Australia. Geology 36, 15–18.

Compton, J.S., Wiltshire, J.G., 2009. Terrigenous sediment export from the western margin of South Africa on glacial to interglacial cycles. Marine Geology 266, 212–222.

Damuth, J.E., Hayes, D.E., 1977. Echo character of the east Brazilian continental margin and its relationship to sedimentary processes. Marine Geology 24, 73–95.

Damuth, J.E., 1975. Echo characters of the western equatorial Atlantic floor and its relationship to the dispersal and distribution of terrigenous sediments. Marine Geology 18, 17–45.
Dingle, R.V., 1980. Large allochthonous sediment masses and their role in the construction of the continental slope and rise of southwestern Africa. Marine Geology 37, 33–35.
Dingle, R.V., Robson, S., 1985. Slumps, canyons and related features on the continental margin off East London, SE Africa (SW Indian Ocean). Marine Geology 67, 37–54.
Dingle, R.V., Siesser, W.G., Newton, A.R., 1983. Mesozoic and Tertiary Geology of Southern Africa. Balkema, Rotterdam, p. 375.
Dingle, R.V., Goodlad, S.W., Martin, A.K., 1978. Bathymetry and Stratigraphy of the northern Natal Valley (SW Indian Ocean): a preliminary account. Marine Geology 28, 89–106.
Dingle, R.V., Birch, G.F., Bremner, J.M., De Decker, R.H., Du Plessis, A., Engelbrecht, J.C., Fincham, M.J., Fitton, T., Flemming, B.W., Goodlad, S.W., Gentle, R.I., Martin, A.K., Mills, E.G., Moir, G.J., Parker, R.J., Robson, S.H., Rogers, J., Salmon, D.A., Siesser, W.G., Simpson, E.S.W., Summerhayes, C.P., Westall, F., Winter, A., Woodborne, M.W., 1987. Deep-sea sedimentary environments around southern Africa (SE-Atlantic & SW-Indian Oceans). Annals South African Museum 98, 1–27.
Eschard, R., 2001. Geological factors controlling sediment transport from platform to deep basin: a review. Marine and Petroleum Geology 18, 487–490.
Farre, J.A., McGregor, B.A., Ryan, W.B.F., Robb, J.M., 1983. Breaching the shelfbreak; passage from youthful to mature phase in submarine canyon evolution. In: Stanley, D.J., Moore, G.T. (Eds.), The Shelfbreak: Critical Interface on Continental Margins. Soc. Econ. Palaeontol. Mineral. Spec. Pub., vol. 33, pp. 25–39.
Flemming, B.W., 1980. Sand transport and bedform patterns on the continental shelf between Durban and Port Elizabeth (southeast African continental margin). Sedimentary Geology 26 (1–3), 179–205.
Flood, R.D., 1980. Deep-sea sedimentary morphology: modelling and interpretation of echo-sounding profiles. Marine Geology 38, 77–92.
Goff, J.A., 2001. Quantitative classification of canyon systems on continental slopes and a possible relationship to slope curvature. Geophysical Research Letters 28, 4359–4362.
Goodlad, S.W., 1986. Tectonic and Sedimentary History of the Mid-Natal Valley (SW Indian Ocean). In: Marine Geoscience Unit Bulletin, vol. 15. Joint Geological Survey/University of Cape Town, p. 415.
Green, A.N., 2009. Sediment dynamics on the narrow, canyon-incised and current-swept shelf of the northern KwaZulu-Natal continental shelf, South Africa. Geo-Marine Letters 29, 201–219.
Green, A.N., 2011a. Submarine canyons associated with alternating sediment starvation and shelf-edge wedge development: northern KwaZulu-Natal continental margin, South Africa. Marine Geology 289, 114–126.
Green, A.N., 2011b. The late Cretaceous to Holocene sequence stratigraphy of a sheared passive upper continental margin, northern KwaZulu-Natal, South Africa. Marine Geology 289, 17–28.
Green, A.N., Garlick, G.L., 2011. Sequence stratigraphic framework for a narrow, current-swept continental shelf: the Durban Bight, central KwaZulu-Natal, South Africa. Journal of African Earth Sciences 60, 303–314.
Green, A.N., Uken, R., 2008. Submarine landsliding and canyon evolution on the northern KwaZulu-Natal continental shelf, South Africa, SW Indian Ocean. Marine Geology 254, 152–170.
Green, A.N., Goff, J.A., Uken, R., 2007. Geomorphological evidence for upslope canyon forming processes on the northern KwaZulu-Natal shelf, South Africa. Geo-Marine Letters 27, 399–409.
Green, A.N., Uken, R., Ovechkina, M., 2008. Nannofossil age constraints for the northern KwaZulu-Natal shelf-edge wedge: implications for continental margin dynamics, South Africa, SW Indian Ocean. Continental Shelf Research 28, 2442–2449.
Jobe, Z.R., Lowe, D.R., Uchytil, S.J., 2011. Two fundamentally different types of submarine canyons along the continental margin of Equatorial Guinea. Marine and Petroleum Geology 28 (3), 843–860.
Jokat, W., 2009. The Expedition of the Research Vessel "Pelagia" to the Natal Basin and the Mozambique Ridge in 2009 (Project AISTEK III). Alfred-Wegener-Institute for Polar and Marine Research, Bremerhaven, p. 67.
Jokat, W., 2006. Southeastern Atlantic and Southwestern Indian Ocean: Reconstruction of the Sedimentary and Tectonic Development Since the Cretaceous, AISTEK-II: Mozambique Ridge and Mozambique Basin. Report of the RV "Sonne" Cruise SO-183, Project AISTEK-II 20 May to 7 July 2005 Reports on Polar and Marine Research. Alfred-Wegener-Institute for Polar and Marine Research, Bremerhaven, p. 71.
Laberg, J.S., Guidard, S., Mienert, J., Vorren, T.O., Haflidason, H., Nygard, A., 2007. Morphology and morphogenesis of a high-latitude canyon; the Andøya canyon, Norwegian Sea. Marine Geology 246, 68–85.
Lastras, G., Acosta, J., Muñoz, A., Canals, M., 2011. Submarine canyon formation and evolution in the Argentine Continental Margin between 44°30′S and 48°S. Geomorphology 128, 116–136.
Leinweber, V.T., Jokat, W., 2011a. Is there continental crust underneath the northern Natal Valley and the Mozambique Coastal Plains? Geophysical Research Letters 38, L14303.
Leinweber, V.T., Jokat, W., 2011b. The Jurassic history of the Africa-Antarctica Corridor – new constraints from magnetic data on the conjugate continental margins. Tectonophysics. http://dx.doi.org/10.1016/j.tecto.2011.11.008.
Martin, A.K., Goodlad, S.W., Hartnady, C.J.H., du Plessis, A., 1982. Cretaceous palaeopositions of the Falkland Plateau relative to southern Africa using Mesozoic seafloor spreading anomalies. The Geophysical Journal of the Royal Astronomical Society 71, 567–579.
Martin, A.K., Flemming, B.W., 1988. Physiography, structure and geological evolution of the Natal continental shelf. In: Schumann, E. (Ed.), Lecture Notes on Coastal and Estuarine Studies off Natal, South Africa. Springer, New York, pp. 11–46.
Martin, A.K., Hartnady, C.J.H., 1986. Plate tectonic development of the south-west Indian Ocean: a revised reconstruction of East Antarctica and Africa. Journal of Geophysical Research 91, 4767–4786.
Miller, K.G., Mountain, G.S., Browning, J.V., Kominz, M., Sugarman, P.J., Christie-Blick, N., Katz, M.E., Wright, J.D., 1998. Cenozoic global sea level, sequences, and the New Jersey transect: results from coastal plain and continental slope drilling. Reviews of Geophysics 36, 569–601.
Miller, K.G., Kominz, M., Browning, J.V., Wright, J.D., Mountain, G.S., Katz, M.E., Sugarman, P.J., Cramer, B.S., Christie-Blick, N., Pekar, S.F., 2005. The Phanerozoic record of global sea-level change. Science 310, 1293–1298.
Mitchell, N.C., 2004a. Form of submarine erosion from confluences in Atlantic USA continental slope canyons. American Journal of Science 304, 590–611.
Mitchell, N.C., 2005. Interpreting long-profiles of canyons in the USA Atlantic continental slope. Marine Geology 214, 75–99.
Moore, A.E., Blenkinsop, T.G., 2006. Scarp retreat versus pinned drainage divide in the formation of the Drakensberg escarpment, southern Africa. South African Journal of Geology 109, 455–456.
McGregor, B.A., 1981. Smooth seaward-dipping horizons - an important factor in sea-floor stability? Marine Geology 34, 3–4.
Partridge, T.C., Maud, R.R., 2000. Macro-scale geomorphic evolution of southern Africa. In: Partridge, T.C., Maud, R.R. (Eds.), The Cenozoic of Southern Africa. Oxford University Press, New York, pp. 3–18.
Pratson, L.F., Ryan, W.B.F., Mountain, G.S., Twitchell, D.C., 1994. Submarine canyon initiation by downslope-eroding sediment flows: evidence in late Cenozoic strata on the New Jersey continental slope. Geological Society of America, Bulletin 106, 395–412.
Ridente, D., Foglini, F., Minisini, D., Trincardi, F., Verdicchio, G., 2007. Shelf-edge erosion, sediment failure and inception of Bari canyon on the Southwestern Adriatic Margin (Central Mediterranean). Marine Geology 246, 193–207.
Schlüter, P., Uenzelmann-Neben, G., 2007. Seismostratigraphic analysis of the Transkei Basin: a history of deep sea current controlled sedimentation. Marine Geology 240, 99–111.
Schlüter, P., Uenzelmann-Neben, G., 2008. Indications for bottom current activity since Eocene times: the climate and ocean gateway archive of the Transkei Basin, South Africa. Global and Planetary Change 60, 416–428.
Shone, R.W., 2006. Onshore post-Karoo Mesozoic deposits. In: Johnson, M.R., Anheuser, C.R., Thomas, R.J. (Eds.), The Geology of South Africa. The Geological Society of South Africa, Johannesburg/Council for Geoscience, Pretoria, pp. 541–553.
Toole, J.M., Warren, B.A., 1993. A hydrographic section across the subtropical South Indian Ocean. Deep Sea Research I 40, 1973–2019.
Tucholke, B.E., 1979. Furrows and focuses echoes on the Blake Outer Ridge. Marine Geology 31, 13–20.
Türkay, M., Pätzold, J. (Eds.), 2009. Southwestern Indian Ocean – Eastern Atlantic Ocean, Cruise No 63, January 24–March 30, 2005. Universität Hamburg, p. 98. METEOR-Berichte 09-3.
Vachtman, D., Mitchell, N.C., Gawthorpe, R., 2012. Morphologic signatures in submarine canyons and gullies, central USA Atlantic continental margins. Marine and Petroleum Geology, 1–14.
Walford, H.L., White, N.J., Sydow, J.C., 2005. Solid sediment load history of the Zambezi Delta. Earth and Planetary Science Letters 238, 49–63.
Wigley, R.A., Compton, J.S., 2006. Late Cenozoic evolution of the outer continental shelf at the head of the Cape Canyon, South Africa. Marine Geology 226, 1–23.

Geo-Mar Lett
DOI 10.1007/s00367-014-0383-1

ORIGINAL

A new pathway for Deep water exchange between the Natal Valley and Mozambique Basin?

Errol Wiles · Andrew Green · Mike Watkeys · Wilfried Jokat · Ralf Krocker

Received: 8 July 2014 / Accepted: 2 September 2014

Abstract Although global thermohaline circulation pathways are fairly well known, the same cannot be said for local circulation pathways. Within the southwest Indian Ocean specifically there is little consensus regarding the finer point of thermohaline circulation. We present recently collected multibeam bathymetry and PARASOUND data from the northern Natal Valley and Mozambique Ridge, southwest Indian Ocean. These data show the Ariel Graben, a prominent feature in this region, creates a deep saddle across the Mozambique Ridge at ca. 28°S connecting the northern Natal Valley with the Mozambique Basin. Results show a west to east change in bathymetric and echo character across the northern flank of the Ariel Graben. Whereby eroded plastered sediment drifts in the west give way to aggrading plastered sediment drift in the midgraben, terminating in a field of seafloor undulations in the east. In contrast, the southern flank of the Ariel Graben exhibits an overall rugged character with sediments ponding in bathymetric depressions in between rugged sub/outcrop. It is postulated that this change in seafloor character is the manifestation of deep water flow through the Ariel Graben. Current flow stripping, due to increased curvature of the graben axis, results in preferential deposition of suspended load in an area of limited accommodation space consequently developing an over-steepened plastered drift. These deposited sediments overcome the necessary shear stresses, resulting in soft sediment deformation in the form of down-slope growth faulting (creep) and generation of undulating sea-floor morphology. Contrary to previous views, our works suggests that water flows from west to east across the Mozambique Ridge via the Ariel Graben.

E. Wiles (✉) · A. Green · M. Watkeys
Geological Sciences, School of Agricultural, Earth and Environmental Sciences, University of KwaZulu-Natal, Private Bag X 54001, Durban 4000, South Africa
e-mail: eawiles@yahoo.com

W. Jokat · R. Krocker
Alfred-Wegener-Institute for Polar and Marine Research, Am Alten Hafen 26, Bremerhaven 27568, Germany

Introduction

The global transfer of heat and nutrients is driven by thermohaline circulation (THC) within the ocean basins. The THC system comprises a network of bottom, deep and surface currents that conserve mass and energy in the World's oceans by the creation of a complex system of circulation cells. The southwest Indian Ocean (SWIO) is a dynamic region of ocean exchange between the Indian, Atlantic and Southern Oceans representing a pivotal component of the THC system. In general, both bottom and deep water circulation pathways around the globe and within the SWIO are well known and constrained. The residence times of these deep and bottom waters have significant implications for long-term climate state as well as CO_2 sequestration (Martin 1981a; Martin 1981b; Ben-Avraham et al. 1994; Srinivasan et al. 2009). As a result, the greater THC system has garnered increased attention over the past two decades, particularly in light of their potential roles driving both palaeo and future climate change (Martin 1981a; Martin 1981b; Raymo et al. 1990; Winter and Martin 1990; Raymo et al. 1997; Schmieder et al. 2000; Srinivasan et al. 2009; Gutjahr et al. 2010). However, at a more localised scale, THC pathways are often poorly constrained. Many factors, including the Earth's rotation (Coriolis Effect), ocean basin macrotopography, ocean gateways, prevailing winds, and glacial/ inter-glacial cycles have a direct impact on THC circulation and transport volumes. This research examines deep water bottom currents in the context of seafloor macrotopography and interprets these in light of several possible deep water circulation systems in the Natal Valley, SWIO.

Since the initial research thrust in the Natal Valley (cf. Martin 1981a; Martin 1981b; Dingle et al. 1978; Dingle et al. 1987,

Published online: 27 September 2014

Winter and Martin 1990), little additional research associated with the Natal Valley has been undertaken; this is especially true for the deep, northern portions of the Natal Valley. Notable exceptions include studies on the interactions between bottom water currents (those deep currents in contact with the seafloor) and sediments from the Natal Valley (Niemi et al. 2000; Wiles et al. 2013), and submarine canyons of the upper slope (Green et al. 2007; Green and Uken 2008; Green 2011a).

This paper presents a new, higher resolution dataset of the area, highlighting several key seafloor and subsurface features that reveal a potential new deep water pathway across the Mozambique Ridge (via the Ariel Graben) to the Mozambique Basin, as described by new multibeam bathymetry and high frequency seismic data from the Natal Valley, SWIO. The aim of this paper is to reconcile this with the major THC systems in the area.

Physical setting

Geology and physiography

Bound to the west by the south-east African continental margin and to the east by the Mozambique Ridge, the Natal Valley is a north–south orientated basin located in the SWIO (Fig. 1). To the south the Natal Valley merges (below 4000 m) with the Transkei Basin. Shoaling northward, the Natal Valley extends toward the extensive low-lying coastal plains of southern Mozambique (Dingle et al. 1978; Goodlad 1986). The Natal Valley, divided in to a northern and southern portion at 30°S, is the product of two distinct spreading centres. The northern portion of the basin opened ca. 183–158 Ma (Leinweber and Jokat 2011), while the southern portion was the result of spreading from 138.9–130.3 Ma (Leinweber and Jokat 2012). The basin was fully developed by 90 Ma (Martin and Hartnady 1986; Ben-Avraham et al. 1994).

The western margin of the Natal Valley exhibits an anomalously narrow, 4–15 km wide, coast-parallel shelf (Dingle and Robson 1985; Green 2011a; Green 2011b; Cawthra et al. 2012). Departure from the narrow shelf is observed offshore of the Limpopo and Thukela rivers where sediment cones prograde into the Natal Valley (Dingle et al. 1978; Martin 1981a; Martin 1981b; Martin 1987). Over the past 65 Ma, sediment input into the Natal Valley has been estimated at ca. 23 $m^3/km^2/yr$; the Limpopo and Thukela rivers delivering the bulk of sediment to the basin, amounting to the deposition of an 800 m thick layer of sediment within the basin (Flemming 1980). Oligocene to present day sedimentation is characterised by erosion and redistribution throughout the Natal Valley and Transkei Basin (Martin 1981a; Martin 1981b; Niemi et al. 2000).

Bathymetric features pertinent to this study are the Central Terrace, Naudé Ridge, Mozambique Ridge (Dana Plateau in particular), Ariel Graben, Tugela cone and Limpopo cone (Fig. 1). The Central Terrace is a north–south orientated

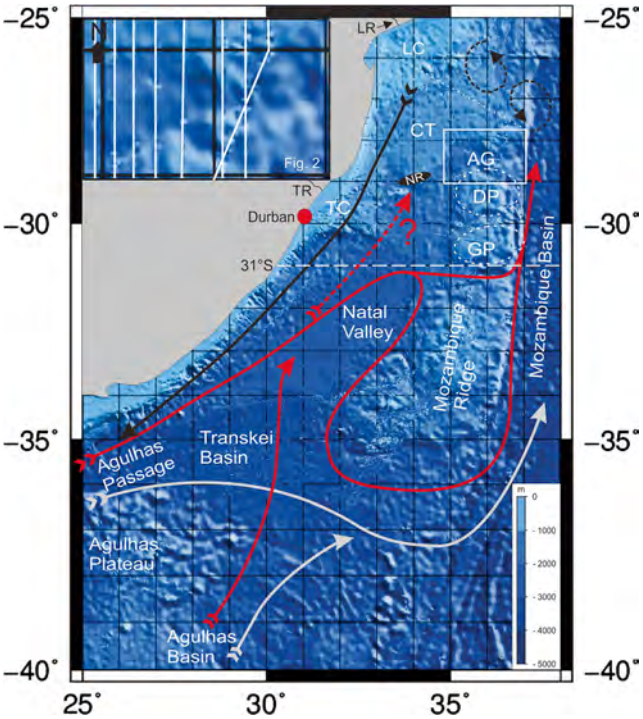

Fig. 1 The general bathymetry (The GEBCO_08 Grid, version 20091120) of the southwest Indian Ocean (modified after Wiles et al. 2013). Presently known THC pathways are shown; black arrow illustrates the Agulhas Current, red—the North Atlantic Deep Water, and grey—the Antarctic Bottom Water (after Bang and Pearce 1976; Casal et al. 2006; Dingle et al. 1987; Toole and Warren 1993; Schlüter and Uenzelmann-Neben 2008; van Aken et al. 2004). Eddies associated with the Mozambique and East Madagascar Currents are shown by dashed circular arrows (Quartly and Srokosz 2004). The Tugela Cone (TC), Limpopo Cone (LC) and Central Terrace (CT) are located west of the study area (white box), which is enlarged to show the ship tracks. The Dana (DP) and Galathea Plateaus (GP) of the northern Mozambique Ridge are indicated by dashed circles. North of the Dana Plateau lies the Ariel Graben (AG), a west/east saddle across the Mozambique Ridge The most prominent rivers flowing in to this Natal Valley region are the Thukela River (TR) in South Africa, and the Limpopo River (LR) in Mozambique. The Naudé Ridge (NR) is a buried basement high. A more detailed overview of the study area is provided in Fig. 2

basement high that provides the northern bathymetric depth constraint within the northern Natal Valley (Figs. 1 and 2). The Central Terrace has a smooth convex surface flanked to the east and west by prominent valleys, whereas the southern flank comprises a steep, smooth slope that extends down to the deep central northern Natal Valley (Dingle et al. 1978). The steep southern slope is the topographic expression of the Naudé Ridge, a prominent basement high now overlain by sediment (thickness of 1 s TTWT) (Dingle et al. 1978). The Tugela and Limpopo cones represent fan shaped features prograding into the Natal Valley from offshore of the Thukela and Limpopo rivers respectively (Fig. 1). The Tugela cone exhibits a steep, west to east southern flank, while the eastern flank has a more moderate gradient and hummocky surface. Numerous terraces create complex bathymetry over the surface of the cone, which is crosscut by the Tugela canyon

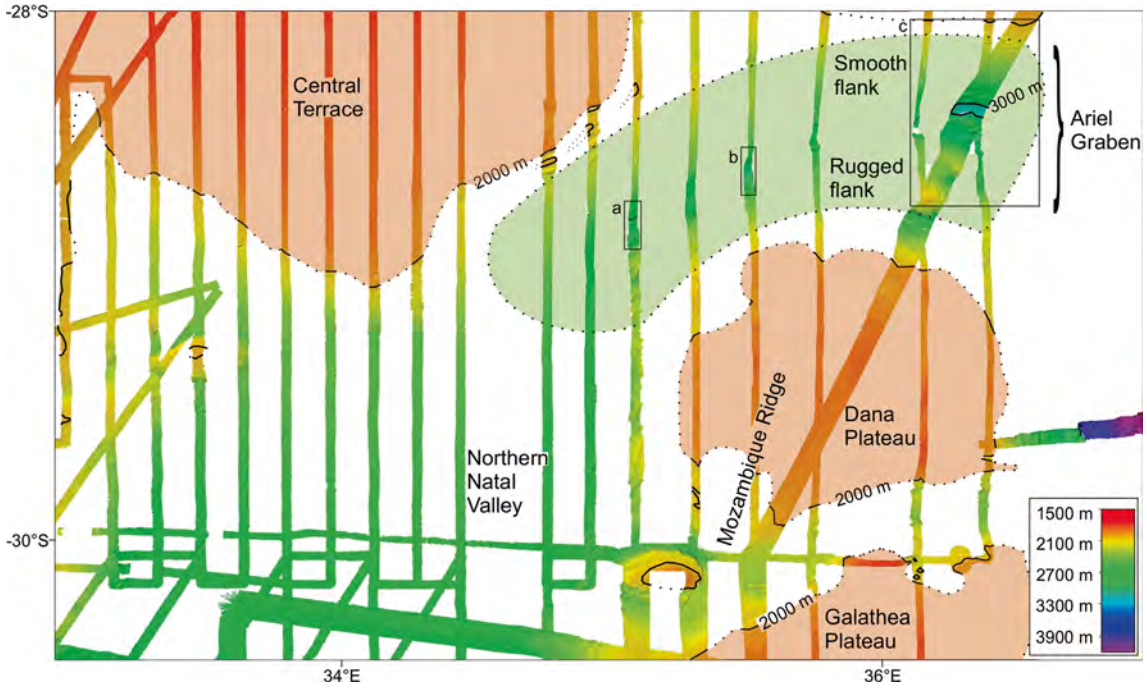

Fig. 2 An overview of the northern Natal Valley and northern Mozambique Ridge. Note the 2000 m isobaths to the NW (Central Terrace) and SE (Dana Plateau), as well as the saddle created by the Ariel Graben. Boxes *a*, *b*, and *c* show areas enlarged in Figs. 3, 4, 5 and 6, and are referred to in text

(Dingle et al. 1978). The Pleistocene age Tugela canyon delivers what little sediment crosses the sediment starved shelf to the Tugela fan which has been winnowed and modified by sweeping of the NADW (Wiles et al. 2013). The Limpopo cone lies north of the Tugela cone, and northwest of the Central Terrace, extending 300 km south of the Limpopo River (Martin 1981a). This sedimentary cone is separated from the continental shelf of southern Mozambique by a narrow valley, similar to that of the Central Terrace to the southeast (Dingle et al. 1978). To the east of the Natal Valley the north/south orientated Mozambique Ridge provides further bathymetric constraint in the form of numerous submarine plateaus. Of importance in this study are the northern Dana and Galathea plateaus (Fig. 1). The northern Dana Plateau is the larger or the two, measuring 120×130 km in dimension, and rising to a depth of 1795 m below the sea surface. The northern flanks of the Dana Plateau deepen into the Ariel Graben (comprising the southern flank of the Ariel Graben), a west/east orientated 12 km wide saddle that crosses the Mozambique Ridge at 28°30'S (Figs. 1 and 2). South of the Dana Plateau the Galathea Plateau rises to shallower depths (1600 m) extending 150 km in an east/west orientation, and 80 km north/south.

Current state of knowledge regarding circulation in the Natal Valley

Circulation within the Natal Valley, and surrounding SWIO, is complex owing to the macrotopography of the basins and the adjacent narrow continental shelf (Fig. 1). Two main circulation systems are recognised, The Agulhas Current and the North Atlantic Deep Water (NADW).

The Agulhas Current is a fast (4 knots), poleward flowing, wide (ca. 100 km) geostrophic current that dominates the upper ocean flow along the western boundary of the Natal Valley (Bang and Pearce 1976; Dingle et al. 1987, Martin 1981a; Martin 1981b; Donohue and Toole 2003; Lutjeharms 2007, McDonagh et al. 2008) (Fig. 1). The precise source area for the Agulhas Current is unknown; however sedimentological studies suggest this source area lies between 26°S and 30°S offshore the east African coast (Flemming 1980; Martin 1981a; Martin 1981b; Lutjeharms 2006a, 2006b). This is a dynamic region influenced by several water masses. Southward flowing eddies from the Mozambique Channel meet with eddies of the East Madagascar Current, with additional input from the Agulhas Return Current (Stramma and Lutjeharms 1997; de Ruijter et al. 2003; Quartly and Srokosz 2004; Quartly and Srokosz 2004; Lutjeharms 2007). A deep-reaching current, the Agulhas Current is considered by some to progressively extend to depths of as much as 2500 m by 32°S along South Africa's southeast coast (Bang and Pearce 1976; Pearce 1977; Dingle et al. 1987; Beal and Bryden 1999; Donohue and Toole 2003). However, in some instances it has only been the upper 500 m of the Agulhas Current that was intensely studied (Pearce 1977), whereas the structure below 1000 m was estimated or shown to be shallower than the sea bottom (Donohue et al. 2000). As such a complete understanding of the variability of depth changes and the

influencing factors of the Agulhas Current remains elusive (Lutjeharms 2006a).

The northern section of the current system is remarkably stable, owing to the steep, linear continental shelf of northern South African margin that steers the current flow (de Ruijter et al. 1999; Lutjeharms 2006a; Lutjeharms 2007). A consequence of this stable linear flow path is that the southward flow associated with the Agulhas Current terminates ca. 200 km offshore (Lutjeharms 2006b). Inshore of this northern Agulhas Current, Beal and Bryden (1997) describe an undercurrent at ca. 31°S flowing northward along the continental slope at 1200 m depth, and directly beneath the surface core of the Agulhas Current. Numerical models have produced comparable flows at ca. 34°S, with the depth of the undercurrent varying from 300–2500 m (see Lutjeharms 2006a).

Other authors consider the bottom water circulation within the Natal Valley to be governed by the northeasterly flowing NADW, a deep western boundary current. Two possibly contemporaneous pathways have been proposed to describe the passage of NADW (ca. $1.2x10^6$ $ms^{-1)}$ into the Natal Valley (Fig. 1). The first (southern) pathway is facilitated by the South Atlantic Current. This pathway is envisaged as transporting NADW around the southern tip of Africa. The NADW core then bifurcates; the northern branch (confined to a depth of 2000–3500 m, and salinity of 34.83 %) continuing northeastward, via the Agulhas and Transkei basins, into the Natal Valley. In contrast, the southern branch of NADW continues eastward beneath the meandering Agulhas Return Current and does not enter the Natal Valley (Toole and Warren 1993; van Aken et al. 2004).

The second (northern) NADW pathway is considered to flow along the African continental slope at depths between 2000 and 2500 m. This NADW core passes, via the Agulhas Passage, into the Transkei Basin on its pathway into the Natal Valley (Toole and Warren 1993; van Aken et al. 2004; Schlüter and Uenzelmann-Neben 2008). Confined by shoaling bathymetry within the Natal Valley, the NADW is believed to return southward along the eastern boundary of the Natal Valley (constrained by the western slopes of the Mozambique Ridge) (Dingle et al. 1987; McDonagh et al. 2008). Van Aken et al. (2004) considered some leakage across a saddle in the Mozambique Ridge at ca. 31°S and at depths of 2500–3000 m.

Within the southern Natal Valley a net northeastward flow of NADW, west of 32°E was confirmed (Beal and Bryden 1999; Donohue et al. 2000; Donohue and Toole 2003, McDonagh et al. 2008). It is this deep northward flow of the NADW which is likely responsible for winnowing of the Tugela fan in the mid-western Natal Valley (Wiles et al. 2013).

Further north, hydrographic observations from the Mozambique Channel showed a variable northward flowing undercurrent along the western channel at 1500–2400 m depth, inshore of the southward migrating Mozambique Current eddies (de Ruijter et al. 2002; DiMarco et al. 2002; Ullgren et al. 2012). The deep core of this undercurrent comprises NADW (flowing at $4x10^6 m^3 s^{-1}$) which, at 2000 m, is able to cross the shallowing sill of the Mozambique Channel (2500 m) and continue into the Somali Basin (Donohue and Toole 2003; van Aken et al. 2004). The NADW that does not cross this sill is considered to return southward along the eastern side of the Mozambique Channel and Basin (Donohue and Toole 2003).

Seafloor/current interactions

In the northernmost and shallowest portions of the Natal Valley, seafloor/current interactions were recorded as areas of non-deposition on the Limpopo Cone and Central Terrace (Martin 1981a, 1981b; Preu et al. 2011). This interaction between the Agulhas Current and the northernmost Natal Valley has a minimum age of Early/Middle Miocene (Martin 1981a; Preu et al. 2011). Although initially variable, the Agulhas Current pathways were thus fairly stable following the Early Miocene. Erosion and redistribution of sediment on the Limpopo cone and Central Terrace, between depths of 400–1500 m, can therefore be attributed to the net southward flow of the Agulhas Current.

Deeper into the Natal Valley (ca. 2500–3000 m) and further south (ca. 33°S), Dingle et al. (1987) recognise recirculation of NADW within the Natal Valley based on the location, orientation, depth and character of sediment drifts in the basin. Through interactions with the seafloor sediments, the NADW has developed two elongate, north/south orientated, sediment drifts. The western drift and eastern drift associated with northward and southward flow respectively since the Late Eocene (Dingle et al. 1987).

Material and methods

A portion of data from two recent research cruises, AISTEK II (20th of May-7th of July, 2005) aboard the R/V Sonne (Jokat 2006) and AISTEK III (9th of April-1st June, 2009) aboard the R/V Pelagia (Jokat 2009), are used in this study. AISTEK II investigated the Mozambique Basin and Ridge using a SIMRAD EM120 multibeam echosounder. A Kongsberg EM300 multibeam echosounder was used to acquire bathymetry data over the Mozambique Ridge and Natal Valley during the AISTEK III survey. Both multibeam data sets were processed onboard using CARIS HIPS and exported as xyz ASCII

files. Interactive Visualization Systems' DMagic (version 7.3.1a) was used to grid the data, which were then displayed in Fledermaus (version 7.3.1a) for interpretation. The final bathymetry data have an output matrix of ~35 m, providing a relatively high resolution dataset. Specific portions of these data are presented in this study to illustrate the results and discussion graphically.

A 3.5 kHz (AISTEK III) and a parametric ATLAS PARASOUND echosounder (AISTEK II) were used to collect seafloor and sub-bottom data during the respective cruises. These data sets provide very high frequency seismic data with a vertical resolution ca. 1 m. Due to technical difficulties, complete seismic coverage along track was in some instances not achievable. In-house designed software, in addition to SEISEE (version 2.17.1.), were used to process the data. These data were incorporated into SEISEE for visualization and interpretation of the echo character. Band pass filter adjustments and colour gains were applied to the data.

Results

A wide, channel-like feature is evident in the multibeam bathymetric data, leading from the mid-Natal Valley across the Mozambique Ridge toward the Mozambique Basin (Fig. 2). Confined to the north–west by the Central Terrace, and the south–east by the Dana Plateau (Mozambique Ridge), the channel is located in the bathymetric depression associated with the Ariel Graben (Fig. 2). Rugged bathymetry is more common on the northern flanks of the Dana Plateau (i.e., southern flank of the Ariel Graben) than on the Central Terrace, where seafloor is smooth (Fig. 2). This rugged bathymetry is confined to depths of 2000–3000 m on the northern flank of the Dana Plateau where there is a significant amount of basement control on topography. Evidence of this is manifest in the highly irregular, rugged bathymetry, and seismic character presented in Figs. 3 and 4. Although the Ariel Graben has created an overall west to east orientated saddle, the actual depression follows a curved path (Fig. 2). The degree of change in channel axis orientation increases more rapidly in the west in the vicinity of box c (Fig. 2).

Boxes a and b (Fig. 2.) are enlarged in Figs. 3 and 4 respectively. These figures illustrate in detail the bathymetry and shallow seismic character of this portion of the Mozambique Ridge. The northern flanks of the channel return distinct bottom echoes, with several discontinuous sub-bottom echoes (profile A—A' in Fig. 3, and profile B—B' in Fig. 4). The seafloor is smooth, with no apparent basement outcrop or subcrop visible within the limit of penetration (20 m) and coverage. The gradient of the northern flank is variable, (0.3°–2.1°, total slope average is 1°), typically increasing with depth (north to south toward the channel) to a maximum of 5.7° nearest the channel. Steepest gradients (5°–6°) are noted in the central region of the saddle across the Mozambique Ridge (Figs. 3 and 4).

The channel floor ranges in width from 4385 m to 5100 m with a variable echo character. In the western portions of the channel, hyperbolic reflectors are evident in the 3.5 kHz profile (profile A—A' in Fig. 3). The hyperbolae are of a similar height above the seafloor, and vary from individual to overlapping in organisation. Bathymetric data show this area to be rough / undulating. Smooth seafloor in the bathymetry is associated with distinct seafloor returns and continuous and sub-parallel sub-bottom reflector packages (profile B—B' in Fig. 4). An elongate terrace, orientated parallel to the base of the southern flank, is evident in both the bathymetry and shallow seismic data suggesting some degree of lateral and vertical erosion (profile B—B' in Fig. 4).

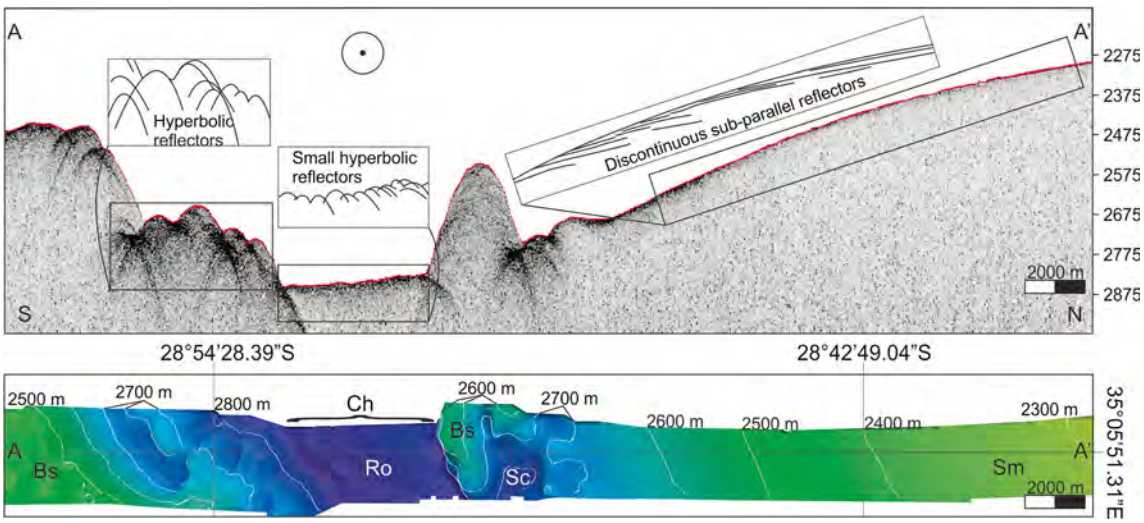

Fig. 3 Enlarged bathymetry of box a in Fig. 2. The contrast between the smooth seafloor (Sm) of the northern flank and the rugged seafloor (Bs), reflecting some basement control, of the southern flank is evident in the multibeam bathymetry (*bottom*) and high frequency seismic record (profile A—A', *top*). Note the apparent scouring (Sc) around basement outcrop in the saddle floor

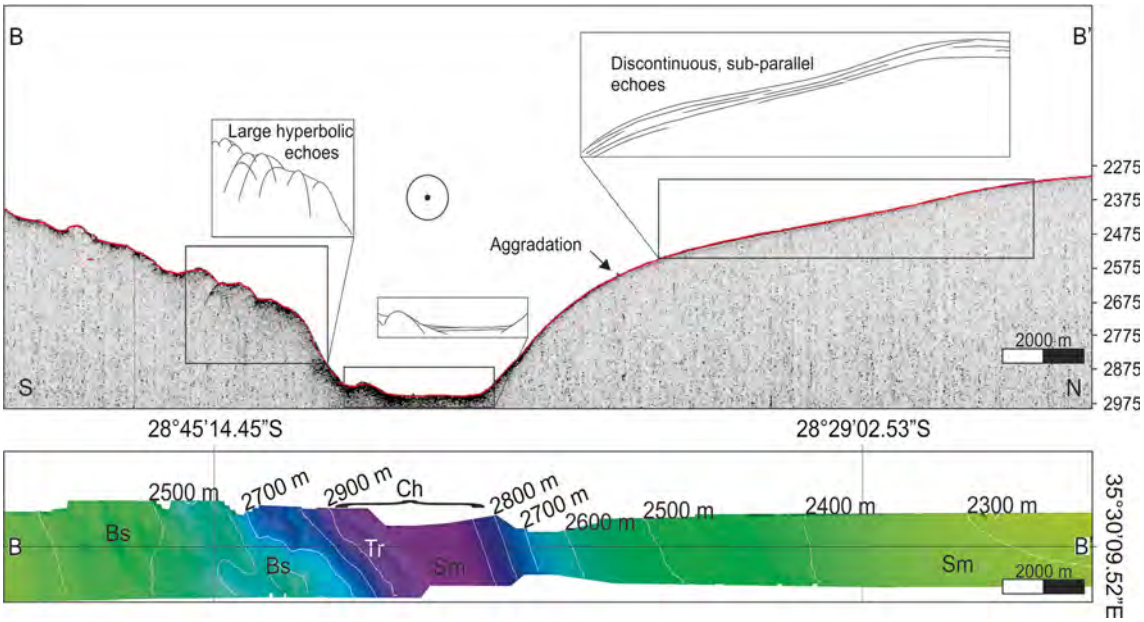

Fig. 4 Enlarged bathymetry of box b in Fig. 2. The contrast between the smooth seafloor (Sm) of the northern flank and the rugged seafloor (Bs) of the southern flank of the Ariel Graben is clear in the multibeam bathymetry (*bottom*) and high frequency seismic record (profile B—B', *top*). Note the change in character of the floor of the saddle. A terrace (Tr) is apparent at the base of the southern flank

The southern flanks of the channel are distinct from the northern flanks in both bathymetric and seismic character. Large, irregular, hyperbolae, ranging in size, amplitude and spacing (over-lapping to 1 km) dominate the seismic profiles (Figs. 3 and 4). Intense overlapping is focused on the more rugged areas, while individual hyperbolae are observed where the bathymetry is less complex. Rugged bathymetry associated with such echoes, exhibit highly variable gradients (0.3°–19.6°). Overall, the channel floor is relatively flat, while the profile of the channel is "U"-shaped. Scouring has modified this "U" shape in certain areas of the lower channel flanks suggesting sustained reworking and removal of sediment (Fig. 3).

There is a notable eastward change in character of the seafloor on the northern flanks of the channel (Fig. 5). At depths between 2100 m and 3000 m, the seafloor displays an undulating morphology (Fig. 5 and profile C—C' in Fig. 6). These undulations are straight crested and parallel/sub-parallel to the local isobaths, with crest long axes orientated west to east. Spacing between the crests is variable. The middle zone (2330–2677 m) is typified by undulations with 600–900 m wavelengths, whereas the upper and lower zones have distances of 1000–1200 m between crests. Cross- sectional symmetry of these features varies from symmetrical to asymmetrical, with broad crests and narrow troughs (Fig. 5). When asymmetrical, the down-slope (south-facing) limb is longer (511.76 m average) than the up-slope (north-facing) limb (323.53 m average) (Table 1). The lower limbs are also steeper than the upper limbs; calculated averages being 3.80° and 1.55°, respectively (Table 1). Overall the total slope on which the undulations are found is south-facing with a gradient of 1.54°, however, the area affected by undulations is slightly steeper with an average slope of 1.75°. Beyond 3000 m (the lower limit of the undulations), the gradient increases to 4.71° at the flank/channel floor transition. North of the undulations (above 2100 m) the seafloor becomes smooth once more, reflecting similar characteristics to that of the western portion of the study area (Fig. 5 and profile D—D' in Fig. 6). The total slope average in this eastern region is 0.54°, thus steeper than to the west. The channel floor, no longer flat, is ca. 440 m wide at 3160 m depth. The profile now has a more "V"-shaped section.

The southern flank of the channel is more rugged than the northern flank (Fig. 5). Hyperbolic echoes (from the 3.5 kHz echo trace) are associated with rugged bathymetry (profile E—E' in Fig. 6). Distinct bottom echoes, with several sub-parallel sub-bottom reflector packages are noted in areas of flat lying bathymetry (profile E—E' in Fig. 6). These packages onlap the rugged subcrop, showing varied package thickness and amplitude. The lowermost packages comprise low amplitude, transparent packages that thicken from south to north, while toward the seafloor surface, high amplitude packages of uniform thickness are evident. The gradient of the southern flank is highly variable, reaching a maximum of 10.5° in the rugged areas, whereas areas of subdued bathymetry exhibit low gradients (0.18°). The total gradient is 1.34° but is a poor indicator of the seafloor character due to marked variability in the gradient of the area (Fig. 7). The variation of the rugged southern flank is far greater and widespread than that of the north (Fig. 7). Only in the eastern portions of the study area, on the northern flank, does the gradient begin to vary as the undulation field is encountered (Fig. 7).

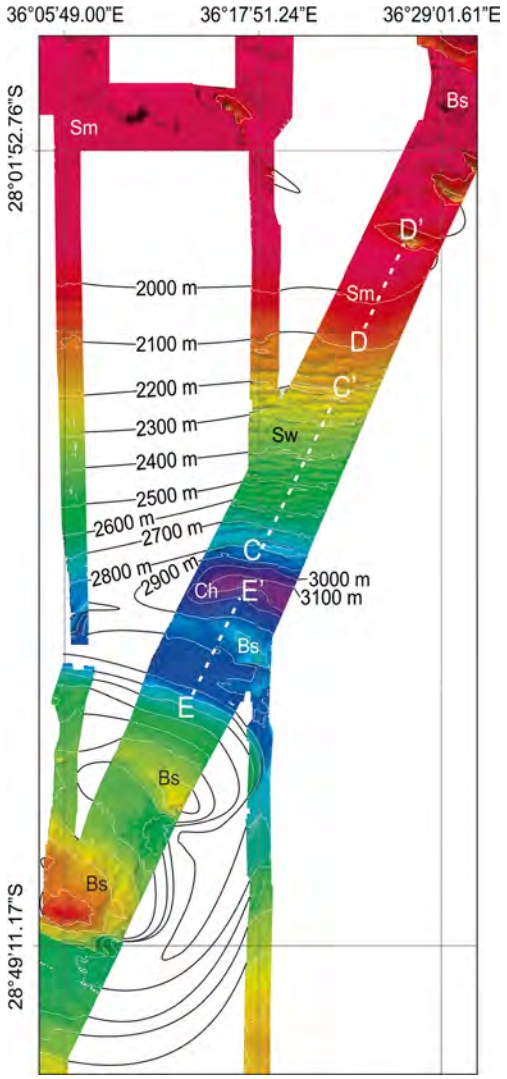

Fig. 5 The eastern region of the Ariel Graben revealed in the multibeam data (See Fig. 2, Box c for location). Note elements of basement control (Bs), smooth seafloor (Sm), and undulation field (Sw). The channel floor (Ch) is now narrower than in the west toward the Natal Valley. Profiles C—C', D—D', and E—E' shown in Fig. 6

Discussion

Echo character contrasts

There is distinct contrast in the echo character of the Ariel Graben's northern and southern flanks. The northern flank (western area) shows distinct, high amplitude, bottom echoes with several discontinuous parallel/sub-parallel sub-bottom reflectors. This echo character is synonymous with the development of crude plastered drifts, as described from other regions (cf. Damuth 1975; Damuth 1980; Jacobi 1982; Faugères et al. 1999; Stow and Mayall 2000; Masson et al. 2002; Maldonado et al. 2003; Stow et al. 1996), and the same deposit is envisioned in this study (Figs. 3, 4 and 6). This is further demonstrated by the areas of smooth seafloor (Sm in Figs. 3, 4 and 5) where current-plastering has created a uniform surface relief. This seafloor character has similar associations to plastered drifts, discussed from other regions by multiple authors (Damuth 1975; Damuth 1980; Jacobi 1982; Faugères et al. 1999; Stow and Mayall 2000; Masson et al. 2002; Maldonado et al. 2003; Stow et al. 1996). Along the northern flanks of the eastern Ariel Graben, seafloor undulations (Fig. 5) are associated with large, individual hyperbolic echoes (Fig. 6) that approach the IIB-2 character of Damuth (1975) scheme. The origin of this echo character is said to be varied; bottom current and gravity-driven processes are postulated as possible formative processes, with setting being an important consideration. In the case presented by Damuth (1975) IIB-2 echoes are located adjacent to levees and distributary channels of the Amazon cone. However; more consolidated gravity controlled flows and mass movements may also result in type IIB-2 echoes being recorded from the respective deposits.

The floor of the Ariel Graben (Ch in Figs. 3, 4, and 5) has a varied echo character. In the west it is rough, with small overlapping hyperbolae (IIIC of Damuth 1975) showing evidence of erosional/depositional bedforms. Such bedforms from other basins have been ascribed to erosion in the bottom boundary layer (Flood 1980) and syndeposition (Tucholke 1979) related to bottom water circulation or gravity driven processes (Damuth 1975) depending on the setting.

The southern flank of the Ariel Graben is rugged, dominated by large hyperbolae. Such a strongly reflective, hyperbolic echo character typifies basement highs or outcrop (Damuth and Hayes 1977; Damuth 1980; Lee et al. 2002). In this case, the lower northern flank of the Dana Plateau is cropping out due to an overall lack of sediment deposition on the southern flank. As shown in Fig. 6 (profile E—E'), ponds of sediment (discontinuous sub-parallel reflectors) are present in troughs and depressions of the southern flank. This suggests a sediment starved environment on the southern flank of the Ariel Graben, and implies differential deposition within the study area.

Interpretation of bathymetric and 3.5 kHz data

The development of a crude plastered sediment drift in the west (on the northern flank) gives way to soft sediment deformation fields in the east of the northern flank of the Ariel Graben. This demonstrates changes in the depositional/erosional setting from west to east through the Ariel Graben along the northern flank. The plastered drifts are typical of depositional features associated with bottom water current circulation (Stow et al. 1996), yet the transition to the field of undulations is atypical and requires that others factors be involved in their formation.

The presence of these undulations could be explained by several processes including contour current/seafloor

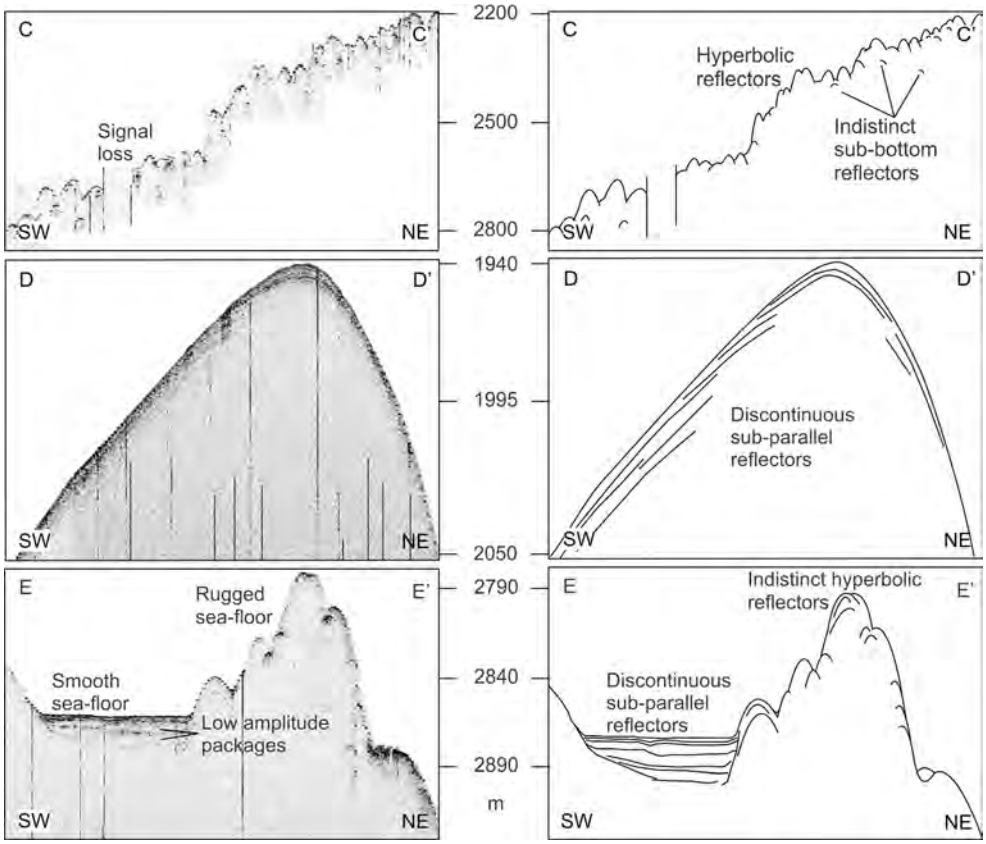

Fig. 6 Seismic character of profiles C—C', D—D', and E—E' (see Fig. 2, Box c, and Fig. 5 for location). Undulating sea floor is associated with hyperbolic echoes with indistinct sub-bottom returns. This is in contrast to the discontinuous sub-parallel reflectors of profile D—D', which is associated with smooth sea floor. On the southern flank of the Ariel Graben, hyperbolic echoes are similarly associated with rugged seafloor (Bs in Fig. 5), while horizontal, discontinuous sub-parallel echoes are evident in troughs adjacent to the rugged sea floor

interactions, turbidity current activity and mass-wasting/soft sediment deformation. Although the undulation dimensions are similar to features created by turbidity currents (see Table 2 for a comparison). In the setting presented here, the formative process associated with IIB-2 echoes is potentially related to deposition by turbidity currents. However, the undulation field is not associated with any deep sea canyon/channel/fan system. The nearest continental shelf that could shed sediment directly to the Ariel Graben is 380 km to the west. Apart from being sediment starved (Green 2009; Flemming 1980), this margin is separated from the Ariel Graben by the Central Terrace, disrupting the pathway of sediment by turbidity current. The Mozambique Ridge is obviously a feature which could play host to turbidity currents, however, in the setting of the Ariel Graben this is unlikely. There is no suitable staging area/source, directly to the north of the Ariel Graben, for the generation of turbidity driven flows. Hence, given the location of the undulation field of this study, deposits associated with turbidity currents are highly improbable.

Furthermore, from a morphological perspective, the character of the undulations is atypical of the surface expression of turbidites (Faugères et al. 2002; Wynn and Stow 2002). The wave-form (i.e., the general morphology of the undulations) dimensions of the undulations are larger in the upslope and downslope areas, decreasing in dimension toward the middle of the flank as opposed to the general decrease in wave dimension downslope (i.e., with distance from the source) expected of turbidity current-fed bedforms.

Table 1 Length and gradient characteristics of undulations

ID	Upslope limb (m)	Downslope limb (m)	Upslope limb (°)	Downslope limb (°)
1	550	650	1.66	−3.88
2	500	550	0.86	−5.64
3	400	600	2.81	−3.17
4	500	700	0.54	−3.15
5	400	600	2.11	−4.66
6	400	600	1.71	−2.80
7	400	450	0.65	−4.25
8	200	450	0.86	−5.09
9	200	400	1.18	−4.62
10	300	300	1.79	−3.28
11	300	400	0.41	−3.98
12	150	350	4.21	−5.59
13	200	350	0.26	−2.87
14	200	350	0.16	−3.15
15	200	800	3.04	−3.48
16	200	400	2.26	−5.46
17	200	750	1.78	−5.84
Average	323.53	511.76	1.55	−3.80

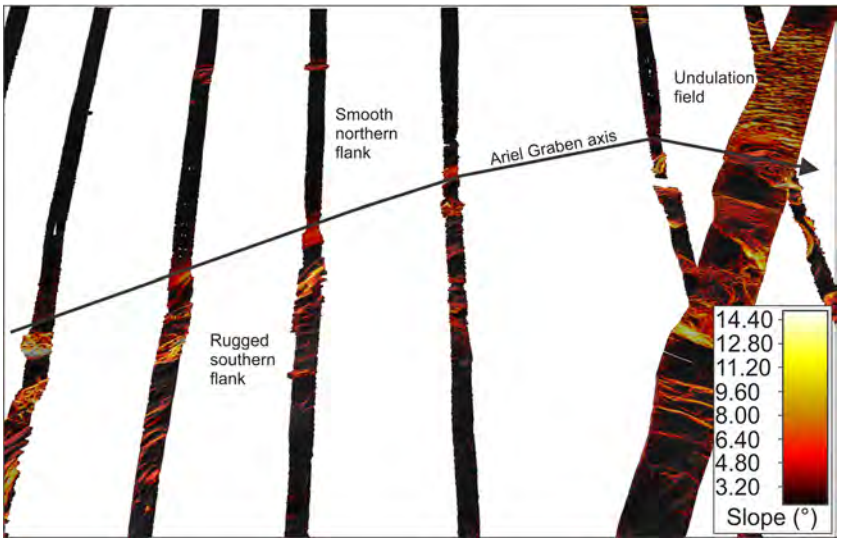

Fig. 7 3D perspective view slope map for the Ariel Graben looking south to north from the Dana plateau across the Ariel Graben. The strips of data reflect the slope of the seafloor as calculated from the bathymetry data from the same area. Note the difference in slope and relief between the northern and southern flanks of the Ariel Graben. The northern flank is relatively uniform, the exception being the undulations to the east which exhibit regular variance in gradient over short distances. In contrast, the southern flank exhibits varied gradients throughout the study area reflecting an irregular seafloor relief. The change in the orientation of the Ariel Graben (*from west to east*) is shown by the black arrow

With regards the genesis of sediment waves by bottom current interaction, the dimensions of the wave-forms observed in this study are similar to those of fine-grained bottom sediment waves (cf. Wynn and Stow 2002; Table 2 this study). Such fine-grained bottom sediment waves are found in sediment drift environments on the basin floor, lower slope and rise. At odds with this interpretation are the general orientations of the wave-form crests themselves. Typically, the crests of fine-grained bottom current sediment wave systems are oblique to the slope, or perpendicular to the flow direction of the current, with evidence of upslope and up-current migration of bedforms. In this study, the crests are parallel/subparallel to the maximum slope, orientated west–east; ~90° to the expected orientation (north–south) had they been directly developed by a current flowing west to east through the graben. As with a turbidity current-induced setting, the decrease then increase of the wave-form dimensions is in contrast to that of a bottom current sediment wave setting that generally produces decreasing wave-form dimensions with increased transport distance (Faugères et al. 2002; Wynn and Stow 2002).

The final alternative of downslope creep appears to be a viable option for the genesis of these features. There has been much discussion concerning the distinction between current generated sediment waves and undulations generated by creep/soft sediment deformation (Dillon et al. 1993; Gardner et al. 1999; Holbrook 2001; Lee and Chough 2001; Holbrook et al. 2002; Lee et al. 2002; Trincardi et al. 2004; Schwehr et al. 2007; Shillington et al. 2012). The debate stems from the similarities in bathymetry and seismic characteristics of these features. However, having excluded generation by bottom or turbidity current, soft sediment deformation is a likely formative process. In addition, the dimensions and characteristics of the seafloor undulations in this study (Table 2) are comparable to those associated with creep as described by Wynn and Stow (2002).

In keeping with the discussion in section Echo character contrasts and in the context of the bathymetry signatures discussed above, it is clear that the northern flank of the Ariel Graben is dominated by sediment cover, whereas the southern flank of the Ariel Graben exhibits basement control on sedimentation in a sediment starved setting with ponds of sediment filling low lying areas amidst the rugged bathymetry of the Dana Plateau's northern flank. The local outcrop of basement is likely to increase turbulence and promote the resuspension and redistribution of sediment rather than deposition. The net result is preferential deposition on the northern, rather than southern flank of the Ariel Graben. The resultant uneven depositional regime is at odds with the uniform distribution of sediment thicknesses attributed to pelagic deposition. Preferential drift deposition on the northern flank of the Ariel Graben is thus the likely driver of *downslope creep* here.

Significance of creep

Seafloor undulations generated by soft sediment deformation are often related to seismic activity. Examples from the Adriatic and Californian continental slopes describe such occurrences of seismically induced soft sediment deformation. However, such settings are far removed from the deep Ariel Graben of the Mozambique Ridge. The former two regions have recent and sustained seismic histories accounting for

Table 2 Summary of characteristics for different types of sediment waves, and also soft sediment deformation features (modified after Wynn and Stow 2002)

Wave-formingprocess	Turbidity current	Turbidity current	Bottom current	Bottom current	Soft sediment deformation (e.g. creep folds)	This study
Sediment grain Size	Fine-grained (mud and silt dominated)	Coarse-grained (sand and gravel dominated)	Fine-grained (mud and silt dominated)	Coarse-grained (sand and gravel dominated)	Varied: usually fine-grained (mud/silt dominated)	Unknown: presumed fine-grained
Environment	Channel levees, continental slope/rise	Canyons, channels and canyon/channel mouths	Sediment drifts on basin floor/lower slope/rise	Topographic ridges, continental slopes, b-c passages	Varied: potentially any submarine slope	Ariel Graben northern flank
Wavelength	Up to 7 km	Usually up to 1 km, rarely larger	Up to 10 km	Up to 200 m	Up to 10 km	600 m – 1.2 km
Wave height	Up to 80 m	Up to 10 m	Up to 150 m	A few metres	Up to 100 m	35–70 m
Key features	Usually on slopes of 0.1 to 0.7° Wave dimensions progressively decrease downslope Wave asymmetry usually decreases downslope Crests are roughly parallel to regional slope	Crests aligned perpendicular to flow direction Can show decrease in dimensions at channel margin Morphology is often irregular/disrupted Migration direction variable	Wave dimensions decrease near edge of wave field Wave symmetry decreases near edge of wave field Waves on slopes are aligned oblique to slope Most waves on slopes migrate upcurrent and upslope Crests are straight or slightly sinuous	Can occur as straight waves or barchans Both types aligned perpendicular to flow Barchans common where sediment supply is poor, migration is upcurrent Ripple patterns show peak flow near barchan crest	Most common on slopes of >2° Orientated perpendicular to maximum slope Do not show true lateral migration Usually show broard crests and narrow troughs Typically random scatter of dimensions	Orientated perpendicular to maximum slope Usually show board crests and narrow troughs Dimensions increase toward the edges, up and down slope.
Key examples	Monterey Fan levees (Normark et al. 1980) Bounty Channel levees (Carter et al. 1990) Toyama Channel levees (Nakajima and Satoh 2001) Var Fan levees (Migeon et al. 2000, 2001) Canary Islands slopes (Wynn et al. 2000a, b)	Var Canyon (Malinverno et al. 1988) Stromboli Canyon (Kidd et al. 1998) Valencia Channel mouth (Morris et al. 1998) Canary Islands (Wynn et al. 2000a) Laurentian Fan (Piper et al. 1985)	Argentine Basin (Flood et al. 1993) Rockall Trough (Howe 1996) Blake-Bahama Ridge (Flood 1994) Gardar Drift (Manley and Caress 1994) Falkland Trough (Cunningham and Barker 1996)	NW European slope (Kenyon 1986) Iceland-Faroe Ridge (Dorn and Werner 1993) Carnegie Ridge (Lonsdale and Malfait 1974) Gulf of Cadiz (Kenyon and Belderson 1973) Various sites (Lonsdale and Speiss 1977)	South Korea Plateau (Lee and Chough 2001) Beaufort Sea (Hill et al. 1982) Tingin Fjord (Syvitski et al. 1987) Landes Marginal Plateau (Kenyon et al. 1978) New England slope (O'Leary and Laine 1996)	

extensive soft sediment deformation fields (cf. Dengler et al. 1993; Tinti et al. 1995), whereas the Mozambique Ridge is comparatively stable (Leinweber and Jokat 2012). Recent findings suggest that there may be some tectonic activity associated with the southward propagation of the East African Rift System (Saria et al. 2014; Wiles et al. 2014). However, seismically induced deformation seems unlikely at this location as the soft sediment deformation is restricted to a specific area within the region rather than a wide-spread occurrence in line with seismically-induced deformation fields. High sedimentation rates, storm waves, and biological processes may also induce downslope movements through the increase of applied shear stress or reduction of the critical shear strength of sediments (Stow et al. 1996). At the depth of the undulations, storm waves are not considered, while biological activity is an unknown variable. A high sedimentation rate is therefore suggested as the most prominent factor in this instance, likely delivered by deep water bottom-interacting currents in the area.

Sediment redistribution via the Agulhas current or NADW?

In the northernmost Natal Valley, sediment redistribution at depths of between 400 and 1500 m on the Central Terrace, Limpopo Cone and adjacent continental shelf has been attributed to action of the Agulhas Current (Flemming and Hay 1988; Martin 1981a, 1981b; Preu et al. 2011). However, it is unlikely that the Agulhas Current at 27°S is as deep seated as it is to the south (32°S), where it reaches depths of 2500 m (Bang and Pearce 1976; Dingle et al. 1987, Beal and Bryden 1997; Donohue and Toole 2003). We attribute this to three reasons. Firstly, in this source region the Agulhas Current is still forming from the amalgamation of eddies from the north and east (Preu et al. 2011). Secondly, the Central Terrace lies in ca. 1500 m of water, so a deeper extension of the current to 2500 m is not possible. Thirdly, the observation by previous authors of a northerly flowing NADW in the west and a southerly flowing NADW in the east of the Natal Valley implies recirculation of this current system whereby NADW passes beneath the Agulhas Current at a deeper level. On this basis we consider the alternative hypothesis, bottom current activity and sediment re-organisation by the NADW.

Oceanographic constraints to potential NADW flow and a revised pathway

As a deep western boundary current plastered up against the east coast of South Africa by the Coriolis Effect, it is unlikely that its northward passage would be impeded until obstacles to that flow are encountered (Dingle et al. 1987; van Aken et al. 2004; Martínez-Méndez et al. 2008; McDonagh et al. 2008). The shoaling of the northern Natal Valley provides the necessary bathymetric restriction to change the pathway of the NADW. However this restriction within the known depth range of NADW is gradual and asymmetrical. The northern Natal Valley does not terminate in a horseshoe between 2000–3500 m (Fig. 8), but rather the Tugela cone and Central Terrace (fronted by the Naude' Ridge) provide initial restrictions from the west and northwest respectively (Fig. 8). These restrictions would force the NADW to shift from its original north northeast flow direction towards the northeast. The 2000 m isobath marks the shallow edge of the central terrace, and consequently the northward limit of NADW flow in the northern Natal Valley. Continuing to the northeast, the 2000 m isobaths of the Central Terrace merges with the top of the Ariel Graben's northern flank (Figs. 2 and 8). The Dana Plateau, located south east of the Central Terrace, rises to a minimum depth of 1795 m and consequently restricts the direct eastward flow of NADW into the Mozambique Basin (Fig. 8). The Dana Plateau thus offers a potential point divergence for NADW flow whereby a portion of the water mass can continue northeast into the Ariel Graben, while the remainder recirculates southward along the eastern margin of the Natal Valley.

Once the NADW enters the Ariel Graben its passage is likely defined by the graben long-axis; the orientation of which is not constant. From west to east the axis migrates in a clockwise manner, not confined to the orientation of the saddle axis. The average gradient of the graben flanks, particularly the northern flank, typically increases from west to east with the steepest gradient found where the saddle axis changes direction to the east (Fig. 7). It is in the east that the maximum axis curvature takes place and it is here that the upper portion of the NADW is likely to over-spill on to the northern flank, effectively over-shooting the bend in the graben axis. This over-spilling results in reduced velocity, and deposition of suspended load on the northern flank. Coriolis Effect is likely to also play a role. Deflection to the left (north in this case) further promotes preferential deposition of the northern flank of the Ariel Graben thereby compounding the result of over-spilling in the region of undulations. Such rapid sedimentation is said elevate pore pressure, and create weak planes within the deposited sediments (Shillington et al. 2012). Subsequent slow gravity-driven downslope motion and deformation generates the region of seafloor undulations on the northern flank of the Ariel Graben. Hence, this area represents an over-steepened plastered drift, developed in response to over-spilling of NADW in the Ariel Graben, the failure of which is manifest as seafloor undulations generated by down slope creep (Fig. 8).

The relevance of a revised deep water pathway

The complex macrotopography of the southwest Indian Ocean (SWIO), as demonstrated by Dingle et al. (1987), van Aken et al. (2004) and Casal et al. (2006), represents a significant

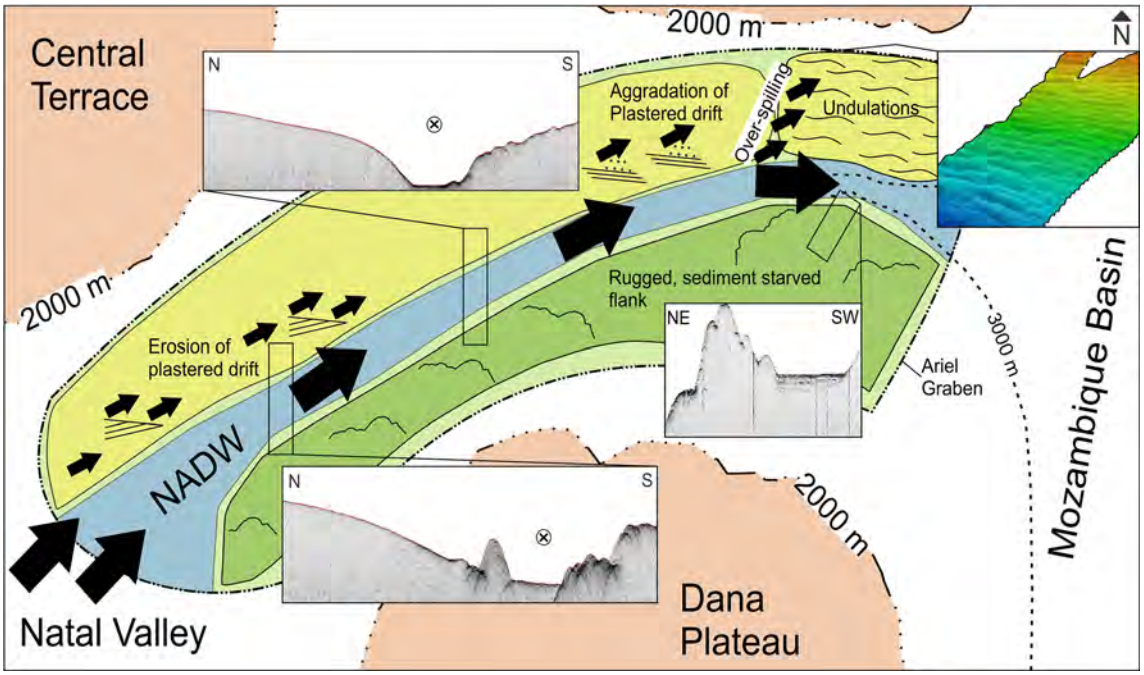

Fig. 8 Schematic of the study area (refer to Figs. 1 and 2) illustrating the proposed NADW pathway through the Ariel Graben. Once the water mass has entered the Ariel Graben its passage is determined by the axis of the graben. Proximally northeast orientated, the graben axis changes to east–southeast towards the distal areas in the east

factor in the control of deep THC flow (Donohue and Toole 2003). In this study, a previously unrecognised northern-most pathway for deep water exchange between the Natal Valley and the Mozambique Basin at 28°S is proposed (Fig. 9). The recognition of this pathway means the Natal Valley system and its effect on the SWIO region should be re-evaluated as the THC system and global climate are strongly linked (Martin 1981b; Martin 1987; Flemming and Hay 1988; Winter and Martin 1990; Martínez-méndez et al. 2008; Blome et al. 2012; Li et al. 2013; Menary and Scaife 2014).

With respect to NADW circulation interglacial periods typically see increased flow of NADW, while glacial periods are associated with reduced flow (Ben-Avraham et al. 1994; Alley et al. 1999; Rutberg et al. 2000). Increased flow, especially the proposed northern incursion of NADW, has implications for the ocean basins in which this water body is found, affecting deep water exchange between sub-basins within the SWIO (Fig. 9). The forcing of this deep water mass into rugged regions of shoaling bathymetry of the northern Natal Valley and Mozambique Ridge has the potential to increase upwelling in these regions, resulting in increased diapycnal mixing between water masses (Polzin et al. 1997).

As long-lived CO_2 sinks, such diapycnal mixing could be of ecological and climatological significance. It is suggested that CO_2 flushing from deep water masses is a step-wise process that includes elevated nutrient supply to the mid-depths, subsequently resulting rapid rage expansion of species, increased productivity and CO_2 sequestration within the mid-Ocean (Galbraith et al. 2007; Henry et al. 2014). These have important ramifications for the east coast of Africa's future fishery potentials.

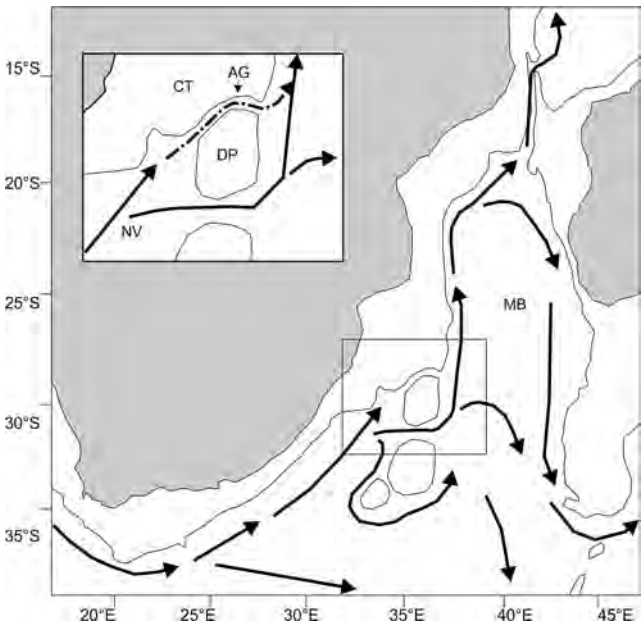

Fig. 9 The postulated passage of deep water (2000–3000 m), in this case NADW, through the SWIO is shown by black arrows, after van Aken et al. (2004). The 2000 m isobaths are shown for reference by the solid black line. The inset shows the study area, where the Ariel Graben creates a saddle across the Mozambique Ridge. The suggested NADW pathway across this saddle, through the Ariel Graben, is illustrated by the black dot-dash line. Abbreviations in insert: *CT* Central Terrace, *AG* Ariel Graben, *DP* Dana Plateau, *NV* Natal Valley

Conclusion

The Ariel Graben creates a deep west to east saddle across the Mozambique Ridge at ca. 28°S. This deep saddle in the Mozambique Ridge provides the potential for deep water exchange between the northern Natal Valley, and Mozambique Basin. A west to east change in character in the Ariel Graben is recorded in the sub-surface and expressed in the morphology of the seafloor and linked to deep water sediment trasnport. Evidence of this transport is manifest as crudely developed plastered drifts in the west and a field soft sediment deformation, of limited extent, in the east of the study area. Here current flow stripping due to increased curvature of the graben axis, results in preferential deposition of suspended load in accordance of reduced current velocity in an area of limited accommodation space. This results in an oversteepened plastered drift. Deposited sediments overcome the necessary shear stresses, resulting in soft sediment deformation in the form of down-slope growth faulting (creep) and generation of undulating seafloor morphology. The observed seafloor and subseafloor characteristics are considered to be associated with a newly postulated NADW passage through the Ariel Graben, as opposed to influence by deep-reaching Agulhas Current activity.

Acknowledgments We wish to thank the BMBF (Bundesministerium fur Bildung und Forschung) for funding the scientific projects (contract numbers 03G0183A, 03G0730A). The crews of RV Sonne (AISTEK II) and RV Pelagia (AISTEK III) are acknowledged for their excellent support and expertise in the data acquisition phases. The financial assistance of the National Research Foundation (Innovation Scholarship) (83799) towards this research is hereby acknowledged. Opinions expressed and conclusions arrived at, are those of the authors and are not necessarily to be attributed to the DAAD-NRF. Prof. Dr. BW Flemming and Dr. AK Martin are thanked for their welcomed reviews of the initial manuscript. Their input added greatly to the revised manuscript.

References

Alley RB, Clark PU, Keigwin LD, Webb RS (1999) Making sense of millennial-scale climate change. In: Clark PU, Webb RS, Keigwin LD (eds) Mechanisms of Global Climate Change at Millennial Time Scales. AGU Geophys Monogr 112:385–494

Bang ND, Pearce AF (1976) Large-scale circulation of surface water of the south Indian Ocean. In: Heydorn AEF (ed) Ecology of the Agulhas current region–an assessment of biological responses to environmental parameters in the south–west Indian Ocean. Proceedings of the marine freshwater conference, port Elizabeth. CSIR, Pretoria, pp 4–10

Beal LM, Bryden HL (1997) Observations of an Agulhas undercurrent. Deep-Sea Res I 44:1715–1724. doi:10.1016/S0967-0637(97)00033-2

Beal LM, Bryden HL (1999) The velocity and vorticity structure of the Agulhas current at 32° S. J Geophys Res 104(C3):5151–5176

Ben-Avraham Z, Niemi TM, Hartnady CJH (1994) Mid-tertiary changes in deep ocean circulation patterns in the natal valley and Transkei basin, southwest Indian ocean. Earth Planet Sci Lett 121(3–4):639–646

Blome MW, Cohen AS, Tyron CA, Brooks JR (2012) The environmental context for the origins of modern human diversity: a synthesis of regional variability in African climate 150,000–30,000 years ago. J Hum Evol 62:563–592

Carter L, Carter RM, Nelson CS, Fulthorpe CS, Neil HL (1990) Evolution of Pliocene to recent abyssal sediment waves on Bounty Channel levees, New Zealand. Mar Geol 95:97–109

Casal TGD, Beal LM, Lumpkin R (2006) A North Atlantic deep-watereddy in the Agulhas Current system. Deep-Sea Res I 53:1718–1728

Cawthra HC, Neumann FH, Uken R, Smith AM, Guastella L, Yates AM (2012) Sedimentation on the narrow (8 km wide), oceanic current-influenced continental shelf off Durban, KwaZulu-Natal, South Africa. Mar Geol 323–325:107–122

Cunningham AP, Barker PF (1996) Evidence for westward-flowing Weddell Sea Deep Water in the Falkland Trough, western South Atlantic. Deep-Sea Res 43:643–654

Damuth JE (1975) Echo characters of the western equatorial Atlantic floor and its relationship to the dispersal and distribution of terrigenous sediments. Mar Geol 18:17–45

Damuth JE (1980) Use of high-frequency (3.5–12 kHz) echograms in the study of near- bottom sedimentation processes in the deep sea: a review. Mar Geol 38:51–75

Damuth JE, Hayes DE (1977) Echo character of the east Brazilian continental margin and its relationship to sedimentary processes. Mar Geol 24:73–95

de Ruijter WPM, Biastoch A, Drijfhout SS, Lutjeharms JRE, Matano RP, Pichevin T, van Leeuwen PJ, Weijer W (1999) Indian-Atlantic interocean exchange: dynamics, estimation and impact. J Geophys Res 104:20885–20910

de Ruijter WPM, Ridderinkhof H, Lutjeharms JRE, Schouten MW, Veth C (2002) Observations of the flow in the Mozambique channel. Geophys Res Lett 29(10):1401–1403

de Ruijter WPM, van Aken HM, Beier EJ, Lutjeharms JRE, Matano RP, Schouten MW (2003) Eddies and dipoles around south Madagascar: formation, pathways and large-scale impact. Deep-Sea Res I 51:383–400

Dengler L, Carver GA, McPherson R (1993) Sources of north coast seismicity. Calif Geol 45:40–53

Dillon WP, Lee MW, Fehlhaber K, Coleman DF (1993) Gashydrates on the Atlantic margin of the United States—controls on concentration. In Howell DG (ed) the future of energy gases. Geol Surv Prof Pap 1570:313–330

DiMarco SF, Chapman P, Nowlin WD Jr, Hacker P, Donohue K, Luther M, Johnson GC, Toole J (2002) Volume transport and property distributions of the Mozambique channel. Deep-Sea Res II: Top Stud Oceanogr 49(7–8):1481–1511

Dingle RV, Robson S (1985) Slumps, canyons and related features on the continental margin off East London, SE Africa (SW Indian Ocean). Mar Geol 67:37–54

Dingle RV, Goodlad SW, Martin AK (1978) Bathymetry and stratigraphy of the northern Natal Valley (SW Indian Ocean): a preliminary account. Mar Geol 28:89–106

Dingle RV, Birch GF, Bremner JM, De Decker RH, du Plessis A, Engelbrecht JC, Fincham MJ, Fitton T, Flemming BW, Goodlad SW, Gentle RI, Martin AK, Mills EG, Moir GJ, Parker RJ, Robson SH, Rogers J, Salmon DA, Siesser WG, Simpson ESW, Summerhayes CP, Westall F, Winter A, Woodborne MW (1987) Deep-sea sedimentary environments around southern Africa (SE-Atlantic & SW-Indian Oceans). Ann S Afr Mus 98:1–27

Donohue KA, Toole JM (2003) A near-synoptic survey of the Southwest Indian Ocean. Deep-Sea Res II 50:1893–1931

Donohue KA, Firing E, Beal L (2000) Comparison of three velocity sections of the Agulhas current and Agulhas undercurrent. J Geophys Res Oceans 105(C12):28585–28593

Dorn WU, Werner F (1993) The contour-current flow along the southern Iceland-Faeroe Ridge as documented by its bedforms and asymmetrical channel fillings. Sediment Geol 82:47–59

Faugères JC, Stow DAV, Imbert P, Viana A (1999) Seismic features diagnostic of contourite drifts. Mar Geol 162:1–38

Faugères JC, Gonthier E, Mulder T, Kenyon N, Cirac P, Griboulard R, Berné S, Lesuavé R (2002) Multi-process generated sediment waves on the Landes plateau (Bay of Biscay, North Atlantic). Mar Geol 182(3–4):279–302

Flemming BW (1980) Sand transport and bedform patterns on the continental shelf between Durban and Port Elizabeth (Southeast African Continental Margin). Sediment Geol 26:179–205

Flemming B, Hay R (1988) Sediment distribution and dynamics of the Natal continental shelf, in Coastal Ocean Studies off Natal, South Africa, Lecture Notes. In: Schumann EH (ed) Coastal estuarine stud, vol 26. Springer, Berlin, pp 47–80

Flood RD (1980) Deep-sea sedimentary morphology: modelling and interpretation of echo-sounding profiles. Mar Geol 38:77–92

Flood RD (1994) Abyssal bedforms as indicators of changing bottom current flow: Examples from the U.S. East Coast continental rise. Paleoceanography 9:1049–1060

Flood RD, Shor AN, Manley PD (1993) Morphology of abyssal mudwaves at Project MUDWAVES sites in the Argentine Basin. Deep-Sea Res 40:859–888

Galbraith ED, Jaccard SL, Pedersen TF, Sigman DM, Haug DH, Cook M, Southon JR, Francois R (2007) Carbon dioxide release from the North Pacific abyss during the last deglaciation. Nature 449:890–893

Gardner J, Prior D, Field M (1999) Humboldt Slide—a large shear dominated retrogressive slope failure. Mar Geol 154:323–338

Goodlad SW (1986) Tectonic and sedimentary history of the mid-Natal Valley (SW Indian Ocean). Joint Geological Survey/University of Cape Town. Mar Geosci Unit Bull 15:415

Green AN (2009) Sediment dynamics on the narrow, canyon-incised and current-swept shelf of the northern KwaZulu-Natal continental shelf, South Africa. Geo-Mar Lett 29:201–219

Green AN (2011a) Submarine canyons associated with alternating sediment starvation and shelf-edge wedge development: Northern KwaZulu-Natal continental margin, South Africa. Mar Geol 289: 114–126

Green AN (2011b) The late Cretaceous to Holocene sequence stratigraphy of a sheared passive upper continental margin, northern KwaZulu-Natal, South Africa. Mar Geol 289:17–28

Green AN, Uken R (2008) Submarine landsliding and canyon evolution on the northern KwaZulu-Natal continental shelf, South Africa, SW Indian Ocean. Mar Geol 254:152–170

Green AN, Goff JA, Uken R (2007) Geomorphological evidence for upslope canyon-forming processes on the northern KwaZulu-Natal shelf, South Africa. Geo-Mar Lett 27:399–409

Gutjahr M, Hoogakker BAA, Frank M, McCave IN (2010) Changes in North Atlantic Deep Water strength and bottom water masses during Marine Isotope Stage 3 (45–35 ka BP). Quat Sci Rev 29:2451–2461. doi:10.1016/j.quascirev.2010.02.024

Henry LA, Frank N, Hebbeln D, Wienberg C, Robinson L, de Flierdt T, Dahl M, Douarin M, Morrison CL, Correa ML, Rogers AD, Ruckelshausen M, Roberts JM (2014) Global ocean conveyor lowers extinction risk in the deep sea. Deep-Sea Res Part I: Oceanogr Res Pap 88:8–16

Hill PR, Moran KM, Blasco SM (1982) Creep deformation of slope sediments in the Canadian Beaufort Sea. Geo-Mar Lett 2:163–170

Holbrook W (2001) Seismic studies of the Blake Ridge: implications for hydrate distribution, methane expulsion, and free gas dynamics. In: Paull C, Dillon W (eds) Natural Gas Hydrates: Occurrence, Distribution, and Detection. American Geophysical Union, Geophysical Monograph 124:235–256

Holbrook W, Lizarralde D, Pecher I, Gorman A, Hackwith K, Hornbach M, Saffer D (2002) Escape of methane gas through sediment waves in a large methane hydrate province. Geology 30(5):467–470

Howe JA (1996) Turbidite and contourite sediment waves in the northern Rockall Trough, North Atlantic Ocean. Sedimentology 43:219–234

Jacobi RD (1982) Microphysiographie du Sud-Est de l'Atlantique Nord et ses conséquences pour la distribution des processus prés du fond marin et des faciès associés, vol 31. Bull Inst Geol Bassin Aquitaine, Bordeaux, pp 31–46

Jokat W (2006) Southeastern Atlantic and Southwestern Indian Ocean: reconstruction of the sedimentary and tectonic development since the cretaceous, AISTEK-II: Mozambique Ridge and Mozambique Basin. Report of the RV "Sonne" Cruise SO-183, Project AISTEK-II 20 May to 7 July 2005 reports on Polar and Marine Research. Alfred-Wegener-Institute for Polar and Marine Research, Bremerhaven, p 71

Jokat W (2009) The expedition of the research vessel "Pelagia" to the Natal Basin and the Mozambique Ridge in 2009 (Project AISTEK III). Alfred-Wegener- Institute for Polar and Marine Research, Bremerhaven, p 67

Kenyon NH (1986) Evidence from bedforms for a strong poleward current along the upper continental slope of NW Europe. Mar Geol 72:187–198

Kenyon NH, Belderson RH (1973) Bedforms of the Mediterranean undercurrent observed with sidescan sonar. Sediment Geol 9:77–99

Kenyon NH, Belderson RH, Stride AH (1978) Channels, canyons and slump folds on the continental slope between south-west Ireland and Spain. Oceanol Acta 1:369–380

Kidd RB, Lucchi RG, Gee M, Woodside JM (1998) Sedimentary processes in the Stromboli Canyon and Marsili Basin, SE Tyrrhenian Sea: results from sidescan sonar surveys. Geo-Mar Lett 18:146–154

Lee SH, Chough SK (2001) High-resolution (2–7 kHz) acoustic and geometric characters of submarine creep deposits in the South Korea Plateau, East Sea. Sedimentology 48:629–644

Lee HJ, Syvitski JPM, Parker G, Orange D, Locat J, Hutton EWH, Imran J (2002) Distinguishing sediment waves from slope failure deposits: field examples, including the "Humboldt Slide", and modelling results. Mar Geol 192:79–104

Leinweber VT, Jokat W (2011) Is there continental crust underneath the Northern Natal Valley and the Mozambique Coastal Plains? Geophys Res Lett 38:L14303

Leinweber VT, Jokat W (2012) The Jurassic history of the Africa-Antarctica Corridor - new constraints from magnetic data on the conjugate continental margins. Tectonophysics 530–531:87–101. doi:10.1016/j.tecto.2011.11.008

Li C, von Storch JS, Marotzke J (2013) Deep-ocean heat uptake and equilibrium climate response. Climate Dynam 40(5–6):1071–1086

Lonsdale P, Malfait B (1974) Abyssal dunes of foraminiferal sand on the Carnegie Ridge. GSA Bull 85:1697–1712

Lonsdale PF, Speiss FN (1977) Abyssal bedforms explored with a deeply towed instrument package. Mar Geol 23:57–75

Lutjeharms JRE (2006a) The Agulhas current. Springer, Berlin, p 329

Lutjeharms JRE (2006b) The coastal oceans of south-eastern Africa. In: Robinson AR, Brink KH (eds) The Sea, vol 14B. Harvard University Press, Cambridge, pp 783–834

Lutjeharms JRE (2007) Three decades of research on the greater Agulhas current. Ocean Sci 3(1):129–147

Maldonado A, Barnolas A, Bohoyo F, Galindo-Zaldívar J, Hernández-Molina J, Lobo F, Rodríguez-Fernández J, Somoza L, Tomás Vázquez J (2003) Contourite deposits in the central Scotia Sea: the importance of the Antarctic circumpolar current and the Weddell gyre flows. Palaeogeogr Palaeoclimatol Palaeoecol 198(1–2):187–221

Malinverno A, Ryan WBF, Auffret G, Pautot G (1998) Sonar images of the path of recent failure events on the continental margin off Nice, France. GSA Spec Pap 229:59–76

Manley PL, Caress DW (1994) Mudwaves on the Gardar sediment drift, NE Atlantic. Paleoceanography 9:973–988

Martin AK (1981a) The influence of the Agulhas current on the physiographic development of the northernmost Natal Valley (SW Indian ocean). Mar Geol 39:259–276

Martin AK (1981b) Evolution of the Agulhas current and its palaeoecological implications. S Afr J Sci 77:547–554

Martin AK (1987) A comparison of sedimentation rates in the Natal Valley, S.W. Indian Ocean, with modern sediment yields in east coast Rivers, Southern Africa. S Afr J Sci 83:716–724

Martin AK, Hartnady CJH (1986) Plate tectonic development of the south West Indian Ocean: A revised reconstruction of East Antarctica and Africa. J Geophys Res 91:4767–4786

Martínez-Méndez G, Zahn R, Hall IR, Pena LD, Cacho I (2008) 345,000-year-long multi-proxy records off South Africa document variable contributions of northern versus southern component water to the deep south Atlantic. Earth Planet Sci Lett 267(1–2):309–321

Masson DG, Watts AB, Gee MJR, Urgeles R, Mitchell NC, Le Bas TP, Canals M (2002) Slope failures on the flanks of the western Canary Islands. Earth Sci Rev 57(1–2):1–35. doi:10.1016/S0012-8252(01)00069-1

McDonagh EL, Bryden HL, King BA, Sanders RJ (2008) The circulation of the Indian Ocean at 32°S. Prog Oceanogr 79:20–36

Menary M, Scaife A (2014) Naturally forced multidecadal variability of the Atlantic meridional overturning circulation. Climate Dynam 42(5–6):1347–1362

Migeon S, Savoye B, Faugeres J-C (2000) Quaternary development of migrating sediment waves in the Var deep-sea fan: distribution, growth pattern, and implication for levee evolution. Sediment Geol 133:265–293

Migeon S, Savoye B, Zanella E, Mulder T, Faugeres J-C, Weber O (2001) Detailed seismic-reflection and sedimentary study of turbidite sediment waves on the Var Sedimentary Ridge (SE France): significance for sediment transport and deposition and for the mechanics of sediment-wave construction. Mar Pet Geol 18:179–208

Morris SA, Kenyon NH, Limonov AF, Alexander J (1998) Downstream changes of large-scale bedforms in turbidites around the Valencia channel mouth, north-west Mediterranean: implications for paleoflow reconstruction. Sedimentology 45:365–377

Nakajima T, Satoh M (2001) The formation of large mudwaves by turbidity currents on the levees of the Toyama deep-sea channel, Japan Sea. Sedimentology 48:435–463

Niemi TM, Ben-Avraham Z, Hartnady CJH, Reznikov M (2000) Post-Eocene seismic stratigraphy of the deep ocean basin adjacent to the southeast African continental margin: a record of geostrophic bottom current systems. Mar Geol 162(2–4):237–258

Normark WR, Hess GR, Stow DAV, Bowen AJ (1980) Sediment waves on the Monterey Fan levee: a preliminary physical interpretation. Mar Geol 37:1–18

O'Leary DWO, Laine E (1996) Proposed criteria for recognizing intrastratal deformation features in marine high resolution seismic reflection profiles. Geo-Mar Lett 16:305–312

Pearce AF (1977) Some features of the upper 500m of the Agulhas current. J Mar Res 35(4):731–753

Piper DJW, Shor AN, Farre JA, O'Connell S, Jacobi R (1985) Sediment slides and turbidity currents on the Laurentian Fan: sidescan sonar observations near the epicentre of the 1929 Grand Banks earthquake. Geology 13:538–541

Polzin KL, Toole JM, Ledwell JR, Schmitt RW (1997) Spatial variability of turbulent mixing in the abyssal ocean. Science 276:93–96

Preu B, Spieß V, Schwenk T, Schneider RR (2011) Evidence for current-controlled sedimentation along the southern Mozambique continental margin since Early Miocene times. Geo-Mar Lett 31(5–6):427–435. doi:10.1007/s00367-011-0238-y

Quartly GD, Srokosz MA (2004) Eddies in the southern Mozambique channel. Deep-Sea Res Part II: Top Stud Oceanogr 51(1–3):69–83

Raymo ME, Ruddiman WF, Shackleton NJ, Oppo DW (1990) Evolution of Atlantic-pacific gradients over the last 2.5 m.y. Earth Planet Sci Lett 97:353–368

Raymo ME, Oppo DW, Curry W (1997) The mid-Pleistocene climate transition: a deep sea carbon isotopic perspective. Paleoceanography 12:546–559

Rutberg RL, Hemming SR, Goldstein SL (2000) Reduced north Atlantic deep water flux to the glacial southern ocean inferred from neodymium isotope ratios. Nature 405:935–938

Saria E, Calais E, Stamps DS, Delvaux D, Hartnady CJH (2014) Present-day kinematics of the East African rift. J Geophys Res Solid Earth 119:3584–3600. doi:10.1002/2013JB010901

Schlüter P, Uenzelmann-Neben G (2008) Indications for bottom current activity since Eocene times: the climate and ocean gateway archive of the Transkei basin, South Africa. Global Planet Change 60:416–428

Schmieder F, von Dobeneck T, Bleil U (2000) The Mid-Pleistocene climate transition as documented in the deep South Atlantic ocean: initiation, interim state and terminal event. Earth Planet Sci Lett 179:539–549

Schwehr K, Driscoll N, Tauxe L (2007) Origin of continental margin morphology: Submarine-slide or downslope current-controlled bedforms, a rock magnetic approach. Mar Geol 240:19–41. doi:10.1016/j.margeo.2007.01.012

Shillington DJ, Seeber L, Sorlien CC, Steckler MS, Kurt H, Dondurur D, Çifçi G, İmren C, Cormier MH, McHugh CMG, Gürçay S, Poyraz D, Okay S, Atgın O, Diebold JB (2012) Evidence for widespread creep on the flanks of the Sea of Marmara transform basin from marine geophysical data. Geology 40(5):439–442

Srinivasan A, Garraffo Z, Iskandarani M (2009) Abyssal circulation in the Indian ocean from a resolution global hindcast. Deep-Sea Res I: Oceanogr Res Pap 56(11):1907–1926

Stow DAV, Mayall M (2000) Deep-water sedimentary systems: New models for the 21st century. Mar Pet Geol 17(2):125–135

Stow DAV, Reading HG, Collison JD (1996) Deep seas. In: Reading HG (ed) Sedimentary environments: processes, facies and stratigraphy. Blackwell Science, Oxford, pp 395–453

Stramma L, Lutjeharms JRE (1997) The flow field of the subtropical gyre of the south Indian ocean. J Geophys Res 102:5513–5530

Syvitski JPM, Burrell DC, Skei JM (1987) Fjords: Processes and Products. Springer Verlag, New York, p 379

Tinti S, Maramai A, Favali P (1995) The gargano promontory: an important Italian seismogenetic–tsunamigenic area. Mar Geol 122:227–241

Toole JM, Warren BA (1993) A hydrographic section across the subtropical South Indian Ocean. Deep-Sea Res I 40:1973–2019

Trincardi F, Cattaneo A, Correggiari A, Ridente D (2004) Evidence of soft sediment deformation, fluid escape, sediment failure and regional weak layers within the late quaternary mud deposits of the Adriatic Sea. Mar Geol 213(1–4):91–119

Tucholke BE (1979) Furrows and focuses echoes on the Blake outer ridge. Mar Geol 31:13–20

Ullgren JE, van Aken HM, Ridderinkhof H, de Ruijter WPM (2012) The hydrography of the Mozambique channel from six years of continuous temperature, salinity, and velocity observations. Deep-Sea Res I Oceanogr Res Pap 69:36–50

van Aken HM, Ridderinkhof H, de Ruijter WPM (2004) North Atlantic deep water in the south-western Indian ocean. Deep-Sea Res I 51:755–776

Wiles E, Green A, Watkeys M, Jokat W, Krocker R (2013) The evolution of the Tugela canyon and submarine fan: a complex interaction between margin erosion and bottom current sweeping, southwest Indian Ocean, South Africa. Mar Pet Geol 44:60–70

Wiles E, Green A, Watkeys M, Jokat W, Krocker R (2014) Anomalous seafloor mounds in the northern natal valley, southwest Indian Ocean: implications for the east African rift system. Tectonophysics 630:300–312. doi:10.1016/j.tecto.2014.05.030

Winter A, Martin, AK (1990) Late Quaternary history of the Agulhas Current. Paleoceanography 5(4):479–486

Wynn RB, Stow DAV (2002) Classification and characterisation of deep-water sediment waves. Mar Geol 192:7–22

Wynn RB, Masson DG, Stow DAV, Weaver PPE (2000a) Turbidity current sediment waves on the submarine slopes of the western Canary Islands. Mar Geol 163:185–198

Wynn RB, Weaver PPE, Ercilla G, Stow DAV, Masson DG (2000b) Sedimentary processes in the Selvage sediment-wave field, NE Atlantic: new insights into the formation of sediment waves by turbidity currents. Sedimentology 47:1181–1197

Appendix B

Seafloor morphology in the Mozambique Channel: Evidence for long-term persistent bottom-current flow and deep-reaching eddy activity

Monika Breitzke[a,*], Errol Wiles[b], Ralf Krocker[c], Michael K. Watkeys[b] and Wilfried Jokat[c]

Submitted to Marine Geology

[a]Department of Geosciences, Universität Bremen, Klagenfurter Straße, D-28359 Bremen, Germany

[b]School of Agricultural, Earth and Environmental Sciences, University of KwaZulu-Natal, Private Bag X 54001, Durban 4000, Republic of South Africa

[c]Alfred-Wegener-Institute for Polar and Marine Research, Am Alten Hafen 26, D-27568 Bremerhaven, Germany

[*]*Corresponding author:* E-mail adress: Monika.Breitzke@uni-bremen.de, Phone: ++49 421 218 65343, Fax: ++49 421 218 65369

Abstract

New high-resolution bathymetric and sub-bottom profiler data of the Mozambique Channel show a large variety of bedforms which were formed by strong bottom currents. The most spectacular bedforms are giant erosional scours in the southwestern study area. Here, northward flowing Antarctic Bottom Water (AABW) is topographically blocked to the north and deflected eastward due to the shallowing bathymetry of the Mozambique Channel. SW-NE trending undulating bedforms aligned parallel to the deflected AABW allow to trace the AABW flow path eastward. A W-E trending channel indicates the northernmost extension of the AABW. NW-SE oriented undulating bedforms in the west, hummocky bedforms in the east and arcuate, cross-cutting features in-between reflect a different current regime in the central study area. LADCP based current velocity sections show that the western part lies in the range of deep-reaching anticyclonic eddies, so that the undulating bedforms are aligned parallel to a part of the swirl. The cross-cutting features mark the eastern boundary of the eddy, where a northward flow direction prevails. The origin of sediment ridges and depressions in the northeastern study area is not clear. Bottom currents which interact with the topography of the Bassas da India complex and the Zambezi Channel may contribute to their formation. All bedforms are draped with sediments indicating that the present-day current velocities are not strong enough to erode sediments. Hence, the microtopography must originate from geologic times when bottom-current velocities were stronger. Assuming a published sedimentation rate of 20 m/Myrs and a drape of at least 50 m thickness the microtopography may have developed during Pliocene and earlier.

Keywords: seafloor morphology; bedforms; bottom currents; deep-reaching mesoscale eddies; Mozambique Channel; SW Indian Ocean

1. Introduction

Since the early publication of seabed photographs showing distinct current-induced sedimentary features such as ripples, scours or current lineations on the deep-seafloor (Heezen and Hollister, 1964, 1971; Heezen et al., 1966; Hollister and Heezen, 1972) numerous studies have been conducted to investigate the influence of bottom currents on the architecture and morphology of continental margins and abyssal planes in detail (Niemi et al., 2000; Bulat and Long, 2001; Kuijpers et al., 2002; Wynn and Stow, 2002; Masson et al., 2004; Hernández-Molina et al., 2006; 2009; 2010; Hanquiez et al., 2007; Schlüter and Uenzelmann-Neben, 2007, 2008). These studies reveal a wide variety of bedforms and architectural elements created by the mobilization, erosion, transportation and deposition of sediments. The types of bedforms that are created mainly depend on the bottom-current velocity and grain size of the sediment (Stow et al., 2009). The locations where they develop result from the interplay between the regional oceanography, the bottom-current velocity, the sediment supply and the large-scale morphology of the seafloor (Bulat and Long, 2001; Kuijpers et al., 2002; Wynn and Stow, 2002; Masson et al., 2004). Seismic reflection techniques are commonly applied to investigate the vertical architecture of large-scale sedimentary features to decipher the bottom-water history over millions of years. In contrast, hydro-acoustic imaging tools such as multibeam and sidescan sonars map the lateral extent of medium- and large-scale bedforms on the seafloor in detail, thus providing information on the most recent bottom-current activity that shaped the seafloor persistently.

The Mozambique Channel plays an important role in the exchange of water masses between the Indian and Atlantic Oceans via Agulhas leakage, which is a crucial component in the global ocean circulation and climate system (Lutjeharms, 2006; Beal et al., 2011). Whereas much oceanographic research has been done to understand the composition, flow path and velocities of the ocean currents in this region (Sætre and Jorge da Silva, 1984; Sætre, 1985; de

Ruijter et al., 2002; Di Marco et al., 2002; Chapman et al., 2003; Ridderinkhof and de Ruijter, 2003; Schouten et al., 2003; Lutjeharms, 2006; Harlander et al., 2009; Ridderinkhof et al., 2010; Swart et al., 2010) their influence on the morphology of the seafloor has only rarely been studied. Only Kolla et al. (1980a; 1980b) mapped several microtopographic zones in the Mozambique Basin and Channel, which differ in their echocharacter type. A broad zone with smooth, flat seafloor and lack of acoustic penetration in the northeastern Mozambique Basin was associated with coarse-grained turbidite deposits transported by the submarine Zambezi Channel. Fine-grained sediment waves along the western and eastern margins of the Mozambique Basin were attributed to the flow of Antarctic Bottom Water (AABW). Hyperbolic echoes with almost no acoustic penetration in the central southern Mozambique Channel were supposed to indicate wavy bedforms, too but with scales, composition and formation mechanism different from the fine-grained sediment waves.

These descriptions of the seafloor morphology are only based on a coarse grid of analogue 3.5 kHz recordings. Detailed bathymetric maps and high-resolution digital seismic images of the shallow subsurface are not available up to now. This paper presents new high-resolution multibeam bathymetry and narrow-beam sub-bottom profiler data collected in the Mozambique Channel during RV Sonne cruise SO-183 (Jokat, 2006). The data show a wealth of current-controlled and mass-wasting features, which are analysed with the objectives

(1) to describe the shape, size, orientation and sedimentation pattern of the bedforms and interpret them in terms of sedimentation processes,

(2) to classify the bedforms into morphological types, map their spatial distribution and thus refine the microtopographic classification of Kolla et al. (1980a),

(3) to relate the spatial distribution of the bedform types to the present-day ocean current regime,

(4) to discuss stratigraphic constraints for the formation of the bedforms taking additional

information on the sedimentology, paleoceanography and formation of other sedimentary features off SE-Africa into account.

2. Regional setting

2.1 Physiography

The Mozambique Channel is located between the landmasses of Southeast Africa and Madagascar (Figures 1, 2). It reaches its narrowest width at ~17°S, broadens southward and merges into the Mozambique Basin, which is bordered by the Mozambique Ridge in the West and the Madagascar Ridge in the East. The water depths shallow northward from ~5000 m in the northern Mozambique Basin to ~2500 m at the narrows of the Mozambique Channel with a significant increase in the slope angle from ~0.05° to ~0.3° at ~27°S (Figure 3). Most parts of the Mozambique Channel are covered with sediments of the upper Mozambique Fan (Droz and Mougenot, 1987; Kolla et al., 1980b). In the study area the large-scale morphology is dominated by the Zambezi Channel, which is structurally confined by the N-S trending Davie Ridge in the East and the volcanic islands and seamounts Bassas da India, Europa Island, Jaguar Seamount and Hall Tablemount in the West (Figure 2). South of ~25°30'S the Zambezi Channel branches into several distributary channels. Two prominent valleys join the Zambezi Channel (Droz and Mougenot, 1987): (1) The Serpa Pinto Valley, which originates from the northern Mozambique margin, runs parallel to the Davie Ridge and is almost completely filled with sediments today. (2) The Tsiribihina Valley, which is the most prominent tributary from the Madagascan margin. The Zambezi Channel has a U-shaped cross-section and a flat channel floor, which appears to be erosional south of ~20°S (Droz and Mougenot, 1987). The channel is flanked by asymmetric convex-shaped levees. Due to the Coriolis force the eastern levee is higher, has a smooth seafloor and contains more terrigenous sediments than the

western levee, which returns hyperbolic echoes in 3.5 kHz recordings (Droz and Mougenot, 1987; Kolla et al., 1980a; 1980b).

2.2 Geology

The Mozambique Channel developed in Late Jurassic to Early Cretaceous times (~155 - 125 Ma) when the Somali Basin north of Madagascar and the Mozambique Basin south of Bassas da India opened during the break-up of Gondwanaland, and Madagascar drifted southward along the Davie Fracture Zone from a position off Tanzania, Kenya and Southern Somalia to its present position (Heirtzler and Burroughs, 1971; Bunce and Molnar, 1977; Scrutton et al., 1981; Rabinowitz et al., 1983; Coffin and Rabinowitz, 1987; König and Jokat, 2010). Open marine sedimentation started in the Early Cretaceous (Droz and Mougenot, 1987). The modern Mozambique Fan began to evolve with the deposition of the first channel-levee system (Serpa Pinto series) during a sea level lowstand at the beginning of the Oligocene (~34 Ma) with the Serpa Pinto Valley acting as main feeding path (Droz and Mougenot, 1987). During the middle Miocene (~15 - 11 Ma) an uplift of the Davie Ridge with concomitant graben formation led to an abandonment of the Serpa Pinto Valley (Droz and Mougenot, 1987). Simultaneously, tectonic activity on the East African continent and formation of the East African Rift system caused the migration of the main feeding path to the Zambezi Valley and the deposition of the second channel-levee system (Zambezi series) in the southern upper Mozambique Fan (Droz and Mougenot, 1987). Today it is not clear, if the Zambezi Valley is still active as feeding path, if its activity has decreased, or if it has completely been abandoned in Pleistocene times (<2 Ma), when another now filled paleovalley under the present shelf prevented the sediments from reaching the Zambezi Canyon 100 km northward (Beiersdorf et al., 1980; Walford et al., 2005). The evolution of the Zambezi Delta on the shelf is characterized by periods of elevated sediment flux (1) in the Late Cretaceous (~90 - 65 Ma)

caused by a period of high denudation in Southern Africa, (2) in the Oligocene (~34 - 24 Ma) due to a potential rapid regional uplift of Southern Africa, and (3) since the Late Miocene (~10 Ma) associated with a doubling of the Zambezi catchment size from Pliocene (~5 - 2 Ma) to Pleistocene times (≲2 Ma) (Walford et al., 2005). The shape of the sediment deposition in the Zambezi Delta changed from a lobate pattern in Cretaceous to Oligocene times (~121 - 24 Ma) to a linear belt since the Early Miocene (≲24 Ma) probably due to the onset of the Mozambique Current (Walford et al., 2005).

Knowledge about the lithology, sedimentology and age of the sediments covering the Mozambique Fan is only available from sediment cores of maximum ~10 m length (Kolla et al., 1980a; 1980b). Most of the sediments are derived from the landmasses of Africa and Madagascar and discharged by rivers like the Zambezi or the Tsiribihina River (Kolla et al., 1980a; 1980b; Droz and Mougenot, 1987). Generally, the uppermost surface sediments are more calcareous than the underlying sediments indicating that they are of Holocene age (Kolla et al., 1980b). West of the Zambezi Channel the sediments are typically composed of interbedded hemipelagic silty clays, calcareous sediments and fine-grained turbidites, whereas east of the channel fine- to coarse-grained turbidites become more and pelagic calcareous components less important (Kolla et al., 1980b). The overall carbonate content ranges from <10% in the northern Mozambique Basin to ~50 - 75% in the Mozambique Channel west of the Zambezi Channel and decreases to ~10 - 50% east of the Zambezi Channel due to dilution by terrigenous components from the Madagascan margin (Kolla et al., 1980a). The carbonate compensation depth (CCD) shallows from >5000 m water depth in the southern Mozambique Basin to <4500 m in the Mozambique Channel due to a northward increasing dilution by terrigenous components (Kolla et al., 1980a). The amount of quartz components in the total non-carbonate fraction is high (12 - >20%) along the Zambezi Channel and decreases west- and eastward from the channel (6 - 10%). Similarly, coarse-grained, poorly sorted sands

dominate on the channel floor, whereas grain sizes decrease west- and eastward of the channel, too (Kolla et al., 1980a; 1980b). A dating of several sediment cores indicates that most of the turbidite deposition in the Mozambique Fan occurred in Pleistocene times prior to 18000 yrs, though some turbidites were obviously also deposited after 18000 yrs, but definitely not after 11000 yrs during Holocene times (Kolla et al., 1980a; 1980b). Holocene-Pleistocene sedimentation rates (<80000 yrs) amount to ≥20 m/Myrs in the upper fan where hyperbolic echoes occur (Kolla et al., 1980a), to 15 - 20 m/Myrs in the area where fine-grained sediment waves were found (Kolla et al., 1980a), and to 10 - 20 m/Myrs in the area with a smooth seafloor south of the Zambezi Channel mouth (Kolla et al., 1980a).

2.3 Oceanography

The present-day circulation pattern in the Mozambique Channel is dominated by southward moving anticyclonic eddies (Sætre and Jorge da Silva, 1984; Sætre, 1985; de Ruijter et al., 2002; Schouten et al., 2003; Swart et al., 2010) and northward flowing deep western-boundary currents which are topographically blocked by the shallowing bathymetry (Kolla et al., 1976; 1980a; Boswell and Smythe-Wright, 2002; Donohue and Toole, 2003; van Aken et al., 2004).

The formation of the anticyclonic Mozambique Channel eddies (MCE) north of ~17°S is strongly coupled with the circulation in the Indian Ocean (Schott et al., 2009) (Figure 1). Here, the South Equatorial Current (SEC), fed by the Indonesian throughflow (ITF), impinges on the eastern coast of Madagascar and bifurcates into the Northeast Madagascar Current (NEMC) and the Southeast Madagascar Current (SEMC) (Schott et al., 2009). The NEMC surrounds the northern tip of Madagascar and bifurcates off the East African coast into the East African Coastal Current (EACC) and a flow through the Mozambique Channel (Schott et al., 2009). This flow was formerly considered to be a persistent Mozambique Current (MC)

(Sætre and Jorge da Silva, 1984; Sætre, 1985; Di Marco et al., 2002), but based on recent hydrographic measurements and satellite altimetry observations it actually appears as a train of large (~300 km diameter) anticyclonic eddies, which cause a discontinuous, temporarily variable southward flow along the Mozambican margin and a weaker northward flow in the middle of the Channel (de Ruijter et al., 2002; Ridderinkhof and de Ruijter, 2003; Schouten et al., 2003; Ridderinkhof et al., 2010; Swart et al., 2010). The SEMC follows the East Madagascan coastline southward, where a part is retroflected back to the Indian Ocean as South Indian Ocean Counter Current (SICC) (Nauw et al., 2008). The other part is assumed to shed temporarily variable cyclonic eddies (Chapman et al., 2003; de Ruijter et al., 2004; Quartly and Srokosz, 2004; Quartly et al., 2006) which cross the Southern Mozambique Channel via two potential paths. The first path follows a straight WSW-directed line (Chapman et al., 2003; de Ruijter et al., 2004; Quartly et al., 2006). The other path hugs the southern tip of Madagascar, heads northwestward into the Channel and at ~23° - 24°S turns west- and then southward (Chapman et al., 2003). Both paths join the MCEs off the Inharrime Terrace off Maputo and form the southward-directed Agulhas Current (AC) (Lutjeharms, 2006; Beal et al., 2011).

The deep western-boundary currents are fed by Antarctic Bottom Water (AABW) and North Atlantic Deep Water (NADW). Intensified by the Coriolis force both water masses spread northward along the western margin of the Mozambique Basin (Read and Pollard, 1999; Boswell and Smythe-Wright, 2002; Donohue and Toole, 2003; van Aken et al., 2004) (Figure 1). After entering the Mozambique Channel the AABW is topographically blocked to the north at ~25°S due to the decreasing water depth (Figure 3), so that it is forced to upwell and mix with overlying water masses and/or to turn east- and then southward forming a weak return current along the eastern margin of the Mozambique Basin (Kolla et al., 1976; 1980a; Donohue and Toole, 2003). The NADW continues flowing northward along the Southeast

222 African margin up to ~20°S, where decreasing water depths again form a topographic bound
223 (Figure 3). Here, one portion of the NADW is also deflected east- and southward resulting in
224 another weak return current along the western Madagascan margin. The other portion travels
225 farther northward and flows through the deep gap west of the Davie Ridge into the Somali
226 Basin (Kolla et al., 1980a; Donohue and Toole, 2003; van Aken et al., 2004).
227 The lateral distribution of the water masses in the Mozambique Channel is rather uniform
228 along WOCE section I4 at 24°40'S (Donohue and Toole, 2003) and along a meridional
229 section at 40°E (Boyer et al., 2009) (Figure 3). The AABW with potential temperatures $\Theta <$
230 0.8°C and salinities S between 34.69 - 34.74 psu (Kolla et al., 1980a) is restricted to water
231 depths below ~4000 m and extends to maximum ~26 - 25°S. The overlying NADW with its
232 high salinity core (S = 34.78 - 34.84 psu) and potential temperatures of 1.2 - 2.2°C (Kolla et
233 al., 1980a) covers water depths between ~2200 - 3500 m. South of ~24°S warmer, low-
234 salinity Antarctic Intermediate Water (AAIW; $\Theta \simeq 3$ - 8°C, $S \simeq 34.4$ - 34.6 psu) is
235 encountered between ~800 - 1500 m water depth. Farther north the AAIW is mixed with more
236 saline (>34.6 psu) Red Sea Water (RSW), which - entrained by MCEs - moves southward
237 through the Channel (de Ruijter et al., 2002; Swart et al., 2010). Warm, high-salinity tropical
238 surface waters (TSW; $\Theta \simeq 10$ - 25°C, $S \simeq 34.7$ - 35.6 psu) form the uppermost layer and are
239 brought southward by MCEs, too (Donohue and Toole, 2003).
240 A rough overview on the current velocity structure across the Mozambique Channel provide
241 LADCP measurements along WOCE section I4 (Donohue and Toole, 2003) (Figure 4a). The
242 main cores of the NADW and AAIW are banked against the Mozambican continental slope in
243 ~2000 - 2500 m and ~700 - 1200 m depth. They flow northward with maximum cross-track
244 velocities of ~0.2 m/s and form the Mozambique Undercurrent west of ~37°30'E (de Ruijter
245 et al., 2002; Donohue and Toole, 2003; van Aken et al., 2004). A region with weak (<0.1 m/s)
246 southward flow east of the Mozambique Undercurrent is interpreted as deep-reaching

continuation of an anticyclonic MCE visible in the upper western part of the section with near-surface speeds of ~0.3 - 0.4 m/s. A deep-reaching cyclonic eddy in the eastern part of the section (at ~42°E) with cross-track velocities of ~0.4 m/s close to the sea surface and ~0.1 m/s close to the seafloor might be associated with the (S)EMC. Southward cross-track velocities of ~0.1 m/s along the western Madagascan margin are considered to indicate the return current of the NADW.

Detailed information on the current velocity structure of deep-reaching MCEs comes from the ACSEX-1 cruise (Ridderinkhof, 2000; de Ruijter et al., 2002). Then, the exact positions of three MCEs were derived from satellite altimetric observations of the sea level anomalies in the Mozambique Channel before LADCP based velocity sections were measured at ~17°S, ~20°S and ~24°S (Figure 4b-d). All three sections show high surface speeds of up to 1.0 m/s, downward decreasing velocities, a strong southward flow along the Mozambican margin and a northward flow in the middle of the Mozambique Channel resulting from the western and eastern halves of the anticyclonic eddies. Additionally, the velocity section at ~24°S indicates that the eddy with its centre at ~38°20'S reaches down to the seafloor in >3000 m water depth, where current velocities still amount to ~0.1 m/s. The narrow band of the northward Mozambique Undercurrent is obvious west of ~37°15'E with its NADW and AAIW cores and current velocities >0.1 m/s. As this section nearly coincides with the western part of WOCE section I4 but was measured ~5 years later, the differences between both sections may roughly reflect the temporal variability of the current velocity regime.

3. Data acquisition

The data presented in this paper were acquired during the R/V *Sonne* cruise SO-183 (Jokat, 2006). The cruise was primarily dedicated to collect marine magnetic and gravity data on the

Mozambique Ridge and in the Mozambique Channel to unravel the break-up of Gondwanaland in this region in detail. High-resolution bathymetry and sub-bottom profiler data were collected simultaneously with non-optimized line spacing and orientation. Rather, the N-S line orientation was chosen to run perpendicular to the expected magnetic anomalies, and the line spacing was optimized such that the magnetic anomalies could be correlated from one line to the next. This led to a grid of 16 parallel, non-overlapping bathymetric stripes which cover an area of ~500 km × 700 km side lengths intermittently with a line spacing of ~30 km and a total length of ~11800 km (Figure 2). The ship speed was ~10 - 11 kn.

The high-resolution bathymetry data were collected using the hull-mounted Kongsberg-Simrad EM120 multibeam sonar. Two CTD casts were run, one in the northern and one in the southern part of the study area, to determine sound velocity profiles for the post-processing of the multibeam data (Jokat, 2006). This post-processing comprises an editing, cleaning and outlier rejection of the bathymetric and the navigation data and was done using the CARIS-HIPS software (Jokat, 2006). Subsequently, the data were gridded with 0.05' (~93 m) cell size, and the gaps between the bathymetric stripes were masked using the GMT software (Wessel and Smith, 1991).

The sub-bottom profiler data were acquired using the hull-mounted narrow-beam parametric ATLAS PARASOUND system. It was operated with a (parametric) frequency of 4 kHz, and the emitted sinusoidal signals had a duration of 2 periods (~0.5 ms) (Jokat, 2006). The water and sub-bottom depths in the seismogram sections were computed from the two-way travel times of the reflected signals assuming a constant sound velocity of 1500 m/s. A Butterworth filter of 2 - 6 kHz passband (72 dB/octave) and a routine, which removes the average noise level from the data were applied as post-processing routines to optimize the display of the data. To enhance reflections from deeper layers the seismogram sections were normalized to individually selected maximum amplitudes. That is, amplitudes higher than this maximum

297 value are clipped while reflections from deeper layers appear enhanced in the grey-shaded
298 images.
299
300
301 **4. Bathymetric maps and microtopographic classification**
302 The hill-shaded coloured map (Figure 5) provides an overview on the acquired bathymetric
303 data. From a visual inspection of this map and of the PARASOUND recordings a
304 microtopographic classification has been established (Figure 6). Four main microtopographic
305 zones and several sub-zones have been identified (Figure 6, Table A1). The main zones
306 consider the overall morphology and divide the study area into regions with smooth (type S),
307 undulating (type B) and rough seafloor (type R) and the Zambezi & Tsiribihina Channels
308 (type Z). The sub-zones take the PARASOUND reflection pattern and the shape, size and
309 orientation of the bedforms into account. In the following chapters the most prominent
310 morphological features are discussed and displayed as enlarged hill-shaded maps combined
311 with the PARASOUND sections and depth profiles running along the central line of each
312 bathymetric stripe.
313
314 **4.1 Undulating seafloor**
315 Most of the study area is covered with undulating bedforms (Figure 6). Based on their overall
316 appearance this area is sub-divided into a southern (type BS), a central (type BC) and a
317 northern bedform area (type BN) and the southeastern Zambezi Channel levee (type BE).
318
319 *Southern bedform area (BS1 - BS7)*
320 Generally, the most prominent characteristics of the southern bedform area are deep, steep-
321 walled channels, furrows or scours, which incise the undulating bedforms intermittently. The

most spectacular of these features occur in the southwest (type BS1). Here, numerous closely spaced, large erosional scours of up to ~450 m depth, up to ~20 km length and ~3 - 7 km width corrugate the seafloor repeatedly (Figure 7). They show asymmetric cross-sections with steep (>10°) southern and shallower northern flanks. They are filled with layered sediments of ~25 - 35 m thickness, which are intermittently intercalated with transparent lenses. Farther southward (type BS2) small sediment drifts with erosional southern flanks and diffuse or small internal hyperbolic echoes and distinctly layered upslope migrating sediment waves of ~45 m height and ~3 - 4 km wavelength are found (Figure 8).

NE-SW to ENE-WSW trending wavy bedforms occur in the southeast (types BS3, BS4). Their average wavelength and height decrease eastward from ~2.5 - 3 km and ~60 - 80 m (Figure 9a) to ~1.5 - 2 km and ~20 - 30 m (Figure 9b). The larger bedforms (type BS3) show very steep flanks (>10°). The smaller bedforms (type BS4) are intermittenly incised by ~60 m deep, ~2 - 3 km wide and ~8 - 15 km long furrows oriented W-E or NW-SE. The PARASOUND reflection pattern is diffuse. The reflection strength is very weak and the signal penetration very low in the larger bedforms, but increase eastward towards the Zambezi Channel to ~20 - 40 m penetration in the smaller bedforms.

A W-E trending ~100 m deep, ~5 km wide and ~100 km long channel (type BS7) marks the northernmost limit of the southern bedform area (Figure 10). In the north the channel is bordered by an almost flat ~20 km broad terrace covered with small wavy bedforms of ~300 m wavelength and <5 m height. They show prolonged subbottom reflections down to ~10 - 15 m depth. Weakly reflecting layered sediments with ~20 - 25 m signal penetration cover the channel floor, the ridge south of the channel and the scours south of the ridge.

Microtopographic zones BS5 and BS6 (without Figures) indicate transition zones between other morphological types. Zone BS5 comprises small irregular, highly variable bedforms, which do not show any distinct orientation. In contrast to the adjacent zone BS3 these

bedforms are composed of sediments which cause moderate/strong prolonged or parallel subbottom reflections down to ~20 - 30 m depth. Zone BS6 is characterized by small undulating bedforms with diffuse prolonged subbottom reflections similar to the adjacent zone BS4. But in contrast to zone BS4 they are mainly oriented NW-SE.

Central bedform area (BC1 - BC8)

The sedimentary structures in the central bedform area have a completely different orientation than in the southern bedform area. Pronounced NW-SE trending undulating bedforms (type BC1) of ~2 km wavelength, ~55 - 60 m height and up to >10 km long wave crests occur in the west (Figure 11a). Steep flanks (>10°) are again typical for these very regular undulating bedforms, as well as intermittently bifurcating wave crests. The PARASOUND seismogram sections show a prolonged diffuse reflection pattern with successive hyperbolic echoes and ~5 - 15 m signal penetration. In north- and northeastward direction between Mount Bourcart and an unnamed seamount the regularity of the bedforms diminishes and their undulations and flanks become smoother (types BC2, BC3) (without Figures). Weakly reflecting parallel-bedded sediments are typical for the western part of zone BC2 (cf. zone R2), whereas diffuse prolonged reflections are typical for the northeastern part of zone BC3.

In the east hummocky bedforms (type BC4) of ~1.0 - 1.5 km wavelength, ~35 - 55 m height, steep flanks (>10°) and with either no or two (W-E and NE-SW) preferential orientations cover two gently sloping hills (Figure 11b). Their PARASOUND reflection pattern is similar to that of type BC1 in the west. The northern local hill is surrounded by small undulating bedforms (type BC5) (without Figure) with rather long (>20 km) wave crests, which follow the local topographic contour lines. The hummocky bedforms of the southern hill become more linear towards the Zambezi Channel (type BC6) (without Figure), where they are mainly oriented NE-SW. Both local hills are separated by a ~15 km wide depression with an almost

372 flat seafloor (type BC7) (without Figure) and a diffuse prolonged reflection pattern with ~5 -
373 15 m signal penetration.
374 The western NW-SE oriented undulating bedforms are separated from the eastern hummocky
375 bedforms by an area with arcuate cross-cutting features (type BC8), which form up ~140 m
376 deep, steep-walled (>10°) convex-bended "channels" and "ridges" and surround a local
377 topographic high of ~35 - 40 km diameter (Figure 12). Smaller NW-SE oriented grooves
378 cross these "channels" and "ridges", particularly in the eastern part. All structures are draped
379 with an at least ~40 m thick sequence of layered sediments which reflect moderately in the
380 upper ~15 m and weakly in greater subbottom depths.
381 A moat which surrounds an unnamed seamount and has a diameter of ~50 - 60 km occurs
382 north of these arcuate bedforms (Figure 13). Diffuse reflecting slumps are found at the foot of
383 the seamount, while flat parallel-bedded distinctly reflecting sediments fill the moat and
384 change to sediment waves of ~1.5 km wavelength and ~10 - 60 m height (cf. zone BC3)
385 farther away from the seamount. However, in contrast to the undulating bedforms in the
386 central (Figures 11a, b) and southern bedform area (Figures 9a, b) they show distinct parallel
387 subbottom reflections with a signal penetration of ~20 m, similar to the moat (Figure 13).
388
389 *Northern bedform area (BN1 - BN2)*
390 In the northern bedform area highly variable structures ranging from arcuate sedimentary
391 features (type BN1) over an amalgamation of holes and elongate depressions to undulating
392 bedforms (type BN2) are found (Figure 14). The arcuate features form either large convex-
393 bended sediment blocks or "ridges" of ~30 - 35 km length which rise up from a flat seafloor
394 to ~40 - 85 m height. They occur northeast of the Bassas da India complex. Slumps initiated
395 on the northern flanks of Europa Island are deposited at its foot and are visible at the southern
396 end of the PARASOUND section of line A. At the northern end of this line two normal faults

occur which displace the parallel-bedded sediments by few metres. The amalgamation of holes and elongate depressions is located farther eastward near the confluence of the Zambezi and Tsiribihina Channels and is accompanied northward by small sedimentary "ridges" (line B) and northeastward by irregular hummocky or almost circular structures close to the western Zambezi Channel bank. The holes, elongate depressions and irregular features reach depths of ~25 - 75 m and diameters/widths of ~1 - 10 km. All bedforms of zone BN1 and of the northern part of zone BN2 are again draped with a sediment sequence showing distinct parallel subbottom reflections down to ~40 - 50 m depth. Farther southward the penetration decreases to ~20 m and steep bedform flanks (>10°) occur more frequently.

Southeastern levee of the Zambezi Channel (BE1)

Undulating bedforms (type BE1) of ~10 - 25 m height and ~5 - 6 km wavelength are found on the southeastern levee of the Zambezi Channel (Figure 15). They are oriented W-E, NE-SW or NW-SE depending on their position relative to the loop(s) of the Zambezi Channel and either do not migrate (in the northern part) or migrate upslope (in the southern part). They show distinct parallel subbottom reflections down to ~30 - 50 m depth.

4.2 Smooth seafloor

A smooth seafloor occurs on the Mozambican continental slope (type S1), north and south of the Bassas da India complex (types S2, S3), on the eastern levee of the Zambezi Channel (type S4) and in the Zambezi cone (type S5). As the bathymetry of these microtopographic zones does not show pronounced variations only selected PARASOUND sections, which illustrate the dominant sedimentation processes, are shown. An exception is a prominent slide, which is displayed as both enlarged hill-shaded map and PARASOUND section.

Mozambican continental slope (S1)

The northwestern Mozambican continental slope is characterized by downslope mass-wasting processes which occur mainly in water depth between ~2900 - 3300 m. The debris flow and slump deposits form transparent lenses and diffuse reflecting sediment bodies, which are intercalated in the undisturbed layered sediment sequence (Figure 16a). Southeastward the number of mass-wasting deposits decreases, and the sedimentation pattern changes to an undisturbed parallel-bedded strongly reflecting succession, which fills a small bowl-shaped basin and onlaps a bathymetric high (Figure 16b).

Few small channels and a slide scar of ~7 km length and on average ~4 km width incise the northwesternmost part of the study area (Figure 17). A closer inspection of the bathymetry and the PARASOUND section exhibits, that this scar reflects a multiphase slope failure with at least two, possibly up to four events. Event 1 occurred farthest upslope and left a narrow, slightly bended scar with a prominent steep headwall along its northern and eastern side. The PARASOUND section, which crosses the scar ~10 km downslope from the northern headwall, shows a ~30 m high step and a prominent change in the reflection pattern from a transparent ~15 - 20 m thick sediment package to a parallel-bedded distinctly reflecting sequence. Farther downslope one, possibly two other events characterized by headwalls with three (event 2) and two (event 3) "fingers" are mapped within the scar of the first event. Again, the PARASOUND section exhibits ~30 and ~15 m high steps, but only minor changes in the reflection pattern and strength. A potential fourth event with a broad triangular scar might have been occurred farther eastward. In the PARASOUND section the subbottom of this slope failure is associated with the transparent sediment package north(-east) of slope failure 1. The transition to the undisturbed seafloor farther northward is marked by a slight change in the slope inclination and in the reflection pattern to a strongly reflecting sequence.

North and south of the Bassas da India complex (S2 - S3)

The seafloor north (type S2) and south (type S3) of the Bassas da India complex is covered with a thick slightly undulating succession, which shows fine-scale distinct parallel subbottom reflectors (Figure 18). At the northern and southern foot of the seamount complex it covers large slump deposits which form ~15 km long and ~75 - 100 m thick transparent sediment bodies. The signal penetration depth reaches ~40 - 60 m in the northern (line Hall Tablemount) and ~20 - 40 m in the southern area (line Jaguar Seamount).

Eastern levee of the Zambezi Channel (S4)

A flat seafloor with a small sediment wave field and fine-scale distinct parallel subbottom reflectors is typical for the upper ~20 - 50 m of the eastern levee of the Zambezi Channel (Figure 19). The number of the subbottom reflectors, their reflection strength and the signal penetration are high close to the Zambezi and Tsiribihina Channels, but decrease southward.

Zambezi cone (S5)

The Zambezi cone encloses the triangular area south of the Zambezi Channel mouth, where the main channel branches into several distributary channels. The cone is covered with flat strongly reflecting sediments (Figure 20). The reflection pattern clearly changes laterally. South of the Zambezi Channel mouth (line Zambezi 1) a thick sequence with distinctly reflecting parallel-bedded sediments and a signal penetration depth of ~40 - 60 m is found (Figure 20a). Southward transparent lenses of mass-wasting deposits lie on top of this sequence and cause significantly reduced reflection amplitudes. ~60 km westward the reflection pattern along the entire line Zambezi 2 resembles the pattern found at the southern end of line Zambezi 1 (Figure 20b). Reflections are diffuse and only penetrate ~20 m. Transparent mass-wasting deposits occur in the middle and (buried) undulating bedforms at

472 the southern end of the line. Another ~90 km westward (line Zambezi 3) the signal
473 penetration decreases to ~10 m (Figure 20c). The reflection pattern is diffuse, and a thin
474 transparent veneer of ~2 - 4 m thickness lies on the top.
475
476 **4.3 Zambezi and Tsiribihina Channels**
477 The Zambezi and the Tsiribihina Channel follow a gently meandering course (Figures 5, 6).
478 Near their confluence both channels are narrowest and deepest (type Z1) (without Figure) and
479 have a width and depth of ~4 km and ~630 - 750 m (Zambezi Channel) and ~2 km and ~570 -
480 650 m (Tsiribihina Channel). Close to its mouth the width of the Zambezi Channel doubled to
481 ~8 km, while its depth diminished to ~150 - 300 m. Reflections from the channel floors are
482 strong, diffuse and prolonged and penetrate down to ~5 - 10 m depth.
483 Both channels show U-shaped cross-sections in agreement with Droz and Mougenot's (1987)
484 findings. In the north the channel walls are steep (>10°) and return either no reflections or
485 weak hyperbolic echoes with no signal penetration (type Z2) (without Figure). Southward the
486 cross-sections become smoother and small terraces occur within the channel. Here, the
487 reflections are strong and prolonged or hyperbolic depending on the course of the
488 PARASOUND line relative to the channel and reach a penetration depth of ~20 - 30 m. The
489 areas within the meander loops are covered with flat or slightly undulating sediments
490 depending on the distance to the channel and show distinct parallel subbottom reflections
491 down to ~40 - 45 m depth or small/moderate hyperbolic echoes.
492
493 **4.4 Rough seafloor**
494 The seamounts and islands have a steep (>10°) rough topography, which returns weak,
495 evanescent reflections or large diffraction hyperbolae (type R1) (without Figure). The signal
496 penetration is usually <5 m.

An unusually strong anomalous reflection pattern occurs north of a ~70 - 75 km long depression south of the bowl-shaped basin at the foot of the Mozambican continental slope (Figure 21a-b). The parallel subbottom reflections of this basin and their onlap on the ascending slope are discernible in the northern part of lines D1 - D3 (Figure 21b). Along line D1 this reflection pattern changes abruptly into an anomalous pattern with strong prolonged stacked hyperbolic echoes, which extend southward to an ~11 km wide, ~110 m deep semi-circular depression. In this depression and farther southward the reflections become abruptly weaker. Another depression of ~8 - 10 km width and ~110 m depth occurs at the southernmost end of line D1, but is not associated with a change in the reflection pattern. Along line D2 undulating asymmetrical bedforms with prolonged echoes are found instead of the anomolous prolonged stacked hyperbolic echoes. Their reflection strength changes abruptly to weaker amplitudes already more than ~10 km north of the depression. The depression itself reveals a rugged topography here and is covered with weakly reflecting, parallel-bedded sediments, which also extend farther southward. Along line D3 a strong, prolonged reflector appears from greater subbottom depth approximately parallel to that part of lines D1 and D2 where the undulating asymmetrical bedforms and the strong prolonged stacked hyperbolic echoes occur. The seafloor above this emerging reflector returns diffuse echoes which change to small undulating W-E oriented bedforms farther southward. The depression at the southern end of line D3 is not as pronounced as in the other two lines, but appears as a slightly undulating seafloor covered with parallel-bedded, weakly reflecting sediments. The signal penetration amounts to ~20 - 35 m in the strongly reflecting northern parts and to ~10 - 25 m in the weaker reflecting southern parts.

4.5 Comparison with the microtopographic classification of Kolla et al. (1980a)

A comparison of the microtopographic classification established in this paper with the zones

II - IV described by Kolla et al. (1980a) illustrates that zone II almost coincides with zone S5 representing the Zambezi cone (Figure 6). Zone III encompasses zones BS2, BS3 and BS4 and thus partially contradicts the interpretation in this paper. Here, fine-grained sediment waves associated with a weak northward AABW flow were found only in zone BS2, whereas the undulating bedforms in zones BS3 and BS4 are interpreted as elongate contourite mounds or a series of grooves and ridges aligned parallel to the deflected AABW. Zone IV comprises the western and northern parts of the southern bedform area and nearly the whole central and northern bedform areas. Thus, the microtopographic classification here identifies much more different types of hyperbolic echoes and relates them to the present-day AABW flow and the deep-reaching eddies of the MC and (S) EMC.

5. Interpretation and discussion

Most of the bedforms obviously developed under the influence of bottom currents. In the following chapters we try

(1) to relate the different bedform types to the present-day ocean current regime,

(2) to discuss whether the bedforms are still active today,

(3) to discuss stratigraphic constraints for the formation of the bedforms.

5.1 Distribution of bedforms vs ocean current regime

Southern bedform area (~4700 - 3500 m water depth)

The southern part of the southern bedform area lies in the water depth range of the AABW (<4000 m) which according to the meridional distribution of the water masses (Figure 3) extends northward to ~26 - 25°S. The northern part already lies in the transition zone between AABW and NADW (~4000 - 3500 m). Current velocity measurements are not available for

547 this part of the study area, but a rough southward extrapolation of the LADCP based current
548 velocity sections at 24°40'S and 24°S (Figure 4) indicates that today none of the survey lines
549 is affected by strong western boundary currents. Rather all lines experience weak bottom
550 currents of <0.1 m/s.
551 Hence, the small sediment drifts and sediment waves in zone BS2 (Figure 8) located in ~4700
552 - 4500 m water depth on a gently ascending slope (~0.05°) developed under the influence of a
553 weak northward AABW flow. They are considered to indicate the northernmost extension of
554 the sediment wave field mapped by Kolla et al. (1980a) along the western margin of the
555 Mozambique Basin (Figure 6). The weak bottom currents of <0.1 m/s today agree with the
556 bottom-current velocities of ~0.08 - 0.1 m/s derived by Kolla et al. (1980a) via a modelling
557 approach for the formation of the sediment waves. Especially, the erosional southern flanks of
558 the sediment drifts and the upslope migration of the sediment waves indicate a persistent
559 northward flow in this part of the study area (Figure 22).
560 The internal hyperbolic echoes in the sediment drifts and the limited spatial extent of
561 sediment waves in zone BS2 point to some turbulences in the water column preventing a
562 widespread smooth, distinctly layered deposition of fine-grained sediments. The reason for
563 such turbulences might be, that north of ~27°S the ascending slope of the Mozambique
564 Channel steepens from ~0.05° to ~0.3° (Figure 3), so that the water depth decreases rapidly
565 from ~4500 to ~4000 m within a distance of ~100 km. This bathymetric ramp forms a
566 topographic barrier for the northward flowing AABW, so that it must upwell and mix with the
567 overlying water masses and/or flow aside (Figure 22). This upwelling and mixing is probably
568 strongest in the western part of zone BS1, where numerous closely spaced giant erosional
569 scours corrugate the seafloor (Figure 7). Here, probably two forces interact: (1) The
570 northward flowing AABW is decelerated and reflected by the bathymetric ramp leading to a
571 south- and upward-directed force. (2) Simultaneously, the Coriolis force pushes the AABW

572 westward against the eastern flank of the Mozambique Ridge. The superposition of both
573 forces might produce clockwise rotating vortices, which erode the giant scour hollows.
574 Furthermore, the south- and upward-directed force might promote retrogressive erosion
575 leading to the asymmetrical cross-sections of the scour hollows.
576 However, it is rather unlikely that the present-day current velocities of <0.1 m/s are strong
577 enough to erode scour hollows of several hundred metres depth, tens of kilometres length and
578 several kilometres width. According to Hjulström's curve current velocities of at least 0.2 m/s
579 are necessary to erode unconsolidated clay, silt and fine sand up to 0.5 mm grain size, and
580 even higher velocities for coarser grain sizes (Tucker, 2004). Therefore, the scours must have
581 been eroded during geologic times when the bottom-current velocities were stronger than
582 today, whereas the present-day current velocities allow only transportation and deposition of
583 particles from suspended load, thus keeping the hollows open. This agrees with weakly
584 reflecting sediments on the ridges between the hollows and an at least ~25 - 35 m thick
585 sediment infill in the hollows. Transparent lenses intercalated in these infills also point to
586 mass-wasting deposits, which might have been swept into the hollows by bottom currents in
587 addition to the undisturbed hemipelagic deposition.
588 Similar giant erosional scours with pronounced scarps, asymmetric cross-sections and partial
589 infill with Pliocene-Holocene sediments were found at the southwestern end of the Faroe-
590 Shetland Channel (Bulat and Long, 2001; Stoker et al., 2003; Long et al., 2004; Masson et al.,
591 2004). These "Judd Deeps" occur at the narrowest part of the deep-water passage, where the
592 throughflow is accelerated to maintain the cross-sectional volume transport. Additionally,
593 deeper penetrating reflection seismogram sections show similar buried features above a Late
594 Oligocene-Early Miocene unconformity leading to the interpretation that the erosion of the
595 scours is related to the onset of a high-energy bottom-current flow through the Faroe-Shetland
596 Channel (Bulat and Long, 2001; Stoker et al., 2003). Due to the similarity of these scours one

can speculate that (1) regions where (strong) bottom currents are topographically forced to change their flow direction are prone to the formation of giant erosional scours and (2) the formation of the giant erosional scours in the Mozambique Channel might also be related to a prominent change in the AABW flow intensity. If deeper lying tectonic structures or unconformities additionally foster the erosion is neither clear for the Faroe-Shetland nor for the Mozambique Channel.

Farther south- and eastward the undulating bedforms of zones BS3 and BS4 (Figure 9a, b) are aligned parallel to the local topographic contour lines pointing to a generation by a contour current. This is probably that portion of the AABW that does not upwell, but is deflected eastward against the Coriolis force and flows along the slope of the shallowing Mozambique Channel (Figure 22).

The alignment of these bedforms, their steep flanks and the almost evanescent diffuse internal reflection pattern arise questions, which mechanism might have formed them. An interpretation as fine-grained sediment waves seems to be rather unlikely, because these usually show a distinct internal stratification, shallower flanks and an orientation oblique or parallel to the topographic contour lines depending on whether they are generated by bottom or by turbidity currents (not evident here) and wave crests oblique or perpendicular to the flow direction (Wynn and Stow, 2002). The alignment of the bedforms here parallel to the topographic contour lines and parallel the bottom-current flow direction rather points to small elongate contourite mounds as have also been described for the northern Rockall Trough (Howe, 1996; Stoker et al., 1998; Masson et al., 2002) and the northeastern Faroe-Shetland Channel (Bulat and Long, 2001). Another potential mechanism might be turbulences or marginal eddies (Stow et al., 2008) associated with the topographic deceleration and deflection of the AABW. They might promote the formation of longitudinal vortices forming grooves and sedimentary "ridges" parallel to the contour lines (Allen, 1997). Such turbulences

might also explain the diffuse reflection pattern and the intermittently incised furrows as a product of short-term, locally increased current velocities (Hollister and McCave, 1984). In any case the eastward decreasing height of the bedforms may be attributed to a successively decreasing current velocity of the deflected AABW caused by its flow against the Coriolis force. The very low signal penetration in zone BS3 might either be explained geometrically by the steep bedforms flanks (>10°), which mainly diffract the narrow-beam PARASOUND signal. Or it might be due to missing fine grain sizes, which have been winnowed here and deposited farther eastward in zone BS4 due to the slower AABW current velocity, thus causing the greater signal penetration in the smaller bedforms. Whether these bedforms are still active, i.e. migrate or change their shape and position, can hardly be identified due to the lack of internal stratification.

The channel in the northwesternmost part of the southern bedform area (zone BS7, Figure 10) lies in the transition zone between AABW and NADW and is interpreted as a contourite channel which indicates the northernmost extension and a flow path of the eastward deflected AABW (Figure 22) during the time when the channel was eroded. Layered sediments covering the "ridge(s)" and filling the channel and the giant erosional scours south of the channel prove that today only weak bottom currents are active which do not erode sediments but keep the channel open. The locally confined terrace with very small sediment waves north of the channel illustrates that the flow was/is not only restricted to the deep channel.

Central bedform area (~3500 - 3000 m water depth)

The central bedform area lies completely in the water depth range of the NADW. The current velocity sections across the whole Mozambique Channel at 24°40'S and across its western half at 24°S (Figure 4) show that this area is mainly affected by deep-reaching eddies, which have bottom-current velocities of <0.1 m/s and produce a southward flow in the western and

647 eastern parts of the study area and a northward flow in the middle of the Mozambique
648 Channel. The Mozambique Undercurrent and the NADW return current influence this area, if
649 at all, only along its western and eastern margins west of ~37°E and east of ~42°E.
650 The very regular undulating bedforms (zone BC1) (Figure 11a) in the west are aligned
651 oblique to the topographic contour lines and lie in the range of the southward flow of the
652 anticyclonic MCEs. Due to their steep flanks, diffuse hyperbolic echoes, low signal
653 penetration and lack of internal stratification it is difficult to discern, whether these bedforms
654 are active. Their bathymetric image and their scales resemble a network of elongate contourite
655 mounds mapped on the slope of the Faroe-Shetland Channel (Bulat and Long, 2001) rather
656 than actual sediment waves. Therefore, we again prefer the term elongate contourite mounds
657 for the undulating bedforms here. Their crests are aligned oblique to the southward flow, but
658 parallel to a part of the swirl of an anticyclonic MCE (Figure 22).
659 The formation of the hummocky bedforms (zone BC4) (Figure 11b) in the east is more
660 difficult to explain. In the planform these bedforms resemble (subaerial) star dunes, which are
661 typically generated by two different wind directions (Anderson and Anderson, 2011). For
662 subaqueous bedforms this implies that two different (W-E and NE-SW) flow directions must
663 be active simultaneously or alternately. Comparisons with modelling computations reveal that
664 the ocean circulation in the Eastern Mozambique Channel is subject to a strong seasonal
665 variability (Chapman et al., 2003), which might cause different flow directions and thus form
666 the hummocky bedforms (Figure 22). Furthermore, the small undulating bedforms, which
667 surround the northern hill seem to reflect the footprint of an eddy, which might be related to
668 the northern path of the (S)EMC (Chapman et al., 2003) (Figure 1). Additionally, one can
669 speculate, if the two gently sloping hills covered with the hummocky bedforms are actually
670 large drift bodies, which accumulated in the centre and along the margin of an eddy.
671 The arcuate cross-cutting features (zone BC8) (Figure 12) in the middle of the central

672 bedform area approximately mark the eastern boundary of an anticyclonic MCE, where a
673 northward flow direction prevails (Figure 22). The course of these sedimentary features seems
674 to be topographically controlled by the almost circular bathymetric high. In contrast, the
675 origin of the smaller grooves crossing the arcuate "channels" and "ridges" is not as obvious,
676 but might again be attributed to a seasonally variable (S)EMC eddy in the eastern part. The
677 ~40 m thick sediment drape indicates again that the formation of these >100 m deep
678 structures must have happened during geologic times, when bottom currents were stronger
679 than today and capable to erode sediments, whereas today sediment transportation and
680 deposition prevails and keeps the structures open.
681 Similarly, the moat surrounding an unnamed seamount north of the arcuate "channels" and
682 "ridges" (Figure 13) is also considered to be generated by a topographically controlled weak
683 northward flow (Figure 22), as well as the small sediment wave field south of the moat and
684 the small W-E oriented undulating bedforms of zone BC3 (without Figure) north of the moat
685 and south of the Bassas da India complex.
686
687 *Northern bedform area (~3200 - 2900 m water depth)*
688 The northern bedform area lies in the water depth range of the NADW, too. Knowledge of
689 current velocities in this area is rare. A rough northward extrapolation of the current velocity
690 section at 24°40'S (Figure 4) implies that northward bottom currents of <0.1 m/s velocity
691 must be anticipated. If the eddy between ~40°30'E and ~42°30'E can also be extrapolated or if
692 it is only a temporarily variable phenomenon is unclear. However, it is worth to mention that
693 the region east of the Bassas da India complex lies outside the main travel corridor of the
694 MCEs (Schouten et al., 2003).
695 The formation mechanism of the highly variable bedforms in this area is not really evident.
696 The arcuate, convex-bended features in zone BN1 (Figure 14) may point to deep-reaching

eddies or bottom currents, which locally interact with the topography of the Bassas da India complex. Similarly, the close vicinity and sometimes sudden change of different topographic features such as the amalgamation of holes, elongate depressions, small "ridges" and hummocky or circular structures in zone BN2 (Figure 14) may suggest an interaction of bottom currents with the topographic incisions of the Zambezi and Tsiribihina Channels (Figure 22). If deeper lying structures or unconformities (additionally) affect or cause these features remains unclear due to the limited penetration of the PARASOUND data. But again, the ~40 - 50 m thick drape on all sedimentary features exhibiting vertical heights and depths of nearly 100 m indicates, that these features must have been formed during geologic times, when bottom currents were stronger, while today sediment deposition and transportation dominates and keeps the structures open.

Southeastern levee of the Zambezi Channel (~3500 - 3200 m water depth)

The southeastern levee of the Zambezi Channel also lies in the water depth range of the NADW. According to the current velocity section at 24°40'S (Figure 4) a southward flow with bottom-current velocities <0.1 m/s prevails. However, the wave crests of the sediment waves (Figure 15) are aligned parallel to the local topographic contour lines suggesting that turbidity currents associated with the sediment transport in the Zambezi Channel formed the waves (Figure 22) rather than bottom currents (Wynn and Stow, 2002).

5.2 Sedimentary processes in regions with smooth and rough seafloor

Mozambican continental slope (~3300 - 2900 m water depth)

The Mozambican continental slope lies in the water depth range of the NADW as well. A rough interpolation between the current velocity sections at 20°S and 24°S (Figure 4) yields that most of the continental slope is influenced by the southward flow of the anticyclonic

MCEs with bottom-current velocities <0.1 m/s. Only the part east of ~38°30'E might rather experience a weak northward flow associated with the eastern part of the MCEs. The Mozambique Undercurrent with its main NADW core in ~2500 m depth and bottom-current velocities >0.1 m/s passes the study area along its northwesternmost corner north of 21°S.

The most prominent morphological feature is the slide scar on the northwestern continental slope (Figure 17). Its morphology and dimension resemble bottleneck slides, as have also been found on the NE Faroe continental margin (van Weering et al., 1998) and on the NW slope of the Hatton Bank (MacLachlan et al., 2008) in current-controlled environments. Though it is the only slide scar detected here this region seems to be rather prone to slope instabilities, as the scar itself exhibits up to four failure events, and several mass-wasting deposits occur near the scar, too (Figure 16). A timing of the failure events is impossible because no sediment cores are available for ground-truthing. However, as at least ~30 thick layered sediments are covering the gliding planes, all failure events seem to be rather "old". As well, no definite failure mechanism can be derived from the bathymetric and PARASOUND data. But a comparison with the similar multiphase slope failure on the NW slope of the Hatton Bank (MacLachlan et al., 2008) suggests that bottom currents might have promoted the failure(s). According to Sultan et al. (2004) an oversteepening of the slope or a removal of the (stabilizing) foot support can cause slope failures. Here, a northwestward increasing slope gradient and the influence of the Mozambique Undercurrent passing the head of the slope failure in the northwest (Figure 22) might have lead to an accumulation of (oversteepened) contouritic successions, which occasionally fail leaving either slide scars on the slope or are deposited as transparent lenses or diffuse reflecting debris flows. Additionally, the displaced mass is missing, at least in the available bathymetric stripes, which might also point to a destabilizing effect of the southward flowing MCEs at the foot of the scar and their capability to remove the displaced sediments.

747 The undisturbed parallel-bedded strongly reflecting layers filling the bowl-shaped basin in the
748 southeast are interpreted as coarse-grained turbidites (Damuth and Hayes, 1977; Damuth,
749 1980) transported down the Mozambican continental slope (Figure 16).
750
751 *North and south of the Bassas da India complex (~3200 - 2900 m water depth)*
752 The more fine-scale distinct reflection pattern of the parallel-bedded sequences north and
753 south of the Bassas da India complex (Figure 18) indicates that more fine-grained sediments,
754 probably distal turbidites, are deposited here than in the bowl-shaped basin (Damuth, 1980;
755 Damuth and Hayes, 1977). Additionally, the larger signal penetration north of the Bassas da
756 India complex point to a shadowing effect of the seamounts. They form a topographic barrier
757 for the turbidite suspension clouds from the Mozambican continental slope, so that less
758 terrigenous particles reach the area in the south resulting in lower sedimentation rates and
759 higher carbonate contents than in the north, thus causing higher signal attenuation (Damuth
760 and Hayes, 1977; Damuth, 1980). The weakly undulating bedforms in the north are
761 considered to be soft sediment deformations caused by slow downslope creeping of soft fine-
762 grained sediments (Wynn and Stow, 2002), whereas the undulating bedforms in the south
763 might be formed by weak bottom currents, possibly at the northern/northwestern margin of a
764 (S)EMC eddy. The thick transparent bodies of slides and debris flow are assumed to originate
765 from the flanks of the seamount complex.
766
767 *Eastern levee of the Zambezi Channel (~3200 - 2800 m water depth)*
768 The reflection pattern of the eastern levee of the Zambezi Channel can be interpreted
769 accordingly. Here, fine-grained terrigenous overspill sediments are considered to generate the
770 fine-scale distinct parallel subbottom reflectors. Their thickness decreases with greater
771 distance from the channel leading to a weaker reflection pattern. The formation of the small

772 sediment wave field can probably be attributed to currents resulting from the overspill of
773 sediments from both the Zambezi and the Tsiribihina Channel rather than to bottom currents.
774
775 *Zambezi Channel and cone (~4400 - 4000 m water depth)*
776 The Zambezi cone lies in the water depth range of the AABW. According to the southern
777 bedform area weak bottom currents of <0.1 m/s can be expected due to the eastward deflected
778 AABW.
779 The strong prolonged or hyperbolic reflections from the channel floor indicate that no
780 sediments are deposited today. If the channel floor is even eroded is difficult to discern
781 because the steep channel walls cause large hyperbolic echoes, which mask potentially
782 outcropping layers in the PARASOUND data.
783 The suspension clouds transported through the channel are deposited as parallel-bedded
784 turbidite sequence within a narrow band southeast of the channel mouth (Figure 20). Very
785 strong reflection amplitudes suggest that it consists of coarse-grained sediments. The diffuse
786 reflection pattern south and west of the parallel-bedded turbidite sequence points to a chaotic
787 or turbulent deposition of coarse-grained sediments in this part of the cone or indicates the top
788 of a huge debris flow or sandy lobe. If this kind of deposition is characteristic for the marginal
789 cone and/or if bottom currents have an influence is not clear. Today, the AABW flow is too
790 weak to mobilize and transport coarse-grained sediments. If the thin transparent veneer on top
791 of the diffuse reflection pattern in line Zambezi 3 indicates a thin pelagic cover cannot
792 unambiguously be answered, too. If it is a pelagic cover this implies that today the suspension
793 clouds do not reach the marginal cone, but are restricted to an area closer to the channel
794 mouth. This again implies that today less sediment is transported through the channel than in
795 times when the cone developed. However, the channel still seems to be active, as obviously
796 no sediments are deposited on the channel floor. Furthermore, the boundary between the

northwestern Zambezi cone and the southern bedform area (zones BS2, BS3, BS4) seems to mark (1) the boundary between the regions, where sediments are too coarse to be moved and are fine enough to develop undulating bedforms under the influence of a bottom current or (2) the southern boundary of the flow path of the deflected AABW at all.

Rough topography (~3300 - 2900 m)

The origin and formation of the unusually strong anomalous reflection pattern and the elongate depression(s) in zone R2 is not evident. The vicinity of Mount Bourcart and an unnamed seamount suggests that tectonic or submarine volcanic activity might play an important role. However, one can only speculate (1) if the elongate depression(s) are collapse structures caused by volcanic eruptions and/or gas outbursts or if they are (in-)active faults, which connect both seamounts and are draped with sediments today, (2) if the unusually strong anomalous reflection pattern north of the depression(s) indicate sediment compositions including volcanic particles, ashes and/or glasses or even lava flows, or if it is associated with deeper structures, and (3) if the strongly reflecting emerging structure in line D3 points to another buried seamount or lava flow, or if it is just an older sedimentary structure.

5.3 Discussion of stratigraphic constraints for the formation of the bedforms

Most of the morphological features described above reach up to ~100 m height, extend over several kilometres lengths and widths and are draped with at least ~20 - 50 m thick sediments. This leads to the conclusion that the bottom-current velocities today are weak enough to allow sediment deposition, but must have been stronger during the geologic times when the morphological features were formed. Kolla et al. (1980a) determined Holocene-Early Pleistocene (<80000 yrs) sedimentation rates of 15 - 20 m/Myrs and >20 m/Myrs for their microtopographic zones III and IV (Figure 6) and concluded that the sediment waves in the

822 Mozambique Basin developed in Pleistocene times and earlier. If these sedimentation rates
823 can be extrapolated to times >80000 yrs and an average rate of 20 m/Myrs is assumed, the
824 sediment drape visible in the PARASOUND data has an age of ~1 - 2.5 Ma and the large
825 morphological features developed before Middle Pleistocene/Late Pliocene times.
826 Studies on sediment drifts in the Transkei Basin and Natal Valley indicate an onset of the
827 proto-AABW at the Eocene/Oligocene boundary (~36 Ma) and of the proto-NADW since the
828 Middle Miocene (~15 Ma) (Niemi et al., 2000; Schlüter and Uenzelmann-Neben, 2007,
829 2008). Their current-velocities increased during the Middle Miocene associated with changes
830 in the extent and built-up of the polar ice sheets (Schlüter and Uenzelmann-Neben, 2008,
831 2007). Thus, the giant erosional scours and the other morphological features in the southern
832 bedform area, which lie in the water depth range of the AABW today, must be younger than
833 Eocene/Oligocene age. Probably, they originate from Middle Miocene times.
834 Studies on sediment drifts in the Limpopo cone and on the Inharrime Terrace (Preu et al.,
835 2011) and an analysis of the sediment depocentres in the Zambezi Delta (Walford et al., 2005)
836 point to an onset of the MC (and the associated eddies) in the Early/Middle Miocene (~24 - 15
837 Ma), possibly due the closure of the eastern Mediterranean connection and the narrowing of
838 the Indonesian gateway and the associated establishment of a strong westerly equatorial
839 surface current in the Indian Ocean at ~14 Ma (Gourlan et al., 2008). Also termed Miocene
840 Indian Ocean Equatorial Jet (MIOJet) this strong surface current might have triggered the
841 onset and controlled the strength of the MC, similar to the present-day ITF and SEC. Based
842 on the morphology of a depositional unit on the Inharrime Terrace highest MC velocities
843 obviously occurred in Middle Miocene-Late Pliocene times (Preu et al., 2011), in agreement
844 with an increase in the MIOJet strength between ~14 - 9 Ma and relative stable conditions
845 until ~4 Ma (Gourlan et al., 2008). Thus, the large morphological features in the central and
846 northern bedform areas, which were linked to the present-day deep-reaching eddies of the MC

847 and (S)EMC, possibly formed during Middle Miocene-(Late) Pliocene times in agreement
848 with the time spans estimated above for the deposition of the sediment drape and for the
849 evolution of the bedforms from Kolla et al.'s (1980a) sedimentation rates.
850 The weak bottom-current velocities, which allowed the deposition of the sediment drape, can
851 possibly be explained with the progressive shallowing and final closure of the Indonesian
852 gateway during Pliocene times (~4 - 2.5 Ma). This gradually reduced the MIOJet to the
853 present-day ITF and thus reduced the SEC and the flow through the Mozambique Channel
854 and around the southern tip of Madagascar, too (Gourlan et al., 2008; Karas et al., 2009).
855
856
857 **6. Summary and conclusions**
858 High-resolution bathymetric and narrow-beam subbottom profiler data collected in the
859 Mozambique Channel between 21°S - 27°S show a large variety of current-controlled
860 bedforms. Their shape, size, orientation and reflection pattern have been analysed and linked
861 to the recent and to paleoceanographic current regimes.
862 (1) The region south of 25°S lies in the depth range of the northward flowing AABW. Its
863 interaction with the seafloor is strongest in the southwest, where giant erosional scours
864 indicate that the ascending slope of the Mozambique Channel acts as a topographic barrier,
865 which forces one portion of the AABW to upwell possibly in clockwise rotating vortices. The
866 other portion, forced by the topography of the Mozambique Ridge, is deflected eastward
867 against the Coriolos force and leaves furrows and small elongate contourite mounds along its
868 flow path. A W-E trending contourite channel at ~25° marks the northernmost extension of
869 the AABW in the present-day transition zone between AABW and NADW.
870 (2) The region north of 25°S lies in the depth range of the NADW. Its main core is included in
871 the northward flowing Mozambique Undercurrent, which affects the study area only

872 marginally.
873 (3) Between 25°S - 22°20'S and east of 37°30' E the seafloor is strongly shaped by deep-
874 reaching eddies, in the west by the southward and swirling flow and in the middle by the
875 northward flow of the MCEs and in the east by seasonally variable EMC eddies. Typical
876 bedforms are small elongate contourite mounds in the west, arcuate bedforms and a moat in
877 the middle and hummocky bedforms in the east.
878 (4) North of 22°20'S and east of 40°E numerous abruptly changing morphological features
879 point to a potential interaction of bottom currents with the Bassas da India complex and the
880 Zambezi/Tsiribihina Channels in a region which lies outside the main corridor of the
881 southward travelling MCEs.
882 (5) The northwestern Mozambican continental slope seems to be prone to slope failures and
883 mass wasting possibly caused by the destabilizing influence of the Mozambique Undercurrent
884 and the MCEs.
885 (6) The regions north and south of the Bassas da India complex exhibit an undisturbed
886 deposition of fine-grained distal turbidites within a hemipelagic sequence and a shadowing
887 effect of the seamounts against the terrigenous input from the Mozambican continental slope.
888 (7) The Zambezi Channel seems to be active because no fine-grained sediments are visible on
889 the channel floor. In the Zambezi cone coarse-grained turbidites are deposited only southeast
890 of the channel mouth. Westwards, chaotic or turbulent deposited sediments lie on the top.
891 (8) Two huge elongate depressions between Mount Bourcart and an unnamed seamount and
892 unusually strong anomalous reflection patterns point to tectonic or submarine volcanic
893 activity in this region.
894 (9) Bedforms scales of ~100 m height and several kilometres length and width on the one
895 hand side and an at least ~20 - 50 m thick sediment drape on the other hand side leads to the
896 conclusion that the bedforms developed during geologic times, when the bottom currents

were stronger than today. From comparisons with previous studies on sediment deposits in the Transkei Basin, Limpopo cone and Zambezi Delta and rough Holocene-Pleistocene sedimentation rates a time interval from approximately Middle Miocene to (Late) Pliocene was estimated for the formation of the bedforms and from (Late) Pliocene to today for the sediment drape. Increased AABW current velocities during the Miocene cooling trend associated with the extent and built-up of the polar ice sheets and the onset of the MC triggered by the establishment of a strong MIOJet due to the narrowing of the Indonesian gateway are discussed as potential paleoceanographic scenarios that forced the formation of the bedforms. A subsequent decrease in the MIOJet and MC strength caused by the final closure of the Indonesian gateway is considered as scenario that forced the deposition of the sediment drape.

(10) Deeper penetrating seismic data, ideally combined with information about the turbidity, vorticity and current velocity structure in the water column, sediment cores and a more complete bathymetric coverage are necessary to answer the questions: When did the bedforms develop? How is the development of the bedforms related to processes in the water column? Did deeper lying structures promote the evolution of bedforms? What is the origin of the huge depression and anomalous reflection pattern in the vicinity of Mount Bourcart?

Acknowledgment

We thank the captain and crew of the RV Sonne cruise SO-183 for their efficient help and support during the expedition. Eric Firing (Department of Oceanography, University of Hawai'i at Manoa) kindly provided the LADCP data from WOCE section I4 and Herman Ridderinkhof (Royal Netherlands Institute for Sea Research) the LADCP data from the ACSEX-1 cruise via the CODIS data management group. The maps and the bathymetry sections were produced using the free software GMT (Wessel and Smith, 1991), the hydrographic sections using the free software Ocean Data View (Schlitzer, 2011). The analysis and interpretation of the data were done within two cooperation projects between the Alfred-Wegener-Institute for Polar and Marine Research, Bremerhaven and the Universität Bremen. The project was funded by the German Bundesministerium für Bildung und Forschung (BMBF) under contract no. 03G0183A.

928 **References**

929 Allen, P.A., 1997. Earth surface processes. Blackwell Science, Oxford.

930 Amante, C., Eakins, B.W., 2009. ETOPO1 1 Arc-Minute Global Reflief Model: Procedures,
931 Data Sources andf Analysis NOAA Technical Memorandum NESDIS NGDC-24, p. 19 pp.

932 Anderson, R.S., Anderson, S.P., 2011. Geomorphology. Cambridge University Press,
933 Cambridge.

934 Beal, L.M., de Ruijter, W.P.M., Biastoch, A., Zahn, R., SCOR/WRCP/IAPSO Working
935 Group 136, 2011. On the role of the Agulhas system in ocean circulation and climate.
936 Nature 472, 429-436.

937 Beiersdorf, H., Kudrass, H.R., von Stackelberg, U., 1980. Placer deposits of Ilmenite and
938 Zircon on the Zambezi Shelf. Geologisches Jahrbuch, Reihe D 36, 5-85.

939 Boswell, S.M., Smythe-Wright, D., 2002. The tracer signature of Antarctic Bottom Water and
940 its spread in the Southwest Indian Ocean: Part I - CFC-derived translation rate and
941 topographic control around the Southwest Indian Ridge and the Conrad Rise Deep Sea
942 Research I 49, 555-573.

943 Boyer, T.P., Antonov, J.I., Baranova, O.K., Garcia, H.E., Johnson, D.R., Locarnini, R.A.,
944 Mishonov, A.V., O'Brien, T.D., Seidov, D., Smolyar, I.V., Zweng, M.M., 2009. World
945 Ocean Database 2009. U.S. Goverment Printing Office, Washington, D.C.

946 Bulat, J., Long, D., 2001. Images of the seabed in the Faroe-Shetland Channel from
947 commercial 3D seismic data. Marine Geophysical Researches 22, 345 - 367.

948 Bunce, E.T., Molnar, P., 1977. Seismic reflecting profiling and basement topography in the
949 Somali Basin: Possible fracture zones between Madagascar and Africa. Journal of
950 Geophysical Research 82, 5305-5311.

951 Chapman, P., Di Marco, S.F., Davis, R.E., Coward, A.C., 2003. Flow at intermediate depths
952 around Madagascar based on ALACE float trajectories. Deep Sea Research II 50, 1957-
953 1986.
954 Coffin, M.F., Rabinowitz, P.D., 1987. Reconstruction of Madagascar and Africa: Evidence
955 from the Davie Fracture Zone and Western Somali Basin. Journal of Geophysical Research
956 92, 9385-9406.
957 Damuth, J.E., 1980. Use of high-frequency (3.5 - 12 kHz) echograms in the study of near-
958 bottom sedimentation processes in the deep-sea: A review. Marine Geology 38, 51 - 75.
959 Damuth, J.E., Hayes, D.E., 1977. Echo character of the East Brazilian continental margin and
960 its relationship to sedimentary processes. Marine Geology 24, 73 - 95.
961 de Ruijter, W.P.M., Ridderinkhof, H., Lutjeharms, J.R.E., Schouten, M.W., Veth, C., 2002.
962 Observations of the flow in the Mozambique Channel. Geophysical Research Letters 29.
963 de Ruijter, W.P.M., van Aken, H.M., Beier, E.J., Lutjeharms, J.R.E., Matano, R.P., Schouten,
964 M.W., 2004. Eddies and dipoles around South Madagascar: formation, pathways and large-
965 scale impact. Deep-Sea Research II 51, 383-400.
966 Di Marco, S.F., Chapman, P., Nowlin Jr., W.D., Hacker, P., Donohue, K., Luther, M.,
967 Johnson, G.C., Toole, J., 2002. Volume transport and property distributions of the
968 Mozambique Channel. Deep Sea Research II 49, 1481-1511.
969 Donohue, K., Toole, J., 2003. A near-synoptic survey of the Southwest Indian Ocean. Deep
970 Sea Research II 50, 1893-1932.
971 Droz, L., Mougenot, D., 1987. Mozambique Upper Fan: Origin of depositional units. AAPG
972 Bulletin 71, 1355-1365.
973 Gourlan, A.T., Meynadier, L., Allègre, C.J., 2008. Tectonically driven changes in the Indian
974 Ocean circulation over the last 25 Ma: Neodymium isotope evidence. Earth and Plaenetary
975 Science Letters 267, 353 - 364.

976 Hanquiez, V., Mulder, T., Lecroart, P., Gonthier, E., Marchès, E., Voisset, M., 2007. High-
977 resolution seafloor images in the Gulf of Cadiz, Iberian margin. Marine Geology 246, 42 -
978 59.
979 Harlander, U., Ridderinkhof, H., Schouten, M.W., de Ruijter, W.P.M., 2009. Long-term
980 observations of transport, eddies and Rossby waves in the Mozambique Channel. Journal
981 of Geophysical Research 114, 1-15.
982 Heezen, B.C., Hollister, C.D., 1964. Deep-sea current evidence from abyssal sediments.
983 Marine Geology 1, 141 - 174.
984 Heezen, B.C., Hollister, C.D., 1971. The face of the deep. Oxford University Press, Inc., New
985 York.
986 Heezen, B.C., Hollister, C.D., Ruddiman, W.F., 1966. Shaping of the continental rise by deep
987 geostrophic contour currents. Science 152, 502 - 508.
988 Heirtzler, J.R., Burroughs, R.H., 1971. Madagascar's paleoposition: New data from the
989 Mozambique Channel. Science 174, 488-490.
990 Hernández-Molina, F.J., Llave, E., Stow, D.A.V., García, M., Somoza, L., Vásquez, J.T.,
991 Lobo, F.J., Maestro, A., Díaz del Río, V., León, R., Medialdea, T., Gardner, J., 2006. THe
992 contourite depositional systm of the Gulf of Cádiz: A sedimentary model related to the
993 bottom current activity of the Mediterranean outflow water and its interaction with the
994 continental margin. Deep-Sea Research II 53, 1420 - 1463.
995 Hernández-Molina, F.J., Paterlini, M., Somoza, L., Violante, R., Arecco, M.A., de Isasi, M.,
996 Rebesco, M., Uenzelmann-Neben, G., Neben, S., Marshall, P., 2010. Giant mounded drifts
997 in the Argentine Continental Margin: Origins, and global implications for the history of
998 thermohaline circulation. Marine and Petroleum Geology, 1508 - 1530.

999 Hernández-Molina, F.J., Paterlini, M., Violante, R., Marshall, P., de Isasi, M., Somoza, L.,
1000 2009. Contourite depositional system on the Argentine Slope: An exceptional record of the
1001 influence of Antarctic water masses. Geology 37, 507 - 510.
1002 Hollister, C.D., Heezen, B.C., 1972. Geologic effects of ocean bottom currents: Western
1003 North Atlanttic, in: Gordon, A.L. (Ed.), Studies in Physical Oceanography. Gordon and
1004 Breach Science Publishers New York, pp. 37 - 66.
1005 Hollister, C.D., McCave, I.N., 1984. Sedimentation under deep-sea storms. Nature 309, 220 -
1006 225.
1007 Howe, J.A., 1996. Turbidite and contourite sediment waves in the northern Rockall Trough,
1008 North Atlantic Ocean. Sedimentology 43, 219 - 234.
1009 Jokat, W., 2006. Southeastern Atlantic and southwestern Indian Ocean: reconstruction of the
1010 sedimentary and tectonic development since the Cretaceous, AISTEK-II:Mozambique
1011 Ridge and Mozambique Basin, Report of the RV "Sonne" cruise SO-183, Project AISTEK-
1012 II 20 May to 7 July 2005 Reports on Polar and Marine Research. Alfred-Wegener-Institute
1013 for Polar and Marine Research, Bremerhaven, p. 71 pp.
1014 Karas, C., Nürnberg, D., Gupta, A.K., Tiedemann, R., Mohan, K., Bickert, T., 2009. Mid-
1015 Pliocene climate change amplified by a switch in Indonesian subsurface throughflow.
1016 Nature Geoscience 2, 434 - 438.
1017 Kolla, V., Eittreim, S., Sullivan, L., Kostecki, J.A., Burckle, L.H., 1980a. Current-controlled,
1018 abyssal microtopography and sedimentation in Mozambique Basin, Southwest Indian
1019 Ocean. Marine Geology 34, 171-206.
1020 Kolla, V., Kostecki, J.A., Henderson, L., Hess, L., 1980b. Morphology and Quaternary
1021 sedimentation of the Mozambique Fan and environs, southwestern Indian Ocean.
1022 Sedimentology 27, 357 - 378.

1023 Kolla, V., Sullivan, L., Streeter, S.S., Lanhset, M.G., 1976. Spreading of Antarctic Bottom
1024 Water and its effects on the sea floor of the Indian Ocean inferred from bottom-water
1025 potential temperature, turbidity, and sea-floor topography. Marine Geology 21, 171 - 189.
1026 König, M., Jokat, W., 2010. Advanced insights into magmatism and volcanism of the
1027 Mozambique Ridge in the view of new potential field data. Geophysical Journal
1028 International 180, 158-180.
1029 Kuijpers, A., Hansen, B., Hühnerbach, V., Larsen, B., Nielsen, T., Werner, F., 2002.
1030 Norwegian Sea overflow through the Faroe-Shetland gateway as documented by its
1031 bedforms. Marine Geology 188, 147 - 164.
1032 Long, D., Bulat, J., Stoker, M.S., 2004. Sea bed morphology of the Faroe-Shetland Chaannel
1033 derived from 3D seismic datasets, in: Davies, R.J., Cartwright, J.A., Stewart, S.A., Lappin,
1034 M., Underhill, J.R. (Eds.), 3D Seismic Technology: Application to the Exploration of
1035 Sedimentary Basins. Geological Society, London, Memoirs, pp. 53 - 61.
1036 Lutjeharms, J.R.E., 2006. The Agulhas Current. Springer, Berlin Heidelberg New York.
1037 MacLachlan, S.E., Elliot, G.M., Parson, L.M., 2008. Investigations of the bottom current
1038 sculpted margin of Hatton Bank, NE Atlantic. Marine Geology 253, 170 - 184.
1039 Masson, D.G., Howe, J.A., Stoker, M.S., 2002. Bottom-current sediment waves, sediment
1040 drifts and contourites in the northern Rockall Trough. Marine Geology 192, 215 - 237.
1041 Masson, D.G., Wynn, R.B., Bett, B.J., 2004. Sedimentary environment of the Faroe-Shetland
1042 and Faroe Bank Channels, northeast Atlantic, and the use of bedforms as indicators of
1043 bottom-current velocity in the deep ocean. Sedimentology 51, 1207 - 1241.
1044 Nauw, J.J., van Aken, H.M., Webb, A., Lutjeharms, J.R.E., de Ruijter, W.P.M., 2008.
1045 Observations of the southern East Madagascar Current and undercurrent and
1046 countercurrent system. Journal of Geophysical Research 113, 1-15.

1047 Niemi, T.M., Ben-Avraham, Z., Hartnady, C.J.H., Reznikov, M., 2000. Post-Eocene seismic
1048 stratigraphy of the deep ocean basin adjacent to the southeast African continental margin: a
1049 record of geostrophic bottom current systems. Marine Geology 162, 237 - 258.
1050 Preu, B., Spieß, V., Schwenk, T., Schneider, R., 2011. Evidence for current controlled
1051 sedimentation along the southern Mozambique continental margin since Early Miocene
1052 times. Geo-Marine Letters in press.
1053 Quartly, G.D., Buck, J.J.H., Srokosz, M.A., Coward, A.C., 2006. Eddies around Madagascar -
1054 The retroflection re-considered. Journal of Marine Systems 63, 115-129.
1055 Quartly, G.D., Srokosz, M.A., 2004. Eddies in the Southern Mozambique Channel. Deep-Sea
1056 Research II 51, 69-83.
1057 Rabinowitz, P.D., Coffin, M.F., Falvey, D., 1983. The separation of Madagascar and Africa.
1058 Science 220, 67-69.
1059 Read, J.F., Pollard, R.T., 1999. Deep inflow into the Mozambique Basin. Journal of
1060 Geophysical Research 104, 3075-3090.
1061 Ridderinkhof, H., 2000. RV Pelagia cruise report, Cruise 64PE156, Project ACSEX-I,
1062 Mozambique Channel, 20 March - 13 April 2000. Royal Netherlands Institute for Sea
1063 Research, Texel, Netherlands., p. 13 pp.
1064 Ridderinkhof, H., de Ruijter, W.P.M., 2003. Moored current observations in the Mozambique
1065 Channel. Deep Sea Research II 50, 1933-1955.
1066 Ridderinkhof, H., van der Werf, P.M., Ullgren, J.E., van Aken, H.M., van Leeuwen, P.J., de
1067 Ruijter, W.P.M., 2010. Seasonal and interannual variability in the Mozambique Channel
1068 from moored current observations. Journal of Geophysical Research 115, 1-18.
1069 Sætre, R., 1985. Surface currents in the Mozambique Channel. Deep Sea Research 32, 1457-
1070 1467.

1071 Sætre, R., Jorge da Silva, A., 1984. The circulation of the Mozambique Channel. Deep Sea
1072 Research 31, 485-508.
1073 Schlitzer, R., 2011. Ocean Data View, http://odv.awi.de.
1074 Schlüter, P., Uenzelmann-Neben, G., 2007. Seismostratigraphic analysis of the Transkei
1075 Basin: A history of deep sea current controlled sedimentation. Marine Geology 240, 99 -
1076 111.
1077 Schlüter, P., Uenzelmann-Neben, G., 2008. Indications for bottom current activity since
1078 Eocene times: The climate and ocean gateway archive of the Transkei Basin, South Africa.
1079 Global and Planetary Change 60, 416 - 428.
1080 Schott, F.A., Xie, S.-P., McCreary Jr., J.P., 2009. Indian Ocean Circulation and climate
1081 variability. Reviews of Geophysics 47.
1082 Schouten, M.W., de Ruijter, W.P.M., Van Leeuwen, P.J., Ridderinkhof, H., 2003. Eddies and
1083 variability in the Mozambique Channel. Deep Sea Research II 50, 1987-2003.
1084 Scrutton, R.A., Heptonstall, W.B., Peacock, J.H., 1981. Constraints on the motion of
1085 Madagascar with respect to Africa. Marine Geology 43, 1-20.
1086 Stoker, M.S., Akhurst, M.C., Howe, J.A., Stow, D.A.V., 1998. Sediment drifts and
1087 contourites on the continental margin off northwest Britain. Sedimentary Geology 115, 33
1088 - 51.
1089 Stoker, M.S., Long, D., Bulat, J., 2003. A record of mid-cenozoic strong deep-water erosion
1090 in the Faroe-Shetland Channel, in: Mienert, J., Weaver, P. (Eds.), European Margin
1091 Sediment Dynamics. Springer, Berlin, pp. 145 - 148.
1092 Stow, D.A.V., Hernández-Molina, F.J., Llave, E., Sayago-Gil, M., Díaz-del-Río, V., Branson,
1093 A., 2009. Bedform-velocity matrix: The estimation of bottom current velocity from
1094 bedform observations. Geology 37, 327 - 330.

1095 Stow, D.A.V., Hunter, S., Wilkinson, D., Hernández-Molina, F.J., 2008. The nature of
1096 contourite deposition, in: Rebesco, M., Camerlenghi, A. (Eds.), Contourites. Elsevier,
1097 Amsterdam, pp. 143 - 156.
1098 Sultan, N., Cochonat, P., Canals, M., Cattaneo, A., Dennielou, B., Haflidason, H., Laberg,
1099 J.S., Long, D., Mienert, J., Trincardi, F., Urgeles, R., Vorren, T.O., Wilson, C., 2004.
1100 Triggering mechanisms of slope instability processes ad sediment failures on continental
1101 margins: a geotechnical approach. Marine Geology 213, 291 - 321.
1102 Swart, N.C., Lutjeharms, J.R.E., Ridderinkhof, H., de Ruijter, W.P.M., 2010. Observed
1103 characteristics of Mozambique Channel eddies. Journal of Geophysical Research 115, 1-
1104 14.
1105 Tucker, M.E., 2004. Sedimentary Petrology. Blackwell Publishing, Oxford.
1106 van Aken, H.M., Ridderinkhof, H., de Ruijter, W.P.M., 2004. North Atlantic deep water in
1107 the south-western Indian Ocean. Deep Sea Research I 51, 755 - 776.
1108 van Weering, T.C.E., Nielsen, T., Kenyon, N.H., Akentieva, K., Kuijpers, A.H., 1998.
1109 Sediments and sedimentation at the NE Faeroe continental margin; contourites and large-
1110 scale sliding. Marine Geology 152, 159-176.
1111 Walford, H.L., White, N.J., Sydow, J.C., 2005. Solid sediment load history of the Zambezi
1112 Delta. Earth and Planetary Science Letters 238, 49-63.
1113 Wessel, P., Smith, W.H.F., 1991. Free software helps map and display data. EOS
1114 Transactions American Geophysical Union 72, 441 and 445-446.
1115 Wynn, R.B., Stow, D.A.V., 2002. Classification and characterisation of deep-water sediment
1116 waves. Marine Geology 192, 7 - 22.
1117
1118

Figure Captions

Figure 1. Map of the western Indian Ocean showing the study area (white box), the surface (yellow) and the bottom/deep water current flow (red) around Madagascar and off SE-Africa, and the positions of LADCP based current velocity sections measured during the WOCE program (dashed purple line) (Donohue and Toole, 2003) and the ACSEX-1 cruise (solid purple lines) (Ridderinkhof, 2000). The bathymetry is based on the ETOPO1 grid (Amante and Eakins, 2009). SEC, South Equatorial Currrent; NEMC, Northeast Madagascar Current; SEMC, Southeast Madagascar Current; SICC, South Indian Ocean Counter Current; EACC, East African Coastal Current; MC, Mozambique Current; MCE, Mozambique Channel eddy; AC, Agulhas Current; AABW, Antarctic Bottom Water; NADW, North Atlantic Deep Water.

Figure 2. Detailed map of the study area including the survey lines. Bathymetry based on ETOPO1 (Amante and Eakins, 2009).

Figure 3. Salinity fields (colour-coded grid) and potential temperatures (white contour lines) (a) across the Mozambique Channel at 24°40'S and (b) along 40°E. The data are extracted from the high-resolution CTD (W-E section at 24°40'S) and from the low-resolution OSD data set (N-S section at 40°E) of the World Ocean Database (Boyer et al., 2009) and are compiled with Ocean Data View (Schlitzer, 2011). AABW, Antarctic Bottom Water; NADW, North Atlantic Deep Water; AAIW, Antarctic Intermediate Water; RSW, Red Sea Water; TSW, Tropical Surface Water.

Figure 4. LADCP based meridional velocities (a) across the Mozambique Channel at 24°40'S (redrawn after Donohue and Toole (2003)) and (b) - (d) across 3 Mozambique Channel eddies at 24°S, 20°S, 17°S (redrawn after Ridderinkhof (2000) and de Ruijter et al. (2002)). Red colours indicate northward, blue colours southward flow directions. WOCE section I4 was collected betwen 14 - 18 June 1995, the ACSEX-1 sections between 26 March - 08 April 2000. For the location of the sections refer to Figure 1.

Figure 5. Hill-shaded coloured map of the acquired bathymetric data. The sections and PARASOUND profiles displayed in Figures 7 - 21 are marked and labeled with their figure numbers.

Figure 6. Microtopographic classification of the study area. Overlain are (i) line drawings of the seafloor morphology along the acquired bathymetric stripes, (ii) smoothed bathymetric contour lines (every 500 m) based on the ETOPO1 grid (cf. Figures 1, 2) and (iii) the boundaries of microtopographic zones II (smooth, flat seafloor), III (sediment waves) and IV (hyperbolic echoes) defined by Kolla et al. (1980a) (dashed yellow lines).

Figure 7. (a) Hill-shaded bathymetry section typical for microtopographic zone BS1. (b) PARASOUND section and (c) depth profile along the central line of the bathymetric stripe shown in (a). The white lines indicate the positions of the PARASOUND blow-ups marked by red boxes and illustrating the sedimentary infill of the scour hollows. VE, vertical exaggeration.

Figure 8. (a) Hill-shaded bathymetry section typical for microtopographic zone BS2. (b) PARASOUND section (parts 1, 2) and (c) depth profile along the central line of the bathymetric stripe shown in (a).

Figure 9. Hill-shaded bathymetry sections typical for microtopographic zones (a) BS3 and (b) BS4, and PARASOUND sections and depth profiles along the central lines of the bathymetric stripes. The PARASOUND sections display the reflection pattern along those parts marked by red boxed in the depth profiles and by white lines in the bathymetric stripes.

Figure 10. (a) Hill-shaded bathymetry section typical for microtopographic zone BS7. (b) PARASOUND section along the black line in bathymetric stripe C. To illustrate the reflection pattern of the terrace north of the channel the section marked by the red box is blown-up in the inset. (c) Depth profiles along the central lines of the bathymetric stripes A - E shown in (a). The dashed black and red arrows indicate the AABW flow path in the bathymetry section

and along the depth profiles.

Figure 11. Hill-shaded bathymetry sections typical for microtopographic zones (a) BC1 and (b) BC4, and PARASOUND sections and depth profiles along the central lines of the bathymetric stripes. The PARASOUND sections display the reflection pattern along those parts marked by red boxes in the depth profiles and by black lines in the bathymetric stripes.

Figure 12. (a) Hill-shaded bathymetry section typical for microtopographic zone BC8. (b) PARASOUND section along the black line in bathymetric stripe C. (b) Depth profiles along the central lines of the bathymetric stripes A - C shown in (a).

Figure 13. (a) Hill-shaded bathymetry section of a moat surrounding an unnamed seamount north of microtopographic zone BC8. (b) PARASOUND sections recorded north and south of the seamount along the black lines in the eastern bathymetric stripe. (c) Depth profile along the central line of the eastern bathymetric stripe shown in (a).

Figure 14. (a) Hill-shaded bathymetry section typical for the adjacent microtopographic zones BN1 and BN2. (b) PARASOUND sections along the black lines in the bathymetric stripes A and B.

Figure 15. (a) Hill-shaded bathymetry section typical for microtopographic zone BE1. (b) PARASOUND section and (c) depth profile along the central line of the bathymetric stripe shown in (a). The PARASOUND section confines to the black line shown in the bathymetric stripe and the red box marked in the depth profile.

Figure 16. PARASOUND sections recorded along the (a) northwestern and (b) southeastern part of microtopographic zone S1 on the Mozambican continental slope.

Figure 17. (a) Hill-shaded bathymetry section of a slide in the northwestern part of microtopographic zone S1 and (b) PARASOUND section along the central black (left) or white (right) line of the bathymetric stripes. The left and right stripes display the seafloor morphology of the slide area with different colour scales, the middle stripe the same data with

1194 an interpretation of four potential failure events (dashed lines). The colour scale used for the
1195 display of the left and middle stripes is the same as for the whole map (Figure 5) and as used
1196 for Figures 7 - 21. For the display of the right bathymetric stripe the water depth range of the
1197 slide area is spread over the full colour scale to further enhance small-scale depth variations.
1198 **Figure 18.** PARASOUND sections recorded (a) north and (b) south of the Bassas da India
1199 complex in microtopographic zones S2 and S3.
1200 **Figure 19.** PARASOUND section recorded on the eastern levee of the Zambezi Channel in
1201 microtopographic zone S4.
1202 **Figure 20.** PARASOUND sections recorded in the Zambezi cone in microtopographic zone
1203 S5. The three lines run parallel to each other from 26°20'S to 26°50'S and show the changing
1204 sedimentation pattern from East to West, i.e. from a position southeast of the Zambezi
1205 Channel mouth to a position ~150 km farther westward.
1206 **Figure 21.** (a) Hill-shaded bathymetry and (b) PARASOUND sections typical for
1207 microtopographic zone R2. The left bathymetry section in (a) displays the seafloor
1208 morphology and the positions of the PARASOUND sections (black lines), the right
1209 bathymetry section the interpretation of the elongate depression (dashed line). The red dashed
1210 lines in (b) mark the elongate depression and the transition from the turbidite-filled bowl-
1211 shaped basin to a bathymetric high.
1212 **Figure 22.** Interpretative map displaying the flow directions of the currents that shaped the
1213 seafloor, as derived from the bedforms. The black and red columns at the left-hand side
1214 approximately indicate the latitudinal spread of the AABW and NADW. Black solid arrows
1215 indicate the floww directions of the AABW, red solid arrows the flow directions of an MCE,
1216 red open arrows the potential flow directions of an EMC eddy and the blue open arrows the
1217 flow directions of overspill sediments from the Zmabezi and Tsiribihina Channels. Underlain
1218 is the microtopographic classification as defined in Figure 6.
1219

Appendix

Table A1 provides an overview on the morphological characteristics, the bedform scales, the PARASOUND signal penetration depth and the location of the microtopographic zones identified in the study area (Figure 6).

Figure 1

Click here to download high resolution image

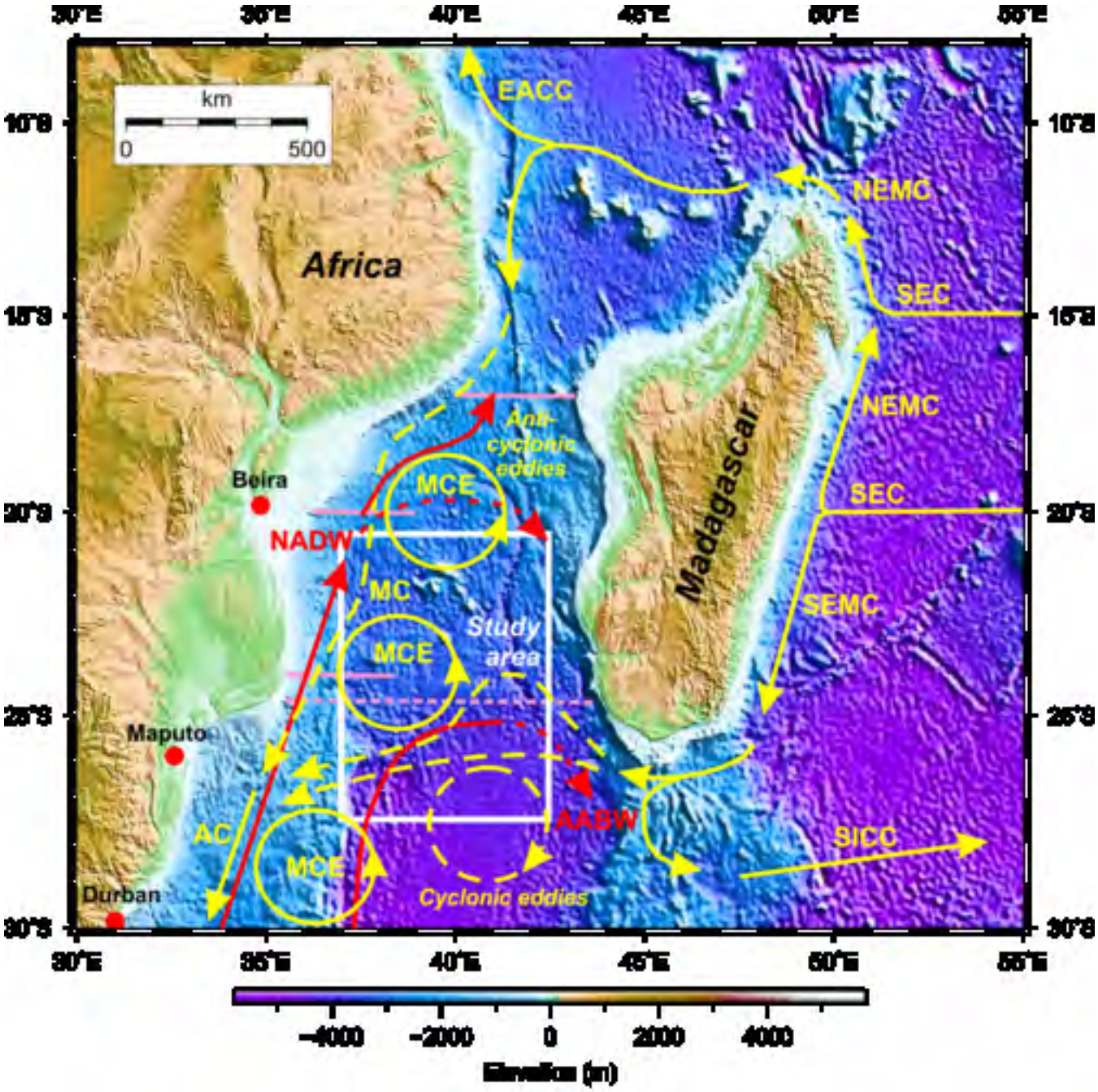

Brelizke et al.,
Fig. 1

Figure 2

Click here to download high resolution image

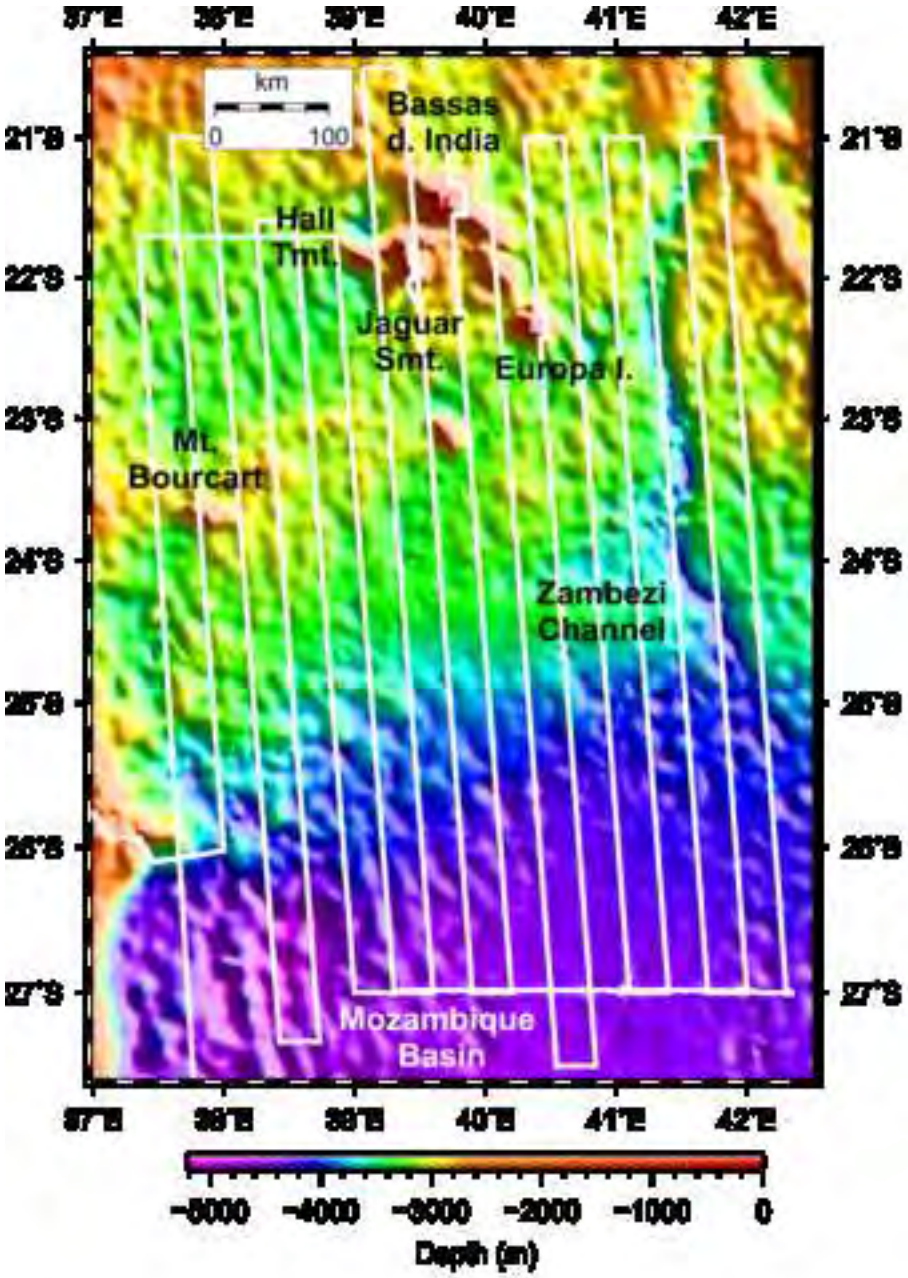

Brelizko et al., Fig.2

Figure 3

Click here to download high resolution image

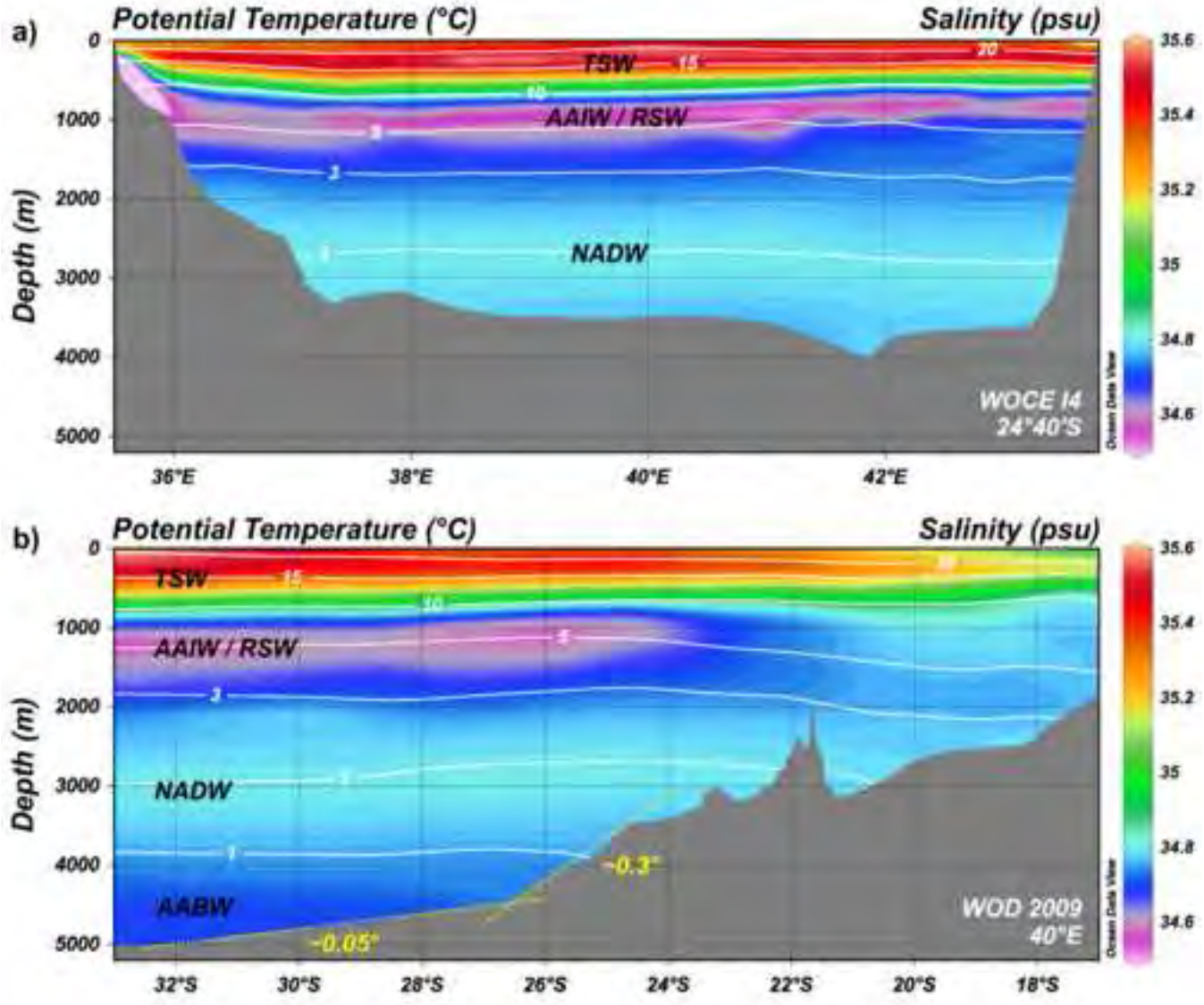

Breitzke et al., Fig. 3

Figure 4

Click here to download high resolution image

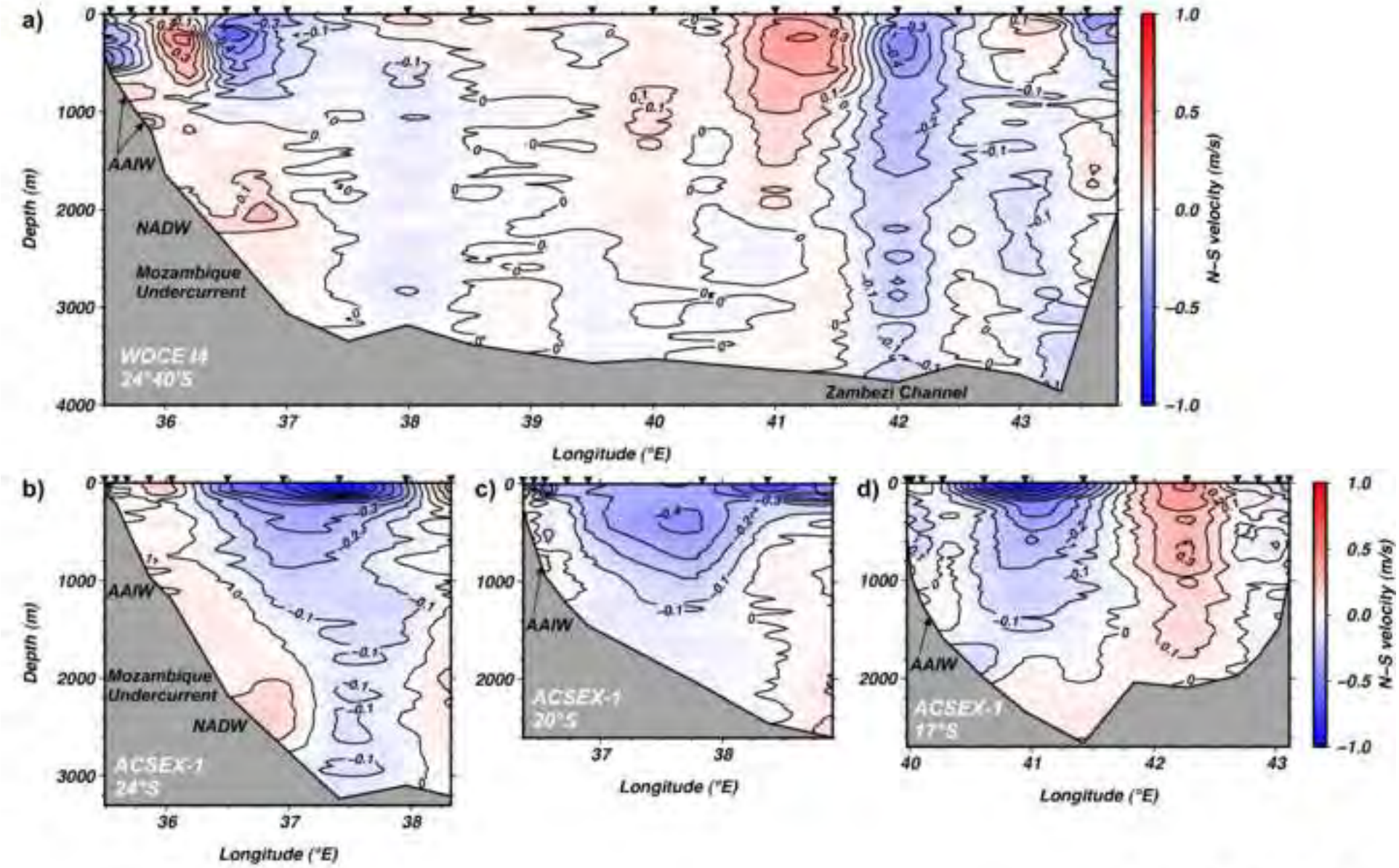

Breitzke et al., Fig. 4

Figure 5

Click here to download high resolution image

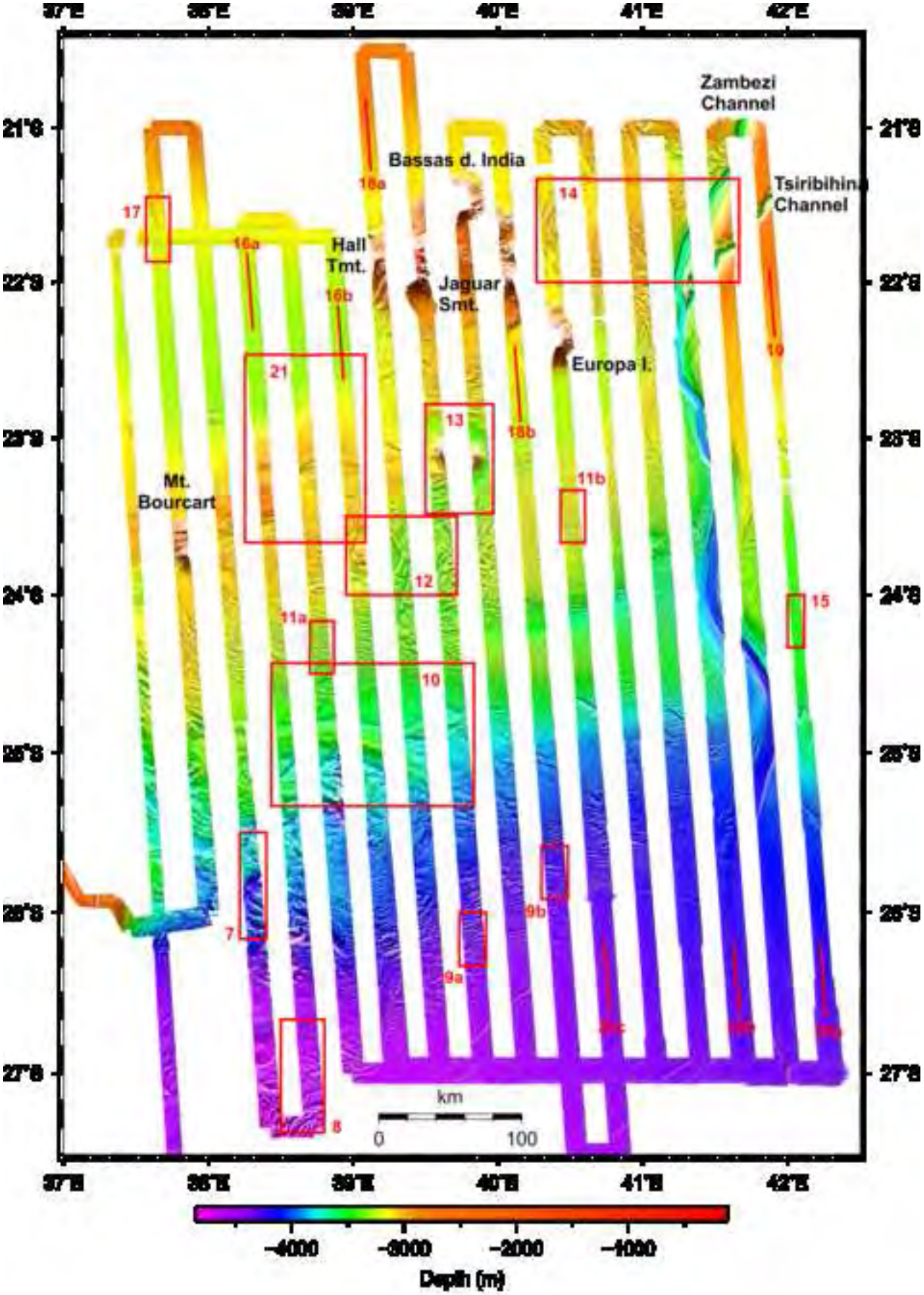

Brolizio et al., Fig. 5

Figure 6

Click here to download high resolution image

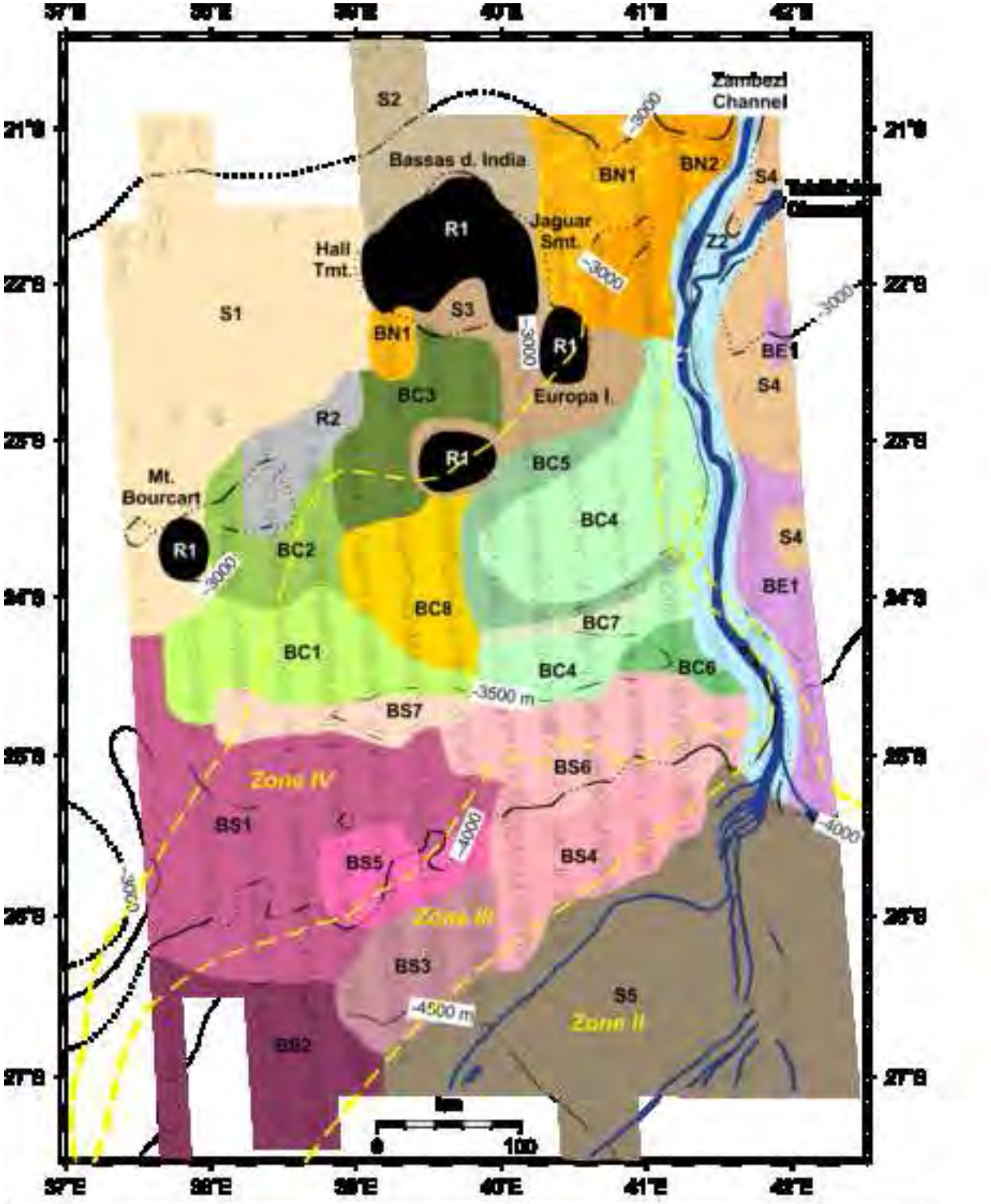

Droxler et al., Fig. 6

Figure 7

Click here to download high resolution image

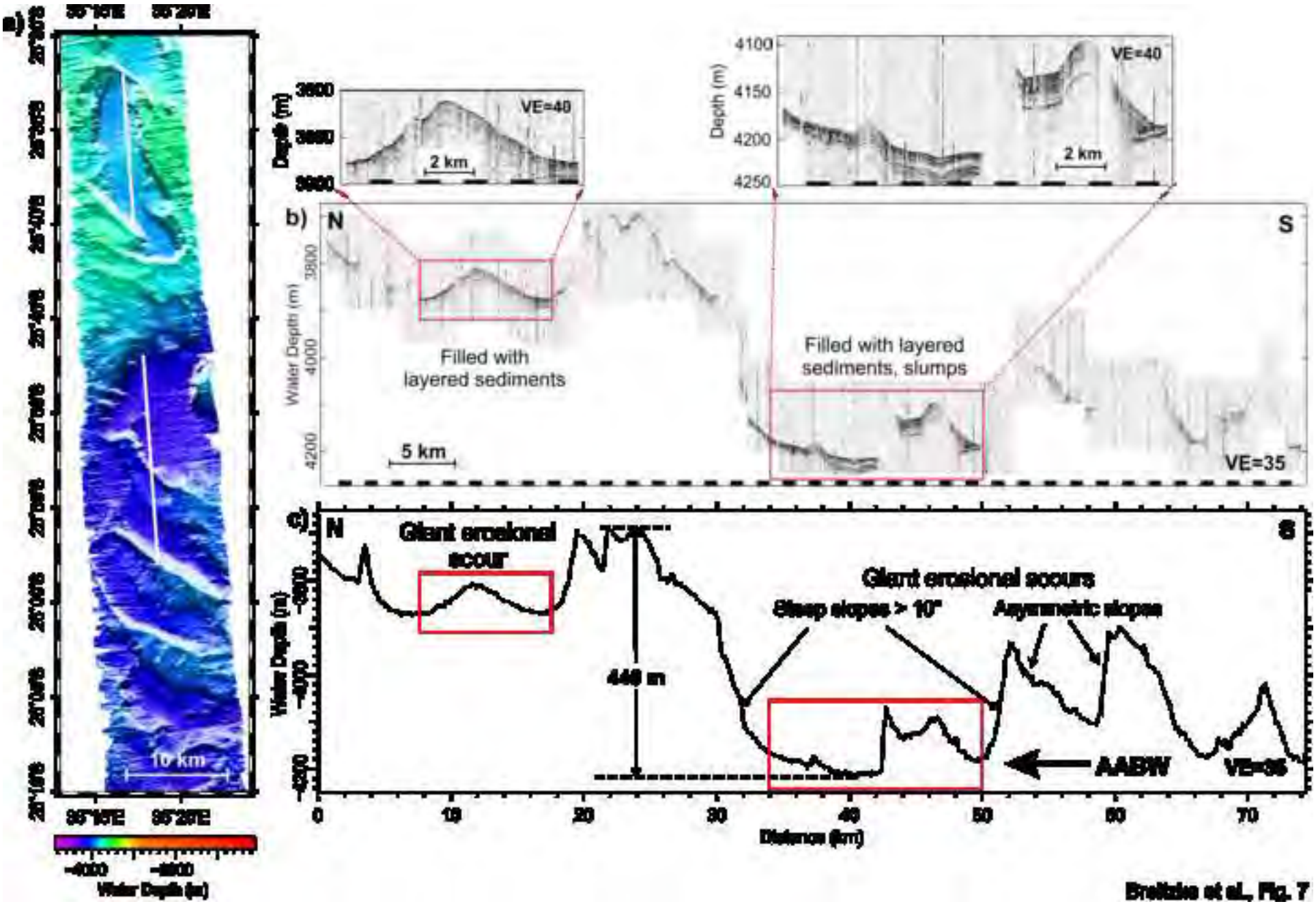

Figure 8

Click here to download high resolution image

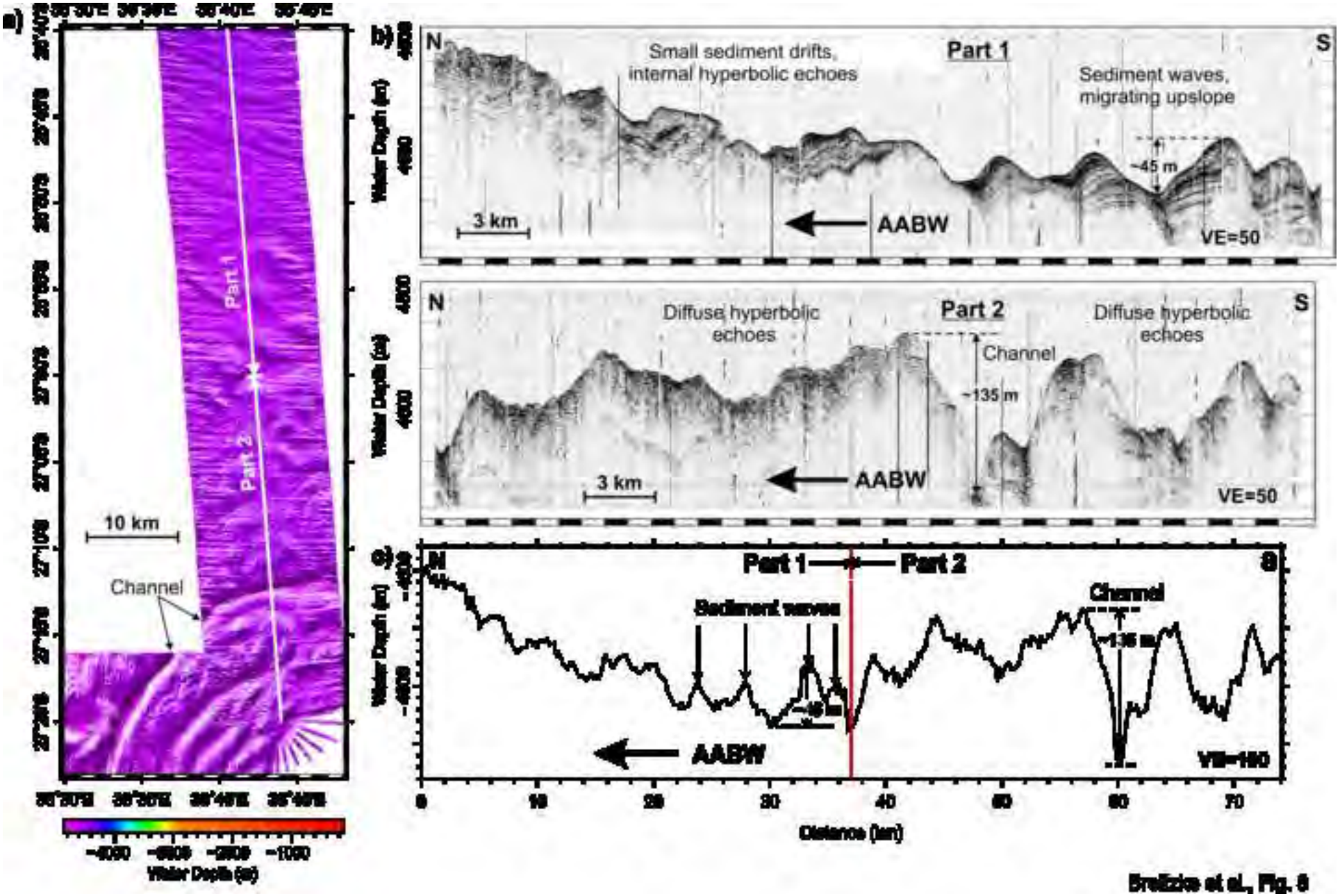

Breilzie et al., Fig. 8

Figure 9

Click here to download high resolution image

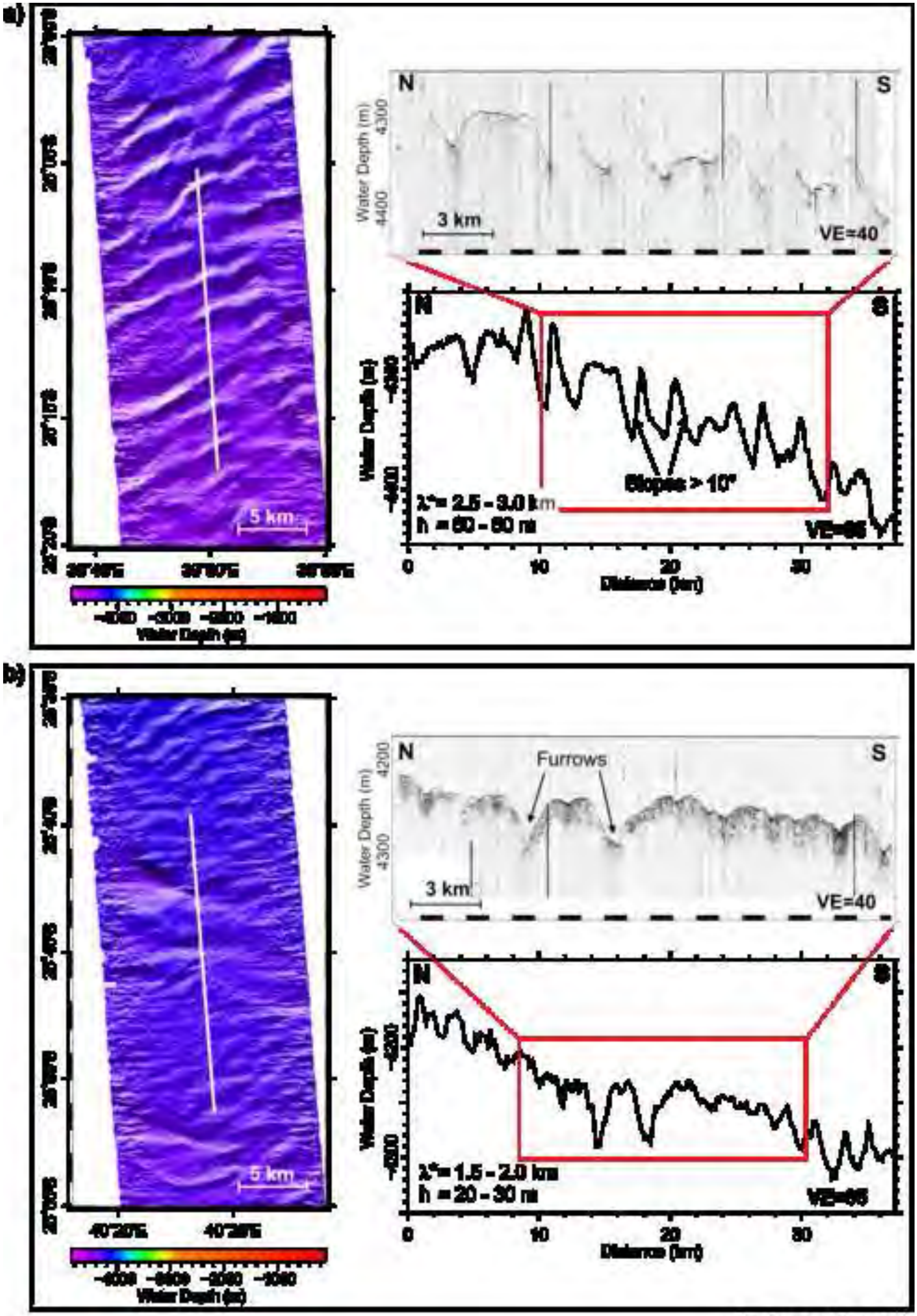

Breitzke et al., Fig. 9

Figure 10

Click here to download high resolution image

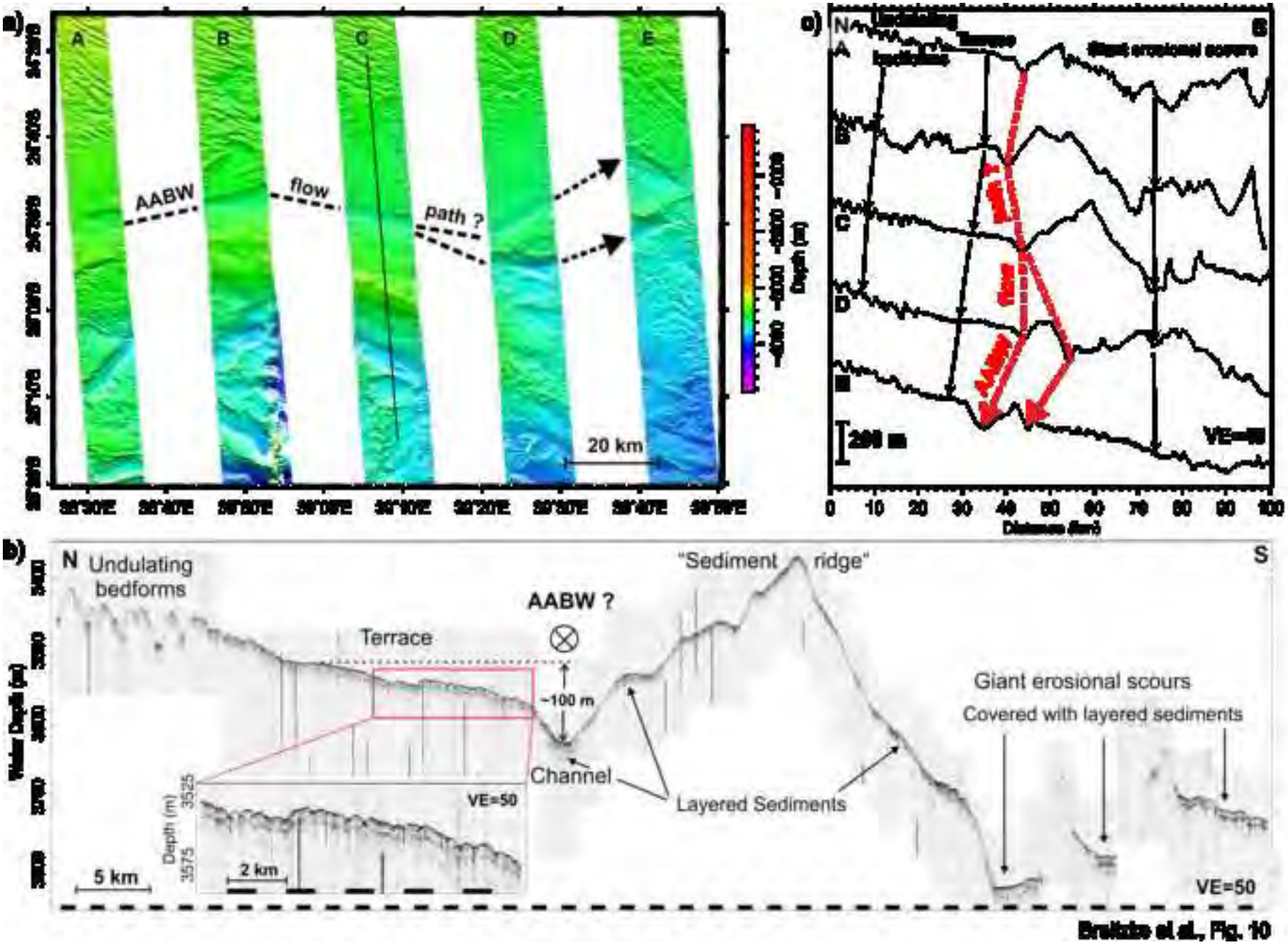

Bruketa et al., Fig. 10

Figure 11
Click here to download high resolution image

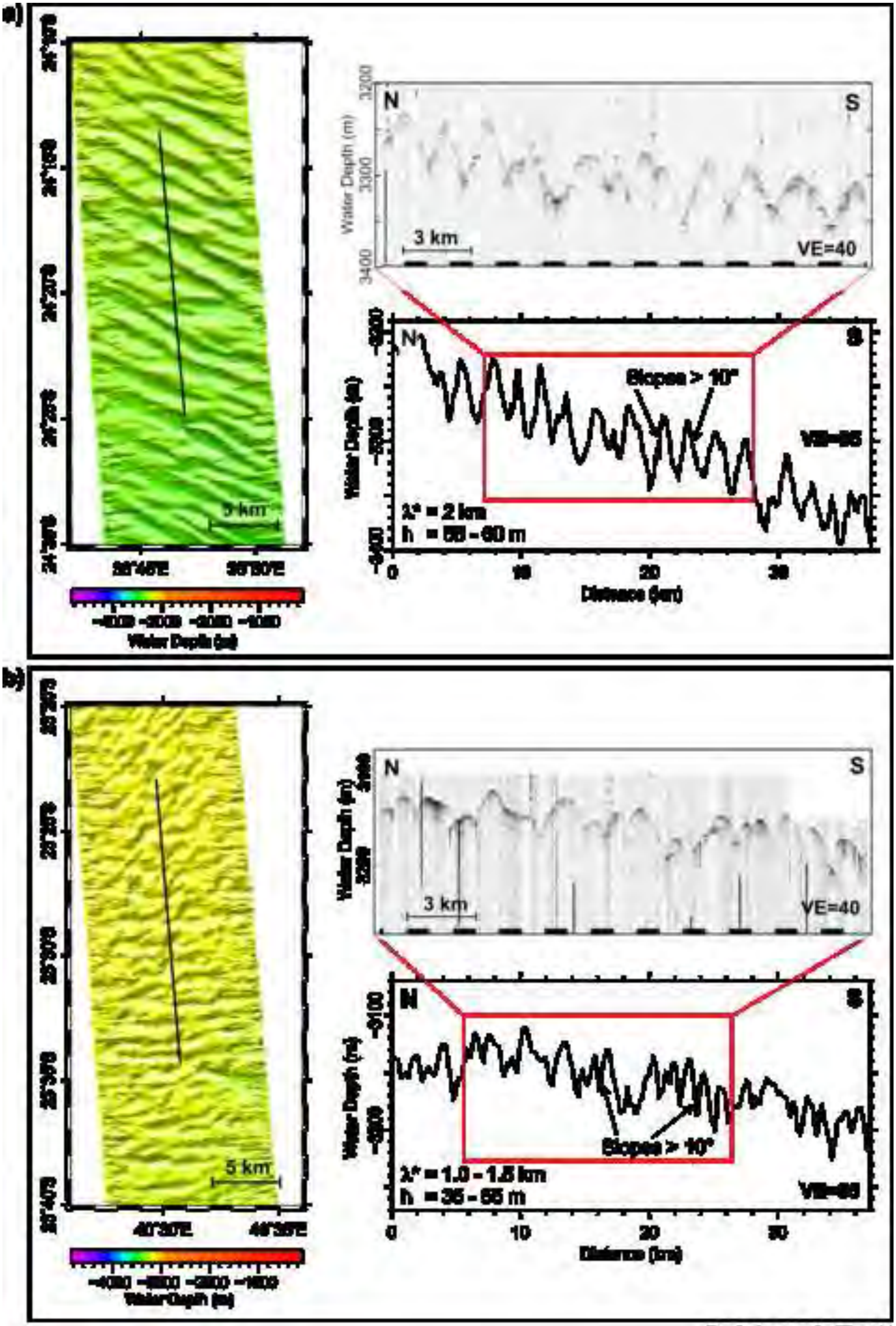

Bouziane et al., Fig. 11

Figure 12

Click here to download high resolution image

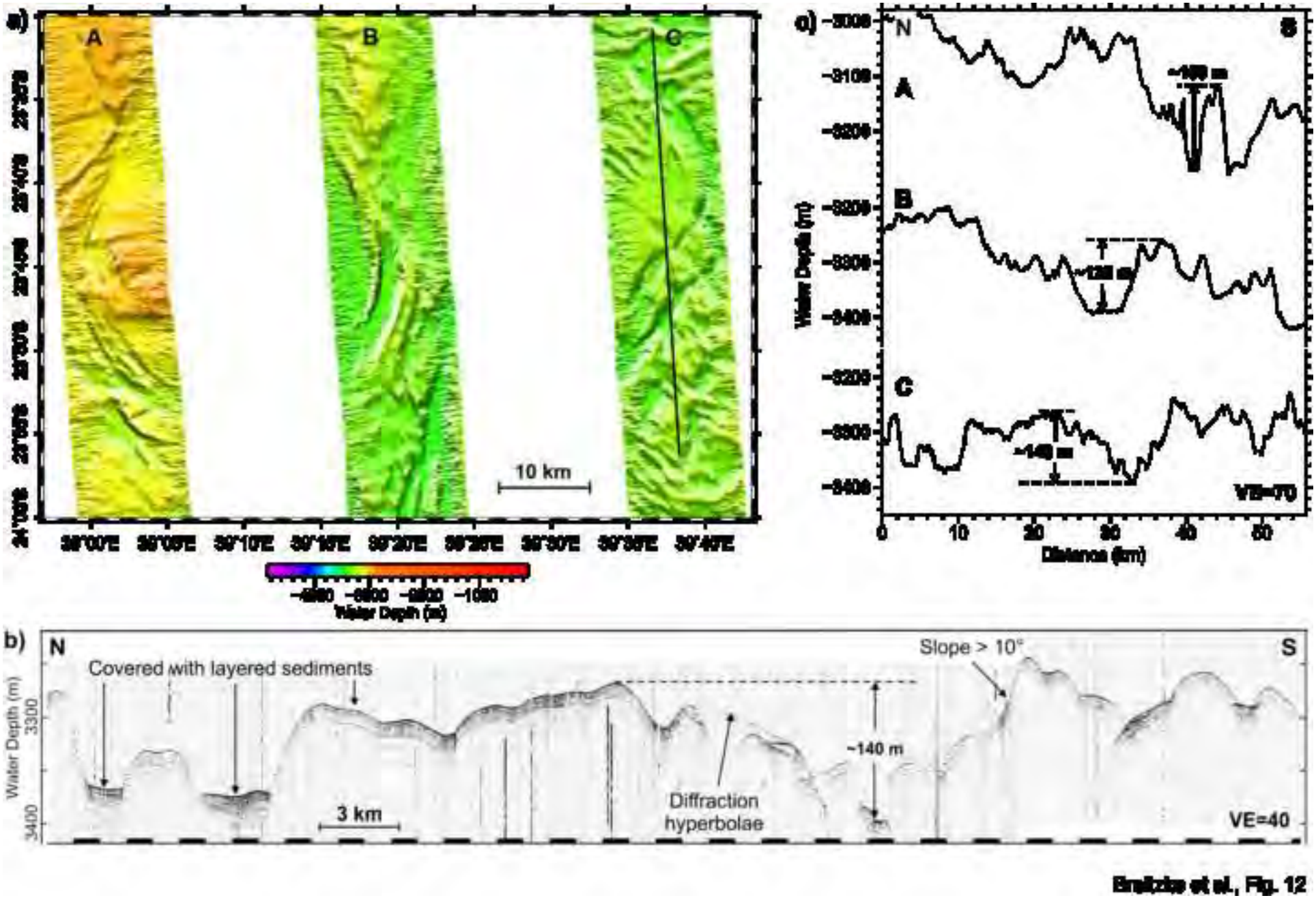

Bralower et al., Fig. 12

Figure 13

Click here to download high resolution image

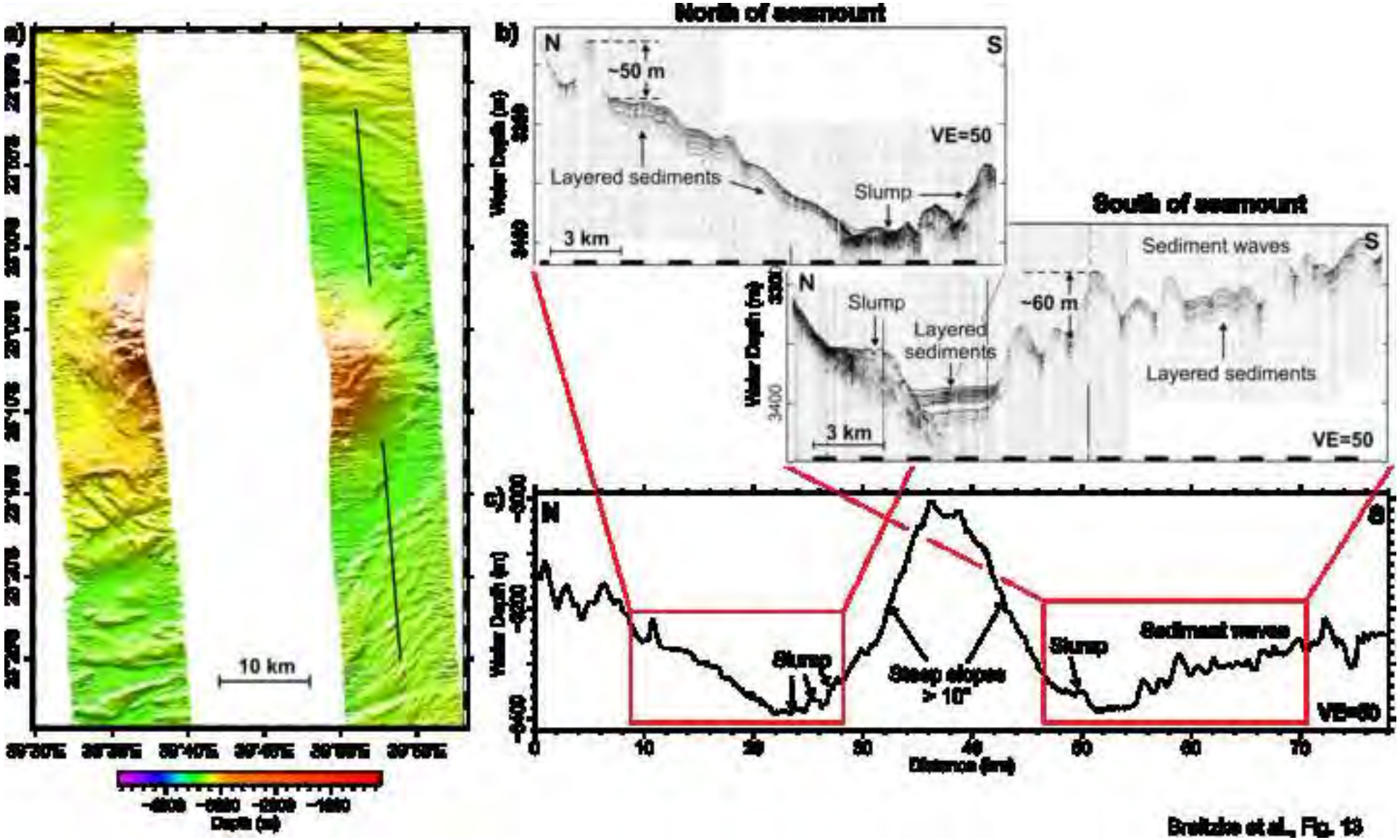

Bruhzke et al., Fig. 13

Figure 14

Click here to download high resolution image

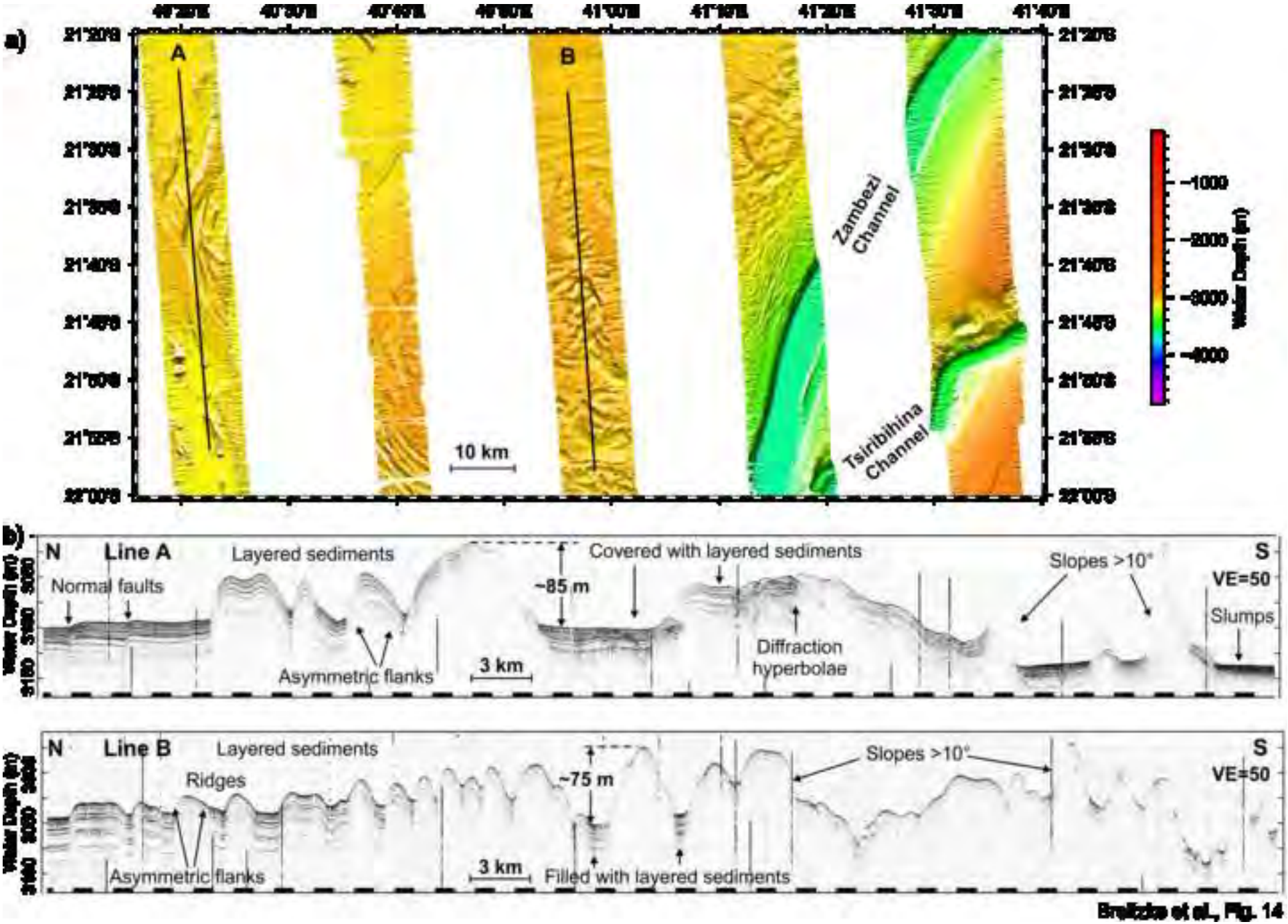

Brailsford et al., Fig. 14

Figure 15

Click here to download high resolution image

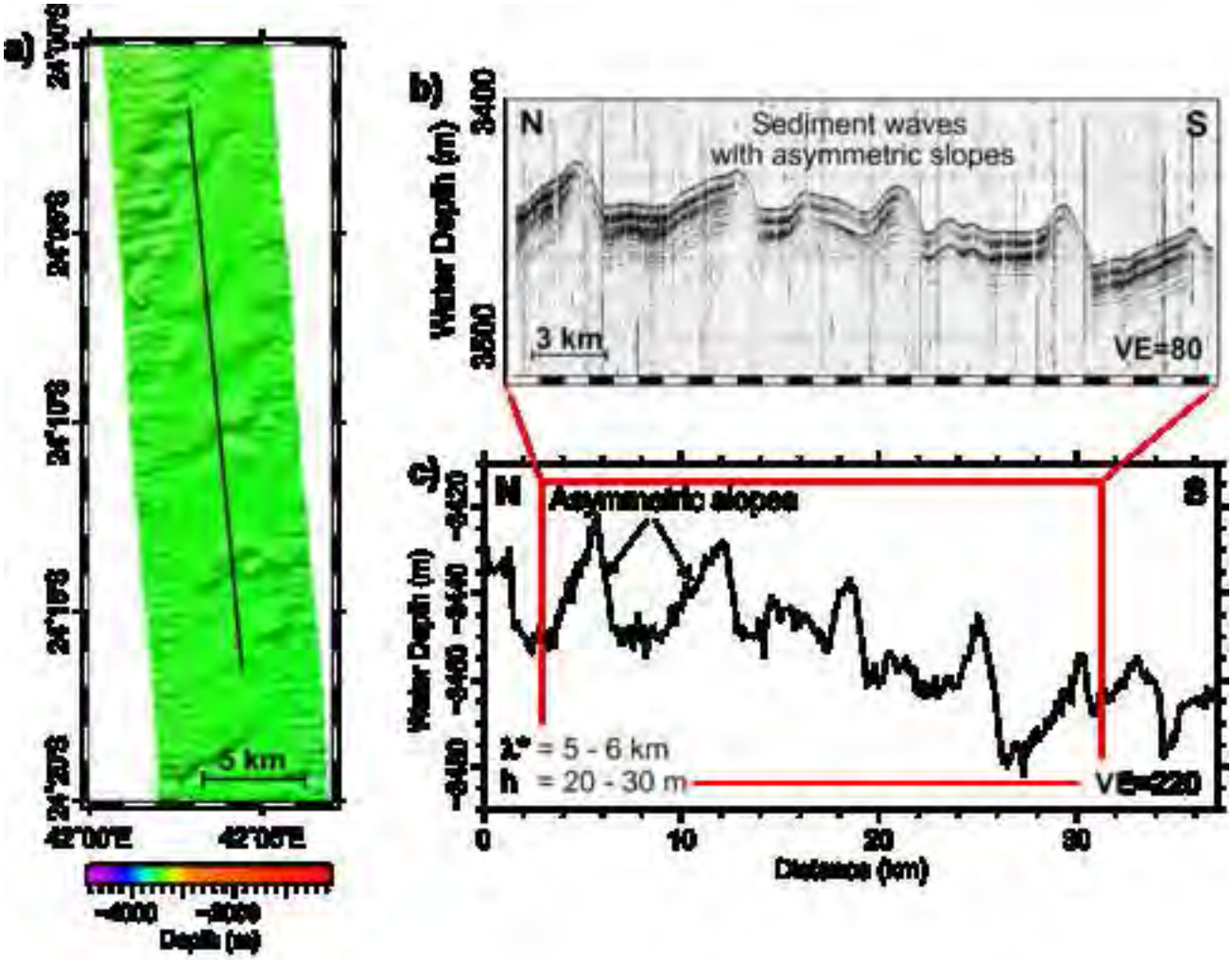

Brenicke et al.,
Fig. 15

Figure 16

Click here to download high resolution image

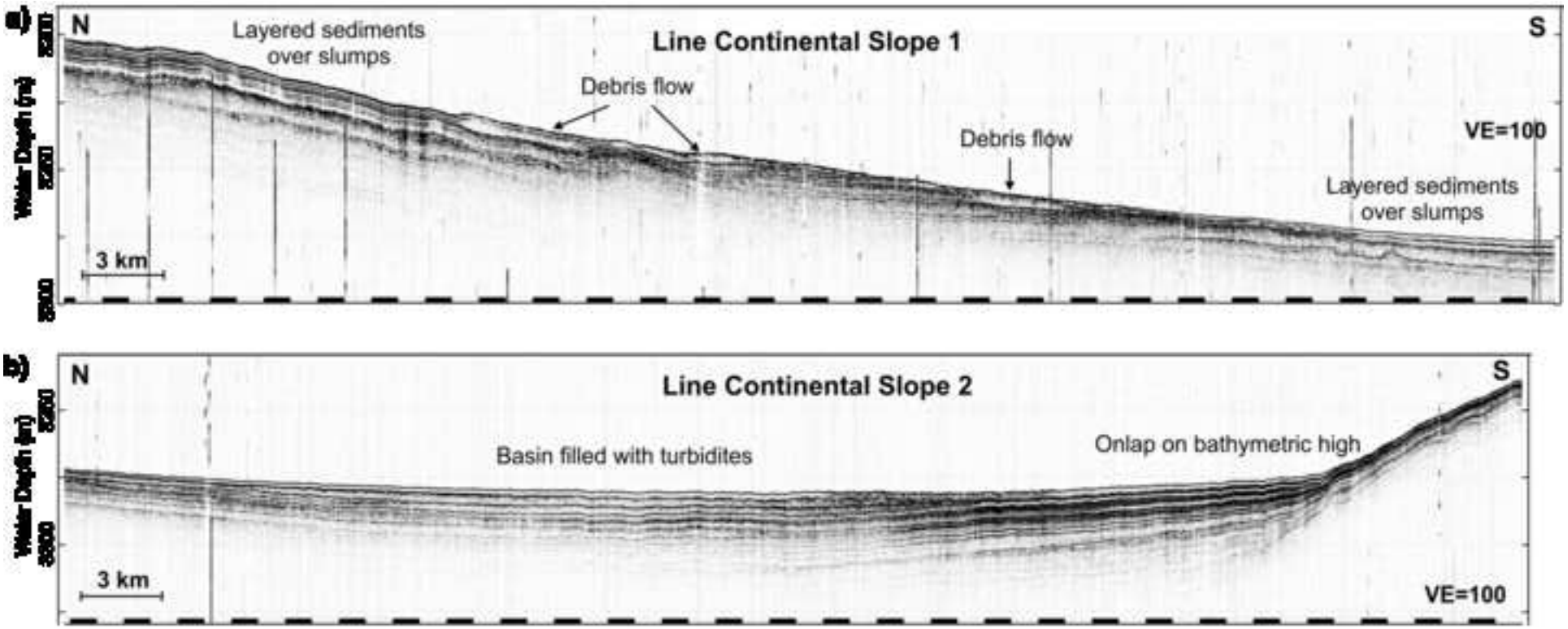

Brekke et al., Fig. 16

Figure 17

Click here to download high resolution image

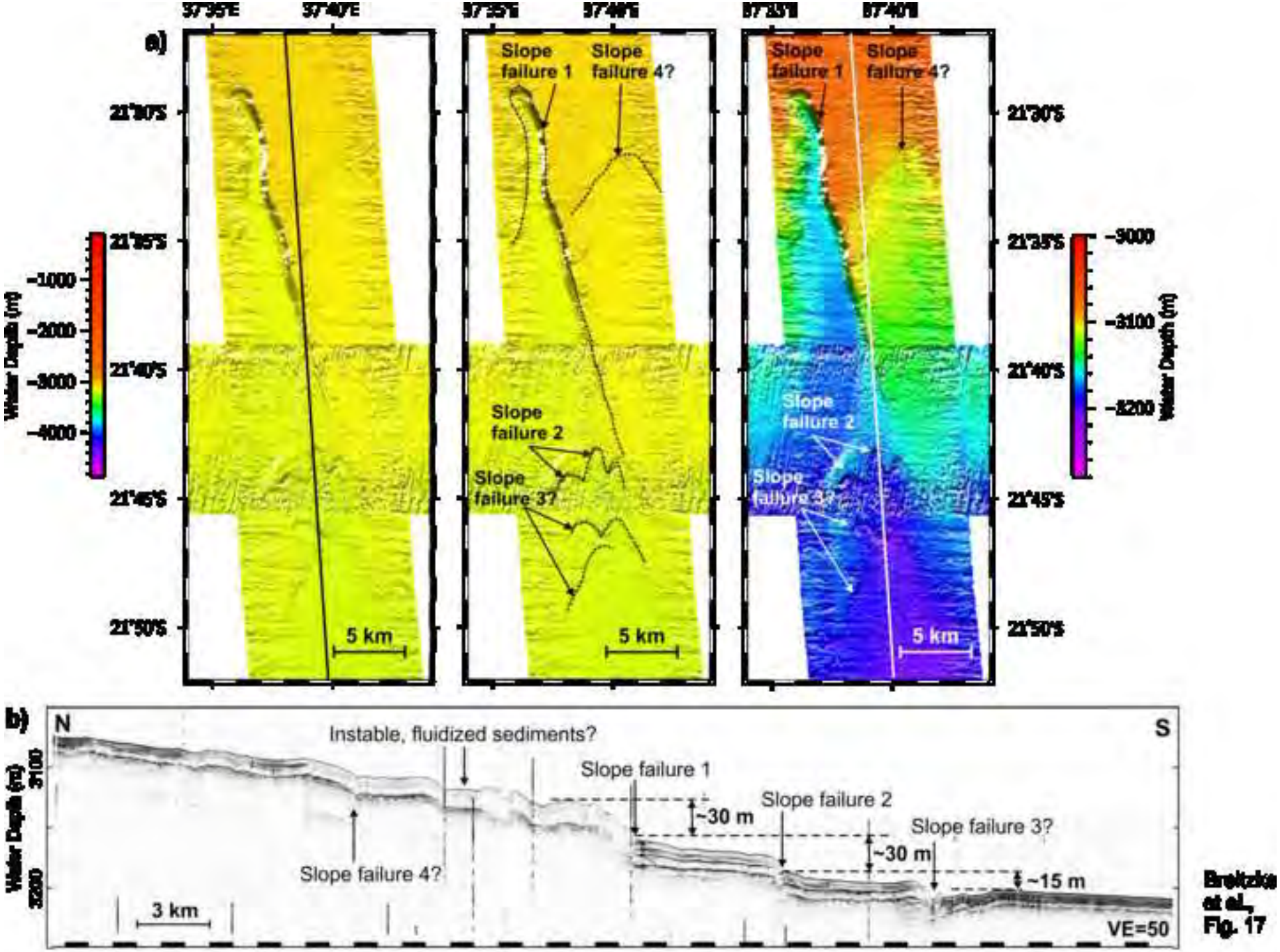

Breitzke et al., Fig. 17

Figure 18

Click here to download high resolution image

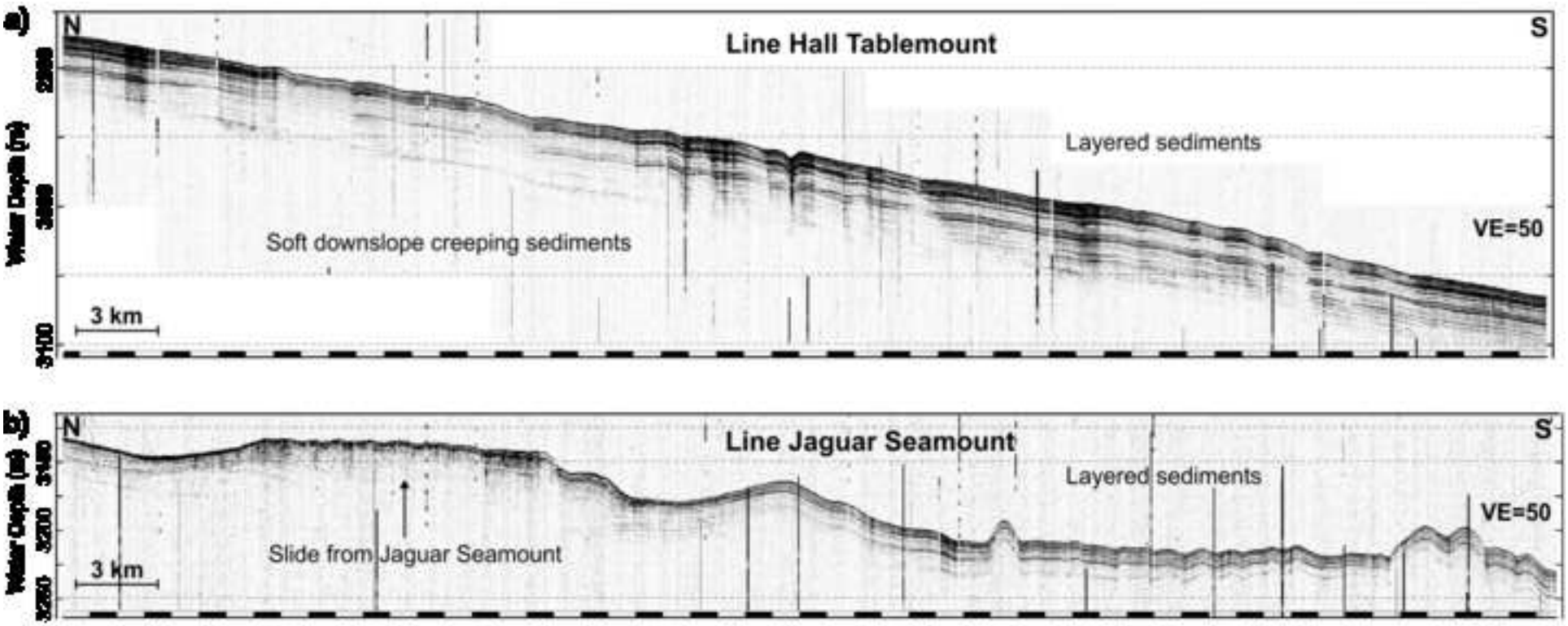

Brückmann et al., Fig. 18

Figure 19

Click here to download high resolution image

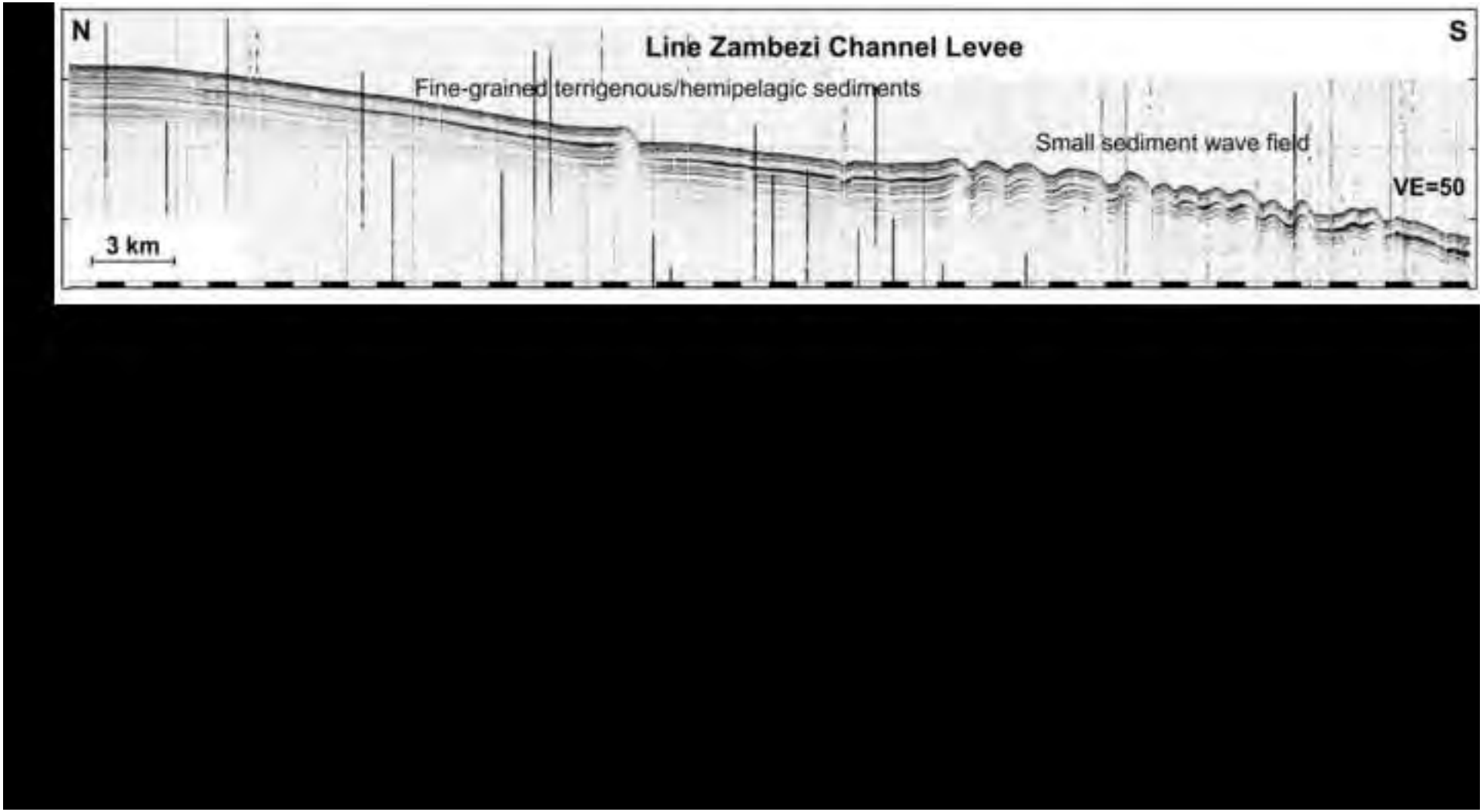

Figure 20

Click here to download high resolution image

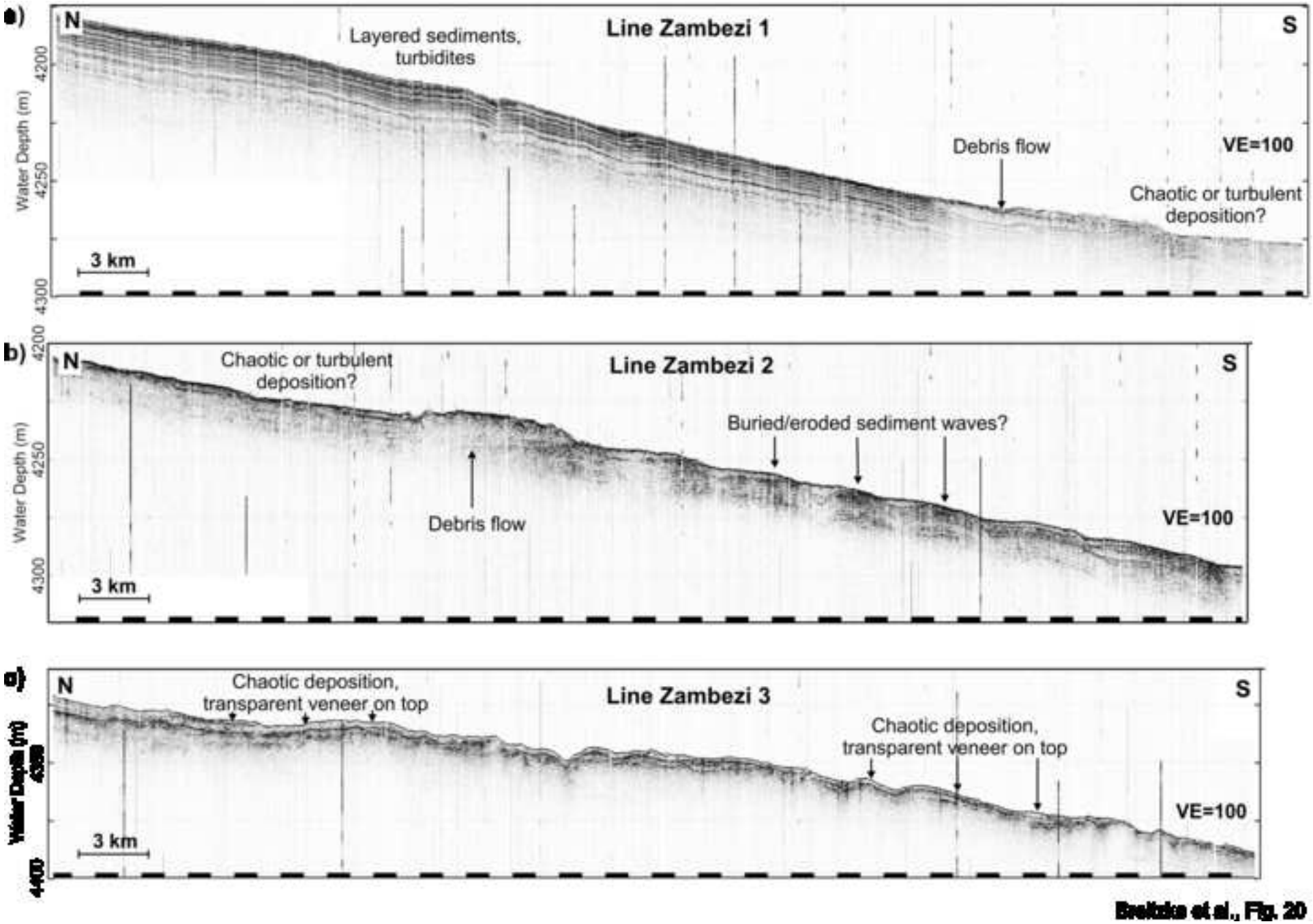

Bellaiche et al., Fig. 20

Figure 21a

Click here to download high resolution image

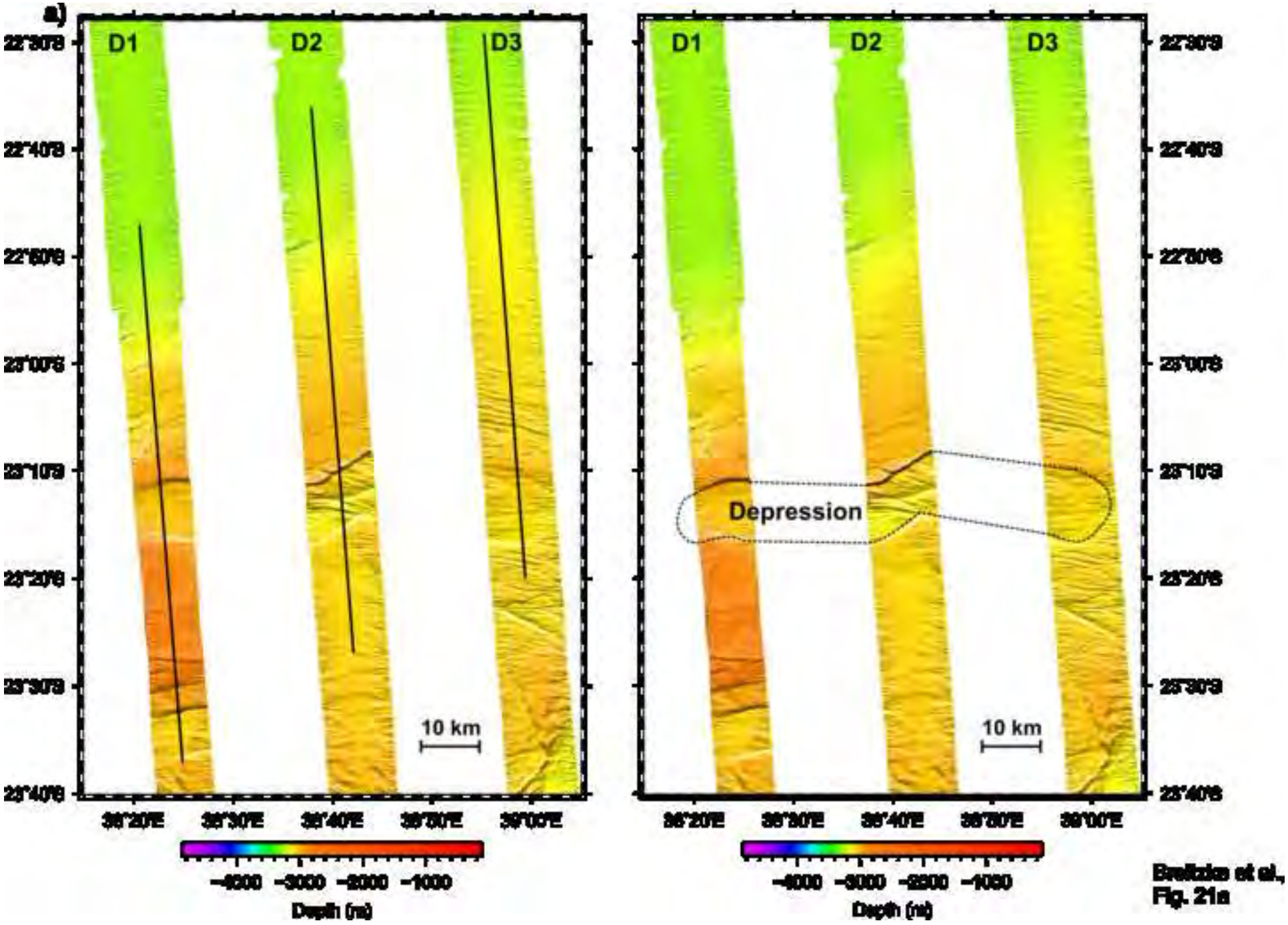

Figure 21b

Click here to download high resolution image

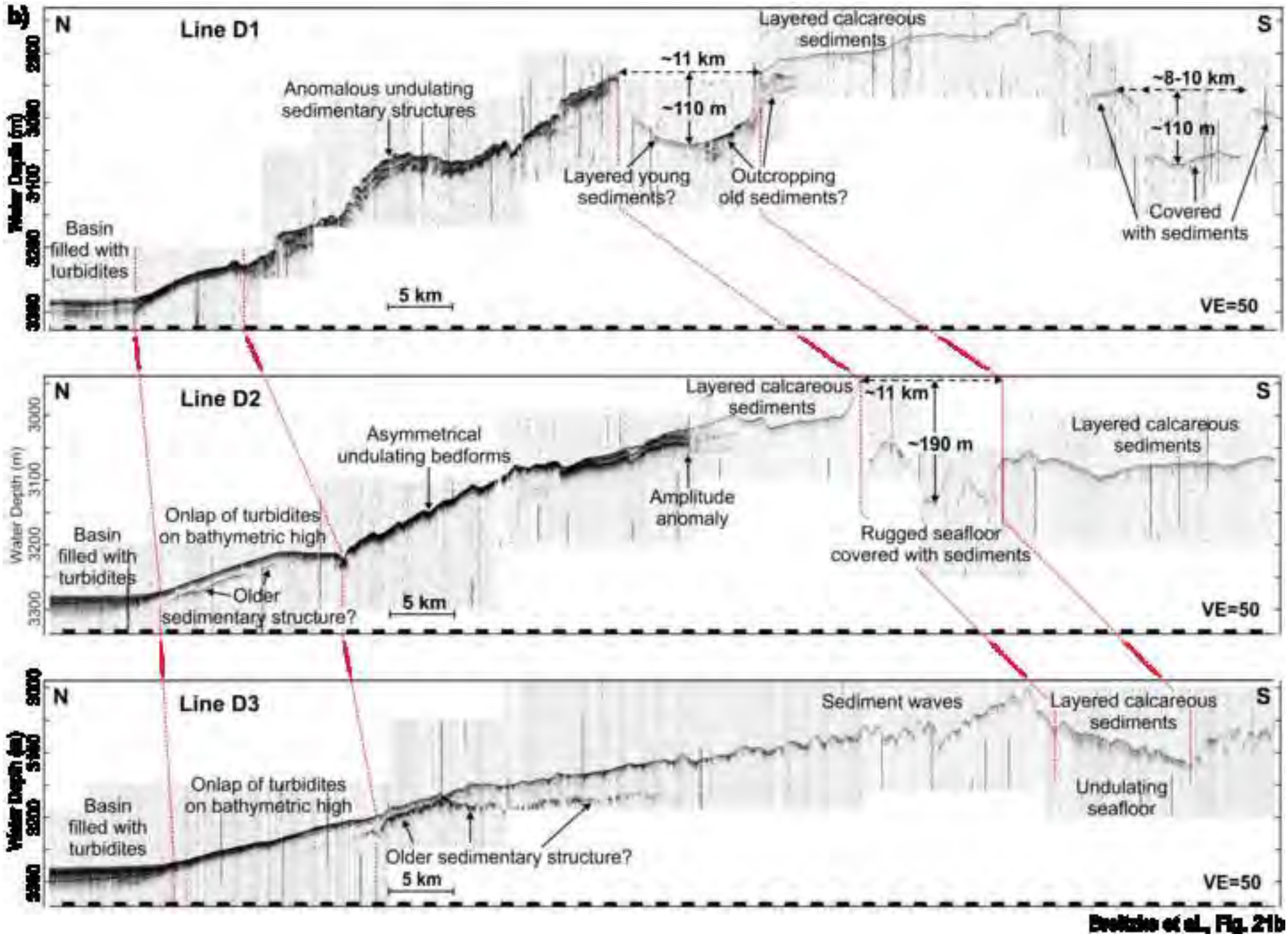

Figure 22

Click here to download high resolution image

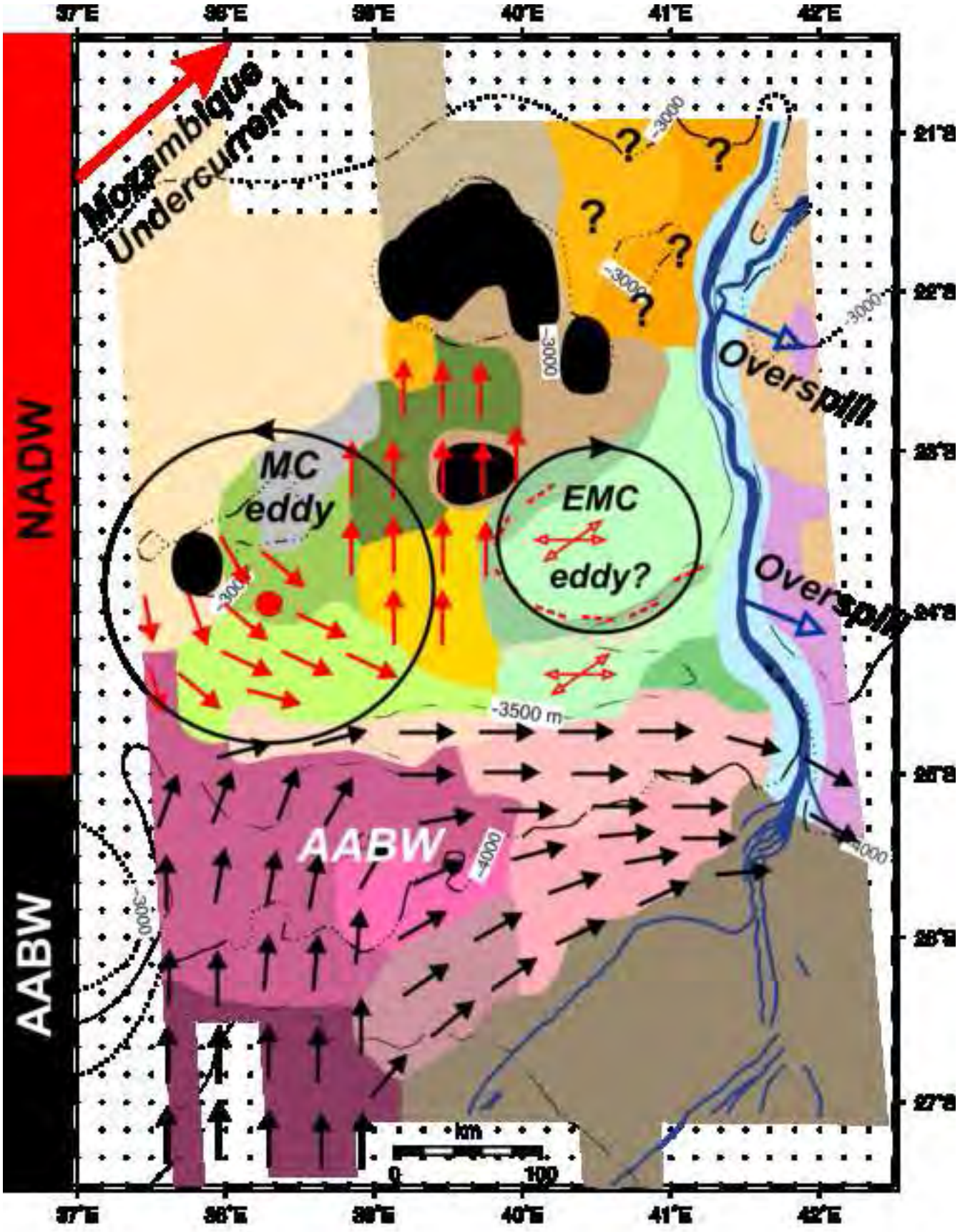

Brodzike et al., Fig. 22

Table A1
Click here to download Table: Table_A1.docx

Table A1. Morphology and PARASOUND reflection pattern of the microtopographic zones mapped in the study area (Figure 6).

Type	Description	Bedform scales	PARASOUND penetration depth	Location (Figure in this paper)
Undulating seafloor - southern bedform area				
BS1	Large steep, asymmetric erosional scours, mainly oriented NW-SE. The southern flanks are steeper than the northern flanks. The seafloor in and between the scour hollows is covered with parallel-bedded sediments.	Erosional scours: up to ~20 km length, ~3 - 7 km width, up to ~450 m depth	~25 - 35 m for the sediments in and between the scour holllows.	Southwestern Mozambique Channel **(Figure 7)**
BS2	Large undulating bedforms, sediment waves and small sediment drifts, mainly oriented NE-SW, with distinct parallel subbottom reflectors or diffuse small internal wavy or hyperbolic echoes. Sediment waves are migrating upslope. Sediment drifts show erosional southern flanks.	Sediment waves: $\lambda^* \approx$ 3 - 4 km $h \approx$ 25 - 45 m Sediment drifts: height up to ~100 m	~40 - 60 m	Southwestern Mozambique Channel **(Figure 8)**
BS3	Undulating bedforms with steep flanks and weak, diffuse reflection pattern, mainly aligned NE-SW.	Bedforms: $\lambda^* \approx$ 2.5 - 3 km $h \approx$ 60 - 80 m	~0 - < 5 m	Southern Mozambique Channel **(Figure 9a)**
BS4	Undulating bedforms with diffuse reflection pattern, mainly aligned NE-SW to ENE-WSW, intermittently incised by W-E to NW-SE oriented furrows. Similar to BS3, but with lower bedform height and higher acoustic penetration.	Bedforms: $\lambda^* \approx$ 1.5 - 2 km $h \approx$ 20 - 30 m Furrows: ~8 - 15 km length, ~2 - 3 km width, ~60 m depth.	~20 - 40 m	Southeastern Mozambique Channel, west of Zambezi Channel mouth **(Figure 9b)**
BS5	Small irregular, highly variable bedforms without distinct orientation. Prolonged to parallel subbottom reflectors.	Bedforms: $\lambda^* \approx$ 1 - 1.5 km $h \approx$ 5 - 30 m	~20 - 30 m	Southwestern Mozambique Channel **(without figure)**

BS6	Small undulating bedforms with diffuse, prolonged reflection pattern, mainly oriented WNW-ESE, NW-SE or W-E.	Bedforms: $\lambda^* \approx 1$ - 2 km h ≈ 5 - 20 m	~10 - 20 m	Southeastern Mozambique Channel, west of the Zambezi Channel **(without figure)**
BS7	Almost flat terrace with very fine-scale W-E trending undulating bedforms, located north of a slightly sinuous, deep contourite channel.	Bedforms: $\lambda^* \approx 0.3$ km h ≲ 5 m Contourite channel: ~5 km wide, ~100 m deep,	~10 - 15 m	Southwestern Mozambique Channel **(Figure 10)**
Undulating seafloor - central bedform area				
BC1	Regularly undulating bedforms, mainly aligned NW-SE, intermittently bifurcating. Diffuse, prolonged reflection pattern with hyperbolic echoes.	Bedforms: $\lambda^* \approx 2$ km h ≈ 55 - 60 m	~5 - 15 m	Central western Mozambique Channel **(Figure 11a)**
BC2	Small, slightly undulating bedforms with weak, parallel subbottom reflectors, mainly oriented NW-SE. Similar to type BC3 but smaller in height.	Bedforms: $\lambda^* \approx 1.5$ - 2 km h ≈ 10 - 40 m	~15 - 20 m	Central western Mozambique Channel **(without figure)**
BC3	Small undulating bedforms, mainly oriented W-E. Occuring in the transition zone between S3 and BC2. Weak, prolonged reflection pattern or hyperbolic echoes.	Bedforms: $\lambda^* \approx 0.5$ - 1.5 km h ≈ 10 - 60 m	~5 - 10 m	Central Mozambique Channel, south of Bassas da India, west of an unnamed seamount **(without figure)**
BC4	Undulating, hummocky bedforms showing two preferential orientations - NE-SW and W-E. They cover two gently sloping local topographic highs, possibly drift bodies. Diffuse, prolonged reflection pattern with hyperbolic echoes.	Bedforms: $\lambda^* \approx 1$ - 1.5 km h ≈ 35 - 55 m	~5 - 15 m	Central eastern Mozambique Channel, west of the Zambezi Channel **(Figure 11b)**
BC5	Small undulating bedforms following the topographic contour lines at the foot of the northern local topographic high covered with sediments of type BC4.	Bedforms: $\lambda^* \approx 1$ - 2 km	~5 - 15 m	Central eastern Mozambique Channel, west of the Zambezi

	Oriented NW-SE, W-E or NE-SW depending on the contour lines. Diffuse, prolonged reflection pattern, sometimes with hyperbolic echoes.	h ≈ 20 - 30 m		Channel **(without figure)**
BC6	Small undulating bedforms, mainly oriented NE-SW. Occurring in a meander loop of the Zambezi Channel, on the western levee. Parallel or prolonged subbottom reflections.	Bedforms: $\lambda^* \approx 1 - 2$ km h ≈ 5 - 40 m	~15 - 20 m	Central eastern Mozambique Channel, west of the Zambezi Channel **(without figure)**
BC7	Almost flat seafloor in a W-E oriented elongate depression between the two local topographic highs covered with sediments of type BC4. Diffuse, prolonged reflection pattern.	Depression: ~15 km wide (N-S)	~5 - 15 m	Central eastern Mozambique Channel, west of the Zambezi Channel **(without figure)**
BC8	Arcuate cross-cutting bedforms forming convex-bended "channels" and "ridges" and surrounding a local topographic high. Channel floors and ridge crests are covered with sediments showing weak, distinct parallel subbottom reflectors.	Height from channel floors to ridge crests: up to ~140 m Diameter of the arcuate bedforms: ~35 - 40 km	~15 - 40 m	Central Mozambique Channel **(Figure 12)**
	<u>For comparison:</u> North of zone BC8 occurs a moat which surrounds the unnamed seamount south of Bassas da India. Filled with distinctly reflecting, parallel-bedded sediments.	Moat diameter: ~55 - 60 km	~30 - 40 m	Central Mozambique Channel **(Figure 13)**
Undulating seafloor - northern bedform area				
BN1	Flat seafloor intermittently interrupted by arcuate bedforms forming large "sediment blocks" or convex-bended "ridges". The bedforms are covered with distinctly reflecting, parallel-bedded sediments, similar to type S2.	Height of the ridge crests: ~ 40 - 85 m; Diameter of the arcuate bedforms: ~30 - 35 km	~40 - 50 m	Central Mozambique Channel, east of the Bassas da India complex **(Figure 14)**

BN2	Highly variable morphological features such as irregular or elongate depressions, holes and hummocky bedforms or slightly undulating NE-SW oriented bedforms close to the western Zambezi Channel bank. The structures are covered with distinctly reflecting, parallel-bedded sediments, similar to types BN1 and S2.	Bedform height: ~20 - 75 m; Bedform length: ~1 - 10 km	~10 - 50 m, depending on the steepness of the bedform flanks and the position relative to the Bassas da India complex and the Zambezi Channel	Central Mozambique Channel, west of the Zambezi and Tsiribihina Channel confluence **(Figure 14)**
Undulating seafloor - southeastern Zambezi Channel levee				
BE1	Undulating bedforms and sediment waves with distinct parallel subbottom reflectors, oriented either W-E, NE-SW or NW-SE depending on their position relative to the Zambezi Channel (loops). Sediment waves either migrate upslope or do not migrate.	$\lambda^* \approx 5$ - 6 km h ≈ 10 - 25 m	~30 - 50 m	Southeastern Zambezi Channel levee **(Figure 15)**
Smooth seafloor				
S1	Flat or slightly undulating seafloor with distinct, parallel subbottom reflectors, with intermittently intercalated transparent lenses of mass wasting deposits and incised by few small channels and slide scars, especially in the northwestern part.	-	~20 - 50 m, increasing from NW - SE	Mozambican continental margin **(Figures 16, 17)**
S2	Flat or slightly undulating seafloor with distinct, parallel subbottom reflectors covering thick transparent slump deposits at the northern foot of the Bassas da India complex.	-	~40 - 60 m	North of Bassas da India complex **(Figure 18a)**
S3	Flat or slightly undulating seafloor with distinct, parallel subbottom reflectors covering thick transparent slump deposits at the southern foot of the Bassas da India complex.	-	~20 - 40 m	South of Bassas da India complex **(Figure 18b)**
S4	Flat seafloor with distinct parallel subbottom reflectors in the north close to the Zambezi and Tsiribihina Channels and weak subbottom reflectors at	-	~20 - 50 m, decreasing southward	Eastern Zambezi Channel levee **(Figure 19)**

	greater distance to the submarine channels.			
S5	Flat or slightly undulating seafloor with (i) strong, distinct, parallel subbottom reflectors southeast of the Zambezi Channel mouth or (ii) diffuse reflection pattern covered with a transparent veneer and intermittently incised by small distributary channels in the southwestern part of the Zambezi cone.	-	~40 - 60 m in areas with parallel subbottom reflectors; ~10 - 20 m in areas with diffuse reflection pattern	Zambezi cone, southeastern Mozambique Channel **(Figure 20)**
Zambezi & Tsiribihina Channels				
Z1	Strong prolonged, diffuse echoes from the channel floors.	Zambezi Channel: i) northern part: ~630 - 750 m deep, ~4 km wide; ii) southern part: ~150 - 300 m deep, ~8 km wide Tsiribihina Channel: ~570 - 650 m deep, ~2 km wide	~5 - 10 m	Zambezi & Tsiribihina Channel **(without figure)**
Z2	Strong prolonged, diffuse echoes from the channel walls and terraces, small to moderate hyperbolic echoes from the terraces within the meander loops, and layered sediments on a terrace in the southernmost meander loop on the western levee of the Zambezi Channel.	-	~15 - 20 m in case of hyperbolic echoes, ~20 - 30 m in case of prolonged, diffuse echoes from the channel walls, ~40 - 45 m in case of the layered sediments in the meander loop	Zambezi & Tsiribihina Channel **(without figure)**
Rough seafloor				
R1	Large diffraction hyperbolae or almost evanescent echoes due to rough topography and steep slopes.	-	0 - < 5 m	Bassas da India, Jaguar Seamount, Hall Tablemount, Europa Island, unnamed

				seamount, Mount Bourcart **(without figure)**
R2	Large elongate depression oriented W-E. Bordered by seafloor with slightly undulating bedforms oriented W-E or NW-SE, similar to types BC2, BC3. North of the depression the seafloor is covered by sediments showing an unsually strong, anomalous reflection pattern. South of the depression the seafloor is covered with sediments shwoing weak parallel subbottom reflectors.	Depression: ~110 - 190 m height, ~11 km width (N-S), ~70 - 75 km length (W-E)	~20 - 35 m in case of the unusually strong, anomalous reflection pattern, ~10 - 25 m in case of the weak parallel subbottom reflectors	Central western Mozambique Channel, northeast of Mount Bourcart **(Figure 21)**

λ^* = apparent wavelength of the bedform measured along the ship's track
h = height of the bedform

Appendix C

Cliff-top storm deposits (55-63m amsl) from Morgan Bay, South Africa

Smith, A.M.,† Green, A.N.,† Cooper, J.A.G.,†+ Dixon, S.,† Pretorius, L.,† Wiles, E.,† Guastella, L.A. ‡

† Geological Sciences, School of Agricultural, Earth and Environmental Sciences,
University of KwaZulu-Natal, South Africa
asconsulting@telkomsa.net

+ School of Environmental Science, University of Ulster, Coleraine BT52 1SA, UK

‡ Department of Oceanography, University of Cape Town, Private Bag X3, Rondebosch, Cape Town, 7701, South Africa.

www.cerf-jcr.org

www.JCRonline.org

ABSTRACT

Smith, A.M, Green, A.N, Cooper, J.A.G. *et al*., 2014. Cliff-top storm deposits (55-63m amsl) from Morgan Bay, South Africa. In: Green, A.N. and Cooper, J.A.G. (eds.), *Proceedings 13th International Coastal Symposium* (Durban, South Africa), *Journal of Coastal Research*, Special Issue No. 70, pp. 349-353, ISSN 0749-0208.

Cliff-top storm deposits (CTSDs) occur south of Morgan Bay, South Africa at elevations varying from ±55- to 63m. These occur as a ±10m-wide horizontal fringe of shell breccia mixed into a very thin (>15cm) sandy soil on the cliff top platform. Visually it is evident that the shell breccia is of various ages. Comparisons with proven wave breccia from this area indicate the same source. We suggest that this breccia was deposited as fall-out from wave and wind-borne plumes produced by wave bores striking the cliff base. These bores would likely have been produced by waves at least ~40m in height. Alternative interpretations, such as a perched marine desposit or tsunamiite are rejected in favour of CTSDs produced by multiple large wave events.

ADDITIONAL INDEX WORDS: *Shell breccia, storm deposits, storm waves, tsunami.*

INTRODUCTION

Cliff-top storm deposits (CTSDs) range from shelly material to boulders located on marine cliff-tops. CTSDs at heights of up to 50m have been described from Shetland, Orkney, Caithness and the Outer Hebrides in Scotland and from the Aran Islands in Galway Bay, Ireland (Hall *et al*., 2006). In this paper we describe CTSDs from marine cliff-tops up to 60m high from the Eastern Cape coastline, South Africa.

ENVIRONMENTAL SETTING

Morgan Bay, on the Eastern Cape Coast of South Africa, faces the Indian Ocean (Fig. 1). The location climate is warm temperate (Cooper *et al*., 2013) and the sea temperatures vary from 22°C in summer to 14°C in winter. Average daily air temperatures vary from 14°C to 23°C. The driest months are June, July and August and are followed by the spring rains. Coastal winds are bimodal: southwesterly and northeasterly in roughly equal proportions (Cooper *et al*., 2013). Marine storms are common in September, although less common, tropical cyclone swells are also experienced (South African Weather Service).

The regional geology comprises gently dipping Beaufort sandstones that have been intruded by thick dolerite sills (Fig. 3A). A well-developed shore platform coated by boulders is present on the adjacent coast, but not at the foot of the sea cliffs where the CTDS are found. Morgan Bay is a small tourist village within a headland-bound bay. It is fronted by a narrow rocky beach, which grades from a boulder beach in the south to a sandy beach in the north. The southern headland is flanked to the south by plunging cliffs up to 65 m high, whereas the northern headland is subdued and capped by a high coastal dune (Smith *et al*., 2011). CTSDs (Hall *et al*., 2006) were found on the tops of exposed bluffs which collectively form the southern headland. These headlands are aligned south-south easterly and project into the Indian Ocean. They have elevations varying from ~16 to ~63m amsl (Fig. 2). In some instances a well-defined step is present on these cliffs where the dolerite-sandstone contact coincides with sea level (Fig. 2B). The immediate cliff top area is relatively flat but slopes gradually landward. The cliffs are relatively undisturbed by human activity and contemporary cliff-top land use is restricted to cattle grazing and hunter gathering.

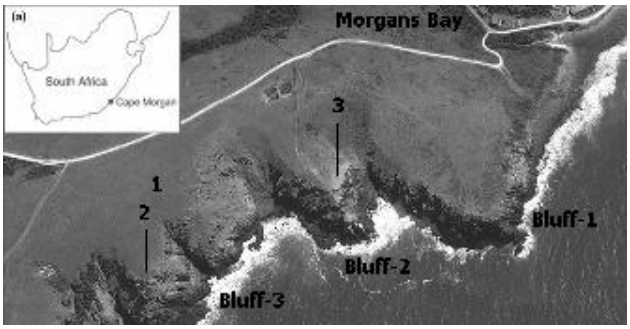

Figure 1A: Location of field area (32°42′14″S 28°20′10″E28 ºE; 34 ºS); B: The sample sites.

OCEANIC ENVIRONMENT

Bathymetry

The shelf is very narrow (±10km wide) and consequently swell attenuation due to bottom friction is minimal. The coast is microtidal, with a mean high tide of 1.25 m and a high astronomical tide (HAT) of 2.08 m (http://www.satides.co.za/).

Meteorology

Swells and seas are generally produced by cold fronts and cut-off-low pressure systems, although tropical storms and cyclones can also contribute. The wave record extends from 1992 (for the port of East London 40km south) to the present (van der Borch and van Werolde, 2004; CSIR wave rider buoy). The prevailing

DOI: 10.2112/SI70-059.1 received 21 December 2013; accepted 21 February 2014.

swell systems move in association with the west-to-east synoptic weather patterns and produce a net south-to-north littoral drift although this can reverse through topographic forcing and during easterly swells.

Wave climate

Wave heights of 8 m and periods of 11–17 s are common during winter storms (Smith *et al*., 2011). The average significant wave height is 4.45 m, with a period of 14 s. The mean peak period is 13.7 secs (vdbvW, 2004). The longest period measured was 18.3s, associated with a comparatively low 5.24 H_{mo} swell in 1993 (the swell propagation direction is not available)(Rousouw and Rousouw, 1999). Most swells approach from 170 to 190º with a measured range varying from 62 to 224º (vdBvW, 2004). Extreme events (>4m H_{mo}) occur between March and September, (van der Borch and van Werolde, 2004).

Between 31st August and the 1st September 2008, 9 to 10.7 m waves were generated by an extremely deep cold front that passed south-west of the country during equinox tides (Table 1) (Guastella and Rossouw (2013). This high swell caused considerable coastal flooding at Morgan Bay and elsewhere in the Eastern Cape. A high swell which struck on the March (2007) equinox had higher swells (Table 1) but passed without much notice, whereas the 2008 September equinox event had an unusually high (7-8m) runup and caused significant flooding and damage to coastal infrastructure. This was probably due to the fact that the 2008 September equinox swell came from an unusually eastely direction (Table 1). It is also possible that the nearshore and inner shelf had not fully recovered from the high swells of 2007, as was the case during the austral winter (2007) erosion in KwaZulu-Natal to the north (Smith *et al*., 2010). It appears that 10 m (H_{max}) swells are not uncommon on a decadal scale (Table 1). However, storm damage was extreme during the 09/2008 event which had a comparatively low swell height. The 1997 event appeasr anomalous, however it is likely that its propagation direction (Table 1) was too far west and that most of the energy would have been lost to friction as the swells wrapped in across the shelf.

METHODS

The cliffs below the CTSDs show several important morphological characteristics. There is a small 1 m-wide step at the upper sill-sandstone junction (Fig. 2A). In addition there are rock projections reminiscent of marine stacks at this boundary.

Figure 2: An oblique view (from the south) of the lower sampled site (#3) showing stack (A) development two thirds of the way up the cliff. B) A closer oblique view of the Morgan Bay cliff showing the stepped edge (arrowed) due to rock removal.

Figure 3: Shell debris in situ on cliff-top platform at an elevation of 60 m.

Table 1. The largest swells on record for East London, 40km south of Morgan Bay.

Date	H_s (m)	H_{max} (m)	T (s)	Bearing	Source
06/1997	9.3	13.79	15.5	?SW	CSIR
02/2007	4.59	7.98	12.5	173	CSIR
03/2007	6.25	10.13	13.3	155	CSIR
05/2007	4.97	10.3	10.3	148	CSIR
09/2008	4.73	8.76	11.1	145	CSIR

The cliff-top edge can also show a distinct step (Fig.2B). No marine platform is present below the highest cliffs. Both Bluffs 2 and 3 (Fig. 1) are capped by a flat cliff-top platform, whereas Bluff 1 slopes steeply northeast. The cliff-top platform is a grassland, with occasional stunted bushes, although the inter-Bluff areas can be more densely vegetated. Rock outcrop is present. The soil is sandy and very thin, varying from zero to about 15cm.

Field mapping was employed to describe the extent of the CTSDs on the cliff-top platform. Four sites were investigated of which three were sampled.

RESULTS

The cliff top sampled deposit locations were recorded and samples were taken for microscopy (both optical and SEM) anyalysis (Table 2). These samples were compared with unequivocal wave deposits from the storm swash terrace (e.g. McKenna *et al*., 2012) at the cliff base. The results of this are described below.

Shell Breccia

Scattered marine shell breccia debris was noted within the thin soil horizon (zero to 20 cm thick) on the flat surface above the cliff edge, at elevations of up to ~63 amsl (Fig.2). No bedding is preserved, most likely having been destroyed by terrestrial bioturbation. The sample characteristics are described in Table 2.

3rd Bluff-South

Samples were taken from the highest (±63m) locality investigated. Two samples were collected (Fig.4) (Table 2). At this locality the shell breccia occurs within the soil, commonly exposed in mole hills and as a lag deposit concentrated in the base of sandstone tarn pools. Material has been washed in from the

surrounding soil to concentrate in the tarn pools. Shell breccia deposition is patchy, but only found within 10m of the cliff edge. Occasional rounded shale and quartzite pebbles (0.5 to 1 cm diameter) are present in the CTSDs. Careful inspection of this locality showed that the shell fragments become more numerous and larger towards the cliff edge (Table 2). The CTSDs form a 10m-wide shell breccia fringe adjacent to the cliff edge, the clasts of which fine rapidly inland. No shell breccia was seen more than 10m inland from the cliff edge.

2nd Bluff-South

On the cliff-top platform (±49m), shell fragments are exposed in mole hills within 10m of the cliff edge (Table 2). The cliff top soil is composed of very fine sand. A single sample (3) was taken.

1st Bluff-South and Inter- Bluff areas

This site is steeply inclined (±16m highest point) and no shell breccia was found here, or in the intervening area, consequently it was not sampled (Fig.1).

General observations

Comparison with unequivocal wave deposits show a strong similarity with wave shell breccia. They too comprise granules, very coarse sand and shell hash of variegated composition (Fig. 4A and B).The CTSDs are only found on cliff-top platforms where they form a 10m-wide detrital shell breccia fringe adjacent to the cliff edge, the clasts of which fine rapidly inland showing that the shell breccia is related to the marine environment. shell breccia was only found on horizontal surfaces. The absence of CTSDs on Bluff 1 may be related to the geomorphology, as there is no cliff-top platform. Instead it slopes steeply to the northeast and would make it less likely that material would settle, but rather flow back down the back slope.

Binocular microscope and SEM analysis

No detailed statistics was attempted as the sample is small. A detailed textural examination revealed a combination of older and younger shell clasts (Fig. 5A and B). SEM analysis of surface weathering features on the shell fragments showed variable degrees of weathering, implying that the breccia clasts are of variable age. The breccia in sample 3 was less weathered and younger than that of sample 1 (Table 2). The shell fragments from sample 2 were more etched than those of sample 3, suggesting them to be older. Further, sample 2 fragments showed evidence of a patchy biological layer, such as might be expected to cover a younger shell fragment (Fig. 5A and B).

DISCUSSION

There is no evidence that the Morgan Bay cliffs have been overtopped by "green water" but the presence of shell breccia in the soil indicates relatively recent introduction of marine debris to the cliff top. The cliff edge often shows a prominent step, associated with stacks at the top of the dolerite. The cliff top is also associated with a prominent step, reminiscent of marine quarrying, however, no loose boulders were noted landward of the cliff edge. In contrast the cliff step is littered with fallen boulders. The cliff-top socket may be the result of extreme wave quarrying but the lack of a boulder fringe argues against this. Optical and SEM inspection of the CTSD breccia shows various degrees of weathering and indicates that the breccia is of variable ages, but absolute dating is beyond the scope of this study, however the more weathered fragments were found at higher levels.

Table 2. Summary of sample properties and locations.

Sample	Dimensions	From cliff edge	Elevation (amsl)	Location
1	1<5 mm most 1-2 mm	5 m	±63 m	Bluff 3
2	<20mm most 4-5 mm	10 m	±62 m	Bluff 3
3	<30m most 5-10 mm	5 m	±49 m	Bluff 2
No sample taken	Not present	Not present	±16 m	Bluff 1
Cliff Base	variable	n/a	8 m	Storm surge terrace

This coastline faces the Indian Ocean and is very exposed to high swell and storm waves. The cliff-top shell breccia is clearly ocean-derived as proved by their similarity to unequivocal wave deposits and the proximity to the cliff edge. Waves are known to spray sand (Cooper *et al*., 1999) and further CTSDs have been described from cliff tops in Scotland and Ireland (Hanson and Hall, 2006). In Shetland, at the Villians of Hamnavoe and Eshaness Lighthouse, CTSDs are present at an elevation of 50 m (Hall *et al*, 2006). They interpreted this as air throw debris produced by very large waves striking the cliff and the ensuing debris being transported onshore by strong winds.within the spray. In the Morgan Bay case wave scour is recognized at an elevation of 40 m, well below the CTDS. In the Morgan Bay case, the position of the CTDs on Bluff 2 and Bluff 3 would suggest that the source is a giant southeasterly swell and associated onshore wind (Fig. 2). Hanson *et al*. (2008) state that 10m high waves can form vertical jets capable of transporting large blocks. In the Morgan Bay case no unequivocal large blocks were observed on the cliff tops but the runoff from such might be capable of eroding the cliff edge. In Morgan Bay the cliffs have clearly been eroded at the dolerite sandstone contact and this must be due to wave action. This is at a level of ~40m. If the wave spray height in figure 6 is used, then simply scaling up the 2008 September Equinoctial event statistics indicates that air throw deposits could easily have been flung 60m upward. For the observed CTSDs to exist on the Morgan Bay cliffs, we theorise that waves in the 40m (H_{max}) category must have ocurred from time to time. We propose that these CTSDs are the result of spray thrown up by bores from very large broken waves striking the cliff (Fig. 6).

The relationship between H_s and H_{max} is probably dependent on wave period and swell order (Table1). Long-range swells are better ordered than storm seas. For this research the proxy used in

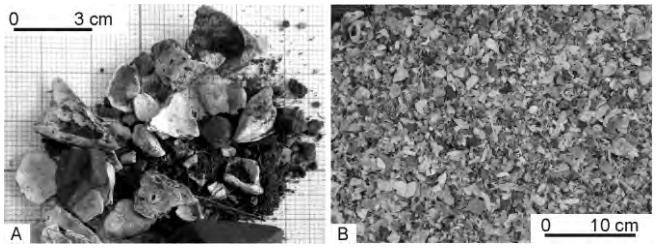

Figure 4. Comparison between (A) CTSD shell hash and pebble deposit of sample 1 and (B) storm wave-deposited sheet of variegated shell hash and pebble material. Note the similarity.

this study is wave height, as period and direction are unknown for ancient swells and we can only surmise direction (a probable southeasterly or coast-normal wave propagation direction).
On a global scale, satellite altimetry has indicated that 100 foot waves (33 m) occur several times per year, one such wave was recently surfed at Nazare, Portugal.

The Agulhas Current flows southwestward, off Morgan Bay, and is famous for 'rogue waves', with a 30 m example having been recorded in 1977 (Faulkner, 2006). Rogue waves are defined variously as $H_{max}/Hs>2$ (Wolfram *et al*., 2000) or 2 x H_s (O'Brien *et al*. 2013) or >2.4 x H_s (Faulkner, 2006). Using the maximum H_{mo} (9.m), waves > 20m are quite possible at Morgan Bay. The largest wave surfed in SA (2008) was in Cape Town (1000km south) and estimated to be 22 m. The open ocean tug Wolraad Woltemade sailed over a 21 m swell in 2001 off Cape Town (Candy, pers. com.). On breaking, this swell could conceivably have had a +30 m face. Clearly 20 m waves are not uncommon on the South African coast. The age of the proposed Morgan Bay CTSDs is not known, consequently we have no idea what the prevailing climatic regime was, but the preservation does point to a Holocene age of deposition.

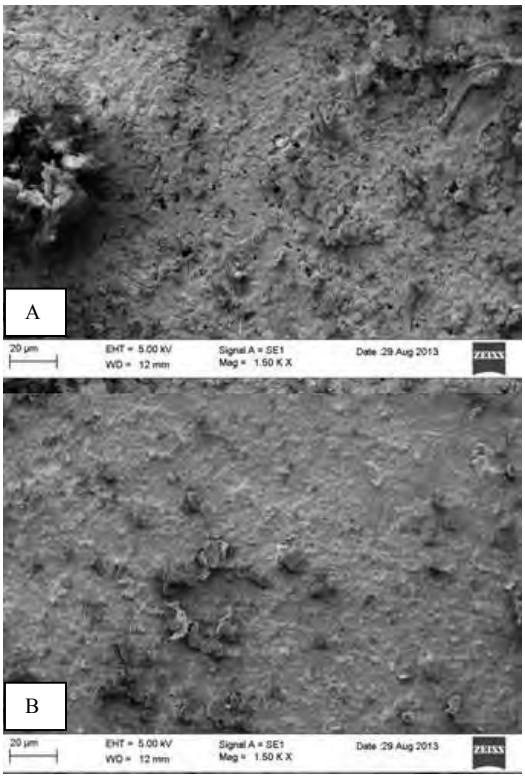

Figure 5. Photomicrographs of shell surface textures. A and B are fragments from sample 1, showing older weathered and younger less weathered material, respectively.

Figure 6. September (2008). Spray from a wave bore (H_s=4.73; Hmax~ 8m), reaching a height of ~12m against a ±16m cliff at Morgan Bay. Photo R. Smith.

Alternate Formative mechanisms

Probable wave deposits at a high elevation automatically attract a tsunamiite hypthesis for their genesis. No tsunamiite deposits are on record for the South African coastline and although such an origin cannot be ruled out, it seems unlikely as the CTSDs are clearly the product of multiple events.

An alternative hypothesis is that the shelly debris were deposited at a raised shoreline during a period of higher sea level. A Tertiary age boulder horizon ('Boulder Bed'), dated at 4 Ma (Erlanger *et al*., 2012) is well known at about 70m amsl from the South African coast (Davies, 1970; Erlinger, 2012). The "Boulder Bed"is located 10m above and several hundred metres landward of the highest proposed CSTDs (site 1). No shell material has ever been found to be associated with the 'Boulder Bed'. The "Boulder Bed" is a very distinctive unit (0.5-1 m thick) comprising very-well rounded cobbles and small boulders. These boulders can be recognized within colluvium below the outcrop. No such clasts have been found to be associated with the CTSDs. Finally the shell debris is from extisting marine species that occur around the base of the cliffs, thus precluding an ancient raised shoreline origin.

CONCLUSIONS

CTSDs are found at levels of up to ±63m amsl at Morgan Bay. This deposit comprises a shelly breccia fringe adjacent to the marine cliff top. Comparisons with wave breccia from the lower supratidal (6m amsl) show them to be similar but older based on micro-textural characteristics of the shell debris. The CTSD fragments are variable in age. We suggest that this breccia was emplaced as air throw from wave and wind-borne plumes produced by the bores of broken waves struck the base of the cliffs. These bores would likely have been produced by waves ~40 m in height. Both a tsunamiite and perched beach origin were considered as alternative means of emplacement, however these origins seem unlikely.

LITERATURE CITED

Candy, R., pers. com. CSIR wave rider buoy. http://wavenet.csir.co.za/OnlineData/EastLondon/eastlondonwaveD.htm

Cooper, J.A.G. and Jackson, D.W.T., 1999. Wave spray-induced sand transport and deposition during a coastal storm, Magilligan Point, Northern Ireland. *Marine Geology*, 161, 377-383.

Cooper, JAG, Smith, A.M. and Green, A.N., 2013. Backbeach deflation aprons: morphology and sedimentology. *Journal of Sedimentary Research*, 83, 395-405.

Davies, O 1970). Pleistocene beaches of Natal. *Annals of the Natal Museum*, 20, 403-442.

Erlanger, E.D., Granger, D.E., Gibbon, R.J., 2012. Rock uplift rates in South Africa from isochron burial dating of fluvial and marine terraces. *Geology*, 40, 1019-1022.

Draper, L., 1964. "Freak" Ocean Waves, Oceanus, X:4. Reprinted in Rogue Waves 2004: Proceedings of a Workshop.

Faulkner, D., 2000. Rogue Waves – Defining Their Characteristics for

Marine Design. Rogue Waves 2000: Proceedings of a Workshop.
Guastella, L.A., Rossouw, M., 2012. What will be the impact of increasing frequency and intensity of coastal storms along the South African coast? *Reef Journal*, 2, 129-139.
Hall, A.M., Hansom, J.D., Williams, DM., Jarvis, J., 2006. Distribution, geomorphology and lithofacies of cliff-top storm deposits: examples from the high-energy coasts of Scotland and Ireland. *Marine Geology*, 232, 131-155.
Hansom, J.D., Barltrop, N.D.P. and Hall, A.M.., 2008. Modelling the processes of cliff-top erosion and deposition under extreme storm waves. *Marine Geology*, 253, 36-50.
O'Brien, L., Dudley, J.M., and Dias, F., 2012. Extreme wave events in Ireland: 14 680 BP. *Natural Hazards and Earth Systems Science*, 13, 625–648, 2013.
McKenna, J., Cooper, J.A.G., Jackson, W.T., 2012. Storm Swash Terraces: A Previously Overlooked Element of the Cliff-Shore Platform System. *Journal of Sedimentary Research*, 82, 260-269.
Rossouw, J., Rossouw, M., 1999. Re-evaluation of recommended design wave methods. Proceedings of the 5th International Conference on Coastal and Port Engineering in Developing Countries (COPEDEC), Cape Town, South Africa, April 1999.

Beachrock facies variability and sea level implications: a preliminary study

Christopher S. Kelly†, Andrew N. Green†, J. Andrew G. Cooper†‡, Errol Wiles†

†Geological Sciences
School of Agriculture, Earth and Environmental Sciences
University of KwaZulu-Natal, Westville, South Africa
christopher.kelly@fulbrightmail.org
greena1@ukzn.ac.za
eawiles@yahoo.com

‡ School of Environmental Sciences
Centre for Coastal and Marine Research
University of Ulster
Coleraine, UK
jag.cooper@ulster.ac.uk

www.cerf-jcr.org

www.JCRonline.org

ABSTRACT

Kelly, C.S., Green, A.N., Cooper, J.A.G. and Wiles, E. 2014. Beachrock facies variability and sea level implications: a preliminary study. *In:* Green, A.N. and Cooper, J.A.G. (eds.), *Proceedings 13th International Coastal Symposium* (Durban, South Africa), *Journal of Coastal Research*, Special Issue No. 70, pp. 736-742, ISSN 0749-0208.

In spite of the worldwide abundance of beachrocks and their acknowledged utility as an indicator of former sea level position, some studies have expressed doubt as to their position of cementation on paleo shorelines. These criticisms are not, however, coupled with nuanced sedimentological studies of beachrocks. Instead, few beachrock studies acknowledge any facies and therefore disregard important signatures of the depositional environment and, consequently, utility as paleo sea level indicators. This study presents detailed sedimentological descriptions and interpretations from two beachrock localities along the subtropical, microtidal, wave-dominated eastern coastline near Durban, South Africa. The outcrops record the migration of a paleo inlet and deposition in sub, inter, and supra tidal environments. Understanding the inferred depositional environment, and observed stratigraphic relationships between various beachrock facies is critical to teasing out the local evolution of shoreline and relative sea level. The outcrops studied here record multiple episodes of Holocene sea level rise and fall.

ADDITIONAL INDEX WORDS: *beachrock, facies, sea level, South Africa*

INTRODUCTION

Beachrocks are common features of tropical and subtropical coastlines. They exhibit diverse sedimentological and morphological characteristics (Vasdoukas *et al.*, 2007). Beachrocks form at or near mean sea level, due to cementation of clasts by calcium carbonate (High-Magnesian Calcite or Aragonite) in the vadose/phreatic zone of the intertidal zone (e.g. Vasdoukas *et al.*, 2007). They have important implications for coastal evolution by preferentially preserving shorelines (Cawthra, 2012; Green *et al.*, 2014) and modifying shoreline dynamics (Cooper, 1991). In microtidal settings beachrocks have been particularly useful in constraining former sea level positions (Ramsay, 1995; Ramsay and Cooper, 2002; Desruelles *et al.* 2009; Cooper, 2011, Vacchi *et al.* 2012). Some concerns, however, have been expressed regarding the reliability of these features as sea-level indicators due to the often diachronous nature of their cementation, the range in thicknesses in relation to the known tidal range and the argument that they may also be supratidal in origin (Kelletat, 2006). Most authors implicitly dismiss or under-describe the facies variations that may occur within beachrocks and superimpose this term broadly on all rocks formed at or near

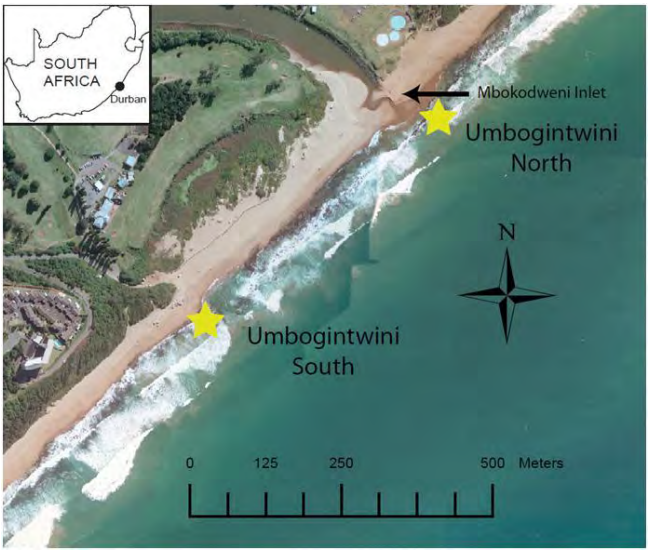

Figure 1. The two study sites from the east coast of South Africa. Umbogintwini North (30.0089° S, 30.9368° E) and South (30.0118° S, 30.9329° E) are denoted by the yellow stars. The study area is approximately 19.5 km south of Durban.

DOI: 10.2112/SI70-124.1 received 08 November 2013; accepted 21 February 2014.

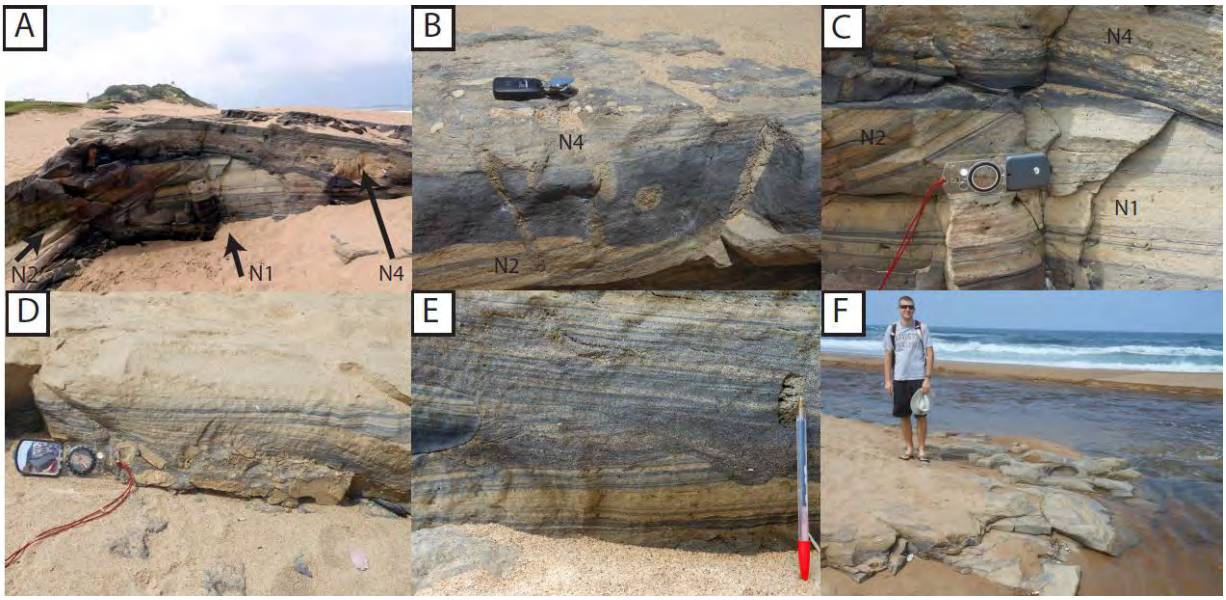

Figure 2. Beachrock units at Umbogintwini North (A-F). **A.** Dip section of Umbogintwini North. Note the erosional surface marking the contact between planar cross bedded sandstone of Facies N1 and overlying steeply dipping Facies N2. **B.** The erosional contact between Facies N2 and N4 with overlying heavy mineral layer and sandy infills of crab burrows (Facies N4). Note the intraformational beachrock and pebbles included as larger clasts. **C.** The contacts between Facies N1, N2, and Facies N4. Note the steeply dipping trough cross bedding of Facies N2 as an inlet migration indicator. **D.** Seaward imbricated pebbles at the base of Facies N4 and overlying antidunes. **E**. Landward oriented antidunes truncating seaward- dipping heavy mineral laminae of Facies N4 **F.** Upper surface of Facies N4 potholed to seaward

mean sea level by carbonate diagenesis. This may be the result of the variability within beachrocks worldwide (Vousdoukas *et al.*, 2007) and the seemingly less diverse sedimentary structures preserved in more temperate occurrences of beachrock (Vacchi *et al.*, 2012; Kelletat, 2006; Knight, 2007) Despite the potential for detailed sedimentological description and interpretation from beachrocks in subtropical settings (Caron, 2011), relatively little attention has been given to the nature of the sedimentary facies preserved and their original environment of deposition. This paper investigates a series of beachrocks on the east coast of South Africa that exhibit major facies variability.

REGIONAL SETTING

The east coast of KwaZulu-Natal South Africa is predominantly a microtidal, wave dominated coastline (Davis and Hayes, 1984; Davis, 1964; Schumann and Orren, 1980). The Quaternary coastal geology surrounding Durban is mainly comprised of Pleistocene-Holocene aged calcareous arenites (Krige, 1932; McCarthy, 1967). These abut a series of rubified palaeo-dune sands that comprise an ancient dune complex of suspected Mio-Pliocene age, termed the Berea Ridge (Krige, 1932; McCarthy, 1967). The Berea Ridge forms a ~ 100 km long coast-parallel ridge that in many instances extends all the way to the shoreline where it is exposed amidst younger Holocene dune sands. The calcareous arenites around Durban have been described by several authors (Cooper and Flores, 1991; Cooper and Liu, 2004; Cawthra, 2012) and are considered to represent the intertidal and supratidal cementation of beachrock and aeolianite respectively.

This paper examines two such outcrops from the East coast of South Africa at Umbogintwini, approximately 19.5 km south of Durban (Figure 1) (Juckes, 1976). The sites are spaced approximately 500 m from each other, situated on either side of the modern Mbokodweni Estuary, a small, temporarily-open closed estuary (Figure 1).

OBSERVATIONS

The sedimentary facies for both Umbogintwini North (Figure 2) and South (Figure 3) are described in terms of their sedimentary features and stratigraphic relationships. Facies of each site are described below.

Umbogintwini North

The exposed portion of outcrop at Umbogintwini North is approximately 30m long and 10 m wide, preserved under the sand of a contemporary barrier beach. Presently, the Mbokodweni inlet abuts the outcrop. Historical literature (Juckes, 1976) from Umbogintwini South and recent aerial photography (Google Earth), however, show that beach cover and inlet position are in perpetual flux. The position of the modern inlet, and even the degree of exposed beachrock, is ephemeral.

Facies N1

This facies is a flat lying to very shallowly dipping planar cross-bedded medium sandstone (Figure 2a). Cross beds dip to the northeast and southwest, the laminae of which are marked by heavy mineral lags. These are truncated by isolated J-shaped sandy burrows (*Psilonichnus* ichnofacies) (Figure 2b). The upper surface of the unit is marked by a strongly erosional boundary that truncates the foresets of Facies 1N (Figure 2a). This surface dips landwards at 30° forming a broad coast-perpendicular scour depression.

Facies N2

Sandstone with high-angle (25°) trough cross beds infills the lower scoured surface. The trough cross-beds are marked by abundant heavy mineral laminae that dip to the south-southwest (Figure 2c). The unit is 50 cm thick and has a notable absence of gravel or shell debris. Facies N2 is truncated laterally to the north by Facies 3.

Facies N3

This facies comprises high angle, planar cross bedded medium sandstone. Bedding planes are marked by heavy mineral laminae that dip to the east at 20° (Figure 2c). Isolated burrows are present. The unit is <40 cm thick and pinches to the north forming a lens like structure. Facies N3 is in turn truncated by a well-defined erosional surface, undulating along strike to form a series of runnels, each approximately 15-20 cm wide and 10 cm deep. This surface itself dips seaward at approximately 15-20 degrees.

Facies N4

This Facies rests on an erosional surface, and its base comprises a 10-20 cm-thick heavy mineral horizon of almost pure heavy minerals interspersed with cobbles to small boulders of intraformational beachrock (Figure 2b, c, and d). This unit is heavily bioturbated, burrows occurring as sandy, quartz-rich infills of material derived from the upper unit (*Skolithos* ichnofacies). The basal surface is marked by smaller cobbles and pebbles in a heavy mineral matrix. On the basal erosion surface, pebbles are seaward imbricated with long axis in the direction of current flow and grade into a crudely planar bedded pebble horizon (Figure 2d). Gravel clasts decrease in frequency with stratigraphic height, with occasional isolated shell debris evident in this horizon. The upper portions of Facies 4 are marked by seaward dipping heavy minerals laminae, some of which are truncated by a series of antidunes that overlie the pebble clasts (Figure 2e). Antidunes grade into smaller scale, rippled trough cross-sets. The upper surface of the outcrop is potholed to seaward (Figure 2f).

Umbogintwini South

Beachrock at Umbogintwini South is exposed in a 30 m outcrop, thinning to the south to just 5-10 meters, and stretching 100 m south. There is undoubtedly more beachrock buried underneath several meters of sand to both the north and south of the ouctrop. Juckes (1976) described a bone-bearing beachrock just seaward of this study site temporarily exposed in the wake of an intense storm in 1966. He also discovered intact fossilized crabs in some of the burrows preserved in now-buried beachrock at the same locality.

Facies S1

This basal facies is a >2m thick, planar laminated fine to medium sandstone with occasional large sigmoidal trough cross-beds (Figure 3a). The planar laminations dip seawards at 4° and are marked by laminae scale heavy mineral partings. Several heavy mineral-rich foresets converge tangentially to seaward forming a thick seaward-pinching horizon (Figure 3b). Some small antidunes are preserved in dip section. This layer is truncated by several sand-filled sub-horizontal burrow structures (*Thallasinoides* ichnofacies). The upper surface of this unit is truncated by a landward dipping 9° erosional surface with a well-developed heavy mineral lag (Figure 3c). This erosional surface is most prominent moving seaward in downdip section.

Facies S2

This comprises a series of steeply both landward and seaward dipping trough cross beds with 20 cm thick cosets, dipping at approximately 20° (Figure 3c). Each set is marked by gritty to very coarse sand horizons in an overall medium sand dominated succession. In strike section, Facies S2 forms a lens-like unit within Facies S1.

Facies S3

Overlying Facies S2, with an erosional contact is Facies S3, a <20 cm thick flat-lying, finely planar laminated medium to fine sandstone (Figure 3d). Occasional heavy mineral layers are evident.

Facies S4

This is a thin, <50 cm thick, veneer of trough cross-bedded, pebbly medium sandstone (Figure 3d). The pebbles comprise bioclasts including bivalves and oysters (*Crassostrea sp.*), occasional intraformational calcareous arenite clasts, and well-rounded dolerite (Figure 3e). The trough cross-bed sets vary in thickness (between 5-20 cm) and dip both seaward and landward.

Facies S5

This consists of re-cemented blocks of Facies S1 and 3S. Blocks are slabby (0.3 m x 1 m x 1 m) and appear to have collapsed and have been subsequently re-cemented onto the outcrop (Figure 3e). The contact itself forms a stylolite core where the blocks have sutured to the underlying platform, in addition to a thin coating of mixed bioclastic and pebble rich gully-fill (Figure 3d). This takes the form of a loosely consolidated and crudely bedded conglomeritic veneer, onlapping the sutured contact (Figure 3e).

Facies S6

Facies S6 includes an alongshore-oriented gully fill that extends for over 100 m (Figure 3f). The fill is a polymict conglomerate of pre-existing cobbles and small boulders of serpulid bioherms, mixed whole shells of non-life position oysters (*Saccostrea* sp.), cobbles of beachrock, arkosic sandstone, dolerite and sparse shale pebbles. These components rest in a very poorly sorted fine sand to grit matrix.

Facies S7

This occurs as a thin drape of rhizolithic, poorly consolidated, fine sandstone (Figure 3g). Facies S7 is mixed with red sands of the Berea Ridge, against which the succession onlaps, that have cascaded via the processes of slope creep and wash. The surface of the outcrop of Facies S6 and Facies S7 is marked by a series of small (20 cm diameter, 10 cm depth) potholes that have not been infilled (Figure 3h).

DISCUSSION

Northern study site interpretations

Given the planar cross-bedded sand together with the heavy mineral laminae and *Psilonichnus* ichnofacies, we interpret Facies 1 as being deposited in the swash zone. The bidirectional upper flow regime planar sets are in keeping with swash runup and backwash, marked by thin lags of heavy minerals in the intertidal zone (Reineck and Singh, 1986). Facies N2 and Facies N3 are interpreted as inlet facies that record both northward and southward migration of the inlet.

The large scale scour geometry and steeply dipping cross-sets of the scour fill are akin to records described by Reddering (1983) for the migration of microtidal inlets.

In describing the mesoscale migration of inlets, Seminack and Buynevich (2013) show steeply dipping sigmoidal-oblique foresets overlying channel lag facies in a broad "cut-and-fill" structure. The abrupt basal contacts observed also resemble those previously described in the inlet facies models of Fitzgerald *et al.* (2012).

The prominent erosional surface that truncates the inlet migration sequence represents an increasing energy regime associated with the deposition of Facies N4; this interpretation is supported by the overlying thick heavy mineral accumulations, seaward imbricated pebbles, upper flow regime planar bedding and antidunes. The most commonly observed occurrences of modern antidunes on the foreshore are in the swash zone (Hayes *et al.*, 1972; Hayes, 1976). Broome and Komar (1979) found that the formation of "backwash ripples" in the swash zone, instead of mirroring stream antidunes, is initiated by supercritical backwash flow colliding with the subcritical wave bore and undergoing an hydraulic jump. In gravelly microtidal settings, gravel imbrication in the swash zone is attributed to the forces of entrainment of blade-shaped gravel clasts via swash and winnowing of spherical gravel via backwash (Postma and Nemec, 1990). When extrapolated to pebble-sized clasts on a sandy beach, energy requirements increase, although the process itself is similar, and consequently the only likely zone of deposition is the swash zone. Thus, the facies assemblages of this unit are characteristic of storm-deposited antidune sequences in the swash zone as neither the process of massive scale winnowing nor pebble imbrication are typical of a normal fair-weather swash regime. As such, these provide a reliable indicator of the palaeo-swash zone in a microtidal setting.

Southern study site interpretations

The predominant planar cross-bedding structures, *Thallasinoides* ichnofacies and isolated antidunes suggest deposition of Facies S1 in a swash-dominated intertidal environment. The antidunes similarly represent occasions of storminess when flows reached supercritical levels (See Facies N4 Discussion); the heavy mineral layers are associated with current winnowing during the build-up, development, and decay of, these bedforms.

The trough cross-bedded and coarser components of the overlying Facies S2 are representative of a longshore trough associated with a low tide terrace at a shallow subtidal shoreline position. This unit is well-established in sedimentary literature and steeply dipping, coarse sand deposits, and trough cross-bedding, are classic markers of the longshore trough facies (Hunter *et al.*, 1979 and Greenwood and Mittler, 1985).

Facies S3 is interpreted as a backbeach unit.

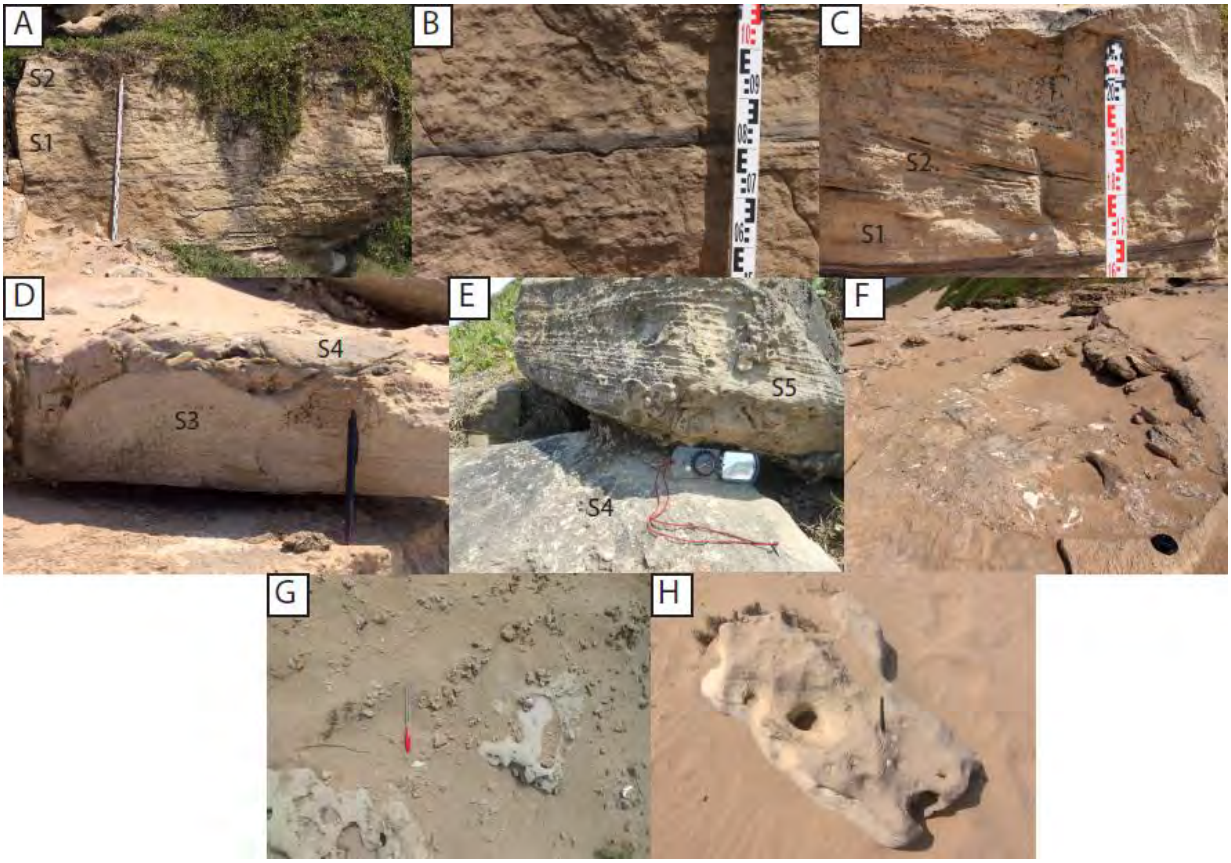

Figure 3. Outcrop photographs from Umbogintwini South (A-H). **A.** Facies 1 truncated by an erosional surface on which Facies S2 occurs. **B.** Seaward-pinching heavy mineral-rich laminae in Facies S1. **C.** Erosional contact between Facies S1 and trough cross bedded Facies S2. **D.** Facies S3 flat-lying planar laminated sandstone and overlying bioclastic gully-fill of Facies S5. **E.** Re-cemented Facies S5 collapsed blocks with stylolite-core cement of bioclastic and pebble composition attached to Facies S4, a bioclast-rich, trough cross bedded medium sandstone. **F.** Polymict conglomeratic gully fill (Facies S6) comprised of serpulid bioherms, *Saccostrea* sp. oysters, beachrock cobbles and pebbles. **G**. Loosely consolidated rizolithic fine sandstone of Facies S7. **H.** Between Facies S6 and S7 potholes occur that have not been infilled.

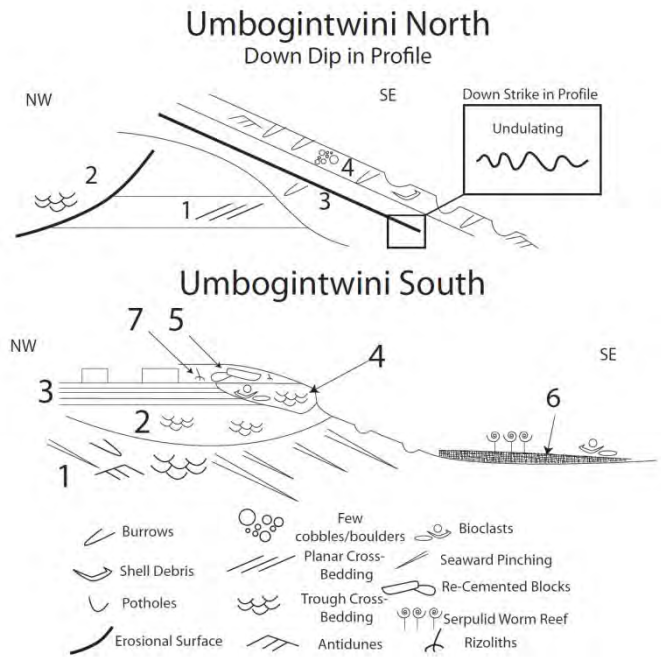

Unit	Dep Env.	~SL	Δ SL
N1	Swash zone	level	
N2	Migrating inlet	level	rise
N3	Migrating inlet	level	
N4	Swash zone	level	rise
S1	Basal foreshore	level	
S2	Longshore trough	higher	rise
S3	Backbeach	lower	fall
S4	Longshore trough	higher	rise
	Subaerial exposure	lower	fall
S5*	Supra/intertidal re-cementation	lower /level	rise
S6*	Longshore trough	higher (<S4)	fall
S7*	Aeolian dune	lower	fall

Figure 4. Schematic figure depicting the stratigraphic relationships, sedimentary structures, and basic geometry of the beachrock facies, and table summarizing depositional interpretations for each facies along with inferred relative sea level position. Chronology for the starred facies is not constrained. Abbreviations: Depositional Environment (Dep Env.), SL (sea level), and change in (Δ)

The flat-lying, planar bedded sand and the reduced presence of heavy minerals suggests a higher position up the shore profile with fewer high energy events. This unit is similar to the backbeach facies reported by Ramsay and Mason (1990) at Sodwana Bay l, ~300 km north of Durban.

We interpret the trough cross-bedding of Facies S4 to represent conditions produced by 3-D barform migration in a subtidal longshore tough depositional environment. Bioclastic debris were likely derived from the reworking of bioherm features to seaward, together with the incorporation of dolerite pebble ejecta from the palaeo-inlet and reworking of intraformational beachrock.

Facies S5 (re-cemented blocks of older facies), seems to represent a previously unrecognised beachrock facies. Additionally, the cementation style is unique to sea level position (an *intertidal* gully fill), and, as such, has remarkable potential in identifying palaeo-shoreline position.

Facies S6 is comparable with the longshore runnel complex of Cooper and Flores (1991). The inclusion of coarse material as rip up clasts of whole serpulid reef, pebbles of reworked Facies S1-S4S and the inclusion of non-life-position oyster clasts suggest storm deposition and subsequent winnowing by longshore currents in the shallow intertidal zone to leave a lag. The scoured runnel morphology lends further credence to this interpretation. The rizolithic nature of Facies S7 points to deposition by an aeolian dune. Similar facies were documented by Cooper and Flores (1991) in the area and signify a regional phase of dune building.

Local sea level history

Our interpretations of depositional environments in light of the microtidal setting of the coastline permits an interpretation of relative sea level fluctuations during the Holocene period. These are described in figure 4, a schematic of the two outcrops in section and the relative fluctuations in sea level for each facies.

Umbogintwini North

During the deposition of Facies N1 in the swash zone, sea level was approximately level with the modern position of the unit. The two migrating inlet facies, Facies N2 and N3, potentially record a shifting base level and consequent change in sea level. The contact between the intertidal Facies N1 and inlet Facies N2 marks the base of the inlet channel which incised to base level. Sea level thus rose from the time of deposition of Facies N1 to Facies N2. The transition from Facies N2 to Facies N3 marked the southward and seaward migration of the inlet, evidenced by its overall orientation. This configuration can be explained by changing longshore sediment supply that caused the reconfiguration of the inlet (e.g. Cooper, 1989; Green *et al.*, 2013). The later transition to the swash zone of Facies N4 implies a rise in sea level and translation of the shoreline over the inlet sequence.

Umbogintwini South

Sea level would have been at approximately the elevation of the basal foreshore Facies S1 at the time of its deposition. From the time of cementation of Facies S1 to S2, sea level had risen, as evidenced by the imposition of a subtidal longshore trough with an erosion surface truncating the lower unit. The along-strike depression formed in this erosional surface is interpreted as a rip channel, and the coarser material as the infill deposit. This is also consistent with rising sea levels. This phase of deposition was followed by a fall in sea level marked by the deposition of Facies S3 in the backbeach. Sea levels then rose again, causing an additional longshore trough to be superimposed over Facies S3

and infilled by the bioclastic-rich Facies S4. The inclusion of reworked beachrock, inlet pebbles, and bioclasts implies a lengthy period of shoreline stability during the deposition of Facies S4.

A sea level low was likely to have followed this period, exposing the previously cemented facies and causing the collapse of the blocks of Facies S2. The stylolitic contacts between these clasts would have initially developed in the supratidal environment where the blocks had collapsed and been shifted into position by possible wave activity (e.g Reddering, 1988) with a later cementation phase as intertidal gully fill once sea level had risen to that elevation. At the point of deposition of Facies S6, sea level would have been at a relatively higher position, but lower than that experienced during the time of deposition of Facies S4, due to Facies 4's similar depositional environment but higher vertical elevation. A key indicator constraining the age disparity between Facies S6 and the stratigraphically higher complex of Facies S4 and S5, is an unfilled pothole surface between the two. The unfilled nature of the potholes also suggests that sea level never subsequently reached this point. Finally, the aeolian Facies S7 was deposited at a time of lower relative sea level than Facies S4, and probably also Facies S6. This inference is consistent with the distance from mean sea level to modern dune cordons.

CONCLUSION

Our detailed sedimentological analysis of beachrock from two sites along the microtidal east coast of South Africa reveals the migration of a paleo inlet, and formation of beachrock in sub, inter, and supratidal settings. Particularly from the latter, we infer at least three cycles of Holocene sea level rise/fall. Although we cannot yet assess this history chronologically , three full cycles of transgression and regression are broadly consistent with previous regional sea level studies conducted by Ramsay and Cooper (2002), Compton (2006), and Norström *et al.* (2012). By more completely understanding the sedimentological characteristics of beachrock at a given locality, geoscientists can more accurately assess the coastal environment in which it formed. This study demonstrates the utility of such an analysis to the position of formation of beachrock, and thus relative sea level history.

Future efforts to age-date the cement of key sea level datums from these sites will help to further resolve the poorly-constrained Holocene sea level history of southeast Africa.

ACKNOWLEDGEMENTS

We are grateful to Mr Riaan Botes for his assistance with GIS-based figures. Additionally, we thank the U.S. Fulbright Student Program and the University of KwaZulu-Natal in their support of this research collaboration.

LITERATURE CITED

Broome, R. and Komar, P.D., 1979. Undular hydraulic jumps and the formation of backlash ripples on beaches. *Sedimentology*, 26, pp.543–559.

Caron, V., 2011. Contrasted textural and taphonomic properties of high-energy wave deposits cemented in beachrocks (St. Bartholomew Island, French West Indies). *Sedimentary Geology*, 237(3-4), pp.189–208.

Cawthra, H.C., 2012. New Insights into the Geological Evolution of the Durban Bluff and Adjacent Blood Reef, South Africa. *South African Journal of Geology*, 115, pp.291–308.

Cooper, J.A.G., 1989. Fairweather versus flood sedimentation in Mhlanga Lagoon, Natal: implications for environmental management. *South African Journal of Geology*, 92. pp. 279-294.

Cooper, J.A.G. 1991. Beachrock formation in low latitudes: implications for coastal evolutionary models. Marine Geology, 98, 145-154.

Cooper, J.A.G. 2011. Sea Level Studies: Sedimentary indicators of relative sea-level changes - high energy coasts. In: Elias, S.A. (ed) Encyclopedia of Quaternary Science. Second Edition. Elsevier.4, 385-395.

Cooper, J.A.G.. and Flores, R.M., 1991. Shoreline deposits and diagenesis resulting rom two Late Pleistocene highstands near +5 and +6 metres, Durban, South Africa. *Marine Geology*, 97, pp.325–343.

Cooper, M.R. and Liu, K., 2004. The Cainozoic palaeontology and stratigraphy of KwaZulu-Natal . Part 4 . The post-Karoo geology of the Durban area , with special reference to the Isipingo Formation. *Durban Museum Novitates*, 29, pp.1–23.

Compton, J.S., 2006. The mid-Holocene sea-level highstand at Bogenfels Pan on the southwest coast of Namibia. *Quaternary Research*, 66(2), pp.303–310.

Davies, J. L., 1964. A morphogenic approach to world shorelines. *Zeitschrift für Geomorphologie*, *8*, 127-142.

Davis, R. A., & Hayes, M. O., 1984. What is a wave-dominated coast?. *Marine Geology*, *60*(1), 313-329.

Desruelles, S., Fouache, É., Ciner, A., Dalongeville, R., Pavlopoulos, K., Kosun, E., Coquinot, Y., and Potdevin, J.-L., 2009, Beachrocks and sea level changes since Middle Holocene: Comparison between the insular group of Mykonos–Delos–Rhenia (Cyclades, Greece) and the southern coast of Turkey: Global and Planetary Change, v. 66, no. 1-2, p. 19–33.

Fitzgerald, D.M., Buynevich, I. V and Hein, C., 2012. Morphodynamics and Facies Architecture of Tidal Inlets and Tidal Deltas. In R. a. Davis, R. a. J. Davis, and R. W. Dalrymple, eds. *Principles of Tidal Sedimentology*. Springer Netherlands, pp. 301–333.

Google Earth, 2013. http://www.earth.google.com [Nov. 15, 2013].

Green, A.N., Cooper, J.A.G., Le Vieux, A.M., 2013. Unusual barrier/inlet behaviour associated with active coastal progradation and river-dominated estuaries, *J. Coast. Res.* 69, 35-45.

Green, A.N, Cooper, J.A.G. and Satzmann, L. 2014. Holocene shelf stratigraphy in the context of a stepped sea level rise: stratigraphic signature of meltwater pulses. Geology. (in press)

Greenwood, B. and Mittler, P.R., 1985. Vertical Sequence and Lateral Transitions in the Facies of a Barred Nearshore Environment. *Journal of Sedimentary Petrology*, 55(3), pp.0366–0375.

Hayes, M.O., 1976. Transitional-coastal depositional environments. In M. O. Hayes and T. K. Kana, eds. *Terrigenous Clastic Depositional Environments: Am. Assoc. Petroleum Geologists Field Course Notes*. University of South Carolina, pp. 32–111.

Hayes, M.O., Anan, F.S. and Bozeman, R.N., 1972. Sediment dispersal trends in the littoral zone; a problem in paleogeographic reconstruction. In *Coastal Environments of Northeastern Massachusetts and New Hampshire*. University of Massachusetts, pp. 290–315.

Juckes, L.M., 1976. A bone-bearing beachrock at Umbogintwini, Natal. *Transactions of the Geological Society of South Africa*, 79, pp.301–303.

Hunter, R.E., Clifton, E.H. and Phillips, L.R., 1979. Depositional Processes, Sedimentary Structures, and Predicted Vertical Sequences in Barred Nearshore Systems, Southern Oregon Coast. *Journal of Sedimentary Petrology*, 49(3), pp.0711–0726.

Kelletat, D., 2006. Beachrock as Sea-Level Indicator? Remarks from a Geomorphological Point of View. *Journal of Coastal Research*, 226, pp.1558–1564.

Knight, J., 2007. Beachrock Reconsidered. Discussion of: Kelletat , D., 2006. Beachrock as Sea-Level Indicator? Remarks from a Geomorphological Point of View. Journal of Coastal Research, 22(6), 1558–1564. *Journal of Coastal Research*, 234(July), pp.1074–1078.

Krige, L.J., 1932. The Geology of Durban. *Transactions of the Geological Society of South Africa*, 35, pp.37–67.

McCarthy, M.J., 1967. Stratigraphical and Sedimentological Evidence from the Durban Region of Major Sea-level Movements since the Late Tertiary. *Transactions of the Geological Society of South Africa*, 70, pp.135–165.

Norström, E., Risberg, J., Gröndahl, H., Holmgren, K., Snowball, I., Mugabe, J.A., and Sitoe, S.R., 2012, Coastal paleo-environment and sea-level change at Macassa Bay, southern Mozambique, since c 6600 cal BP: Quaternary International, v. 260, p. 153–163.

Postma, G. and Nemec, W., 1990. Regressive and transgressive sequences in a raised Holocene gravelly beach, southwestern Crete. *Sedimentology*, 37, pp.907–920.

Ramsay, P.J., 1995. 9000 Years of Sea-Level Change Along the Southern African Coastline. *Quaternary International*, 31(1989), pp.71–75.

Ramsay, P.J. and Cooper, J.A.G., 2002. Late Quaternary Sea-Level Change in South Africa. *Quaternary Research*, 57(1), pp.82–90.

Ramsay, P.J. and Mason, T.R., 1990. Development of a Type Zoning Model for Zululand Coral Reefs, Sodwana Bay, South Africa. *Journal of Coastal Research*, 6(4), pp.829–852.

Reddering, J.S. V, 1983. An inlet sequence produced by migration of a small microtidal inlet against longshore drift : the Keurbooms Inlet , South Africa. *Sedimentology*, 30, pp.201–218.

Reddering, J.S. V. 1988. Pseudo-stylolites produced by abrasion, Robberg, southern Cape. South African Journal of Geology , 91, pp. 415-416.

Reineck, H.E. and Singh, I.B., 1986. *Depositional Environments* 2nd ed., New York: Springer.

Schumann, E. H., & Orren, M. J. , 1980. The physico-chemical characteristics of the south-west Indian Ocean in relation to Maputaland. *in* M.N. Bruton and K.H. Cooper, eds. *Studies on the ecology of Maputaland.* Rhodes University and The Wildlife Society of Southern Africa, Grahamstown-Durban, 8-11.

Seminack, C.T. and Buynevich, I. V., 2013. Sedimentological and Geophysical Signatures of A Relict Tidal Inlet Complex Along A Wave-Dominated Barrier: Assateague Island, Maryland, U.S.A. *Journal of Sedimentary Research*, 83(2), pp.132–144.

Vacchi, M., Rovere, A., Zouros, N., Desruelles, S., Caron, V., and Firpo, M., 2012, Spatial distribution of sea-level markers on Lesvos Island (NE Aegean Sea): Evidence of differential relative sea-level changes and the neotectonic implications: Geomorphology, v. 159-160, p. 50–62.

Vousdoukas, M.I., Velegrakis, a. F. and Plomaritis, T. a., 2007. Beachrock occurrence, characteristics, formation mechanisms and impacts. *Earth-Science Reviews*, 85, pp.23–46.

Appendix D

Geophysical Research Abstracts
Vol. 16, EGU2014-112, 2014
EGU General Assembly 2014

Soft sediment deformation associated with the passage of North Atlantic Deep water through the deep Ariel Graben, Mozambique Ridge southwest Indian Ocean.

Errol Wiles (1), Andrew Green (1), Mike Watkeys (1), Wilfried Jokat (2), and Ralph Krocker (2)

(1) Geological Sciences, School of Agricultural, Earth and Environmental Sciences, University of KwaZulu-Natal, Private Bag X 54001, Durban 4000, South Africa, (2) Alfred-Wegener-Institute for Polar and Marine Research, Am Alten Hafen 26, D-27568 Bremerhaven, Germany

Interactions between bottom water currents and seafloor sediments are well known. Bottom current generated bedforms are varied both morphologicaly and sedimentologicaly. Sediment transport and deposition, associated with bottom water circulation, plays a significant role is sculpting seafloor morphology in all ocean basins. Indeed, bedforms have been used to great effect to define the presence, direction and strength of bottom water circulation globally. Here we present new multibeam swath bathymetry and high frequency seismic data from the Natal Valley and Mozambique Ridge, southwest Indian Ocean. These data show a deep (-3200 m) channel-like feature (Ariel Graben, situated at 28° 30”S on the Mozambique Ridge) connecting the northern Natal Valley to the Mozambique Basin. A distinct W – E change in seafloor morphology and seismic character is noted moving from the Natal Valley through the Ariel Graben. The northern flank of the graben exhibits smooth plastered drifts which give way to undulating seafloor in the east. The plastered drifts are characterised by distinct bottom echoes, with several discontinuous sub-bottom reflections. In contrast, the undulating seafloor is characterised by distinct hyperbolic echoes, with occasional indistinct sub-bottom reflectors. The W – E orientated undulations are straight crested, parallel / sub-parallel to the local isobaths. Wavelength is variable, ranging from 600 m to 1200 m. Cross-sectional symmetry of these features varies from symmetrical to asymmetrical, with board crests and narrow troughs. When asymmetrical, the lower (south-facing) limb is the longer (511.76 m average) than the upper (north-facing) limb (323.53 m average). The lower limbs are also steeper than the upper limbs; calculated averages being 3.80° and 1.55°, respectively. Overall, the slope on which the undulations are found, is south-facing with a gradient of 1.54°, however, the area affected by undulations is slightly steeper (average slope of 1.75°). Beyond -3000 m, the lower limit of the undulations, the gradient increases to 4.71°. The total slope average in this eastern region is 0.54° steeper than in the west area. The channel floor, no longer flat, is ca. 440 m wide at -3160 m depth. The Ariel Graben represents a deep saddle across the Mozambique Ridge at 28°30”S. This saddle provides a northern-most passage for the transport of NADW from the northern Natal Valley to the Mozambique Ridge. Evidence of this transport is manifest as crudely developed plastered drifts in the west and a soft sediment deformation field in the east of the study area. Here, current flow stripping, due to increased curvature of the saddle axis, results in deposition of suspended load in accordance with reduced current velocity. The steepened northern graben flank in this area provides limited accommodation space which promotes high sedimentation. Deposited sediments overcome the necessary shear stresses, resulting in soft sediment deformation in the form of down-slope growth faulting and generation of undulating sea-floor morphology.

SOUTHERN AFRICAN MARINE SCIENCE SYMPOSIUM: Waves of Change

15-18 July 2014 Stellenbosch, South Africa

Anatomy, high frequency seismic character and depositional processes of the lower Zambezi Channel, Mozambique Basin, SWIO.

Errol Wiles [1,a], Andrew Green [a], Mike Watkeys [a], Wilfried Jokat [b], Ralph Krocker [b]

[1]eawiles@yahoo.com

[a] Marine Geology Research Unit, Discipline of Geological Sciences, School of Agricultural, Earth and Environmental Sciences, University of KwaZulu-Natal, Westville, South Africa.

[b] Alfred Wegener Institute for Polar and Marine Research, Bremerhaven, Germany.

Deep-sea channels represent preferential sediment transport conduits to the deep ocean floor, funnelling gravity flows from canyons towards deep-sea fans. Deposits associated with these deep-sea channels may accumulate over millions of years, providing longstanding records of changing climate, hinterland tectonics, and ocean circulation. In the southwest Indian Ocean (SWIO), where tectonic activity has a complex and protracted history, such systems are especially important. To this end we investigate the anatomy and shallow seismic character of the lower Zambezi channel in order to better understand this system. New swath bathymetric and sub-bottom data collected in the northern Mozambique Basin reveal an unprecedented view of the lower 530 kilometres of the Zambezi channel. Due to apparent morphological differences between the Zambezi channel and other deep-sea channels, a number of questions are raised regarding the evolution of this system as well as how it should be classified. Findings show a straight (1.08 sinuosity) deep-sea channel which exhibits a down slope change in seismic character and channel morphology. Initially 4.2 km wide in the north, the channel floor widens to 10 km wide before opening in to a frontal splay in the south. This downstream widening is accompanied by a reduction in channel relief with depth. Several levees and terraces suggest a history of vertical erosion, with little horizontal movement of the channel axis over time. A knick point (1.1 ° change in gradient) in the main channel is associated with the confluence of the Zambezi and Tsiribihina Channels. This confluence is classified as a pure, unequal, asymmetrical type, with a confluence width to tributary width ratio of 1.05, comparable to channels of the Niger Delta, and examples form the US Atlantic margin.